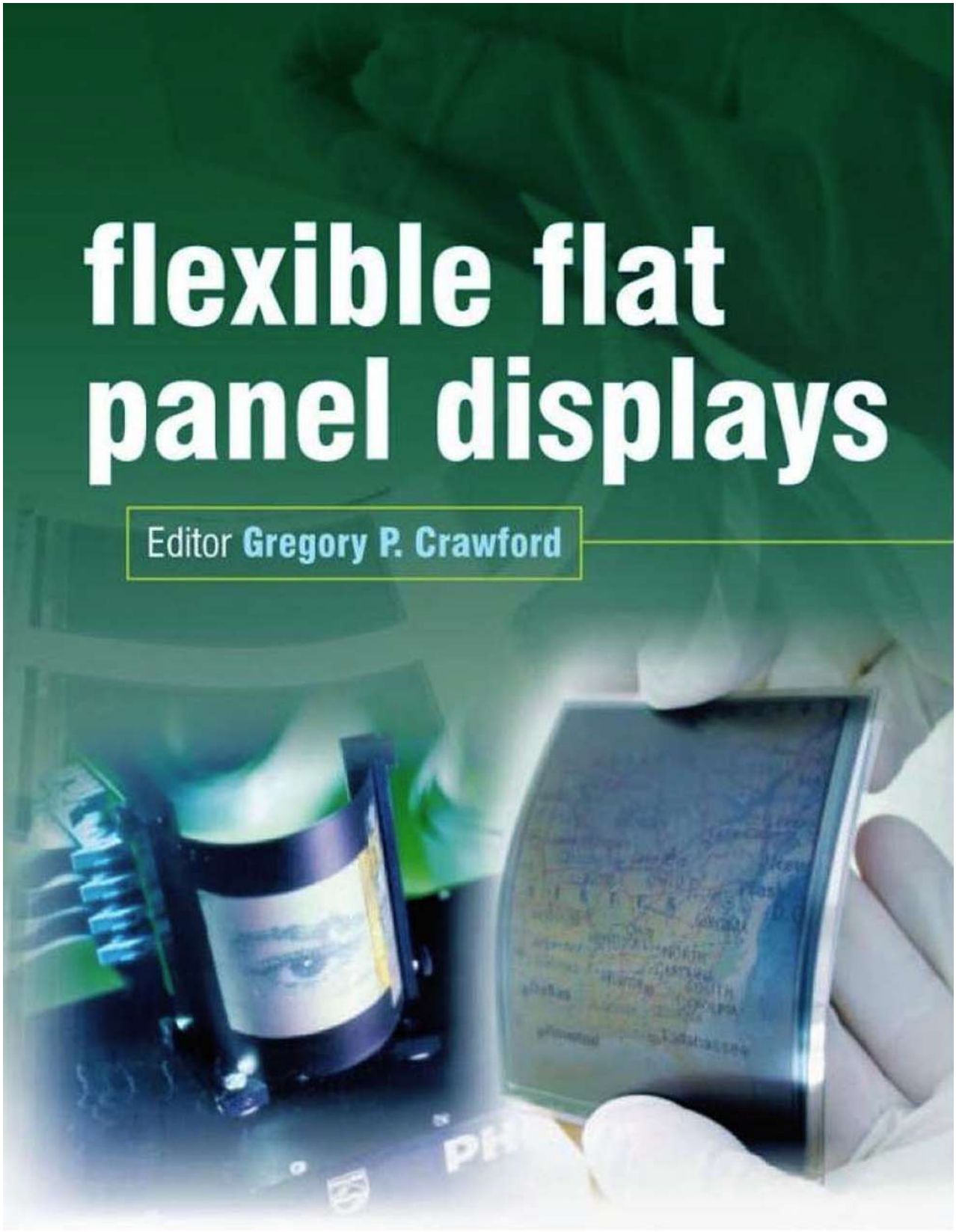
flexible flat panel displays

Editor **Gregory P. Crawford**



WILEY SID Series in **Display Technology**

Petitioner Samsung Ex-1011, 0001

Flexible Flat Panel Displays

Flexible Flat Panel Displays Edited by G. P. Crawford
© 2005 John Wiley & Sons, Ltd., ISBN 0-470-87048-6

Petitioner Samsung Ex-1011, 0002

Wiley-SID Series in Display Technology

Editor:
Anthony C. Lowe
The Lambent Consultancy, Braishfield, UK

Display Systems:
Design and Applications
Lindsay W. MacDonald and **Anthony C. Lowe (Eds)**

Electronic Display Measurement:
Concepts, Techniques, and Instrumentation
Peter A. Keller

Projection Displays
Edward H. Stupp and **Mathew S. Brennesholz**

Liquid Crystal Displays:
Addressing Schemes and Electro-Optical Effects
Ernst Lueder

Reflective Liquid Crystal Displays
Shin-Tson Wu and **Deng-Ke Yang**

Colour Engineering:
Achieving Device Independent Colour
Phil Green and **Lindsay MacDonald (Eds)**

Display Interfaces:
Fundamentals and Standards
Robert L. Myers

Digital Image Display:
Algorithms and Implementation
Gheorghe Berbecel

Flexible Flat Panel Displays
Gregory P. Crawford (Ed)

Polarization Engineering for LCD Projection
Michael G. Robinson, Jianmin Chen, Gary D. Sharp

Published in Association with the *Society for Information Display*



Petitioner Samsung Ex-1011, 0003

Flexible Flat Panel Displays

Edited by

Gregory P. Crawford

Brown University, USA



John Wiley & Sons, Ltd

Petitioner Samsung Ex-1011, 0004

Copyright © 2005 John Wiley & Sons Ltd, The Atrium, Southern Gate, Chichester,
West Sussex PO19 8SQ, England

Telephone (+44) 1243 779777

Email (for orders and customer service enquiries): cs-books@wiley.co.uk
Visit our Home Page on www.wiley.com

All Rights Reserved. No part of this publication may be reproduced, stored in a retrieval system or transmitted in any form or by any means, electronic, mechanical, photocopying, recording, scanning or otherwise, except under the terms of the Copyright, Designs and Patents Act 1988 or under the terms of a licence issued by the Copyright Licensing Agency Ltd, 90 Tottenham Court Road, London W1T 4LP, UK, without the permission in writing of the Publisher. Requests to the Publisher should be addressed to the Permissions Department, John Wiley & Sons Ltd, The Atrium, Southern Gate, Chichester, West Sussex PO19 8SQ, England, or emailed to permreq@wiley.co.uk, or faxed to (+44) 1243 770620.

This publication is designed to provide accurate and authoritative information in regard to the subject matter covered. It is sold on the understanding that the Publisher is not engaged in rendering professional services. If professional advice or other expert assistance is required, the services of a competent professional should be sought.

Other Wiley Editorial Offices

John Wiley & Sons Inc., 111 River Street, Hoboken, NJ 07030, USA

Jossey-Bass, 989 Market Street, San Francisco, CA 94103-1741, USA

Wiley-VCH Verlag GmbH, Boschstr. 12, D-69469 Weinheim, Germany

John Wiley & Sons Australia Ltd, 33 Park Road, Milton, Queensland 4064, Australia

John Wiley & Sons (Asia) Pte Ltd, 2 Clementi Loop #02-01, Jin Xing Distripark, Singapore 129809

John Wiley & Sons Canada Ltd, 22 Worcester Road, Etobicoke, Ontario, Canada M9W 1L1

Wiley also publishes its books in a variety of electronic formats. Some content that appears in print may not be available in electronic books.

Library of Congress Cataloging-in-Publication Data

Flexible flat panel displays / edited by Gregory P. Crawford.
p. cm.
Includes bibliographical references and index.
ISBN-13 978-0-470-87048-8 (alk.paper)
ISBN-10 0-470-87048-6 (alk. paper)
1. Information display systems. 2. Liquid crystal displays.
3. Electroluminescent display systems.
I. Crawford, Gregory Philip.
TK7882.I6F54 2005
621.3815′422–dc22 2005003238

British Library Cataloguing in Publication Data

A catalogue record for this book is available from the British Library

ISBN-13 978-0-470-87048-8 (HB)
ISBN-10 0-470-87048-6 (HB)

Typeset in 10/12pt Times by Thomson Press (India) Limited, New Delhi
Printed and bound in Great Britain by Antony Rowe Ltd., Chippenham, Wiltshire
This book is printed on acid-free paper responsibly manufactured from sustainable forestry in which at least two trees are planted for each one used for paper production.

Petitioner Samsung Ex-1011, 0005

Contents

List of Contributors **xvii**

Foreword **xxiii**

Series Editor's Foreword **xxv**

Preface **xxvii**

1 Flexible Flat Panel Display Technology **1**
Gregory P. Crawford

1.1 Introduction 1
1.2 Manufacturing 4
1.3 Enabling Technologies 5
1.3.1 Flexible substrates 6
1.3.2 Barrier layers 6
1.3.3 Inorganic conducting layers and mechanical properties 7
1.3.4 Organic conducting layers and mechanical properties 7
1.3.5 Optical coatings 7
1.3.6 Thin film transistors 7
1.3.7 Electro-optic materials 8
1.3.8 Flexible display prototypes 8
1.3.9 Markets 8
1.4 Conclusions 9
References 9

2 Engineered Films for Display Technologies **11**
Bill A. MacDonald, Keith Rollins, Duncan MacKerron, Karl Rakos, Robert Eveson, Katsuyuki Hashimoto, and Bob Rustin

2.1 Introduction 11
2.2 Polymer Substrates 12
2.3 Properties 13
2.3.1 Optical properties 13
2.3.2 Birefringence 14
2.3.3 Thermal properties 14
2.3.4 Moisture and solvent resistance 19
2.3.5 Surface treatment 20

Petitioner Samsung Ex-1011, 0006

2.3.6 Barrier 23
2.3.7 Mechanical properties of the composite structure 24
2.4 Polyester Films in Application 27
2.4.1 Novel low-temperature processes for building silicon-based TFTs 28
2.4.2 Adapting existing silicon processes to reasonably low temperature 29
2.4.3 Organic-based TFTs with processing temperatures below 200 °C 30
2.4.4 Use of Teonex in flexible displays 30
2.5 Concluding Remarks 31
Acknowledgements 31
References 31

3 Flexible Glass Substrates 35
Armin Plichta, Andreas Habeck, Silke Knoche, Anke Kruse, Andreas Weber, and Norbert Hildebrand
3.1 Introduction 35
3.2 Display Glass Properties 36
3.2.1 Overview of display glass types 36
3.2.2 Glass properties 37
3.3 Manufacturing of Thin "Flexible" Glass 41
3.3.1 Float and downdraw technology for special glass 41
3.3.2 Limits 42
3.4 Mechanical Properties 45
3.4.1 Thin glass and glass/plastic substrates 45
3.4.2 Mechanical test methods for flexible glasses 45
3.5 Improvement in Mechanical Properties of Glass 48
3.5.1 Reinforcement of glass substrates 48
3.6 Processing of Flexible Glass 50
3.6.1 Cleaning 51
3.6.2 Separation 51
3.7 Current Thin Glass Substrate Applications and Trends 53
3.7.1 Displays 53
3.7.2 Touch panels 53
3.7.3 Sensors 54
3.7.4 Wafer-level chip size packaging 54
References 55

4 Barrier Layer Technology for Flexible Displays 57
Gordon L. Graff, Paul E. Burrows, Rick E. Williford, and Robert F. Praino
4.1 Introduction 57
4.2 Development of Thin Film Vapor Barrier Systems 58
4.2.1 Organic electronics: packaging needs 59
4.2.2 Single-layer gas barrier films on polymeric substrates 59
4.2.3 Multilayer gas barrier films for OLEDs 60
4.3 Measurement Techniques 61
4.3.1 Steady-state transmission tests 61
4.3.2 The calcium test 62
4.3.3 Defect characterization 63
4.4 Theories of Vapor Barrier Permeation 63

Petitioner Samsung Ex-1011, 0007

4.5 Deconvolution of Experimental Data 64
4.5.1 Transient and steady-state permeation models 65
4.5.2 Methods to determine in situ properties 67
4.5.3 Implications for multilayer barrier systems 72
4.6 Discussion 73
4.7 Conclusions 74
Acknowledgements 75
References 75

5 Transparent Conducting Oxide Materials and Technology 79
David C. Paine, Hyo-Young Yeom, and Burag Yaglioglu
5.1 Introduction 79
5.2 Materials Selection and Characterization 80
5.2.1 Transparent conducting materials classes: why oxides? 80
5.2.2 Transparent conducting oxides: general considerations 81
5.3 Indium-Based Binary Oxides 84
5.3.1 Background 84
5.3.2 Crystalline indium tin oxide 86
5.3.3 Amorphous indium tin oxide 90
5.3.4 Amorphous indium zinc oxide 92
5.4 Future Directions for Transparent Conducting Oxides 94
5.4.1 Novel materials 94
5.4.2 Manufacturing considerations 95
5.5 Summary 96
References 97

6 Mechanics of ITO on Plastic Substrates for Flexible Displays 99
Piet C. P. Bouten, Peter J. Slikkerveer, and Yves Leterrier
6.1 Introduction 99
6.1.1 Plastic substrates contain thin brittle layers 99
6.1.2 Thermoelastic properties of thin films 100
6.1.3 Mechanical loading and internal stresses 101
6.1.4 Failure modes of thin brittle films 102
6.2 Failure of Brittle Layers under Tensile Stress 103
6.2.1 Mechanical test methods 103
6.2.2 Characteristic failure modes 104
6.2.3 Experimental analysis of uniform layers 104
6.2.4 Experimental analysis of patterned layers 108
6.2.5 Discussion on failure mechanics 109
6.3 Failure of Brittle Layers under Compressive Stress 112
6.3.1 Some pictures of characteristic failure modes 112
6.3.2 Mechanism of buckling failure 113
6.3.3 Buckling strain 114
6.3.4 Discussion 115
6.4 The Failure Situation in a Display 117
6.4.1 Summary of the failure results 117
6.4.2 More complex situations 118
6.4.3 What does it mean for a product? 118
6.5 Conclusions 119
Acknowledgements 119
References 120

Petitioner Samsung Ex-1011, 0008

7 Stability of Externally Deformed ITO Films **121**
Jeong-In Han
7.1 Introduction 121
7.2 Mechanical Properties of Thin Films 122
7.2.1 Numerical analysis of mechanical stress induced by bending force 123
7.2.2 Experimental results for bending-induced mechanical stress 127
7.3 Conclusions 131
References 132

8 Conductive Polymers **135**
L. "Bert" Groenendaal
8.1 Introduction 135
8.2 Historical Overview 138
8.3 Overview of Polymerization Methods 139
8.3.1 Chemical oxidative polymerizations 139
8.3.2 Chemical reductive polymerizations 140
8.3.3 Polymerizations based on organometallic cross-coupling reactions 141
8.3.4 Electrochemical polymerizations 144
8.4 Overview of Conductive Polymer Types 145
8.4.1 Polyacetylene and derivatives 145
8.4.2 Polyaniline and derivatives 148
8.4.3 Polypyrrole and derivatives 151
8.4.4 Polythiophene and derivatives 153
8.4.5 Other conductive polymers 156
8.5 Applications for Conductive Polymers 156
8.6 Outlook 158
References 159

9 Mechanical Reliability of Conductive Polymers for Rollable Display Applications **163**
Darran R. Cairns
9.1 Introduction 163
9.2 Electromechanical Properties of Transparent Anodes 165
9.2.1 ITO-coated PET in tension 166
9.2.2 PEDOT:PSS in tension 169
9.2.3 Cyclic loading in tension 169
9.3 Environmental Degradation of PEDOT:PSS 171
9.4 Cyclic Mandrel Loading of Flexible Anodes 172
9.5 Conclusions 174
References 175

10 Optical and Functional Coatings for Flexible Displays **179**
Matthew E. Sousa and Gregory P. Crawford
10.1 Introduction 179
10.2 Thin Film Polarizers 180
10.2.1 Thin crystal film polarizers 180
10.2.2 Cholesteric film polarizers 182

Petitioner Samsung Ex-1011, 0009

10.3 Thin Film Retarders 184
10.3.1 Thin crystal film retarders 184
10.3.2 Reactive mesogen retarders 185
10.4 Color Filters 186
10.5 Alignment Layers 188
10.5.1 Linear polymerized photopolymer alignment layers 189
10.5.2 Multidomain linear polymerized photopolymer alignment layers 189
10.6 Antireflective Coatings 190
10.7 Summary 191
References 191

11 Patterning Techniques and Semiconductor Materials for Flexible Electronics 195
John A. Rogers and Graciela Blanchet
11.1 Introduction 195
11.2 Large-Area Patterning Techniques 197
11.2.1 Contact printing with high-resolution stamps 197
11.2.2 Thermal transfer printing 202
11.2.3 Combining contact and thermal transfer printing 204
11.3 Printable Semiconductors and Devices 205
11.3.1 Conventional organic semiconductors 205
11.3.2 New printable semiconductors for flexible circuits 209
11.4 Prototype Circuits and Systems 212
11.5 Conclusions 214
Acknowledgements 214
References 215

12 Printed Organic Electronics 219
Raj B. Apte, Robert A. Street, Ana Claudia Arias, Alberto Salleo, Michael Chabinyc, William S. Wong, Beng S. Ong, Yiliang Wu, Ping Liu, and Sandra Gardner
12.1 Introduction 219
12.2 System Requirements 220
12.3 Transistor Requirements 222
12.3.1 Fabrication methods 224
12.3.2 Contact resistance 224
12.3.3 Short-channel effects 226
12.3.4 Bias stress and chemical stability 226
12.4 Organic Semiconductors 229
12.4.1 High-performance polythiophene designs 231
12.4.2 Poly(dialkylterthiophene) 232
12.4.3 Poly(dialkylquaterthiophene) 235
12.5 Digital Lithography 237
12.5.1 Subtractive printing 237
12.5.2 Additive printing 238
12.6 Prospects 240
Acknowledgements 240
References 241

Petitioner Samsung Ex-1011, 0010

13 Rollable Active Matrix Displays with Organic Electronics **245**
Edzer Huitema, Gerwin Gelinck, Erik van Veenendaal, Fred Touwslager, and Pieter van Lieshout
13.1 Introduction 245
13.2 Flexible Display Overview 246
13.3 Organic Electronics Technology 247
13.4 Display Design and Processing 248
13.5 Transistor Requirements 249
13.5.1 Field-effect mobility effects 250
13.5.2 Leakage current effects 252
13.6 Transistor Characteristics 253
13.7 Functional Displays 255
13.8 Driver Integration 256
13.8.1 32-Stage shift registers 258
13.8.2 120-Stage shift registers 259
Acknowledgement 260
References 260

14 Mechanics of TFT Technology on Flexible Substrates **263**
Sigurd Wagner, Helena Gleskova, I-Chun Cheng, James C. Sturm, and Z. Suo
14.1 Introduction 263
14.2 Deformation of a TFT Backplane 264
14.2.1 Mechanical stresses introduced during shaping 264
14.2.2 Mechanical stresses introduced during fabrication 265
14.3 Stress, Strain and Curvature of a Film/Substrate Couple 267
14.3.1 Stiff substrate 267
14.3.2 Compliant substrate 268
14.3.3 Bending by externally applied moment 269
14.4 Effects of Mechanical Strain on a-Si TFTs 270
14.5 Shaping of TFT Backplanes by Plastic Deformation 272
14.6 Case Studies of Stiff TFT Films on Organic Polymer Substrates 275
14.6.1 Evaluating built-in stress in a device film 275
14.6.2 Controlling mask overlay alignment by adjusting built-in stress 279
14.6.3 Determining Electrical Failure of a-Si TFTs after Bending 280
14.7 Summary and Outlook 281
References 282

15 OLED Displays on Plastic **285**
Mark L. Hildner
15.1 Introduction 285
15.2 PLED Basics 286
15.2.1 Conjugated polymers 286
15.2.2 Light-emitting diodes 287
15.2.3 OLED display types 289
15.3 Plastic Substrates for OLED 289
15.3.1 Substrate requirements 289
15.3.2 Plastic base film 290

Petitioner Samsung Ex-1011, 0011

15.3.3 Barrier 291
15.3.4 Composite substrate 292
15.4 Substrate Processing Issues 293
15.4.1 Processing issues 293
15.4.2 Film stress 294
15.4.3 Dimensional stability 295
15.4.4 Substrate fixturing 298
15.5 Passive Matrix Display Fabrication 298
15.5.1 PMOLED structure 298
15.5.2 Substrate patterning 299
15.5.3 Active material application 302
15.5.4 Cathode and encapsulation 303
15.5.5 Device operation 304
15.6 Active Matrix for OLED on Plastic 304
15.6.1 Structure 304
15.6.2 TFT requirements 305
15.7 Conclusion 307
Acknowledgements 308
References 308

16 Encapsulated Liquid Crystal Materials for Flexible Display Applications 313
Gregory P. Crawford
16.1 Introduction 313
16.2 History of Encapsulated Liquid Crystals 314
16.3 Encapsulation Techniques 318
16.4 Conformed Polymer-Dispersed Liquid Crystals 319
16.5 Holographic Polymer-Dispersed Liquid Crystals 321
16.6 Prefabricated Templates Impregnated with Liquid Crystal 325
16.7 Summary 325
References 326

17 Cholesteric Liquid Crystals for Flexible Displays 331
J. William Doane and Asad Khan
17.1 Introduction 331
17.2 Basic Properties of Cholesteric Displays 332
17.2.1 Cholesteric domains 334
17.2.2 Display brightness and view angle 335
17.2.3 Degree of circular polarization and brightness 336
17.2.4 Effect of cell thickness: brightness versus contrast 337
17.2.5 Drive voltage threshold and multiplexing 338
17.3 Drive Schemes, Chips and Circuitry 341
17.3.1 Conventional drive 341
17.3.2 Dynamic drive 341
17.3.3 Cumulative drive 342
17.3.4 Active matrix drive 342
17.4 Power Consumption 342
17.5 Full Color 343
17.5.1 Stacked color displays 344

Petitioner Samsung Ex-1011, 0012

17.5.2 Color patterning 345
17.5.3 Black and white 345
17.6 Droplet Dispersions for Flexible Displays 345
17.6.1 Emulsification 346
17.6.2 Droplet morphology 347
17.6.3 Phase separation 347
17.7 Toward Flexible Displays 350
17.7.1 Displays from emulsions 350
17.7.2 Displays from PIPS processes 351
17.7.3 Conducting polymer electrodes 352
17.8 Conclusions 352
References 352

18 Paintable LCDs: Single-Substrate LCDs Produced by Photoenforced Stratification 355
Roel Penterman, Stephen I. Klink, Joost P. A. Vogels, Edzer A. Huitema, Henk de Koning, and Dirk J. Broer
18.1 Introduction 355
18.2 Photoenforced Stratification 356
18.3 Experimental Procedures 357
18.4 Single UV Exposure 359
18.5 Two-step UV Exposure 359
18.6 Paintable Displays 362
18.7 Improved Paintable LCD Technology 364
18.8 Conclusion 367
Acknowledgements 367
References 368

19 Electrophoretic Imaging Films for Electronic Paper Displays 369
Karl Amundson
19.1 Introduction 369
19.2 Scattering Imaging Films for Displays 370
19.3 Electrophoresis and Electrophoretic Imaging 372
19.3.1 Electrophoretic switching speed 373
19.3.2 Image stability and waveforms 374
19.3.3 Integration of films into displays 374
19.3.4 Failure modes and their remedies 377
19.4 Current Electrophoretic Display Development Efforts 378
19.4.1 Microencapsulated electrophoretic displays 378
19.4.2 Microcellular air-gap electrophoretic displays 383
19.4.3 In-plane electrophoretic displays 385
19.5 Flexible and Conformable EPID Displays 387
References 389

20 Gyricon Materials for Flexible Displays 393
Nicolas Sheridon
20.1 Introduction 393
20.2 Electro-Optical Response 394
20.3 Image Storage 396

Petitioner Samsung Ex-1011, 0013

20.4 Brightness and Contrast 398
20.5 Addressing Methods 401
20.5.1 Multiple fixed-image addressing with printed circuit boards 402
20.5.2 Linear electrode array (stylus wand) addressing 403
20.6 Fabrication 405
20.7 Conclusions 406
References 406

21 Roll-to-Roll Manufacturing of Flexible Displays 409
Abbie Gregg, Lara York, and Mark Strnad
21.1 Background 409
21.1.1 Some Challenges 410
21.2 Objective 411
21.3 Device Scenario 411
21.4 Product Design 412
21.4.1 Process and tool tables 412
21.5 Tools 414
21.5.1 Tools for roll-to-roll processing 414
21.5.2 Develop, etch, strip 416
21.6 Device Inspection 416
21.6.1 Darkfield technologies 417
21.6.2 Batch web coater for EB deposition 417
21.7 Die Punch for Alignment and Registration 418
21.8 Evaporator: Thermal Cathode for LEP Device 418
21.9 Evaporator: OLED 418
21.10 Exposure: Proximity 419
21.11 Exposure: Step and Repeat 419
21.12 Inkjet Deposition 420
21.12.1 Litrex 140L inkjet system 420
21.13 Lamination 420
21.13.1 Preco 2430 P 420
21.13.2 Schmid CSL 4000 421
21.14 Laser Processing 421
21.15 Roll Coater: Photoresist 421
21.15.1 Toray model 1-2 421
21.15.2 Systronic RC 4000 421
21.16 Screen Printer 422
21.16.1 Preco 422
21.17 Oven for Low-Temperature Curing 422
21.17.1 Gruenberg model 4/MM6H100.83M 422
21.18 Sputtering 422
21.19 Materials Discussion 423
21.19.1 PEFT substrate 423
21.20 Thermal Budget for Plastic Substrates 424
21.21 Interleaf or Slip Sheet 424
21.22 Materials List 424
21.23 Processing Issues 424
21.23.1 Moisture and oxygen resistance 424
21.23.2 Cleanliness and particles 425
21.23.3 Defects and yield 425

Petitioner Samsung Ex-1011, 0014

21.24 Material Handling in Roll-to-Roll Processing 425
21.24.1 Lift cart 426
21.24.2 Leader material 427
21.24.3 Loading new rolls of material 428
21.24.4 Resist coater 429
21.24.5 Web edge in photoresist process 429
21.24.6 Cleanliness 429
21.24.7 Throughput of handling equipment 429
21.24.8 Tension control 429
21.24.9 Intermittent processing and alignment 431
21.24.10 Punch 431
21.24.11 Roll-to-roll optical alignment 431
21.24.12 Price of interleaf handling 432
21.24.13 Corrosion prevennttion: wet process 433
21.24.14 Lamination with prepunched windows 433
21.24.15 Integration of vision systems for alignment 434
21.24.16 Minienvironment enclosures 434
21.24.17 Web handling 435
21.24.18 Tension control systems 436
21.24.19 Web transport systems 437
21.24.20 Advanced roll-to-roll processing 438
21.25 Results from the Cost Model 439
21.25.1 Glossary of modelling terms 439
21.25.2 Yields 440
21.25.3 Cost results 441
21.25.4 Cost components 441
21.25.5 Cost by category 442
21.25.6 Factory size issues 442
21.25.7 Tool spacing limitations 443
21.25.8 Minimum realistic capital investment 443
21.25.9 Summary of results 443
21.25.10 Obstacles, technical issues and concerns 444
Bibliography 445

22 High-Resolution Full-Color Flexible TFT LCDs Based on Amorphous Silicon 447
Jin Jang, Sung Hwan Won, Bo Sung Kim, Mun Pyo Hong, and Kyu Ha Chung
22.1 Introduction 447
22.2 Effect of He Dilution on SiN_x Deposition 450
22.3 a-SI:H TFT on Plastic with an Organic Gate Insulator 452
22.4 Fabrication of an a-SI:H TFT Array on Plastic 456
22.5 a-SI:H TFT LCD on Plastic 459
22.5.1 Color filter on plastic 459
22.5.2 LC cell 460
22.5.3 Driver IC bonding and driving 460
References 461

23 All-Plastic Color TFT LCDs Based on Low-Temperature Poly-Si 463
Akihiko Asano
23.1 Introduction 463

Petitioner Samsung Ex-1011, 0015

23.2 Overview of the Process 465
23.2.1 TFT device process 465
23.2.2 Transfer process 466
23.2.3 Cell process 467
23.3 Results of the Transfer Process 467
23.3.1 Transferred device pattern 467
23.3.2 Influence on TFT characteristics 468
23.4 Changes in TFT Characteristics with Substrate Bending 470
23.5 Display Properties of Plastic LCDs 473
23.5.1 Specification and structure 473
23.5.2 Display performance 474
23.5.3 Displayed image on curved LCD 475
23.6 Problems to Solve 475
23.7 Summaries and Future Prospect 477
Acknowledgements 477
References 477

24 TFT Transfer Technology 479
Sumio Utsunomiya, Satoshi Inoue, and Tatsuya Shimoda
24.1 Introduction 479
24.2 TFT Transfer Process Sequence 481
24.3 Transfer Mechanism 483
24.4 TFT Performance 485
24.5 Applications 487
24.5.1 SUFTLA TFT LCD 487
24.5.2 SUFTLA TFT OLED 489
24.6 Summary 493
References 493

25 Markets and Applications of Flexible Displays 495
Kimberly Allen
25.1 Introduction 495
25.2 Why Flexible? 496
25.2.1 Lightweight displays 497
25.2.2 Rugged displays 497
25.2.3 Curved displays 497
25.2.4 Roll-up displays 497
25.2.5 Roll-to-roll manufacturing 498
25.3 Supporting Technologies 498
25.3.1 Substrate materials 499
25.3.2 Semiconductor material classes 501
25.3.3 Processing transistors on plastic 502
25.3.4 Flexible display manufacturing processes 505
25.4 Flexible Display Technologies 506
25.4.1 Liquid crystal displays 506
25.4.2 Organic light-emitting diode displays 507
25.4.3 Electrophoretic displays 508
25.4.4 Other types of display 509
25.5 Market Forecast 510
25.5.1 Top-level market view 511

Petitioner Samsung Ex-1011, 0016

25.5.2 Market by display technology 512
25.5.3 Market by application 513
25.6 Regional Development 518
25.7 Investment and Commitment 519
25.8 What Will it Take? 520
25.8.1 New substrate material 520
25.8.2 Full-color process 521
25.8.3 A ‘‘champion’’ leading to critical mass 521
25.8.4 Compelling applications 521
25.8.5 Ultra low cost production 522
25.9 Conclusion 522
References 523

Index **525**

Petitioner Samsung Ex-1011, 0017

List of Contributors

Kimberly Allen
iSuppli Corp.
2901 Tasman Drive
Suite 201
Santa Clara CA 95054
United States

Karl Amundson
E Ink Corporation
733 Concord Ave.
Cambridge, MA 02138
United States

Raj B. Apte
Electronic Materials Laboratory
Palo Alto Research Center
3333 Coyote Hill Road
Palo Alto, CA 94304
United States

Ana Claudia Arias
Electronic Materials Laboratory
Palo Alto Research Center
3333 Coyote Hill Road
Palo Alto, CA 94304
United States

Akihiko Asano
Sony Corporation
Process Development Department
Mobile Display Company
Micro Systems Network Company
4-14-1 Asahi-cho
Atsugi-City, 243-0014
Japan

Graciela Blanchet
DuPont Central Research
Experimental Station
Wilmington, DE 19880
United States

Piet C. P. Bouten
Philips Research Laboratories
Prof. Holstlaan 4
5656 AA Eindhoven
Netherlands

Dirk J. Broer
Philips Research Laboratories
Prof. Holstlaan 4
5656 AA Eindhoven
Netherlands

Paul E. Burrows
Pacific Northwest National Laboratory
Materials Science Division
PO Box 999
Richland, WA 99354
United States

Petitioner Samsung Ex-1011, 0018

Darran R. Cairns
3M Touch Systems
Optical Systems Division
300 Griffin Brook Park Drive
Methuen, MA 01821
United States

Michael Chabinyc
Electronic Materials Laboratory
Palo Alto Research Center
3333 Coyote Hill Road
Palo Alto, CA 94304
United States

I-Chun Cheng
Department of Electrical Engineering and
Princeton Institute for the Science and
Technology of Materials
Princeton University
Princeton NJ 08544
United States

Kyu Ha Chung
Samsung Electronics Co., Ltd
LCD R&D Center
Giheung-eup, Yongin
Korea

Gregory P. Crawford
Brown University
Division of Engineering
Box D
Providence, RI 02912
United States

Henk de Koning
Philips Research Laboratories
Prof. Holstlaan 4
5656 AA Eindhoven
Netherlands

J. William Doane
Kent Displays, Inc.
343 Portage Blvd.
Kent, OH 44240
United States

Robert Eveson
DuPont Teijin Films
PO Box 2002
Wilton
Middlesbrough TS90 8JF
United Kingdom

Sandra Gardner
Xerox Research Centre of Canada
2660 Speakman Drive
Mississauga, Ontario L5K 2L1
Canada

Gerwin Gelinck
Philips Research Laboratories
Prof. Holstlaan 4
5656 AA Eindhoven
Netherlands

Helena Gleskova
Department of Electrical Engineering and
Princeton Institute for the Science and
Technology of Materials
Princeton University
Princeton NJ 08544
United States

Gordon L. Graff
Pacific Northwest National Laboratory
Materials Science Division
PO Box 999
Richland, WA 99354
United States

Abbie Gregg
Abbie Gregg, Inc.
1130 East University Drive
Suite 105
Tempe, AZ 85281
United States

L. Bert Groenendaal
Agfa-Gevaert NV
R&D Materials/Chemistry Department
Septestraat 27
B-2640 Mortsel
Belgium

Petitioner Samsung Ex-1011, 0019

Andreas Habeck
Schott AG
D-55014 Mainz
Germany

Jeong-In Han
Information Display Research Center
Korea Electronics Technology Institute
Pyungtaek, Kyunggi 451-860
Korea

Norbert Hildebrand
Schott North America Inc.
Elmsford, NY 10523
United States

Mark L. Hildner
DuPont Displays
6780 Cortona Drive
Santa Barbara, CA 93117
United States

Mun Pyo Hong
Samsung Electronics Co., Ltd
LCD R&D Center
Giheung-eup, Yongin
Korea

Edzer A. Huitema
Philips Research Laboratories
Prof. Holstlaan 4
5656 AA Eindhoven
Netherlands

Satoshi Inoue
Seiko Epson Corporation
Technology Platform Research Center
281 Fujimi, Fujimi-machi
Nagano 399-0293
Japan

Jin Jang
Kyunghee University
Department of Information Display
Hoegi-dong, Dongdaemoon-gu,
Seoul
Korea

Asad Khan
Kent Displays, Inc.
343 Portage Blvd.
Kent, OH 44240
United States

Bo Sung Kim
Samsung Electronics Co., Ltd
LCD R&D Center
Giheung-eup, Yongin
Korea

Stephen I. Klink
Philips Research Laboratories
Prof. Holstlaan 4
5656 AA Eindhoven
Netherlands

Silke Knoche
Schott AG
D-55014 Mainz
Germany

Anke Kruse
Schott AG
D-37581 Bad Gandersheim
Germany

Yves Leterrier
Ecole Polytechnique Fédérale de
Lausanne (EPFL)
Laboratoire de Technologie des
Composites et Polymères (LTC)
CH-1015 Lausanne
Switzerland

Ping Liu
Xerox Research Centre of Canada
2660 Speakman Drive
Mississauga, Ontario L5K 2L1
Canada

Bill A. MacDonald
DuPont Teijin Films
PO Box 2002
Wilton
Middlesbrough TS90 8JF
United Kingdom

Petitioner Samsung Ex-1011, 0020

Duncan MacKerron
DuPont Teijin Films
PO Box 2002
Wilton
Middlesbrough TS90 8JF
United Kingdom

Beng S. Ong
Xerox Research Centre of Canada
2660 Speakman Drive
Mississauga, Ontario L5K 2L1
Canada

David C. Paine
Brown University
Division of Engineering
Box D
Providence, RI 02912
United States

Roel Penterman
Philips Research Laboratories
Prof. Holstlaan 4
5656 AA Eindhoven
Netherlands

Armin Plichta
Schott AG
D-55014 Mainz
Germany

Robert F. Praino
Vitex Systems Incorporated
3047 Orchard Parkway
San Jose, CA 95134
United States

Karl Rakos
DuPont Teijin Films
PO Box 2002
Wilton
Middlesbrough TS90 8JF
United Kingdom

John A. Rogers
University of Illinois at Urbana-Champaign
Departments of Materials Science and Engineering, and Chemistry
1304 West Green Street Urbana,
IL 61801
United States

Keith Rollins
DuPont Teijin Films
PO Box 2002
Wilton
Middlesbrough TS90 8JF
United Kingdom

Bob Rustin
DuPont Teijin Films
PO Box 411
Hopewell, VA 23860
United States

Alberto Salleo
Electronic Materials Laboratory
Palo Alto Research Center
3333 Coyote Hill Road
Palo Alto, CA 94304
United States

Nicolas Sheridon
Director of Research
Gyricon, LLC
3333 Coyote Hill Rd.
Palo Alto, CA 94304
United States

Tatsuya Shimoda
Seiko Epson Corporation
Technology Platform Research Center
281 Fujimi, Fujimi-machi
Nagano 399-0293
Japan

Peter J. Slikkerveer
Philips Research Laboratories
Prof. Holstlaan 4
5656 AA Eindhoven
Netherlands

Petitioner Samsung Ex-1011, 0021

Matthew E. Sousa
Brown University
Division of Engineering
Box D
Providence, RI 02912
United States

Robert A. Street
Electronic Materials Laboratory
Palo Alto Research Center
3333 Coyote Hill Road
Palo Alto, CA 94304
United States

Mark Strnad
Abbie Gregg, Inc.
1130 East University Drive
Suite 105
Tempe, AZ 85281
United States

James C. Sturm
Department of Electrical Engineering and
Princeton Institute for the Science and
Technology of Materials
Princeton University
Princeton NJ 08544
United States

Z. Suo
Division of Engineering and Applied
Sciences
Harvard University
Cambridge MA 02139
United States

Fred Touwslager
Philips Research Laboratories
Prof. Holstlaan 4
5656 AA Eindhoven
Netherlands

Sumio Utsunomiya
Seiko Epson Corporation
Technology Platform Research
Center
281 Fujimi, Fujimi-machi
Nagano 399-0293
Japan

Pieter van Lieshout
Philips Research Laboratories
Prof. Holstlaan 4
5656 AA Eindhoven
Netherlands

Erik van Veenendaal
Philips Research Laboratories
Prof. Holstlaan 4
5656 AA Eindhoven
Netherlands

Joost P. A. Vogels
Philips Research Laboratories
Prof. Holstlaan 4
5656 AA Eindhoven
Netherlands

Sigard Wagner
Department of Electrical Engineering and
Princeton Institute for the Science and
Technology of Materials
Princeton University
Princeton NJ 08544
United States

Andreas Weber
Schott AG
D-31073 Grünenplan
Germany

Rick E. Williford
Pacific Northwest National
Laboratory
Materials Science Division
PO Box 999
Richland, WA 99354
United States

Sung Hwan Won
Kyunghee University
Department of Information Display
Hoegi-dong, Dongdaemoon-gu, Seoul
Korea

Petitioner Samsung Ex-1011, 0022

William S. Wong
Electronic Materials Laboratory
Palo Alto Research Center
3333 Coyote Hill Road
Palo Alto, CA 94304
United States

Yiliang Wu
Xerox Research Center of Canada
2660 Speakman Drive
Mississauga, Ontario L5K 2L1
Canada

Burag Yaglioglu
Brown University
Division of Engineering
Box D
Providence, RI 02912
United States

Hyo-Young Yeom
Brown University
Division of Engineering
Box D
Providence, RI 02912
United States

Lara York
Abbie Gregg, Inc.
1130 East University Drive
Suite 105
Tempe, AZ 85281
United States

Petitioner Samsung Ex-1011, 0023

Foreword

Flexible displays have prompted many popular news stories and myths, like the roll-up newspaper in the side of your phone or inside a pen case. Some may call them dreams, perhaps even some of the authors in this book picture these applications in their minds for motivation and imagine big new markets in the assuredly display-centric world of the future.

Not me. Call me a cynic. As a marketing guy, I know hype when I see it. As a physicist, I know many challenges and hurdles remain to be overcome. As a businessman, with many years of the large and unique display business under my belt, I also know that economics beats technology and/or features every time. When I first saw DOS software from Microsoft and the network application from AOL, I felt that both the interface and performance could be improved. I also felt that better technologies and solutions should exist – but both thrived on a more simple economic model and straightforward marketing push. The best technical solution rarely wins, but the most economically successful does.

Flat displays, which have recently become a huge economic force (due largely to the TFT LCD industry I call home) had great features going for them for many years (thin, light, low-power, ergonomic; all of which contributed to making them desirable to the consumer via better interior design elements) but had huge economic and technical hurdles to overcome (which they did with the tireless efforts of hundreds of companies in their supply chain over the past two decades). Now they have developed from an enabling technology (for notebooks and cellphones) to a huge replacement technology (for PC monitors and even HDTVs) and have shifted from a high-priced technical wonder to a widespread consumer product workhorse. They also showed that 20–30 companies working together can accomplish more than one or two could ever dream of, even if the one or two had better technology.

We stand at the precipice of a similar evolutionary possibility for the flexible display. Will it punch through the many technical and economic barriers to enable better, cheaper and perhaps even new types of display devices, or will the flexible display category stay stuck in the lab for many years as AMOLEDs have so far, and carbon nanotubes certainly may?

As a scientist, and a display and product guy, I am thrilled to see the economic progress that the field has achieved over the past few years, much of it well reflected by the diverse yet deep selection of chapters in this book. As a realistic businessman, however, I know that all of the new design opportunities these types of displays could enable are inconsequential compared to the real economic driving forces behind the work in this volume: cheaper manufacturing costs and lighter, more durable flat displays. If you can build a bendable TFT

Petitioner Samsung Ex-1011, 0024

on plastic, then perhaps the benefits of roll-to-roll manufacturing and higher throughput (and maybe lower capex costs) could be achieved for mainstream flat panel applications. That – and not foldable or bendable end-user displays – is the real prize, with the rest, if any, being icing on the cake.

What is the state of the art today? Well, that's what this book tries to answer, or at least it takes a wide snapshot of a large and dynamic band of an enormous sea of scientific and technological effort being done in pursuit of the dream of a truly flexible display. As in many scientific endeavors, the hype around future industrializations and applications sometimes seems to get ahead of the results (OLEDs?), but hopefully this book will help to calibrate the flexible display world as we know it, and point toward some areas of great progress and promise.

The hype has been that you could easily foresee a world of bendable, printable, plastic displays, easily made in high volume with a low-cost manufacturing process. They are envisioned to be thinner lighter, more ergonomic and having higher resolution than today's ''flat'' (but usually glass) inflexible displays. Of course, to date, the reality is one of high costs and low volumes, difficult manufacturing, and poor conformability without a clear market, process, or even supply chain. Thus, one might claim, there is poor visibility to see where the focus or efforts should be.

But take heart – remember it was not so long ago when TFT LCDs were an expensive display alternative for the niche portable PC application and measured less than 9 in in diagonal. Few people a decade or so ago could imagine a world of hundreds of millions of much larger-sized LCDs shipping as PC notebooks and even mainstream monitors, let alone flat TVs at 37 in wide or even 42 in wide as is commercially available today. The next ten years could see equally dramatic changes in the world of flexible displays, and I for one am excited by the peek into the future provided by the efforts and vision displayed in this book. The devil, of course, is in the detail. But the creativity and diligent efforts displayed in the work represented in these chapters is truly admirable. From printable electronics to stampable, flexible, rollable display substrates, from electronic ''paper'' to conductive polymers – the achievements so far are breathtaking and the implications often staggering, yet much work will lie ahead. I hope that you'll join me in the excitement over the possibilities herein, and bend a page or two quickly, to get started in this enlightening tour of our potential future.

Bruce Berkoff

Executive Vice President of Marketing
LG.Philips LCD, Seoul, Korea
December 2004

Petitioner Samsung Ex-1011, 0025

Series Editor's Foreword

Every advance in technology needs champions. Here you will find, written by a worldwide collection of such champions, the most comprehensive collection of essays on the subject of Flexible Displays ever published.

''Holy Grail'' is a term often used by those in pursuit of the difficult and challenging. It is mentioned more than once in the following chapters and the implication that the vision described in this book will be difficult to achieve is apt. However, if scientists and engineers had not attacked in the past and did not continue to attack the daunting tasks involved in developing new concepts and applications of technology, we would not now be enjoying the benefits of advanced display technology and future progress would be slow or non-existent.

No one can predict with certainty if or when flexible displays will emerge into the mainstream of display technology. Certainly, some major reductions in cost will be required, as well as performance improvements — in some cases, such as the oxygen and water permeability of polymeric substrates for use with OLEDs, orders of magnitude improvement. But success will require even more than this; compelling applications in the market place. We should be mindful that the debate continues whether the market would prefer a direct view rollable display or one which projects images directly on to the retina.

However, that is not really the point. A major effort in industry and academia is now under way, and advances will undoubtedly be made from this push to develop flexible displays. These will involve the development of flexible glass and polymeric substrates, barrier layers, organic conductors and semiconductors and new display effects. This effort will produce enormous benefits, not only for display technology in general but for other potentially low cost and revolutionary technologies unrelated to displays.

So, I congratulate Greg Crawford in his enthusiasm and zeal to achieve his objective of creating an ubiquitous range of flexible displays in many different applications. Immerse yourselves in this vision of the future and you will learn not just about flexible displays, but about developments which will, in other ways, be of great relevance to the future.

Anthony Lowe

Series Editor
Braishfield, England

Petitioner Samsung Ex-1011, 0027

Preface

No one really knows what the future holds in any industry, but if researchers have their way in the flat panel industry it is almost certain that truly flexible displays will emerge on the commercial market in the not too distant future. The development of flexible display technology promises to reshape the global flat panel display landscape and open up compelling new applications for displays which do not exist today. At first glance flexible flat panel displays may appear to be modified renditions of current flat panel display technology, but they will differ in many significant ways. These differences will determine how they will serve existing display product applications, as well as new markets in which the flexible and robust nature of the display will enable unique applications. In order for flexible flat panel displays to become a reality, widespread transformations will need to occur industry-wide. In particular, the infrastructure for manufacturing, processing, and assembly will take on a completely new look especially if roll-to-roll methods are implemented.

The recent convergence of many technologies (substrates, conducting layers, barrier layers, electro-optic materials, thin film transistor technologies, and manufacturing processes) is accelerating the flexible flat panel display concept closer to commercial reality. Many flexible flat panel display prototypes have been developed by several display companies around the world. Many smaller entrepreneurial firms focused on display components are growing up around the flexible display concept and betting on the paradigm shift to flexible in the future. The field is truly interdisciplinary, combining basic principles from nearly all engineering and science disciplines. From a purely scientific and technical perspective, the thrust towards flexible flat panel displays will uncover many new research and development opportunities and challenges for engineers, physicists, chemists, and material scientists. There are many obstacles and challenges that may prevent flexible flat panel displays from realizing their full commercial potential, but these obstacles and challenges represent great opportunities for technologists and high-technology companies.

The overriding purpose of the book is to condense the basic knowledge needed to understand the various technologies associated with the burgeoning field of flexible flat panel displays into a single volume. The book encompasses many chapters focused on the fundamentals and applications of flexible flat panel displays written by researchers who

Petitioner Samsung Ex-1011, 0028

are authorities in their respective fields. The authors come from industry and academia to ensure a balance of fundamental science, engineering, and high technology. The chapters are all self-contained and organized to bring the reader from the component level, through display system and assembly, to the possible manufacturing routes. I believe this collection of contributed papers by internationally renowned researchers, exclusively covering the science and technology of flexible flat panel displays, will further accelerate and stimulate the development of this exciting field.

Finally, I am indebted to my esteemed colleagues who graciously devoted their time and expertise in preparing contributions for this book. If not for their excellent contributions, such a collection of state-of-the art chapters in this rapidly expanding field would not be possible. I am confident that their time and dedication to this endeavor have been well rewarded. I am also grateful to the National Science Foundation's Materials Research Science and Engineering Center on Micro- and Nanomechanics of Structural and Electronic Materials (DMR 0079964) at Brown University for its continued support over the years of my flexible display research. I also wish to thank John Wiley for all of its assistance throughout the preparation of this book. So many John Wiley employees were involved in the book's attractive presentation, which is greatly appreciated. From a personal level, I have enjoyed my interaction with the authors and it is my hope that this book will serve the flat panel display industry for many years to come.

Gregory P. Crawford

Brown University, Providence, RI

Petitioner Samsung Ex-1011, 0029

1

Flexible Flat Panel Display Technology

Gregory P. Crawford

Division of Engineering, Brown University, Providence RI

1.1 Introduction

The manufacturing of flat panel displays is a dynamic and continuously evolving industry. Improvements of flat panel displays are made rapidly as technology improves and new discoveries are made by display scientists and engineers. The cathode ray tube and active matrix liquid crystal display (LCD) recently celebrated their 100th and 25th anniversary, respectively. The arrival of portable electronic devices has put an increasing premium on durable, lightweight and inexpensive display components. In recent years, there has been significant research investment in the development of a flexible display technology. Figure 1.1 shows the evolution away from the bulky CRT display to the thin active matrix LCD for desktop applications, and the much anticipated paper-like flexible flat panel display of the future. To enable a flexible flat panel display, a flexible substrate must be used to replace conventional glass substrates, which can be either plastic or thin glass. Flexible flat panel display technologies offer many potential advantages, such as very thin profiles, lightweight and robust display systems, the ability to flex, curve, conform, roll, and fold a display for extreme portability, high-throughput manufacturing, wearable displays integrated in garments and textiles, and ultimate engineering design freedom (e.g. odd-shaped displays) as shown in Figure 1.2(a). Many of these potential advantages have been the principal

Flexible Flat Panel Displays Edited by G. P. Crawford
© 2005 John Wiley & Sons, Ltd., ISBN 0-470-87048-6

Petitioner Samsung Ex-1011, 0030

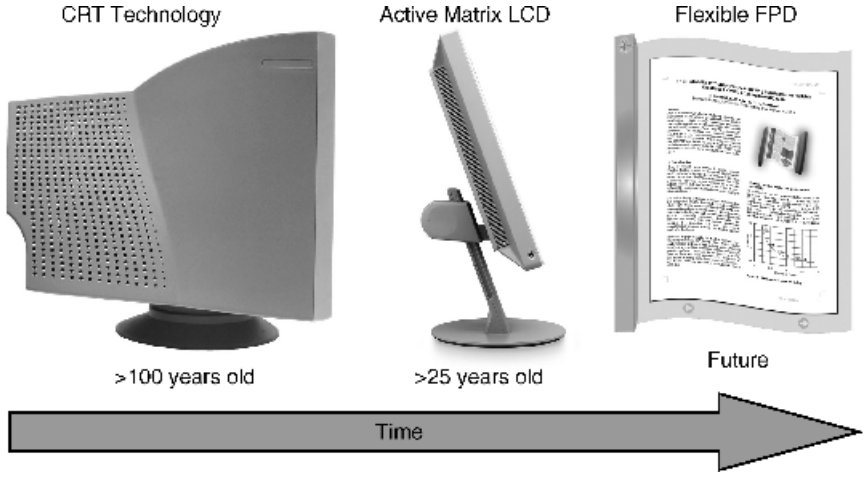


Figure 1.1 Evolution of display technology

driving force behind much of the effort and resources dedicated towards the development of flexible flat panel display configurations.

There are also many new compelling product categories enabled by the promise of plastic display technology. An electronic newspaper, for example, could eventually update headlines throughout the day. If plastic displays on televisions and computers could become

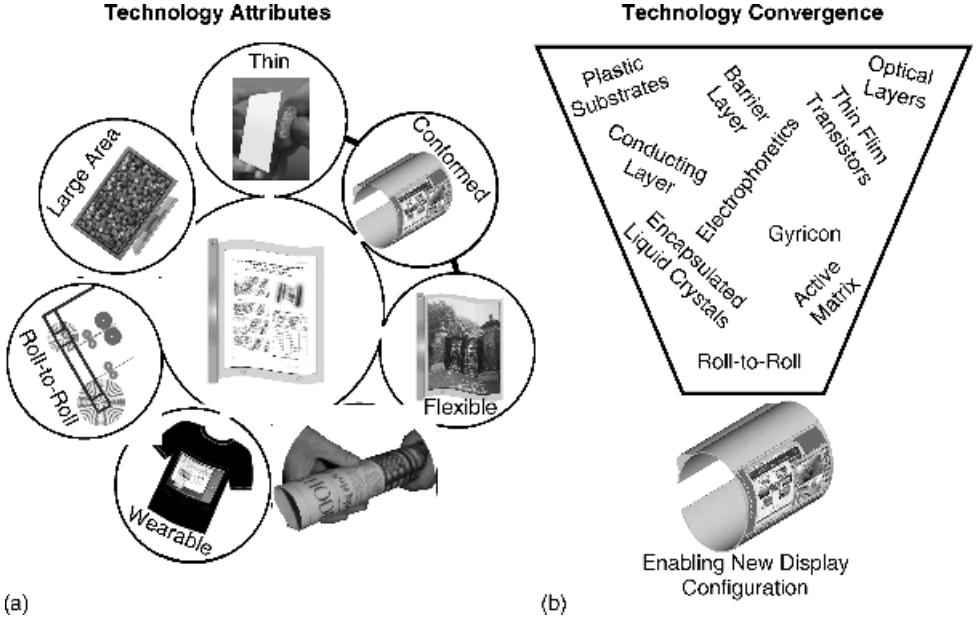


Figure 1.2 (a) The technology attributes of flexible displays and (b) the convergence of the many technologies that are making flexible flat panel displays feasible

Petitioner Samsung Ex-1011, 0031

analogous to fabric or paper, they would no longer dominate our physical and aesthetic worlds. We could make them fade from sight when not in service. The television could simply disappear into a painting or tapestry. Your PDA could roll up into a pen that you could stick into your shirt pocket. Instead of adapting our aesthetic sensibilities to incorporate technology into our lives, technology could better reflect our imagination and creativity.

The broad definition of a flexible flat panel display is as follows (Slikkerveer 2003):

> A flat panel display constructed of thin (flexible) substrates that can be bent, flexed, conformed, or rolled to a radius of curvature of a few centimeters without losing functionality.

Defining a flexible display is akin to defining modern art (Slikkerveer 2003). Because the diversity of the application space for flexible display technology is so vast, it is hard to propose an all-encompassing definition. The term ''flexible display'' means different things to different people. Flexible displays may only be flexed once during their lifetime; for example, during manufacturing to create a permanently conformed display. For a rollable display application, however, the display may be rolled and unrolled more than 100 times per day.

The ability to flex a display has fascinated researchers for many years, only today they are being seriously considered for a number of applications and moving closer to the marketplace (Howard 2004; Ong 2004; Kinkade 2004; Hogan 2003; Hellemans 2000; Savage 1999). One of the primary reasons for the increased interest is that many of the necessary enabling technologies for flexible displays are maturing to the extent where reasonable-looking prototypes are being produced by many research and development organizations. As illustrated in Figure 1.2(b), the convergence and evolution of technologies such as flexible substrates, barrier layers, conducting layers, electro-optic materials, optical and functional thin film materials, and thin film transistors (TFTs) is making possible new flexible display concepts.

Flexible display technology can potentially result in many compelling applications not satisfied by a rigid glass-based display. Figure 1.3 shows several artistic renditions of flexible display concepts, such as a large-area, wall-sized reflective screen for use in a conference room setting that could be rolled away when not in use (a), a small portable rollable display (b), an irregular-shaped display used in the steering wheel of an automobile (c), a conformed display integrated in an automobile filling up the entire dashboard (d), a wristband display that is permanently conformed throughout its lifetime (e), and a switchable mask for children, also permanently conformed. Also, there may be a temptation to believe flexible displays will replace glass-based displays for many other applications. While this may be possible at some point in the future, it will be difficult for flexible displays to compete solely on cost alone in the inexpensive and small display module market (e.g. super twisted nematic displays) or in the high-end, high-performance market such as desktop and laptop screens. For the time being, flexible displays will most likely enter the marketplace in a unique way where their positive attributes are clearly capitalized on. The market outlook for flexible displays is surveyed in Chapter 25.

Flexible flat panel display technology constitutes an eclectic research field and potentially large industry in the future. Its highly interdisciplinary range combines basic principles from engineering, physics, chemistry, and manufacturing. The following chapters will provide a comprehensive overview of this exciting and multidisciplinary field.

Petitioner Samsung Ex-1011, 0032



Figure 1.3 Various flexible flat panel display concepts: (a) a direct-view large-area screen; (b) a rollaway display system; (c) an odd-shaped display integrated in a steering wheel of an automobile; (d) a permanently conformed display covering the entire dashboard of an automobile; (e) a permanently conformed display that securely fits around the wrist; and (f) a child's switchable mask. Renditions courtesy of Suraj Gorkhali, Brown University

1.2 Manufacturing

Although it may be somewhat of an overstatement, the words ''holy grail'' are often used to describe the flat panel display community desire to achieve a commercialized flexible display technology (Kincade 2004). One reason why these words are often used is because flexible displays, in principle, are amendable to a roll-to-roll manufacturing process which

Petitioner Samsung Ex-1011, 0033

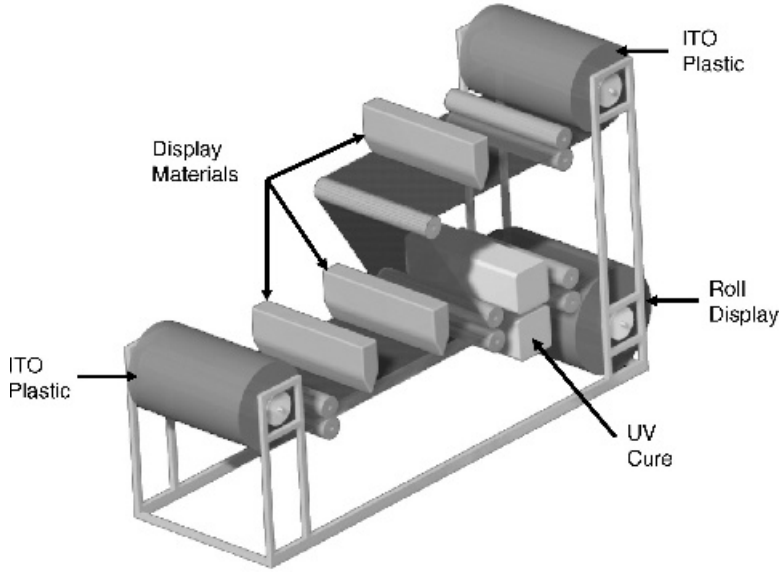


Figure 1.4 A simple schematic diagram of a roll-to-roll manufacturing process

would be a revolutionary change from current batch process manufacturing (Chapter 21). Figure 1.4 shows a simple conceptual illustration of a roll-to-roll manufacturing process where display materials are deposited on indium-tin-oxide (ITO) coated plastic substrates, processed, and rolled back up.

As compared to a batch process, which handles only one component at a time, roll-to-roll processing represents a dramatic deviation from current manufacturing practices. If and when roll-to-roll manufacturing technology matures for display processing, it promises to reduce capital equipment costs, reduce display part costs, significantly increase throughput, and it may potentially eliminate component supply chain issues if all processes are performed with roll-to-roll techniques. Although batch processing can still be employed to manufacture flexible flat panel displays, many researchers and technologists believe that roll-to-roll manufacturing will ultimately be implemented.

1.3 Enabling Technologies

The technology of flexible displays includes many components and supporting technologies. Anticipating a new market opportunity, the display industry has been developing display materials targeted specifically at flexible flat panel display requirements. These technologies must be compatible and converge to enable a truly flexible display. The necessary technologies include robust flexible substrates, conducting transparent conducting oxides and/or conducting polymers, electro-optic and reflecting materials, inorganic and organic electronics, and packaging technologies. In addition, many processes must also be developed and optimized in concert with the materials development, such as roll-to-roll manufacturing,

Petitioner Samsung Ex-1011, 0034

coating technology, and printing. In reality, these components and processes cannot be optimized independently since a flexible display is a complex system of linked components that must be co-developed in order to function efficiently. It should be made clear that not all technologies described in this book will survive the flexible flat panel race. Since the field is still racing towards commercialization at a rapid pace, it is not at all clear which technologies will win and ultimately become commercialized. The book provides an overview of nearly all the technologies competing in the flexible display landscape, and each topic area provides several solutions for the specific needs of a flexible flat panel display.

1.3.1 Flexible Substrates

There are two choices for flexible substrates, which include polymeric and thin glass. Since the flexible substrate represents the fundamental starting component for the display, flexible substrates arguably face the greatest challenges in terms of compatibility with all of the other necessary display layers that need to be integrated onto them. Chapter 2 focuses on polymer films engineered for flexible display technologies. A number of issues are discussed such as process temperature limitations as a function of polymer type, optical properties, thermal properties, and surface smoothness properties. One of the biggest challenges for polymeric substrates is the process temperature required by subsequent display layers (Lueder 2002). It is highly unlikely that flexible displays in the foreseeable future will be completely organic, but rather they will be a hybrid of inorganic and organic layers and components. However, the process temperatures for many inorganic layers have been decreasing (Chapter 5) and the thermal stability of polymer substrates has greatly improved (Chapter 2). This represents one example where technologies are converging in an optimal way to enable flexible displays.

The other solution for flexible substrates is organic based (Chapter 3). Glass has the ultimate barrier properties and is resistant to display process temperature and chemicals, but it lacks the flexibility and ease of handling found in polymeric substrates. Chapter 3 discusses a glass manufacturing process which can process thin glass down to 30 μm thicknesses. In order to improve mechanical stability for flexibility and processing, a polymeric layer is deposited on the glass. This hybrid solution enables one to capitalize on the positive attributes of glass, as well as to enable it to be more flexible and process handling friendly.

1.3.2 Barrier Layers

When polymeric substrates are employed in flexible display applications, a barrier layer is required to protect the enclosed functional materials and layers from oxygen and water permeation (Chapter 4). Oxygen and water permeation through a flexible substrate is of particular importance to organic light-emitting diode (OLED) devices (Chapter 15). Although single-layer barrier layers do provide the packaged materials with some protection, it appears that multiple layers are necessary for OLED applications for long-term stability. Chapter 4 discloses an inorganic/organic hybrid multilayer solution to create a barrier layer that is beginning to satisfy the demanding requirements of an OLED material.

Petitioner Samsung Ex-1011, 0035

1.3.3 Inorganic Conducting Layers and Mechanical Properties

Indium tin oxide (ITO) is the typical conducting layer used in display technologies. However, the process temperatures required for ITO on glass to obtain low sheet resistance and high optical throughput properties is incompatible with plastic substrates. Therefore lower-temperature processes have to be developed for ITO in order for it to be considered for flexible display applications (Chapter 5). Although ITO has excellent sheet resistance and optical properties, it does have one shortcoming in the flexible display realm. When ITO is deposited on a polymeric substrate, it can crack (buckle) under tensile (compressive) strain. For a flexible display application, ITO cracking can cause catastrophic failure (Chapter 6). Because of the importance of ITO in display applications, there is significant emphasis on the mechanics of ITO in this book (Chapters 6 and 7). The mechanics of ITO on polymeric substrates is becoming better understood in flexible display applications. In addition, the models and fundamentals learned by studying ITO on polymeric substrates can also be applied to other components, such as inorganic thin film transistors (TFTs) on plastic.

1.3.4 Organic Conducting Layers and Mechanical Properties

Conducting polymers are also being considered for flexible display applications (Chapter 8). Although their sheet resistance and optical properties are not as attractive as ITO, they do have exceptional mechanical properties (Chapter 9) and low process temperatures. Chapter 8 describes the fundamentals of the underlying chemistry of conducting polymers and Chapter 9 investigates the mechanics of conducting polymers as compared to ITO. As ITO and conducting polymer technology compete for the conducting substrate solution, there is a new conducting substrate technology based on nanotechnology. Flexible and transparent electrodes have been formed from carbon nanotube dispersions in combination with wet coating processes and printing techniques (Arthur *et al.* 2004).

1.3.5 Optical Coatings

Optical coatings will play an important role in flexible flat panel displays. Many optical films that are used on conventional glass-based displays will be applicable to flexible display configurations. Polarizers, retarders, color filters, antireflection films, and alignment layers for liquid crystals are discussed in Chapter 10. This is an area of research and development that has not been specifically targeted towards the flexible display field, but it does constitute a crucial set of elements in certain flexible display configurations. For example, the paintable LCDs presented in Chapter 18 require thin film polarizers. Additionally, when super twisted nematic (STN) displays are used in a flexible configuration, they require thin film polarizers, retarders, color filters, and backlights (Slikkerveer *et al.* 2004).

1.3.6 Thin Film Transistors

For many electro-optic materials, such as OLEDs (Chapter 15), polymer-dispersed liquid crystals (Chapter 16), paintable LCDs (Chapter 18), electrophoretics (Chapter 19) and

Petitioner Samsung Ex-1011, 0036

Gyricon materials (Chapter 20), an active matrix backplane will be required for high resolution. Considerable work is being dedicated to developing various processes to print and pattern organic electronics on polymeric substrates (Chapters 11, 12, 13). There is also significant research and development in developing processes for inorganic TFTs on foil (Chapter 14) and polymer substrates (Chapter 24). The failure mechanisms of TFTs on flexible substrates are also critical to the future success of flexible displays, as discussed in Chapter 14. The success of TFTs for plastic substrates to date has been an enabler for flexible flat panel displays and constitutes a very vital component. They have enabled the development of high-resolution prototypes.

1.3.7 Electro-Optic Materials

The various types of electro-optic materials for flexible display applications essentially fall into three categories – emissive, reflective, and transmissive – analogous to the categories for glass-based displays. For emissive applications, OLED materials are being developed that can be small molecule or high molecular weight (Chapter 15). In order to have a truly low-power display, a reflection mode of operation will have to be implemented on flexible substrates. Polymer-dispersed liquid crystals (Chapter 16), chiral liquid crystal dispersions (Chapter 17), encapsulated electrophoretics (Chapter 19), and bichromic ball composites (Chapter 20) all operate in the reflective mode. For electronic book and surrogate paper applications, an efficient reflective mode display is critical to eliminate the need for a power-hungry backlight. Chapter 19 discloses a unique process to paint liquid crystals onto a flexible substrate. Although this technique currently uses a transmissive display mode, the process may be applicable to other materials that can operate in reflection.

1.3.8 Flexible Display Prototypes

The primary reason for the interest in flexible displays also arises from the early success of prototypes manufactured by a number of organizations. A number of display system papers are also presented, including a high-resolution LCD based on amorphous silicon (Chapter 22), a full-color LCD based on low-temperature polysilicon (Chapter 23), and an OLED display that was manufactured using a TFT transfer process (Chapter 24). Clearly the ability to prototype high-quality flexible display prototypes has had a tremendous impact on the continued interest and investment in the flexible display arena. The prototypes show the industry what is possible.

1.3.9 Markets

Although the future is difficult to predict, the book culminates with a chapter dedicated to the market analysis for flexible flat panel displays. There are many applications in which flexible flat panel displays are suitable for today, but we still do not know what clever applications the industry will come up with once flexible flat panel displays enter the marketplace and how the early adopters react to the new technology.

Petitioner Samsung Ex-1011, 0037

1.4 Conclusions

The recent development of many components and supporting technologies for flexible flat panel display applications, such as substrates, conducting layers, barrier layers, electro-optic materials, thin film transistor technologies, and manufacturing processes, is accelerating the flexible flat panel display concept towards the marketplace. Very impressive flexible flat panel display prototypes have been manufactured by several display groups around the world, which continues to drive interest and development in the field. The fundamental purpose of the book is to provide a comprehensive work that covers the knowledge needed to understand the various technologies associated with the burgeoning field of flexible flat panel displays and to disclose the state of the art in the field. The book is all-encompassing, with chapters focused on the fundamentals and applications of flexible flat panel displays written by active researchers in their respective fields. The authors come from industry and academia to ensure a well-balanced treatment of the subject matter, which covers fundamental science, engineering, and the state of the art in flexible display technology.

References

Authur, D., Glatkowski, P., Wallis, P. and Trottier, M. (2004) Flexible transparent circuits from carbon nanotbues. *SID Digest of Technical Papers* **XXXV**, 582–585.

Hellemans. A. (2000) Polymer matrix augurs flexible displays. *IEEE Spectrum* **37**, 18–21.

Hogan, H. (2003) Never too thin. *Photonics Spectra* **37**, 66–72.

Howard, W. E. (2004) Better displays with organic films. *Scientific American*, 76–81.

Kincade, K. (2004) Flexible displays open new windows of opportunity. *Laser Focus World* **40**, 65–69.

Lueder, E. (2002) Plastic substrates for flat panel displays. *Proceedings of the 7th Asian Symposium on Information Display*, 13–14.

Ong, B. (2004) Flat-panel displays – semiconductor ink advances flexible displays. *Laser Focus World* **40**, 85–88.

Savage, N. (1999) Flexible displays – electronic paper coming to market. *Laser Focus World* **35**, 42–46.

Slikkerveer, P. J. (2003) Bending the rules. *Information Display* **3**, 20–24.

Slikkerveer, P., Bouten, P., Cirkel, P., de Goede J., Jagt, H., Kooyman, N., Nisato, G., van Rijswijk, R. and Duineveld (2004) A fully flexible color display. *SID Digest of Technical Papers* **XXXV**, 770–774.

Petitioner Samsung Ex-1011, 0038

2

Engineered Films for Display Technologies

Bill A. MacDonald, Keith Rollins, Duncan MacKerron, Karl Rakos, Robert Eveson, Katsuyuki Hashimoto, and Bob Rustin

DuPont Teijin Film

2.1 Introduction

While today's display industry is, to a very large extent, based on rigid, glass-based devices with the dominant space occupied by LCDs, there is an emerging flexible display industry which is forecast to show significant growth towards the end of this decade and into the next (Allen and Mentley 2003) and which will have the opportunity to exploit the display technologies of OLED and e-paper in addition to LCD. The challenges involved in converting the concept of flexible displays into consumer and other user reality are significant and will require considerable multi-disciplinary efforts. A whole range of issues must be addressed including user acceptance, supply chain investments, display technology development (e.g. OLED, e-paper, flexible backplane). In the complexity of these considerations, it is possible to lose sight of the criticality regarding the development and supply of high-quality flexible substrates which are optimised for device manufacture. The supply of such materials requires the substrate to be robust to a set of performance characteristics which are a challenge to all commercially available plastics; significant research efforts are being made today to develop the plastic-based materials which will therefore be required and fully functional in finished devices. The goal of much of this research is to define the ''engineered substrates'' which will be a key

Flexible Flat Panel Displays Edited by G. P. Crawford
© 2005 John Wiley & Sons, Ltd., ISBN 0-470-87048-6

Petitioner Samsung Ex-1011, 0040

platform in the establishment of a flexible displays industry. There is currently considerable interest in flexible displays (Slikkerveer 2002, 2003), and many electronic-based companies and new entrants are presently actively researching flexible displays based on primarily liquid crystal displays (LCD) (Kim *et al.* 2003), organic light-emitting diodes (OLEDs) (Heeks and Hough 2003; Innocenzo *et al.* 2003) and electrophoretic displays (Chen *et al.* 2003).

Flexible displays offer substantial rewards in terms of being able to develop displays that are thinner, lighter, robust, conformable and can be rolled away when not required. In addition, plastic-based substrates coupled with the recent developments in solution deposition and inkjet printing for laying down OLED materials (MacPherson *et al.* 2003) and active matrix thin film transistor (TFT's) arrays (Sirringhaus *et al.* 2003) open up the possibility of cost-effective processing in high volumes using roll-to-roll processing (van den Berg 2001). Flexible displays can be built on metal foil, very thin glass coated with a polymer and a variety of plastics; this review will concentrate on plastic films and biaxially oriented polyester films in particular. To replace glass, a plastic substrate needs to be able to offer the properties of glass, i.e. clarity, dimensional stability, thermal stability, barrier, solvent resistance, low coefficient of thermal expansion (CTE) coupled with a smooth surface. No plastic film offers all these properties, so any plastic-based substrate will almost certainly be a multilayer composite structure. This chapter will discuss and contrast the leading candidates for plastic-based flexible substrates and discuss examples of the polyester films in use. Note that this is a fast-evolving field and some of the results discussed in the literature may not represent what the flexible substrate suppliers would (or will in the future) present as their preferred tailored candidates. This chapter tries to present a comparison based on current knowledge of the available substrates.

2.2 Polymer Substrates

This review will focus only on plastic films that have been given serious consideration as flexible substrates for flexible electronics. The main candidates are shown in Figure 2.1, which lists the substrates in terms of increasing glass transition T_g (MacDonald 2004; MacDonald *et al.* 2003).

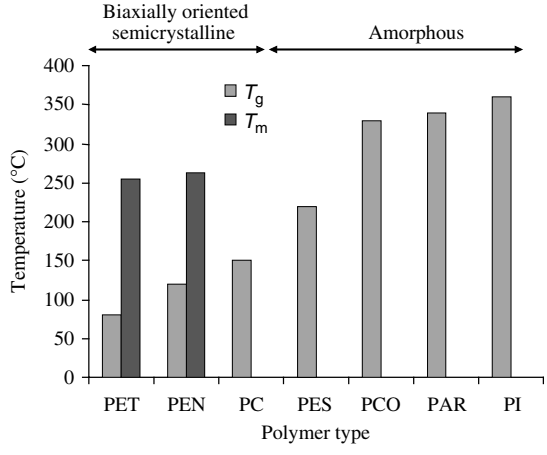


Figure 2.1 Comparison of a range of plastics by glass transition

Petitioner Samsung Ex-1011, 0041

The polymers can be further categorised into films that are semicrystalline, amorphous and thermoplastic, and amorphous but solvent cast. The group of thermoplastic semicrystalline polymers includes polyethylene terephthalate (PET), e.g. DuPont Teijin Films Melinex polyester film (Melinex); polyethylene naphthalate (PEN), e.g. DuPont Teijin Films Teonex polyester film (Melinex); and polyetheretherketone, e.g. Victrex PEEK. PEEK, with a T_g of $\sim$140 °C and a T_m of 340 °C, is in the upper temperature range for the semicrystalline thermoplastic polymers that can still be melt processed. Polyethylene terephthalate and polyethylene naphthalate films are prepared by a process whereby the amorphous cast is drawn in the machine direction and the transverse direction. The biaxially oriented film is then heat set to crystallise the film. PEEK film is prepared by an extrusion process but is not biaxially oriented. Polymers with T_g values higher than 140 °C that are semicrystalline tend generally to have melting points that are too high to allow the polymers to be melt processed without significant degradation. The next category is polymers that are thermoplastic but noncrystalline; these range from polycarbonate (PC), e.g. Teijin PURE-ACE and GE Lexan (PURE-ACE) with a T_g of $\sim$150°C, to polyethersulphone (PES), e.g. Sumitomo Bakelite Sumilite (Sumilite) with a T_g of $\sim$220 °C. Although thermoplastic, these polymers may also be solvent cast to give high optical clarity. The third category is high-T_g materials that cannot be melt processed and includes aromatic fluorene-containing polyarylates (PAR), e.g. Ferranias Arylite (Arylite); polycyclic olefin (PCO), also known as polynorbornene, e.g. Promerus Appear (Appear); and polyimide (PI), e.g. DuPont Kapton (Kapton).

This review will focus primarily on the crystalline biaxially oriented films which have different properties compared to amorphous films (both melt and solvent cast) and for simplicity these two basic categories will be used when comparing and contrasting the properties of the film types.

2.3 Properties

2.3.1 Optical Properties

The clarity of the film is important for bottom-emissive displays where one is viewing through the film and a total light transmission (TLT) of $>$ 85% over 400–800 nm coupled with a haze of less than 0.7% are typical of what is required for this application. All the base films described above meet this criterion, except for polyimide which is yellow; polycarbonate in particular has excellent optical properties; see Table 2.1 (MacDonald 2004). The percentage transmission of Teonex Q65 is shown in Figure 2.2.

Table 2.1 Basic properties of films used for base substrates

	PET	PEN	PC	PES	PAR	PCO	PI
CTE (−55 to 85 °C) ppm/°C	15	13	60–70	54	53	74	17
Transmission at 400–700 nm (%)	$>$ 85	$>$ 85	$>$ 90	90	90	91.6	yellow
Water absorption (%)	0.14	0.14	0.2–0.4	1.4	0.4	0.03	1.8
Young's modulus (GPa)	5.3	6.1	1.7	2.2	2.9	1.9	2.5
Tensile strength (MPa)	225	275	NA	83	100	50	231

Note: The information in this table is taken from different datasheets and should only be taken as illustrative.

Petitioner Samsung Ex-1011, 0042

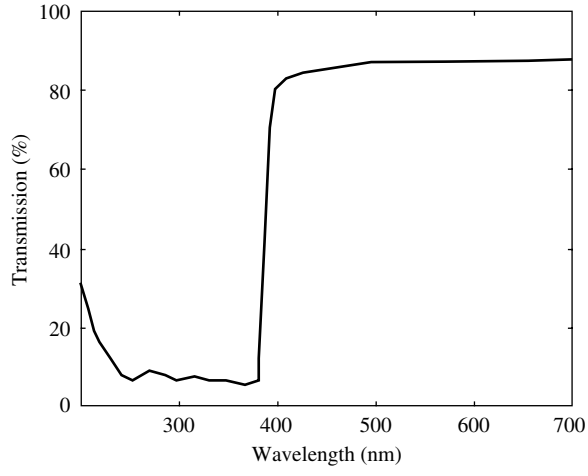


Figure 2.2 Percentage transmission of Teonex Q65

For top-emissive displays, clarity in the base substrate is not essential and this opens up the possibility of building display devices on non-transparent substrates such as stainless steel or polyimide which is yellow. However, top-emissive displays will still need an optically clear barrier film as an encapsulant.

2.3.2 *Birefringence*

Biaxially oriented films such as polyethylene terephthalate and polyethylene naphthalate are birefringent. The dependence on light of known polarisation in LCDs means that birefringent films, which would change the polarisation state, are unlikely to be used as substrates. Films based on amorphous polymer are not birefringent and are more suitable for LCDs. Birefringence is not an issue with OLED or electrophoretic displays.

2.3.3 *Thermal Properties*

Thermal and dimensional stability are critical in enabling a film to withstand the high temperatures required for deposition of barrier coatings and indium tin oxide coatings; to ensure precision registration of the different layers in the final device; and for the multilayer device to be able to withstand thermal cycling during its manufacture. Plastic films undergo a variable and undesirable change in dimensions at T_g, due to molecular relaxation events associated with the increased mobility of the polymer chains and also 'shrinkage' or 'expansion' associated with the relaxation of residual strain within the oriented parts of the film

Petitioner Samsung Ex-1011, 0043

structure. With biaxially oriented polyesters this is a consequence of the film manufacturing conditions. However, it is important to consider what are the key property requirements when choosing materials for device manufacture. T_g is an obvious characteristic to focus on initially.

Polymers undergo a change in physical and mechanical properties at the glass transition T_g. However, for OLED and/or active matrix backplane manufacture it is not the change in mechanical properties that is of prime importance, but rather the control of the dimensional reproducibility as the film is cycled in temperature. This is manifested in two ways. Firstly, there is the shrinkage a film undergoes when it is heated then cooled to the starting temperature. Low levels of shrinkage are desired to make accurate alignments on the substrates after each thermal processing step. Secondly, there is the natural expansion of the film as the temperature is cycled, as measured by the coefficient of linear thermal expansion (CLTE); this is often called the coefficient of thermal expansion (CTE). A low CLTE typically < 20 ppm/°C is desirable to match the thermal expansion of the base film to the layers which are subsequently deposited. A mismatch in thermal expansion means that the deposited layers become strained and cracked under thermal cycling.

Polyethylene terephthalate and polyethylene naphthalate films with T_g values of 78 and 120 °C, respectively, would at first sight be considered to have too low a T_g to impart the thermal and dimensional stability necessary to support OLED manufacture. However, the dimensional stability of polyethylene terephthalate and polyethylene naphthalate films can be enhanced by a heat stabilisation process (MacDonald 2004; MacDonald *et al.* 2003), in which the internal strain in the film is relaxed by exposure to high temperature while under minimum line tension. The majority of polymer films, when heated to temperatures above the nominal T_g, show some tendency to shrink or expand along selected axes. Shrinkage at a given temperature is measured by placing the sample in a heated oven for a given period of time. The percentage shrinkage is calculated as the percentage change of dimension of the film in a given direction or molecular axis before and after the heating process. Heat-stabilised polyethylene naphthalate film exhibits minimal shrinkage of order $< 0.1\%$ and typically $< 0.05\%$ when exposed to temperatures of up to 180 °C for 30 min. In addition, once heat stabilised, the T_g effects described above are essentially negated and polyethylene naphthalate film remains a dimensionally reproducible substrate up to 200 °C, i.e. within the performance requirements of a flexible substrate for an OLED display. Polyethylene terephthalate film exhibits minimal shrinkage up to 150 °C.

How the dimensions change with temperature and time is clearly illustrated by results from thermal mechanical analysis carried out using a TMA-7 thermomechanical analyser (Perkin Elmer). These data compare heat-stabilised 125 μm polyethylene naphthalate film to non-heat-stabilised 125 μm polyethylene naphthalate film (Figure 2.3) (MacDonald 2004; MacDonald *et al.* 2003) and heat-stabilised polyethylene naphthalate film to heat-stabilised polyethylene terephthalate film (Figure 2.4).

In the evaluation, the films have been heated and subsequently cooled between 8 °C and 140 °C, 160 °C, 180 °C and 220 °C, respectively, and any permanent change in dimensions on cooling back to room temperature before the next heating cycle are recorded on the *y*-axis. This is illustrated in Figure 2.3 where heat-stabilised polyethylene naphthalate film reproducibly follows the same expansion and contraction path as the sample is heated through T_g and to higher temperatures and then cooled. Under the same conditions, non-stabilised polyethylene naphthalate film remains dimensionally stable up to 120 °C, but shrinks above

Petitioner Samsung Ex-1011, 0044

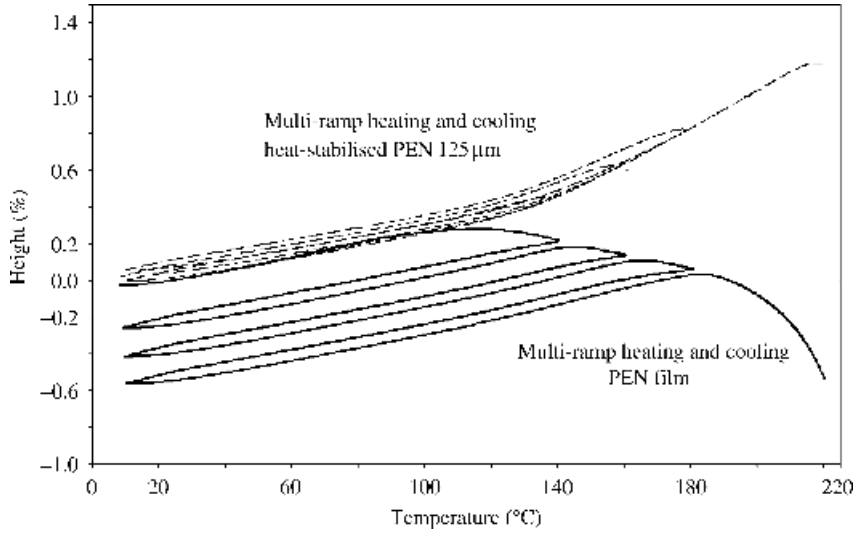


Figure 2.3 Thermomechanical analysis of 125 µm PEN and heat-stabilised 125 µm polyethylene naphthalate films

this temperature. Heat-stabilised polyethylene terephthalate film follows the same expansion and contraction path up to 150 °C (Figure 2.4).

The rates of expansion against temperature vary and are known to depend on factors such as draw ratio, heat-setting temperatures and subsequent heat treatment or thermal mechanical history.

In a further experiment, samples of Teonex Q65 were heated from 20 °C to the isothermal temperature (150, 160, 180 or 200 °C) at 20 °C/min, then held isothermally at the selected

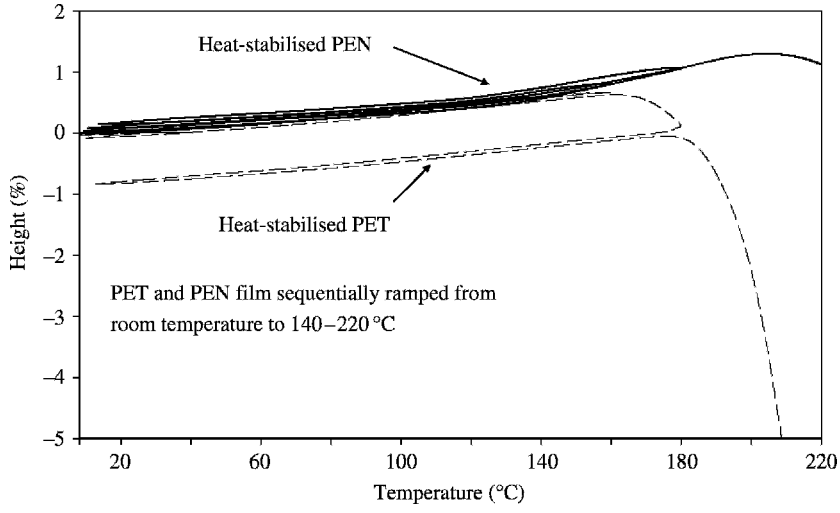


Figure 2.4 Thermal analysis of heat-stabilised polyethylene terephthalate and heat-stabilised polyethylene naphthalate films

Petitioner Samsung Ex-1011, 0045

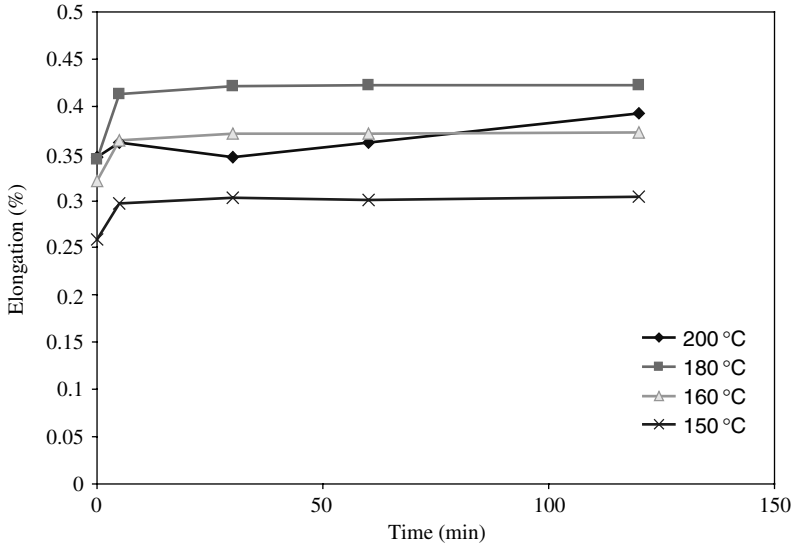


Figure 2.5 Thermomechanical analysis of polyethylene naphthalate film

temperature for two hours. The samples were examined using the Perkin Elmer TMA-7 in extension analysis mode. The specimen had length ∼12.5 mm, width 5 mm and thickness 0.125 mm. The applied load was 20 mN (tension = ∼30 000 N/m^2). Figure 2.5 shows the percentage elongation just as the isothermal conditions are approached, which was at approximately 5 min (the first point on the graph). The films show the natural expansion of the films on heating, but once the selected temperature has been reached there is no change in dimensions on heating for up to 2 h. The film heated to 200 °C is exhibiting shrinkage as well as the natural expansion of the sample.

The amorphous family of polymers exhibit very low shrinkages when cycled to temperatures below their respective T_g values and therefore the higher the T_g, the higher the operating window.

Research has shown that the shrinkage values of amorphous and semicrystalline films can be pushed further by annealing the films at elevated temperatures for extended periods of time. Polyimide, polyarylate and polycyclic olefin films exhibited shrinkages of < 10 ppm per hour when annealed at 300 °C for 10–100 h (Angiolini *et al.* 2003). Polyethersulphone exhibited a similar shrinkage when annealed at 180 °C for a similar period of time (Young *et al.* 2003). Polyethylene naphthalate shrinkages of 25 ppm during thin film transistor backplane processing, after an annealing process have recently been reported (Sarma *et al.* 2003).

The coefficient of linear thermal expansion (CLTE) values (MacDonald 2004; MacDonald *et al.* 2003) for polyethylene naphthalate are generally lower than for most equivalent polyethylene terephthalate based films (by ∼25%) and the higher glass transition, T_g, for polyethylene naphthalate film means that relaxation events (related to increased molecular mobility) would therefore occur at relatively higher temperatures (Table 2.2).

At T_g polymers normally exhibit a threefold increase in CLTE. However it can be seen from Figures 2.3 and 2.4 that with the heat-stabilised polyethylene terephthalate and polyethylene naphthalate films there is only a small change in the natural expansion of the film.

Petitioner Samsung Ex-1011, 0046

Table 2.2 Coefficient of linear thermal expansion (ppm/°C) for heat-stabilised polyethylene naphthalate film

	−50 °C to 0 °C	0 °C to 50 °C	50 °C to 100 °C	100 °C to 150 °C
Machine direction	13	16	18	25
Transverse direction	8	11	18	29

Using the information in Figure 2.5 it is possible to calculate the CLTE for the temperature range over which the sample is heated, here encompassing the T_g process.

Notice from Table 2.3 that the CLTE of Teonex Q65 in the range from 20 °C to the isothermal temperature (150, 160, 180 °C) is about 25 ppm/ °C (the sample heated to 200 °C shows a lower CTLE due to the shrinkage effect mentioned above). The CLTE below T_g is of

Table 2.3 Coefficient of linear thermal expansion for heat-stabilised polyethylene naphthalate film over temperatures covering the glass transition temperature

Temperature range (°C)	Elongation(%)	CLTE (ppm/°C)
20–150	0.3	23
20–160	0.37	26
20–180	0.42	26
20–200	0.36	20

order 15–20 ppm/ °C; the change at T_g is relatively small. This contrasts favourably with the quoted coefficient of expansion of amorphous polymers, typically 50 ppm/°C (Won *et al.* 2003) below T_g but it can increase by a factor of 3 above T_g. A low CLTE is essential to match the CLTE of inorganic coatings and is a unique feature of the Teonex Q65 family being both semicrystalline and biaxially oriented.

Once shrinkage, or additional expansion effects (principally due to release of residual strain effects within the oriented parts of the structure) have been removed by the heat stabilisation process outlined above, the changes in the CLTE value with temperature are essentially predictable. The differential measured along the two principal axes, machine direction (MD) and transverse direction (TD), reflects the degree of orientation within each molecular axis within the plane of the polyethylene naphthalate film; that is, the lower the CLTE value, the higher the degree of orientation. The CLTE value for unoriented isotropic polyethylene naphthalate by comparison is measured at ∼35 ppm/°C.

Taking the CLTE and shrinkage data together, heat-stabilised polyethylene terephthalate and polyethylene naphthalate films are therefore dimensionally predictable substrates below the temperature ranges at which they have been heat stabilised. It is the ability to firstly limit and secondly to predict changes in dimension with temperature that are exploited in the OLED and TFT manufacturing process.

In addition to dimensional stability, another important factor is the upper processing temperature (T_{max}) that a film can be used at. Although T_g does not define T_{max} for the semicrystalline polymers, it largely defines it for the amorphous polymers. Figure 2.6 shows

Petitioner Samsung Ex-1011, 0047

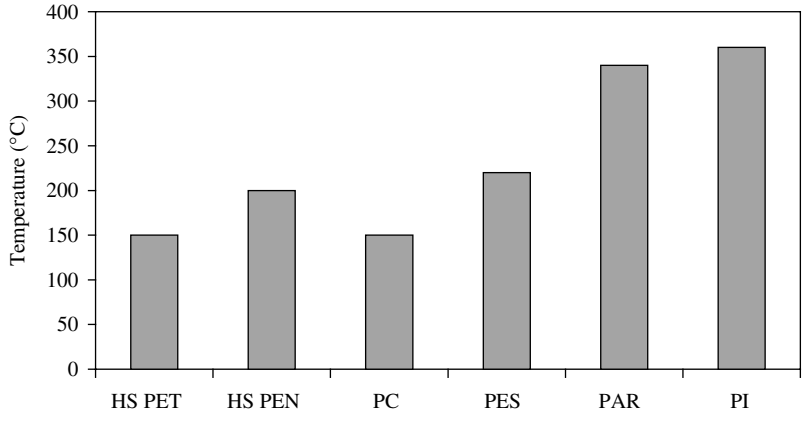


Figure 2.6 Upper operating temperature of base substrates

the upper operating temperature if the effect of heat stabilisation is taken into account. However, again the picture is not quite as simple, as the films based on amorphous polymers may be hardcoated to give solvent resistance (Section 2.3.5) and T_{max} is then defined by the thermal stability of the hardcoat. This can bring T_{max} down to 220 °C for some of the solvent-cast amorphous polymers.

2.3.4 Moisture and Solvent Resistance

A wide range of solvents and chemicals can potentially be used when laying down the various layers in display depending on the processing steps involved. Amorphous polymers in general have poor solvent resistance compared to semicrystalline polymers (Table 2.4).

Table 2.4 Table of solvent resistance

	Unit	Q65	PET	PC	PES
Ketone	Acetone	Good	Good	(Fair)	(NG)
	MEK	Good	Good	(Fair)	(—)
Alcohol	Methanol	Good	Good	(Good)	(—)
	Ethanol	Good	Good	(Good)	(Good)
	Isopropanol	Good	Good	(Good)	(—)
	Butanol	Good	Good	(Good)	(—)
Ester	Ethyl acetate	Good	Good	(Fair)	(Good)
Hydrocarbon	Formalin	Good	Good	(NG)	(—)
	Tetrachroloethane	Good	Good	(—)	(Good)
Acid	10% HCI	Good	Good	(—)	(Good)
	10% $HN0_3$	Good	Good	(—)	(Good)
	10% H_2SO_4	Good	Good	(—)	(Good)
	Acetic acid	Good	Good	(—)	(—)
Alkali	10% NaOH	Good	Fair	(—)	(Good)

Petitioner Samsung Ex-1011, 0048

This deficiency is overcome by the application of a hardcoat to the amorphous resins, which significantly improves the solvent and chemical resistance to solvents such as NMP, IPA, acetone, methanol, THF, ethyl acetate, 98% sulphuric acid, glacial acetic acid, 30% hydrogen peroxide and saturated bases such as sodium hydroxide (Angiolini *et al.* 2003).

Polymers absorb water and the amounts of water they absorb can have a very detrimental effect on their dimensional stability. This will become increasingly important as processing moves towards roll-to-roll. Polyethylene terephthalate and polyethylene naphthalate films have an inherent advantage over the amorphous polymers films, as they are semicrystalline and biaxially oriented and they will typically absorb approximately 1400 ppm of moisture at equilibrium (the exact figure depends on temperature and relative humidity). Polyethersulphone and polyimide films are particularly problematic and will absorb over 1% moisture at equilibrium (Sumilite and Kapton). Polycyclic olefin film is an exception to this and has a very low moisture absorption level of 300 ppm (Appear).

Although pre-annealing the substrate can greatly reduce shrinkage and careful process design can reduce the effects of swelling due to solvents and water, it is very likely that alignment equipment will require special adaptations. With polyethylene terephthalate and polyethylene naphthalate films, a hardcoat is not required to give solvent resistance.

2.3.5 Surface Treatment

The surface smoothness and cleanliness of the flexible substrates are essential to ensure the integrity of subsequent layers such as barrier and conductive coatings (Section 2.3.6). With polyethylene terephthalate and polyethylene naphthalate films, improvements in surface quality can be achieved through control of recipe and film process. This is demonstrated in Figure 2.7, which highlight the substantial reduction of surface defect peaks with two different grades of polyethylene naphthalate film (MacDonald 2004; MacDonald *et al.* 2003). A 2.5 mm square area of industrial grade polyethylene naphthalate (Figure 2.7(a)), as measured using conventional non-contacting, white light, phase-shifting interferometry techniques (the instrument used was a Wyko NT3300 surface profiler), contains over ten peaks greater than 100 nm in height and numerous peaks over 50 nm. Compare this with the optical grade polyethylene naphthalate (Teonex Q65) in Figure 2.7(b), where only five peaks greater than 50 nm exist throughout the same measured area, indicating how the surface quality can be controlled by recipe and process optimisation alone. The surface defects which remain in the Teonex Q65, however, are still detrimental to the performance of thin overlying layers. To remove them entirely requires the application of a coating layer, typically comprised of a scratch-resistant material. This acts to smooth over all the underlying polyethylene naphthalate film surface defects and additionally helps to prevent surface scratches on handling. The coated film surface is now ''surface engineered'' for the deposition of subsequent layers.

The degree of smoothness Teonex Q65 surface-engineered film provides over that of its corresponding pretreated substrate is best shown through atomic force microscopy (AFM) analysis. Figure 2.8 shows the surface of the Teonex Q65 with a pretreat coating present to give adhesion to the subsequent smoothing, antiscratch coating compared to surface-engineered Teonex Q65.

Measurements over much larger sampling areas (1.2 cm), using white light interferometry (WYKO, PSI mode and with 1.6 μm lateral resolution), demonstrate the consistent

Petitioner Samsung Ex-1011, 0049

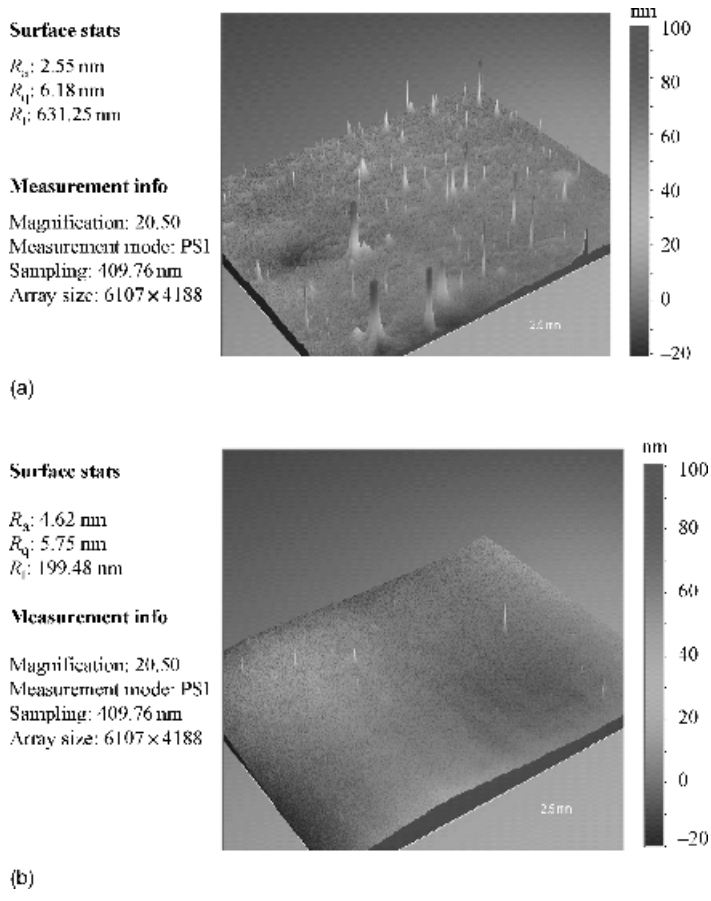


Figure 2.7 (a) Surface smoothness of industrial grade polyethylene naphthalate. (b) Surface smoothness of Teonex Q65

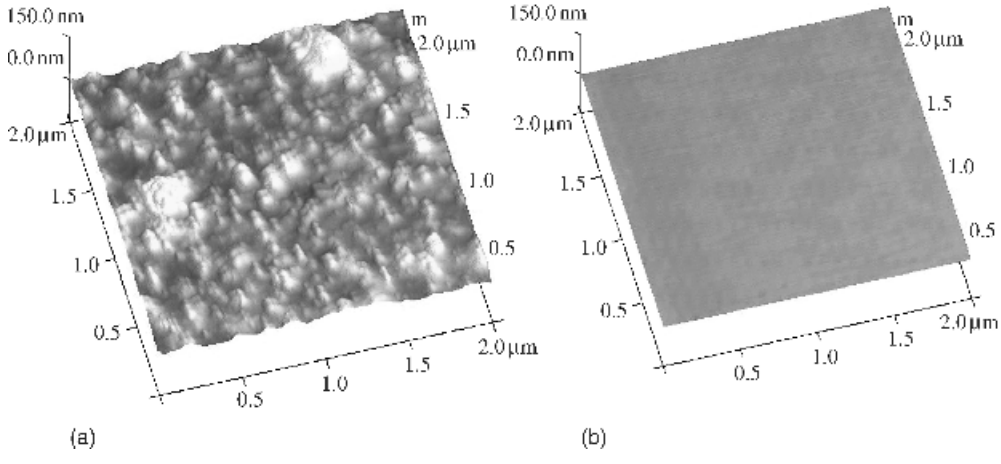


Figure 2.8 AFM analysis of pretreated and surface-engineered polyethylene naphthalate

Petitioner Samsung Ex-1011, 0050

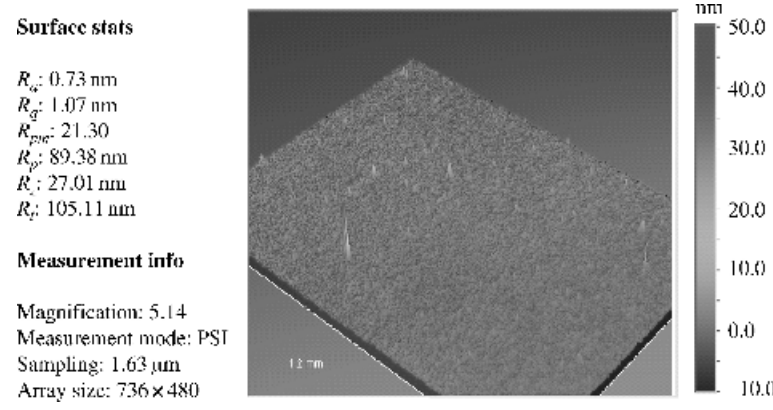


Figure 2.9 Surface smoothness of Teonex Q65 with an adhesion pretreat

smoothness. Figure 2.9 shows the surface of the pretreated film and Figure 2.10 shows the surface of the surface-engineered film. Combining numerous measurements to deliver large sampling areas (5 cm × 5 cm) reveals low surface peak heights with resultant Sa (Ra) roughness values of less than 1 nm. Such levels are necessary to ensure good integrity for subsequent barrier layers, conductive coatings and pixel array resolution.

Surface-engineered Teonex Q65 also exhibits extremely low levels of surface defects (extreme surface peak heights) too. For the same 5 cm × 5 cm sampling area, only approximately 5 defect counts are detected, between 0.2 and 0.3 µm maximum height; this is shown in Figure 2.11. The film therefore provides a very good smooth clean surface, enabling good coating quality further downstream in the product manufacture.

Polyarylate and Polycyclic olefin films are also surface coated to both improve surface quality and also give solvent resistance (Angiolini *et al.* 2000).

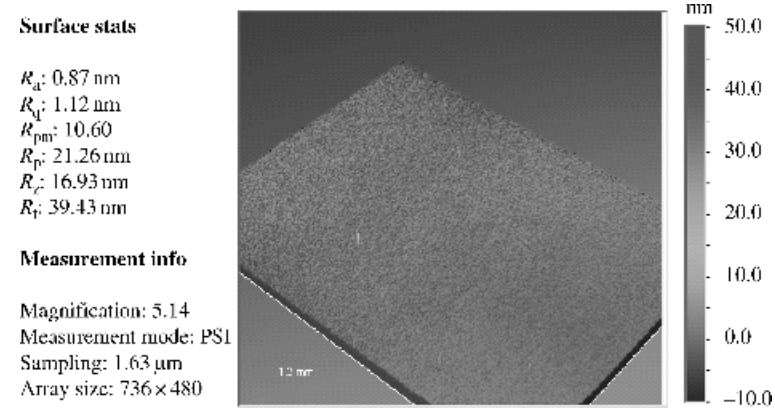


Figure 2.10 Surface smoothness of surface-engineered Teonex Q65

Petitioner Samsung Ex-1011, 0051

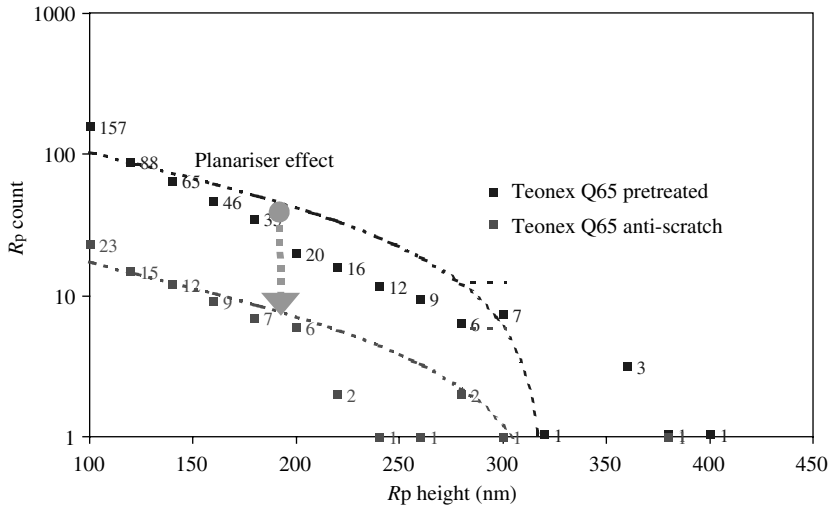


Figure 2.11 Surface peak defect R_p (highest point): frequency distribution of surface-engineered Teonex Q65. White light interferometry measurements, 1.6 μm from lateral resolution, approximately 5 cm × 5 cm sampling area in total

2.3.6 *Barrier*

One of the key properties of any substrate that replaces glass will be to offer glass-like barrier properties. OLED materials in particular are 10 000 times more sensitive than LCDs to moisture and oxygen. This is because the OLED and component layers are of order 50 nm, and any peak that protrudes from the surface by 100 nm or more is likely to cause a defect. In addition, the OLED materials are themselves chemically unstable in the presence of air and moisture; they degrade, thereby creating black spots and ruining a display.

The plastic substrates that are under consideration as flexible substrates typically have barriers of order 1–10 g/m^2 per day for water vapour transmission rate and about 1–10 mL/m^2 per day for oxygen. OLED displays will require water vapour transmission rates of $< 10^{-6}$ g/m^2 per day and oxygen transmission rates of $< 10^{-5}$ mL/m^2 per day. No polymer at present meets these extremely demanding requirements.

Barrier coatings on films have been extensively researched for several years (Prins and Hermans 1959; Jamieson and Windle 1983; Philips *et al.* 1993; Rossi and Nulman 1993; Amberg *et al.* 1998; Moosheimer and Langowski 1999; Henry *et al.* 2001; Smith *et al.* 2002; Henry *et al.* 2002) because of the need to prolong the shelf life of packaged food products by reducing water and oxygen ingress, and metal and dielectric layers are now routinely coated on polymers for this purpose with great success. However, the permeability specification for OLED applications is several orders of magnitude lower than for food packaging (Nisato *et al.* 2003; Maixner, 2002) and for optical applications it is not possible to use opaque metal films.

In principle, a perfect layer of silica only a few nanometres thick should reduce the diffusion of water and oxygen to acceptable levels (just as the 2–3 nm native oxide layer on

Petitioner Samsung Ex-1011, 0052

silicon wafers protects the wafer surface from further oxidation). The problem in practice is that thin film coatings can have defects that provide easy paths for water and oxygen molecules to penetrate (Rossi and Nulman 1993). Also, surface defects on the polymer substrates cause pinholes in the final coating and lead to catastrophic failure of barrier properties. However, even clean, pinhole-free coatings are not perfect. In the particular case of vacuum-deposited thin film barrier coatings, this is due to the tendency of such films to show columnar growth and to exhibit densities less than the density of the bulk material (Henry *et al.* 2001). Water and oxygen molecules can then diffuse through the nanospacings between columns (Langowski *et al.* 2002). This effect is enhanced on the relatively rough surfaces of normally processed polymer sheet. Heating substrates to elevated temperatures can help reduce columnar growth, but this is not an option with all polymer substrates.

Thin film diffusion barrier encapsulants and substrates based on vacuum-deposited organic/inorganic multilayers offer a promising route to transparent packaging for OLED displays (Langowski *et al.* 2002; Bright 2002; Graff *et al.* 2001) and several organisations are currently developing optically transparent multilayer barrier coatings for flexible substrates. This will be discussed in Chapter 4.

Bottom emission displays are currently encapsulated in metal cans. The move towards higher-specification displays will require active matrix addressing and this will probably require silicon-based thin film transistors on the substrate. These may partially block light, thereby reducing the display efficiency and putting a limit on resolution. A transparent barrier film opens up the possibility of designing the display so that the light exits the top of the display, significantly boosting the efficiency and enabling much higher resolution.

The requirements for OLED displays are particularly demanding. In the course of developing barrier technologies for this application it is likely that films with improved barrier performance, such as water permeability in the range of 10^{-3} g/m^2 per day, will be developed and will find application in less demanding devices such as electronic paper.

2.3.7 Mechanical Properties of the Composite Structure

Production of glass-based displays currently involves moving batches of glass between the different processing stages. The mechanical difference, particularly stiffness, between rigid glass and flexible substrates will probably require very different methods of processing. Polyethylene terephthalate and polyethylene naphthalate films are inherently stiffer than amorphous films, with their Young's modulus being typically three times higher, an artefact of being semicrystalline and biaxially oriented (Table 2.1). Young's modulus is independent of thickness and does not indicate how stiffness will change with thickness. Another way to express this is by defining the rigidity as follows:

$$D = \frac{Et^3}{12(1-n)}$$

where E is the tensile or Young's modulus, t is the thickness and n is Poisson's ratio (0.3–0.4). Assuming a Young's modulus of 2 GPa for amorphous films and 6 GPa for polyethylene

Petitioner Samsung Ex-1011, 0053

Table 2.5 Comparative rigidity of amorphous and semicrystalline films

Material	Thickness (μm)	Rigidity/ 10^4(N m)	Rigidity relative to 125μm amorphous film
Amorphous	125	5	1
Amorphous	200	20	4
Teonex Q65	125	15	3
Teonex Q65	200	61	12

naphthalate film, it can be seen that 200 μm polyethylene naphthalate film is four times more rigid than 125 μm polyethylene naphthalate film and 12 times more rigid than a 125 μm amorphous film (Table 2.5). This stiffness may prove to be an advantage in the current batch-based display manufacturing process.

The final engineered substrate for flexible displays will be a multilayer structure. Issues such as adhesion at the interface between the different layers under thermal cycling and environmental testing, curl, the wetting characteristics, and ability to withstand flex testing, will be critical to determining their robustness in use. However, note that flexible displays include displays that are curved but are not flexed during use, displays that are mildly flexible but do not undergo severe treatment such as rolling, and rollable displays. The performance requirements of each type will be very different, and the rollable category is particularly demanding. To date there has been very little published work in this area and there is an important need to define test protocols and determine how the structures behave on testing. Published work to date has focused on the behaviour of transparent conductive coatings on flexible substrates during flexing (Gorkhali *et al.* 2003; Bouten 2002); (see Chapter 6).

The planarising coatings under development within DuPont Teijin Films are optimised to survive a boil test in water. The choice of pretreat on the Teonex Q65 before application of the planarising coating is critical. The proprietary planarising coatings do not show significant thermal degradation as measured by weight loss until over 300 °C (Figure 2.12). The coating demonstrated is more thermally stable than acrylic-based coatings, which start to show significant thermal degradation above 250 °C.

In their final application, flexible displays are subjected to some degree of bending. All polymer film substrates are sufficiently compliant to undergo bending deformation even to the level required for rollable displays. Of more interest is the effect of bending on the supported barrier or conductive layers, which may have very low fracture strains yet whose integrity is critical for its final function. Consequently, a predictive model, based on simple beam theory, has been written and extended to allow the calculation of internal stress for a multilayer stack that is subjected to deformations such as three-point bending, two-point bending and pure bending. This model is proving to be a powerful tool for assessing specific materials in multilayer electronic stacks and their performance in real designs.

Figure 2.13 illustrates two of the bending geometries. In one calculation the three-point bend of a polyethylene naphthalate film, coated with a silica-based hardcoat (solely for illustration, the modulus was taken as around 40 GPa and Poisson's ratio as 0.2) was considered as a model for a common mode of bending in a flexible display. It was found that

Petitioner Samsung Ex-1011, 0054

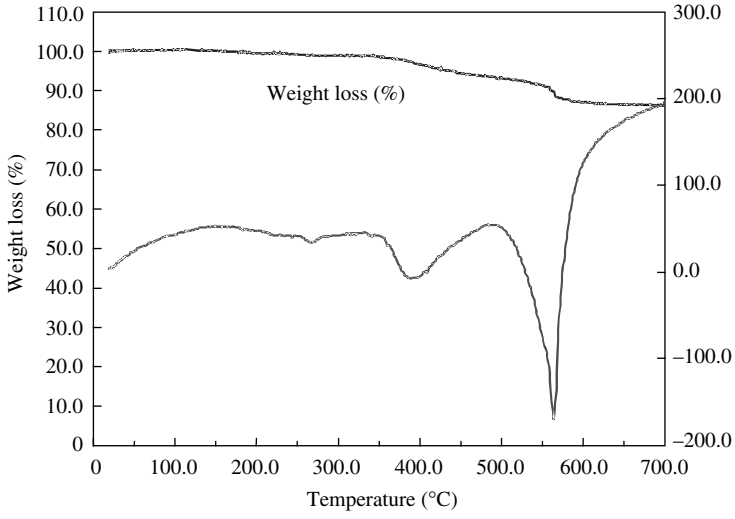


Figure 2.12 Thermogravimetric analysis of the coating used as a smoothing coat

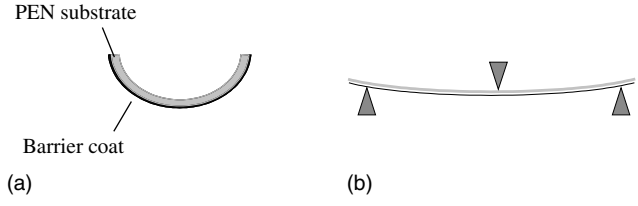


Figure 2.13 Bending geometries

under deflections of 10 mm, a sheet of polyethylene naphthalate (100 mm × 100 mm × 125 μm thick) caused a strain in the second layer of 0.07%.

The strain and also stress predicted for each layer was a function of the geometry and the material characteristics. In contrast, when the same polyethylene naphthalate/hardcoat laminate was subjected to pure bending with a radius equivalent to that reported for rollable displays, the corresponding strain in the inorganic layer was calculated to be 0.6%.

The data, summarised in Table 2.6, become useful when considered with the fracture strain or fracture stress measured elsewhere for each layer. A sample of the polyethylene

Table 2.6 Percentage strain of films having different thicknesses

Laminate layer	Thickness (mm)	Deformation	Strain (%)
PEN	125	Pure bending, radius 10 mm	0.8*
Hardcoat	2	Pure bending, radius 10 mm	0.6
PEN	125	Three-point bending, 10 mm in centre	0.11*
Hardcoat	2	Three-point bending, 10 mm in centre	0.07

*Refers to comprehensive strain on PEN surface.

Petitioner Samsung Ex-1011, 0055

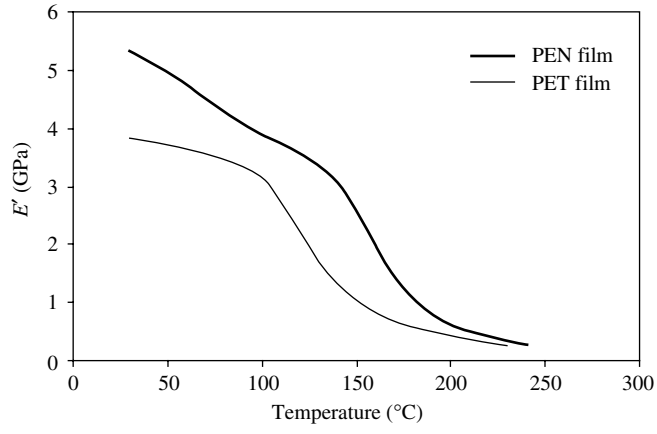


Figure 2.14 Change in stiffness with temperature for polyethylene terephthalate and polyethylene naphthalate film

naphthalate/hardcoat laminate that was strained in tension developed cracks initially in the inorganic coating at low strains before complete fracture of the polyethylene naphthalate substrate above 50% strain. The onset of cracking by the hardcoat layer occurs at around 1% strain, and this may limit its application in demanding rollable displays. This model does not necessarily represent film structures under development but illustrates how, through coupling an awareness of the architecture supported by the polyethylene naphthalate with some simple materials science and mechanical theory, we can obtain an early indication of design strengths and faults.

One of the main drivers in moving to plastic substrates is that it opens up the possibility of roll-to-roll processing (R2R) and the process and economic advantages this brings. Under these conditions a winding tension will clearly be present and polymer film substrates with low moduli will be susceptible to internal deformation, particularly at elevated process temperatures. Figure 2.14 shows a comparison between polyethylene terephthalate and polyethylene naphthalate films. The storage modulus $E^{'}$ is recorded using dynamic mechanical/thermal analysis (DMTA) and as the temperature is increased, the stiffness of both materials is seen to fall. However, in the region 120–160 °C polyethylene naphthalate is significantly stiffer and stronger, with a modulus almost twice that of polyethylene terephthalate.

2.4 Polyester Films in Application

There is considerable activity in polyester films and by the time this book comes to press, values reported here will probably have been improved significantly. In some application areas, only preliminary results are being disclosed, so the companies involved will be mentioned but the technologies will not be discussed in any detail.

There are two possible methods of fabrication for flexible displays:

- standard polysilicon TFT fabrication on glass substrates and transfer of the array to a polymer substrate;
- direct fabrication on the polymer substrate itself.

Petitioner Samsung Ex-1011, 0056

The first approach has been demonstrated by several research groups (Asano and Kinoshita 2002; Berge *et al.* 2003) and offers the benefits that the TFT array can be manufactured on existing production lines once the transfer process has been established (Chapter 22). The cost will always be higher than for a glass-based display because of the wasted glass substrate and the additional transfer process. However, low-temperature flexible substrates can subsequently be used and the probable factor that will drive the substrate choice will be cost.

Direct fabrication is a more attractive option, but there are significant issues concerning active matrix technology and manufacturing equipment. There are three basic approaches and although detailed discussion is beyond the scope of this chapter, they can be used to highlight the pros and cons of the various options (Young *et al.* 2003):

- To develop novel low-temperature processes ($< 200\,^{\circ}$C) for building silicon-based TFTs that can be carried out on the lower-temperature substrates (semicrystalline and amorphous melt-processable films). This option has the benefit of using lower-cost substrates but may require new processing technology for silicon-based TFTs to achieve the desired mobilities.
- To adapt existing silicon processes to reasonably low temperature (250–300 °C) for use on higher-temperature films (amorphous solvent-cast films). This route exploits existing silicon processing technology but will probably require new substrate development as none of the existing amorphous cast films offer the ideal property mix (CLTE < 20 ppm/ °C, good colour and ability to withstand a processing temperature of 300 °C).
- To exploit organic-based TFTs with processing temperatures $< 200\,^{\circ}$C depending on the coating process. The inkjet printing of organic-based TFTs is a genuine game-changing technology which pushes processing temperatures down below 120 °C; at these processing temperatures, polyethylene terephthalate starts to become viable as a substrate and has a considerable cost advantage over the other film options.

Before discussing examples, it is worth emphasising that the work reported in the literature was carried out over the past few years using the films available at that time and may not reflect subsequent advances in tailoring films for this application.

2.4.1 Novel Low-Temperature Processes for Building Silicon-Based TFTs

FlexICs has pioneered ultra low temperature polysilicon (ULTPS) thin film transistors on plastic technology (Pellingro 2003). FlexICs has based its ULTPS process technology on standard semiconductor CMOS technologies. The TFTs employ a top-gate self-aligned device structure incorporating metal gates and a single additional metallisation level. Industry-standard LTPS TFT processes typically employ special display glass substrates, and contain one or more process steps in which the temperature is raised to 350–400 °C. FlexICs has developed a TFT process in which the plastic substrate is never subjected to temperatures above 100 °C. For this purpose, FlexICs uses an excimer laser annealing (ELA) technique similar to that used in standard polysilicon-on-glass TFT processes. However, FlexICs has developed a proprietary thick dielectric film (silicon dioxide) which is placed between the plastic substrate and the silicon film during laser annealing, protecting the plastic substrate

Petitioner Samsung Ex-1011, 0057

from damage during this process. The use of this thick dielectric film prevents the temperature of the plastic substrate from exceeding 250 °C even though the silicon film is heated to over 1500 °C as it is melted by the excimer laser pulse. Even although the surface region of the plastic does reach 250 °C, it is only for a very brief period of time (less than a millisecond) and the plastic film remains undamaged. FlexICs has also focused on overcoming issues associated with fabricating on polymer films such as distortions related to a mismatch in CLTE between organic and inorganic layers, and curl. These include heat treatment to reduce shrinkage, balancing the film structure by depositing inorganic coatings on both sides of the film to reduce curl and reduce distortion, controlling moisture exposure and minimising as-deposited film stresses. By controlling these factors, FlexICs has been able to reduce the distortion of polyethylene naphthalate film from 200 ppm to 20 ppm (i.e. 3 μm over 150 mm). FlexICs has reported NMOS processes offering electron mobilities of $> 250\ \mathrm{cm^2V^{-1}s}$ and threshold voltages of 5 V, and PMOS processes offering hole mobilities of $50\ \mathrm{cm^2V^{-1}s}$ and threshold voltages of -5 V on polyethylene naphthalate film. This performance is comparable with low-temperature polysilicon (LTPS) TFTs on glass technology.

Amorphous silicon TFT is currently the workhorse of the well-established active matrix LCD technology. The conventional a-Si TFTs are fabricated at a typical processing temperature of 300 °C. In recent years, significant progress has been made in the process temperature reduction and a-Si TFTs have been successfully fabricated on polyimide using a process temperature of 150 °C with a performance comparable to the 300 °C process with respect to mobility, threshold, voltage and leakage current. Honeywell (Sarma *et al.* 2003), working with DuPont Displays, DuPont Teijin Films and Princeton University, has developed an a-Si TFT process with 150 °C maximum temperature on heat-stabilised polyethylene naphthalate film with a planarising surface treatment, using plasma–enhanced chemical vapour deposition. Before fabrication the sample was preannealed at temperatures over the processing temperature. This reduced the shrinkage from 500 ppm to 25 ppm. Problems related to mismatch of CLTE were overcome by choice of thin film materials and optimisation of the TFT array fabrication process. The engineered surface on the polyethylene naphthalate film overcame issues associated with surface imperfections. TFTs on polyethylene naphthalate with a mobility of $0.7\ \mathrm{cm^2V^{-1}s}$ and a threshold voltage of 2.4 V were reported. This performance is comparable to conventional TFTs fabricated at temperatures over 300 °C and is comparable with 150 °C TFT on glass. This mobility was sufficient for driving an OLED display, and a 64×64 pixel active matrix OLED test display using an a-Si TFT backplane fabricated on polyethylene naphthalate at 150 °C was demonstrated. This technology will be discussed in Chapter 12. The above examples illustrate that polyethylene naphthalate film can reach the demanding product requirements required for a flexible substrate for active matrix backplanes.

2.4.2 *Adapting Existing Silicon Processes to Reasonably Low Temperature*

Researchers at Philips have reported building polycrystalline silicon TFTs on polyimide, polyarylate, polynorbonene and polyethersulphone (Young *et al.* 2003). The use of poly-Si necessitated the use of higher processing temperatures and the substrates listed above were focused on. The films before use were all annealed for extended periods of time (10–100 h) at 300 °C for polyimide, polyarylate, polynorbonene and 180 °C for polyethersulphone. After this treatment, shrinkages reached < 10 ppm/h. An SiO_2 layer was deposited on the

Petitioner Samsung Ex-1011, 0058

films to aid adhesion to the substrate, to provide thermal insulation and to provide a barrier. The barrier was good enough for LCD displays and nearly good enough for OLED displays. Amorphous silicon was deposited on top and then laser annealed in different environments. Using this process led to NMOS TFTs with a mobility of 100 $cm^2V^{-1}s$ and a threshold voltage of 3.9 V, and PMOS devices with a mobility of 52 $cm^2V^{-1}s$ and a threshold voltage of −6 V. It was only possible to make NMOS poly-Si TFTs on polyethersulphone because of maximum temperature processing limitations, but at the time of the work it had superior surface quality compared to the higher-temperature films. This highlights how more than one factor must be considered when choosing substrates for study.

2.4.3 Organic-Based TFTs with Processing Temperatures below 200 °C

Various printing such as screen printing and inkjet printing have been demonstrated in the manufacture of TFTs on glass and this technology is currently being translated to plastic. Minimum resolution of screen printing is tens of microns, insufficient for most application.

Several printing methods can achieve micrometre resolution. DuPont report a dry thermal transfer printing on polyethylene terephthalate (Blanchet *et al.* 2003); see Chapter 10. DuPont claim that this technology overcomes issues associated with the sequential application of liquid layers. TFTs with a carrier mobility of 0.3 $cm^2V^{-1}s$ as well as a flexible 5000-transistor array have been made.

Infineon has developed a process for fabricating polymer gate dielectric pentacene TFTs and integrated circuits with printed gate electrodes on polyethylene naphthalate film. Infineon uses microcontact printing which involves a soft lithography technique to pattern the surface of the polyethylene naphthalate film with hydrophobic and hydrophilic areas. The resolution of the process is theoretically better than 1 μm, but Infineon limited features to 5 μm as it believes that features below 5μm are unrealistic for large-volume manufacture, considering the dimensional stability limits of the substrate. The Infineon process reaches temperatures of 200 °C briefly to cross-link the polyvinyphenol gate dielectric. Polyethylene naphthalate film was heated to 200 °C before processing, and this reduced shrinkage from 0.5% to 0.02%. TFTs with mobilities similar to that achieved on glass by this technique have been reported (Zschieschang *et al.* 2003)

Plastic Logic has employed a photolithographically defined polyimide barrier on glass to enhance the resolution attained by inkjet printing (Burns *et al.* 2003). It is currently translating this technology to flexible substrates and developing active matrix backplanes on polyethylene terephthalate.

PolyIC has also reported organic-based TFTs on polyethylene terephthalate using different printing processes.

2.4.4 Use of Teonex in Flexible Displays

Flexible OLED displays on heat-stabilised Teonex Q65 have been demonstrated by DuPont Displays and will be discussed in Chapter 13. Polymer Vision is developing and demonstrating prototype rollable displays. These combine organic-based active matrix driving electronics with a reflective ''electronic ink'' front plane on 25 μm Teonex film.

Petitioner Samsung Ex-1011, 0059

2.5 Concluding Remarks

No single display technology will serve all applications, and several technologies will coexist. This means that several of the substrates discussed in this chapter will probably find use, and the choice of a substrate for a particular application will depend on the operating requirements of that particular technology. Significant advances have been made in the development of substrates for flexible displays and possible trends that will influence future work are

- further advances in barrier technologies to meet the exacting requirements of OLED displays;
- new understanding of the relationship between multilayer structures and the properties of the final device in use, leading to optimisation of product design;
- lower-temperature processing of TFTs opening up wider use of lower-temperature substrates;
- advances in fabrication technology that set new challenges to the substrate suppliers;
- the need to simplify the substrate structure for roll-to-roll processing.

The fabrication technology for flexible displays is still largely batch based; the move to a roll-to-roll process will open up a new set of requirements on the film associated with roll handling, in addition to a general requirement to simplify the substrate structure. Flexible displays is a continuously evolving field and it is essential that the material suppliers and device fabricators work closely together to create the synergy required to bring flexible displays to the market.

Acknowledgements

The authors acknowledge contributions from Philip Willcocks of ICI, and David Bird of DuPont Teijin Films.

References

Allen, K. and Mentlley, D. E. (2003) Flexible Displays-Emerging Display Technologies, iSuppli/ Stanford Resources.

Amberg, S., Hoffmann, M., Bader, H. and Gessler, M. (1998) Inorganic-organic hybrid polymers with barrier properties for water vapour, oxygen and flavours. *Journal of Sol-Gel Science and Technology* **1/2**, 141–146.

Angiolini, S., Avidano, M., Bracco, C., Barlocco, C., Bracco, R., Bacskay, J., Lipian, J.-H., Neal, P. S., Rhodes, L. S., Shick, R. A., Zhao X.-M. and Freeman, G. (2000) High performance plastic substrate for flexible flat panel displays. *Society For Information Display, Digest of Technical Papers*, 1–4.

Angiolini, S., Avidano, M., Bracco, R., Barlocco, C., Young, N. G., Trainor, M. and Zhao, X.-M. (2003) High performance plastic substrates for active matrix flexible FPD. *Society For Information Display, Digest of Technical Papers*, 1325–1327.

Petitioner Samsung Ex-1011, 0060

Asano, A. and Kinoshita, T. (2002) *Society For Information Display, Digest of Technical Papers*, 37–37.
Berg, van den, R. (2001) *Displays Europe.*, Autumn, 15–19.
Berge, C., Wagner, T., Brendle, W., Craff-Castillo, C., Schubert, M. B. and Werner, J. H. (2003) Flexible monocrystalline Si films for thin film devices from transfer processes. *Materials Research Society Symposium Proceedings* **769**, paper H2.7.1, 53–58.
Blanchet, G. B., Loo, Y. L., Rogers, J. A., Gao, F. and Fincher, C. R. (2003) Large area, high resolution, dry printing of conducting polymers for organic electronics. *Applied Physics Letters* **82**, 463–465.
Bouten, P. C. T. (2002) Failure test for brittle conductive layers on flexible display substrates, *22nd International Display Research Conference, Conference Proceedings*, 313–316.
Bright, I. C. (2000) US Patent 20020022156A1.
Burns, S. E., Cain, P., Mills, J., Wang, J. and Sirringhaus, H. (2003) Inkjet printing of polymer thin film transistor circuits. *MRS Bulletin* **28**, 829–834 and references therein.
Chen, Y., Au, J., Kazlas, P., Ritenour, A., Gates, H. and McCreary, M. (2003) *Nature* **423**, 136.
Gorkhali, S. D. R. Cairns, D. R. and Crawford, G. P. (2003) Reliability of transparent conducting substrates for rollable displays: a cyclic loading inverstigation. *Society for Information Display, Digest of Technical Papers,* 1332–1335.
Graff, G. I., Gross, M. E., Shi, M. K., Hall, M. G., Martin, P. M. and Mast, E. S. (2001) WO 01/82389 A1.
Heeks, K. and Hough S. (2003) *Information Display* **4/5**, 14–19.
Henry, B. M., Erlat, A. G., Grovenor, C. R. M., Deng, C. S., Briggs, G. A. D., Miyamoto, T., Noguchi, N., Niijima, T. and Tsukahara, Y. (2001) The permeation of water vapour through gas barrier films. *44th Annual Technical Conference Proceedings of the Society of Vacuum Coaters*, 469–475.
Henry, B. M., Erlat, A. G., Grovenor, C. R. M., Briggs, G. A. D., and Tsukahara, Y. (2002) Gas permeation studies of metal oxide/polymer composite films. *45th Annual Technical Conference Proceedings of the Society of Vacuum Coaters*, 514–518.
Innocenzo, J. G., Wessel, R. A., O'Regan, M. and Sellars, M. (2003) *Society For Information Display, Digest of Technical Papers*, 1329–1335.
Jamieson, E. H. H. and. Windle, A. H. (1983) Structure and oxygen-barrier properties of metallized polymer film. *Journal of Material Science* **18**, 64–80.
Kim, Y. H., Park, S. K., Han, J. I., Moon, D. G. and Kim, W. K. (2003) *Society For Information Display, Digest of Technical Papers*, 996–999.
Langowski, H. C., Melzer, A. and Schubert, D. (2002) Ultra high barrier layers for technical applications. *45th Annual Technical Conference Proceedings of the Society of Vacuum Coaters*, 471–475.
MacDonald, W. A., Rollins, K., Eveson, R., Rakos, K., Rustin, B. A., and Handa M. (2003) New developments in polyester films for flexible electronics. *Materials Research Society Symposium Proceedings* **769**, paper H9.3, 283–290.
MacDonald, W. A. (2004) Engineered films for display technologies. *Journal of Materials Chemistry* **14**, 4–10.
MacPherson, C., Anzlowar, M., Innocenzo, J., Kolosov, D., Lehr, W., O'Regan, M., Sant, P., Stainer M., Sysavat, S. and Venkatesh, S. (2003) *Society For Information Display, Digest of Technical Papers*, 1191–1193.
Maixner, R. D. (2002) Future trends in permeation measurement. *45th Annual Technical Conference Proceedings of the Society of Vacuum Coaters*, 461–464.
Moosheimer, U. and Langowski, H.-C. (1999) Permeation of oxygen and moisture through vacuum web coated films. *42nd Annual Technical Conference Proceedings of the Society of Vacuum Coaters*, 408.
Nisato, G., Kuilder, M., Bouten, P., Moro, L., Philips, O. and Rutherford, N. (2003) Thin film encapsulation for OLEDs: evaluation of multilayer barriers using the Ca test. *Society For Information Display, Digest of Technical Papers*, 550–553.
Pelligrino, P. W. (2003) USDC Flexible Microelectronics and Displays Conference, February 3–4, Phoenix, Arizona.

Petitioner Samsung Ex-1011, 0061

Philips, R. W., Markantes, T. M. and LeGallee, C. (1993) Evaporated dielectric colorless films on PET and OPP exhibiting high barriers towards moisture and oxygen. *36th Annual Technical Conference Proceedings of the Society of Vacuum Coaters*, 293–301.

Prins, W. and Hermans, J. (1959) Theory of permeation through metal coated polymer films. *Journal of Physical Chemistry* **63**, 716.

Rossi, G. and Nulman, M. (1993) Effect of local flaws in polymeric permeation reducing barriers. *Journal of Applied Physics* **74**, 5471.

Sarma, K. R., Chanley, C., Dodd, S., Roush, J., Schmidt, J., Srdanov, G., Stevenson, M., Wessel, R., Innocenzo, J., Yu, G., O'Regan, M., Macdonald, W. A., Eveson, R., Long, K., Gleskova, H., Wagner, S. and Sturm, J. C. (2003) Active matrix OLED using 150oC a-Si TFT backplane built on flexible plastic substrate. *Proceedings from SPIE Aerosense, Techologies and Systems for Defense and Security*, 180–191.

Sirringhaus, H. Burns, S. E., Kuhn, R. C., Jacobs, K., MacKenzie, J. D., Etchells, M., Chalmers, K., Devine, P., Murton, N., Stone, N., Wilson, D., Cain, P., Brown, T., Arais, A. C., Mills, J. and Friend, R. H. (2003) *Society For Information Display, Digest of Technical Papers*, 1084–1087.

Slikkerveer, P. J. (2002) *Conference Proceedings from 22nd International Display Research Conference*, 273–276.

Slikkerveer, P. J. (2003) *Information Displays* **3**, 20–24.

Smith, A. W., Copeland, N., Gerrard, D. and Nicholas D. (2002) PECVD of SiOx barrier films. *45th Annual Technical Conference Proceedings of the Society of Vacuum Coaters*, 525.

Young, N. D., Trainor, M. J., Yoon, S.-Y., McCulloch, D. J., Wilks, R. W., Pearson, A., Godfrey, S., Green, P. W., Roosendaal, S. and Hallworth E. (2003) Low temperature poly-Si on flexible polymer substrates for active matrix displays and other applications. *Materials Research Society Symposium Proceedings* **769**, paper H2.1, 17–28.

Zschieschang, U., Klauk, H., Halik, M., Schmid, G. and Dehm, C. (2003) Flexible organic circuits with printed gate electrodes. *Advanced Materials* **15**, 1147–1151.

Petitioner Samsung Ex-1011, 0062

3

Flexible Glass Substrates

Armin Plichta,[1] Andreas Habeck,[1] Silke Knoche,[1] Anke Kruse,[1] Andreas Weber,[1] and Norbert Hildebrand[2]

[1]Schott AG and [2]Schott North America Inc.

3.1 Introduction

Since the development of display technology, glass has played an important role. From the early days of CRT bulbs to today's special TFT-LCD and PDP glass types, glass development has gone hand in hand with display technology advances.

Today, in order to be competitive in the traditional CRT market, LCD technology has improved by processing glass substrates with a size of roughly 4 m^2 (Gen 7). A new trend for the smaller displays is under discussion: How can displays be made thinner to accommodate a new product characteristic such as flexibility? Despite the fact that flexibility is not defined, four different grades can be distinguished according to application: (a) ultra thin and flat displays (mobiles, PDAs, laptops), (b) ultra thin and curved displays (mobiles, automotive), (c) ultra thin and bendable displays (smartcards), and last but not least (d) ultra thin and ''highly'' flexible displays (e.g. rollable or wearable displays). Since glass substrates are the standard substrate material at the moment, flexibility can only be achieved by reducing the substrate thickness significantly. This chapter will discuss in detail the pros and cons of the next generation of glass substrates in the thickness range of 0.2 mm to 30 μm.

Flexible Flat Panel Displays Edited by G. P. Crawford
© 2005 John Wiley & Sons, Ltd., ISBN 0-470-87048-6

Petitioner Samsung Ex-1011, 0064

3.2 Display Glass Properties

3.2.1 Overview of Display Glass Types

With the multitude of material and product properties required by the different display technologies there exists not one, but several display glass types.

Glass describes a material in a ''frozen liquid'' state (Scholze 1988). From a practical viewpoint, soda lime glass for hollow glass and for window glass applications is produced in the highest volume today. Soda lime glass has a high content of SiO_2 (70–75%) (network builder) and lower amounts of Na_2O (12–16%) and CaO (10–15%) (network modifier). Mixed in the right proportions during melting, the mixture will not crystallize during cooling and will form a new material – glass. Adding B_2O_3 or Al_2O_3 to the SiO_2 network creates new glass types, the borosilicates or aluminosilicates, or if both oxides are present the aluminoborosilicates.

Within these glass types the composition of the network builders and the modifiers may still be varied, resulting in a large variety of glass types with different material properties. Most glass types used for flat panel displays are in the borosilicate and aluminosilicate glass families.

Plastic substrates are used today in various applications, but glass is the favorite choice for high-tech applications. Glass has many advantages over plastic:

- Optical properties:
  - high transmission rate in the visual range,
  - high homogeneity of the refractive index,
  - no retardation,
  - high UV resistance.

- Thermal properties:
  - high temperature stability,
  - high dimensional stability,
  - low thermal expansion coefficient,
  - no outgassing.

- Chemical properties:
  - high resistance to chemical attack,
  - excellent barrier properties against water and oxygen.

- Mechanical properties:
  - high scratch resistance,
  - high scrub resistance.

Petitioner Samsung Ex-1011, 0065

3.2.2 Glass Properties

From our day-to-day experiences we are familiar with some glass properties that make this material so important for display technologies. We can easily look through it, and it is strong and passive enough to encapsulate the more sensitive components of a display. When we look in more detail, we see that glass exhibits many different properties that make it the material of choice for all types of display technology today.

Optical properties

Glass has been used in optical components for centuries. Clear glass types show a very high internal transmittance, typically over 98% for a 1 mm thick glass sheet in the visible part of the electromagnetic spectrum. With a refractive index of $\sim$1.5, a luminous transmittance of $> 90\%$ ($t = 1$ mm) is typical for all display glass types.

Figure 3.1 shows the optical transmission for D263. For some special applications, glass with optical filter properties is used. A typical example would be the use of neutral optical density or color enhancement filters for improving daylight readability.

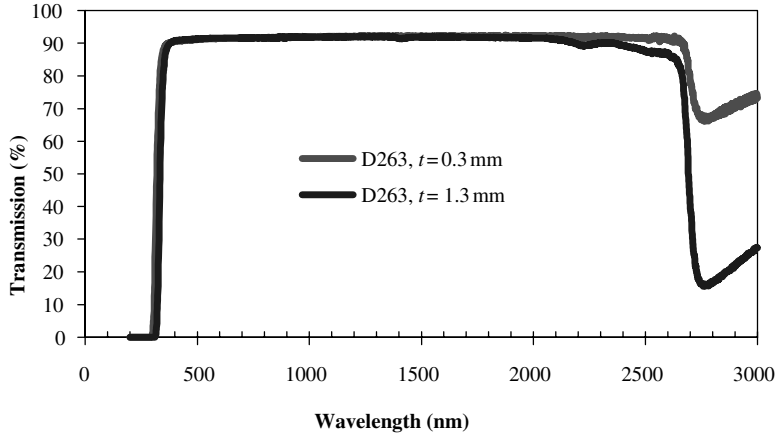


Figure 3.1 Transmission of D263 in the visible and near-IR spectrum

Another important optical glass property is the very low stress birefringence for glass. Even very thin glass sheets (down to 30 μm thickness) show these very low values, making them the ideal substrate material for LCD technologies.

Chemical properties

During the display manufacturing process, many different chemicals are used to form specific display components. Resistance to any form of chemical attack is important for any display substrate material. Silicates, especially borosilicates and aluminoborosilicates, have a very high resistance to chemicals.

Petitioner Samsung Ex-1011, 0066

The chemical durability of glass as it concerns various chemicals is measured in material loss per exposed area, typically expressed in milligrams per square centimeter (mg/cm^2). The chemical attack is a function of temperature, time and concentration of the respective chemical. For glass, three types of chemical attack are generally considered. Acid, base and water attack describe the reaction of a glass type to aqueous solutions with different pH values.

As an example, Figure 3.2 shows the chemical durability of a standard borosilicate glass (Borofloat) against various chemicals. Although glass is not completely inert to chemical attack, typically it does not cause any significant degradation of the substrate material. Based on an SiO_2 network, glass typically shows the lowest chemical durability against chemicals containing fluorine followed by strong base chemicals; different glass types will react differently.

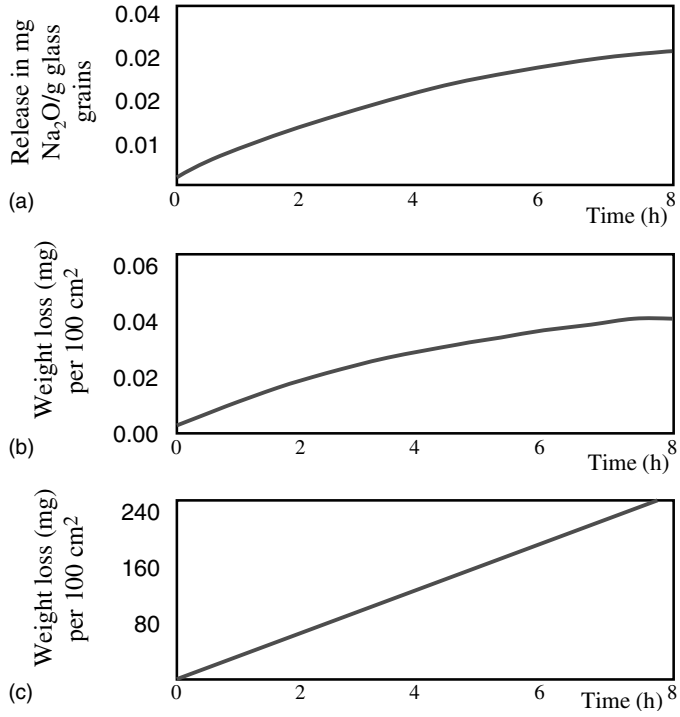


Figure 3.2 Chemical durability of Borofloat against (a) water attack, (b) acid attack, and (c) alkali attack

Thermal properties

During the manufacturing process, glass is brought into the liquid state (melting) and subsequently cooled to room temperature. Since the glass does not solidify like other materials, it does not show a long-range molecular order. Scientifically, glass is typically not in its thermodynamically lowest energy state at room temperature, consequently, some

Petitioner Samsung Ex-1011, 0067

material properties are not only a function of the glass composition, but also a function of the cooldown speed. The slower the glass is annealed, the more dense or compact it becomes. Further processing steps in the manufacture of displays may require elevated temperatures. During such a temperature cycle, glass may show a further dimensional change – thermal shrinkage. The amount of thermal shrinkage depends on temperature, time and the glass type.

The control of thermal shrinkage is very important for thin display technologies. If the thermal shrinkage is too large, processing of multiple mask steps in photolithographic processes may become difficult (misalignment of registration marks), leading to lower yield. The same is true if the front and the back substrate show any differences in thermal shrinkage. For example, AF37 (Schott) shows shrinkage below 10 ppm.

Another important and more commonly known thermal property is the coefficient of thermal expansion (CTE). As a solid, glass exhibits a linear thermal expansion up to a temperature around the transformation temperature T_g. Looking at the length change ($\Delta l/l$) of a piece of glass, one can see the change in behavior around T_g in Figure 3.3. For most glass types used today in the flat panel display industry, a linear behavior can be assumed from $-50\,^{\circ}\mathrm{C}$ to above $450\,^{\circ}\mathrm{C}$.

Some display technologies require high temperature steps. This is pushing the development of high strain point glass types with a T_g above $600\,^{\circ}\mathrm{C}$. The CTE value depends on the glass composition. Most borosilicate and aluminoborosilicate glass types used in the flat panel industry have a CTE of approximately $4 \times 10^{-6}\,\mathrm{K}^{-1}$ (AF45 Schott, CTE $= 4.5 \times 10^{-6}\,\mathrm{K}^{-1}$), which allows a better CTE match to Si layers used in active matrix display technologies. ''TFT glasses'' such as AF37 (Schott), 1737 (Corning), AN100 (Asahi) show similar CTE values of approximately $3.7 \times 10^{-6}\,\mathrm{K}^{-1}$. Display technologies not requiring active matrix backplanes use glass types with higher CTE values above $7 \times 10^{-6}\,\mathrm{K}^{-1}$.

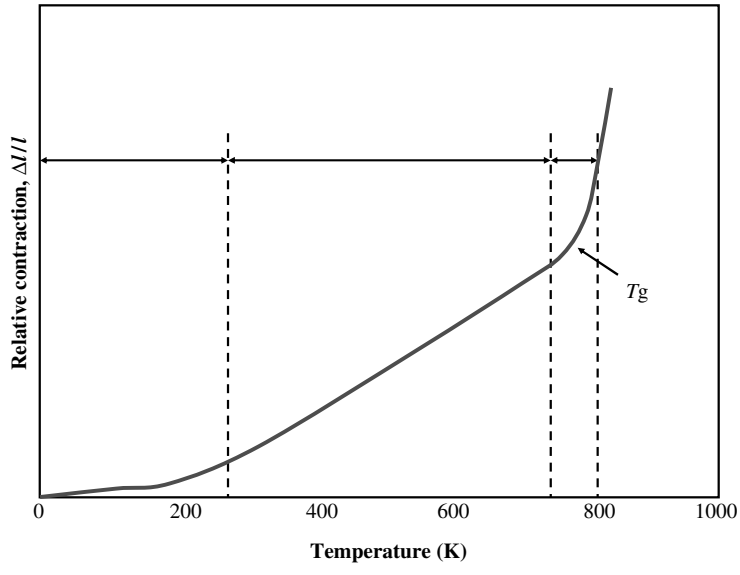


Figure 3.3 Length change of glass as a function of temperature

Petitioner Samsung Ex-1011, 0068

Surface properties

Based on the composition, structure and manufacturing process, glass has a very smooth surface, which is created by surface tension during solidification. The silicate structure gives glass a hard surface that can be polished to a very low surface roughness if necessary (e.g. glasses produced by float technology must be polished). Typical roughness values for display substrates are $R(\text{RMS}) \leq 1$ nm.

Depending on the production process, the glass substrate may exhibit other longer-range surface deformations such as warp, waviness or thickness deviation. These features differ with the various manufacturing processes; for the downdraw process some features exhibit unidirectional structures, whereas for the float process the structures are bidirectional.

Figure 3.4 shows the contribution of the single quality features to the real appearance of a display glass substrate.

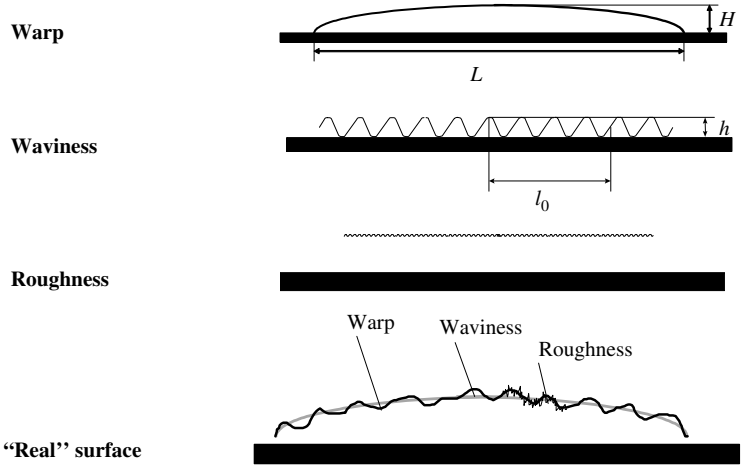


Figure 3.4 Contribution of single quality features to the real glass substrate

Based on a silicate structure, glass surfaces have a high tendency to absorb water molecules. As this process starts directly after manufacturing, the glass surface changes over time this surface change may influence thin film deposition processes at a later stage.

Permeability

Water and oxygen easily attack all kinds of organic materials, leading to chemical changes within a display thus limiting its lifetime. However, glass has a very low permeability to gases and moisture — an important factor for all display technology. Very low permeation is inherent in the silicate structure, which is not only very dense, but also forms very strong bonds to oxygen and water. Permeation values for oxygen and water through glass sheets therefore is so low that they are below the detection limit and, typically, it is assumed that glass sheets do not show any oxygen or water permeation.

Petitioner Samsung Ex-1011, 0069

3.3 Manufacturing of Thin "Flexible" Glass

A clear definition of ''thin'' does not exist, however, due to the progress of TFT LCD technology, which uses 0.7 mm ''thick'' glass, some people are using this thickness as the upper limit for thin glass. The lower limit is defined by the so-called microsheet with a thickness of 50 μm (Kessler *et al.* 1997).

In principle, glass becomes what is commonly understood as ''flexible'' below a thickness of approximately 200 μm (Plichta *et al.* 2003). The production of thin glass for the flat panel display modules has to keep pace with the increase in size and quality levels, therefore several process developments and upscaling procedures are ongoing. However only two production principles have survived and are in the frame: float technology and downdraw (DD) technology.

Float technology can produce glass substrates with a thickness down to 0.4 mm but DD technology offers the potential to produce glass down to 50 μm, or even down to 30 μm, which is the technical limit today. Both production technologies will be described in this section.

3.3.1 Float and Downdraw Technology for Special Glass

Figure 3.5 shows the principal flow of a glass production facility. The common processes of all glass productions are mixing of raw materials (I), melting (II), refining (III) and homogenization (IV) of the glass melt; and annealing (VI) and cutting (VII) of the glass sheet. For float technology (Va), the hot forming is performed horizontally on a liquid tin bath, whereas for DD technology, the hot forming takes place in a vertical direction (Vb). In general, float technology offers throughputs of over 500 tons/day, whereas current draw technologies are limited to approximately 8 tons/day.

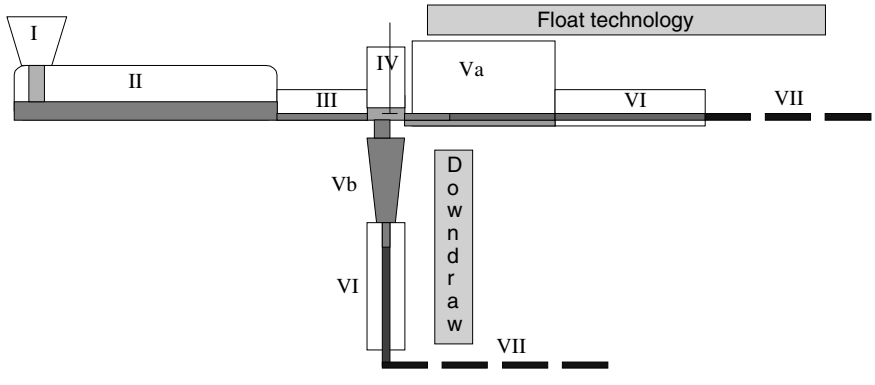


Figure 3.5 Basic process steps of modern glass production: I = mixing raw materials, II = melting, III = refining, IV = homogenization, Va = float technology, Vb = downdraw (DD) technology, VI = annealing, VII = cutting

Petitioner Samsung Ex-1011, 0070

After hot forming, annealing (VI) is necessary to cool down the continuous glass ribbon and to relax the mechanical stress induced during hot forming. The refining step (III) reduces the bubble content of the glass melt. Depending on the glass type, various refining agents such as antimony oxide, tin oxide or alkali halogenide can be used. Homogenization is performed with a stirrer. All tubes and hot-forming equipment for molten glass after the refining are made of precious metal alloys.

The DD processes for special glasses are developed mainly at Corning and Schott although they are also used by other glass manufactures around the globle. Corning uses the so-called overflow fusion process (Lapp *et al.* 1994). Schott uses a special nozzle slot design for the production of thin and ultra thin glasses with high-quality surface features, as well as a float technology for the production of large-size standard TFT glasses.

Production of ultra thin glass of thickness 100 μm and below is now a reality. Every year several hundred tons are produced by the DD technology for use as microscopy cover slides, glass touch panels and for wafer-level chip size packaging.

3.3.2 Limits

Display glass substrates must fulfill a multitude of requirements. For LCD displays the surface quality is decisive to assure exact control of LCD geometry. The quality features of the end product can be controlled from the glass production processes. Table 3.1 summarizes the relation of the glass production processes to important quality parameters required for display technology.

Table 3.1 Relation of production process and corresponding quality features

Process	Quality features	General requirements
Raw materials	Glass composition including optical, thermal and electrical properties	Alkaline content $< 0.1\%$ for TFT displays Optical transmission visible range $> 90\%$ CTE < 4 ppm/K for TFT
Melting	Inclusions (stones, quartz)	<30 μm
Refining	Bubbles	<30 μm
Homogenization	Uniform glass properties	
Hot forming	Surface properties: waviness, wave, surface roughness, thickness	Waviness < 100 nm Wave < 20 nm Surface roughness < 1 nm Thickness $= 0.7$ mm Thickness deviation within a sheet < 10 μm, from sheet to sheet < 40 μm
Annealing	Flatness (warp) Shrinkage	Warp < 150 μm Shrinkage < 10 ppm
Cutting into oversized sheets	Size tolerance	± 0.5 mm

Petitioner Samsung Ex-1011, 0071



Figure 3.6 Large thin glass sheet, 50 μm thick, produced by the DD technology

Thickness limits for production

The float technology is limited for thin glass production in terms of thickness and surface quality. The thinnest glass currently available is 0.4 mm thick, whereas the DD technology limit for production is currently at 30 μm or 50 μm. This shows that only the DD technology is in a position to follow the trend to thinner and even flexible displays. Figure 3.6 gives an impression of the state of the art of thin glass production using DD technology. Figure 3.7

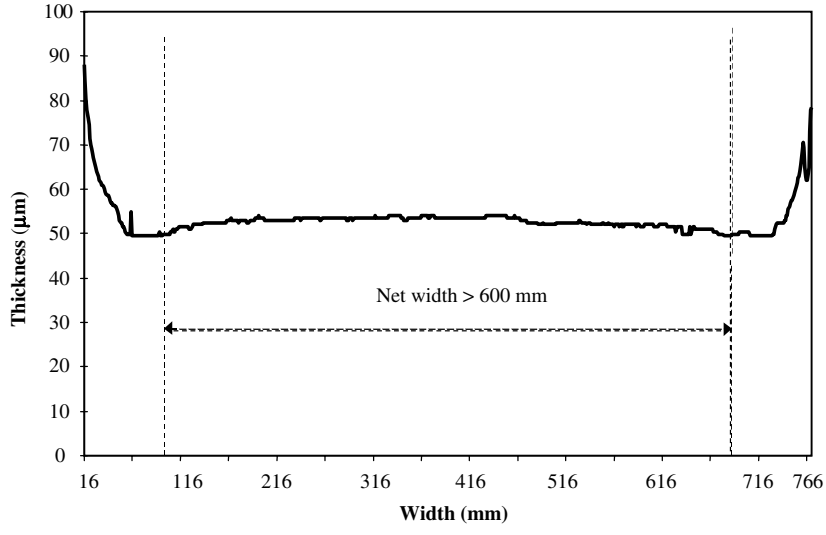


Figure 3.7 Thickness data for a large 50 μm thin glass sheet produced by the DD technology

Petitioner Samsung Ex-1011, 0072

shows the thickness data for thin glass sheet, 50 μm thick, produced by DD technology over a net width of > 600 mm.

Surface quality limits for production

Glass sheets produced by the float technology need to be polished to achieve the required surface quality features, whereas current DD technologies are providing excellent surface quality without any postprocessing.

The allowed surface deviations for LCD technology are in the submicron range. Figure 3.8 illustrates in detail the surface quality requirements. An evaluation window is defined (in this

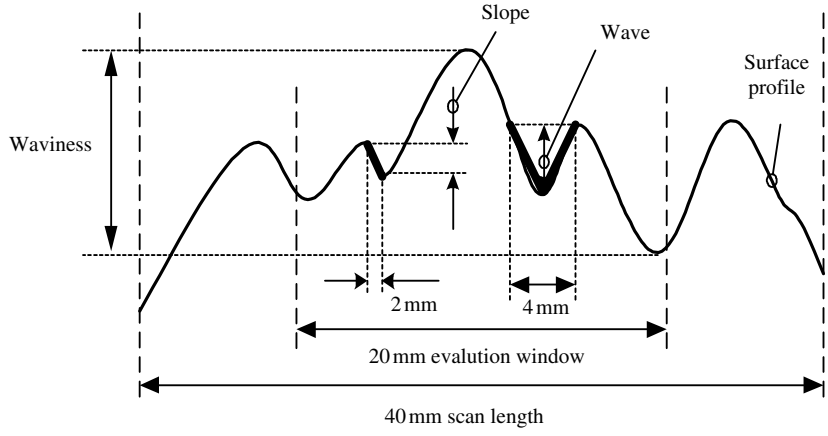


Figure 3.8 Detailed diagram of surface quality requirements for LCD technology

case 20 mm) within the scan length of the measurement equipment. Within the evaluation window, the maximum wave and slope of the sample are determined over shorter spans. Here are some typical values of the specification for LCD glass substrates:

- waviness 20 pv (peak-to-valley): < 0.100 μm;
- wave $20^*/4^\dagger$: < 0.020 μm;
- slope $20^*/2^\ddagger$: < 0.025 μm.

Moreover, the available advanced DD technologies offer excellent roughness quality features. The drawn surface shows roughness data in the range of 1 nm RMS roughness without any special treatment. In summary, DD technology is the sole production technology achieving economic production of high-quality flexible glass sheets.

* Scan length in mm
† Wave length in mm
‡ Slope length in mm

Petitioner Samsung Ex-1011, 0073

3.4 Mechanical Properties

3.4.1 Thin Glass and Glass/Plastic Substrates

System manufacturers tend to regard the glass strength as a subordinate property. ''Hard'' product features such as optical transmission, dimensional stability within the system design and during processing, chemical barrier qualities or electric material characteristics as functional sizes take precedence over mechanical properties. Nevertheless, the glass strength is a highly important property, because it determines the mechanical strength of glass parts. For this reason, the mechanical peculiarities of glass in manufacturing or during usage are discussed in many articles (Rawson 1988; ICG 2003). However, the manufacturing of curved, bendable or rollable displays will require glass sheets with a thickness of less than 100 μm.

3.4.2 Mechanical Test Methods for Flexible Glasses

Thin sheet glasses usually have surfaces of very good mechanical quality. Microdefects may be induced in the glass surface by mishandling it, in the sense of mechanically damaging it or causing abrasion. This applies to handling during the manufacturing process, as well as to the typical wear and tear by customer usage. In short, the strength of a glass part depends on its entire history, which involves mechanical or chemical traces placed on the glass surface. The stronger these traces, the more reduced the strength and the lifetime, and the higher the loss probability of a glass part. Of course, it is assumed as a basic condition that in the final product the mechanical requirements for the use of brittle materials have been considered.

In most mechanical laboratories, the surface strength of brittle materials is evaluated by a standard procedure, the so-called ring-on-ring procedure (DIN EN 1288). Care must be taken that reproducible tension profiles in the test objects are obtained by choosing test setups with suitable dimensions, in particular for the testing of ultra thin sheet glass applications (Section 3.5).

Much more critical than the weakening of the surface strength by surface damages is the breaking edge produced when the glass sheets are cut into smaller pieces. In most cases this breaking edge is responsible for the failure of a glass component. We will primarily deal with this type of failure.

Low-cost manufacturing is usually carried out by the time-parallel processing of many single structures on a large-area glass substrate. The necessary separation of these single structures, e.g. displays, induces serious, strength-relevant injuries in the glass surface or glass body when carried out with standard separation procedures such as diamond scribing, wheel cutting, dicing, and laser cutting.

Figure 3.16 shows the broken edge characteristic of an ultra thin glass sheet cut into smaller pieces by diamond scribing (substrate thickness 100 μm). Looking from above, we see the typical fine trace of the initial cracking with strong injuries in the form of microcracks or chips, followed by mist and twist hackle marks. In the lower part, opposite the initial cracking, the breaking edge is almost smooth. With unfavorable breaking, this part may also be damaged by chips or cracks. From each of the surface structures displayed here, a crack may originate under local tension, hence causing the failure of the glass component

The heterogeneity of the fracture patterns with respect to the correlated sheet surfaces required different mechanical tests to be carried out for a complete characterization of the

Petitioner Samsung Ex-1011, 0074

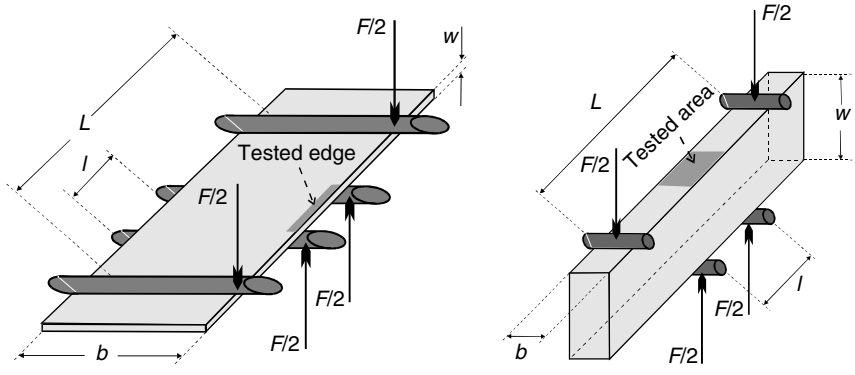


Figure 3.9 Four-point bending test

edge quality. As a standard test procedure, static (three) four-point bending tests (Figure 3.9) are carried out in a first step. Depending on the position of the test bodies, the already optically visible directional dependence of the mechanical edge quality can be taken into account.

For glass, the strength is not defined as a material constant (in contrast to other materials, e.g. metals), but as a statistical dimension, i.e. as the probability of fracture under load or under varying environmental conditions, for example. After the destructive tests have been carried out, the acquired data are analyzed with various statistical standard tools (Sachs 2002; DIN 55303). It is very important – and must be emphasized to the manufacturers of the final devices – that the necessary statistical test procedures (e.g. χ^2 or *t*-test) which verify the statistical hypotheses can only be executed when a sufficient number of valuable breaking events are available. This is the only way to acquire solid results.

In addition to the described static tests, it is useful to investigate in the laboratory the impact of short-term loads, such as when a PDA is dropped, or during processing on the production line (e.g. use of stoppers to position thin sheets). The main focus is again on the critical breaking edge of the glass substrate. A test setup is shown in Figure 3.10.

When the mallet is equipped with a cladding and the thin sheet glass is placed on a cantilever support, it is possible to simulate the conditions for transport on a production line and for display assembly. It is also possible to generate ''wear and tear damage'' and its relevance for the durability of the glass item may then be investigated with the static test methods described above.

Ultra thin sheet glasses naturally tend to break under smaller loads than ''thick'' sheets, because mechanical stresses, assuming the same load, are approximately inversely proportional to the square of the glass thickness.

In fact, ultra thin sheet glasses are at least ''as strong'' as thick sheets, but their dimensions make them more sensitive to mishandling in the production line or at the customer.

Consequently, the demands on the mechanical stability are higher for flexible substrates because the substrates, and therefore the breaking edges, are much more stressed. The two-point bending procedure is suitable for testing such stresses (Figure 3.11). This test procedure has been established for telecommunication fibers (Matthewson 1986) and adapted for ultra thin sheet glasses. In this test, ultra thin sheet glasses are placed between

Petitioner Samsung Ex-1011, 0075

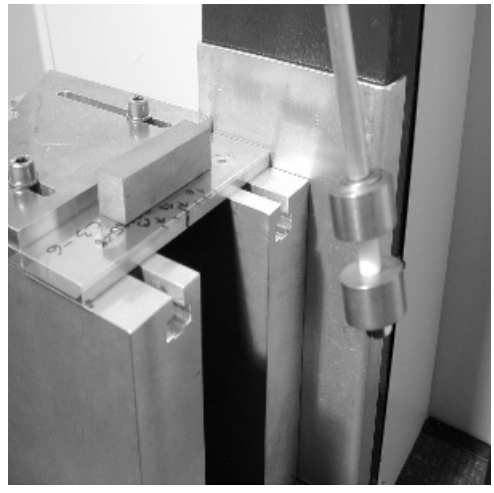


Figure 3.10 Edge impact test

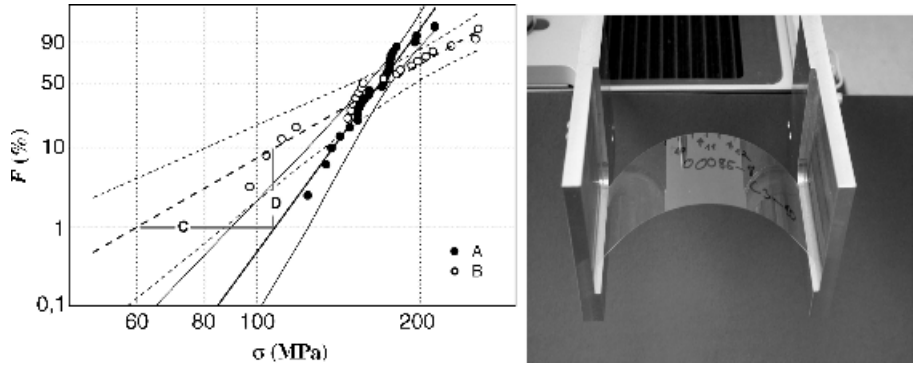


Figure 3.11 Setup for the two-point bending procedure and the influence of edge positioning

two traveling jaws, which are then tightened until the test piece fails. As can be seen in Figure 3.11, today's cutting technologies and suitable polymer coatings, applied especially to the breaking edge region, enable durable glass bending radii of 30 mm with a predicted loss probability of <1%. Corresponding results, for example the process influence and the enhancement of the already high breaking edge quality by effective edge coating, are explained in Section 3.5.1.

As an example for the demonstrated heterogeneity of cutting edges (Figure 3.16) and the influence on the fracture strength, Figure 3.11 shows the strength distribution of the upper edge (A, initial scribing) and the lower edge (B). As can be seen, the edges of the ultra thin sheet glasses have high strength (parameter of the Weibull distribution $\sigma_0 > 160$ MPa). However, depending on the positioning, strength σ differs by almost 100% for an identical failure probability $F = 1\%$ (C) or the failure probability at the edge bottom is expected to

Petitioner Samsung Ex-1011, 0076

increase by a factor of 10 under a load of 110 MPa (D). These results indicate that attention should be paid to the positioning of the glass sheets when bend ultra thin sheet glasses are being processed.

3.5 Improvement in Mechanical Properties of Glass

The properties of glass in Section 3.2.1 are important for different display technologies. The most important advantage of plastic is the low breakage probability. Even the flexibility, which plastic is said to have, can be achieved by glass. Thus, bending radii of 31 mm for glass of thickness 100 μm and 12 mm for 50 μm thin glass (at a failure rate of 1%) were measured by Schott (Plichta *et al.* 2002).

There are several methods to achieve the lowest possible breakage rate for glass:

- careful handling with suitable equipment,
- thermal or chemical hardening,
- use of multilayer and compound glasses,
- coating.

Of these general possibilities for glass treatment, only coating can be considered for thin glasses. Hardening can only be used for thick glasses, and compound glasses reduce the flexibility. Therefore coating is the only chance to reduce the breakage rate and to keep the flexibility of the thin glass.

3.5.1 Reinforcement of glass substrates

The reinforcement coating has two positive effects on the glass strength. First of all, the possible damage to the glass can be blocked by a surface coating, which means the number of microcracks is reduced. Secondly, the coating results in a compressive stress on the glass surface. Therefore the growth of already existing cracks can be reduced or even stopped.

Principal methods of reinforcement

A reinforcement of glass for display applications can be achieved by

- lamination with plastic foil;
- thin layer coating such as a plasma despoiled hardcoat;
- thick layer coating, e.g. of polymers.

When using these coating processes, the advantageous properties of both materials can be combined. That means the excellent barrier properties and the dimensional stability of the glass can be combined with the resistance of damage to plastic.

Strength tests have shown that the breakage rate of glass depends not only on the damage of the surface, but also or even more heavily on the damage at the edges of the substrate. The

Petitioner Samsung Ex-1011, 0077

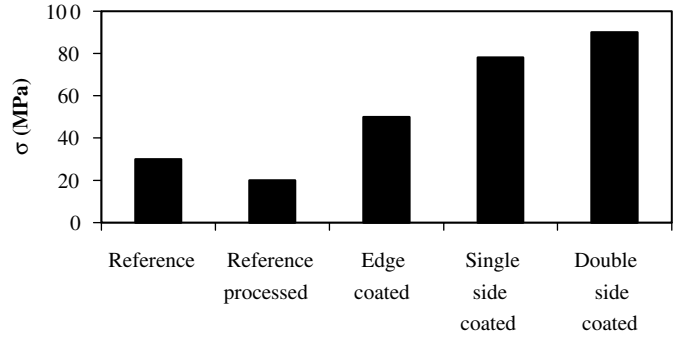


Figure 3.12 Influence of edge and surface (including edges) coating on the edge strength (P2 coating) at a failure probability of 1%

protection of the substrate surface is important, but the protection of the edges is even more critical as approximately 90% of the breakage is caused by damaged edges.

Figure 3.12 shows the influence of the edge and surface coating on the strength. When the surface is coated, the edges are also coated. It shows the positive influence of edge coating against the uncoated substrate. However, the highest strength values were achieved by a combined coating of the edge, as well as of the surface.

Materials for reinforcement coatings

The influence of the coating material on the achievable edge strength σ is shown in Figure 3.13. In the histogram, uncoated glass substrates (Ref.) are compared with polymer-coated glass substrates (P1, P2 and P3). P1, P2 and P3 represent different polymer materials. Notice that the strength of uncoated substrates is decreased due to handling (Proc.). In this case the processed substrates went through the coating process without applying a polymer. Substrates coated with a polymer show a higher strength after the same handling steps when compared to the uncoated substrates.

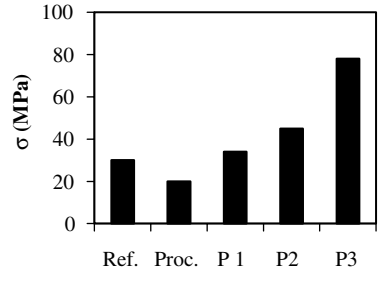


Figure 3.13 Edge strength σ of processed (coated) substrates at a failure probability of 1%: Ref. = reference glass (not processed); Proc. = processed glass without coating; P1, P2, P3 = processed glass with different coatings

Petitioner Samsung Ex-1011, 0078

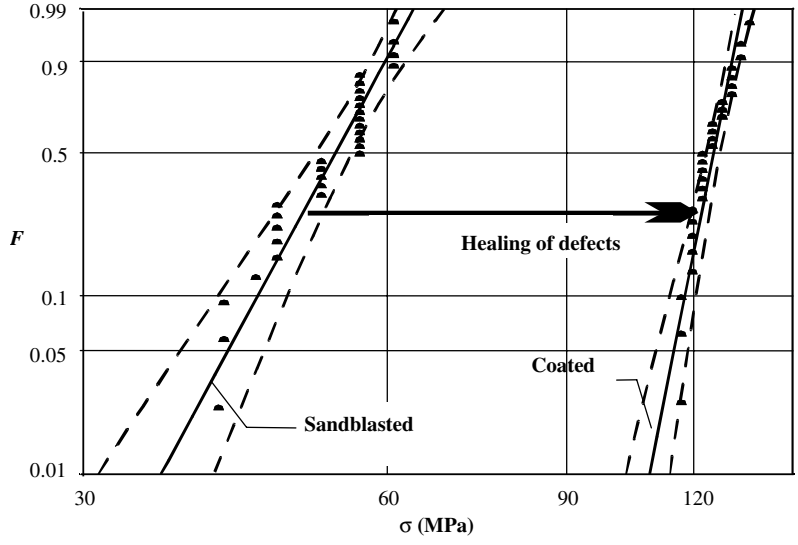


Figure 3.14 Improved surface strength of damaged (sandblasted) glass surface by coating

Due to a suitable polymer coating, significant protection of the glass can be achieved, thus reducing the damaging influences of processing and handling steps. Such a coating can also reduce the influence of already existing defects. Figure 3.14 shows the ''healing'' effect of a polymer coating. In this test, the substrate surfaces were sandblasted and the surface strength σ was measured before and after coating. The amount of glass breakage in the manufacturing process is reduced if the glass surfaces are coated, and the process becomes more stable to minor handling mistakes in production. Both effects are crucial for increased ''robustness'' of ultra thin glass applications (Plichta *et al.* 2003).

3.6 Processing of Flexible Glass

When manufacturing displays, there are some important aspects for both the substrate supplier and the display manufacturer, such as transportation issues, cleaning methods and separation methods. Moreover, a mass production manufacturing process is not yet available. This holds for any kind of flexible substrate, glasses as well as plastics. The current situation for mass production of displays involves the use of standard manufacturing equipment, which allows only minor changes in material properties to keep the product cost-competitive. An important material property is the so-called sagging, which depends mainly on the Young modulus E of the substrates. Sagging values describe how much a substrate is allowed to sag under special conditions of the handling equipment.

Sagging specifications and substrate flexibility run counter to each other. This means if flexible substrates are to be processed with standard manufacturing equipment there are only two choices: modify all automated handling steps or modify the substrate so that its stiffness becomes comparable to that of thicker standard substrates. The first choice involves building a new production line. This is the reason why new display technologies have a greater advantage in manufacturing flexible displays, as standard equipment is not yet available (e.g. OLED).

Petitioner Samsung Ex-1011, 0079

On the other hand, advanced LCD technology must also be able to deal with ''flexible'' substrates if we consider the new Gen 7 glass substrates. The traditional sagging value for these substrates is nearly 1 m instead of several millimeters of sagging tolerated for smaller substrate sizes. Nevertheless, the LCD industry has developed solutions to overcome this problem with new handling concepts.

From the viewpoint of plastic substrates, the idea of roll-to-roll processing is favored as it is more cost-effective. Following this concept, a lot of other issues need to be resolved and can't be discussed here. In any case, glass-based flexible displays can only use batch processes, because even if rolling glass ribbons is possible, the practical use is limited due to low yield related to glass breakage. In summary, these are the reasons why current efforts are made to manage the glass substrates only with standard equipment benefiting from possible cost savings and therefore making the product cost-competitive. With this background information the focus of activity is on cleaning, cutting and transportation of flexible glass substrates.

3.6.1 Cleaning

Every substrate must be cleaned before processing. How intensive the cleaning has to be depends on the contamination of the substrates. Such contamination can be particles caused by the environment such as dust, glass particulates due to the cutting process, or organic compounds such as fingerprints or paper prints due to handling, storage and transportation. In order to remove such contamination, different cleaning techniques need to be combined. The basic cleaning methods are

- brush cleaning;
- megasonic (400 kHz to 3 MHz) and ultrasonic (25–100 kHz) cleaning;
- cleaning by hydrodynamic forces (laminar and turbulent flow, drag and lift forces, spray);
- dry ice cleaning;
- UV/ozone cleaning;
- laser cleaning.

When cleaning standard glass sizes, good cleaning results are achieved by using commercially available equipment. However, for cleaning ultra thin glasses or very large sizes like Gen 7 and above, new concepts, e.g. a substrate holder, are necessary. The challenge here is the flexibility of those substrates.

Based on commercially available ultrasonic washing equipment, very good cleaning results have been achieved for coated substrates at a thickness of 100 μm. For 300 mm × 300 mm substrates STN LCD quality has been achieved.

3.6.2 Separation

There are several methods of separation of glass and displays. Depending on the accuracy and shape, several methods are used:

Petitioner Samsung Ex-1011, 0080

- sawing;
- guillotining;
- cutting:
  - water jet cutting (rarely used),
  - laser cutting (full-body cut, laser scribing),
  - cutting by wheel (hard-metal wheel or diamond wheel),
  - cutting by diamond.

At present the most commonly used separation methods are conventional cutting by wheel or diamond and by laser

When speaking of conventional cutting, this implies a mechanical scribe process followed by a breaking step. This process causes fragmentation, as can be seen in Figure 3.15, which may generate glass particles. In order to avoid such glass particles, the full-body laser cut was developed. The full-body cut uses a laser beam to apply heat to the glass. The glass is then immediately cooled, which generates a stress-induced cut that results in complete separation.

For thin glass sheets below 200 μm, the conventional cutting process is being utilized in a newly developed process. When properly adjusted, this conventional cutting equipment produces edge quality and strength results as good as those of a laser-cut substrate. After the substrate is diamond scribed, the following breaking step results in a high edge quality as shown in Figure 3.16.

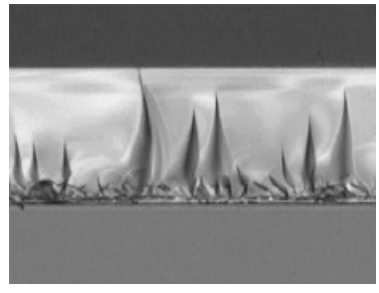


Figure 3.15 Edge quality of standard cutting equipment (using a diamond wheel)

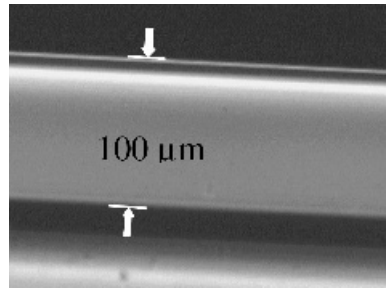


Figure 3.16 Edge quality of improved cutting equipment (using a diamond)

Petitioner Samsung Ex-1011, 0081

3.7 Current Thin Glass Substrate Applications and Trends

In today's world there are numerous buzzwords such as ''miniaturization'' and ''multi-functional,'' forcing the industry to look for alternative material compositions. One decisive point for all of the handheld and energy-saving applications is the thickness, and thus the weight, of the materials used. Talking about display applications, and microelectro mechanical systems (MEMS), the substrate material glass has played an important role and still plays an important role. Thanks to different production technologies (drawing, floating, casting, etc.) and different chemical compositions (soda-lime, borosilicate, aluminosilicate, etc.) the substrate material glass can serve a huge variety of applications and sometimes it might not even seem that glass is present inside the product.

3.7.1 Displays

The leading technology now and in the future is TFT (active matrix), and the second is the family of TN/STN (passive matrix). Besides these two major technologies there are smaller markets for OLED and PolyLED, LCOS, ELD, PDP and many more. One demanding area is the handheld communication market (e.g. mobile phones, PDAs and laptops), which requires higher functionality, easier handling and reduced weight. The mobile phone market began some years ago with passive matrix black and white displays and substrate thicknesses of 1.10 mm and 0.70 mm. Today no new mobile phone is equipped with such thick substrate materials. The main market is driven with 0.50 mm and 0.40 mm thick substrates for the main displays and 0.30 mm for the subdisplays. The leading mobile phone makers are now focusing on a thickness less than 0.30 mm for both displays. This request can easily be fulfilled for the passive matrix displays using STN/CSTN technology by using thinner glass substrates; the rising TFT makers use alternatives like etching or polishing down the TFT panels (which are mainly being produced in 0.70 mm glass thickness). Both ways are acceptable to the industry, as both technologies can comply with the requirement for lightweight and good picture quality.

The mainstream TN technology passive matrix is still using a 0.70 mm thickness with the exception of watch displays, which for quite some time have already used a 0.30 mm thick substrate. And, who knows how much thinner these displays will become in the future? The same trend can be seen for laptops, for example, using TFT substrates. First prototypes have been presented to the public already with glass substrates as thin as 0.30 mm and even thinner (for curved displays).

3.7.2 Touch Panels

Touching is one of the most instinctive human actions. Therefore touch panels (Figure 3.17) can be found in many industrial environments, hospitals, tourist centers, schools, retail and automotive industries. Touch screens make access to using computers easier, as clearly defined menus eliminate the need for keyboards. Thin glass touch panels with low reflectance are used in car navigation systems, as well as for other applications. Thin glass substrates with thickness of about 200 μm offer the advantage of furnishing the device with the required flexibility to recognize the ''touch'' of a wide variety of objects.

Petitioner Samsung Ex-1011, 0082

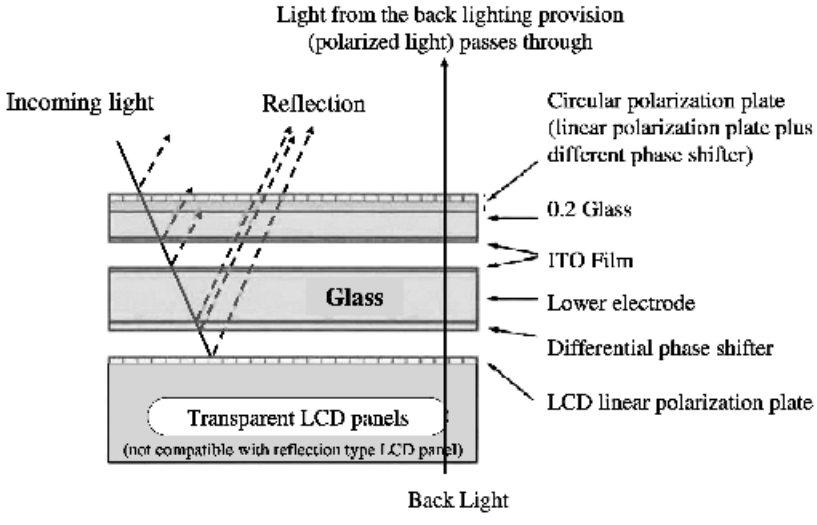


Figure 3.17 Principal structure of a touch panel

Flexible glass sheets provide touch panels with better scratch resistance than plastic, which is beneficial in rough environments.

3.7.3 Sensors

The market for sensors is very large and growing, as sensors can be found in industry and in our daily lives, as well. Small to ultra small sensors are offered from all manufacturers. Again, a suitable material for this application is glass. Sensors used, for example, in the automotive industry for airbags, temperature control, gasoline control, etc., are already very small parts, which is important. They need to become smaller and lighter in weight to help reduce gasoline or energy consumption and keep the environment cleaner.

Promising growth can be seen in CCD and CMOS image sensors, especially with applications for new cell phones with or without camera systems. Digital cameras also require small parts with low weight and high transparency as well as a number of high-technology features combined in a small part with special glass covers or windows using glass thicknesses of approximately 0.30 mm. Many manufacturers are involved in this market, but the real volume is done by only a few.

3.7.4 Wafer-Level Chip Size Packaging

An alternative technology using a glass/silicon/glass sandwich developed by Shellcase/Israel uses glass substrates as thin as 100 μm. This enables the manufacturer to produce miniaturized packages well suited for use in handheld communication devices such as portable computers, mobile phones, and wireless communication as well as in the medical field. A total package thickness of 330 μm to 730 μm definitely requires highly precise thin glass substrates.

Petitioner Samsung Ex-1011, 0083

References

ICG (2003) Advanced course on the strength of glass: basics and test procedures. Research Association of the German Glass Industry (HVG).

Kessler, T., Wegener, H., Togawa, T., Hayashi, M. and Kakizaki, T. (1997) Large microsheet glass for 40-in. class PALC displays. *Proceedings of the 4th International Display Workshops*, 347–349.

Lapp, J. C., Bocko, P. L. and Nelson, J. W. (1994) Advanced glass substrates for flat panel displays. *SPIE Proceedings* **2174**, 129.

Matthewson, M. J., Kurkjian, C. R. and Gulati, S. T. (1986) Strength measurement of optical fiber bending. *Journal of the American Ceramics Society* **69**(11), 815–821.

Plichta, A., Deutschbein, S., Weber, A. and Habeck, A. (2002) Thin glass-polymer systems as substrates for flexible displays. *SID Proceedings*.

Plichta, A., Weber, A. and Habeck, A. (2003) Ultra thin flexible glass substrates. *MRS Proceedings*.

Rawson, H. (1988) Why do we make the glass so weak? A review of research on damage mechanisms. *Glastechnische Berichte* **61**(9), 231–246.

Sachs, L. (2002) *Angewandte Statistik*, Springer Verlag.

Scholze, H. (1988) *Glas*, Springer Verlag.

Petitioner Samsung Ex-1011, 0084

4

Barrier Layer Technology for Flexible Displays

Gordon L. Graff,[1] Paul E. Burrows,[1] Rick E. Williford,[1] and Robert F. Praino[2]

[1]Pacific Northwest National Laboratory and [2]Vitex Systems Incorporated

4.1 Introduction

Organic light-emitting devices (OLEDs) are currently used in emissive displays for car stereos, cell phones, electric razors and digital cameras. The thin film structure offered by OLEDs holds promise for the near-term introduction of flexible full-color displays on lightweight plastic substrates. However, the extreme sensitivity of OLEDs to water vapor induced degradation places severe demands on the barrier performance of flexible, thin film coatings.

This chapter will briefly summarize the development of thin film barrier layers in various applications, and describe the OLED vapor barrier technical requirements (Section 4.2). Section 4.3 is a brief summary of relevant experimental methods used to measure gas permeation in thin films. Attempts are made to delineate the advantages and disadvantages of each measurement technique. In Section 4.4 we describe some of the historical analytical and modeling approaches that have been invoked to explain the measured analytical results and discuss some of the more important shortcomings of those modeling concepts. Section 4.5 presents an approach suitable to describe gas diffusion in multilayer thin film

Flexible Flat Panel Displays Edited by G. P. Crawford
© 2005 John Wiley & Sons, Ltd., ISBN 0-470-87048-6

Petitioner Samsung Ex-1011, 0086

structures. Transient permeation measurements are used to extract physically reasonable values for the in situ effective diffusivity and solubility of the various polymer and oxide layers, as well as estimates of defect size and spatial density consistent with those parameters. The implications of these results are that lag times for permeant breakthrough in multilayered barrier systems are extremely long and are likely to dominate many of the results reported to date, rather than the commonly measured steady-state flux. These findings are then discussed in relation to practical OLED encapsulation in Section 4.6, along with the need for new techniques for further improving the barrier quality. Section 4.7 is a conclusion.

4.2 Development of Thin Film Vapor Barrier Systems

This section briefly describes representative applications of thin film vapor barriers over the past three decades, the exponential increase of barrier performance requirements necessitated by the advent of organic electronics, and the evolution of barrier structural/materials designs to respond to those needs.

The use of vacuum-deposited thin films as gas diffusion barriers is ubiquitous in today's world. Since the early 1970s thin metal films deposited on polymeric substrates have been used as gas barrier coatings for packaging of foods (Schiller *et al.* 2001). In 2001 about 11 billion square meters of aluminized polyester (PET) and polypropylene (OPP) were produced for snack foods, beverages, etc. Metallized plastics are also used extensively in packaging of sensitive electronic components (such as integrated circuits), medical components (instruments and pharmaceuticals) and decorative applications (such as mylar balloons and wrapping paper). In these applications, a thin film of Al metal, typically 10–100 nm thick, is flash evaporated onto a moving web of polymeric substrate in a large vacuum chamber using a roll-to-roll (r2r) configuration (Baxter 1993; Watts 1991). The thin Al film reduces the permeability of atmospheric gases by as much as 1000 times over the native polymeric substrate. For example, a typical 1 mil (25.4 μm) PET film has an oxygen transmission rate (OTR) of 58 cm^3(STP)/m^2/day/atm at 25 °C while aluminized mylars (PET) have values of 0.1–10 cm^3(STP)/m^2/day/atm at 25 °C (Schwarz Packaging Systems 2003).

In the past ten years an increasing need has arisen for *transparent* flexible packaging with gas barrier properties equivalent to those of the opaque metallized films. Transparent barrier packaging enables viewing of the product, microwavability and fewer environmental concerns (better recyclability) (Krug *et al.* 1993). For these applications, metal oxides and nitrides, such as SiO_x, Si_3N_4, AlO_x, TiO_x and ITO, have been extensively investigated. Due to the high melting temperatures and dielectric nature of these materials, high-rate vacuum deposition presents a substantial challenge. In addition, thermal limitations of the polymeric substrate typically require inorganic film deposition at substrate temperatures below 100 °C. Transparent barrier films have been deposited using thermal and electron beam evaporation, DC, AC, RF and microwave sputtering, reactive magnetron sputtering, CVD, plasma-enhanced CVD, and exotic routes such as electron cyclotron resonance plasma-enhanced CVD (ECR-PECVD). Though many factors affect the final properties of vacuum-deposited thin films, most researchers agree that the process providing the highest density, lowest defect number and smallest defect size produces the best barrier film. The factors affecting the quality of the barrier film will be discussed more completely in the following sections.

Petitioner Samsung Ex-1011, 0087

4.2.1 Organic Electronics: Packaging Needs

With the advent of thin film organic electronics (organic transistors, conducting polymers, and OLEDs) the fabrication of ''flexible'' electronics and devices has become a reality. Flexible organic light-emitting test pixels (OLEDs) were first demonstrated by Gustaffson *et al.* (1992) using polymeric electroluminescent layers in 1992 and later by Gu *et al.* (1997) using small molecule (nonpolymeric) organic emitters. The total display thickness, including anode, organic emitting layers, cathode and current collector is $\sim$3000 Å (0.3 μm), orders of magnitude thinner than liquid crystal displays (LCDs). Despite the potential advantages of thin, flexible, emissive displays, the commercialization of OLED devices is hindered by their extreme sensitivity to water vapor. Low work function metals, such as Ca and Li, are required to obtain efficient electron injection from the cathode to the organic luminescent layers. Hydrolysis of the cathode metals (from leaks in the vapor barriers) creates nonconductive regions in the electrode resulting in nonemissive ''black spots'' and pixel shrinkage (Burrows *et al.* 1994; Kolosov *et al.* 2001). Hermetic sealing (encapsulation) of the OLED device is required to achieve lifetimes that exceed a few hours. Display manufacturers require packaging methods with demonstrated water vapor permeation rates (WVTR) of $< 10^{-5}$ g/m^2 per day at 25 °C and 40% relative humidity (RH) (Weaver *et al.* 2002). Currently, commercially available thin film packaging materials have WVTR values of $\sim$0.5–1.0 g/m^2 per day at 25 °C and 100% RH, and developmental materials rarely obtain WVTR values as low as 0.01 g/m^2 per day at 25 °C and 100% RH. These permeation rates are 3–4 orders of magnitude above those required for successful OLED encapsulation. Similar encapsulation requirements are likely for other organic electronic applications, particularly those involving current injection.

4.2.2 Single-Layer Gas Barrier Films on Polymeric Substrates

OLED devices deposited on PET substrates survive only a matter of hours when exposed to atmospheric conditions due to the high diffusion of oxygen and water vapor through the native polymeric substrate. The vacuum deposition (PVD or CVD) of a thin inorganic barrier film (single-layer approach) on native polymeric substrates can dramatically improve the overall barrier performance. This is especially impressive when one considers that the inorganic film is 100–1000 times thinner than the substrate. Table 4.1 provides a survey of OTR (oxygen permeation rates) and WVTR values (25 °C) obtained for single-layer inorganic coatings deposited on polymeric substrates.

The presence of the inorganic thin film improves the barrier performance by a factor of 10–100 over the native substrate due to the lower diffusivity (D), solubility (S) and resulting permeability ($P = DS$) of the inorganic layers relative to the polymeric substrates. For example, the diffusivity of O_2 in PET or acrylic is $\sim 10^{-9}$ cm^2/s at 20 °C while the O_2 diffusivity in *bulk* SiO_2 is $\sim 10^{-15}$ cm^2/s at 1500 °C. Polycrystalline Al_2O_3 has a *bulk* diffusivity of $\sim 10^{-13}$ cm^2/s at 2000 °C. From the bulk diffusivity values, one would expect that the room temperature gas permeation (WVTR) through these inorganic materials should be immeasurably low (basically zero). The published data demonstrate that diffusivities of thin, vacuum-deposited inorganic films are many orders of magnitude above those of the bulk materials. This is due to the presence of microscopic defects in the deposited film (Chatham 1996; Prins and Herman 1959; Jamieson and Windle 1983; Rossi

Petitioner Samsung Ex-1011, 0088

Table 4.1 Comparison of OTR and WVTR values of PET and nylon substrates containing inogranic thin film coatings

Normalized to 1 mil thickness	OTR (cm^3(STP)/m^2 per day per atm)	WVTR (g/m^2 per day) at 90–100% RH	Deposition method
PET/SiO_x a	2.0	1.1	Evaporation
PET/SiO_x c	0.08	0.5	PECVD
PET/AlO_x	1.5	5.0	Evaporation
PET/AlO_xN_y	2.8	4.3	Sputtering
PET/DLC	2	1.5	PECVD
PET/ITO	1.56	0.2	Sputtering
PET/Al	0.31–1.55	0.31–1.55	Evaporation
Nylon/Al	0.8	3.1	Evaporation
PET/7 mm Al foil	0.001	—	Lamination
PET	79	10.7	—

and Nulman 1993; da Silva Sobrinho *et al.* 2000; Hanika and Langowski 2003; Roberts *et al.* 2002; Erlat *et al.* 2000, 1999; Henry *et al.* 2001).

4.2.3 Multilayer Gas Barrier Films for OLEDs

Multilayer organic/inorganic thin film encapsulation is routinely used in the semiconductor industry for passivation and hermetic packaging of integrated circuits (Wong 1993). The electronic devices are first overcoated with a polymeric material, such as silicone, polyimide or parylene, followed by PECVD deposition of Si_3N_4. A similar approach was used by early developers in an attempt to directly encapsulate OLED display devices fabricated on glass or silicon substrates (Harvey *et al.* 1998, 1997; Rogers *et al.* 1998, So *et al.* 1998). These thin film methods were not successful at attaining the required barrier performance and the addition of metal ''cans'' or glass ''lids'' was required to hermetically seal the sensitive OLED device.

Shaw and Langlois (1994) reported a four orders of magnitude decrease in OTR (from 1000 to 0.1 cm^3(STP)/m^2/day/atm) using an oriented polypropylene (OPP) substrate overcoated with alternating thin film layers of acrylate polymer and aluminum metal (OPP/acrylate/Al/acrylate). In such structures, each polymer–metal layer pair is called a dyad. Affinito *et al.* (1996b) achieved OTR and WVTR values below instrument detection limits (< 0.0155 cm^3(STP)g/m^2/day/atm at 25 °C) using a multilayer organic/inorganic thin film barrier structure deposited on a PET substrate (PET/1 μm acrylate/25 nm AlO_x/0.24 μm acrylate). The same group later correlated critical process parameters (such as surface roughness, particulate, and the thin film deposition method) with improvements in multilayer barrier performance (Affinito *et al.*, 1997).

Recent publications have shown that OLEDs encapsulated using multilayer organic/inorganic thin films show extended operating lifetimes of greater than 1000 h (Weaver *et al.* 2002; Nisato *et al.* 2003; Moro *et al.* 2004). A typical multilayer structure used for OLED encapsulation is shown in Figure 4.1. The thin (∼40 nm), lighter-colored layers are inorganic AlO_x, and the darker layers are organic (acrylate) polymers.

Petitioner Samsung Ex-1011, 0089

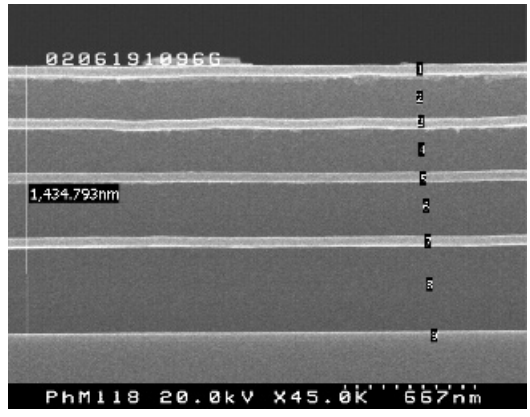


Figure 4.1 SEM cross section of a typical multilayer organic/inorganic barrier stack

Based on the increase in transparency of a thin film of calcium as it oxidizes, a WVTR of 8×10^{-5} g/m^2 per day at 25 °C and 40% RH was reported for five dyads (AlO_x–polyacrylate pairs) on a PET substrate, with the permeability of the epoxy edge seal reported as a limiting factor in the test (Nisato *et al.* 2001). Using actual OLED test pixels, fabricated directly on multilayer PET/barrier substrates (Weaver *et al.* 2002), a continuous operation test showed that the device decayed to 50% of its initial luminance in 3800 h, compared to 10 700 h for an equivalent device made on glass. Again, leakage through the epoxy edge seal limited the results. By calculating the percentage of inactive pixel area, a total package WVTR of 2×10^{-6} g/m^2 per day at 25 °C and 40% RH was inferred, in good agreement with the measurements made using the Ca test (Nisato *et al.* 2003, Moro *et al.* 2004). We note, however, that neither of these results strictly represents equilibrium permeation, since moisture accumulates inside the package during the experiment. Furthermore, the mechanism of vapor permeation through multilayered barrier films has not been clearly identified. Identification of this mechanism is an objective of this chapter.

4.3 Measurement Techniques

The previous section described the evolution of thin film barrier systems in response to an increasing demand for performance. This section will briefly outline some techniques used to characterize barrier structures. A serious challenge facing barrier film developers is the inability to accurately measure gas permeation in a range useful for organic electronics ($< 10^{-5}$ g/m^2 per day at 25 °C and 40% RH). A second challenge is the difficulty of characterizing defect sizes and spatial densities in vacuum-deposited thin films, particularly when attempting to quantify multilayer structures with buried layers.

4.3.1 Steady-State Transmission Tests

Some of the simplest or straightforward measurement techniques, such as gravimetry, capacitive/resistive humidity sensors, or mass spectroscopy, lack the sensitivity to be useful

Petitioner Samsung Ex-1011, 0090

for OLED applications. The most widely used methods for measuring gas permeation follow test protocols such as ASTM D3985 (OTR) and ASTM F1249 (WVTR) designed to measure steady-state rate of transmission. In these tests the membrane is positioned in a flow cell with the upstream side of the sample exposed to a constant concentration of test gas. A sweep gas is used to maintain the downstream test gas concentration at zero, thus establishing a constant driving force for diffusion. The test treats the barrier assembly as a homogeneous material and no information is produced concerning defect sizes or distributions. The resolution of commercially available equipment (Mocon Corporation, 7500 Boone Avenue North, Minneapolis, MN) is 0.005 cm^3(STP)/m^2/day/atm (OTR) and 0.005 g/m^2 per day (WVTR), and laboratory services are available with a factor of 10 improvement in sensitivity (0.0005). These sensitivities are insufficient to evaluate the performance of modern barrier systems, particularly those involving multilayer structures. However, using these techniques, it is possible to obtain the entire history of the gas fluence versus time, from which the transient diffusion data can be analyzed (Section 4.4)

Recently, a flow-cell test (ASTM F1249 type) has been developed using radioactive (tritiated) water (HTO) as the probe gas (Dunkel 2004). Detection resolution is reported to be 0.1 μCi or 2×10^{-7} g/m^2 per day, approximately three orders of magnitude below existing commercial equipment, and in a range useful for OLED devices. Like the Mocon equipment, this experimental method measures average permeation over a given sample area and yields no information concerning the defect sizes or number densities. In addition, the test must be conducted in a licensed radioactive laboratory.

4.3.2 The Calcium Test

Studies have shown that a primary degradation mechanism for OLEDs is hydrolysis of the moisture-sensitive cathode (Ca or Li) (Aziz *et al.* 1988; Kolosov *et al.* 2001; Liew *et al.* 2000). Based on this information, research began into the use of reactive metals as test probes for water vapor ingress and the subsequent development of the ''calcium test''. The test optically monitors the degradation of thin, vacuum-deposited, calcium layers (< 100 nm thick) onto test substrates. The chemical reaction of water vapor with the thin Ca layer produces a transparent oxide or hydroxide resulting in increased light transmission. Accelerated aging conditions such as 60–85 °C and 85–90% RH are used to increase diffusion rates and reduce analysis time. Details of the test are described extensively by Nisato *et al.* (2001, 2003). The detection limit is approximately 10^{-7} g/m^2 per day at 60 °C and 90% RH, but the test is often limited by ''edge sealing'' effects (Nisato *et al.* 2001; Moro *et al.* 2004). One possible advantage of this test is the ability to visualize coating defect sizes and number densities. This is particularly important in OLED displays, where the existence of large flaws will generate unacceptable dark spots. Other advantages include the ability to provide data concerning diffusion in the plane of the barrier assembly, compatibility with accelerated aging conditions, and the generation of transient WVTR data (see next section). The test has serious limitations when attempting to evaluate fundamental materials properties (such as diffusivity) due to the lack of a constant concentration gradient across the test structure. Even so, the Ca test has widespread adoption in the OLED community largely due to its direct correlation with OLED device lifetime.

Petitioner Samsung Ex-1011, 0091

4.3.3 Defect Characterization

As barrier designs advance from single- to multilayer, and from opaque to transparent materials, the need to characterize defects size and spatial density has become increasingly important. With opaque, metallized films it is possible to make direct observations of defects using transmission optical microscopy. This technique was used to measure defect size and spatial density in aluminized polyester films (Jamieson and Windle 1983; Chatham 1996). For transparent barrier layers, da Silva Sobrinho *et al.* (2000) used a reactive oxygen plasma to etch cavities in the underlying polymer through defects existing in the inorganic layer. This provided sufficient contrast to allow characterization using optical microscopy. As film quality continues to improve, direct observation of defects has become increasingly challenging. Roberts *et al.* (2002) and Erlat *et al.* (1999, 2004) reported measurements on nanometer-sized film defects using transmission electron microscopy (TEM) and atomic force microscopy (AFM), though data collection and interpretation are tedious and complicated. Defect size or spatial separation sometimes makes direct observation virtually impossible. This is particularly true for multilayered systems, where the more impervious oxide layers are buried and thus not accessible to optical or electron probes. One configuration of the calcium test, in which the thin film barrier is deposited *directly upon* the calcium layer, may be useful in identifying (quantifying) defects since the areas of vapor diffusion appear as bright spots in the semi-opaque film (Figure 4.2), though this approach would only image the layer immediately adjacent to the Ca. To date, there are no reports of direct defect characterization using the Ca test.

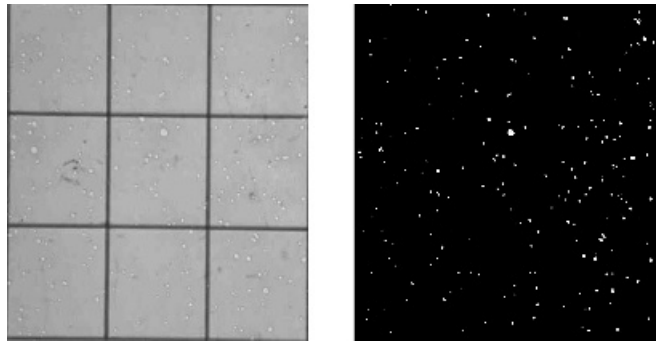


Figure 4.2 Optical micrograph (left) of Ca deposited on a five-dyad PET/barrier substrate after 1632 h of atmospheric exposure. Image analysis (right) of optical view after converting grayscale to pure black and white. White regions are reacted Ca. Total image area = 2.25 mm^2

4.4 Theories of Vapor Barrier Permeation

The previous sections summarized the evolution of barrier structures, and measurement techniques for permeation, defect sizes, and defect densities. In this section we introduce the use of theoretical models to describe gas permeation in thin film barrier structures. The existence of multiple gas transport mechanisms and defect size regimes makes identification

Petitioner Samsung Ex-1011, 0092

of permeation-controlling phenomena extremely challenging using purely empirical approaches. The measured experimental ''signals'' are actually the convolution of several phenomena. Some theory and modeling is useful to provide a means to deconvolute these signals, and thus identify controlling mechanisms. This section offers a brief perspective on the development of several thin film barrier models, evolving from simpler analyses limited to steady-state conditions for single barrier layers, to the transient analyses useful for understanding multilayered systems.

Simple one-dimensional, series resistance models (ideal laminate theory) were first used to describe enhanced barrier performance observed by deposition of inorganic thin films onto polymeric substrates (Decker and Henry 2002; Roberts *et al.* 2002). The permeability (P) through the multilayer structure is modeled as resistors in series using the diffusivity (D) and solubility (S) of the respective *bulk* materials ($P = DS$), and the total permeability of the laminate is calculated by

$$1/P_{\mathrm{T}} = 1/P_1 + 1/P_2 + \cdots + 1/P_n$$

where P_{T} is the total permeability through the structure and P_1, $P_2, \ldots P_n$ are the permeability rates through the respective layers. The model predicts permeation rates that are many orders of magnitude below those observed in practice due to the huge discrepancy between the permeation of *bulk* and *thin film* inorganic materials. Chatham (1996) also showed that permeation in thin film barrier structures does not follow the thickness dependence predicted by these simple models.

Such deficiencies led to the development of ''surface coverage'' and ''pinhole/defect models'' more consistent with experimental observations (Prins and Hermans 1959; Jamieson and Windle 1983; Rossi and Nulman 1993; Decker and Henry 2002). These models assume that diffusion through defects in the inorganic thin film dominates the steady-state permeability, and good correlations between permeation and defect size/spatial density have been measured (da Silva Sobrinho *et al.* 2000) using single-layer systems.

For alternating organic/inorganic layers (called dyads), another theory (polymer interlayer theory) proposes that vapor transmission through the stack is dominated by in-plane diffusion through the polymer layers, between widely spaced defects in the oxide layers (Hanika *et al.* 2002, 2003; Schaepkens *et al.* 2004). As the thickness of the polymeric layer is reduced, particularly below the defect radius, the conductance of the diffusing gas species becomes severely limited. In practice the polymeric interlayers are capable of covering asperities or debris commensurate with the film thickness, helping to eliminate nanometer- and submicron-sized surface asperities and particulate that can create discontinuities in the thin (< 50 nm) inorganic layers. By further thinning the polymer layers, the potential ''conductance–limiting'' benefits might be overwhelmed by the negative consequences of exposed debris and asperities (Graff *et al.* 2004).

4.5 Deconvolution of Experimental Data

This section describes the mathematical models employed to deconvolute experimental data for single and multilayered barrier systems in order to identify the controlling mechanisms for gas diffusion. In particular, a method is developed for extracting the diffusivity (D) and

Petitioner Samsung Ex-1011, 0093

solubility (S) of individual layers in a multilayer barrier stack. These measured materials properties can then be inserted into well-established Fickian models for steady-state and transient permeation.

4.5.1 Transient and Steady-State Permeation Models

To model permeation through a single layer of thickness l, we employed the classical solution (Crank 1975) for the concentration profile of vapor as a function of distance and time; $C(x,t)$. We assume that the vapor is saturated in the carrier gas at a fixed concentration of C_1 on the ''upstream'' side of the layer and maintained at zero on the downstream side by a sweep gas, i.e. an infinite source and sink, respectively. A noncondensable gas is also assumed. Fick's second law then gives the well-known solution

$$C(x,t) = C_1\left(1 - \frac{x}{l}\right) - \frac{2C_1}{\pi}\sum_{n=1}^{\infty}\frac{1}{n}\sin\left(\frac{n\pi x}{l}\right)\exp\left(-\frac{Dn^2\pi^2 t}{l^2}\right), \tag{4.1}$$

where D is the diffusivity of the vapor in the layer. The flux, F, is obtained by differentiation with respect to distance in accordance with Fick's first law. The flux at the downstream surface $(x = l)$ can then be integrated over time to give the total mass transmitted (the fluence, Q) through the layer:

$$Q(t) = \int_{t'=0}^{t} F(x = l, t)\,\mathrm{d}t' = \frac{DtC_1}{l} - \frac{lC_1}{6} - \frac{2lC_1}{\pi^2}\sum_{n=1}^{\infty}\frac{(-1)^n}{n^2}\exp\left(-\frac{Dn^2\pi^2 t}{l^2}\right). \tag{4.2}$$

As t becomes large, an asymptotic analysis shows that this equation reduces to a linearly increasing fluence (the steady-state regime) offset by a delay, referred to as the lag time:

$$Q(t \to \infty) = \frac{DC_1}{l}\left(t - \frac{l^2}{6D}\right). \tag{4.3}$$

The slope of this line (DC_1/l) is the measured steady-state flux, F_{ss}, and the lag time for a single-layer barrier film is

$$L = l^2/6D. \tag{4.4}$$

A schematic representation of time-dependent diffusion through a single layer of a material is shown in Figure 4.3.

The above result for L can then be used to find the apparent solubility of the single-layer barrier. The permeability P is calculated from the measured steady-state flux F_{ss}, the thickness l and the pressure gradient across the film, ΔP:

$$P = F_{ss}l/\Delta P = DS. \tag{4.5}$$

Petitioner Samsung Ex-1011, 0094

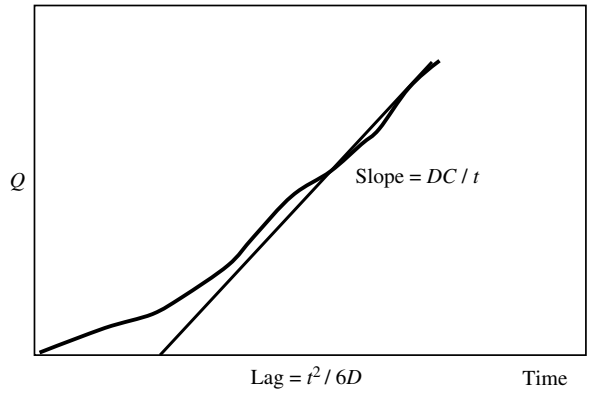


Figure 4.3 Conceptual plot of cumulative permeation data, defining lag time and steady-state regimes for a single-layer system

With D given from the measured lag time L, then S can be found from the flux by

$$S = F_{ss} l / D \, \Delta P. \tag{4.6}$$

For a multilayered system with n layers, a series resistance model (often called the ideal laminate theory) is often used to give the following steady-state flux equation:

$$F_{ss} = \frac{P_{H_2O}}{l_1/D_1S_1 + l_2/D_2S_2 + l_3/D_3S_3 + \cdots + l_n/D_nS_n}, \tag{4.7}$$

where the subscripts $1, 2, \ldots, n$ denote the layer number; 1 is the upstream inlet side and n is the downstream outlet side. P_{H_2O} is the water vapor pressure on the upstream side. In contrast to the case for a single layer, solubility appears in the lag time equation for multilayers:

$$L = \frac{\sum_{i=1}^{n} \left\{ \frac{l_i^2}{2D_i} \sum_{m=1}^{n} \left[\frac{l_m}{D_m} \prod_{j=1}^{m-1} K_j \right] - \frac{l_i^3}{3D_i^2} \prod_{j=1}^{i-1} K_j \right\} + \sum_{i=1}^{n} \left\{ \frac{l_i}{D_i} \prod_{j=1}^{i-1} K_j \sum_{\beta=i+1}^{n} \left[\frac{l_\beta}{\prod_{j=1}^{\beta-1} K_j} \sum_{m=\beta}^{n} \left[\frac{l_m}{D_m} \prod_{j=1}^{m-1} K_j \right] - \frac{l_\beta^2}{2D_\beta} \right] \right\}}{\sum_{i=1}^{n} \left[\frac{l_i}{D_i} \prod_{j=1}^{i-1} K_j \right]}, \tag{4.8}$$

where

$$K_j = S_j / S_{j+1}. \tag{4.9}$$

Equation (4.8) (Ash *et al.* 1965) provides a relatively simple means to analyze transient data. It is useful today because the large aspect ratios (i.e. widths/thicknesses) common in thin

Petitioner Samsung Ex-1011, 0095

film systems are not always amenable to more complex computational tools (such as finite element analyses). This will be demonstrated below when the spatial density of defects in the oxide layers is discussed.

This analysis shows that understanding permeation through multilayer stacks requires knowledge of the solubility and diffusivity of each constituent layer. There are several challenges associated with obtaining this knowledge. First, it is impractical to experimentally measure, in situ, material properties such as the effective D and S for each layer in a multilayer system. This is important because the thin film properties often differ substantially from the ''bulk'' values, particularly with films deposited on low-temperature substrates. Second, the multilayer organic/inorganic barrier structures are known to reduce substrate-induced defects via surface planarization, therefore a simple analysis of single oxide layers deposited on PET may not accurately represent the individual layers existing within a multilayer stack. Thirdly, defects are known to have an important influence on barrier permeation behavior (Chatham 1996; Prins and Hermans 1959; Jamieson and Windle 1983; Rossi and Nulman 1993; da Silva Sobrinho *et al.* 2000; Hanika and Langowski 2003; Roberts *et al.* 2002). However, direct imaging of defects in buried layers to determine their sizes and spatial densities is usually not possible. Analytical methods to deduce the effective properties for the various thin film layers are described below.

4.5.2 Methods to Determine In Situ Properties

In this section we deduce the values of D and S for single barrier layers used in a multilayer stack shown schematically in Figure 4.4. The vapor barrier consists of (in sequence from the upstream side) a PET substrate, an acrylic smoothing layer (denoted P1), a sputtered aluminum oxide (AlO_x) barrier layer and a second acrylic smoothing layer (denoted P2). More barrier plus smoothing layers (i.e. AlO_x/P2 dyads) can be added to reduce permeability, so that the general barrier designation is (PET/P1/AlO_x/P2/AlO_x/P2/AlO_x/...). Structures containing two or more dyads are difficult to measure on standard permeation

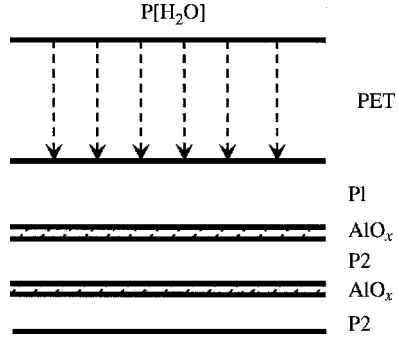


Figure 4.4 Schematic of the multilayer structure used in this study. The plastic substrate is polyester (PET), the P1/P2 layers are vacuum-deposited acrylic polymers, and the AlO_x is sputtered aluminum oxide

Petitioner Samsung Ex-1011, 0096

equipment due to their low permeability. The (PET/P1/AlO_x/P2) layer thicknesses (μm) used in this study were (177.7/0.34/0.037/0.20).

Sample preparation was accomplished using a custom-built roll coater described in the literature (Affinito *et al.* 1996b 1996a, 1995). To measure permeation, samples were analyzed according to ASTM F1249 on a Mocon 3/31G instrument (Mocon Testing Services, Minneapolis, MN). For films with permeability below the resolution limit of such tests we used results from the nonequilibrium Ca test as described in the literature (Nisato *et al.* 2001, 2003; Moro *et al.* 2004).

Given that D and S for the PET substrate were known from handbooks (Brandrup and Immergut 1989), the first test configuration (PET/P1) was designed to evaluate the diffusivity and solubility of the P1 and P2 polymer smoothing layers. After thorough drying, water vapor permeability experiments were conducted at 100% relative humidity and 38 °C. Typical data are shown in Figure 4.5. Analyses employing both the single-layer and multilayer equations given above showed that the diffusivity and solubility of the P1 and P2 layers were in good agreement with the handbook values for PET: $D_P = 8.5 \times 10^{-9}$ cm^2/s and $S_P = 0.17$ g/cm^3/atm. This is reasonable because the thicknesses (and volumes) of the P1 and P2 layers were very small relative to the PET substrate.

The four-layer system (PET/P1/AlO_x/P2) is the simplest structure in which $D(AlO_x)$ and $S(AlO_x)$ are likely to be representative of the oxide barrier layers used in an ultra-low permeation structure. The P1 ''smoothing'' layer decouples the inorganic layer from surface roughness or debris while the P2 overcoat layer protects the delicate oxide layer from damage. Representative data for water vapor permeation are shown in Figure 4.6. Here we need to use Equations (4.7) and (4.8) to determine D and S values for the layers.

Several series of calculations were executed before a solution was found. The first employed ''bulk'' values of D and S for the alumina layer ($D = 10^{-30}$ cm^2/s) (Burger and Morgan 1980), for which no solution could be found that remotely agreed with the data for both the lag time (L) and the steady-state flux (F_{ss}). The second series of calculations

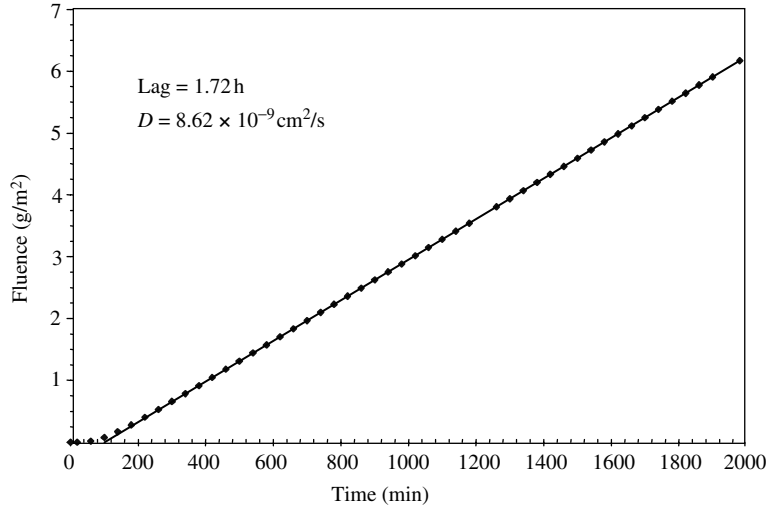


Figure 4.5 Representative data from the (PET/P1) water vapor permeation experiments

Petitioner Samsung Ex-1011, 0097

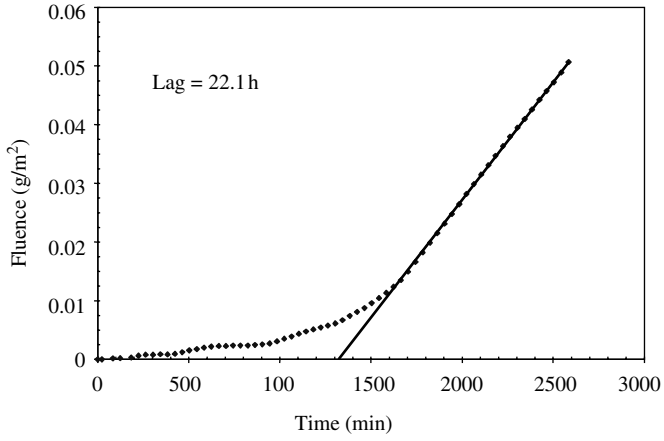


Figure 4.6 Representative data from the four-layer system (PET/P1/AlO_x/P2) water vapor permeation experiments showing a lag time of approximately 22 h

allowed D and S for the alumina layer to vary as needed to match the measured L and F_{ss}. A nonlinear root solver was employed in these simulations. Although solutions could be found that matched either L or F_{ss}, there were no reasonable solutions that matched both simultaneously.

The third series of calculations explored the only remaining parameter that could realistically vary in the multilayer stack–the length of the diffusion path. It was postulated that the diffusion path was not limited, nor even dominated, by diffusion normal to the plane of the barrier layers (i.e. in the z direction alone, as in the ideal laminate theory). A simple sketch revealed that a realistic diffusion path was in the plane of the barrier, through the P1 and/or P2 polymer interlayers, between the defects in successive oxide layers. Even for a single oxide layer, this path appeared reasonable by analogy to the flow paths water must take as it drains through widely spaced pinholes in the bottom of a bucket. This is shown schematically in Figure 4.7.

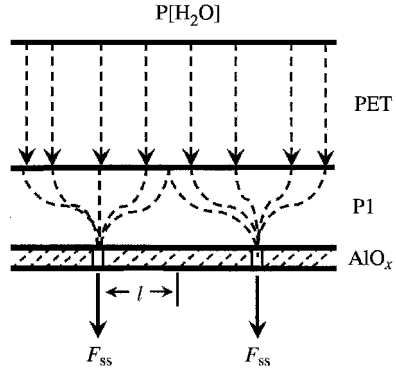


Figure 4.7 Flow paths for water vapor through defects in AlO_x coating when the defects are small and spaced far apart

Petitioner Samsung Ex-1011, 0098

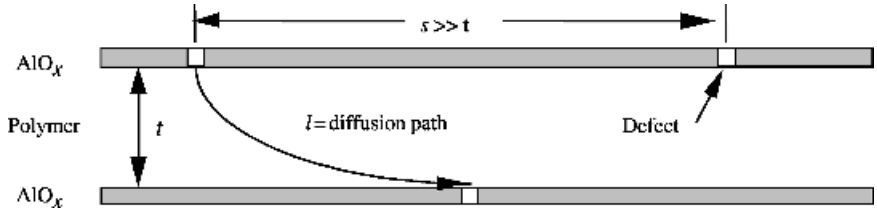


Figure 4.8 The multilayer geometry provides a long effective diffusion path when the defects in adjacent AlO_x layers are widely spaced. For large defect spacings and thin polymer layers the diffusion path (l_{eff}) is approximately one-half the defect spacing

The same concept for multiple alumina layers is shown in Figure 4.8. Allowing the diffusion path l(P1) to vary along with D and S for the alumina gave a series of solutions (i.e. D, S, and l_{eff} triplets) that simultaneously matched the data for both L and F_{ss}. For example, $D(AlO_x) = 1.4 \times 10^{-13}\,cm^2/s$ and $S(AlO_x) = 0.02\,g/cm^3/atm$ for an effective polymer layer thickness (diffusion path length), l_{eff}, of 100 μm (Graff *et al.* 2004). The *effective* diffusivity of the alumina layer required to satisfy the experimental measurements was orders of magnitude larger than the bulk value ($\sim 10^{-30}\,cm^2/s$). This is further evidence that the thin film alumina layer contained defects that increased permeation.

Some of the above solutions gave defect spatial densities (i.e. the inverse square of the defect spacing) that were in good agreement with data from the literature, indicating that those solutions were physically reasonable. This value was verified by relating the effective diffusivity of the alumina layer derived above ($D(AlO_x) = 1.4 \times 10^{-13}\,cm^2/s$) with that predicted by theory for a defected alumina layer. There are three components to this theory of effective diffusivity: a classical (Crank 1975) effective medium approximation of the diffusivity of the alumina layer, the assumption that the diffusivity of polymer interlayers is isotropic (da Silva Sobrinho *et al.* 2000), and an approximation of the diffusion path length through the polymer interlayers. These are described in the following three paragraphs.

The effective diffusivity (D_{eff}) of defective AlO_x can be estimated using an area fraction model (Crank 1975), assuming that defects of area $A_D = \pi r_e^2$ are filled with polymer where r_e is the effective radius of the defect (described below). With s as the defect spacing (i.e. 1 defect per distance s in the x or y direction on the AlO_x surface), the area fraction of defects is $f_D = A_D/s^2$, and that of the solid (bulk material) $f_b = A_b/s^2$. The effective diffusivity of the defected AlO_x layer is then

$$D_{eff}(AlO_x) = D_{P1} f_D + D_{AlO_x} f_b, \tag{4.10}$$

where $D_{P1} = 8.5 \times 10^{-9}\,cm^2/s$ and $D_{AlO_x} = 10^{-30}\,cm^2/s$. Since essentially all the vapor flows through the defects, the diffusivity contribution of the "bulk" alumina is negligible. Increasing D_{AlO_x} by ten orders of magnitude (to $D_{AlO_x} = 10^{-20}\,cm^2/s$) produced nearly identical values for the resulting effective diffusivity (D_{eff}).

After diffusing through defects in the alumina layer, the vapor diffuses through the polymer interlayers. With wide spacing between defects in the oxide layers, the primary diffusion path through the polymer interlayers is in the plane of the barrier assembly, rather

Petitioner Samsung Ex-1011, 0099

than normal to the plane as usually assumed for the ideal laminate theory. For this reason, the model must account for spreading of the defect size due to isotropic diffusion in the polymer layers. da Silva Sobrihno *et al.* (2000) showed that the defect exhibits an effective radius given by

$$r_e = (2tr + r^2)^{1/2}, \tag{4.11}$$

where r is the defect physical radius and t is the physical thickness of the polymer layer into which the gas diffuses. For a defect of $0.5\,\mu m$ physical radius and a polymer thickness of $0.34\,\mu m$, the effective defect radius is $\sim 0.77\,\mu m$ due to the three-dimensional nature of the diffusion. Although included for completeness in the present model, the differences between r and r_e are probably within measurement uncertainties for today's experimental methods.

The large defect spacings suggest that the length of the effective diffusion path can be adequately approximated by a simple Pythagorean argument. For a polymer physical thickness t and defect spacing s, when $t << s$ the effective diffusion path length is approximately

$$l(\mathrm{P1}) = [t^2 + (s/2)^2]^{1/2} \sim s/2, \tag{4.12}$$

as shown schematically in Figure 4.8.

An alumina diffusivity model was constructed from the above three approximations, and used to generate the defect diffusivity map in Figure 4.9. For a defect spacing of $s = 200\,\mu m$ and an effective diffusivity of $1.4 \times 10^{-13}\,cm^2/s$, the defect diameter is approximately $1\,\mu m$. This defect diameter is in reasonable agreement with general observations from a large variety of thin film sources, as shown in Table 4.2. From Figure 4.9 it is also apparent that a verifiable solution is possible since the effective diffusivity defines the curve on which the solution resides. By measuring either defect diameter or defect spatial density and

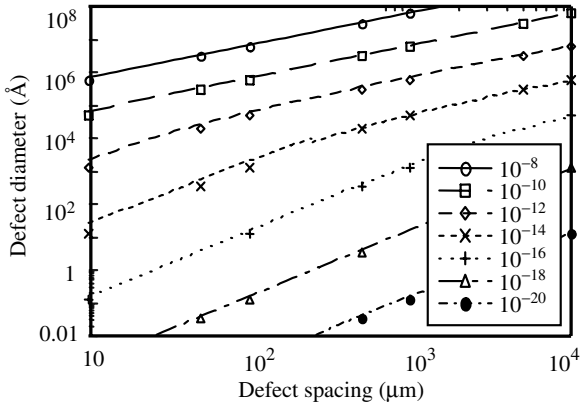


Figure 4.9 Graph showing the relationship between defect size and spacing for different values of effective diffusivity in the AlO_x layer. The calculations are based on a simple area fraction model described in the text

Petitioner Samsung Ex-1011, 0100

Table 4.2 Measured defect size and spatial densities for a number of vacuum-deposited, single-layer inorganic films deposited on polymeric substrates

Defect radius (μm)	Defect density (mm^{-2})	Coating material	Deposition method	Substrate	Reference
0.6	11–1100	SiO_2	PECVD	PET	da Silva Sobrinho *et al.* (2000)
0.6	5–1000	Si_3N_4	PECVD	PET	da Silva Sobrinho *et al.* (2000)
1.0	25–400	Al	Evaporation	PET	Jamieson and Windle (1983)
1.0	100–300	Al	Evaporation	PET	Chatham (1996)
2–3	200	Al	Sputtering	PET	Hanika *et al.* (2002)
0.5–1.4	600	AlO_xN_y	Sputtering	PET	Erlat *et al.* (2001)
0.4	100–1000	Al	Evaporation	BOPP	Hanika Langowski (2003)
0.5	700	AlO_xN_y	Sputtering	PET	Erlat *et al.* (2004)

extrapolating to the appropriate D_{eff} curve, the other defect parameter can be used for verification of the results, thus closing the analytical loop.

There are several features of this analysis worth noting. First, the model has a sound theoretical foundation since all equations originated from classical, well-established literature. Second, the analysis has closed the analytical loop by allowing experimental verification of the derived defect diameters and/or spatial densities. Third, the model is capable of providing unique answers, because the number of equations (three, one each for L, F_{ss}, and D_{eff}) equals the number of unknowns (D_{eff}, S, and l_{eff}). We anticipate that this general method will be useful to the industry for designing multilayer thin film barrier systems.

4.5.3 Implications for Multilayer Barrier Systems

In previous work (Graff *et al.* 2004), we have shown that a multilayer series resistance model predicts minimal improvement in the steady state WVTR (F_{ss}) of a multi-dyad stack when the above derived transport parameters are used (i.e. $D_{\text{PET}} = D_{\text{P1}} = D_{\text{P2}} = 8.5 \times 10^{-9}\,\text{cm}^2/\text{s}$, $S_{\text{PET}} = S_{\text{P1}} = S_{\text{P2}} = 0.17\,\text{g/cm}^3/\text{atm}$, $D_{\text{AlO}_x} = 1.4 \times 10^{-13}\,\text{cm}^2/\text{s}$, $S_{\text{AlO}_x} = 0.02\text{g/cm}^3/\text{atm}$, $p_{\text{H}_2\text{O}} = 0.0666\,\text{atm}$ at 38 °C, the physical thicknesses 177 and 0.037 μm for the PET and AlO_x, and an effective thickness of 100 μm for the polymer interlayers). Figure 4.10 shows the F_{ss} obtained for a five-dyad structure ($\sim 10^{-2}\,\text{g/m}^2$ per day) is orders of magnitude above that required for successful OLED encapsulation ($\sim 10^{-6}\,\text{g/m}^2$ per day). The steady-state flux calculation does not accurately predict the demonstrated performance of multilayered vapor barrier films, even when corrected to accommodate the defected oxide layers.

However, the results of the lag time computations, using the same parameters mentioned above, are of particular note (Figure 4.10). As the defect spacing increases from 100 to 1000 μm, the lag time for a five-dyad barrier increases from ~73 days to approximately 2 years. In essence, the multilayer defect spacing model described in this chapter predicts success simply by *delaying* the ingress of water vapor to the OLED, rather than by *preventing* it. During this time delay, the vapor flux is transient, and is much smaller in magnitude than the ultimate steady-state value. This can be seen by comparing the slopes of the data curves in the transient and steady-state regions (Figure 4.6).

Petitioner Samsung Ex-1011, 0101

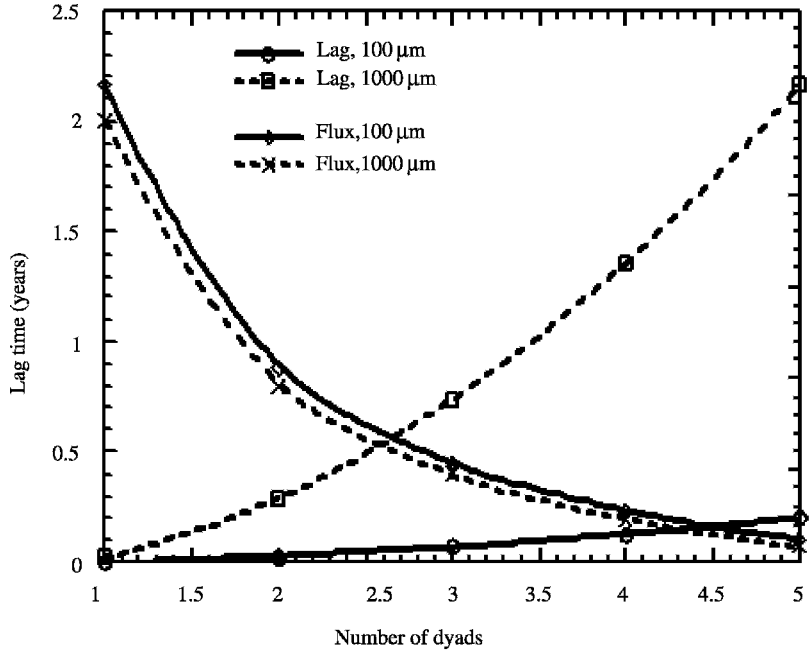


Figure 4.10 Comparison of relative sensitivity of lag time versus steady-state flux given an order of magnitude change in defect spacing

4.6 Discussion

The previous sections showed that more advanced analytical methods were needed to understand the controlling mechanisms of modern vapor barriers. This need was generated by the natural evolution of barrier designs and materials as performance requirements became more demanding. Along with the primary performance requirement for WVTR $< 10^{-6}\,\mathrm{g/m^2}$ per day came the need for good reliability through a robust design. These factors led to multilayer designs that decouple defects between successive barrier layers. This decoupling is possible due to the small defect size and low spatial density inherent in ''ultra high quality'' barrier layers. The multilayer approach enables attainment of unprecedented barrier performance using inorganic ''barrier'' layers that are manufacturable without seeking the single, perfect, defect-free layer. Successful OLED encapsulation using a single inorganic layer requires $D_{\mathrm{eff}} < 10^{-18}\,\mathrm{cm^2/s}$. This equates to a defect size of $\sim$10 nm with $\sim 10^7$ nm (10 mm) spacings, and is extremely challenging to attain for any low-temperature, vacuum-deposited thin film.

The model presented above was developed to deconvolute the experimental data in an effort to identify the controlling mechanism (delayed vapor breakthrough due to a long effective diffusion path length, rather than low vapor transmission rate). In the process, it was also necessary to derive effective transport properties for the various layers. Both of these objectives were met for the simplest multilayer structure (PET/P1/AlO_x/P2). In addition, the solution was shown to be unique (within measurement uncertainties) by

Petitioner Samsung Ex-1011, 0102

comparison of predicted defect sizes and spatial densities to available databases. These uncertainties must be reduced in future work, and improved experimental methods are needed for this purpose.

We also recognize that additional mechanisms may be operative during the transport of water vapor across the barrier stack, particularly in extremely small defects ($< 10\,\text{nm}$). These mechanisms include adsorption, dissociation, and recombination of water molecules on the oxide surfaces or in the polymer free volume. Although recent literature (Roberts *et al.* 2002; Erlat *et al.* 2004) has begun to address the differences between oxygen and water transport through barrier systems, we suggest that the present theory will remain self-consistent with further analyses. The Fickian formalism employed herein implicitly includes all transport mechanisms. In addition, the handbook values of D and S used to benchmark the values derived herein, were also derived based on the same implicit Fickian assumptions. The engineering foundations of the present model thus appear sound. The outcome of such additional analyses would probably fall into the category of materials science or physical chemistry, and could be of significant value for designing new *materials* for multilayer barrier systems, rather than new *structures*.

To be conservative, the properties determined using a simple PET/P1/AlO_x/P2 structure were extended to model n-dyad systems. Experience suggests that the continued planarization afforded by the addition of polymer/AlO_x dyads can lead to successively improved oxide interlayers (lower D_{eff}). In April, 2004 we have neither the mathematical nor experimental techniques to detect such an occurrence. Further work is needed to develop such techniques so that the barrier stack can be optimized with respect to its performance and its manufacturing economics. Such work is in progress. An important aspect of this work will address the variability of barrier samples produced by different methods and at several locations, in an attempt to lower the associated scatter in the data.

4.7 Conclusions

A classical Fickian analysis of permeation data has been developed to determine the diffusivity and solubility of individual thin film layers in a multilayer structure. These materials properties can then be used to predict the transient and steady-state permeation characteristics of multilayer barrier films. The analysis shows that the unprecedented barrier performance of multilayer structures is, primarily due to lag time effects (i.e. the delay in vapor breakthrough due to a long effective diffusion path) rather than low steady-state permeability. The models further indicate that the steady-state permeation rate should be substantially higher than the reported WVTR calculated during the transient period.

The deposition of high-quality, inorganic thin films (low defect size and large defect spacings), combined with a multilayer structure, is necessary to attain superior barrier properties. Inorganic thin films with large numbers of defects (high effective diffusivity) will not meet the performance requirements for OLEDS, even if assembled into a multilayer architecture.

To attain steady-state permeation values useful for OLED encapsulation ($< 10^{-6}\,\text{g/m}^2$ per day at 38 °C and 100% RH) requires a near-perfect deposition of a single-layer inorganic film. This analysis indicates that a defect diameter of less than 1 nm and a defect spacing of $\sim$1 mm are required to attain the necessary F_{ss}. Such films are extremely difficult to deposit using PVD or CVD methods, particularly at low temperatures. This could explain why there

Petitioner Samsung Ex-1011, 0103

have been no reports of successful thin film OLED encapsulation using a single vacuum-deposited barrier layer.

Finally, since diffusion through the polymer interlayers is the dominant diffusion pathway, lowering the permeability (lowering D and S) of the polymer will improve the steady state permeability of the multilayer barrier. Possible improvements include graded organic/inorganic interfaces, surface treatments (such as plasma or ion bombardment) or increased crystallinity in the polymer.

Acknowledgements

The authors gratefully acknowledge the contributions of our colleagues M. E. Gross, W. D. Bennett, P. M. Martin, E. S. Mast, M. R. Zumhoff, M. G. Hall, C. C. Bonham and D. W. Matson for years of dedicated effort in the development of ultrabarrier films. We also appreciate the technical support of L. Moro and N. M. Rutherford at Vitex Systems Incorporated. Partial funding for this work was provided by Vitex Systems Inc., and PNNL's Nanoscience and Technology LDRD Initiative. Pacific Northwest National Laboratory is operated by Battelle for the US Department of Energy under contract DE-AC06-76RLO 1830.

References

Affinito, J. D., Martin, P., Gross, M., Coronado, C. and Greenwell, E. (1995) Vacuum deposited polymer/metal multilayer films for optical applications. *Thin Solid Films* **270**, 43.

Affinito, J. D., Gross, M. E., Coronado, C. A., Dunham, G. C. and Martin, P. M. (1996a) High rate vacuum deposition of polymer electrolytes. *Journal of Vacuum Science Technology A* **14**(3), 733.

Affinito, J. D., Gross, M. E., Coronado, C. A., Graff, G. L., Greenwell, E. N. and Martin, P. M. (1996b) A new method for fabricating transparent barrier layers. *Thin Solid Films* **290/91**, 63–67.

Affinito, J. D., Eufinger, S., Gross, M. E., Graff, G. L. and Martin, P. M. (1997) PML/oxide/PML barrier layer performance differences arising from use of UV or electron beam polymerization of the PML layers. *Thin Solid Films* **308/9**, 19–25.

Anon (1996) *Permeability and other Film Properties*, Plastics Design Library, Norwich, NY.

Ash, R., Barrer, R. M. and Palmer, D. G. (1965) Diffusion in multiple laminates. *British Journal of Applied Physics* **16**, 873–884.

Aziz, H., Popovic, Z., Tripp, C. P., Hu, N. -H., Hor, A.-M. and Gu, X. (1988) Degradation processes at the cathode/organic interface in organic light emitting devices with Mg:Ag cathodes. *Applied Physics Letters* **72**(21), 2642.

Baxter, I. (1993) Advanced resistance deposition technology for productive roll coating. *36th Annual Technical Conference Proceedings, Society of Vacuum Coaters*, 197.

Brandrup, J. and Immergut, E. H. (1989) *Polymer Handbook*, 3rd edn, John Wiley & Sons, Inc., New York.

Burger, L. L. and Morgan, L. G. (1980) *Tritium Safety in Fusion Reactor Designs,* PNNL Report, June.

Burrows, P. E., Bulovic, V., Forrest, S. R., Sapochak, L. S., McCarty, D. M. and Thompson, M. E. (1994) Reliability and degradation of organic light emitting devices. *Applied Physics Letters* **65**(23), 2922.

Chatham, H. (1996) Oxygen diffusion barrier properties of transparent oxide coatings on polymeric substrates. *Surfaces and Coatings Technology* **78**, 1.

Crank, J. (1975) *The Mathematics of Diffusion*, Claredon Press, Oxford.

Petitioner Samsung Ex-1011, 0104

da Silva Sobrinho, A. S., Czeremuszkin, G., Latreche, M. and Wertheimer, M. R. (2000) Defect-permeation correlation for ultrathin transparent barrier coatings on polymers. *Journal of Vacuum Science Technology A* **18**(1), 149.

Decker, W. and Henry, B. (2002) Basic principles of thin film barrier coatings. *45th Annual Technical Conference Proceedings, Society of Vacuum Coaters*, 492–502.

Dunkel, R. (2004) Method of measuring ultra-low water vapor permeation for OLED displays. *Flexible Displays and Microelectronics Conference*, February, 10–12.

Erlat, A. G., Wang, B. -C., Spontak, R. J., Tropsha, Y., Mar, K. D., Montgomery, D. B. and Vogler, E. A. (2000) Morphology and gas barrier properties of thin SiO_x coatings on polycarbonate: correlations with plasma-enhanced chemical vapor deposition conditions. *Journal of Materials Research* **15**(3), 704.

Erlat, A. G., Spontak, R. J., Clarke, R. P., Robinson, T. C., Haaland, P. D., Tropsha, Y., Harvey, N. G. and Vogler, E. A. (1999) SiO_x gas barrier coatings on polymer substrates: morphology and gas transport considerations. *Journal of Physical Chemistry B* **103**, 6047.

Erlat, A. G., Henry, B. M., Ingram, J. J., Mountain, D. B., McGuigan, A., Howson, R. P., Grovenor, C. R. M., Briggs, G. A. D. and Tsukahara, Y. (2001) Characterisation of aluminium oxynitride gas barrier films. *Thin Solid Films* **388**, 78.

Erlat, A. G., Henry, B. M., Grovenor, C. R. M., Briggs, A. G. D., Chater R. J. and Tsukahara, Y. (2004) Mechanism of water vapor transport through PET/AlO_xN_y gas barrier films. *Journal of Physical Chemistry B* **108**, 883–890.

Graff, G. L., Williford, R. E. and Burrows, P. E. (2004) Mechanisms of vapor permeation through multilayer barrier films: lag time versus equilibrium permeation. *Journal of Applied Physics*, **96**(4), 1840.

Gu, G., Burrows, P. E., Venkatesh, S. and Forrest, S. R. (1997) Vacuum-deposited, nonpolymeric flexible organic light-emitting devices. *Optics Letters* **22**(3), 172.

Gustaffson, G., Treacy, G. M., Cao, Y., Klavetter, F., Colaneri, N. and Heeger, A. J. (1992) Flexible light-emitting diodes made from soluble conducting polymers. *Nature* **357**, 477.

Hanika, H., Langowski, H.-C., and Peukert, W. (2003) Simulation and verification of defect-dominated permeation mechanisms in multiple structures of inorganic and polymeric barrier layers. *46th Annual Technical Conference Proceedings*, *Society of Vacuum Coaters*, 592–599.

Hanika, H., Langowski, H.-C. and Moosheimer, U. (2002) Layer defects and the synergetic effect between inorganic and organic barrier layers. *45th Annual Technical Conference Proceedings*, *Society of Vacuum Coaters,* 519–24.

Harvey, T. B. III, Shi, S. Q. and So, F. (1997) Passivation of organic devices, US Patent 5,686,360.

Harvey, T. B. III, Shi, S. Q. and So, F. (1998) Passivated organic device having alternating layers of polymer and dielectric, US Patent 5,757,126.

Henry, B. M., Erlat, A. G., McGuigan, A., Grovenor, C. R. M., Briggs, G. A. D., Tsukahara, Y., Miyamoto, T., Noguchi, N. and Niijima, T. (2001) Characterization of transparent aluminium oxide and indium tin oxide layers on polymer substrates. *Thin Solid Films* **382**, 194.

Jamieson, E. H. H. and Windle, A. H. (1983) Structure and oxygen-barrier properties of metallized polymer film. *Journal of Materials Science* **18**, 64.

Kolosov, D., English, D. S., Bulovic, V., Barbara, P. F., Forrest, S. R. and Thompson, M. E. (2001) Direct observation of structural changes in organic light emitting devices during degradation. *Journal of Applied Physics* **90**(7), 3242.

Krug, T., Ludwig, R. and Steiniger, G. (1993) New developments in transparent barrier coatings. *36th Annual Technical Conference Proceedings*, *Society of Vacuum Coaters,* 302.

Liew, Y. -F., Aziz, H., Hu, N. -X., Chan, H. S., Xu, G. and Popovic, Z. (2000) Investigation of the sites of dark spots in organic light-emitting devices. *Applied Physics Letters* **77** (17), 2650.

Moro, L., Krajewski, T. A., Rutherford, N. M., Philips, O., Visser, R. J., Gross, M. E., Bennett, W. D. and Graff, G. L. (2004) Process and design of a multilayer thin film encapsulation of passive matrix OLED displays. *Proceedings of SPIE* **5214**, 83–93.

Petitioner Samsung Ex-1011, 0105

Nisato, G., Bouten, P. C. P., Slikkerveer, P. J., Bennett, W. D., Graff, G. L., Rutherford, N. and Wiese, L. (2001) Evaluating high performance diffusion barriers: the calcium test. *21st Annual Asia Display, 8th International Display Workshop, Nagoya, Japan*, 1435.

Nisato, G., Kuilder, M., Bouten, P., Moro, L., Philips, O. and Rutherford, N. (2003) Thin film encapsulation for OLEDs: evaluation of multi-layer barriers using the Ca test. *Society for Information Display, 2003 International Symposium, Digest of Technical Papers*, **XXXIV**, 88.

Prins, W. and Hermans, J. J. (1959) Theory of permeation through metal coated polymer films. *Journal of Physical Chemistry* **63**, 716.

Roberts, A. P., Henry, B. M., Sutton, A. P., Grovenor, C. R. M., Briggs, G. A. D., Miyamoto, T., Kano, M., Tsukahara, Y. and Yanaka, M. (2002) Gas permeation in silicon-oxide/polymer (SiO_x/PET) barrier films: role of the oxide lattice, nano-defects and macro-defects. *Journal of Membrane Science* **208**, 75–88.

Rogers, S. P., So, F., Shi, S. Q. and Webb, B. A. (1998) Organic electroluminescent device hermetic encapsulation package, US Patent 5,821,692.

Rossi, G. and Nulman, M. (1993) Effect of local flaws in polymeric permeation reducing barriers. *Journal of Applied Physics* **74**, 5471.

Schaepkens, M., Erlat, A. G., Kim, T. W., Jan, M., Heller, C. M. and McConnelee, P. (2004) Ultra-high barrier coatings on polymer substrates for flexible optoelectronics: water vapor transport and measurement systems. *47th Annual Technical Conference Proceeding, Society of Vacuum Coaters*, 654.

Schiller, N., Straach, S., Fahland, M. and Charton, C. (2001) Barrier coatings on plastic web. *44th Annual Technical Conference Proceedings*, *Society of Vacuum Coaters*, 184.

Schwarz Packaging Systems (2003) Film barrier chart, www.schwarzflex.com/film.htm

Shaw, D. G. and Langlois, M. G. (1994) Use of vapor deposited acrylate coatings to improve the barrier properties of metallized film. *37th Annual Technical Conference Proceedings*, *Society of Vacuum Coaters,* 240.

So, F., Shi, S. Q. and Gorsuch, C. A. (1998) Passivation of electroluminescent organic devices. US Patent 5,731,661.

Watts, I. (1991) 20 years of resistance source development. *34th Annual Technical Conference Proceedings*, *Society of Vacuum Coaters*, 118.

Weaver, M. S., Michalski, L. A., Rajan, K., Rothman, M. A., Silvernail, J. A., Burrows, P. E., Graff, G. L., Gross, M. E., Martin, P. E., Hall, M., Mast, E., Bonham, C., Bennett, W. and Zumhoff, M. (2002) Organic light-emitting devices with extended operating lifetimes on plastic substrates. *Applied Physics Letters* **81**, (16), 2929.

Wong, C. P. (1993) Recent advances in IC passivation and encapsulation: process technologies and materials–polymers for electronic and photonic applications, AT&T Bell Laboratories.

Petitioner Samsung Ex-1011, 0106

5

Transparent Conducting Oxide Materials and Technology

David C. Paine, Hyo-Young Yeom, and Burag Yaglioglu

Division of Engineering, Brown University, Providence RI

5.1 Introduction

Materials that combine optical transparency in the visible spectrum with reasonable electrical conductivity generally fall into three classes: very thin pure metals, highly doped conjugated organic polymers, and degenerately doped wide band gap oxide or nitride semiconductors. The applications of transparent conductors include electrodes for most flat panel display technologies, collector electrodes in solar cells, deicing electrodes on airplane cockpit windows, static dissipation, and electromagnetic shielding. A review of the considerations for the selection of transparent electrode materials is presented in Section 5.2. For display applications, indium oxide materials are almost exclusively used due to their superior combination of environmental stability, relatively low electrical resistivity (1 to $3 \times 10^{-4}\,\Omega$ cm) and high transparency ($>90\%$ at a film thickness of 100 nm) to visible light. The focus of Section 5.3, and much of this chapter, is the indium-based transparent conducting oxides (TCOs) that are now available and which can be processed under conditions that are compatible with heat-sensitive flexible polymeric substrates. These include Sn-doped In_2O_3 (ITO) and Zn-stabilized amorphous indium oxide (IZO).

The first transparent conducting oxide was reported in 1907 by Baedeker (Baedeker 1907), who used a primitive vapor deposition system to deposit thin film CdO that was both optically transparent and electrically conducting. Transparent conducting indium oxide

Flexible Flat Panel Displays Edited by G. P. Crawford
© 2005 John Wiley & Sons, Ltd., ISBN 0-470-87048-6

Petitioner Samsung Ex-1011, 0108

doped with tin was developed for window coatings in the mid 1950s and in the subsequent half-century it has become the material of choice for a variety of high-performance applications. There is, however, significant cost-driven pressure to find a replacement that does not rely on the relatively scarce and expensive element indium. In the 30 years or so after ITO first became available, physical vapor deposition (PVD) processing refinements led to an order of magnitude decrease in resistivity. This initially rapid rate of improvement has slowed and the performance of polycrystalline ITO has reached a performance plateau at a resistivity level of about $1 \times 10^{-4}\,\Omega$ cm. Further improvement in resistivity while maintaining transparency over a wide spectral window will probably require the development of new TCO materials. Alternative transparent conducting oxides based on mixed binary and ternary oxides of the d^{10} cations: Cd^{2+}, Zn^{2+}, Ga^{3+}, In^{3+}, and Sn^{4+} are now under development.

The technological advantages of flexible substrates are enumerated elsewhere in this book but they include the large-scale productivity benefits of roll-to-roll web coating. This approach allows low-cost deposition of very large areas of material and the possibility of multiple inline deposition and patterning processes. Roll-to-roll coating of polymeric substrates with multiple inorganic layers has been used for the fabrication of large-area electronics in which, for example, flexible transistors and solar cells (Sheats 2000; Jackson 2003) have been demonstrated. Today, roll-to-roll web coating is used for the deposition of ITO onto PET substrates for touch screen applications. For this application, plastic rolls up to 2 m in width and hundreds of meters in length are coated in a single inline process.

The deposition of these brittle inorganic materials on plastic while achieving the highest possible optical, electrical, and mechanical performance presents a new set of challenges to the thin film deposition and processing community. Current polymeric substrate materials (e.g. PET, PEN, polyimmide, PMMA, polycarbonate) are heat sensitive and lose integrity if heated to 250–350 °C, temperatures typically used in the DC magnetron sputter deposition of polycrystalline ITO having the lowest achievable resistivity. Even at modest substrate temperatures, say 100–150 °C, the dimensional stability of many polymers is poor and may lead to increased film stress and failure by cracking or debonding from the substrate. At low (i.e. unheated) substrate temperatures, ITO is deposited as an amorphous film over a wide range of processing conditions and techniques. The optoelectronic properties of these amorphous materials are usually inferior to those of the crystalline state. Fortunately, amorphous thin films of doped and undoped indium oxide deposited at room temperature have an optical transmissivity and electrical conductivity that is adequate for present display technologies. However, new transparent conductors and processing methods will be required in order to meet the needs of flexible display technologies currently under development. To provide faster display refresh rates, the transparent conducting electrodes on these displays will require lower resistivity while maintaining high optical transmission. These electrodes will also require increased structural, chemical, and electrical stability.

5.2 Materials Selection and Characterization

5.2.1 Transparent Conducting Materials Classes: Why Oxides?

An initial screening of the available transparent conducting materials can be performed using a figure of merit that considers the ratio of the optical transmittance (often cited

Petitioner Samsung Ex-1011, 0109

at 550 nm and scaled by the tenth power) of a material to its sheet resistance (Haacke 1976):

$$\phi = T^{10}/R_s. \tag{5.1}$$

For this purpose, optical transmittance (T) is given by $T = \exp(-\alpha x)$ where α is the visible absorption coefficient and x is the film thickness. Sheet resistance (R_s) is thickness dependent but is related to a fundamental material property, resistivity (ρ), by $R_s = \rho/x$. Combining these relationships yields

$$\phi = (x/\rho)\ \exp(-10\alpha x). \tag{5.2}$$

It is possible to obtain reasonable figures of merit in thin metals, conducting polymers and degenerately doped wide band gap semiconductors. For example, using the above definition, the maximum figure of merit (ϕ) of silver is approximately $0.023\,\Omega^{-1}$. This is found using the absorption coefficient of $\alpha = 10^6\,\text{cm}^{-1}$ (at a wavelength of 550 nm) and resistivity of $1.6 \times 10^{-6}\,\Omega\,\text{cm}$ to arrive at an optimum film thickness of approximately 1 nm. At this optimum thickness, the optical transmittance is 90% and the sheet resistance is 16.3 Ω/sq. At a thickness of 1 nm there are practical difficulties with the fabrication of conformal contiguous films. Furthermore, surface scattering of the free carriers significantly decreases the effective conductivity in these ultra-thin films. In comparison to silver, ITO has a figure of merit (ϕ), that is an order of magnitude higher ($0.22\,\Omega^{-1}$ with $\rho = 1.6 \times 10^{-4}\Omega\,\text{cm}$ and $\alpha = 10^3\,\text{cm}^{-1}$) at a film thickness of 1000 nm. Note that in comparing ITO to Ag thin films, the optimum figure of merit for ITO thin films occurs at a thickness that is three orders of magnitude higher (1 nm vs. 1000 nm) than for Ag films. Furthermore, at their respective optimum thicknesses, both materials have 90% optical transmissivity while ITO has an order of magnitude lower sheet resistance.

Conjugated organic polymers have undergone intense development since the 1990s when the application of these materials in organic light-emitting diodes was first demonstrated. The resistivity of doped electronic polymers such as *trans*-$(CH)_x$ and polyaniline are reported (MacDiarmid 2002) to be as low as 10^{-5} to $10^{-3}\,\Omega\,\text{cm}$ but practical coatings of these materials suffer from low mobilities ($< 1\,\text{cm}^2/\text{V s}$), low carrier density, and poor transparency. In addition, there are engineering challenges associated with the environmental stability of conducting polymers. It is well known, for example, that conjugated polymer conductors suffer from severe environmental instability including sensitivity to oxygen and moisture and, as such, these materials require robust encapsulation. Although conducting polymers would seem to be a natural choice for flexible substrate applications, it appears that there remains much development work ahead before they have the optical and electrical properties combined with reliability demanded by display applications.

In conclusion, the universal choice for electrode applications requiring optical transparency and low sheet resistance are the transparent conducting oxide class of materials. Within this class, indium oxide materials are currently used in the vast majority of high-performance display applications.

5.2.2 Transparent Conducting Oxides: General Considerations

The primary consideration in the selection of a transparent conductor for use with any class of substrate is the ability to deposit material with adequate optical and electrical properties.

Petitioner Samsung Ex-1011, 0110

Polymeric substrates impose an additional set of restrictions. These materials are often heat sensitive and, in many cases, suffer from dimensional and structural instability when exposed to various solvents, heat, or energetic radiation including ultraviolet light. As such, the deposition of transparent conducting oxides onto polymeric substrates requires a process that uses an inert atmosphere, minimal exposure to energetic radiation, and negligible substrate heating. A critical material requirement is that the mechanisms for doping the wide band gap crystalline oxide can be activated at low process temperatures and are operational in the disordered amorphous state.

Resistivity is a fundamental property that varies inversely with the product of the carrier density (n), mobility (μ), and charge (q) on the electron such that

$$\rho = (q\mu n)^{-1}. \tag{5.3}$$

The mobility of the free carriers in a typical material depends inversely on the concentration of charged and neutral scatter centers combined with phonon scattering. An increased impurity concentration, including intentionally added dopants, and the presence of microstructural defects, such as grain boundaries, will decrease the free carrier mobility since impurities and defects act as additional scatter centers. Oxides with a fundamental band gap of 3 eV or more are insulators at room temperature in the undoped state, hence they must be very heavily doped to become conducting. The doping of these materials must increase the free carrier density enough to move the Fermi level into the conduction band. This highly doped condition is known as a degenerately doped state and represents a severe constraint on the potential candidate materials for transparent conductor applications since it requires a readily ionized source of electron donors in the form of point defects or impurities. These donors must have ionization energies close enough to the conduction band to allow room temperature activation. In some oxides, in particular those with d^{10} cations such as indium oxide, zinc oxide, tin oxide, and cadmium oxide, native stoichiometric point defects like oxygen vacancies are readily ionized and thereby donate electrons. Further doping is usually required (e.g. Al in ZnO, Sn in In_2O_3, Sb in SnO_2) and these impurity ions must find their way to substitutional sites in the parent lattice. One of the processing challenges of using heat-sensitive polymeric substrates is the activation of dopants at low temperatures. Degenerate doping implies an extremely high concentration of ionized dopants, which leads to increased electron scattering and a decrease in carrier mobility (μ).

Extrinsic dopants in the form of intentionally added impurities can be either cationic (e.g. in In_2O_3, tetravalent Sn substitutionally on a trivalent In site) or anionic (F substitutionally on an O site in SnO_2). Note that the native stoichiometric point defects like the oxygen vacancies discussed above are not mobile at room temperature, hence ionic conduction does not play a role in the conductivity of TCO materials at room temperature. Furthermore, all current practical transparent conductors are degenerately doped n-type with either intentionally added impurities or native point defects. The recent discovery of p-type TCO materials (Hiramatsu *et al*. 2003; Nagarajan *et al*. 2001; Stauber *et al*. 1999) that utilize electron acceptor states to create carriers has stirred interest in the concept of transparent electronics based on pn junctions. At present, these materials are not sufficiently conducting for practical use as display electrodes.

For a TCO to be of interest for display applications it must transmit freely across the visible spectrum from approximately 0.4 to 1.5 μm. The short-wavelength (UV) cut-off corresponds to the fundamental band gap of the material, while the long-wavelength (IR)

Petitioner Samsung Ex-1011, 0111

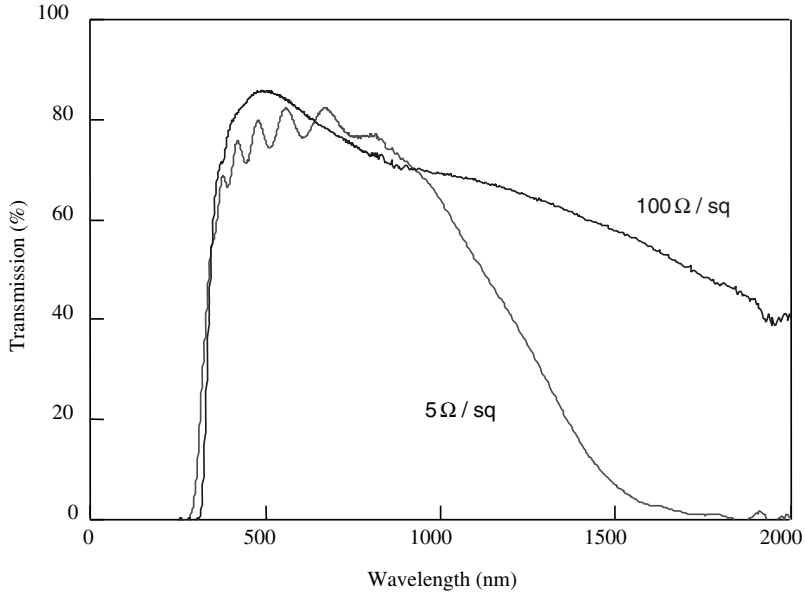


Figure 5.1 Transmission curves for two TCO films of SnO_2 having different sheet resistances. Note the decrease in long-wavelength transmission for the lower-resistivity material. Courtesy of D. Ginley, NREL

edge corresponds to the free carrier plasma resonance frequency. These critical optical properties are directly influenced by the carrier density and mobility in a way that was first described for ITO by Kostlin *et al*. 1975). In general, for a material to be transparent across the visible spectrum its band gap must be greater than 3 eV to allow transmission up to the near-UV (0.4 μm) and its free carrier plasma resonance absorption must be close to, or above, the near-infrared (1.5 μm).

A typical transmission spectrum is presented in Figure 5.1 which shows the transmission window of two films of SnO_2, one with high resistance (100 Ω/sq) the other with low resistance (5 Ω/sq). Between the UV (0.4 μm) and the IR (1.5 μm) wavelengths, the material shows the high transmissivity typical of a dielectric material with only interference effects modifying the transmitted intensity within the spectral window. In Figure 5.1, note the shift to shorter wavelengths at the IR end of the spectrum for the lower-resistivity sample. This shows that an increase in free carrier density decreases the resistivity of the material but also shifts the IR absorption edge to shorter wavelengths, thus narrowing the transmission window. This shift at the IR end of the spectrum is determined by the plasma oscillation of the free carriers that screen the incident electromagnetic wave via intraband transitions within the conduction band. Kostlin *et al*. (1975) points out that the characteristic frequency (ω_p) for IR reflection in ITO is well predicted by the Drude model. The origin of the transmission drop at the IR end of the spectrum is seen from the frequency-dependent dielectric function:

$$\epsilon(\omega) = \epsilon_\infty \left(1 - \frac{\omega_p^2}{\omega^2 + i\omega/\tau}\right), \tag{5.4}$$

Petitioner Samsung Ex-1011, 0112

where τ is the relaxation time associated with the scattering mechanism and ω_p is the plasma resonance frequency. Note that the optical transmission drops sharply near the plasma resonance frequency. The plasma resonance frequency depends on the carrier density (N) and inversely on the effective mass (m^*) of the free carriers and is given by

$$\omega_p^2 = \frac{Ne^2}{\epsilon_0 \epsilon_\infty m^*}. \tag{5.5}$$

Note that any effort to increase the carrier density to reduce resistivity will have the effect of shifting the plasma edge to shorter wavelengths.

The position of the UV edge is also dependent, in part, on the free carrier density in the material. Consider that the UV absorption edge is a result of the band-to-band transfer of electrons across the band gap. In degenerate materials, the Fermi level lies in the conduction band and Fermi statistics indicate that the bottom of this band is effectively filled with carriers. Consequently, the optical band gap (and UV edge) shifts to higher energy (shorter wavelength) with increasing carrier density since absorption by band-to-band transitions requires an electron transition from the top of the valence band to an unoccupied state in the conduction band. This carrier-density-dependant shift is known as the Burnstein–Moss effect (Kostlin *et al*. 1975) and straightforward analysis of the density of states in the conduction band reveals that the UV edge will shift to shorter wavelengths with increasing carrier density (n) since the change in the optical band gap energy (ΔE) increases with carrier density as $\Delta E \sim n^{3/2}$.

The optical performance and electrical performance of TCOs are intimately tied to the fundamental band structure of the material. The band structure, in turn, depends on the periodic distribution of potential in the crystal. This would, at first glance, suggest that amorphous materials where the long-range periodicity of the crystalline structure has been disrupted would yield materials with dramatically different optical and electrical properties. For indium oxide, this proves not to be the case. Both the crystalline and amorphous states of indium oxide are discussed below since both yield useable TCO materials.

5.3 Indium-Based Binary Oxides

5.3.1 Background

The TCOs most widely used in active matrix display applications are crystalline indium tin oxide (c-ITO), amorphous indium tin oxide (a-ITO), and amorphous indium zinc oxide (a-IZO). The amorphous indium oxides (either ITO or IZO) are typically formed by deposition from a ceramic target onto unheated substrates. Although various physical vapor deposition (PVD) methods have been used for the deposition of indium oxide, the most common method is DC magnetron sputter deposition and its variations. This technique is preferred over RF sputtering since, for conducting targets that can dissipate charge, it offers much higher deposition rates.

The microstructure of PVD-deposited thin films is determined by many factors (Chapman 1980). Some of these factors are substrate temperature, atomic flux, background gas pressure, and specifics of the material being deposited, including the details of atom attachment

Petitioner Samsung Ex-1011, 0113

at the growth surface. The use of plasma techniques (as opposed to thermal evaporation methods such as electron beam deposition) has the disadvantage of producing ion damage in the growing film that can increase film resistivity. For this reason, process variables such as sputter gas pressure and target-to-substrate distance are of importance and are adjusted to reduce the energy of ions incident on the growth surface during deposition.

In general, ITO is deposited from sintered ceramic In_2O_3 targets containing between 3 and 10 wt% SnO_2 while IZO targets contain 7–10 wt% ZnO. The oxygen stoichiometry of the target will depend on the process used to manufacture it. In general, a low oxygen target ($In_2O_{3-\delta}$) will appear yellow and, as δ approaches zero, the color will change from green to grey to black. Crystalline ITO deposited onto substrates heated to 250–350 °C offers the lowest resistivity currently available (1 to $3 \times 10^{-4}\,\Omega\,\text{cm}$). Two alternatives to c-ITO that may be processed at room temperature are a-ITO and a-IZO. Compared to c-ITO, both of these amorphous materials have lower carrier densities, hence higher resistivity. Nevertheless, these amorphous materials are, in some applications, favored over crystalline ITO because they offer improved lithographic line definition due to their more controllable wet-etch characteristics. In addition, a-IZO offers the advantage of not requiring the addition of oxygen to the sputter gas since the optimum resistivity is found at or near zero oxygen (Figure 5.2). In some display fabrication processes, a-ITO is crystallized after patterning by performing a postpatterning anneal. These anneals are performed at relatively modest temperatures (around 200 °C) and produce stable crystalline ITO with a resistivity that lies between the resistivities of the as-deposited crystalline and amorphous states. The amorphous-to-crystalline phase transformation also occurs (Paine *et al.*1999) at much lower temperatures (< 120 °C) and, in principle, low-temperature, long time postdeposition anneals of a-ITO could be used to crystallize as-deposited a-ITO. However, the slow kinetics of this reaction (measured in days or weeks) makes it economically infeasible for a production process.

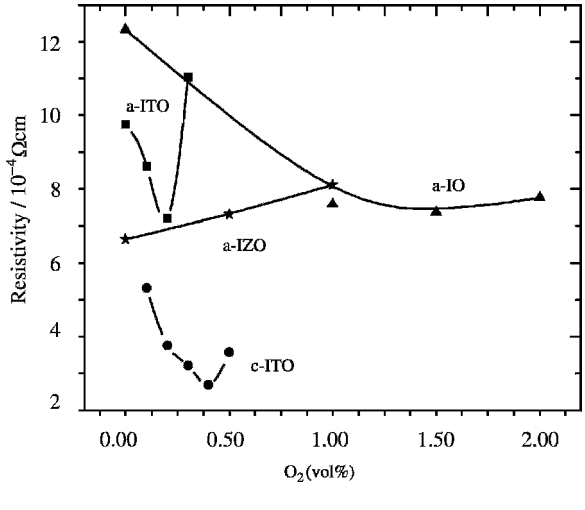


Figure 5.2 DC magnetron sputter deposition oxygen optimization curves for pure amorphous indium oxide (a-IO), a-ITO, c-ITO, and a-IZO. These curves are for films of roughly equivalent thickness (100 nm) and were sputtered at similar total pressure (mtorr) and power (0.25 W/cm^2)

Petitioner Samsung Ex-1011, 0114

The carrier density in ITO depends critically on the precise control of the oxygen stoichiometry of the compound. For this reason, both crystalline and amorphous ITO deposited by conventional DC magnetron sputter techniques require optimization of the oxygen content in the sputter gas. Typical oxygen gas optimization curves taken from work performed in the authors' laboratory are shown in Figure 5.2 for four oxides: a-ITO, a-IO (undoped indium oxide), c-ITO, and a-IZO. The two sets of ITO films were deposited from the same In_2O_3 9.8 wt% SnO_2 target but the a-ITO was deposited onto a substrate at room temperature while c-ITO was deposited at 350 °C. Note that the minimum resistivities of the two sets of ITO films occur at different oxygen contents (c-ITO at 0.4 vol%; a-ITO at 0.2 vol%). Films of a-IZO deposited onto unheated substrates have a minimum in resistivity at 0 vol% oxygen.

Examination of the data presented in Figure 5.2 provides insight into the effectiveness of dopants in the amorphous state. Note that all of the amorphous samples (pure indium oxide, Sn-doped indium oxide, and Zn-stabilized indium oxide) have similar resistivities (6 to $7 \times 10^{-4}\,\Omega$ cm) and that this resistivity is significantly higher than that of crystalline indium oxide (2 to $3 \times 10^{-4}\,\Omega$ cm) deposited in the same reactor.

Hall transport measurements are presented in Table 5.1 and show that all of the optimized amorphous samples, doped or not, have similar free carrier densities (1.8 to $2 \times 10^{20}\,\text{cm}^{-3}$) whereas the c-ITO sample has a much higher free carrier density ($6 \times 10^{20}\,\text{cm}^{-3}$). This suggests that Sn (and Zn for that matter) is not activated in the amorphous state and does not effectively dope indium oxide. In the amorphous state, most of the free carriers arise from some oxygen vacancy-like state.

Table 5.1 Electrical properties of 100 nm thick optimized films of a-ITO and c-ITO, a-IZO, and a-IO

	Resistivity (Ω cm)	Carrier density (cm^{-3})	Mobility ($\text{cm}^2/\text{V s}$)
c-ITO	2.23×10^{-4}	6.03×10^{20}	46.4
a-ITO	7.18×10^{-4}	2.18×10^{20}	41.4
IO	7.48×10^{-4}	1.88×10^{20}	44.5
IZO	6.66×10^{-4}	1.95×10^{20}	48.0

5.3.2 Crystalline Indium Tin Oxide

Crystalline indium oxide has the bixbyite structure (Figure 5.3) consisting of an 80-atom unit cell with the Ia3 space group and a 1 nm lattice parameter in an arrangement that is based on the stacking of InO_6 coordination groups. The structure is closely related to fluorite, which is a face-centered cubic array of cations with all the tetrahedral interstitial positions occupied by anions. The bixbyite structure is similar, except that the MO_8 coordination units (oxygen positioned on the corners of a cube and a metal cation (M) located near the center of the cube) of fluorite are replaced with units that have oxygen missing from either the body or the face diagonal. The removal of two oxygen ions from the metal-centered cube to form the $In–O_6$ coordination units of bixbyite forces the displacement of the cation from the center of the cube. In this way, indium is distributed in two nonequivalent sites with 1/4 of the indium atoms positioned at the center of a trigonally distorted oxygen octahedron (diagonally missing O). The remaining 3/4 of the indium atoms are positioned at the center of a more distorted octahedron that forms with the removal of two oxygen atoms from the face of the octahedron. These two nonequivalent In-centered octahedra are illustrated by the insets of

Petitioner Samsung Ex-1011, 0115

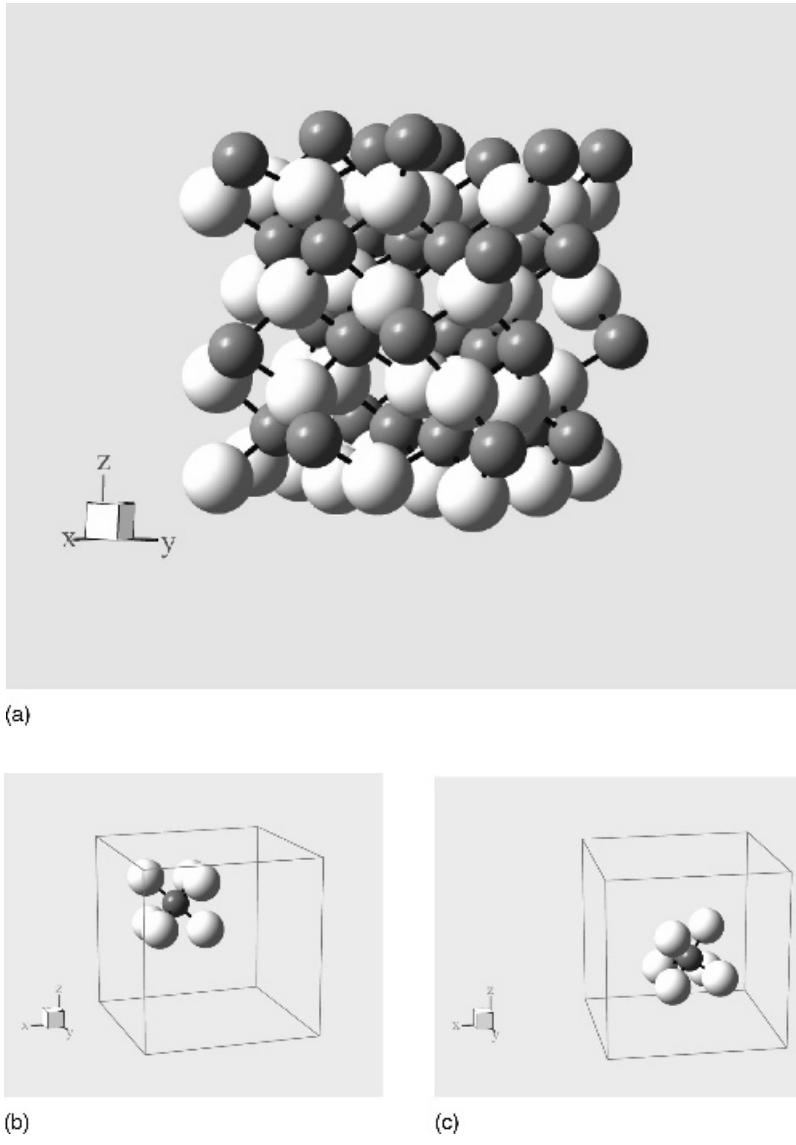


Figure 5.3 The bixbyite unit cell and the two basic nonequivalent InO_6 structural units of bixbyite: (a) unit cell, (b) type 1 In–O octahedra, (c) type 2 In–O octahedra

Figure 5.3. These MO_6 coordination units are stacked such that 1/4 of the oxygen ions are missing from each {100} plane to form the complete bixbyite structure.

When tin-doped indium oxide (ITO) is deposited using DC magnetron sputtering under optimum conditions onto a glass substrate at 250–350 °C, it assumes a ''rice field'' structure similar to that shown in the SEM image presented in Figure 5.4. Cross-sectional TEM reveals that the individual grains of the ITO are typically much wider than the film thickness and that they are subdivided by small-angle grain boundaries.

Petitioner Samsung Ex-1011, 0116

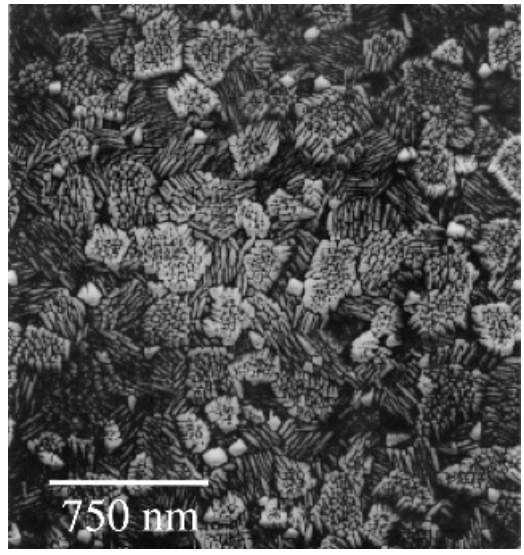


Figure 5.4 High-quality crystalline ITO deposited by DC magnetron sputtering at 350 °C with a resistivity of $1.1 \times 10^{-4}\,\Omega\,\text{cm}$ and transmissivity of better than 90%. Note the presence of subgrain regions known colloquially as the rice field structure

The resistivity of the film shown in Figure 5.4 is $1.1 \times 10^{-4}\,\Omega\,\text{cm}$, indicating that this material is near to the minimum achievable in ITO. The transmission spectrum for this film is presented in Figure 5.5 and shows a wide window over which the transmissivity is better than 90%. The rice field structure is observed in higher kinetic energy deposition processes such as high-density plasma-enhanced deposition and DC magnetron sputtering where the

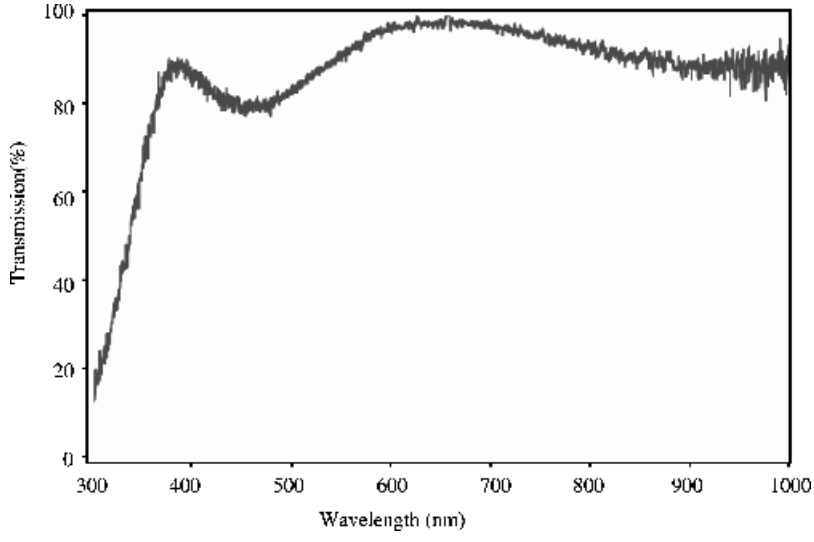


Figure 5.5 Transmission spectrum for crystalline ITO deposited at 250–350 °C to a thickness of 110 nm

Petitioner Samsung Ex-1011, 0117

growing surface is bombarded with energetic ions and reflected neutrals. Depending on the technique and the specifics of the deposition process, the kinetic energies of the particles (neutrals, ions of argon and oxygen, and thin film species such as indium, oxygen, and larger molecules of the two) incident on the growing surface can range from 10 to 400 eV. The rice field structure is only observed in these energetic deposition processes (Shigesato and Paine 1994) and only when deposition occurs on heated substrates (250–350 °C). This surface relief is shown in Figure 5.4 and is actually smoother than films of similar thickness deposited by low kinetic energy processes (Shigesato and Paine 1994) at elevated temperatures. Therefore high-temperature energetic deposition is favored for device processing.

Optimization of DC magnetron sputtered ITO films requires the adjustment of sputter power, total pressure, and, most importantly, the partial pressure of oxygen in the system. A set of typical optimization curves were shown in Figure 5.2 where the film resistivity is plotted for various commonly used indium oxide materials deposited over a range of O_2/Ar ratios. The films were deposited to a thickness of about 100 nm under identical power (0.25 W/cm^2) and total Ar pressure conditions in the same DC magnetron sputter deposition system. Hall transport measurements were made using a Van der Pauw setup and exact film thickness was determined using X-ray reflectivity. Note the clear minimum in resistivity at approximately 0.4 vol% O_2 for c-ITO. Crystalline ITO differs from the other samples plotted in this figure by having the lowest resistivity. Unfortunately, to achieve these low resistivity levels, the substrate must be heated to about 350 °C during deposition and, as such, this approach is not useful for currently available polymeric substrates.

The requirement that the oxygen partial pressure be optimized during deposition arises from the fundamental nature of the doping process in indium oxide. The doping of c-ITO results from two sources: tetravalent Sn substituting for trivalent In in the bixbyite crystal and the creation of doubly charged oxygen vacancies. A more detailed understanding of the point defect doping mechanisms has evolved over the years starting with the Frank and Kostlin (1982). This work was the first to explain the observations that (i) even well below the solubility limit, tin is not fully activated in the indium oxide lattice and (ii) the free carrier density in In_2O_3 depends on both the tin content and the oxygen content of the film. These observations are consistent with the c-ITO oxygen optimization curve shown in Figure 5.2 and can be understood in terms of the simple defect model for doping in ITO that has recently been reviewed by Freeman *et al*. (2000).

Table 5.1 reveals that c-ITO has a much higher carrier density (hence lower resistivity) than a-ITO of identical composition. This is due to the additional carriers provided by substitutional Sn, which is activated in the crystalline state but not in the amorphous state. The minimum in the c-ITO oxygen optimization curve can be understood in terms of the interaction between the activation of Sn and the oxygen partial pressure in the sputter gas. Frank and Kostlin (1982) suggested that tin tends to exist in the bixbyite lattice as neutral interstitial associates. These associates are formed via the reaction

$$2In_{In}^{x} + 2SnO_2 = (2Sn_{In}^{\bullet}O_i'')^{x} + In_2O_3. \qquad (5.6)$$

Here conventional Kroger–Vink notation is used in which the chemical species is appended with a superscript to designate the charge, positive ($^{\bullet}$) or negative ($'$), and a subscript is used to designate the site in the perfect crystal that the species occupies. Experimental evidence that supports the existence of the $2Sn_{In}^{\bullet}O_i''$ interstitial defect was recently acquired using

Petitioner Samsung Ex-1011, 0118

neutron diffraction data (Gonzalez *et al*. 2000). The presence of a neutral interstitial defect allows a self-consistent model to be developed that relates oxygen partial pressure, tin concentration, and free carrier density by considering three doping processes:

- Direct doping with substitutional Sn donors via

$$2In_{In}^{x} + 2SnO_2 = 2Sn_{In}^{\bullet} + 2e' + In_2O_3 + \frac{1}{2}O_{2(g)}. \tag{5.7}$$

  Although this is the simplest mechanism for carrier generation, it does not account for the observation that Sn exists as a neutral species and that Sn is not fully activated.

- At low oxygen potentials, carrier generation occurs via the reduction of electrically inactive neutral Sn interstitial associates via the reaction

$$(2Sn_{In}^{\bullet}O_i'')^{x} = 2Sn_{In}^{\bullet} + \frac{1}{2}O_{2(g)} + 2e'. \tag{5.8}$$

- Also at low oxygen potentials, the creation of doubly charged oxygen vacancies can occur via the reaction

$$O_o^{x} = \frac{1}{2}O_{2(g)} + V_o^{\bullet\bullet} + 2e''. \tag{5.9}$$

Consideration of the thermodynamics of these reactions along with the application of electroneutrality considerations (Frank and Kostlin 1982) reveals that, at high oxygen partial pressure, doubly charged oxygen vacancies and substitutional tin are both consumed as the reactions given in Equations (5.8) and (5.9) proceed to the left. At intermediate and low oxygen potentials (i.e. reducing conditions), these reactions proceed to the right and free carriers are created. Under conditions that are highly reducing, the indium oxide itself is reduced to In metal and the resultant decrease in lattice integrity causes a sharp decrease in conductivity.

5.3.3 Amorphous Indium Tin Oxide

Amorphous indium oxide is formed during physical vapor deposition processing when the InO_x units that evolve from the source or from species arriving on the growth surface are randomly oriented as they are incorporated into the growing film. The restricted mobility of the InO_x clusters at low substrate temperatures prevents the relaxation of the misoriented and distorted coordination units. Although the crystalline bixbyite phase consists of a large 80-atom unit cell, the crystallization of amorphous ITO occurs rapidly at very low homologous temperatures ($T/T_m < 0.19$), and 150 °C is commonly cited (Shigesato *et al*. 1992; Oyama, 1992) as the temperature at which crystallization occurs rapidly. At lower temperatures, crystallization may also proceed but the kinetics are slow and require a time frame of days or weeks.

The plan view TEM, shown in Figure 5.6, reveals the crystallization behavior of a-ITO deposited onto unheated substrates under optimum (lowest resistivity) sputter conditions. In this case, crystallization is initiated from a fixed number of pre-existing nuclei. These nucleation sites are spaced much farther apart than the film thickness (Figure 5.6 (a)). Hence,

Petitioner Samsung Ex-1011, 0119

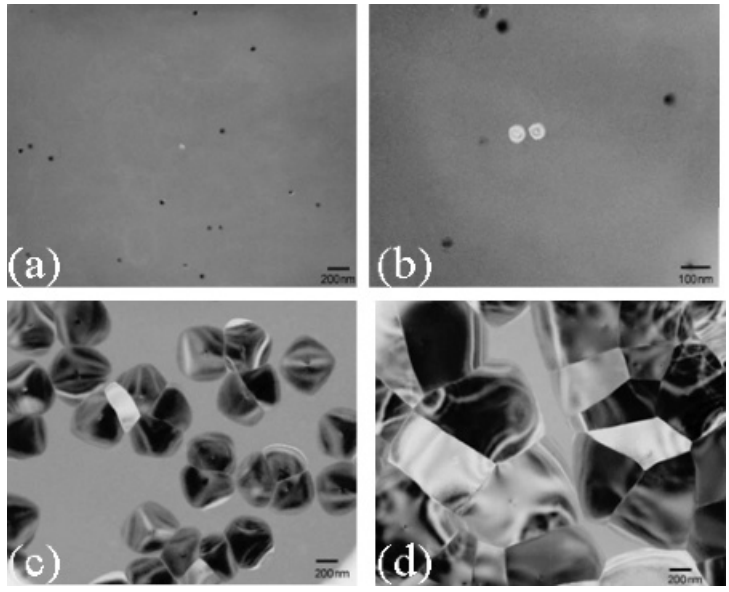


Figure 5.6 In situ TEM showing crystallization of DC magnetron sputter deposited amorphous ITO during annealing at 250 °C for approximately (a) 0, (b) 0.5, (c) 2.5, and (d) 5 h

once the growing indium oxide crystallite reaches a diameter equal to the film thickness, growth is in the form of two-dimensional islands, as seen in Figure 5.6 (b) and (c). Crystallization of the amorphous ITO proceeds by lateral growth of the crystalline islands until adjacent islands impinge and form grain boundaries. Note that crystallization in this case– where the composition of the crystalline phase and the amorphous phase from which it grows are identical–is limited only by the rate of short-range atomic hopping across the amorphous/crystalline phase boundary.

The specific conditions that result in an amorphous or partially amorphous ITO film depend on a wide variety of processing variables, including substrate temperature (Yi 1995; Vink *et al*. 1995), total film thickness (Muranaka *et al*. 1987; Muranaka, 1991), and oxygen partial pressure (Song, 1998). Muranaka showed that layers deposited by reactive evaporation onto substrates at temperatures below 150 °C are initially amorphous but become crystalline as the film increases in thickness. Films up to 55 nm thick were reported to be fully amorphous when deposited at room temperature and showed decreasing amorphous layer thickness with either increasing film thickness or temperature up to 150 °C. Similarly, in DC magnetron sputtered ITO, several authors (Yi 1995; Vink *et al*. 1995) report that very thin films of ITO deposited on substrates that are close to the crystallization temperature ($\sim$150 °C) are only partially crystalline. Thus, the amorphous/crystalline transformation probably plays a role in defining the microstructure in as-deposited films deposited on heated substrates. It certainly plays a critical role in defining the stability and performance of ITO deposited at low temperatures on unheated polymer substrates.

In the crystalline state, ITO is doped to degeneracy by substitutional tetravalent Sn positioned on trivalent In sites and by the presence of doubly charged oxygen vacancies. In the amorphous state, the doping mechanisms are not as well established. However, the data

Petitioner Samsung Ex-1011, 0120

in Table 5.1 suggest that Sn is not efficiently activated in the amorphous state. Pure indium oxide and a-ITO deposited at room temperature under optimized oxygen conditions have very similar carrier densities (1.9 to $2 \times 10^{20}\,\mathrm{cm}^{-3}$ in Table 5.1) and resistivity. Thus, it is clear that Sn is unlikely to be activated in the amorphous state and that free carriers in these materials are contributed primarily by vacancy-like oxygen defects in the amorphous structure. The difficulty of activating Sn in the amorphous state has been reported previously (Morikawa and Fujita 2000; Bellingham *et al*. 1990) and improving the effectiveness of doping amorphous indium oxide remains an area of active research.

The structure of a vacancy in the amorphous state is not well defined, but it is clear that the electronic properties of amorphous ITO depend on the local bonding environment. It would seem likely that the local In–O nearest-neighbor coordination remains unchanged in the amorphous and crystalline states. This is supported by radial distribution function (RDF) analysis of In–O bond lengths in amorphous ITO (Yaglioglu *et al*. 2003). In this work, electron scattering was used to evaluate the mean interatomic spacing in amorphous and crystalline phases of ITO having identical composition. It was shown that the In–O spacing remains the same in both phases.

It is interesting to note that the mean free path of the conduction electrons in amorphous indium oxide is much larger than the scale of the atomic disorder. This suggests that the Fermi electrons can not interact with the atomic disorder in the amorphous phase since it exists on too small a scale. This idea is supported by the RDF analysis mentioned above which showed that the InO_x structural units in the amorphous phase have the same average In–O spacing as measured for c-ITO. Since these units are 1/4 of the 1 nm unit cell dimension, the disorder must exist on a scale of 0.25 nm. In fact, in the amorphous state, ITO that has been optimized with respect to the oxygen content during deposition has a characteristic carrier mobility that is only slightly less than for crystalline films of the same composition (Table 5.1). The amorphous form of ITO possesses no structural discontinuities (grain boundaries, line faults, or planar faults) but Sn in the amorphous state probably exists in an inactive uncharged state similar to the neutral associates mentioned above.

5.3.4 Amorphous Indium Zinc Oxide

Tin-doped indium oxide (ITO) has been the transparent electrode material of choice for high-value, high-performance display applications. To take full advantage of ITO it must be deposited onto heated substrates. The crystalline form of ITO, however, is difficult to wet-etch and there are no dry-etch technologies available for this material. As a result, there has been a trend toward the use of a-ITO despite its higher resistivity when fine line definition or process simplification (Kaijo *et al*. 2001) is required. This trade-off between electrical performance and lithographic patterning has led to the development by Idemitsu Corp. (Kaijou 1999)of amorphous Zn-doped indium oxide. This material is of great current interest because it has better etch characteristics than c-ITO, it has a resistivity that is slightly lower than for a-ITO, it is structurally stable, and it can be deposited onto unheated substrates. It is therefore appropriate for use on glass substrates when lithographic definition is of importance and on heat-intolerant polymeric substrates.

When doped, both ZnO and In_2O_3 are useful transparent conductors. However, their valence state (2+ versus 3+) and cation coordination are quite different (4 versus 6), hence their mutual solid solubility is low. Over a wide range of compositions, the In_2O_3–ZnO

Petitioner Samsung Ex-1011, 0121

phase diagram (Moriga *et al*. 1998) shows that these two oxides react to form a set of homologous compounds (Cannard and Tilley 1988). These compounds consist of planes of {0001} wurtzite-like ZnO interspersed with bixbyite-like {111} planes of In_2O_3 to create a rhombohedral or hexagonal crystal structure with a *c*-axis periodicity determined by the compositional ratio of In and Zn. These homologous compounds indicate a strong tendency for the two cations (Zn and In) to preserve their individual tetrahedral (wurtzite) or octahedral (bixbyite) coordination with oxygen. Many of the $Zn_kIn_2O_{k+3}$ (where $k =$ 3,4,5,6,7,9,11,13,15) homologous compounds show promise for transparent conducting oxide applications (J. Phillips *et al*. 1995; Marcel *et al*. 2002; Minami *et al*. 2000 and references therein), but all of them require high-temperature processing and therefore they are not useful in polymeric substrate applications.

Amorphous ITO undergoes crystallization at remarkably low annealing temperatures and it is found to be crystalline in the as-deposited condition when deposited on substrates at or above 150–200 °C. In contrast, amorphous IZO (10 wt% ZnO) does not begin to crystallize at measurable rates until heated above 500 °C and it is deposited in the amorphous condition unless the substrate is above 350 °C (Jung 2003). The reason for this increased stability of the amorphous phase is that ZnO and In_2O_3 are immiscible and must undergo phase separation to allow crystallization. In Zn-rich IZO amorphous alloys, separation occurs on a microscopic scale and may result in the homologous-layered structures mentioned above. For the 7–10 wt% ZnO levels used for a-IZO, phase separation requires the rejection of Zn from the crystallizing indium oxide structure. The kinetics of phase separation are slow and, as a result, Zn has the effect of stabilizing the amorphous structure. The stabilization of the amorphous phase of IZO (10 wt% ZnO) is closely tied to the need for ZnO to remain tetrahedrally coordinated (which, presumably, is possible in the amorphous state) and the relative insolubility of Zn in bixbyite In_2O_3. A series of TEM images showing the crystallization of IZO in air at 500 °C is presented in Figure 5.7 and reveals a more serrated amorphous/crystalline interface (compared to Figure 5.6) and much slower crystallization kinetics.

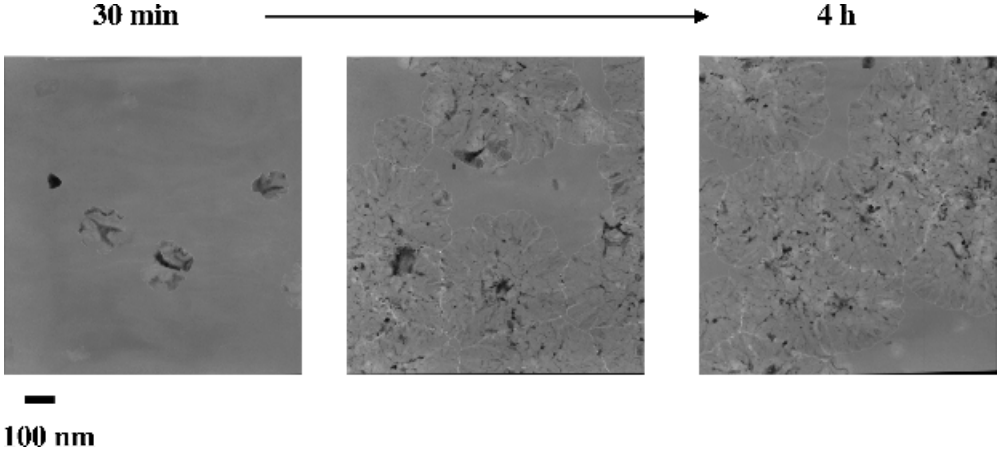


Figure 5.7 TEM image showing the amorphous (a) to crystalline (c) transformation of IZO in air at 500 °C. Note the regions of lighter contrast at the grain boundaries and at the a/c interface indicating the depletion of In

Petitioner Samsung Ex-1011, 0122

Amorphous IZO films doped up to 10 wt% ZnO deposited at low temperatures are structurally (Minami *et al*. 1999) more stable than a-ITO and possess similar or lower resistivities. At higher Zn concentrations (20 at%) Minami reports that the resistivity of IZO increases slightly but that the band gap decreases from 3.8 eV (pure indium oxide) to a minimum of 2.9 eV. Table 5.1 shows that the carrier density of all three amorphous phases is very similar (regardless of dopant). It also shows that the carrier mobility of amorphous IZO is higher than either of the other two amorphous phases and, as a consequence, the resistivity of IZO is the lowest of the three amorphous phases. This is possibly due to the effect of Zn on the band structure of IZO. It has been reported (Minami *et al*. 1999) that Zn decreases the band gap and may also (Jung 2003) modify the band shape in a way that increases the mobility by flattening the bottom of the conduction band.

5.4 Future Directions for Transparent Conducting Oxides

5.4.1 Novel Materials

Development of novel PVD processing methods and the optimization of PVD deposition conditions have led to a reduction in the resistivity of In_2O_3 from about $1 \times 10^{-3}\,\Omega$ cm in the late 1960s to $1 \times 10^{-4}\,\Omega$ cm at present (Minami *et al*. 2000). Minami plotted literature reports of crystalline ITO resistivity as a function of publication year. This plot shows that the rate of resistivity improvement has dropped in recent years to nearly zero. This suggests that the further improvements in carrier density and mobility in ITO necessary to reduce resistivity are unlikely and that new materials systems will be required for improved TCO performance. In addition, there is concern that the world supply of indium metal is limited and may not allow for the economical use of In-containing materials for future technologies, particularly those targeted at large-area low-cost applications. This realization has led in recent years to an intensive search for new TCO materials.

Table 5.2 lists many of the established available binary and single-component transparent conductors. Although Cd-based oxides are known transparent conductors, they are not under wide consideration due to concerns about the toxicity of Cd. There is great current interest in ZnO-based materials, which are attractive from the view point of Zn abundance but, to date, the resistivity of these materials is higher than the state-of-the-art alternatives (ITO and IZO) deposited at room temperature. For example, ZnO:Al (AZO) and ZnO:Ga (AGO) were reactively deposited with a resistivity in the range 10^{-3} to $10^{-4}\,\Omega$ cm and with better than 90% transmission (Kon *et al*. 2002, 2003). The resistivity of these materials, however, is not

Table 5.2 Work function and resistivity of selected (transparent) conductors

Material	Resistivity (Ω cm)	Work function (eV)	Band gap (eV)
Ag	1.6×10^{-6}	5	none
TiN	2×10^{-5}	—	metalloid
In_2O_3:Sn (ITO)	1×10^{-4}	4.7	3.8
ZnO:Al	1.5×10^{-4}	4.5	3.1
SnO_2:F	2×10^{-4}	4.8	3.5

Petitioner Samsung Ex-1011, 0123

Table 5.3 Partial list of known n-type ternary compound oxide conductors

Material	Resistivity (Ω cm)	Work function (eV)	Band gap (eV)
Zn_2SnO_4	1.7×10^{-2}	—	—
$ZnSnO_3$	4×10^{-3}	5.3	3.5
$MgIn_2O_4$	4.3×10^{-3}	4.7	3.4
$GaInO_3$	2.7×10^{-3}	5.4	3.3
$(Ga,In)_2O_3$	5.8×10^{-4}	—	—
$Zn_2In_2O_5$	2.9×10^{-4}	5	2.8
$In_4Sn_3O_{12}$	2×10^{-4}	4.9	3.5

Sources: Phillips *et al.* (1995), Minami *et al.* (1997, 1998, 2000)

lower than that of current ITO materials, and higher substrate temperatures are required to achieve minimum resistivity.

Ternary metal oxides are less well characterized but many have been reported with excellent conductivity and good optical transmissivity.

Table 5.3 lists several candidate ternary oxides and their properties. The SnO_2–In_2O_3 pseudobinary system, for example, has a ternary compound with $In_4Sn_3O_{12}$ stoichiometry that exhibits good conductivity and is stable in acid solutions and in high-temperature oxidizing atmospheres (Minami *et al*. 1997). Other promising ternary compounds that have reasonable conductivity include $GaInO_3$ (J. M. Phillips *et al*. 1994), $MgIn_2O_4$, (Unno *et al*. 2002) and $Zn_2In_2O_5$ (Minami *et al*. 1995). Both $Zn_2In_2O_5$ and $In_4Sn_3O_{12}$ are reported to have a band gap of about 3.4 eV and a work function of 4.8 to 5 eV and are, at present, the most promising of the ternary oxides. Many other multicomponent oxides are also under consideration but the work function and band gap of many of these ternary compounds are not yet well characterized. The prospects for high performance under low-temperature deposition conditions are not good for these ternary oxides. The increased structural complication of ternary oxide compounds requires a greater degree of atomic motion to assume the correct crystalline structure. As such, these ternary compounds typically require process temperatures well above the limit of most polymer substrates.

There are a host of new TCO materials under development that are significantly less costly than the In-based systems. However, most of them require a heated substrate or have lower performance than the currently available materials. At present, it appears that low-cost applications will utilize lower-performance nonindium materials and high-end applications will continue to use indium materials.

5.4.2 Manufacturing Considerations

At present, the largest volume use of transparent conducting materials is in energy-efficient coatings for architectural glass where a spray-deposited thin film of F- or Sb-doped SnO_2 is used to reflect infrared radiation (heat) while allowing the transmission of visible light. Spray coating of SnO_2 at atmospheric pressure allows large-area deposition onto glass with excellent reflectivity in the infrared at very low process and raw materials cost. The economic advantages of large-scale coating operations using PVD processes may also be realized one day for large-area low-cost flexible display applications using roll-to-roll web coating of flexible polymeric substrates.

Petitioner Samsung Ex-1011, 0124

Roll-to-roll vacuum web coating of flexible polymer substrates is an established industry with annual worldwide production of nearly 10 billion square meters of coated plastic. Most of this output is directed to the manufacture of capacitors (40%) and packaging (58%) (Sheats 2002; Lievens 1995), with the balance being made up of a diverse selection of more complex materials such as ITO on PET for touch screen applications. A typical roll-to-roll coater used for capacitor fabrication deposits a 30 nm film of Al onto a PET substrate (1–50 μm thick) that is unrolled in one end of the coater, passed across a PVD source (DC magnetron sputtering or thermal evaporation) at speeds that range from 0.1 to 10 m/s, and is rolled-up at the other end. The web width can be up to 2 m and its maximum length depends only on the capacity of the coater.

Both evaporation and sputtering are used in typical web-coating operations. Thermal evaporation is favored for the deposition of metals with reasonable vapor pressures such as Al since the deposition rate is practically limited only by the rate at which heat can be removed from the web. For the deposition of binary or ternary conducting oxide compounds, DC magnetron sputter deposition, or a variant of it, is probably the only technology that has the long-term stability necessary for web-to-web coating. While it may be possible, for example, to reactively sputter deposit these oxide materials from metal targets in an oxygen ambient, target poisoning results in unacceptable levels of nonuniformity. Furthermore, DC magnetron sputtering is favored over RF sputtering due to its higher deposition rate.

The technology needed to produce complex multilayer structures in a single pass through a web coater is already available. For example, there are reportedly (Kukla *et al*. 1996) commercially available web-to-web sputter tools with ten cathodes that may be installed to allow higher deposition rates or multilayer depositions. These tools may be used to mitigate the effect of high-resisitivity TCO materials by the use of composite multilayer structures. For example, Ag/ITO multilayers have been proposed which combine an optical antireflection function and decreased resistivity.

5.5 Summary

The best available materials today for deposition onto unheated substrates are ITO and IZO. This is despite the efforts of many laboratories to find a low-cost, high-performance replacement for In-based transparent conducting oxides. In the as-deposited state, IZO is always amorphous when deposited at substrate temperatures below 350 °C and remains in this metastable state unless heated to above 500 °C. In contrast, ITO deposited in the amorphous state on unheated substrates can be crystallized at relatively low anneal temperatures (as low as 120 °C). Neither Zn nor Sn contribute carriers in amorphous indium oxide and, consequently, the resisitivity of crystalline ITO deposited at 250–350 °C is significantly lower than for either a-ITO or IZO. Although Zn in IZO does not act as a dopant, it does appear to improve the carrier mobility. As a result, IZO has a slightly lower resistivity than amorphous ITO. The deposition of transparent conducting oxides on flexible polymer substrates is already a commercial success for touch screen applications. Further significant reduction in the resistivity of these In-based binary oxide materials deposited at room temperature appears unlikely. Thus, device designers who wish to use temperature-sensitive polymer substrates must make do with the 5 to $7 \times 10^{-4}\,\Omega\,\text{cm}$ available from a-IZO or a-ITO until an alternative TCO becomes available or until novel flexible materials become available that can withstand elevated temperature processing.

Petitioner Samsung Ex-1011, 0125

References

Baedeker, K. (1907) Uber die elektrische Leitfahigkeit und die thermoelektrische Kraft einiger Schwermetallverbindungen. *Annals of Physics* **22**, 749–766.

Bellingham, J. R., Phillips, W. A., and Adkins, J. C. (1990) Electrical and optical properties of amorphous indium oxide. *Journal of Physics: Condensed Matter* **2**(28), 6201.

Cannard, P. J and Tilley, R. J. D. (1988) New intergrowth phases in the ZnO–In_2O_3 system. *Journal of Solid State Chemistry* **73**, 418–426.

Chapman, B. N. (1980) *Glow Discharge Processes*. John Wiley & Sons, Inc. New York, p. 70.

Frank, G. and Kostlin, H. (1982) Electrical and optical properties of indium oxide. *Applied Physics A* **27**, 197–203.

Freeman, A. J., Poeppelmeier, K. R., Mason, T. O., Chang, R. P. H., and Marks, T. J. (2000) Chemical and thin film strategies for new transparent conducting oxide. *MRS Bulletin* **25**, 45–51.

Gonzalez, G., Cohen, J., Hwang, J. H., Mason, T., Hodges, J., and Jorgensen, J. (2000) Defect structures of indium tin oxide and its relationship to conductivity. In *Proceedings of the International Conference on Mass and Charge Transport in Inorganic Materials*, Vincenzini P. (ed.), Techna, Faenza, Italy.

Haacke, G. (1976) New figure of merit for transparent conductors. *Journal of Applied Physics* **47**, 4086–4088.

Hiramatsu, H., Ueda, K., Ohta, H., Hirano, M., Kamiya, T. and Hosono, H. (2003) *Thin Solid Films* **445**, 304–308.

Jackson, T., MRS Fall Meeting 2003, symposium X.

Jung, Y. S., Seo, J. Y., Lee, D. W. and Jeon, D. Y. (2003) Influence of DC magnetron sputtering on the properties of amorphous indium zinc oxide thin film. *Thin Solid Films* **445**, 63–71.

Kaijo, A., Inoue, K., Matsuzaki, S. and Shigesato, Y. (2001) Practical properties of indium zinc oxide for thin film transistor liquid crystal displays. In *Proceedings of the Fourth Pacific Rim International Conference on Advanced Materials and Processing*.

Kaijou, A., Ohyama, M., Shibata, M. and Inoue, K. (1999) Transparent electrically conductive layer, electrically conductive transparent substrate and electrically conductive material, US Patent 5,972,527.

Kon, M., Song, P. K., Shigestao,Y., Frach, P., Ohno, S. and Suzuki, K. (2002) Al-doped ZnO films deposited by reactive magnetron sputtering in mid-frequency mode with dual cathodes. *Japanese Journal of Applied Physics* **41**, 814–819.

Kon, M., Song, P. K., Shigestao, Y., Frach, P., Ohno, S. and Suzuki, K. (2003) Impedence control of reactive sputtering process in mid-frequency mode with dual cathodes to deposit Al-doped ZnO films. *Japanese Journal of Applied Physics* **42**, 263–269.

Kostlin, H., Jost, R. and Lems, W. (1975) Optical and electrical properties of doped In_2O_3 films. *Physica Status Solidi (a)*, **29**, 87–93.

Kukla, R., Ludwig, R. and Meinel, J. (1996) Overview of Modern vacuum web coating technology. *Surface Coatings Technology* **86/7**, 753–761.

Lievens, H. (1995) Wide web coating of complex materials. *Surface Coatings Technology* **76**/**77**, 744–753.

MacDiarmid, A. G. (2002) Synthetic metals: a novel role for organic polymers, *Synthetic Metals* **125**, 11–22.

Marcel, C., Naghavi, N., Couturier, G., Salardenne, J. and Tarascon, J. M. (2002) Scattering mechanisms and electronic behavior in transparent conducting $Zn_xIn_2O_{x+3}$ oxide thin films. *Journal of Applied Physics* **91**(7), 4291–4297.

Minami, T., Sonohara, H., Kakumu, T. and Takata, S. (1995) Highly transparent and conductive $Zn_2In_2O_5$ thin films prepared by RF magnetron sputtering. *Journal of Applied Physics* **34**, L971–L974.

Petitioner Samsung Ex-1011, 0126

Minami, T., Takeda, Y., Takeda, S. and Kakumu, T. (1997) Preparation of transparent conducting $In_4Sn_3O_{12}$ thin films by DC magnetron sputtering. *Thin Solid Films* **308/9**, 13–18.

Minami, T., Miyata, T. and Yamamoto, T. (1998) Work function of transparent conducting multi-component oxide thin films prepared by magnetron sputtering. *Surface Coatings Technology* **109**, 583–587.

Minami, T., Miyata, T. and Yamamoto, T. (1999) Stability of transparent conducting oxide films for use at high temperatures. *Journal of Vacuum Science and Technology A* **17**, 1822–1826.

Minami, T., Yamamoto, T., Toda, Y. and Miyata, T. (2000) Transparant conducting zinc-co-doped ITO films prepared by magnetron sputtering. *Thin Solid Films* **373**, 189–194.

Moriga, T., Edwards, D., Mason, T. O., Palmer, G. B., Poeppelmeier, K. R., Kannewurf, C. R. and Nakabayashi, I. (1998) Phase relationships and physical properties of homologous compounds in the zinc oxide–indium oxide system. *Journal of the American Ceramic Society* **81**(5), 1310–1316.

Morikawa, H. and Fujita, M. (2000) Crystallization and electrical property change on the annealing of amorphous indium-oxide and indium-tin-oxide thin films. *Thin Solid Films* **359**, 61.

Muranaka, S. (1991) Crystallization of amorphous In_2O_3 films during film growth. *Japanese Journal of Applied Physics Part 2* **30**(12A), L2062.

Muranaka, S., Bando, Y. and Takada, T. (1987) Influence of substrate temperature and film thickness on the structure of reactively evaporated In_2O_3 films. *Thin Solid Films* **151**, 355–364.

Nagarajan, R., Draeseke, A. D., Sleight, A. W. and Tate, J. (2001) p-type conductivity in $CuCr_{1-x}Mg_xO_2$ films and powders, *Journal of Applied Physics* **89**, 8022.

Oyama, T. (1992) Structure of deposited ITO. *Journal of Vacuum Science and Technology A* **10**, 1682.

Paine, D. C., Whitson, T., Janiac, D., Beresford, R., Yang, C. O. and Lewis, B. (1999) A study of low temperature crystallization of amorphous thin film indium-tin-oxide. *Journal of Applied Physics* **85**(12), 8445–8450.

Phillips, J., Cava, R., Thomas, G., Carter, S. A., Kwo, J., Siegrist, T., Krajewski, J. J., Marshall, J. H., Peck, W. F. and Rapkine, D. (1995) Zinc-indium-oxide: a high conductivity transparent conducting oxide. *Applied Physics Letters* **67**(15), 2246–2248.

Phillips, J. M., Kwo, J., Thomas, G. A., Carter, S. A., Cava, R. J., Hou, S. Y., Krajewski, J. J. and van Dover, R. B. (1994) Transparent conducting thin-films of $GaInO_3$. *Applied Physics Letters* **65**, 115–117.

Sheats, J. R. (2002) Roll-to-roll manufacturing of thin film electronics. *SPIE Proceedings* 4688.

Shigesato, Y. and Paine, D. C. (1994) A microstructural study of low resistivity tin-doped indium oxide prepared by d. c. magnetron sputtering. *Thin Solid Films* **238**, 73.

Shigesato,Y., Takaki, S. and Haranoh, T. (1992) Electrical and structural properties of low resistivity tin-doped indium oxide films. *Journal of Applied Physics* **71**, 3356.

Song, P. K. (1998) Study on crystallinity of tin-doped oxide films deposited by DC magnetron sputtering. *Japanese Journal of Applied Physics part 1* **37**(4A), 1870–1876.

Stauber, R. E., Perkins, J. D., Parilla, P. A. and Ginley, D. S. (1999) Thin film growth of transparent p-type $CuAlO_2$. *Electrochemistry Solid State Letters* **2**, 654.

Un'no, H., Hikuma, N., Omata, T., Ueda, N., Hashimoto, T. and Kawazoe, H. (2002) Carrier generation in $MgIn_2O_4$ thin films. *Philosophical Magazine B* **82**, 1155.

Vink, T. J., Walrave, W., Daams, J. L. C, Baarslag, P. C. and van der Meerakker, J. E. A. M. (1995) On the homogeneity of sputter deposited ITO films. Part 1: Stress and mictrostructure. *Thin Solid Films* **266**, 145.

Yaglioglu, B., Yeom, H. Y., Chason, E. and Paine, D. C. (2003) A structural study of the amorphous to crystalline transformation in In_2O_3 thin films. *Material Research Society Symposium Proceedings* **747**, 347–352.

Yi, C. H. (1995) Microstructure of low-resistivity tin-doped indium oxide films deposited at 150–200 °C. *Japanese Journal of Applied Physics Part 2* **34**(2B), 244–247.

Petitioner Samsung Ex-1011, 0127

6

Mechanics of ITO on Plastic Substrates for Flexible Displays

Piet C. P. Bouten,[1] Peter J. Slikkerveer,[1] and Yves Leterrier[2]

[1]Philips Research Laboratories and [2]EPFL Lausanne

6.1 Introduction

6.1.1 Plastic Substrates Contain Thin Brittle Layers

Flexibility of displays is an appealing feature which will change the look and feel of a display altogether from a heavy, expensive and fragile piece of equipment to a thin, lightweight and rugged device that can be used in many new surroundings. Besides flexibility meaning a lack of rigidity, it also indicates improved ruggedness. For a number of display principles that are intrinsically thin, like liquid cystal displays (LCDs) and organic light-emitting diode (OLED) displays, flexibility can be obtained by reducing the thickness of the substrates, while the choice for plastic substrates improves the ruggedness. Although advantageous for flexibility, the properties of polymeric materials seldom match with all requirements set by display processing or display usage, either mechanically (e.g. scratch resistance), chemically (e.g. chemical resistance) or physically (e.g. water permeability). To compensate for this, a plastic display substrate needs to be ''engineered,'' i.e. coated with several layers to improve the properties of the total film. As the generic substrate structure in

Flexible Flat Panel Displays Edited by G. P. Crawford
© 2005 John Wiley & Sons, Ltd., ISBN 0-470-87048-6

Petitioner Samsung Ex-1011, 0128

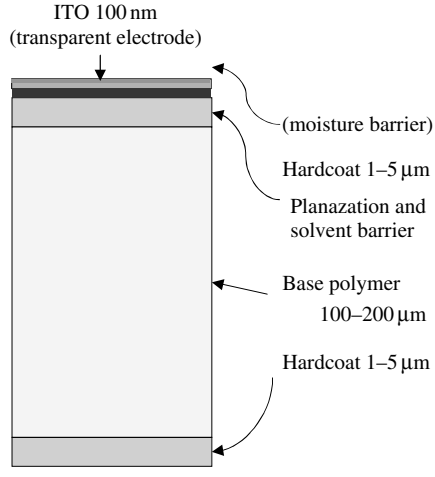


Figure 6.1 Generic substrate structure

Figure 6.1 shows, the base film is often coated on both sides with a 'hardcoat' (HC). This layer increases the scratch resistance of the film, while it also acts as a solvent barrier, improving its chemical stability by preventing direct contact between the process chemicals and the base polymer. On top of the hardcoat, a gas or moisture barrier can frequently be found, while the display side is coated with a transparent electrode material, such as indium tin oxide (ITO).

While the polymer substrate is usually fully organic, the hardcoat might be either organic or partially inorganic (e.g. silica/polymer nanocomposite), and the gas barrier and ITO are mostly inorganic materials (metal oxides and nitrides). Since inorganic materials are commonly stiff and brittle, whereas the polymers are not, the aim of this chapter is to discuss the mechanical failure of these thin brittle layers on top of a polymer base film, with special attention paid to ITO. This work focuses on the two most critical failure modes for flexible displays, tensile failure and compressive failure, which can lead in both cases to interfacial delamination.

This section introduces some fundamental properties of both polymer and inorganic brittle layers and resulting main failure modes. The following two sections focus respectively on the failure under tensile strain, including mechanical test methods used to investigate this class of layered composite materials, and failure under compressive strain. The last section briefly discusses failure in complex situations relevant to manufacture and service of a display device.

6.1.2 Thermoelastic Properties of Thin Films

The base polymer and the additional layers differ significantly in their two main thermo-mechanical properties: the Young's modulus and the coefficient of thermal expansion (CTE). Where the Young's modulus indicates the rigidity of a layer, the differences in CTE are very important, since they can lead to significant strains at changing temperatures, which lead to high stress levels, particularly in thin, high-modulus layers.

Petitioner Samsung Ex-1011, 0129

Table 6.1 Young's modulus and CTE of substrate layers

Material	Young's modulus, E (GPa)	Coefficient of thermal expansion, CTE (ppm/K)
Hardcoat	6.0 ± 0.5	61 ± 1
Base polymer (e.g. Arylite)	2.9	~65
Gas barrier (e.g. SiN_x)	150*	10*
ITO	119 ± 5	7.6

*Estimated values.

These two properties are reported in Table 6.1 for typical materials used for flexible displays (Leterrier *et al.* 2003a). The Young's modulus and CTE of the base polymer were measured by means of tensile testing and thermomechanical analysis, respectively. The Young's modulus of thin layers, E_c, was derived from the moduli of coated and uncoated thin (12 μm) polymer films, using the rule of mixtures, and compared with nanoindentation data of the same layers deposited on glass. A good agreement was obtained between the two methods: for ITO, E_c was found to be 119 GPa with tensile tests and 112 GPa with nanoindentation. The CTE of the thin layers was derived from the measured radius of curvature of coated foils subjected to temperature changes, using classic thermoelastic stress analysis (Leterrier *et al.* 2003a).

6.1.3 Mechanical Loading and Internal Stresses

Bending a display or a display substrate leads to a very well-defined deformation profile. At a given radius of curvature, the outside of the display substrate is stretched while the inside of the film is compressed, with the strain varying linearly over the thickness of the film (Figure 6.2). At a given position in the cross section of the substrate (the neutral plane) the strain does not change upon bending. This location depends on the layer structure of the film and the Young's moduli of all layers. For a homogeneous substrate this neutral plane would be in the centre of the substrate. This bending strain and the strain due to a tensile load are examples of externally applied stains.

Note that bending prescribes the strain profile in the film, not the stress profile. The stress profile is derived from the strain using the Young's modulus of the specific layer. With the strain being the primary parameter, in this chapter we will refer to failure strains, rather than failure stresses.

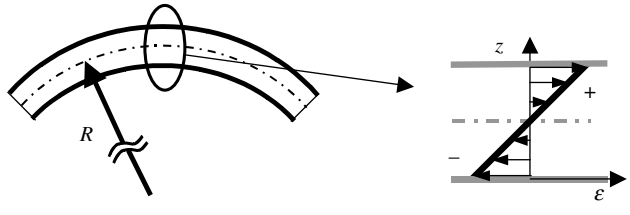


Figure 6.2 Strain distribution in a bend film

Petitioner Samsung Ex-1011, 0130

In contrast to uniaxial bending strains originating from bending, thermal strains induced by temperature changes and differences in CTE are biaxial. In inorganic layers like ITO, compressive thermal stresses usually develop during cooldown after deposition at elevated temperatures. On the contrary, when brought to temperatures higher than deposition conditions, for instance during annealing, the stresses may turn from compressive to tensile. The thermal strains in a multilayer system leads to curving of the structure. Townsend *et al.* (1987) derived equations for the curvature, strain (and stress) distribution and position of the neutral plane, in multilayer substrates.

The thermal strain distribution in the curved sample is an example of an internal strain in the system. Internal stresses (strains) in a stack of layers originate not only from thermal expansion differences. A variety of other mechanisms contribute to this internal strain distribution. Volume or length changes in individual layers, due to ingression of moisture in layer or substrate, for instance, contribute to the internal strain distribution. These strains further evolve throughout manufacture and eventually during service as a result of the application of external mechanical strains on the total substrate or by thermally loading the substrate. They may also change due to time-dependent processes such as viscoelastic creep and physical aging of the polymer substrate. Since the internal stresses can be very significant, they must be taken into account for analysis of measurements and lifetime considerations. Unless otherwise specified, stress or strain in this chapter denotes total amount of stress or strain present in the material, which is the combination of externally applied stress or strain and the internal stress or strain.

The present chapter mainly discusses linear elastic deformations, following Hooke's law $\sigma = \varepsilon E_{\text{eff}}$, where σ is the stress and ε the strain. The effective elastic modulus E_{eff} depends on the actual loading situation: under uniaxial load, it is equal to Young's modulus E (plane stress) or $E/(1-\nu^2)$ (plane strain), where ν is Poisson's ratio. For biaxial load, $E_{\text{eff}} = E/(1-\nu)$.

To describe the difference in mechanical properties of two adjacent layers, we introduce the dominant Dundurs, or elastic mismatch, parameter (Hutchinson and Suo 1992):

$$\alpha = \frac{E_{\text{eff},1} - E_{\text{eff},2}}{E_{\text{eff},1} + E_{\text{eff},2}}. \tag{6.1}$$

Here $E_{\text{eff},1}$ and $E_{\text{eff},2}$ are the effective elastic moduli of neighboring layers (e.g. coating and substrate). For equal moduli $\alpha = 0$. A hard coating on an extremely soft substrate results in $\alpha \to 1$. ITO on the base polymer (Table 6.1) gives $\alpha = 0.95$.

6.1.4 Failure Modes of Thin Brittle Films

The stresses in the multilayer inorganic/organic composite resulting from thermal or mechanical loading may cause a variety of failure mechanisms. These may lead to either cohesive failure of the inorganic layer (e.g. fracture), or adhesive failure between layer and substrate (Figure 6.3). The internal stresses in substrate and coating, e.g. introduced by CTE differences and temperature steps during processing, may affect the extent of the failure pattern considerably. The viscoelastic properties of the base substrate add to the complexity of the failure mechanism.

Petitioner Samsung Ex-1011, 0131

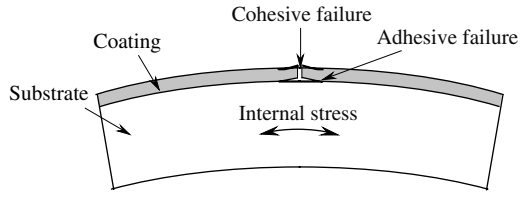


Figure 6.3 The durability of thin film/polymer layered composites is determined by the internal stress (coating and interfacial region), the coating cohesive strength and related crack onset strain, and the coating/substrate adhesion.

6.2 Failure of Brittle Layers under Tensile Stress

6.2.1 Mechanical Test Methods

In this section, two different techniques are used for accurate investigation of the failure mechanisms of ITO films on plastic substrates: a tensile test and the bending test (Figure 6.4). In the tensile test, a film specimen is loaded in tension in situ in a microscope, which allows for simultaneous measurement of electrical resistance and detection of damage in the brittle coating. The coating damage is characterized in terms of crack density as a function of strain (Leterrier 2003). The device uses contactless video extensometry to overcome compliance phenomena (Leterrier *et al.* 2004). Although the method is time-consuming, the detailed observation of failure processes is a key benefit of this method. To examine failure under biaxial strains, samples were loaded by means of a bulging cell, as detailed in a recent work (Leterrier *et al.* 2001).

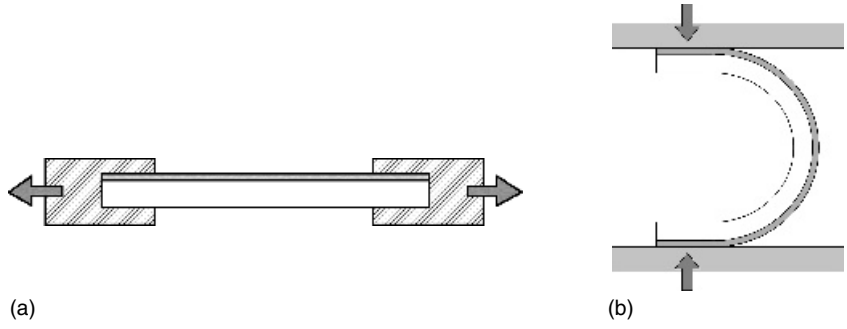


Figure 6.4 Schematic representation of (a) the tensile test, (b) the two-point bending test

The second method is a two-point bending technique (Bouten 2002), in which the film specimen is bent between two parallel plates. For elastic response of the samples, the bending profile of the sample is well defined and the strains are maximal in the sample central between the two plates. Upon bending, the outer surface of the sample is loaded in tension and the inner surface in compression. The electrical resistance of the ITO layer is

Petitioner Samsung Ex-1011, 0132

Table 6.2 Overview of the bending and tensile test methods

Test	Purpose	Advantage	Drawbacks
Two-point bending	Determination of critical strain and failure statistics	Fast and automated	Only conductive coatings
Tensile test	Determination of critical strain and adhesion	Direct observation of failure processes	Time-consuming, no automation

monitored as a function of the distance between the two parallel plates. At a certain strain level, the resistance increases significantly due to cracking of the ITO layer. This test thus determines the conductive failure of the ITO layer. Contrary to the tensile test, the method does not require sophisticated video extensometry.

The advantages and drawbacks of the two test methods are summarized in Table 6.2.

6.2.2 Characteristic Failure Modes

Figure 6.5 shows the typical failure of ITO under uniaxial tension as a sequence of micrographs at increasing strain levels. Here a 100 nm thick ITO layer is coated on a hardcoated polymer substrate. Upon loading, the very first cracks originate at defect sites as a result of localized stress concentrations. Cracks propagate from these defects to finite lengths and, at higher strains, become unstable and span the whole sample width, while the density of cracks increases markedly to beyond 100 cracks/mm. It is evident from the figures that the transition from stable crack growth to unstable propagation occurs when the crack length is several hundred times the coating thickness. At higher strain, the HC layer fails, and the crack density in the ITO saturates.

Biaxial loading of the ITO leads to a markedly different failure pattern, as shown in Figure 6.6. Cracks still initiate from small defects sites and propagate with curved trajectories until reaching another crack, which they intercept at right angles. In some instances, dynamic crack branching takes places, leading to fragments with sharper corners. Detailed analysis of failure processes under 2D loading can be found in Andersons *et al.* (2003).

6.2.3 Experimental Analysis of Uniform Layers

Figure 6.7 shows the resistance change of 100 nm thick ITO layers during loading in two test geometries (two-point bending and tension). Up to a certain strain, the resistance is (nearly) constant then it starts to increase strongly. In this chapter, conductive failure is expressed in terms of crack onset strain (COS), defined as a 10% increase in resistance.

Figure 6.8 plots the crack density (the number of cracks per millimeter) and relative resistivity increase against the applied strain, both measured with the tensile test. The remarkable correlation between optical detection and electrical measurements is evident. The COS corresponds well to the first cracks spanning the whole sample width.

Petitioner Samsung Ex-1011, 0133

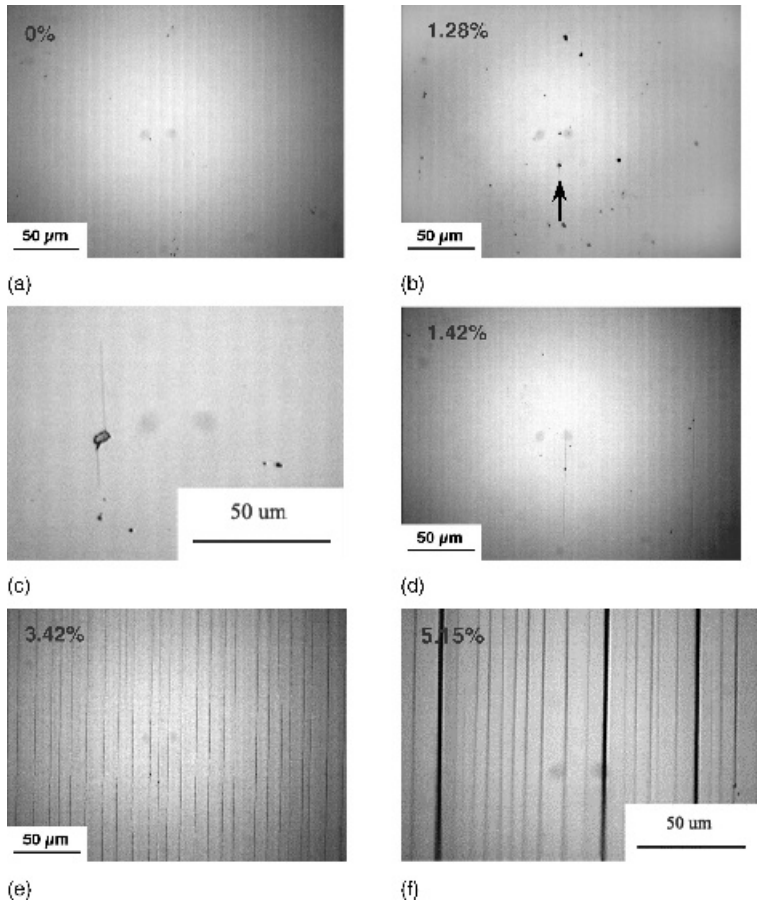


Figure 6.5 Progressive cracking of a 100 nm thick ITO coating on a hardcoated polyester substrate during tensile loading along the horizontal direction; strains are listed in the micrographs; (c) and (d) are at 1.42% strain. Parts (a), (b), (d) and (e) reprinted from ''Mechanical Integrity of Transparent Conductive Oxide Films for flexible Polymer-Based Displays'', vol 460, Leterrier Y., Médico L., Demarco F., Månson J.-A. E., Bouten P., DeGoede J., Nisato G., Nairn J. A., ''Thin Solid Films'', pp. 156–166 (2004) with permission from Elsevier. Parts (c) and (f) reproduced by the permission of SVC

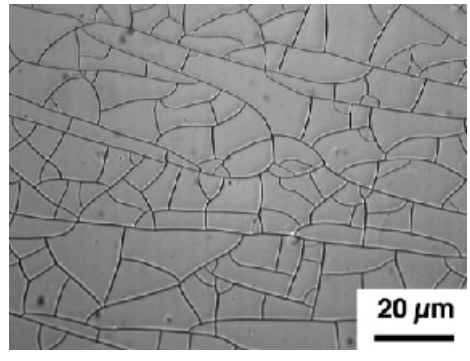


Figure 6.6 Biaxial tensile failure of a 100 nm thick ITO coating on polymer substrate

Petitioner Samsung Ex-1011, 0134

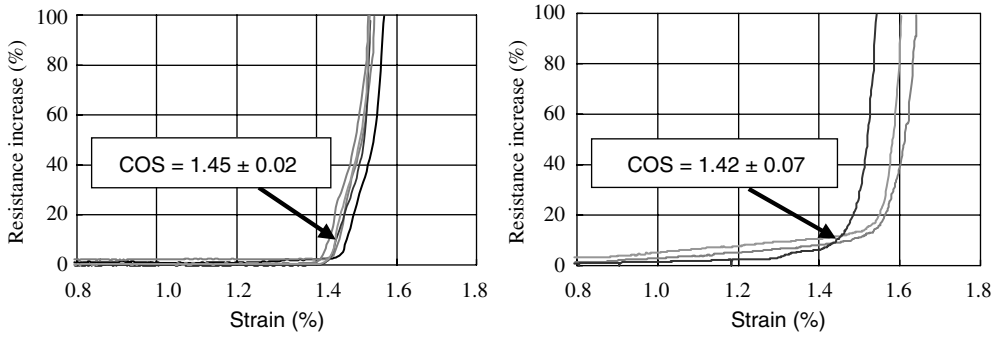


Figure 6.7 Normalized resistance change during bending (left) and tensile (right) loading of 100 nm thick ITO coatings on polymer films, in the vicinity of the critical strain for failure. Reproduced by the permission of SVC

The thickness of the ITO has a significant influence on the critical strains, as shown in Table 6.3 for three thicknesses of ITO and measured with both experimental techniques. The influence of the ITO thickness on cracking is investigated in Section 6.2.5.

Failure of brittle layers is usually a statistical process dominated by the presence of defects in the material, e.g. particles or small surface flaws. As Figure 6.5 shows, thin brittle

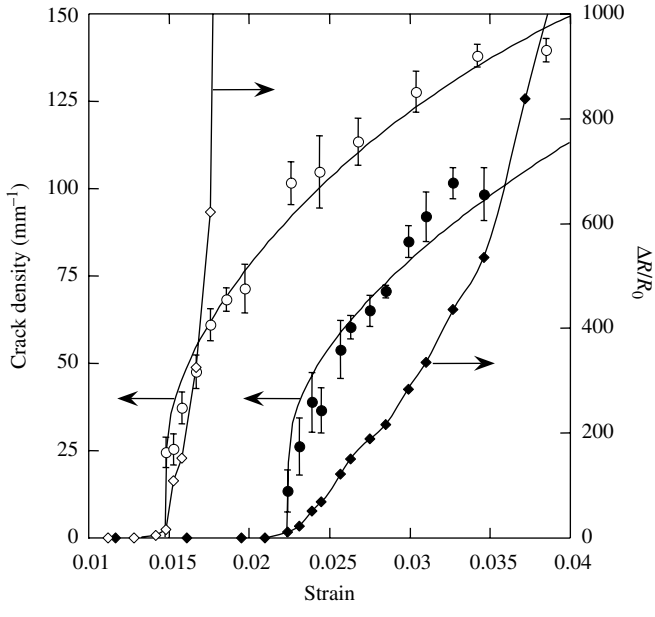


Figure 6.8 Density of tensile cracks and normalized resistance change during tensile loading of ITO coatings on polymer substrate. The coating thicknesses are (•) 50 nm and (○) 100 nm. Reprinted from ''Mechanical Integrity of Transparent Conductive Oxide Films for flexible Polymer-Based Displays'', vol 460, Leterrier Y., Médico L., Demarco F., Månson J.-A. E., Bouten P., DeGoede J., Nisato G., Nairn J. A., ''Thin Solid Films'', pp. 156–166 (2004) with permission from Elsevier

Petitioner Samsung Ex-1011, 0135

Table 6.3 Crack onset strain (COS) of ITO layers

ITO thickness (nm)	Bending COS ($\Delta R/R_0 = 10\%$)	Tensile COS ($\Delta R/R_0 = 10\%$)
50	1.77 ± 0.03	1.83 ± 0.15
100	1.45 ± 0.02	1.42 ± 0.07
200	1.56 ± 0.03	1.45 ± 0.16

Reproduced by permission of SVC

coatings do not seem to be an exception. A defect leads to concentration of stresses. This stress concentration depends on the size and shape of the defect. When the (local) stress exceeds a certain limit, a crack initiates at this ''weak link'' in the structure. The stochastic mechanism of crack initiation can be well described using weakest link statistics, for instance Weibull statistics (Lawn 1993). When plotted in a Weibull plot, the cumulative failure probability against the failure strain gives a straight line. The slope of this line, the Weibull modulus m, is related to the width of the failure strain distribution; for brittle materials like bulk ceramics and glasses, it is typically in the range $5 \leq m \leq 12$.

This Weibull statistic was used to analyze the results of the two-point bending test for uniform ITO layers of two different substrates (A and B). As Figure 6.9 shows, the conductive failure (COS) data are well described with a Weibull distribution. Using a linear fit to the data, the characteristic failure strain ε_0 (i.e. at 63% failure probability) and the Weibull modulus m are obtained: $\varepsilon_0 = 1.44\%$, $m = 55$ for A; $\varepsilon_0 = 1.56\%$, $m = 58$ for B. The values obtained in this present case ($m = 50$–60) are exceptionally high, compared to the typical values for brittle ceramic materials. This narrow distribution of failure strains means that either there is a very well-defined ''weakest link'' in the ITO layers, or the failure mechanism is governed by another well-defined mechanism. Further investigation on this issue is detailed in the next section.

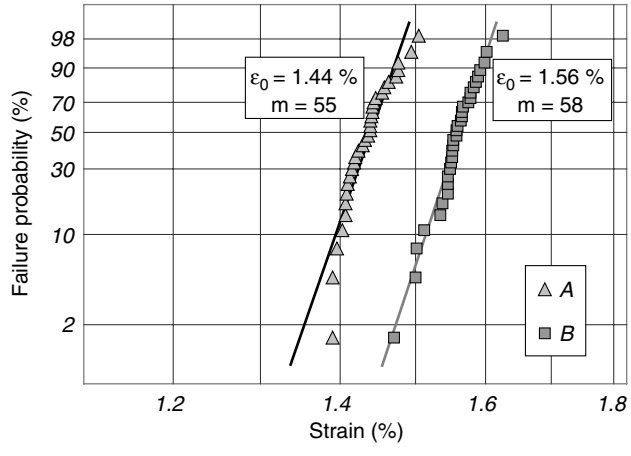


Figure 6.9 Weibull plot showing failure strain of ITO on two composite polymer substrates

Petitioner Samsung Ex-1011, 0136

6.2.4 Experimental Analysis of Patterned Layers

In a display, the ITO layer is often patterned into narrow lines, whose failure behavior might differ from that of uniform layers investigated in above sections. Previous work demonstrated that failure strain distributions of rather wide etched lines (0.3–10 mm) with good edge quality compared quite well to those of uniform layers cut from coated foils, characterized by poor edge quality (Bouten 2003). Apparently the edge quality does not affect the COS.

New data was obtained by testing narrow ITO lines (10–300 μm wide) with the two-point bending method. For each line width, 30 samples (15 mm × 75 mm) containing a single ITO line are tested. The results are summarized in the Weibull plots in Figure 6.10, and compared with data obtained for a uniform ITO layer. The Weibull modulus m and the characteristic failure strain ε_0, fitted from experimental data, are reported in Table 6.4.

The results show a small systematic increase of the characteristic failure strain ε_0 with decreasing line width. More noteworthy is the larger scatter of the measured failure strain for the narrow lines, as reflected by lower values for the Weibull modulus m. These values compare well with those of bulk ceramics ($5 \leq m \leq 12$), where the defect size distribution controls the failure strain.

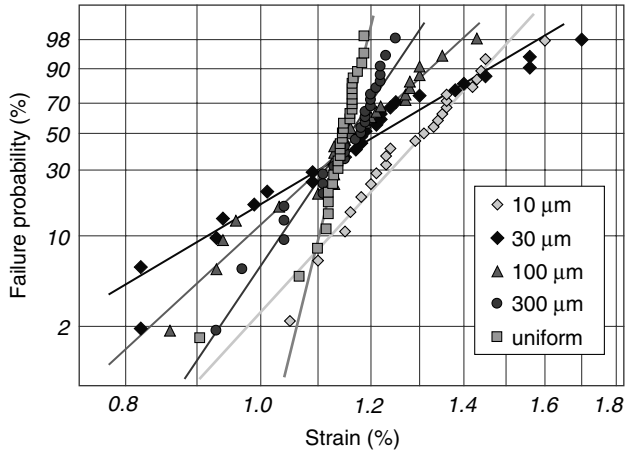


Figure 6.10 Weibull plot showing failure strain of ITO lines of different width

Table 6.4 Weibull values for different line widths

Width (μm)	Weibull modulus m	ε_0 (%)
10	12.1	1.35
30	6.6	1.29
100	10.3	1.22
300	16.5	1.19
15 000	45.6	1.16

Petitioner Samsung Ex-1011, 0137

6.2.5 Discussion on Failure Mechanics

In failure analysis of brittle materials a distinction is made between the crack initiation stage and the crack propagation stage, where the initial crack grows to its full size. The failure of bulk brittle materials is dominated by the initiation of cracks that immediately propagate to full size. Thin brittle films show some significant differences in failure behavior with these bulk materials: the presence of quite long stable cracks, and crack propagation as a dominant failure mechanism will be discussed in this respect.

During crack propagation a new crack surface is formed requiring new surface energy, which is driven by the elastic energy released from the material. The crack propagates when G, the released elastic energy, becomes larger than Γ, the fracture surface energy: $G \geq \Gamma$. The energy release is related to the elastic strain energy $G_0 = \sigma^2 h/2E_{\text{eff}}$ stored in the elastically loaded layer (h is the layer thickness, σ is stress in the layer). Note that σ denotes the total stress in the layer and is a combination of the internal stresses σ_{i} and the external applied stress σ_{appl} ($\sigma = \sigma_{\text{appl}} + \sigma_{\text{i}}$). The energy released for the propagation of a crack in a stressed thin layer on a substrate is

$$G = 2ZG_0, \tag{6.2}$$

where Z is a constant (Hutchinson and Suo 1992). The magnitude of constant Z depends on the crack type and the elastic mismatch of substrate and layer. When layer and substrate have identical elastic properties (Dundurs parameter $\alpha = 0$), the constant $Z = 1.976$. For an ITO layer on HC ($\alpha = 0.90$) and on base polyester ($\alpha = 0.95$), one obtains $Z = 8.48$ and $Z = 13.24$, respectively (Beuth 1992).

Assuming a constant fracture surface energy, Equation (6.2) predicts a crack propagation stress σ_{p}, proportional to $1/\sqrt{Z}$. This leads to a 20% lower crack propagation stress for ITO on base substrate ($\alpha = 0.95$) compared to ITO on hardcoat ($\alpha = 0.90$), which corresponds with the experimental results in a recent study (Leterrier *et al.* 2004).

Equation (6.2) also predicts that the critical stress, hence the critical strain, will decrease with the thickness of the ITO layer as $1/\sqrt{h}$. This decrease seems not to be corroborated by the COS data in Table 6.3. The samples, however, contain different levels of internal stresses (σ_{i}), which determined from the curvature of the film sample were found to be compressive and increasing with layer thickness (Izumi *et al.* 2002). With E_{eff} the internal strain (ε_i) can be calculated. A combination of COS and ε_i gives the intrinsic crack onset strain COS*, a fundamental cohesive property of the material:

$$\text{COS} = \text{COS}^* - \varepsilon_i. \tag{6.3}$$

As shown in Figure 6.11, the decrease of COS* with ITO thickness follows the predicted $1/\sqrt{h}$ scaling, supporting a propagation model for conductive ITO failure. This line represents a constant crack propagation energy (6.2). For the combination of ITO and base substrate, $Z = 13.24$ and $G = 21$ J/m^2. Figure 6.11 and Equation (6.3) indicate clearly the beneficial influence of the internal compressive strain when the coated substrate is loaded in tension.

Petitioner Samsung Ex-1011, 0138

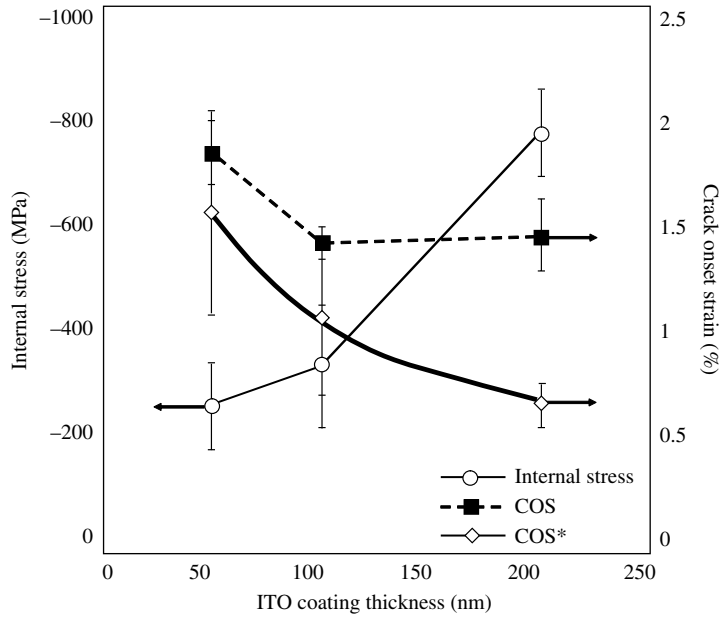


Figure 6.11 Coating thickness dependence of internal stress, measured crack onset strain (COS) and intrinsic crack onset strain (COS^*). The thick continuous line is a power-law fit to the intrinsic crack onset strain data. Reproduced by the permission of Elsevier and SVC

In the initiation-dominated failure of bulk brittle materials, the initiated cracks are unstable and propagate immediately to the full size of the sample. Consequently, failure is governed by the number and size of the defects present in the material. For thin ITO brittle films, however, the failure strain was independent of the rather big defects in the edge of the ITO layer (Bouten 2003). Moreover, the width of the strength distribution for the wide lines and uniform layers is very small, with very high Weibull moduli ($m > 20$, Figure 6.10). Such high values are certainly not characteristic for a size distribution of weakest spots, but are determined by a clearly defined crack propagation limit ε_{p}.

A recent numerical investigation (Ambrico and Begley 2002) predicts the presence of long stable cracks at strain levels below a crack propagation limit ε_{p}. The maximum stable crack length a_p was found to scale with layer thickness h and to be a function of Dundurs' parameter α. The transition to instable crack propagation occurs for $\alpha = 0$ when a_p/h is approximately equal to 5, whereas for $\alpha > 0.90$ it is at $a_p/h > 40$. The very long stable cracks in ITO on base substrate ($> 50\,\mu$m, Figure 6.5(c) and (d)) confirm the model for $\alpha > 0.90$.

The consequence of (i) the characteristic defect sizes in the micrometer range and (ii) the stable-to-unstable transition for cracks of length 10–100 μm could be considerable when ITO is patterned in narrow lines, whose width may interfere with crack initiation and propagation modes. To explain the different behavior observed in the tests with wide and narrow ITO lines (Figure 6.10), we can use the schematic diagram in Figure 6.12.

Petitioner Samsung Ex-1011, 0139

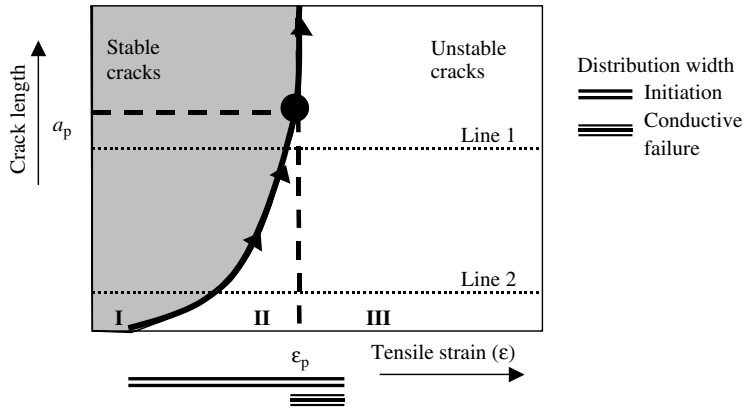


Figure 6.12 Schematic representation of the growth size at increasing strain levels

In this plot of crack length against tensile strain, two regimes are distinguished: a regime where cracks are stable (the shaded area) and one where the cracks are unstable. The solid line represents the unstable-to-stable transition. In the stable area (region I) the cracks will maintain their length until, with increasing tensile strain, they meet the curved solid line. There the crack will grow stably with increasing tensile strain, as the arrows in Figure 6.12 indicate. Upon the crack length exceeding the maximum stable crack length a_p, and the critical crack propagation level ε_p, the crack becomes unstable and grows to the full sample size. In the unstable region, the cracks increase in length (at constant strain) until they meet a stable length (region II, $\varepsilon < \varepsilon_p$) or span the whole layer width (region III).

From stress concentrations around defects in the coating (e.g. dust particles), cracks will initiate. The crack initiation strain depends strongly on the size and the type of defect. To illustrate the width of the distribution of crack initiation strains, a double line is drawn beneath the horizontal axis of Figure 6.12. Depending on the strain at initiation, crack growth could follow three types of route:

- At low strains, the crack might not grow further until at higher strain the stable crack growth curve leaves the horizontal axis.
- At medium strains, the crack grows instantly to the stable crack growth curve (solid line) which it will follow until failure at $\varepsilon = \varepsilon_p$.
- At strains above ε_p, the crack will be completely unstable and grow instantly to the full width of the layer.

For a major part of the initiations, the cracks follow the stable crack growth curve and the final failure of the crack to the size of the sample occurs around the crack propagation limit ε_p. The measured failure distribution (the triple line below the horizontal axis in Figure 6.12) is thus considerably narrower than the crack initiation distribution (the double line).

For narrow lines, where the line width is lower than the maximum stable crack length a_p, the influence of crack initiation increases. With decreasing line width (e.g. from line 1 to line 2 in Figure 6.12), an increasing part of the cracks initiated in regime II lead to

Petitioner Samsung Ex-1011, 0140

immediate failure, since they try to obtain a stable crack length that is longer than the line is wide. Since propagation does not play a role in the ITO line failure here, with decreasing line width, the failure distribution approaches that of a purely initiation-dominated, wide, distribution. This effect is assisted by the decreasing surface area of the ITO with thinner lines, which means a decreasing probability of finding defects per length of the line. This leads to a general shift of the crack initiation probability to higher strain levels.

Both effects are quite clearly observed in Figure 6.10: the wide lines show a narrow distribution in failure strain, determined well-defined crack propagation limit ε_p. The narrow lines show a much wider distribution in the failure strain; crack initiation controls the (electrical) failure of the conducting line. Due to the defect density distribution, the critical cracks in the narrow lines on the tested samples initiate in some of the samples below ε_p, and in other samples above ε_p.

6.3 Failure of Brittle Layers under Compressive Stress

6.3.1 Some Pictures of Characteristic Failure Modes

Thin brittle coatings loaded in compression show a specific type of failure – a combination of delamination and buckling. Figure 6.13(a) shows an atomic force microscope (AFM) image of a well-developed buckling pattern in a biaxial compressively loaded thin layer (100 nm ITO on a polymer substrate). The layer is locally released from the substrate, and deflects upward. The pattern shows an in-plane periodic variation, the so called telephone cord structure, which is characteristic for thin films loaded in biaxial compression. As with tensile failure, this type of pattern starts at a local defect, for instance a hole in the layer (Figure 6.12(b)). At sufficiently high compressive strain the pattern develops in time.

The length scale of the delamination patterns depends on the stiffness of the coating (Figure 6.14). Here parallel ITO lines on a polymer substrate are partly covered by parallel metal lines. A fine-pitch buckling pattern can be seen in the ITO lines, while a significantly coarser buckling pattern is present where the metal stiffens the ITO below. The pattern is not present below the part of the metal line, directly deposited on the substrate (Figure 6.14).

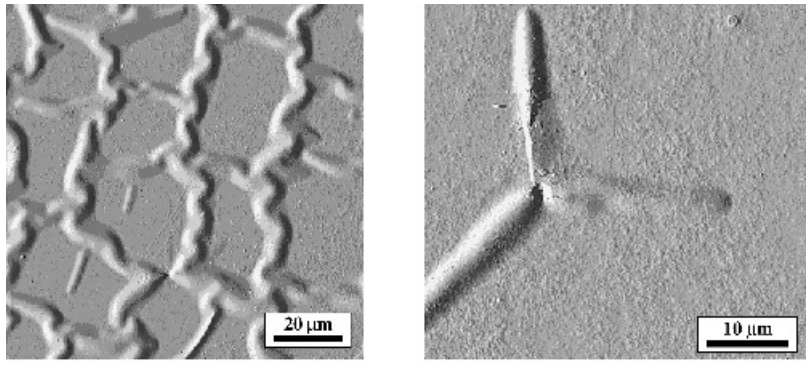


Figure 6.13 AFM images of buckling patterns: (a) biaxially loaded layer (b) initiation point

Petitioner Samsung Ex-1011, 0141

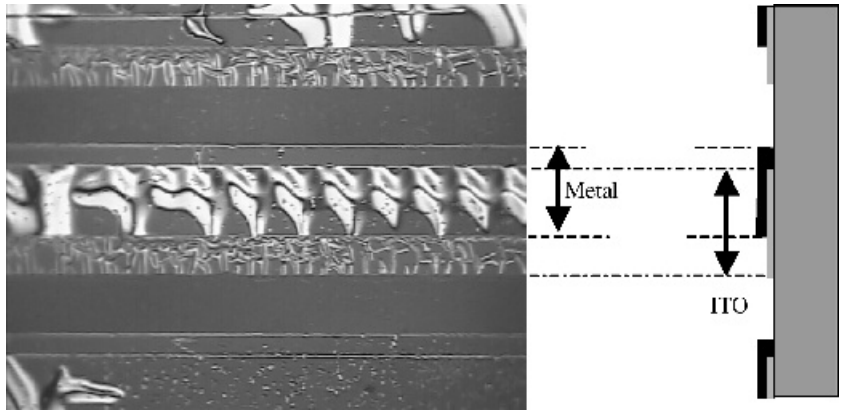


Figure 6.14 Different buckling sizes below 100 nm ITO and 600 nm metal on top of ITO

6.3.2 Mechanism of Buckling Failure

Figure 6.15 shows a schematic cross section of the delaminated buckle. This buckling phenomenon is governed by an energy balance, very much like the failure of the layer in tensile stresses. The buckling release elastic energy from the compressively strained coating and this energy is used to create new free surface by peeling the coating from the substrate surface. It might also be used partially to crack the buckled layer.

For buckling to start the elastic energy released in the buckling process should be larger than the surface energy needed for forming the new free surface. This situation is represented as follows:

$$C_c(\alpha)\varepsilon^2 E_c hb - C_s(\alpha)\varepsilon^2 E_s b^2 \geq 2\Gamma b. \tag{6.4}$$

The left-hand side represents the net release in elastic energy. The first term denotes the elastic energy released from the coating. This energy can be obtained by integrating the product of stress ($\sigma = E_c\ \varepsilon$) and strain ($\varepsilon$) over the volume of the coating (roughly $2bh$). The energy is, however, not only released from the buckle itself. As Figure 6.15 indicates, the buckle allows the coating next to the buckle itself to relieve stress. Since this amount

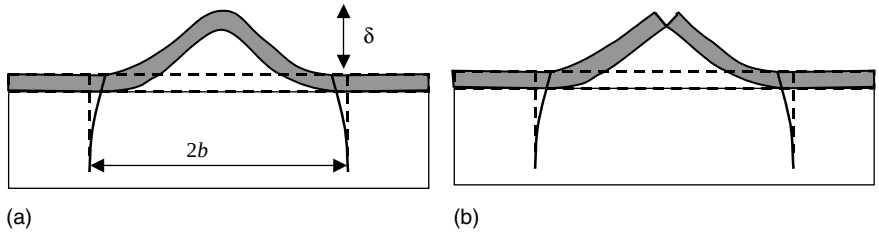


Figure 6.15 Schematic cross section of buckling patterns

Petitioner Samsung Ex-1011, 0142

depends on the difference in Young's moduli between coating and substrate, the coefficient C_c is a function of Dundurs' parameter α. Since the coating next to the buckle itself relieves stress, it deforms the substrate near the edges of the buckle as sketched in Figure 6.15. The energy required for this is taken into account in the second term of Equation (6.4). Being elastic strain energy, this term resembles the first term, except that the thickness of the deformed volume in the substrate is assumed to scale with the length of the buckle (b) and of course the material parameters differ. Again the proportionality constant C_s, introduced to incorporate all other parts of the term, can be expected to be a function of Dundurs' parameter α. The total released elastic energy now needs to exceed the energy required to form the new free surface ($2b\Gamma$ with $2b$ the length of the new surface and Γ the fracture surface energy). In this schematic model we have neglected the elastic energy needed to deform the coating to the shape of the buckle, but also possible cracking in the buckle's tip. Neither is mode mixing around the tip taken into account (Yu and Hutchinson 2002).

The model in Equation (6.4) displays a maximum in the released elastic energy as function of the buckle length (b), which will be the effective buckle length that is realized. This buckle length increases with the Dundurs parameter α and the coating thickness. The coating thickness dependence of the buckle length is in accordance with the observation in Figure 6.14: the buckling pattern below the metal–ITO stack is significantly coarser than that below the ITO layer only. Due to the better adhesion of metal on base substrate (higher Γ) and assisted by a lower Dundurs parameter α, no buckling is observed in the region where the metal directly contacts the substrate.

The first model on delamination buckling of coatings has been derived for materials with equal elastic moduli (Dundurs parameter $\alpha = 0$). Recent work treats also situations for hard thin layers on compliant substrates (Cotterell and Chen 2000; Yu and Hutchinson 2002). This work on compliant substrates shows clearly that the released elastic energy on buckling can be significantly larger than the energy present in the hard layer itself (of width $2b$) before buckling (C_c up to 5).

6.3.3 Buckling Strain

Although the model in the previous section gives some basic insights into the mechanism of delamination buckling, it is very useful to determine the onset of buckling in a practical situation. There are several ways to estimate the strain leading to buckling. In a first approach the length difference between the buckle width $2b$ and the curve length of the buckle itself can be determined from images like Figure 6.13. Both parameters are determined by fitting the profile of a buckle with its analytical shape: $\delta = \delta_0\,[1 - \cos(\pi x/b)]/2$. The values obtained for the situation in Figure 6.13 are $2b = 7.9 \pm 0.5\,\mu\text{m}$ and $\delta_0 = 0.68 \pm 0.06\,\mu\text{m}$. The difference in length of the base of the buckle ($2b$) and its curve length may be interpreted as a relaxed compression $\varepsilon = 2.47(\delta_0/2b)^2$ resulting in $\varepsilon = 1.8\%$. Although straightforward, this approach leads to an overestimate of buckling strain, since it neglects the strain release in the coating next to the buckle itself, as shown in Figure 6.15.

Figure 6.16 illustrates a second approach to determining the buckling strain. It shows a buckling pattern of a 100 nm thick ITO layer on a polymer substrate that is observed when

Petitioner Samsung Ex-1011, 0143

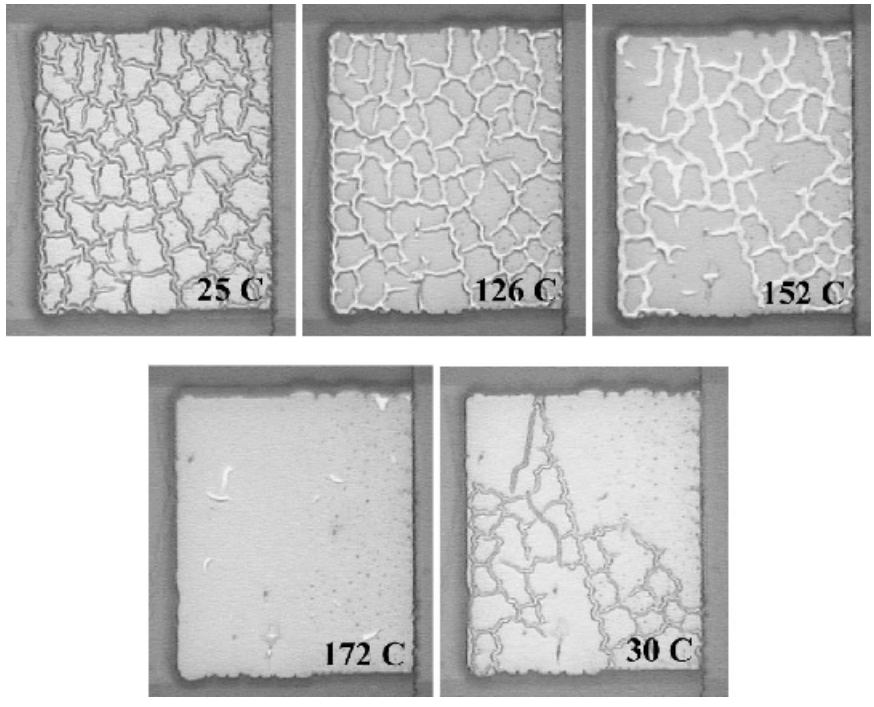


Figure 6.16 Buckling pattern during heating and subsequent cooling

heated on a hot-stage microscope to 210 °C, and subsequently during the cooling cycle. The size of the ITO area is 230 μm × 250 μm and it is bounded by polymer walls. At a temperature of 120 °C the pattern starts to disappear, the major part has disappeared around 160 °C and at 200 °C it has disappeared completely. During and after cooling, the pattern partly reappeared in its original form. According to the thermal expansion difference between base polymer and ITO coating (Table 6.1), a strain difference $\Delta\varepsilon = 0.80\%$ is calculated at a 140 K temperature increase, which might indicate that the compressive strain is driving the buckling.

However, when determining the compressive strain in 100 nm ITO layers from curvature measurements of nonbuckled ITO-coated polymers, a compressive strain of about 0.3% is obtained at room temperature. This is significantly lower than the values obtained from the hot-stage microscopy results and profile measurements.

6.3.4 Discussion

Estimating the buckling strain is not straightforward. All the methods here have some interpretation issues, some of them caused by the thermomechanical behavior of the substrate. Measuring the profile of the buckle is direct, but must be compensated for the strain release of the coating adjacent to the buckled part. Although ready-to-use equations have not been derived yet, model studies on buckling of thin coatings on compliant

Petitioner Samsung Ex-1011, 0144

substrates have been performed (Cotterell and Chen 2000; Yu and Hutchinson, 2002). They show that the total amount of elastic energy released by the buckle (G) is significantly larger than the amount of energy stored in the buckled part of the coating (G_0). This amount increases with the increasing elastic mismatch between a hard coating and a compliant substrate. For a Dundurs parameter $\alpha = 0.95$ (ITO on base polymer, Table 6.1) a factor around $G/G_0 = 5$ is presented. This means that 4/5 of the energy release comes from the nondelaminated part of the coating, which pushes the edges of the buckle inward as illustrated in Figure 6.15. As a crude approximation one could say that by measuring the difference between buckle width and buckle curve length one overestimates the buckling strain by the square root of this factor (elastic energy is proportional to strain squared), This makes the buckling strain closer to 0.8 % than the 1.8% calculated in the previous section.

As sketched in Equation (6.4), surface or adhesion energy Γ – the quality of the adhesion between the coating and the substrate – is a very important parameter in preventing buckling. For coating and substrate of equal elastic modulus (Dundurs' parameter $\alpha = 0$), Hutchinson and Suo (1992) gives simple relations for the adhesion energy Γ with coating layer thickness, the shape of the buckle (height δ_0 and width $2b$) and the stress in the coating before buckling. In the absence of relations for $\alpha > 0$, we will estimate the adhesion energy from Equation (6.4). For this we will use the strain estimate of 1.8%. Although wrong for estimating the strain before buckling, together with $C_c = 1$, this should yield a reasonable estimate of the energy released by the buckle. Neglecting the second term in Equation (6.4), the adhesion energy is estimated to be about 1.9 J/m^2.

This refers to a rather poor adhesion of the ITO layer, which is, unfortunately, not an exception for displays substrates. In comparison Cotterell and Chen (2000) report an adhesion energy $\Gamma = 32$ J/m^2 for a 100 nm ITO layer on PET film. The cracking of the buckled layer, shown in their experiments, together with the significantly lower delamination width ($b \sim 1\mu m$) compared to 4 μm shown here in Figure 6.14 are in agreement with higher adhesion energy.

Where increasing the adhesion energy is the prime parameter for increasing compressive behavior of brittle coatings, decreasing the elastic mismatch between substrate and coating can also have a significant effect. Compliant substrates allow the elastic energy in the coating to concentrate when released in a buckle. This leads to a lower critical buckling strain for more compliant substrates ($\alpha \rightarrow 1$) at similar adhesion energy. This effect might be reduced by placing matching layers with intermediate elastic properties between the substrate and coating (e.g. a hardcoat).

The low strain levels for initiation of buckling delamination found here are a reason for concern, since they can be easily obtained by the combination with the thermal expansion mismatch between coating and substrate and elevated processing temperatures. For example, an SiN_x layer applied at 120 °C on the base polymer substrate results in a compressive strain of 0.55% in the thin layer at room temperature (Table 6.1). This internal compressive strain in the coating is sometimes high enough to initiate buckling delamination at one of the interfaces in the multilayer substrate. The concern increases since it is known that chemicals used in display making might facilitate the delamination processes. Water, for example, leads to reactions at a crack tip, resulting in a serious reduction of the safe service stress of adhesive joints (Kinloch 1987), and glass (Lawn 1993). When the buckling process is driven by chemically assisted reaction, a significantly lower adhesion energy Γ is expected than determined on dry samples.

Petitioner Samsung Ex-1011, 0145

6.4 The Failure Situation in a Display

6.4.1 Summary of the Failure Results

On the basis of conductivity measurements and optical detection, ITO failure is observed at strain levels of about 1%, which is similar to that measured with other brittle layers of comparable thickness (Leterrier, 2003). At lower strain levels, already some stable ITO cracks of limited length are observed, which develop to cracks over the full width of a conducting line above a certain critical strain level. Both the microscopic observation and resistance measurements on narrow ITO lines show that these stable ITO cracks are in the range 10–300 μm. The measurements and theory indicate that the onset of ITO conductivity loss in tension can be delayed by

- reducing the ITO layer thickness;
- using a high-modulus but nonbrittle undercoat for the ITO;
- introducing a moderate level of compressive stress in the ITO layer.

From the electrical measurement data it seems that the minimum achievable radius of curvature for the 100 nm thick ITO-coated film on 100 μm thick polymer substrate could be down to about 3.5 mm. However, this conclusion should be treated with great care. The results show that well before conductive failure occurs (as measured through the crack onset strain), small cracks have already formed; the COS should in fact be renamed the crack propagation strain (CPS). Such flaws do not severely alter the electrical properties of the ITO layer, in contrast to other functional properties like blocking gas permeation (Rossi and Nulman 1993). Nevertheless, such stable cracks are likely to grow under fatigue loading, or as a result of viscoelastic, time-dependent processes such as creep, common to polymer materials used as substrate material. In a curved display, where the layered substrate structure is subjected to constant strain, creep phenomena might lead to ITO film failure earlier than expected from the types of measurement reported above. It is advisable to carry out specific studies on this issue.

In compression loading, the thin brittle layers show delamination and buckling, where the quality of the adhesion between layer and substrate determines the strain at which buckling appears. For rather poor adhesion, buckling is frequently observed without the application of additional external strain. Process-induced thermomechanical stress is then sufficient to develop the buckling pattern. Although the data is still limited, there are indications that compressive failure by buckling occurs at similar or lower absolute strain levels than those by tensile failure. Considering that the coatings often bear compressive stresses from their deposition process, the applied stresses at failure might be considerably lower than those for tensile failure.

Upon pure bending of a symmetrical substrate, the tensile strains at the outside of the curve are equal to the compressive strains at the inside, therefore compressive failure on the inside might occur before tensile failure on the outside. This would make compressive failure the dominant failure mechanism for a thin brittle film, while for bulk brittle material tensile failure is the dominant mechanical failure condition. This difference is caused by compressive failure of coatings not being an intrinsic material property but an adhesive failure between coating and substrate.

Petitioner Samsung Ex-1011, 0146

6.4.2 More Complex Situations

The analysis presented up to now is mainly limited to the testing of simple structures in well-controlled situations. It has been largely limited to simple elastic deformations. A number of factors complicate the situations in real applications of flexible displays:

- The substrates are multilayer composites, consisting of inorganic and polymeric materials. Due to (high-temperature) processing steps and (thermal) history, a complex stress distribution might be present in the structure that could influence the failure strain (positively or negatively).
- This stress distribution can also be time-dependent, due to a time-dependent behavior of polymeric materials in the stack. Origins of this time dependence may be creep and relaxation, volume changes due to solvent (water) uptake and release, and physical aging of the polymeric matrix.
- A temperature change leads to redistribution of the stresses, and to changes in the time constants of relaxation processes, for example. A consequence of all these processes is that the stress situation in critical layers changes with time.

A constant tensile load on a multilayer substrate in a curved display might result in creep behavior of the polymer. Since inorganic materials do not creep, the stress and strain on a brittle functional layer (e.g. the gas barrier) increases with time. They may exceed a critical limit and lead to failure after a certain loading time.

Although this chapter focuses on failure of brittle layers, this is not the only failure that is important in the mechanical reliability of flexible display cells. The base polymer of the substrate is generally a high-modulus polymer. These materials also exhibit brittle failure when they are under load and have cracks that are too large or after a slow viscoelastic crack growth. These cracks often originate out of edge damage from cutting the substrate.

Bending a display or a display film does more than to elongate the outer substrate and to compress the inner substrate. At the display edges (near the seal line for a display cell) or anywhere in the display where curvature changes, there are supplementary shear stresses in the central plane of the display or film. These might be very significant and add to loading by the bending itself and the residual stresses that are present. Depending on the loading conditions, a peel component may also be present in this load. Adhesion failure often starts preferentially at these locations.

6.4.3 What Does it Mean for a Product?

Bending is quite a favorable type of deformation for flexible displays. Although significant tensile and compressive strains are achieved at bending to small radii – a 100 μm thick substrate achieves surface strains of 1% at a curvature radius of 5 mm – there are ways to reduce the strain on brittle layers.

Critical layers in displays can be positioned near the centre of the display. For symmetric cell geometries, this brings the layers close to the neutral plane, which can reduce the strains on the layers by an order of magnitude.

Petitioner Samsung Ex-1011, 0147

At equal tensile and compressive strains, we have seen that the adhesion issues between layers make compressive failure an expected dominant failure mode, especially when considering the additional shear strains near display edges or seal lines, for example. With the complexity of the layer structure in the display substrate and the even greater complexity in the complete display, adhesion between all layers should be a principal concern of any work on flexible displays.

But it is not only the failure mechanisms of the thin layers that have to be taken into account. Failure characteristics of the base substrate and the adhesive seal are also important in the reliability of the flexible display. And it is often the interactions between the materials that determine the failure modes.

6.5 Conclusions

In tension, conductive failure of ITO, measured by its resistivity increase, is predominantly propagation controlled. The failure strains are measured at around 1% and exhibit a narrow failure distribution.

Failure, however is already initiated at lower strains, leading to stable cracks of finite length that contribute weakly to resistivity increase. These small cracks control loss of functional properties such as gas permeation of barrier layers and they do determine the failure of narrow ITO lines. Besides initiation at strain levels below 1%, the distribution of crack initiation is considerably wider than for conductive failure, requiring an additional safety margin for product reliability.

In compression, hard coatings show a buckling delamination phenomenon, which can take place at comparable or lower strain levels than tensile failure. There are reasons to be concerned since these strain levels can easily be reached by the combination of temperature changes and the differences in coefficient of thermal expansion (CTE) of coating and substrate.

For both tensile and compressive stresses failure can be postponed by reducing the (ITO) layer thickness, using a high-modulus but non-brittle undercoat between ITO and substrate and introducing a moderate level of internal stress in the coating opposite to the stress that will be applied externally. This is only possible when the applied stress is known in advance.

So far it seems that the main focus of the literature has been tensile failure of brittle layers on polymer substrates. The analysis in this chapter shows that compressive failure is a very significant failure mechanism, possibly dominant over tensile failure.

Acknowledgements

The authors are indebted to the IST program of the European Union (IST-2001-34215 FLEXled) for funding this work, and to the companies Ferrania Imaging Technologies, Vitex Systems and Unaxis Balzers (Display Division) for the supply of film samples. They would like to thank Giovanni Nisato for all his support and scientific input, Léonard Médico, Fabio Demarco and Judith de Goede for experimental support, Niklas Jansson, Marcel van Gils and Peter Timmermans for numerical simulation work and Kees Mutsaers for sample preparation.

Petitioner Samsung Ex-1011, 0148

References

Ambrico, J. M. and Begley, M. R. (2002) The role of initial flaw size, elastic compliance and plasticity in channel cracking of thin films. *Thin Solid Films* **419**, 144–153.

Andersons, J., Leterrier, Y. and Fescenko, I. (2003) Analysis of the initial fragmentation stage of oxide coatings on polymer Substrates under biaxial tension. *Thin Solid Films* **434**, 203–215.

Beuth, J. L. Jr (1992) Cracking of thin bonded films in residual tension. *International Journal of Solid Structures* **29**, 1657–1675.

Bouten, P. C. P. (2002) Failure test for brittle conductive layers on flexible display substrates. *Proceedings of Eurodisplay* **2002**, Nice, pp. 313–316.

Bouten, P. C. P. (2003) On integrity of flexible displays. *Proceedings of Fracture Mechanics of Ceramics 8*, Houston, forth coming.

Cotterell, B. and Chen, Z. (2000) Buckling and cracking of thin films on compliant substrates under compression. *International Journal of Fracture* **104**, 169–79.

Hutchinson, J. W. and Suo, Z. (1992) Mixed mode cracking in layered materials. *Advances in Applied Mechanics* **29**, 63–191.

Izumi, H., Adurodija, F. O., Kaneyoshi, T., Ishihara, T., Yoshioka, H. and Motoyama, M. (2002) Electrical and structural properties of indium tin oxide films prepared by pulsed laser deposition. *Journal of Applied Physics* **91**, 1213.

Kinloch, A. J. (1987) *Adhesion and Adhesives*, Chapman and Hall, London.

Lawn, B. (1993) *Fracture of Brittle Solids*, 2nd edn, Cambridge University Press, Cambridge.

Leterrier, Y., Pellaton, D., Mendels, D. A., Glauser, R., Andersons, J. and Månson, J.-A. E. (2001) Biaxial fragmentation of thin silicon oxide coatings on poly(ethylene Terephthalate). *Journal of Materials Science* **36**, 2213–2225.

Leterrier, Y., Médico, L., Bouten, P. C. P. and De Goede, J. (2003a) Layer mechanics of optimized materials, IST-2001-34215-FLEXled report D17.

Leterrier, Y. (2003) Durability of nanosized oxygen-barrier coatings on polymers. *Progress in Material Science* **48**, 1–55.

Leterrier, Y., Fischer, C., Médico, L., Demarco, F., Månson, J. -A. E., Bouten, P., Goede, J. de, Nisato G. and Nairn, J. A. (2003b) Mechanical properties of transparent functional thin films for flexible displays. *Proceedings of the 46th SVC Annual Technical Conference, San Francisco*, May 3–8, p. 169.

Leterrier, Y, Médico, L., Demarco, F., Månson, J. A. E., Escola Figuera, M., Kharrazi, Olsson, M., Betz, U. and Atamny, F. (2004) Mechanical integrity of transparent conductive oxide films for flexible polymer-based displays. *Thin Solid Films*, **460**, 156–166.

Rossi, G. and Nulman, M. (1993) Effect of local flaws in polymeric permeation reducing barriers. *Journal of Applied Physics* **74**, 5471–5475.

Townsend, P. H., Barnett, D. M. and Brunner, T. A. (1987) Elastic relationships in layered composite media with approximation for the case of thin-films on a thick substrate. *Journal of Applied Physics* **62**, 4438–44.

Yu, H. and Hutchinson, J. W. (2002) Influence of substrate compliance on buckling delamination of thin films. *International Journal of Fracture* **113**, 39–55.

Petitioner Samsung Ex-1011, 0149

7

Stability of Externally Deformed ITO Films

Jeong-In Han

Information Display Research Center, Korea Electronics Technology Institute

7.1 Introduction

Flexible displays have been one of the most vital issues in the display industry during the past decade due to their potential advantages such as low weight, compactness, robustness and most of all, vast mechanical and design flexibilities compared to the conventional glass-based displays. These flexibilities will open a new era in display technology. Rollable displays, wearable displays and displays with various shapes (not just rectangular) will become a reality using this technology.

At an early stage of the development, simple passive matrix liquid crystal displays (LCDs) using twisted nematic, super twisted nematic or ferroelectric liquid crystals were intensively studied. They were mostly developed for small size mobile phones, smartcards and personal digital assistant (PDA) devices (Matsumoto *et al.* 1993; Wenz and Aastuen 1993; Gardner and Wenz 1995; Park *et al.* 2000). The driving force behind these developments was thin, lightweight, low-power displays matching the resolution of cathode-ray tubes (CRTs). However, in order to satisfy the growing demands of multicolor, high-definition and high-performance displays, recent works mainly focus on active matrix flexible displays using amorphous silicon (a-Si) or low-temperature polycrystalline silicon (LTPS) thin film transistors and they have been successfully demonstrated by a number of major flat panel display manufacturers (Utsunomiya *et al.* 2003; Asano *et al.* 2003; Inoue *et al.* 2003).

Flexible Flat Panel Displays Edited by G. P. Crawford
© 2005 John Wiley & Sons, Ltd., ISBN 0-470-87048-6

Petitioner Samsung Ex-1011, 0150

To realize a mechanically stable display, several issues have to be settled beforehand. Firstly, as the present flexible display technology still uses very similar processes which are compatible with the conventional glass-based technology, appropriate process modifications need to be completed first. Secondly, inorganic materials such as metals and oxides which are used in the current flexible display technology have very different mechanical properties compared to the polymer substrate, therefore cracking and delamination may occur during the fabrication process and in operation. Typically, the Young's modulus (E) of widely used poly(ethylene terephthalate) (PET) substrate is 5.3 GPa, whereas those of indium tin oxide (ITO) and chromium are 118 and 289 GPa, respectively. Also, the thermal expansion coefficients of polymer substrates are much larger than those of inorganic materials, which introduces stresses during the deposition process. These residual stresses along with the external bending stress would lead to the failure of devices. Thus the controlling (minimizing) of these stresses is the key factor in realizing a true flexible display.

Indium tin oxide is a transparent conductive oxide (TCO) material having a relatively high optical transmittance and electrical conductivity. ITO is widely used as the transparent electrode for display devices such as organic light-emitting diodes (OLEDs) and liquid crystal displays (LCDs). However, ITO films are very brittle and easily broken down by externally applied bending forces. This chapter mainly examines how external deformation influences the mechanical stability of ITO thin films on flexible polymer substrates, typically in a bent state. It discusses the mechanical behaviors of thin films under externally applied forces and the effects of buffer layers on reducing the induced stress in the thin films. The mechanical stability was determined by numerical analysis using the Storney formula on double- and triple-layer structures and bulge tests to measure the conductivity changes of patterned ITO islands as a function of bending curvature. Also, the mechanical stresses in film–substrate composites incorporating buffer layers with various Young's moduli are numerically analyzed from external bending stresses.

7.2 Mechanical Properties of Thin Films

The mechanical behaviors of film–substrate composites have been intensively studied by Nix and coworkers (Nix 1989; Mayo and Nix 1988; Weihs *et al.* 1988), Wagner and coworkers (Suo *et al.* 1999; Gleskova *et al.* 1999a; Wagner *et al.* 1999) and many other researchers (Leterrier *et al.* 1999; Cairns *et al.* 2000; Yu *et al.* 2000; Song *et al.* 2001; Petersen *et al.* 1998). Cairns *et al.* have investigated the mechanical properties of ITO films on a PET substrate, focusing on the cracking mechanism and its relation to electrical properties (Cairns *et al.* 2000). According to this report, the change in the electrical resistance can be described as a function of the number of cracks, applied mechanical strain and the thickness of ITO films. Also, the effect of additional polymer coatings on the resistance of ITO films was discussed. Suo *et al.* (1999) have investigated the mechanical stability of bent metallic films on compliant substrates, correlating it with the thickness ratio of the substrate to the metallic film. Leterrier *et al.* (1999) have observed the cracking of a 100 nm thick SiO_2 layer on a PET substrate. These results, estimated using the Kelly–Tyson approach (Kelly and Tyson 1965), suggested that the crack density increases with the strain and approaches a saturation value. Yu *et al.* (2000) have also studied the intrinsic stress in diamond films deposited by chemical vapor deposition (CVD) on silicon substrates using elastic/plastic analysis and correlated it with the film thickness.

Petitioner Samsung Ex-1011, 0151

They investigated the mechanical properties of metallic films on a polymer substrate incorporated with an interfacial fraction energy. Gleskova *et al.* (1999b) calculated the external bending stress in amorphous silicon thin film transistors by considering observed built-in curvature, and Hsueh (2002) suggested a model of elastic deformation of multilayers due to residual stress with no external bending stress.

This chapter reviews the electrical conduction behaviors of micropatterned ITO films corresponding to mechanically deformed film–substrate composites (Park *et al.* 2003). The island structures of the ITO sample were prepared for the precise analysis of surface-fracture-dependent electrical changes of the films which are free from the edge force effect leading to nonuniform stress distribution.

7.2.1 Numerical Analysis of Mechanical Stress Induced by Bending Force

Double-layer structure

During fabrication and application, a flexible electronic device inevitably suffers from an external force with bending movement, leading to significant degradation of device performance. This degradation in the device performance mainly results from cracks formed in the thin electrode films and which lead to the conduction failure. These cracks are readily generated by externally applied bending stresses above a critical limit. Therefore it is necessary to determine the conduction failure mechanism of the electrodes induced by the external mechanical forces for the reliability of organic electronic devices. First, we postulate that ITO films and the substrate have thicknesses of t_f and t_s with corresponding Young's moduli of E_f and E_s.

When an external force is applied to the substrate, mechanical distortion causes the substrate to bend elastically; the bending curvature depends on the substrate's thickness and its Young's modulus. It is assumed that the substrate is isotropic in the plane of the substrate. If the polymer substrate is thin and compliant, a film–substrate composite bends into a cylindrical roll instead of a spherical cap. Hence, we ignore Poisson's ratio in the following analysis.

Under a specific tensile or compression force, a film–substrate composite bends with a constant curvature of R and the bending moment elongates the layer in the upper section of the film–substrate composite compressing the layer in the lower section. Between the elongated and compressed parts, there exists at position z_n a layer called a neutral layer, which is free from any stresses (Figure 7.1).

The local elongation is $\varepsilon_s = (d_x - d_{xo})/d_{xo}$ with d_x and d_{xo} being the infinitesimal length along the long axis of the substrate in the deformed and undeformed states, respectively. Deformation $\varepsilon_s(z)$ is given by

$$\varepsilon_s(z) = \frac{z - z_n}{R}. \tag{7.1}$$

In the substrate, deformation results in a local stress $\sigma(z)$ given by

$$\sigma_s(z) = E_s\varepsilon_s(z) = E_s\left(\frac{z - z_n}{R}\right), \tag{7.2}$$

Petitioner Samsung Ex-1011, 0152

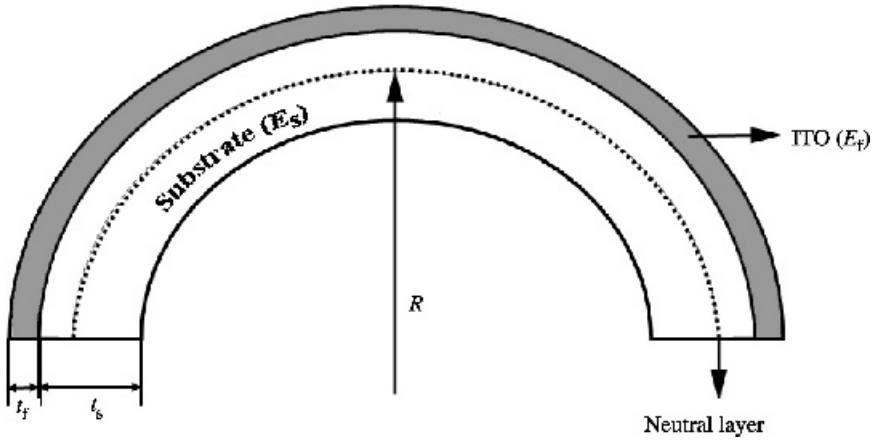


Figure 7.1 A cross-sectional view of a double-layer sturcture in bending state

where E_s is the Young's modulus of the substrate. The position of the neutral layer z_n is derived from the condition that there is no net elongation force acting on the film–substrate composite (force per unit length). Therefore

$$F_s + F_f = 0 \quad \left(F = \sigma t = \int_0^{t_s} \sigma(z)\,dz\right),$$
$$\int_0^{t_s} \frac{E_s}{R}(z - z_n)\,dz + \int_{t_s}^{t_s+t_f} \sigma_f\,dz = 0, \tag{7.3}$$

where F_s is the force acting on the substrate; F_f is the force acting on the film; σ_f is the averaged local stress of the film, assumed to be independent of the position z. Solving (7.3) for z_n results in

$$z_n = \frac{t_s}{2} + \frac{R\sigma_f t_f}{E_s t_s}. \tag{7.4}$$

From the condition that there is no external moment (torque) acting on the film–substrate composite, the averaged local stress of the film (σ_f) is

$$M_s + M_f = 0 \quad \left(M = \int_0^{t} \sigma(z)\,z\,dz\right),$$
$$\int_0^{t_s} \frac{E_s}{R}(z - z_n)^2\,dz + \int_{t_s}^{t_s+t_f} \sigma_f(z - z_n)\,dz = 0, \tag{7.5}$$

Petitioner Samsung Ex-1011, 0153

where M_s and M_f are the moments acting on the substrate and film, respectively. Solving (7.5) for σ_f gives

$$\sigma_f = \frac{E_s t_s^3}{6Rt_f(t_s + t_f)}. \tag{7.6}$$

It is clear from (7.6) that the stress in the film is a function of the Young's modulus of the substrate, the substrate thickness and the film thickness. From (7.2) and (7.6) the strain (ε_f) in the film can be written as

$$\varepsilon_f = \frac{t_s^2}{6Rt_f(t_s + t_f)} \left(\frac{E_s}{E_f}\right) \frac{t_s}{t_f}. \tag{7.7}$$

Triple-layer structure

For a triple-layer structure where an additional buffer layer is inserted between the film and the substrate, the stress–strain relation can be derived in a similar manner. The thickness and Young's modulus of the buffer layer are denoted as t_b and E_b, respectively. In a system containing a buffer layer, the stress–strain relation can be analyzed in terms of a triple-layer structure (Figure 7.2).

To analyze this triple-layer structure, the postulated net force is modified by F_b, the force acting on the buffer layer, given by

$$F_s + F_b + F_f = 0, \tag{7.8}$$

$$\int_0^{t_s} \frac{E_s}{R}(z - z_n)\,dz + \int_{t_s}^{t_s+t_b} \frac{E_b}{R}(z - z_n)\,dz + \int_{t_s+t_b}^{t_s+t_b+t_f} \sigma_f\,dz = 0. \tag{7.9}$$

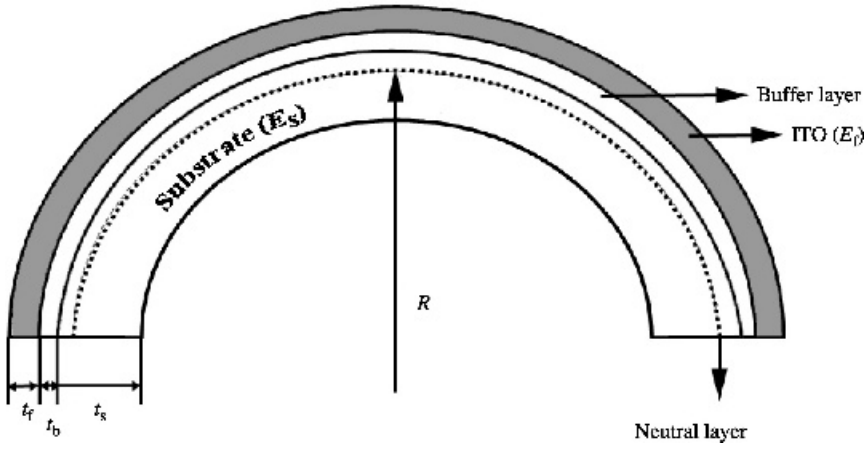


Figure 7.2 A cross-sectional view of a triple-layer sturcture with a buffer layer

Petitioner Samsung Ex-1011, 0154

This expression leads to the neutral layer position as

$$z_{\mathrm{n}} = \frac{E_{\mathrm{s}} t_{\mathrm{s}} + E_{\mathrm{b}}(t_{\mathrm{s}} + t_{\mathrm{b}})}{2(E_{\mathrm{s}} + E_{\mathrm{b}})} + \frac{R\sigma_{\mathrm{f}} t_{\mathrm{f}}}{(E_{\mathrm{s}} + E_{\mathrm{b}})t_{\mathrm{s}}}. \tag{7.10}$$

If $E_{\mathrm{b}} = E_{\mathrm{s}}$, then (7.10) simplifies to

$$z_{\mathrm{n}} = \frac{t_{\mathrm{s}}}{2} + \frac{t_{\mathrm{b}}}{4} + \frac{R\sigma_{\mathrm{f}} t_{\mathrm{f}}}{2E_{\mathrm{s}} t_{\mathrm{s}}}. \tag{7.11}$$

On comparing (7.11) and (7.4), the insertion of a buffer layer with Young's modulus E_{b} can change the position of the neutral layer. If $E_{\mathrm{b}} = E_{\mathrm{s}}$ and $t_{\mathrm{f}} \ll t_{\mathrm{s}}$, the neutral layer position moves toward the ITO film by $t_{\mathrm{b}}/4$ compared to a film–substrate composite in the absence of a buffer layer.

Furthermore, if $E_{\mathrm{b}} \neq E_{\mathrm{s}}$ and $t_{\mathrm{f}} \ll t_{\mathrm{s}}$, then as the value of E_{b} decreases, the position of the neutral layer shifts from mid-surface towards the film and accompanies the ebbing of stress imposed on the film.

Similar to (7.8), we must modify (7.5) by the moment M_{b}, the moment acting on the buffer layer. Therefore

$$M_{\mathrm{s}} + M_{\mathrm{b}} + M_{\mathrm{f}} = 0, \tag{7.12}$$

$$\int_0^{t_{\mathrm{s}}} \frac{E_{\mathrm{s}}}{R}(z - z_{\mathrm{n}})^2 \,\mathrm{d}z + \int_{t_{\mathrm{s}}}^{t_{\mathrm{s}}+t_{\mathrm{b}}} \frac{E_{\mathrm{b}}}{R}(z - z_{\mathrm{n}})^2 \,\mathrm{d}z + \int_{t_{\mathrm{s}}+t_{\mathrm{b}}}^{t_{\mathrm{s}}+t_{\mathrm{b}}+t_{\mathrm{f}}} \sigma_{\mathrm{f}}(z - z_{\mathrm{n}})\mathrm{d}z = 0. \tag{7.13}$$

From (7.13) we can obtain the stress formula on the film–substrate structure containing a buffer layer

$$\sigma_{\mathrm{f}}(z) = \frac{E_{\mathrm{s}} t_{\mathrm{s}}^3 - \beta}{12Rt_{\mathrm{f}}\left(t_{\mathrm{s}} + t_{\mathrm{b}} + \frac{t_{\mathrm{f}} - \alpha}{2}\right)}, \tag{7.14}$$

where

$$\alpha = \frac{E_{\mathrm{s}} t_{\mathrm{s}} + E_{\mathrm{b}}(t_{\mathrm{b}} + t_{\mathrm{s}})}{2(E_{\mathrm{s}} + E_{\mathrm{b}})},$$

$$\beta = 2E_{\mathrm{s}}\alpha t_{\mathrm{s}}(t_{\mathrm{s}} + \alpha) - E_{\mathrm{b}}[(t_{\mathrm{b}} + t_{\mathrm{s}} - \alpha)^3 - (t_{\mathrm{s}} - \alpha)^3].$$

In most applications of thin film electronic devices, the thickness and Young's modulus of ITO films are fixed due to their optimum electrical, optical and chemical properties. Hence, under a constant bending strain, the stress in ITO films with a buffer layer is determined by the Young's moduli and the thicknesses of the buffer layer and polymer substrate. From (7.14) it should be noted that the use of a buffer layer and a substrate with low

Petitioner Samsung Ex-1011, 0155

thicknesses and low Young's moduli enables the reduction of stress in ITO films on polymer substrates.

7.2.2 Experimental Results for Bending-Induced Mechanical Stress

Here we focus on the changes in the sheet resistance as a function of strain which results from the externally induced mechanical force. We provide a model describing the mechanism by which the electrical resistivity of ITO film changes with the imposed strain. Assuming that a film–substrate composite is bent by differential mechanical strain, the change in mechanical strain can be expressed as a function of bending curvature. Moreover, the stress imposed on ITO films can be indicated by the increase of electrical resistivity resulted from delamination and cracks. According to (7.14), the Young's modulus of the substrate is one of the factors determining the mechanical stress. Thus we used a polycarbonate (PC) foil as a substrate because of its low Young's modulus and easy availability. Figure 7.3 shows the stress–strain relations of ITO films on a polymer substrate, which is simulated using (7.14). The stress in ITO films on PC substrates was calculated with $t_s = 100$ μm, $t_b = 0.5$ μm, $t_f = 0.1$ μm and $E_s = 5.3$ GPa. The results of the simulation reveal that a buffer layer having a Young's modulus less than 2.885 GPa is required to improve the mechanical stability of ITO films. This is in good agreement with our experimental results, which show a lower Young's modulus of buffer layers for the improvement of mechanical stability. The measured Young's moduli of buffer layers and metallic films are shown in Table 7.1.

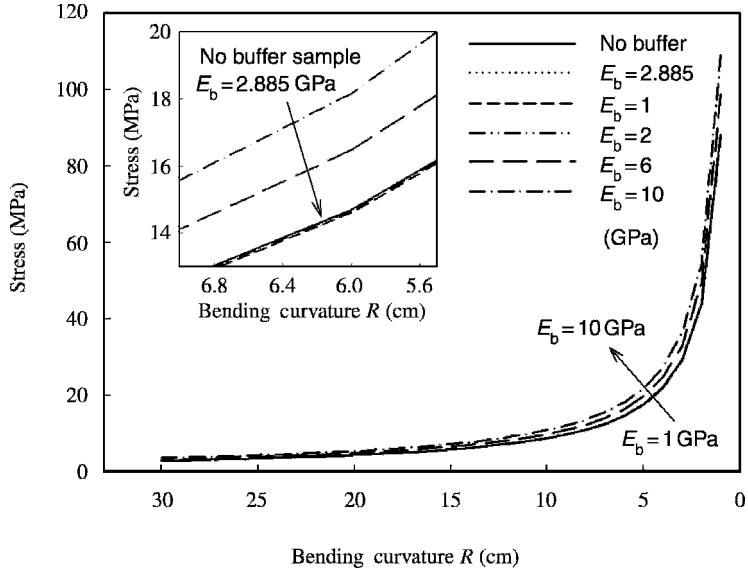


Figure 7.3 Effect of a buffer layer on the stress of mechanically deformed ITO–polymer substrate systems with respect to Young's modulus of the buffer layer. The data in this figure were calculated from (7.14) by considering the ITO films on PC substrate with $t_s = 100$ μm, $t_b = 0.5$ μm, $t_f = 0.1$ μm and $E_s = 5.3$ GPa. The inset figure shows the stress with bending curvature range from 6.9 cm to 5.6 cm

Petitioner Samsung Ex-1011, 0156

Table 7.1 Young's moduli of various substrates, buffer layers and metallic films measured by nanoindentation

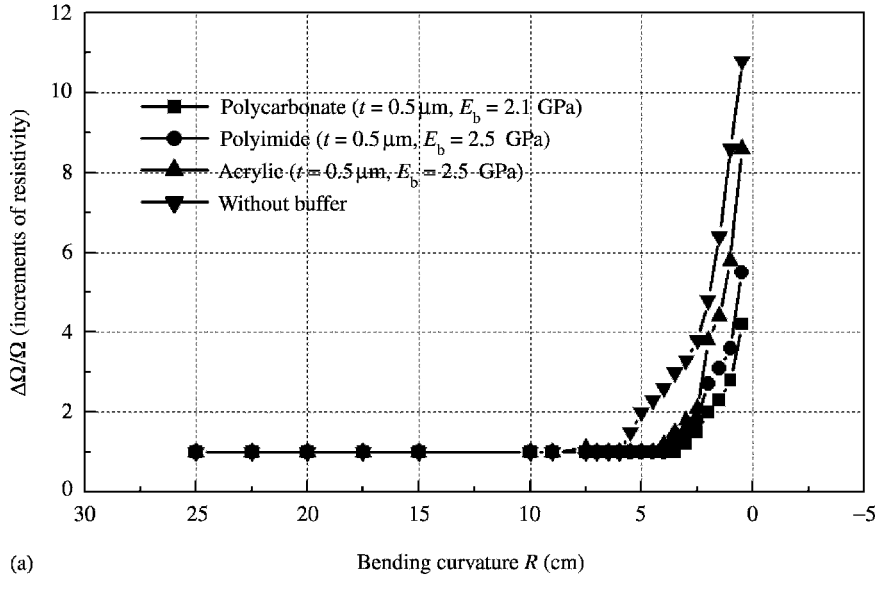
Item	Materials (thickness, μm)	Young's modulus (GPa)
Substrate	PC (100)	5.3
	PES (100)	5.7
	PET (100)	5.53
Buffer layer	Polycarbonate (0.5)	2.1
	Polyimide (0.5)	2.5
	Acrylic resin (0.5)	3.2
	Aluminum film (0.5)	11.5
Metallic film	ITO film (0.1)	118
	Tantalum film (0.1)	140

Figure 7.4(a) shows the relationship between the resistivity variations, the bending curvature and Young's modulus of the buffer layer. It depicts the changes in the electrical resistivity as a function of bending curvature. The values of resistivity in ITO films are vastly changed with buffer materials below 7 cm of the bending curvature; they remain almost independent of buffer materials above this value of bending curvature. If the buffer layer has a fixed thickness and there is ITO film on the buffer layer, the stress imposed on the thin film depends on α, as shown in (7.14). As the α value is mainly determined by the Young's modulus of the buffer layer, the different behaviors of the resistivity changes depicted in Figure 7.4(a) are attributed to the Young's moduli of the buffer layers. The results of Figure 7.4(a) are in excellent agreement with the results from the simulation in Figure 7.3. The ITO film with a buffer layer having lower Young's modulus shows a slower increment of resistivity than the film without a buffer layer, which corresponds to the reduction of stress on the film. Figure 7.4(b) shows the dependence of the stress–strain relation in ITO films on the thickness of polymer substrates. From (7.9) it is also predicted that ITO films on thinner substrates corresponding to the same bending curvature have smaller stresses.

Figure 7.5 compares experimental and simulated results. It shows that the resistivity changes and distributed stress on ITO films which originated from the mechanical defects of films are reduced by using an organic buffer layer, and the reduction is inversely proportional to the Young's modulus of the buffer layer. It is generally well known that the stress originating from mechanical distortion or bending creates numerous cracks in thin films on polymer substrates, leading to a degradation in the conductive properties of ITO films (increment of resistivity of ITO films). Therefore the release of distributed stress on ITO films by adding a buffer layer that is expected from (7.14) and Figure (7.3) would reduce the likelihood of cracks, giving an improvement in the electrical properties of ITO films (reduction of increment of resistivity in ITO films) at the same bending curvature. However, the discrepancy between theoretical predictions and experimental results for the relationship of Young's modulus and mechanical properties seems to be attributed to the interfacial mismatch between ITO films and buffer layers in addition to some uncertainty in the Young's modulus measurements.

For a more obvious comparison of the mechanical stability, a very brittle material tantalum (Ta) was used as the top thin film in the experiment. Figure 7.6(a) shows the

Petitioner Samsung Ex-1011, 0157



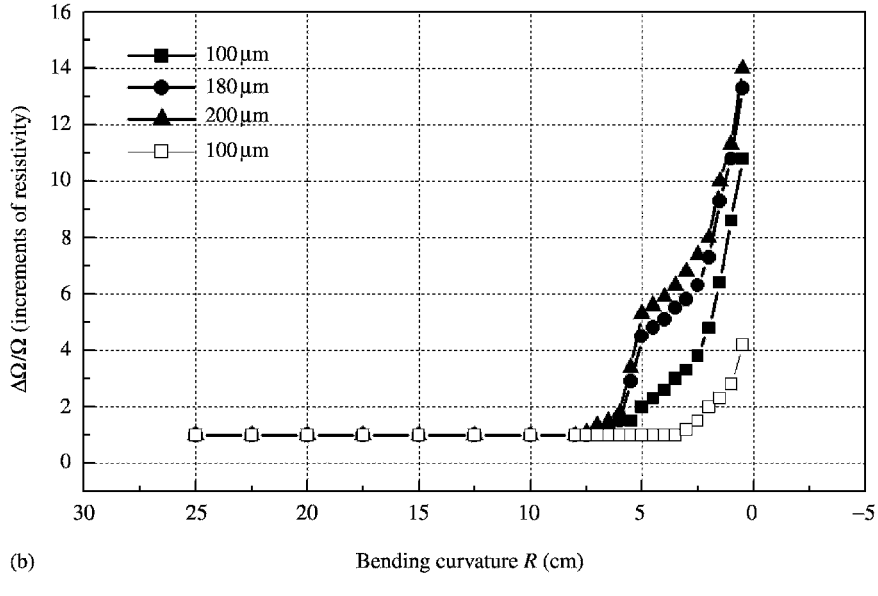


Figure 7.4 Dependence of electrical resistivity in ITO films (a) on the bending curvature and buffer material, and (b) on bending curvature and substrate thickness. In (a) the substrate is 100 μm polycarbonate and the ITO film has $t = 0.1$ μm. In (b) the organic buffer layer $t = 0.1$ μm and $E_b = 2.1$ GPa and the ITO film has $t = 0.1$ μm; the values in the key are substrate thicknesses

Petitioner Samsung Ex-1011, 0158

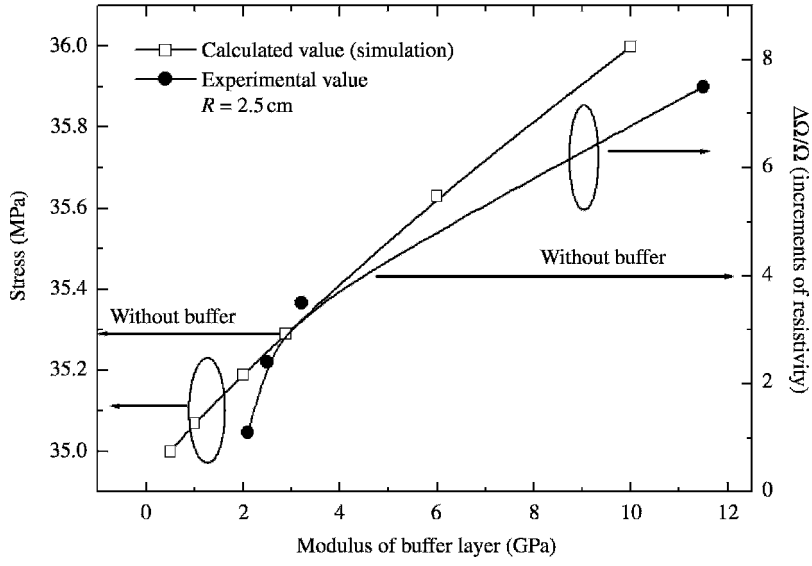


Figure 7.5 Dependence of the increment of electrical resistivity and stress distribution in ITO films on Young's modulus of buffer layers

stress–strain relation of Ta film on a polymer substrate with various buffer layers. The materials used for the buffer layers are polycarbonate and aluminum (Al) of thickness 0.5 μm. These experiments also reveal that Ta thin films including an Al buffer layer (Young's modulus 11.5 GPa) exhibit deterioration of mechanical stability compared to films without a buffer layer. It was also evident that the stress imposed on the conductive film is much larger in tension than in compression. In general, since the polymer substrate has a higher thermal expansion than the Ta films, deposition induces a tensile force on the films concomitant with differential strain. Consequently, an external compressive force reduces the tensile force; on the other hand, an external tensile force increases the differential strain by adding additional force to the original tensile force. Figure 7.6(b) shows the resistivity changes of Ta films under external tensile force. On comparing Figure 7.6(a) and (b), it is evident that the tensile force causes 7–8 times higher stress on the conductive films.

Figure 7.7 shows the increase of cracks in the ITO films on polymer substrates with different bending curvatures. The images were obtained in a stress-free state using a long focal length optical microscope and charge-coupled device camera. The experimental results described here confirm the model of increasing resistance with cracks. As shown in Figure 7.7, the ITO films with a buffer layer exhibit a lower density of cracks than the films without a buffer layer at a similar bending curvature. Another distinct phenomenon found in the experiments is the saturation of crack density at a critical bending momentum (as seen in Figures 7.5 and 7.6). Cairns *et al.* (2000) also suggested that resistivity increases slowly with increasing bending moment until a certain critical point is reached. After that point, even though the crack density is in a saturated state, the electrical resistance increases sharply. It is considered that after the saturation point, the stress imposed on the ITO films generates more dislocation sites in the structure and accordingly accelerates the original cracks to become wider and deeper, causing serious conduction failure.

Petitioner Samsung Ex-1011, 0159

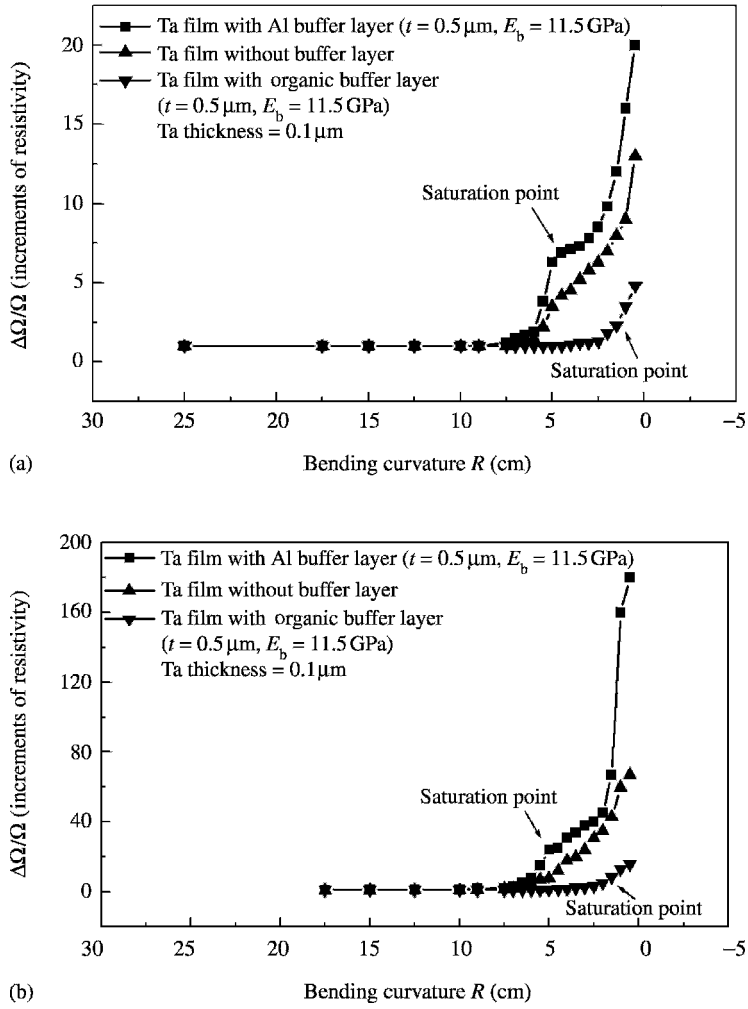


Figure 7.6 (a) Dependence of the increment of electrical resistivity in Ta films on buffer layers after exposure to compressive bending force, and (b) the tensile bending force

7.3 Conclusions

We have studied the stability of mechanically deformed ITO films on polycarbonate substrates. First, we performed a numerical analysis of the mechanical properties of deformed ITO films on compliant substrates using the Storney formula, and then we investigated a triple-layer structure including a buffer layer. Finally, measuring the conductivity variations of patterned ITO islands as a function of bending curvature, the theoretical expectations were compared with experimental results. We discovered that a buffer layer with a Young's modulus lower than a critical value can help to relieve the mechanical stress in the films. Moreover, for the reduction of induced tensile force in ITO

Petitioner Samsung Ex-1011, 0160

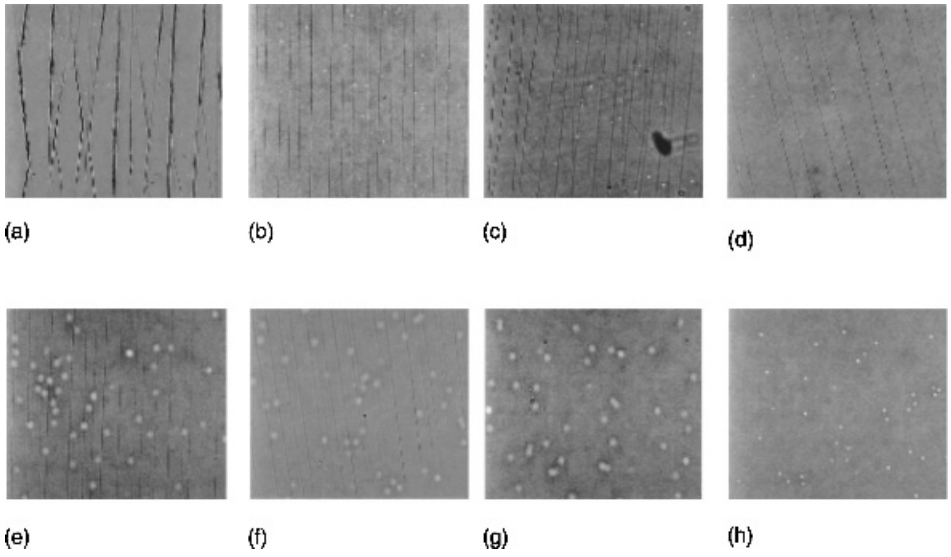


Figure 7.7 Optical images of cracks in ITO films in accordance with bending curvature and buffer layer: (a–d) without buffer, (e–f) with buffer for (a) $R = 1$ cm, (b) $R = 2$ cm, (c) $R = 4$ cm, (d) $R = 10$ cm, (e) $R = 1$ cm, (f) $R = 2$ cm, (g) $R = 4$ cm, (h) $R = 10$ cm

films, it is suggested that an additional layer with an appropriate Young's modulus has to be deposited onto the opposite side of a polymer substrate.

References

Asano, A., Kinoshita, T. and Otani, N. (2003) A Plastic 3.8-in. Low-temperature polycrystalline silicon TFT color LCD panel. *SID Digest*, 988.

Cairns, D. R., Witte, R. P. II, Sparacin, D. K., Sachsman, S. M., Paine, D. C., Crawford, G. P. and Newton, R. R. (2000) Strain-dependent electrical resistance of tin-doped indium oxide on polymer substrates. *Applied Physics Letters* **76**, 1425.

Gardner, T. J. and Wenz, R. P. (1995) STN alignment on rib-spaced plastic LCD substrate. *SID Digest*, 695.

Gleskova, H., Wagner, S. and Suo, Z. (1999a) Rugged a-Si:H TFTs on plastic substrates. *Materials Research Society Symposium Proceedings* **557**, 653.

Gleskova, H., Wagner, S. and Suo, Z. (1999b) Stability of amorphous silicon transistors under extreme in-plane strain. *Applied Physics Letters* **75**, 3011.

Hsueh, C. H. (2002) Modeling of elastic deformation of multilayers due to residual stresses and external bending. *Journal of Applied Physics* **91**, 9652.

Inoue, S., Utsunomiya, S. and Shimoda, T. (2003) Transfer mechanism in surface free technology by laser annealing/ablation (SUFTLA). *SID Digest*, 984.

Kelly, A. and Tyson, W. R. (1965) Tensile properties of fibre-reinforced metals: copper/tungsten and copper/ molybdenum. *Journal of the Mechanics and Physics of Solids* **13**, 329.

Leterrier, Y., Boogh, L., Andersons, J., and Mansons, J. A. E. (1999) *Journal of Polymer Science Part B*, **323**, 63.

Petitioner Samsung Ex-1011, 0161

Matsumoto, F., Nagata, T., Miyabori, T., Tanaka, H. and Tsushima, S. (1993) Color STN-LCD on polymer film substrates. *SID Digest*, 965.

Mayo, M. J. and Nix, W. D. (1988) *Acta Metallurgica* **26**, 2183.

Nix, W. D. (1989) Mechanical properties of thin films. *Metallurgical Transitions A* **20**, 2217.

Park, S. K., Han, J. I., Kim, W. K. and Kwak, M. G. (2000) Development of 2-in. plastic-film STN LCD with uniform cell gap. *SID Digest*, 514.

Park, S. K., Han, J. I., Moon, D. G. and Kim, W. K. (2003) Mechanical stability of externally deformed indium-tin-oxide films on polymer substrates. *Japanese Journal of Applied Physics* **42**, 623.

Petersen, C., Heldmann, C. and Johannsmann, D. (1998) *Journal of Polymer Science Part B*, **325**, 163.

Song, J. Y., Cho, S. I. and Yu, J. (2001) Estimation of the interfacial fracture energy of metal/polymer system in microelectronic packaging. *Materials Research Society Proceedings* **682E**, N6.2.

Suo, Z., Ma, E. Y., Gleskova, H. and Wagner, S. (1999) Mechanics of rollable and foldable film-on-foil electronics. *Applied Physics Letters* **74**, 1177.

Utsunomiya, S., Kamakura, T., Kasuga, M., Kimura, M., Miyazawa, W., Inoue, S. and Shimoda, T. (2003) Flexible color AM-OLED display fabricated using surface free technology by laser ablation/annealing (suftla) and ink-jet printing technology. *SID Digest*, 864.

Wagner, S., Gleskova, H., Ma, E. Y. and Suo, Z. (1999) Compliant substrates for thin-film transistor backplanes. *SPIE Proceedings* **3636**, 32.

Weihs, T. P., Hong, S., Bravman, J. C. and Nix, W. D. (1988) The mechanical deflection of cantilever microbeams: a new technique for testing the mechanical properties of thin films. *Journal of Materials Research* **3**, 931.

Wenz, R. P. and Aastuen, D. J. W. (1993) Plastic microstructure-spaced LCD. *SID Digest*, 961.

Yu, J., Kim, J. G., Chung, J. O. and Cho, D. H. (2000) An elastic/plastic analysis of the intrinsic stresses in chemical vapor deposited diamond films on silicon substrates. *Journal of Applied Physics* **88**, 1688.

Petitioner Samsung Ex-1011, 0162

8

Conductive Polymers

L. ''Bert'' Groenendaal

Agfa-Gevaert N.V.

Dedicated to the memory of our daughter, Summer Groenendaal.

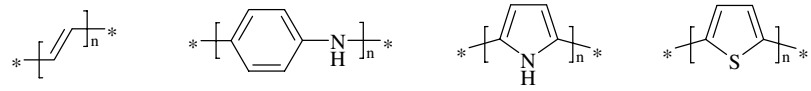
8.1 Introduction

Although each class of polymers has its own specific properties, there is one feature that almost all polymers seem to have in common – they are electrical insulators. For this reason, polymers such as PVC and polyimides have been used and continue to be used as materials that surround the copper in electrical wires or that prevent shorts in electrical circuits. There is, however, one class of polymers that forms an exception to this rule, and they are the conductive polymers (Skotheim 1998; Nalwa 1997; Feast *et al.* 1996; Stenger-Smith 1998; Kiebooms *et al.* 2001; Epstein 1997). Figure 8.1 shows some examples. In contrast to other polymers, conductive polymers have the ability to conduct electricity, just like metals such as copper and iron.

A metal wire can conduct electricity because the electrons in the metal are free to move. How can we then explain the conductivity within these polymers? When describing polymers, we distinguish between sigma (σ) bonds and pi (π) bonds. The σ bonds are fixed and immobile. They form the covalent bonds between the atoms. The π electrons in a conjugated double bond system are also relatively localized, though not as strongly bound as the σ electrons. Before a current can flow along the molecule, one or more electrons have to be removed (oxidation) or inserted (reduction). If an electric field is then applied, the electrons constituting the bonds can move rapidly along the molecular chain. The conductivity of the plastic material, which consists of many polymer chains, will be limited

Flexible Flat Panel Displays Edited by G. P. Crawford
© 2005 John Wiley & Sons, Ltd., ISBN 0-470-87048-6

Petitioner Samsung Ex-1011, 0164



Polyacetylene Polyaniline Polypyrrole Polythiophene

Figure 8.1 Some members of the conductive polymer family

by the fact that the electrons have to ''jump'' from one polymer chain to the next. Hence the chains have to be well packed in ordered rows.

There are two types of doping, oxidative and reductive. In polyacetylene the reactions are written as follows:

- Oxidation (*p*-doping): $[CH]_n + \frac{3}{2}x\ I_2 \rightarrow [CH]_n^{x+} + xI_3^-$.
- Reduction (*n*-doping): $[CH]_n + x\text{Na} \rightarrow [CH]_n^{x-} + x\text{Na}^+$.

The doped polymer is a salt. However, it is not the iodide or sodium ions that move to create the current, but the electrons from the conjugated double bonds (Figure 8.2). Furthermore, if a suitable electric field is applied, the iodide and sodium ions can move either towards or

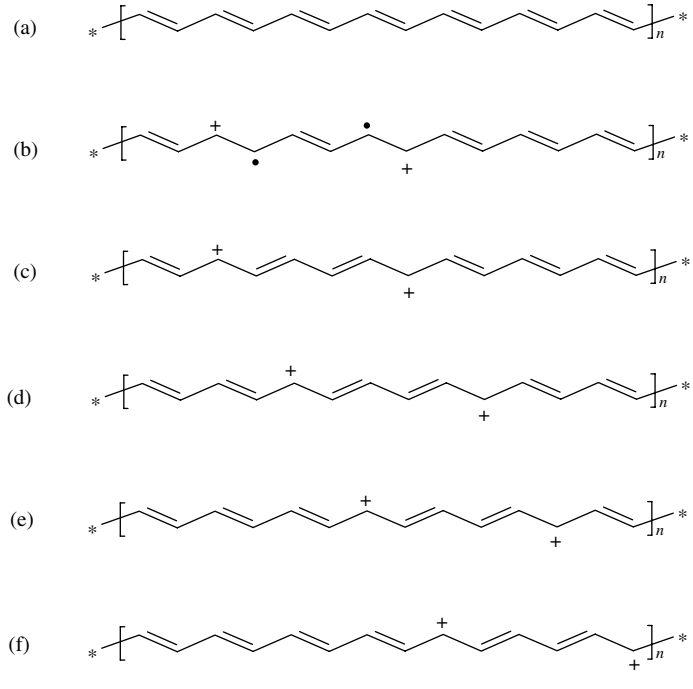


Figure 8.2 Transport of charges within conductive polymers (polyacetylene has been taken as an example): (a) neutral PAc, (b) PAc doped by oxidant, (c) radicals recombine; (d, e, f) transport of charges along the PAc backbone (www.nobel.se/chemistry/laureates/2000/illpres)

Petitioner Samsung Ex-1011, 0165

away from the polymer. This means that the direction of the doping reaction can be controlled and the conductive polymer can easily be switched on and off. In case oxidation the iodine molecule attracts an electron from the polyacetylene chain and becomes I_3^-. The polyacetylene molecule, now positively charged, is called a radical cation, or polaron. The lone electron of the double bond, from which an electron was removed, can move easily. As a consequence, the double bond progressively moves along the molecule. The positive charge, on the other hand, is fixed by electrostatic attraction to the iodide ion, which does not move so readily. If the polyacetylene chain is heavily oxidized, polarons condense pairwise into so-called solitons. These solitons are then responsible, in a complex manner, for the transport of charges along a polymer chain. When the charges reach the end of the polymer chain, they can hop to an adjacent polymer chain and continue their progress. Thus, the nanoscopic charge carriers produce a macroscopic electrical conductivity.

The material's ability to conduct electricity can be expressed in two units: siemens per centimeter (S/cm) for the conductivity (σ) of a material and ohm per square (ohm/sq) for the surface resistance (R_s) of a material. When a certain material has a surface resistance of 1000 ohm/sq, its conductivity can be calculated by considering the material thickness, T (e.g. $T = 200$ nm):

$$R_s = 1000\,\text{ohm/sq} \equiv 1/T\sigma = 1/(200 \times 10^{-7} \times \sigma)$$
$$\sigma = 1/R_s T = 1/(1000 \times 200 \times 10^{-7}) = 50\,\text{S/cm}.$$

In the literature, conductivity values for conductive polymers vary from 10^{-9} S/cm (antistatic) to 10^5 S/cm (metallic conductivity); see Figure 8.3. For comparison, copper exhibits a conductivity of 6×10^5 S/cm. Due to the typical polymer characteristics such as flexibility, processability and low density, there are numerous (potential) applications for conductive polymers. Examples are their use as antistatic material in photographic film or TV screens, as electrode material in capacitors or as anticorrosive material. Section 8.5 gives more examples.

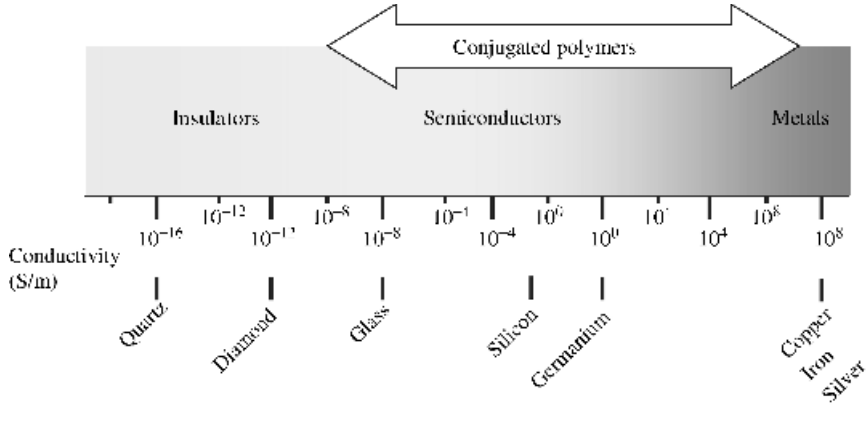


Figure 8.3 Conductive polymers within the conductivity spectrum

Petitioner Samsung Ex-1011, 0166



Figure 8.4 Left to right, Nobel laureates A. J. Heeger, A. G. MacDiarmid and H. Shirakawa

In 2000 the Nobel Prize for Chemistry was awarded to Professors Alan J. Heeger, Alan. G. MacDiarmid and Hideki Shirakawa (Figure 8.4). In the 1970s, together with several graduate students and postdocs, they studied polyacetylene at the University of Pennsylvania. On November 23rd, 1976 they found that if polyacetylene was chemically doped with an oxidant (they first applied bromine, later iodine), this material became nine orders of magnitude more conductive than the nonoxidized species (Shirakawa *et al*. 1977). Although they were not the first to prepare an electrically conductive polymer (Naarman *et al*. 1990), it was this discovery that opened the modern era of conductive polymers. Section 8.2 is a historical overview of conductive polymers from the very early beginning until today.

8.2 Historical Overview

Although conductive polymers are generally considered as a relatively young class of polymers, the first synthesis of such a polymer dates back to the first half of the nineteenth century. At that time, chemistry was not much more than the destructive distillation of coal tar and animal bones which resulted in the discovery of (hetero)aromatics such as benzene (1825), aniline (1826), pyrrole (1834) and thiophene (1882). In the decades that followed, the first accidental polymerizations were performed: polyaniline was prepared chemically in 1834 (Genies *et al.* 1990) and electrochemically in 1862 (Letheby 1862), whereas polypyrrole was first prepared chemically in 1916 (Angeli 1916).

In the 1960s and 1970s the field slowly started developing. Companies started doing research (e.g. BASF in Germany) and the first patents were filed and granted (e.g. DE 1195497, filed February 1, 1963 by BASF, and DE 1178529, filed April 11, 1963 by BASF). In this same period the first inorganic conductor was discovered: $(SN)_x$ (Labes *et al.* 1979).

In 1976 Heeger, MacDiarmid and Shirakawa made the discovery that polyacetylene, when chemically doped with an oxidant, exhibits a high electrical conductivity (Shirakawa *et al*. 1977). Shirakawa, who had been the first to make shiny films of this polymer, had met MacDiarmid at a conference in Japan where they had had discussions about this material. Soon after this conference, Shirakawa went to the University of Pennsylvania as a visiting scientist and in a very short time they made huge progress. This eventually led to the discovery of the remarkable increase (nine orders of magnitude) in electrical conductivity of polyacetylene and the identification of that increase as resulting from a transition from insulator to a metal-like conductor. This culminated in the awarding of the 2000 Nobel Prize

Petitioner Samsung Ex-1011, 0167

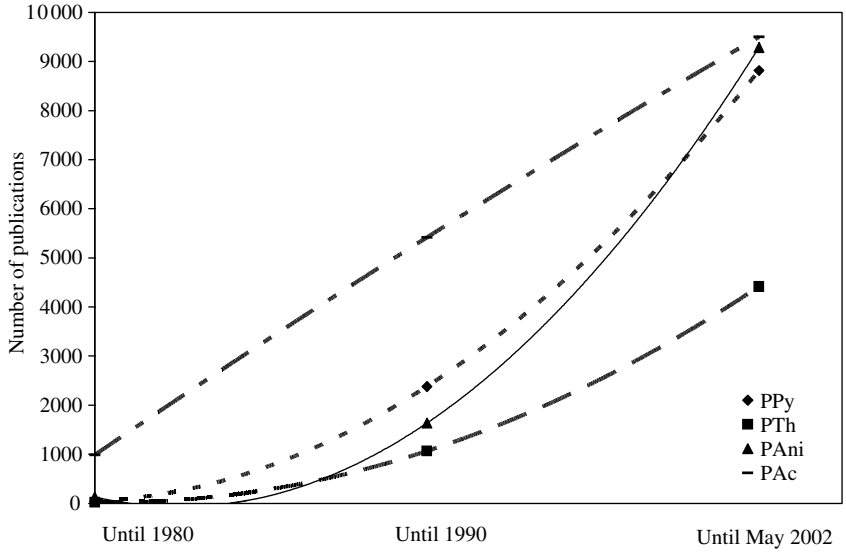


Figure 8.5 Development of PPy, PTh, PAni and PAc expressed by the number of publications (including patents) over the years. This figure is the result of a Scifinder search in May 2002 using the keywords polypyrrole, polythiophene, polyaniline and polyacetylene

for Chemistry to Professors Alan J. Heeger, Alan. G. MacDiarmid and Hideki Shirakawa (Figure 8.4) for their pioneering work that initiated the development of this polymer chemistry (www.nobel.se/chemistry/laureates/2000/index; Shirakawa *et al.* 2001).

Around 1980 the first polypyrroles, polyanilines and polythiophenes were prepared and characterized, and their conductive properties were recognized. In the years that followed, numerous academic and industrial groups started doing research in this field (Figure 8.5), resulting in many breakthroughs ranging from the synthesis of excellent new materials to further increases in conductivity and commercialization of the first conductive polymers.

I will discuss in detail the best-known and most intensively studied conductive polymers, including their synthesis, properties and applications. But first I will briefly consider the different polymerization methodologies that can be used to prepare conductive polymers.

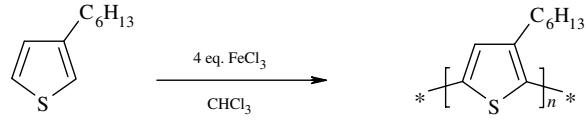
8.3 Overview of Polymerization Methods

Over the years various methods have been developed to prepare conductive polymers. This section is an overview of the best-known and most frequently used polymerization types.

8.3.1 Chemical Oxidative Polymerizations

The chemical oxidative polymerization method is definitely the most frequently used method to prepare conductive polymers (Skotheim 1998; Nalwa 1997; Feast *et al.* 1996; Stenger-Smith 1998; Kiebooms *et al.* 2001). Applying Fe^{3+} salts such as $FeCl_3$ or $Fe(OTs)_3$ in

Petitioner Samsung Ex-1011, 0168



Scheme 8.1 Poly(3-hexylthiophene) obtained by oxidative polymerization (Sugimoto *et al.* 1986; McCullough 1998)

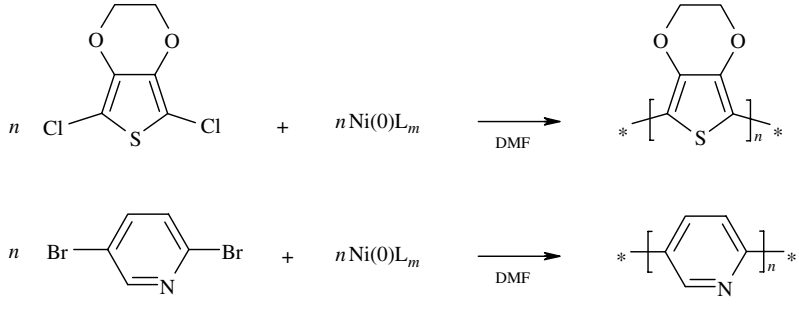
$CHCl_3$, one can easily polymerize a range of monomers into their corresponding polymers. Scheme 8.1 shows an example (Sugimoto *et al.* 1986). Due to the use of equimolar amounts of Fe^{3+} salts, the resulting polymers can be difficult to purify; small amounts of iron salts are easily incorporated, which makes the characterization more difficult.

8.3.2 Chemical Reductive Polymerizations

Reductive chemical polymerizations are far less frequently used to prepare conductive polymers. In contrast to their oxidative analogs, the reductive polymerization results in polymers that are in their reduced state. Yamamoto coupling is one of the most frequently used reductive polymerization reactions. It involves the polymerization of an aryl dihalide (X—R—X) using an Ni^0 complex (Ni^0L) (Yamamato 1999):

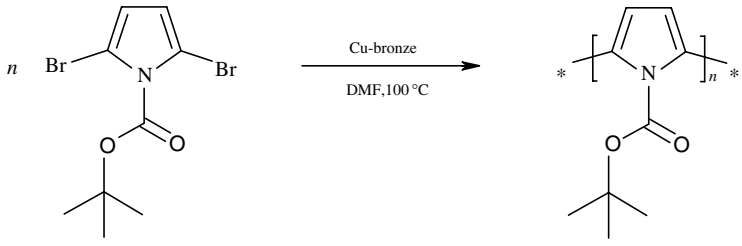
$$\mathrm{X{-}R{-}X + Ni^0L \rightarrow -(R)_{n^-} + NiX_2.}$$

Yamamoto *et al.* and others have applied this coupling methodology for the polymerization of numerous (hetero)aromatics. Frequently used Ni^0 complexes include $Ni(cod)_2$ (cod = 1,5-cyclooctadiene) and $Ni(PPh_3)_4$; the latter is prepared in situ from $Ni(PPh_3)_2Cl_2$, PPh_3 and Zn. Yamamoto coupling is believed to proceed through a multistep cyclic mechanism (Yamamato 1999). Scheme 8.2 shows two illustrative examples of a reductive polymerization using $Ni(0)L_m$ (a mixture of bis(1,5-cyclooctadiene)nickel(0), $Ni(cod)_2$ and 2,2′-bipyridine) as reagent (Yamamato *et al*. 2000).



Scheme 8.2 Examples of Yamamoto-type reductive polymerization reactions (Yamamato *et al.* 2000)

Petitioner Samsung Ex-1011, 0169



Scheme 8.3 Reductive polymerization of a pyrrole derivative via the Ullmann reaction (Groenendaal *et al.* 1995)

Another type of reductive polymerization reaction is the well-known Cu-mediated Ullmann reaction (Fanta 1964, 1974). Several examples can be found in the literature, one of which is shown in Scheme 8.3 (Groenendaal *et al.* 1995).

8.3.3 Polymerizations Based on Organometallic Cross-Coupling Reactions

Over the past three decades a number of organometallic C—C cross-coupling reactions have been developed, e.g. the Suzuki, Kumada, Stille, Negishi, Heck and Sonogashira reactions (Malleron 1997; Yamamoto 1997). Most of these reactions use catalysts containing Pd, Ni or Cu as the active metal, and a number of ligands. Organometallic cross-coupling reactions have been applied many times to prepare conductive polymers such as polythiophenes and polypyrroles. The most frequently used coupling reactions are briefly discussed here along with some illustrative examples of polymerization.

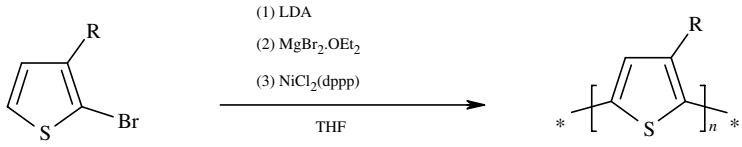
Kumada coupling

The Kumada coupling is a cross-coupling reaction between a Grignard reagent (R—MgX) and an organohalide (R′—X) (Kalanin 1992; Kumada 1980). A group VIII metal (Ni, Pd), that forms a complex with a number of ligands (L), catalyzes the reaction. Well-known catalysts are Ni(dppe)Cl_2, Ni(dppp)Cl_2, Pd(dppb)Cl_2 and Ni(acac)$_2$ (dppe, dppp, dppb = 1,3-bis(diphenylphosphino)ethane, -propane, -butane, respectively; acac = acetyl- acetonate; some of these catalysts are suspected to be carcinogenic).

$$\mathrm{R{-}MgX + R'{-}X \rightarrow R{-}R' + MgX_2.}$$

A disadvantage of the Kumada coupling, its mechanism proceeding via a multistep catalytic cycle, is that it does not tolerate a wide variety of functional groups due to the reactivity of the Grignard reagent. Despite this drawback, it has been applied to several conductive polymer syntheses, mostly of thiophene derivatives. Scheme 8.4 shows the well-known and frequently used synthesis of regioregular poly(3-alkylthiophene)s developed by McCullough *et al.* (1993).

Petitioner Samsung Ex-1011, 0170



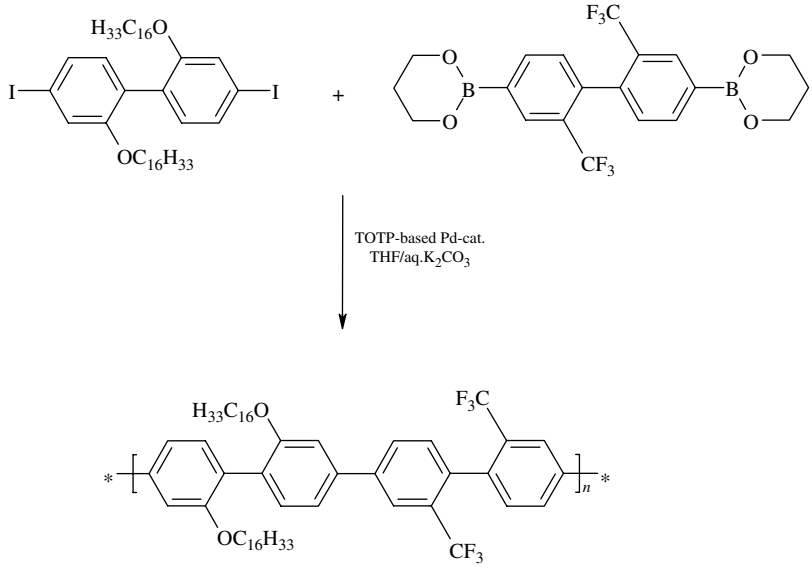
Scheme 8.4 Synthesis of regioregular polythiophenes applying the Kumada methodology (McCullough *et al.* 1993)

Suzuki coupling

The Suzuki coupling is a cross-coupling reaction between an organoboron reagent ($R{-}B(OR')_2$; R=H, (cyclo)alkyl)) and an unsaturated halide, triflate or sulfonate ($R''{-}X$) (Martin and Yang 1993; Miyaura and Suzuki 1995). In general the reaction is catalyzed by tetrakis(triphenylphosphine)palladium(0) ($Pd(PPh_3)_4$) and performed in a two-phase system consisting of an organic solvent (e.g. toluene) and an aqueous basic phase (e.g. Na_2CO_3):

$$R{-}B(OR')_2 + R''{-}X \rightarrow R{-}R'' + X{-}B(OR')_2.$$

The Suzuki reaction, which is also believed to proceed via a multistep cyclic mechanism, has been used many times to prepare π-conjugated polymers; one example is the synthesis of polyphenylenes in Scheme 8.5 (Goodson *et al.* 1998).



Scheme 8.5 Synthesis of polyphenylenes via a Suzuki-type polymerization (Goodson *et al.* 1998)

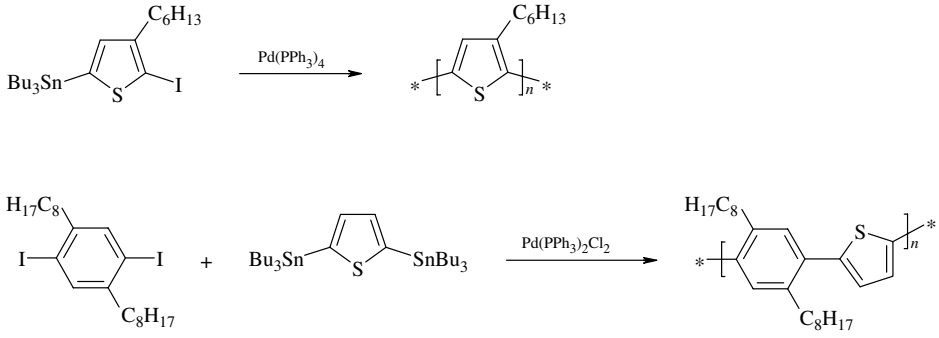
Petitioner Samsung Ex-1011, 0171

Stille coupling

The Stille reaction is a transition-metal-mediated cross-coupling reaction between an organostannane ($R_3Sn{-}R'$) and an unsaturated halide, triflate or sulfonate ($R''{-}X$) that can be performed with a Pd catalyst such as $Pd^0(PPh_3)_4$ or $Pd(PPh_3)_2Cl_2$ in a solvent such as DMF, toluene or dioxane (Stille 1986; Mitchell 1992):

$$R_3Sn{-}R' + R''{-}X \rightarrow R'{-}R'' + R_3Sn{-}X.$$

Although mostly used for the synthesis of small molecules, this coupling reaction has been used several times to synthesize conjugated polymers. Scheme 8.6 shows two examples: one is the synthesis of regioregular poly(3-alkylthiophene)s (Iraqi and Baker 1998) and the other is the copolymerization of phenylene and thienylene units by applying the Stille chemistry (Bao *et al.* 1995).



Scheme 8.6 Polymerization reactions via the Stille methodology (Iraqi and Baker 1998; Bao *et al.* 1995)

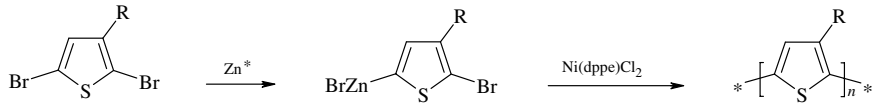
Negishi coupling

The Negishi coupling is a cross-coupling reaction between an organozinc intermediate ($R{-}ZnX$) and an unsaturated halide ($R'{-}X$) (Negishi 1981, 1983). The reaction employs a Pd or Ni catalyst and is performed under mild conditions:

$$R{-}ZnX + R'{-}X \rightarrow R{-}R' + ZnX_2.$$

There are several examples in the literature which use the Negishi coupling methodology to synthesize π-conjugated polymers. One of the best-known examples is the synthesis of regioregular poly(3-alkylthiophene)s as shown in Scheme 8.7 (Chen *et al.* 1995).

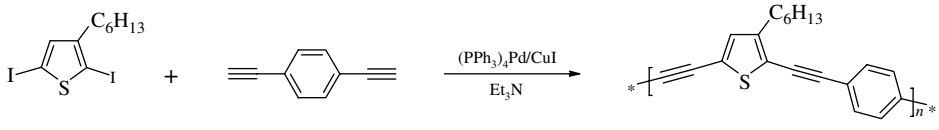
Petitioner Samsung Ex-1011, 0172



Scheme 8.7 Synthesis of regioregular poly(3-alkylthiophene)s applying the Negishi methodology (McCullough 1998; Chen *et al.* 1995)

Heck and Sonogashira coupling

The Heck and the Sonogashira reactions are cross-coupling reactions between an aryl halide and an alkene or alkyne, respectively (Heck 1991). The reactions are mostly Pd-catalyzed and have frequently been used to prepare arylene–ethenylene and arylene–ethynylene oligomers and polymers. Scheme 8.8 shows an example of a Sonogashira type polymerization (Takagi *et al.* 1993; Yamamoto *et al.* 1993).



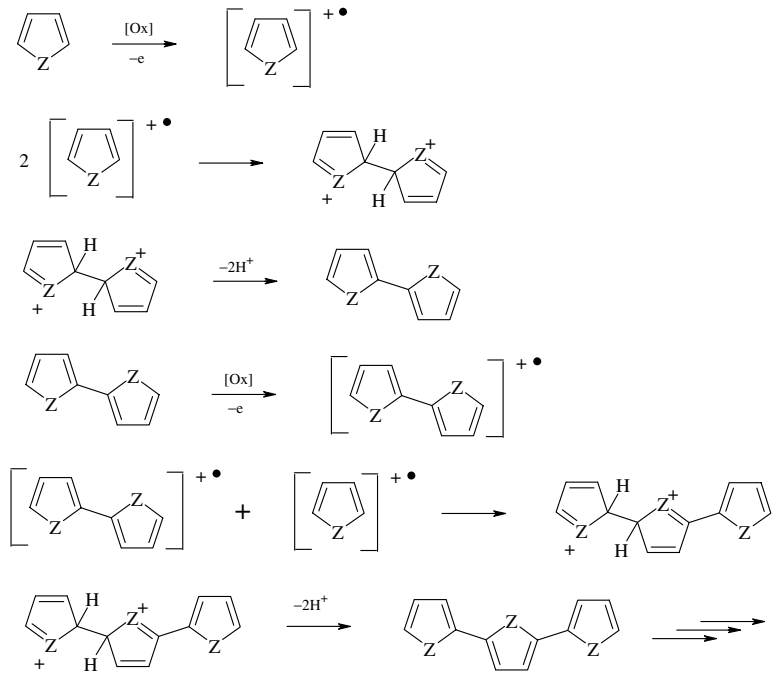
Scheme 8.8 Synthesis of an arylene–ethynylene copolymer via the Sonogashira route

8.3.4 Electrochemical Polymerizations

Besides the chemical polymerization methods discussed above, electrochemical polymerization has also been widely explored during the past decades (Zotti 1997). Depending on the electropolymerization conditions, one can easily obtain films of polyaniline or polyheteroaromatics such as polypyrrole and polythiophene, in aqueous and nonaqueous media. Scheme 8.9 shows the general mechanism.

Electropolymerization has several advantages and disadvantages over chemical polymerization techniques. A first advantage is that after formation of the polymer film from an electrolyte/monomer solution, this film can be directly characterized by cyclic voltammetry, simply by transferring the film into a monomer-free electrolyte solution. A second advantage of electropolymerization is that only small amounts of monomer are needed. This can be an advantage when one has synthesized a new monomer in small quantities and (quickly) wants to study its characteristics and properties. At the same time this is also a disadvantage when one wants to further characterize the resulting polymers and their properties. A third advantage is the fact that the molecule can easily be switched from its reduced state to its oxidized state, and vice versa, by switching the applied potential. In chemically prepared polymers, reduction and oxidation of the polymer are normally performed by using hydrazine and iodine, respectively. Due to the numerous electrochemical studies that have been performed over the years, electrochemical polymerization of conductive polymers has largely contributed to the development of these species. Nevertheless, it is not the method of choice for preparing conductive polymers on a commercial scale.

Petitioner Samsung Ex-1011, 0173



Scheme 8.9 Mechanism for the electrochemical polymerization of a five-membered heteroaromatic monomer

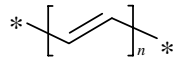
8.4 Overview of Conductive Polymer Types

This section looks at the most frequently studied conductive polymers in more detail: polyacetylene, polyaniline, polypyrrole and polythiophene.

8.4.1 Polyacetylene and Derivatives

Introduction

Acetylene is a bulk chemical that was discovered in the nineteenth century. In the 1950s scientists became interested in its corresponding polymer, polyacetylene (PAc), since it represents the ultimate member of the polyene family:



Polyacetylene

Although the first studies showed that this material is a wideband semiconductor with low intrinsic conductivity, Berets and Smith showed that the conductivity of pressed pellets of

Petitioner Samsung Ex-1011, 0174

PAc could be varied over the range of 10^{-9} to 10^{-2} S/cm by exposure to various Lewis acids and bases (Berets and Smith 1968).

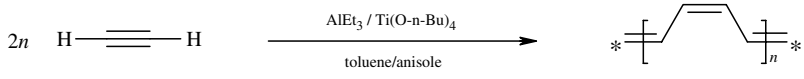
In 1976 Shirakawa, MacDiarmid and Heeger showed that by exposing polyacetylene films to stronger oxidants, conductivities of order 10^2 to 10^3 S/cm could be obtained (Shirakawa *et al.* 1977). These studies initiated the beginning of the modern era of conductive polymers, which in the late 1980s resulted in PAc films with room temperature conductivities (1×10^5 S/cm) (Naarmann and Theophilou 1987; Kaneko *et al.* 1993; Tsukamoto 1992), close to that of copper (6×10^5 S/cm).

Synthesis

Although numerous preparative methods for PAc are known, there are three main synthetic routes to this material.

Shirakawa route

The Shirakawa route is an extension of the initial work described by Natta *et al.* (1958). The polymerization is carried out at the interface of a solution of the initiator system in an inert solvent at $-78\,^{\circ}C$. The initiator concentration used is significantly higher than in Natta's solution phase work, as serendipitously found (Scheme 8.10) (Ito *et al.* 1974; Shirakawa and Ikeda 1980).



Scheme 8.10 Shirakawa's route to polyacetylene (Shirakawa and Ikeda 1980)

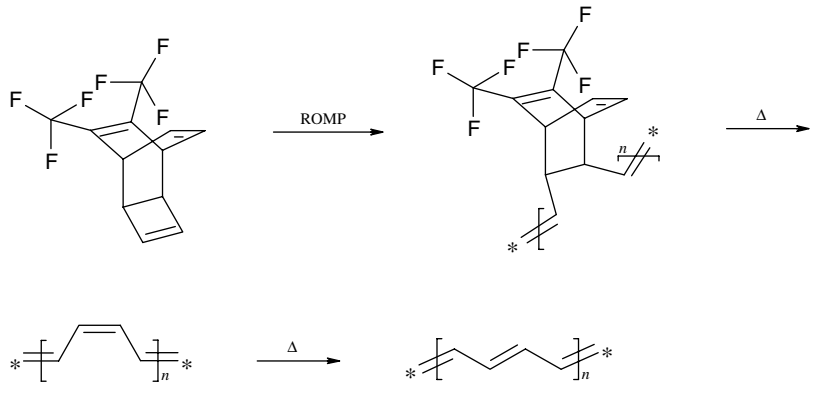
The conditions under which the polymerization is carried out, i.e. concentration, ratios, etc., have a profound effect on the properties and morphology of the films produced. For example, one can obtain a powder, a spongy mass or a film.

Due to its insoluble character, unsubstituted PAc is difficult to characterize. Nevertheless, applying ATR-IR, DSC and other techniques, the most important features can be studied. For example, applying ATR-IR one can observe that the Shirakawa route yields PAc which is mainly *cis* oriented. By reducing the Al/Ti ratio almost pure *trans* PAc can be obtained (Baker *et al.* 1986).

Precursor polymer/Durham route

Due to the reactivity of acetylene resulting in a wide variety of side reactions (formation of benzene, cycloaddition, etc.) as well as to the inherent insolubility and infusibility of polyacetylene, considerable research efforts have been directed towards obtaining PAc by methods that will allow convenient fabrication as well as control over the bulk morphology. In 1980 the Durham group directed by Feast developed an approach that involves the use of prepolymers that can be thermally converted to polyacetylene (Edwards and Feast 1980). Starting from 7,8-bis(trifluoromethyl)tricyclo[4.2.2.$0^{2,5}$]deca-3,7,9-triene and performing a ring opening metathesis type of polymerization with an initiator such as $WCl_6/SnMe_4$, a high molecular weight precursor polymer is obtained which is soluble in common organic

Petitioner Samsung Ex-1011, 0175



Scheme 8.11 Synthesis of polyacetylene via the polymer precursor/Durham route (Edwards and Feast 1980)

solvents and can be purified, characterized and processed by conventional methods. On heating, the precursor polymer can be converted to PAc with the evolution of 1,2-bis(trifluoromethyl)benzene (Scheme 8.11). By controlling the reaction protocol (temperature, time, presence of solvent, etc.), the morphology and properties of the final material can be regulated, yielding amorphous foams or dense oriented films. The dense oriented films have a higher density than films obtained via the Shirakawa route and also possess a much high *trans* content.

In a similar type of reaction Grubbs and coworkers were able to synthesize partially substituted polyacetylenes that are both soluble and highly conjugated (Gorman *et al.* 1993).

Naarmann route

This method, developed by H. Naarmann and colleagues at BASF, is characterized by utilizing silicone oil as a solvent and high-temperature ageing ($> 120\ ^{\circ}C$) of the catalyst, and results in the so-called N-$(CH)_x$ or Naarmann-type PAc films (Haberkorn *et al.* 1988; Naarmann 1990). Although its chemistry is quite similar to the Shirakawa route, this method results in a material that is highly regular, very compact and crystalline in well-defined parallel planes. When it is stretched and doped, the N-(CH)x films show conductivity values of 10^5 S/cm. Due to its synthesis it has a minimal sp^3 fraction, a high *cis* content and high density. Due to these features, the material is considerably more stable than PAc prepared by other methods. The same group also developed the ARA method (addition of reducing agents) for synthesizing PAc. This method also yields highly conductive PAc (Naarmann and Theophilou 1987; Kaneko *et al.* 1993; Tsukamoto 1992).

Properties

What about polyacetylene's electrical and optical properties? PAc is a black material. The highest conductivity values for PAc, i.e. of order 10^5 S/cm, have been obtained by Naarmann and Theophilou (1987) and Tsukamoto *et al.* (1990), applying the high-temperature aging of the catalyst method and I_2 as p-dopant. Other oxidants resulting in highly conductive PAc are AsF_5 and $FeCl_3$. The highest conductivity obtained for reductively doped PAc is

Petitioner Samsung Ex-1011, 0176

5×10^3 S/cm as obtained by Park *et al.* using K as n-dopant (Park *et al.* 1995). Na and Rb also give conductivities in the same range.

The type of polymerization, the reaction conditions, and the experience of the person who is performing the experiment greatly influence the properties of the material. Despite its excellent conductivity values, PAc is an air-sensitive, infusible and insoluble black material. Therefore it is not very likely that this polymer will find its way into industrial applications. It also explains the nonexponential increase in the number of publications on PAc compared to other conductive polymers (Figure 8.5).

8.4.2 Polyaniline and Derivatives

Introduction

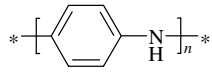
Aniline, the monomer used to prepare polyaniline, has an interesting history (Lawrence and Marshall 1985). It was first obtained by the destructive distillation of indigo by O. Unverdorben in 1826, who named it Krystalline. F. Runge identified it as a constituent of coal tar in 1834 and named it Kyanol. In 1841 C. J. Fritzsche heated indigo with caustic potash and called the product Aniline. In the same year, N. N. Zinin obtained an amine by reduction of nitrobenzene and called it Benzidam. A. W Hofmann proved these products to be identical in 1843 and fixed the name aniline. Since 1854 aniline has been commercially produced, initially for the preparation of dyes, later for numerous other products ranging from agricultural chemicals to rubber chemicals and polymers (Figure 8.6).



Figure 8.6 Chemical plant of the Actien-Gesellschaft für Anilin-Fabrikation, Berlin, during the second half of the nineteenth century. The company is now called Agfa-Gevaert

Petitioner Samsung Ex-1011, 0177

Polyaniline, also known as aniline black, was first prepared by Runge in 1834 (Genies *et al.* 1990). Since then it has been the subject of numerous studies (Trivedi 1997).



Polyaniline

Although the first conductivity measurements were performed at the beginning of the 1960s, it was not until the 1980s that the conducting properties of PAni were really recognized. Since then the number of publications dealing with this conductive polymer grew rapidly (Figure 8.5). The fact that aniline is cheap and conductive PAni can be made soluble and processable has resulted in a competitive race in which industries as well as academic groups have been involved over the years. Nowadays several companies produce polyaniline derivatives for a range of applications.

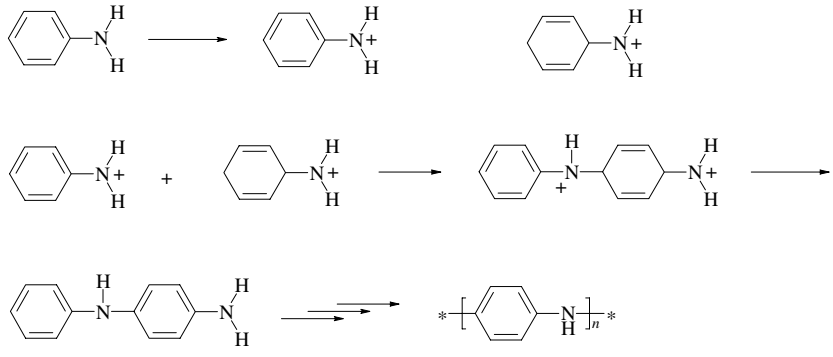
Synthesis

Oxidation of aniline is the most widely employed synthetic route to PAni and can be performed both chemically and electrochemically. Both approaches will be discussed here.

Electrochemical preparation of PAni

The electrochemical method was originally developed by Letheby in 1862 as a test for the determination of small quantities of aniline (Letheby 1862). The method has been improved ever since and has also been applied to all kinds of substituted anilines; the resulting polymers often exhibited conductivity values comparable with that of unsubstituted PAni.

Electrochemical experiments have indicated that oxidative polymerization of aniline occurs at about 0.8 V vs. SCE (Trivedi 1997). Scheme 8.12 shows the mechanism of electropolymerization. In the first step, aniline is oxidized to a radical cation that is resonance stabilized. In the second step, this species couples to a second radical cation (monomeric, oligomeric, or polymeric) after which two H^+ ions are split off, resulting in the formation of larger species. Note that *para* coupling is not exclusive; *ortho* couplings leading to the formation of a disrupted polymer, can also take place. The whole process is diffusion



Scheme 8.12 Mechanism of electrochemical polymerization of aniline to polyaniline

Petitioner Samsung Ex-1011, 0178

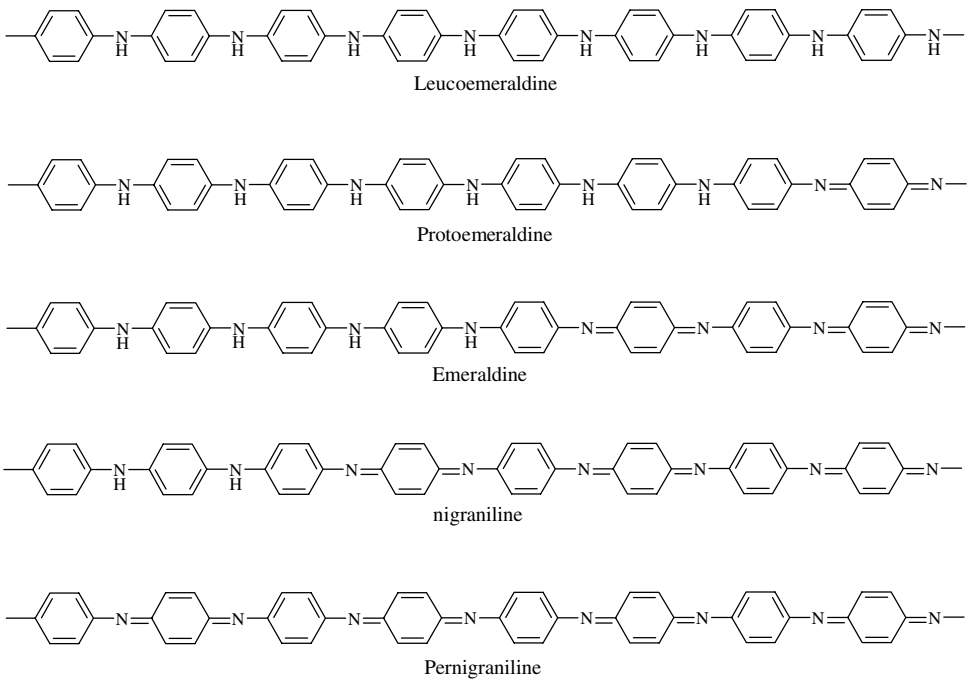


Figure 8.7 Different forms of polyaniline

controlled. As expected, the characteristics of the material obtained greatly depend on the conditions under which polymerization takes place, such as temperature, electrolyte, and pH.

Chemical preparation of PAni

The most preferred method to prepare PAni is to use either HCl or H_2SO_4 with ammonium persulfate as oxidant (Nalwa 1997). This oxidative polymerization is a two-electron exchange reaction, hence the persulfate requirement is one mole per mole of monomer. The resulting blue, nondoped form of PAni, leucoemeraldine, is the primary material from which other forms of PAni can be obtained. The other well-defined oxidation states of PAni, each with its own name as originally attributed by Green and Woodhead, are shown in Figure 8.7 (Green and Woodhead 1910).

In general PAni is insoluble in most common organic and aqueous solvents, irrespective of the method of synthesis. Nevertheless, the emeraldine base can be dissolved in pyridine, DMF and NMP as shown by Epstein and coworkers (Angelopoulos *et al.* 1987). The synthesis of a soluble PAni is of great interest in order to facilitate postsynthesis processing. There are several ways to prepare soluble polymers, e.g. formation of the polymer salt using an anionic dopant which favors dissolution (i.e. protonated PAni is soluble in aqueous acids), or prefunctionalization of the starting monomer with a suitable group. However, prefunctionalization often has a negative effect on the conductivity.

Properties

PAni can occur in a number of well-defined oxidation states. The different states range from the fully reduced leucoemeraldine via protoemeraldine, emeraldine and nigrinaline to the

Petitioner Samsung Ex-1011, 0179

fully oxidized pernigraniline (Green and Woodhead 1910). Unlike most other polyaromatics, the fully oxidized state of PAni is not conducting. As a matter of fact, none of the above states is really conducting. PAni only becomes conducting when the moderately oxidized states, in particular the emeraldine base, are protonated and charge carriers are generated. It is this process, generally called ''protonic acid doping'' (Chiang and MacDiarmid 1986), which makes PAni so unique; no electrons have to be added to or removed from the insulating material to make it conducting. The different oxidation states of PAni can also be generated by doping with oxidants such as iodine, but the resulting conductivity is lower than obtained via protonic acid doping (Wang *et al.* 1991).

The conduction mechanism is believed to involve polaronic carriers; the protonated emeraldine consists of a delocalized poly(semiquinone radical cation) (MacDiarmid 1993). The conductivity is affected by the water content; completely dry samples are five times less conductive than samples containing some water (Scherr *et al.* 1991).

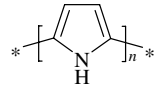
In 1992 Heeger and coworkers reported an extremely useful system composed of camphorsulfonic acid/emeraldine base/*m*-cresol (Cao *et al.* 1992). This three-component system has good solubility in common organic solvents and is compatible with many of the classical polymers. It has led to the preparation of conducting blends with low loading levels of the conducting phase. Camphor sulfonic acid doped PAni has a conductivity of few $\times$ 100 S/cm in the presence of *m*-cresol. The Heeger group also reported a similar system using dodecylbenzenesulfonic acid. The role of *m*-cresol has been explained in terms of secondary doping.

8.4.3 Polypyrrole and Derivatives

Introduction

In May 1834 Friedlieb Ferdinand Runge, at that time working as a chemist at the Chemische Produktenfabrik in Oranienburg, discovered that coal tar contains several interesting compounds (Runge 1834). One of these gave a beautiful bright red color on contact with HCl. He called it pyrrole after the Greek word for ''fiery red oil.'' However, despite many attempts, Runge was not able to separate pyrrole from other products. In 1857 Thomas Anderson, professor of chemistry in Glasgow, was able to isolate this heteroaromatic compound (Anderson 1857). In 1870 Baeyer and Emmerling suggested the correct structure while investigating indole (Baeyer and Emmerling 1870).

Pyrrole was first chemically polymerized in 1916 by oxidation with H_2O_2 to give an amorphous black powder known as pyrrole black (Angeli And Alessandri 1916). However, little further interest was shown in this material until it was electrochemically prepared by Dall'Olio *et al.* (1968). They obtained films of pyrrole black by electrochemical polymerization of pyrrole in 0.1 N sulfuric acid on a Pt electrode. Since then numerous studies have been performed focusing on all aspects of this type of conductive polymer (Figure 8.5).



Polypyrrole

Petitioner Samsung Ex-1011, 0180

Synthesis

Electrochemical polymerization

Electrochemical polymerization of pyrrole is the most commonly employed polymerization method to obtain PPy. Due to pyrrole's low oxidation potential, i.e. 1.20 V vs SCE, it can easily be polymerized in aqueous and organic solvents, providing good quality films on the anode. Numerous studies have been performed to determine the mechanism of this polymerization type, resulting in what has been described in Scheme 8.9 (Z = NH). The type and concentration of the counterion have a considerable influence on the conductivity and the mechanical properties. For example, changing the counterion from oxalate to perchlorate increases the conductivity by a factor of 10 (Jen *et al.* 1986). For more details on the electrochemical polymerization of pyrrole, see Rodriguez *et al.* (1997).

Recently, Reynolds and coworkers synthesized and studied a new class of PPy derivatives, poly(3,4-alkylenedioxypyrroles) (Schottland *et al.* 2000). They have the lowest oxidation potential of all pyrrole derivatives known today. And they exhibit very interesting electrochromic properties – their color changes depending on their oxidation state.

Chemical polymerization

In general, pyrrole blacks have been prepared in the presence of numerous oxidizing reagents, including H_2O_2, PbO_2, $FeCl_3$, nitrous acid, quinones, and ozone. Chemical syntheses with acid or peroxide initiators have mainly resulted in fairly insulating materials. This is associated with the high degree of saturation of the pyrrole rings in such materials, either by oxygen incorporation or by hydrogen saturation. As a result, improved chemical methods have been developed that are able to produce polymers by oxidation while retaining the aromatic characteristics of the pyrrole rings.

A class of oxidants that are often used are the oxidative transition metal ions such as Fe^{3+} and Cu^{2+} (Section 8.3.1). $FeCl_3$, in particular, has been used extensively. It was found that the optimum Fe^{3+}/pyrrole molar ratio is about 2.25; 2 mole equivalents are needed to polymerize all monomer, whereas the remaining 0.25 mole equivalent is needed to oxidize the material.

Structural defects like α–β couplings are inherent to the oxidative polymerization method and are always present in the materials prepared according to the methods described above. This failure to produce perfectly α–α-linked polymers has been overcome by using organometallic coupling methods such as the Stille reaction (Martina *et al.* 1992) and the Ullmann reaction (Groenendaal *et al.* 1995).

Properties

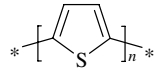
Oxidized PPy is an insoluble black powder that is very stable under ambient conditions and up to temperatures exceeding 300 °C. When electrochemically polymerized onto ITO glass, its films are clearly less transparent than polyaniline or polythiophene films of the same thickness. The neutral form of PPy is difficult to obtain and characterize due to its extreme susceptibility to oxidation – as soon as it ''smells'' oxygen, it starts oxidizing. The conductivity of PPy strongly depends on the oxidizing agent, solvent, concentrations, reaction time, etc. Conductivities up to few × 100 S/cm have been reported by numerous groups (Skotheim 1998; Nalwa 1997; Feast *et al.* 1996; Stenger-Smith 1998; Kiebooms *et al.* 2001; Rodriguez *et al.* 1997).

Petitioner Samsung Ex-1011, 0181

8.4.4 Polythiophene and Derivatives

Introduction

Thiophene was discovered in 1883 by Victor Meyer when a sample of benzene failed to give the characteristic blue indophenine color test during a laboratory demonstration (Meyer 1883). Pursuing this anomaly, Meyer found that his assistant had provided him with high-purity benzene prepared by pyrolysis of calcium benzoate, instead of the conventional benzene derived from coal tar. Subsequently, Meyer isolated thiophene from coal-tar-derived benzene, showed it to be the component responsible for the indophenine color test, established its structure and synthesized it by ring closure of succinic acid with phosphorus pentasulfide.



Polythiophene

Although the first synthesis of oligio- and polythiophenes dates back to the nineteenth century, this area of conductive polymer research really started around 1980. Since then numerous groups have studied polythiophenes with the result that this material has made an enormous contribution to our insight into conductive polymers today. Furthermore, just as for PPy and PAni, polythiophenes have found their way to commercialization.

Synthesis

Electrochemical polymerization

As in the case of polypyrrole, anodic electropolymerization is a very convenient method to prepare polythiophene films. Due to its higher oxidation potential (2.07 V vs SCE), thiophene is more difficult to polymerize than pyrrole (1.20 V vs SCE). Nevertheless, good quality films can easily be prepared on the anode via the mechanism displayed in Scheme 8.9 (X = S). When the electropolymerization is performed under rigorously oxygen- and moisture-free conditions, high conductivity values can be obtained (McCullough 1998; Roncali 1992).

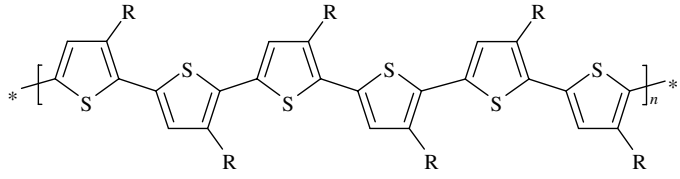
Chemical polymerization

Chemical polymerization of thiophene derivatives is a very broad area, probably the broadest in the conductive polymer field. This section considers the types with the highest impact.

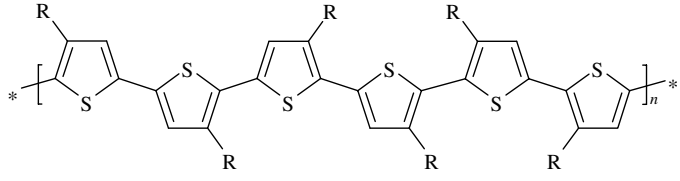
The first type of chemical polymerization of thiophene derivatives is that involving Fe^{3+} salts. In case of 3-alkylthiophenes this method results in soluble poly(3-alkylthiophene)s that can be spincoated or cast onto a substrate. The reaction is normally performed in $CHCl_3$ at 30 °C under a nitrogen atmosphere. After purification by several techniques, polymers are obtained with molecular weights in the range of 10^3 to 10^5 g/mol. Niemi surprisingly found that only solid $FeCl_3$ is active as a polymerization oxidant for 3-alkylthiophenes; the soluble part stays inert (Niemi *et al.* 1992).

A second type of chemical polymerization that has had a large impact is the regioregular polymerization of 3-alkylthiophenes via organometallic coupling reactions. Following a

Petitioner Samsung Ex-1011, 0182



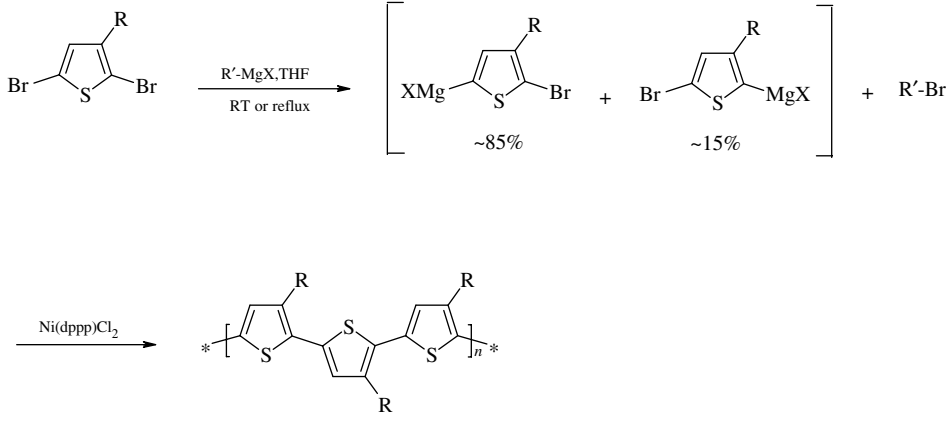
Regioregular(head-to-tail)



Regiorandom

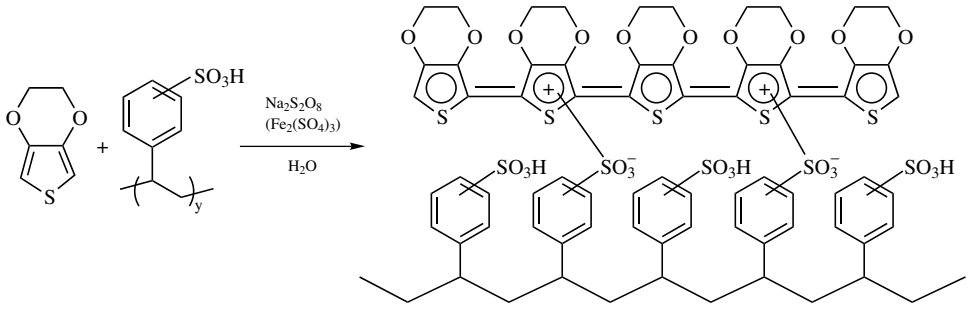
Figure 8.8 Regioregular versus regiorandom poly(3-alkylthiophene)

sequence of selective halogenation/lithiation and subsequent Kumada polymerization (Scheme 8.4) (McCullough *et al.* 1993; McCullough 1998) or Negishi polymerization (Scheme 8.7) (McCullough 1998; Chen *et al.* 1995), high molecular weight poly(3-alkylthiophene)s are obtained in excellent yields. Due to the regioregularity of the side chains (Figure 8.8), the optical and electrical properties of these polymers are much better than those of their regiorandom analogs. Conductivities exceeding 1000 S/cm have been reported showing that order on the nanoscopic scale has a huge influence on the material properties. Recently, McCullough and coworkers serendipitously found a simplified Kumada polymerization, the so-called GRIM (Grignard metathesis) method of Scheme 8.13 (Loewe



Scheme 8.13 Synthesis of regioregular poly(3-alkylthiophene)s via the GRIM method (Loewe *et al.* 2001)

Petitioner Samsung Ex-1011, 0183



Scheme 8.14 Chemical synthesis of poly(3,4-ethylenedioxythiophene)/polystyrenesulfonic acid (PEDT/PSS) (Groenendaal *et al.* 2000)

et al. 2001). In 1994 Inganäs and coworkers were able to regioselectively polymerize 3-(4-octylphenyl)thiophene using $FeCl_3$ (Andersson *et al.* 1994). By adding the $FeCl_3$ slowly and thus maintaining a low Fe^{3+}/Fe^{2+} ratio, this ''soft'' polymerization leads to a polymer with up to 94% head-to-tail couplings.

A final type of polymerization, now a commercial industrial process, involves the chemical polymerization of 3,4-ethylenedioxythiophene in aqueous polystyrenesulfonic acid (Scheme 8.14) (Groenendaal *et al.* 2000). Applying $Na_2S_2O_8/Fe_2(SO_4)_3$ as the oxidant/catalyst systems, a dark blue, aqueous PEDT/PSS dispersion can be obtained. After purification with acidic and basic ion-exchange resins, the resulting polymer dispersion can be coated onto any substrate. Conductivities of PEDT/PSS films range from antistatic ($10^6\,\Omega$/sq) to highly conductive ($< 1000\,\Omega$/sq) depending on the processing conditions. Due to its excellent stability, PEDT/PSS has found its way into several industrial applications.

Properties

The electrical and optical properties of polythiophenes greatly depend on the type of polymerization and the structure of the resulting polymer. Conductivities as high as few $\times$ 100 S/cm have been obtained, although the chemistry involved can sometimes be rather complex. Generally, in contrast to polypyrroles, polythiophenes are more transparent but less stable in their conductive state. This difference in stability is due to the fact that polythiophenes have a significantly higher oxidation potential than polypyrroles. As a result, numerous studies have been performed on neutral polythiophenes. An exception to that stability/conductivity rule are poly(3,4-alkylenedioxythiophene) derivatives; these are both highly conductive and extremely transmissive (Groenendaal *et al.* 2000).

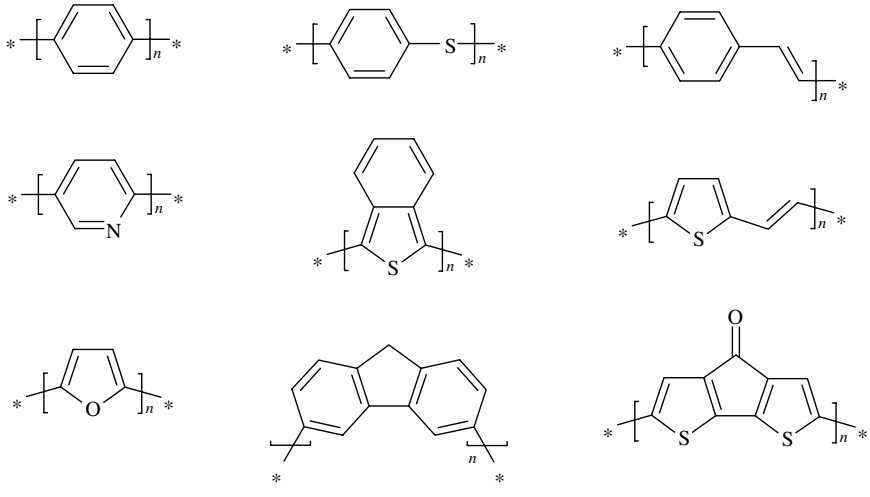
An interesting electrochemical study deals with the relationship between morphology and conductivity, as performed by Garnier and coworkers (Yassar *et al.* 1989). They studied poly(3-methylthiophene) films at various stages of the electropolymerization. The progress of electrochemical polymerization was accompanied by an increasing morphological disorder. The SEM photographs indicated that the surface of a 50 nm film was very smooth whereas that of a 1 μm film was rough. The conductivity of the film decreased rapidly with

Petitioner Samsung Ex-1011, 0184

an increase in thickness. Conversely, when polymer growth was limited to a film of a few nanometers thick, more compact and ordered films were obtained with conductivities as high as 2×10^3 S/cm. From absorption spectra the mean conjugation length was noticeably more extended, as shown by the λ_{max} value of 552 nm in 6 nm thick films.

8.4.5 Other Conductive Polymers

Besides the four conductive polymer families mentioned above there are numerous other systems that have been studied extensively. Scheme 8.15 shows some of these polymers.



Scheme 8.15 Other conductive homo- and copolymers

8.5 Applications for Conductive Polymers

In 1993 Nobel laureate A.J. Heeger estimated that the worldwide market for conductive polymers would reach about $ 1 billion by 2000. Although this number seems rather high, it is very clear that some of the numerous conductive polymers prepared over the past decades have made their way towards commercialization. Three of the main types of polymers discussed here – polyaniline, polypyrrole, and polythiophene – have gone through the whole process of R&D, optimization, scaling-up and production. The following applications are foreseen and/or have been developed based on conductive polymers:

- antistatic coating material,
- electrochromic material in displays and windows,
- electromagnetic interference shielding (EMI),

Petitioner Samsung Ex-1011, 0185

- (bio)sensors and actuators,
- anticorrosion material (corrosion inhibition),
- electrode material in inorganic electroluminescent lamps, capacitors, batteries, etc.,
- membranes,
- electroplating.

Due to the fact that aniline is a cheap bulk chemical, PAni is probably the most investigated conductive polymer in industry. Its applications range from corrosion protection and antistatic materials to electrochromic windows and EMI shielding. Companies that have commercialized polyaniline derivatives are Panipol Ltd (Finland) and Ormecon Chemie (Germany).

A second conducting polymer that has been commercialized is PPy. Its applications range from antistatic material for textiles and fibers to sensors. Companies that have commercialized polypyrrole derivatives are Milliken Corp. (US) and DSM (Netherlands).

A third conductive polymer that has found its way onto the market is polythiophene, or more specifically poly(3,4-ethylenedioxythiophene) (abbreviated as PEDT or PEDOT). Its first application, in the form of a polystyrenesulfonic acid (PEDT/PSS) mixture, was as an antistatic material in photographic films from Agfa-Gevaert. Since then several other applications have been developed or are under development. Some examples are its use as an electrode material in solid electrolyte capacitors, material for through-hole plating of printed circuit boards, antistatic coating for cathode ray tubes and transparent electrode material for inorganic electroluminescent lamps (Figures 8.9 and 8.10). In the devices, the inorganic ITO can be replaced by a PEDT/PSS based transparent electrode (www.agfa.com/sfc/polymer/). Companies that have commercialized PEDT/PSS are Agfa-Gevaert (Belgium) and HC Starck/Bayer (Germany).

A final example of conjugated polymers that have become commercialized are poly(phenylene vinylene) derivatives (PPVs) that have found application in polymer light-emitting diodes (PLEDs). This topic is covered by other chapters in the book.

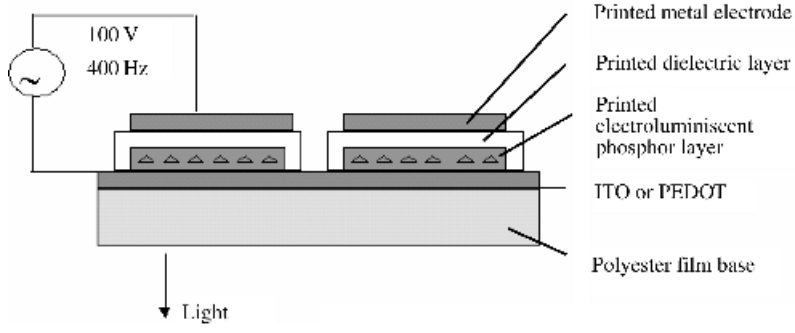


Figure 8.9 PEDT/PSS as electrode material in electroluminescent lamps: surface resistance = 60–2500 Ω/sq and transparency = 85%

Petitioner Samsung Ex-1011, 0186

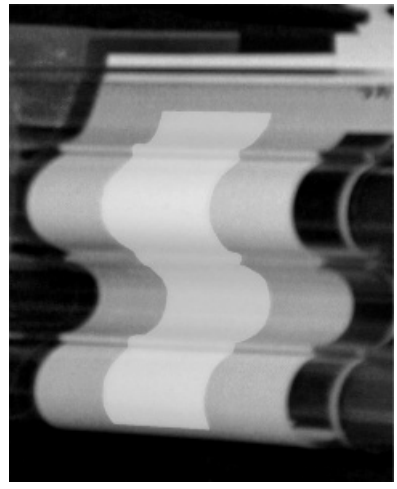


Figure 8.10 A flexible inorganic electroluminescent lamp. PEDOT/PSS is used as transparent electrode

8.6 Outlook

In 1998 J. D. Stenger-Smith wrote, ''Conducting-polymer research is at a critical juncture between laboratory curiosity and commercial viability'' (Stenger-Smith 1998). Although several products are commercially available, he is correct to say that the curiosity phase is almost over. Companies and investors want to see money coming in after many years of investment, and they are right! However, in order to make the step towards commercialization, there are two important questions that have to be answered: Is there a market for a certain product? And is this certain product ready for the market? Only if the answers are both yes does the material have a chance.

The main problem with conductive polymers at the moment is that they are still rather ill-defined and/or their properties are not yet optimized. This means that it will take a few more years before some new products come onto the market because of unreliable and irreproducible synthesis or performance at the moment. For the near future, the market is looking for materials which have conductivities greater than 1000 S/cm, preferably greater than 5000–10 000 S/cm, that are stable, environmentally friendly and easy and reproducible to make.

The compelling question is, what are the optimal properties of the existing materials? The results obtained up to now indicate that low conductivity values are obtainable. However, it might also be that we will have to prepare new materials to reach these values. In addition, the transmission properties must also be retained at high conductivity values. Ultimately the comparison of conductivity and transmission will be made with ITO (Chapter 5). An important aspect for scientists within this field for the coming years will be to synthesize products that are more well-defined and better ordered on the nano-, micro- and macroscopic scales. I hope this comes as a challenge to you!

Petitioner Samsung Ex-1011, 0187

References

Anderson, T. (1857) *Transactions of the Royal Society of Edinburgh, Earth Sciences* **XXI**, 571.

Andersson, M. R., Selse, D., Berggren, M., Jarvinen, H., Hjertberg, T., Inganäs, O., Wennerström, O. and Österholm, J.-E. (1994) *Macromolecules* **27**, 6503.

Angeli, A. (1916) *Gazzetta Chimica Italiana* **46**, 279.

Angeli, A. and Alessandri, L. (1916) *Gazzetta Chimica Italiana* **46**, 283.

Angelopoulos, M., Ray, A., MacDiarmid, A. G. and Epstein, A. J. (1987) *Synthetic Metals* **21**, 21.

Baeyer, A. and Emmerling, H. (1870) *Bernoulli* **3**, 514.

Baker, G. L., Shelburne, J. A. and Bates, F. S. (1986) *Journal of the American Chemical Society* **108**, 7377.

Bao, Z., Chan, W.K. and Yu, L. (1995) *Journal of the American Chemical Society* **117**, 12426.

Berets, D. J. and Smith, D. S. (1968) *Transactions of the Faraday Society* **64**, 823.

Cao, Y., Smith, P. and Heeger, A. J. (1992) *Synthetic Metals* **48**, 91.

Chen, T.-A., Wu, X. and Rieke, R. D. (1995) *Journal of the American Chemical Society* 117, 233.

Chiang, J.-C. and MacDiarmid, A. G. (1986) *Synthetic Metals* **13**, 193.

Dall'Olio, A., Dascola, Y., Varacca, V. and Bocchi, V. (1968) *Comptes Rendus* **C267**, 433.

Edwards, J. H. and Feast, W. J. (1980) *Polymer* **21**, 595.

Epstein, A. J. (1997) *MRS Bulletin* **22**(6), 13.

Fanta, P. E. (1964) *Chemical Review* **64**, 613.

Fanta, P. E. (1974) *Synthesis* **9**.

Feast, W. J., Tsibouklis, J., Pouwer, K. L., Groenendaal, L. and Meijer, E. W. (1996) *Polymer* **37**, 5017.

Genies, E. M., Boyle, A., Lapkowski, M. and Tsintavis, C. (1990) *Synthetic Metals* **36**, 139.

Goodson, F. E., Wallow, T. I. and Novak, B. M. (1998) *Macromolecules* **31**, 2047.

Gorman, C. B., Ginsberg, E. J. and Grubbs, R. H., (1993) *Journal of the American Chemical Society* **115**, 1397.

Green, A. G. and Woodhead, A. E. (1910) *Journal of the Chemical Society, Faraday Transactions* **97**, 2388.

Groenendaal, L., Peerlings, H. W. I., van Dongen, J. L. J., Havinga, E. E., Vekemans, J. A. J. M. and Meijer, E. W. (1995) *Macromolecules* **28**, 116.

Groenendaal, L., Jonas, F., Freitag, D., Pielartzik, H. and Reynolds, J. R. (2000) *Advanced Materials* **12**, 481.

Haberkorn, H., Heckmann, W., Kohler, G., Naarmann, H., Schlag, J., Simak, P., Theophilou, N. and Voelkel, R. (1988) *European Polymer Journal* **24**, 497.

Heck, R. F. (1991) *Comprehensive Organic Synthesis* (eds B. M. Trost and I. Fleming), Pergamon, New York, Vol. 4, p. 833.

Iraqi, A. and Baker, G. W. (1998) *Journal of Materials Chemistry* **8**, 25.

Ito, T., Shirakawa, H. and Ikeda, S. (1974) *Journal of Polymer Science, Polymer Chemistry* **12**, 11.

Jen, K.-W., Miller, G. G. and Elsenbaumer, R. L. (1968) *Journal of the Chemical Society, Chemical Communication,* 1346.

Kalanin, V. N. (1992) *Synthesis*, 413.

Kaneko, H. *et al.* (1993) *Synthetic Metals* **57**, 4888.

Kiebooms, R., Menon, R. and Lee, K. (2001) Chapter 1 in *Handbook of Advanced Electronic and Photonic Materials and Devices* (ed. H. S. Nalwa), Vol. 8, Conducting Polymers, Academic Press.

Kumada, M. (1980) *Pure and Applied Chemistry* **52**, 669.

Labes, M. M., Love, P. and Nichols, L. F. (1979) *Chemical Review* **79**, 1.

Lawrence, F. R. and Marshall, W. J. (1985) *Ullmann's Encyclopedia of Industrial Chemistry* (ed. W. Gerhartz), VCH-Weinheim, Vol. A2, p. 303.

Letheby, H. (1862) *Journal of the Chemical Society* **161**.

Loewe, R. S., Ewbank, P. C., Liu, J., Zhai, L. and McCullough, R. D. (2001) *Macromolecules* **34**, 4324.

Petitioner Samsung Ex-1011, 0188

MacDiarmid, A. G. (1993) Chapter 6 in *Conjugated Polymers and Related Materials*, Oxford University Press 6.
Malleron, J.-L. (1997) *Handbook of Pd-catalyzed Organic Reaction* (eds J.-C. Fiaud and J.-Y. Legros), Academic Press, San Diego, CA.
Martin, A. R. and Yang, Y. (1993) *Acta Chemica Scandinavica* **47**, 221.
Martina, S., Enkelmann, V., Wegner, G. and Schlütter, A.-D. (1992) *Synthetic Metals* **51**, 299.
McCullough, R. D. (1998) *Advanced Materials* **10**, 93.
McCullough, R. D., Lowe, R. D., Jayaraman, M. and Anderson, D. L. (1993) *Journal of Organic Chemistry* **58**, 904.
Meyer, V. (1883) *Chemiche Berichte* **16**, 1465.
Mitchell, T. N. (1992) *Synthesis* 803.
Miyaura, N. and Suzuki, A. (1995) *Chemical Reviews* **95**, 2457.
Naarmann, H. (1990) *Advanced Materials* **2**, 345.
Naarmann, H. and Theophilou, N. (1987) *Synthetic Metals* **22**, 1.
Nalwa, H. S. (ed.) (1997) *Handbook of Organic Conductive Molecules and Polymers*, Vols 1 to 4, John Wiley & Sons, Ltd, Chichester.
Natta, G., Mazzanti, G. and Corradini, P. (1958) *Atti della Accademia Nazionale dei Lincei Rendiconti* **25**, 3.
Negishi, E.-I. (1981) *Pure and Applied Chemistry* **53**, 2333.
Negishi, E.-I. (1983) *Current Trends in Organic Chemistry* (ed. H. Nozaki), Pergamon, Oxford.
Niemi, V. M., Knuuttila, P., Österholm, J. E. and Kolvola, J. (1992) *Polymer* **33**, 1559.
Park, E. B. *et al.* (1995) *Synthetic Metals* **69**, 61.
Rodriguez, J., Grande, H.-J. and Otero, T. F. (1997) Chapter 10 in *Handbook of Organic Conductive Molecules and Polymers*, Vol. 2 (ed. H. S. Nalwa), John Wiley & Sons, Inc., New York.
Roncali, J. (1992) *Chemical Reviews* **92**, 711.
Runge, F. F. (1834) *Poggendorf Annalen* **31**, 65.
Scherr, E. M., MacDiarmid, A. G., Manohar, S. K., Masters, J. G., Sun, Y., Tang, X., Druy, M. A., Glatkowsky, P. J., Cajipe, V. B., Fischer, J. E., Cromack, K. R., Jozefowitcz, M. E., Ginder, J. M., McCall, R. P. and Epstein, A. J. (1991) *Synthetic Metals* **41**, 735.
Schottland, P., Zong, K., Gaupp, C., Thompson, B., Thomas, C., Giurgiu, I., Hickman, R. , Abboud, K. and Reynolds, J. R. (2000) *Macromolecules* **33**, 7051.
Shirakawa, H. and Ikeda, S. (1980) *Synthetic Metals* **1**, 175.
Shirakawa, H., Louis, F.J., MacDiarmid, A. G., Chiang, C. K. and Heeger, A. J. (1977) *Journal of the Chemical Society, Chemical Communication*, 578.
Shirakawa, H., MacDiarmid, A. G and Heeger, A. J. (2001) *Angewandte Chemie International Edition in English* **40**, 2575.
Skotheim, T. A. (1998) *Handbook of Conducting Polymers*, 2nd edn (eds R. L. Elsenbaumer and J. R. Reynolds), Marcel Dekker, New York.
Stenger-Smith, J. D. (1998) *Progress in Polymer Science* **23**, 57.
Stille, J. K. (1986) *Angewandte Chemie International Edition in English* **25**, 508.
Sugimoto, R., Takeda, S., Gu, H. B. and Yoshino, K. (1986) *Chemical Express* **1**, 635.
Takagi, M., Kizu, K., Miyazaki, Y., Kubota, K. and Yamamoto, T. (1993) *Chemistry Letters* **913**.
Trivedi, D. C. (1997) Chapter 12 in *Handbook of Organic Conductive Molecules and Polymers*, Vol. 2 (ed. H. S. Nalwa), John Wiley & Sons, Inc., New York.
Tsukamoto, J. (1992) *Advanced Physics* **41**, 509.
Tsukamoto, J., Takahashi, A. and Kawasaki, K. (1990) *Japanese Journal of Applied Physics* **29**, 125.
Wang, L., Ling, X. and Wang, F. (1991) *Synthetic Metals* **41**, 739.
Yamamoto, T. (1997) Chapter 5 in *Handbook of Organic Conductive Molecules and Polymers*, Vol. 2 (ed. H. S. Nalwa), John Wiley & Sons, Inc., New York.
Yamamoto, T. (1999) *Bulletin of the Chemical Society of Japan* **72**, 621.

Petitioner Samsung Ex-1011, 0189

Yamamoto, T., Takagi, M., Maruyama, T., Kubota, K., Kanbara, H., Kurihara, T. and Kaino, T. (1993) *Journal of the Chemical Society, Chemical Communication*, 797.

Yamamoto, T., Takeuchi, M. and Kubota, K. (2000) *Journal of Polymer Science, Polymer Physics* **38**, 1348.

Yamamoto, T., Shiraishi, K., Abla, M., Yamaguchi, I. and Groenendaal, L. (2002) *Polymer* **43**, 711.

Yassar, A., Roncali, J. and Garnier, F. (1989) *Macromolecules* **22**, 804.

Zotti, G. (1997) Chapter 4 in *Handbook of Organic Conductive Molecules and Polymers*, Vol. 2 (ed. H. S. Nalwa), John Wiley & Sons, Inc., New York.

Petitioner Samsung Ex-1011, 0190

9

Mechanical Reliability of Conductive Polymers for Rollable Display Applications

Darran R. Cairns

3M Touch Systems

9.1 Introduction

As displays permeate our homes, our workplaces, our vehicles and the world around us, designers are hungry for greater freedom in their display applications. Some of the most sought-after attributes of the next generation of displays include large size, a thin profile, low weight, the ability to make curved displays and flexibility. Of course in an ideal world these would all come at a modest price and the displays would also have high contrast, high brightness and maintain their properties indefinitely.

Over the past few years a wide range of flexible displays have been developed in the laboratory. Almost every current display technology has been proposed. Proposed liquid crystal (LC) technologies range from twisted nematic liquid crystal displays (TN-LCDs) (Gardner and Wenz *et al.* 1995) to cholesteric LCDs (West *et al.* 1999), and polymer-dispersed liquid crystal (PDLC) displays (Sheraw *et al.* 2002). Emissive displays have also been developed including flexible organic light-emitting diodes (OLEDs) (Krasnov and Lee 2002), electroluminescent (EL) displays (Chwang *et al.* 2003), field-emitting diodes (FEDs) (Lee and Lee 2003) and even flexible plasma displays (Wedding *et al.* 2004). In addition, a

Flexible Flat Panel Displays Edited by G. P. Crawford
© 2005 John Wiley & Sons, Ltd., ISBN 0-470-87048-6

Petitioner Samsung Ex-1011, 0192

number of display technologies that are envisioned for paper-like display applications are seen as being particularly useful in a flexible format, including encapsulated electrophoretics such as e-ink (Drzaic *et al.* 1998) and the bichromal ball technology Gyricon (Sheridon, 1999).

Due to the difficulties in developing flexible backlights for displays and the high manufacturing cost, much effort has been placed on reflective display technologies. A number of researchers have been particularly attracted to cholesteric displays (Kim *et al.* 1999; West *et al.* 1995; Slikkerveer *et al.* 2002), including Podojil and coworkers (Podojol *et al.* 1998) who use a fast dynamic switching algorithm to obtain high resolution (133 dpi). West and coworkers have actually created a full-color plastic cholesteric liquid crystal display using a vertical stacking approach to improve brightness and resolution, and have also found that substrate birefringence plays a role between the color layers (West *et al.* 1999). The degradation of optics is particularly challenging to the development of high-quality flexible displays. In addition, the precise lamination of multiple optical films provides a severe manufacturing challenge.

Recently, Philips researchers have described a potential solution to this challenge by employing simple coating techniques, comparable to painting, where liquid crystal and polymer materials can be prepared on a single substrate (Penterman *et al.* 2002). This revolutionary approach makes displays cheaper, thinner, and easier to process, and provides great design freedom. In their approach, the complete displays are built from the bottom up on a single substrate by subsequently coating all functional layers on top of each other in utilizing photopolymerization to seal the liquid crystal cell.

An alternative roll-to-roll process has been proposed by researchers at Eastman Kodak. Stephenson et al (Stephenson *et al.* 2004) have fabricated prototype flexible displays using photographic technology. The entire device is coated on to a laser-patterned ITO-coated PET substrate to produce addressing lines. The first coating layer is a cholesteric polymer-dispersed liquid crystal (cPDLC) followed by a dark polymer layer to act as the black state and then a screen-printed polymer thick film conductor ink for addressing electrodes. The resulting display is reflective and therefore does not require a backlight. In the short term, reflective technologies are likely to dominate the flexible display market until robust flexible backlights can be developed. However, Slikkerveer *et al.* (2004) have developed one potential back light solution based on a silicone-elastomer backlight.

Emissive display materials for flexible displays were widely reported at the 33rd Society for Information Display Symposium (Kim and Kafaf 2002; Grove *et al.* 2002; Becker *et al.* 2002; Funamoto *et al.* 2002; Haskal *et al.* 2002; Innocenzo *et al.* 2002). Flexible OLEDs (FOLED) have been demonstrated by researchers for both low molecular weight OLEDs (Gu *et al.* 1997) and polymer OLEDs (Haskal *et al.* 2002). Low molecular weight FOLEDs are vacuum deposited on a polyester substrate which can withstand both the manufacturing and considerable flexing with little degradation of its display characteristics. Polymeric OLEDS have been used to fabricate flexible PLEDS using inkjet printing methods. However, for polymer OLEDS there is still much work needed to develop suitable inks and reliable inkjet heads for mass manufacturing (Miayshita 2002).

One of the major challenges to developing flexible displays is the need to design displays that are not only flexible but that also do not degrade due to permeation of gases. This is particularly important for emissive displays such as OLEDs, EL displays and plasma displays. However, it is also important in transmissive displays where the backlight may be based on an emissive technology. The organic molecules used for OLEDs and EL displays are degraded by H_2O and O_2 molecules (Burrows *et al.* 1994). In addition, for

Petitioner Samsung Ex-1011, 0193

efficient OLEDs, low work function metals such as magnesium are required for the cathode, and these cathode materials are also degraded by water and oxygen permeation (Aziz *et al.* 1998). The low density and small thickness of transparent flexible substrates provide a poor barrier to gas and moisture permeation. Improved barrier layers are being developed to help with this problem, however, a moisture permeation rate of less than 10^{-5} g/m^2 per day (Burrows *et al.* 2001) is required to ensure adequate lifetimes. This is a great challenge and is also below the detection rate of current commercial systems. Plasma displays are similarly vulnerable to gas and moisture permeation.

In a plasma display, a low-pressure gas (typically a Xe-rich mixture) is ionized into a plasma by application of an AC field (Oversluizen *et al.* 2000). The ionized plasma then causes a phosporescent coating to emit colored light. The gas becomes more difficult to ionize as permeation occurs and the phosphor also degrades. One potential solution to gas and moisture permeation is to encapsulate the active material. This approach was reported recently by Wedding *et al.* (2004). By encapsulating an ionizable gas in a dielectric material, a plasma sphere is created. This plasma sphere acts as a barrier to gas permeation and therefore when applied to a flexible substrate the substrate is not required to have good barrier properties. A similar approach is used for commercially available electrophoretics such as e-ink (Drzaic *et al.* 1998).

In e-ink, TiO_2 particles are dispersed in a black ink and encapsulated in a transparent polymer sphere. These polymer spheres are then coated onto an active matrix backplane and a transparent anode completes the device. In this case the barrier properties are provided by the spheres. These spheres can be dispersed in a binder and easily processed or printed on a plastic substrate (Rogers *et al.* 2001; Kawase *et al.* 2002). These materials have a white Lambertian reflection and therefore are well suited for paper surrogate applications (Crawford 2000).

One component common to almost all display types is a flexible anode. At present there are two main candidate materials for transparent conducting electrodes: indium tin oxide (ITO) (Lewis and Paine 2000) and polyethylene dioxythiophene doped with polystyrene sulfonate (PEDOT:PSS) (Kim and Kafafi 2002) coated on PET. Substrate materials include polycarbonate, polyacrylate, polyimide, polyethyleneterephthalate (PET), polyestersulfone (PES) and polyolefins. With a glass transition temperature of $T_g = 210\,^{\circ}\mathrm{C}$, PES allows higher manufacturing temperatures than other plastic substrates; however, PET is currently the most investigated because of its low cost, clarity, and transmission. With low sheet resistances ($< 100\,\Omega/\square$) and good optical throughput ($> 90\%$), the negative aspect of ITO on PET is that it cracks at a relatively low strain ($< 2\%$) (Leterrier *et al.* 2004). However, PEDOT can withstand strain of few $\times$ 10%, but at this time the sheet resistance is much higher ($>$ few $\times$ 2 k$\Omega/\square$) and optical throughput is typically inferior to that of ITO ($< 90\%$) for reasonable sheet resistances. A flexible anode material that does not degrade significantly in service is essential to the development of next-generation flexible displays. In this chapter we will discuss our work on the reliability of flexible anode materials.

9.2 Electromechanical Properties of Transparent Anodes

By far the most common flexible anode material is ITO-coated PET (Chapters 5, 6, and 7). This is an unusual mechanical system with a hard, brittle ceramic material applied to a viscoelastic polymer substrate. When a thin, brittle film adhered to such a substrate is

Petitioner Samsung Ex-1011, 0194

subjected to a tensile stress, multiple cracks form in the brittle layer perpendicular to the applied stress (Leterrier *et al.* 2004). The number of cracks and the strain at which they form depend on the material properties of the film and substrate, the thickness of the film and the interfacial shear strength (Chen *et al.* 1999).

There are a number of complicating factors: the difference in modulii is very large for a polymer–ceramic system; the polymer substrate is very temperature dependent; and the substrate is very flexible, which means deformation by bending is a very real issue. Little work has been carried out previously on these systems, however, SiO_x on PET has been studied by Leterrier *et al.* (1997a, 1997b) and Yanaka *et al.* (1999). These materials were primarily used for food packaging. There is currently burgeoning interest in these materials systems because of the advent of flexible electronic devices.

In considering the mechanical reliability, there are two important parameters: (i) the maximum strain a device can be deformed to once before damage occurs; (ii) the maximum strain a device can be deformed to many times without causing degradation with repeated cycling. In the following sections we will discuss changes in resistance of ITO-coated PET and PEDOT:PSS-coated PET with monotonically increasing tensile strain and during cyclic mandrel loading. In mandrel bending, the strain is constant and is inversely proportional to the mandrel diameter. We will also discuss the effect of temperature on resistance for both flexible anodes.

9.2.1 ITO-Coated PET in Tension

Thin films of ITO were deposited on a 125 μm thick PET (Dupont ST 504) substrate by DC magnetron sputtering in a dedicated commercial roll coater system. Samples with sheet resistances of 61 Ω/□, 70 Ω/□, 100 Ω/□, 300 Ω/□, and 400 Ω/□ were prepared.

Mechanical tests of the ITO-coated PET samples were performed using a miniature tensile testing machine (Rheometric Scientific Minimat 2000) at constant crosshead speed. Samples were processed in the shape of a dog bone with a gauge length of 21.8 mm and a gauge width of 4.7 mm. Care was taken in the cutting of the samples to avoid premature cracking of the ITO layer and samples were viewed on the optical microscope to check for signs of severe damage to the ITO prior to further investigation. The crack evolution with strain was monitored in situ with a long-distance microscope (Infinity Photo-Optical Company, model K2). The resistance as a function of uniaxial strain was measured in situ using a standard four-point measurement technique (Ohring 1992).

In tension, initial cracking occurs perpendicular to the loading direction in the ITO layer at strains close to 2.75% strain, and the number of cracks perpendicular to the loading direction increases rapidly between 2.75% and 3.25% strain then saturates.

Optical micrographs of the early stages of the crack evolution of a 70 Ω/□ (105 nm) ITO layer are shown in Figure 9.1; the strain increases from 2% to 3.3% from left to right. (i) Cracking was first observed at 2.3% nominal strain; (ii) the number of cracks then increased rapidly to 2.6% strain; (iii) at 6% strain, transverse cracking occurs due to lateral contraction; (iv) at 10% strain, tertiary cracks appear parallel to the primary cracks but these tertiary cracks are stopped by the secondary cracks. The fragment length decreases with increasing strain. Lines have been drawn over the cracks in the figure to improve contrast. Figure 9.2 graphs the cumulative probability of fragment length as a function of

Petitioner Samsung Ex-1011, 0195

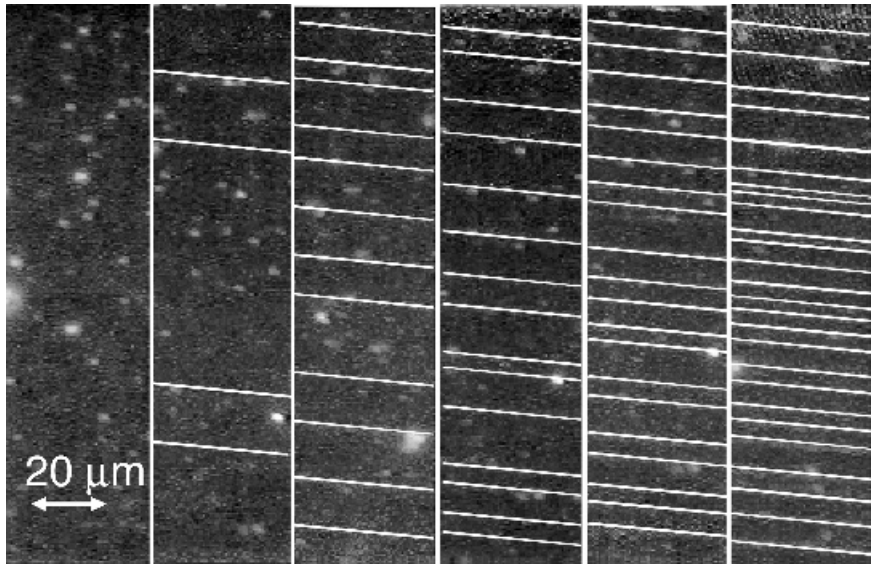


Figure 9.1 Optical micrographs showing the evolution of cracking of the ITO layer in tension. Strain increases from 2% to 3.3% from left to right

strain for this sample. The distribution of fragment length becomes narrower with increasing strain.

The change in resistance as a function of uniaxial strain for the three ITO thicknesses are presented in Figure 9.3. In all cases the resistance increases sharply at some critical strain

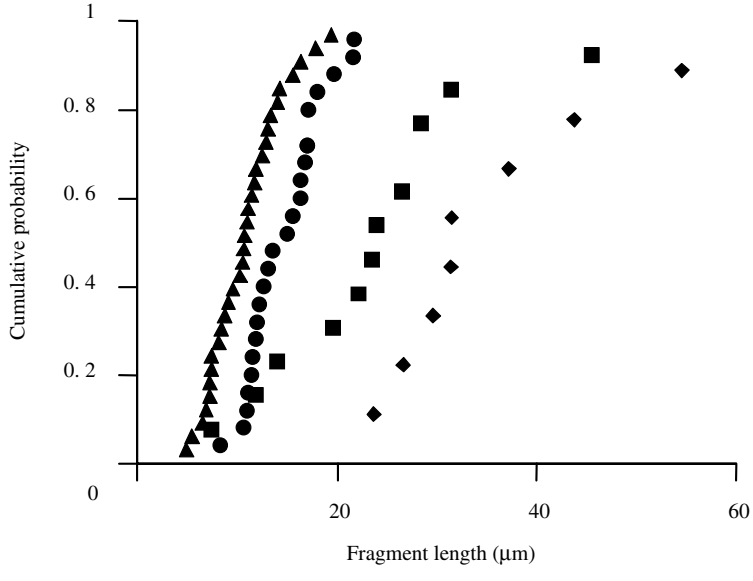


Figure 9.2 Cumulative probability of fragment length for ITO-coated PET at different strains: strained to (◆) 2.4%, (■) 2.6% (●) 3.1%, (▲) 3.7%

Petitioner Samsung Ex-1011, 0196

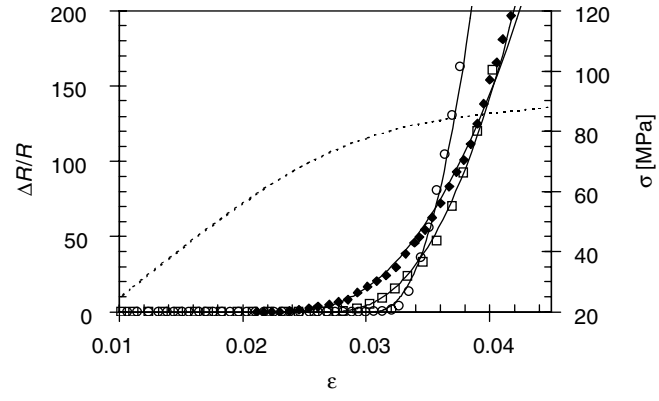


Figure 9.3 Fractional change in resistance $\Delta R/R$ of ITO-coated PET as a function of strain ε (left-hand axis). Experimental data for three thicknesses are shown as points: (◆) 105 nm, (□) 42 nm, and (○)16.8 nm; modeled fits are shown as solid lines. The stress–strain curve for ITO-coated PET (right-hand axis) is shown as a dotted line. Reprinted, with permission, from *Applied Physics Letters* **76**, 1425 (2000)

which depends on ITO film thickness. The resistance of the thickest ITO film increases at the lowest strain, while the resistance of the thinnest ITO layer begins to rapidly increase at the highest critical strain. This is consistent with studies of thin ceramic films on ductile substrates where the critical strain for cracking was inversely proportional to the square root of film thickness (Wang *et al.* 1998). The thickest film begins to increase in resistance at the lowest strain but the rate of increase is less than for the thinner films. At sufficiently high strains, the thinnest sample has increased in resistance by the greatest amount.

It is not surprising that the increase in resistance is due to cracking but it is surprising that the increase in resistance is gradual rather than a sharp catastrophic loss in continuity as the first crack forms across the entire sample width. This implies that there must be some conducting path between neighboring ITO fragments after a crack is formed. From SEM and AFM micrographs (Cairns *et al.* 2000) we conclude that there is very little debris inside the cracks and we therefore postulate that there is some residual conducting layer at the base of the crack. In a previous report (Cairns *et al.* 2000) we have shown that the resistance of a number of these cracks can be described by

$$R_{\text{increase}} = \frac{\rho D^2 L_0 (1+\varepsilon) \sum_{i=1}^{m} (\varepsilon - \varepsilon_{\text{ci}})^2}{V}, \tag{9.1}$$

where ρ is resistivity, D and L_0 length scales, ε the strain of interest, ε_{ci} the strain at which the ith crack formed, m the total number of cracks and V the volume of conducting material in the crack.

While a critical strain of 3% is limiting for flexible displays, ITO-coated PET may still be suitable for use in conformable displays (Cairns *et al.* 2003). It may also be possible to utilize the improved durability of the ITO layer above T_g to fabricate conformal displays with very small radius of curvature features by processing in the following way: (1) heat

Petitioner Samsung Ex-1011, 0197

without distorting above T_g; (2) conform heated display to template; (3) hold display and template at temperature for 1 h; (4) cool display and template; and (5) remove conformal display from template.

9.2.2 PEDOT:PSS in Tension

Figure 9.4 is a graph showing resistance as a function of strain for PEDOT:PSS-coated PET (Agfa Orgacon EL1500) at different temperatures. The resistance increases with increasing strain in each case, but the rate of increase is much less than for ITO-coated PET. This is expected since ITO is a brittle ceramic and known to crack whereas PEDOT:PSS is a polymeric coating. The PEDOT:PSS coating continues to conduct beyond 60% strain, far in excess of the 3% observed for ITO.

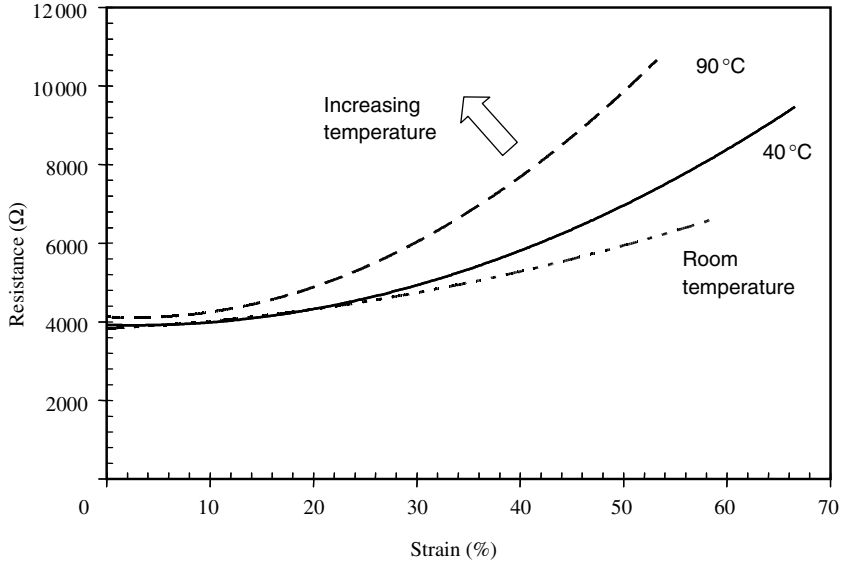


Figure 9.4 Resistance versus strain for PEDOT:PSS-coated PET deformed in uniaxial strain at room temperature, 40 °C, and 90 °C. The rate of increase of resistance with increasing strain increases with temperature

The effect of temperature on the electromechanical properties of PEDOT is dramatic, and increased temperature degrades the electrical conductivity. For samples deformed at 90 °C the resistance had doubled at a strain of 40%, ten times the increase observed at room temperature. While the resistance of the material is still finite, it is important to understand the thermal and/or thermomechanical degradation of PEDOT:PSS. Initial work on the thermal degradation has been reported (Rannou and Nechtschein 1999).

9.2.3 Cyclic Loading in Tension

We have loaded ITO-coated PET (Polar Vision Inc.) and PEDOT:PSS-coated substrates (Agfa Orgacon EL1500) repeatedly around mandrels and monitored the resistance as a

Petitioner Samsung Ex-1011, 0198

function of the number of cycles. Four different mandrel diameters were used: 7.6 mm, 10 mm, 17.6 mm and 25.4 mm. For 7 mil (175 μm) PET substrates the approximate strain in the conducting layer is 0.6%, 0.9%, 1.5% and 2%. This was done in situ using a custom-built testing system (Figure 9.7). The sample had length 20 cm, width 5 cm, and thickness 0.17 mm. This testing can be extended to loading in compression (i.e. with the ITO side on the inside of the substrate).

In addition, tensile samples were deformed in uniaxial tension and the resistance monitored in situ using a four-point resistance configuration. The tensile stress–strain testing was loaded using a miniature tensile tester (Rheometric Scientific Minimat 2000) at a crosshead speed of 0.1 mm/min. Tensile samples had dimensions of 7.8 mm gauge length, 4.7 mm gauge width and 0.17 mm gauge thickness.

ITO-coated PET and PEDOT:PSS-coated PET samples were repeatedly loaded and unloaded to 1.5% strain in uniaxial tension. The resistance was monitored in situ and the results for PEDOT:PSS are shown in Figure 9.5. The resistance increases approximately linearly during the loading portion of the cycle and decreases exponentially during unloading.

This is consistent with the changes in dimensions of the polymer substrate during the loading portion of the cycle. The increase in strain is linear; during unloading the polymer does not spontaneously recover its shape but recovers over time. This is particularly true for the gauge width. The resistance as a function of strain during the loading cycle (assuming no

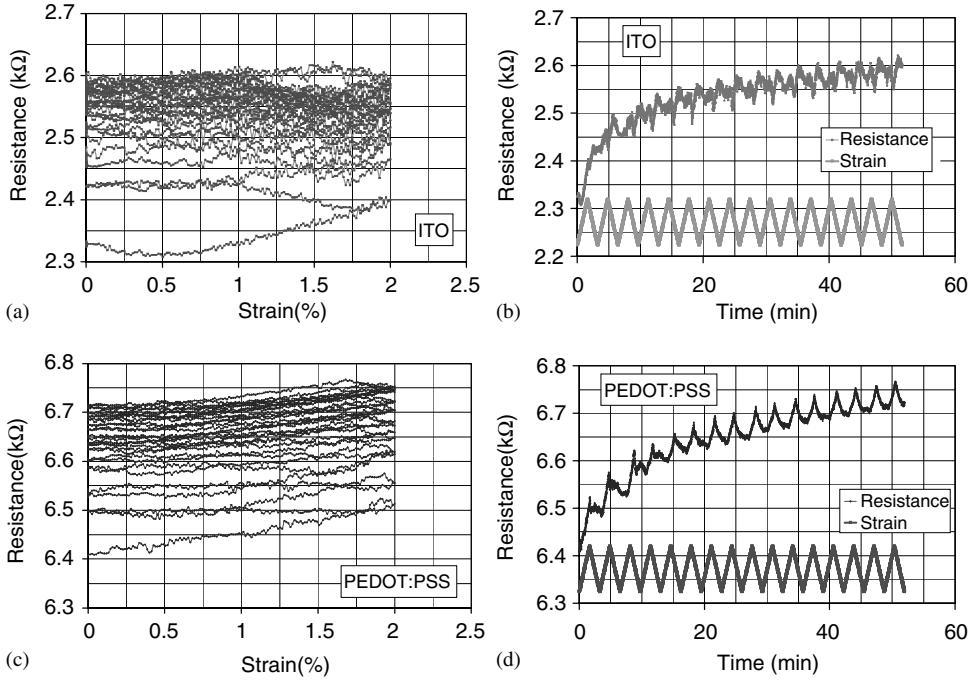


Figure 9.5 Fatigue test data for the cyclic loading of (a, b) ITO-coated PET and (c, d) PEDOT:PSS coated PET loaded in tension

Petitioner Samsung Ex-1011, 0199

cracking) can be quantified in terms of the applied strain, ε, the Poisson's ratio of the substrate, ν_s and the Poisson's ratio of the conducting layer, ν_f, given by

$$R = R_0 \frac{(1+\varepsilon)}{(1-\nu_s)(1-\nu_f)}. \tag{9.2}$$

During the unloading cycle, the substrate does not fully recover before the next loading cycle begins; therefore the gauge width decreases with each cycle until equilibrium occurs between the applied strain and the recovery of the gauge width. This is evident in Figure 9.5 by an underlying increase in resistance that gradually levels off after approximately 50 cycles.

9.3 Environmental Degradation of PEDOT:PSS

To investigate the environmental stability of flexible anodes utilizing PEDOT:PSS, silver electrodes (DuPont Membrane Switch Compound) were applied to a sheet of PEDOT:PSS-coated PET (AGFA ORGACON EL1500 using screen printing. The printed substrate was fired at 100 °C for 5 min to cure the silver. Leads were attached to the electrodes, then the entire device was placed inside a controlled environment chamber and aged at 60 °C and 90% relative humidity (RH). The resistance between two electrodes (3 in × 0.25 in) separated by 1.5 in was monitored in situ using a digital multimeter (Agilent Technoolgies 34401A). The resultant graph of resistance versus aging time is shown in Figure 9.6.

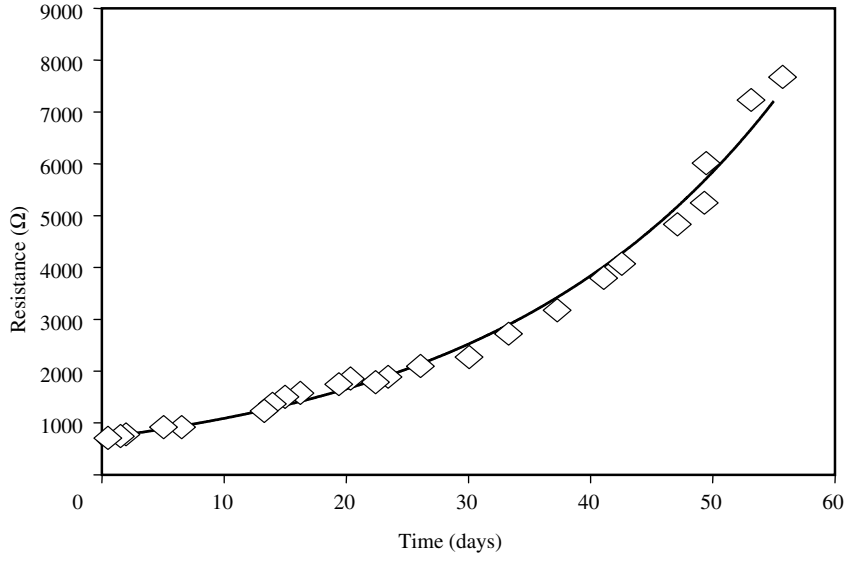


Figure 9.6 Relative sheet resistance and contact resistance versus time at 60 °C and 90% relative humidity for PEDOT:PSS printed with DuPont 5089 Silver Carbon Conductor

Petitioner Samsung Ex-1011, 0200

The increase in resistance is approximately exponential, with the resistance doubling approximately every 20 days. This supports the work of Rannou *et al.* and highlights the need for considering any device designed using PEDOT:PSS.

9.4 Cyclic Mandrel Loading of Flexible Anodes

The change in resistance with increasing strain is important in determining initial design constraints; however, when considering the reliability in service, repeated deformation is necessary. To gain an understanding of the long-term change in resistance due to deformation we designed a cyclic loading rig.

Figure 9.7 is a schematic diagram of the apparatus showing the main components. The system allows loading and unloading of the sample around a mandrel at a precise and controlled rate (Gorkhali *et al.* 2004). This structure has been built on a heavy optical table to reduce external vibration. Samples as big as 3 in wide and 10 in long can be tested with the current configuration. One end of the sample is firmly fastened to the mandrel by a metal plate screwed on to the curved mandrel surface. The other end of the sample is clamped between a pair of thin metal plates, held in place by a low-tension spring. A flat base plate holds the spring and the sample in the horizontal position and prevents it from sagging.

A pair of flat end wires is connected to two fixed ends of the sample. The electrical connection between the wire and the conducting surface is made steady and stable by a layer of thin copper tape. End-to-end resistance of the sample is recorded by an Agilent 34401A 6½ digital multimeter. The mandrel rotates smoothly on a pair of Teflon-coated linear bearings at the two ends. The sprocket is attached to one end of the shaft supporting the mandrel and is rotated by a timing belt connected to an electric stepper motor. The entire system is secured to the optical table using posts and post holders for easy mounting and modifications.

The microstepping motor MDrive M-17 from Intelligent Motion System is used for this purpose. The factory-mounted encoder provided easy control of the motor. The motor is powered by a 24 V DC power source and is controlled by three 5 V TTL input signals for step clock, direction and enable/disable. The motor also has configurations for holding

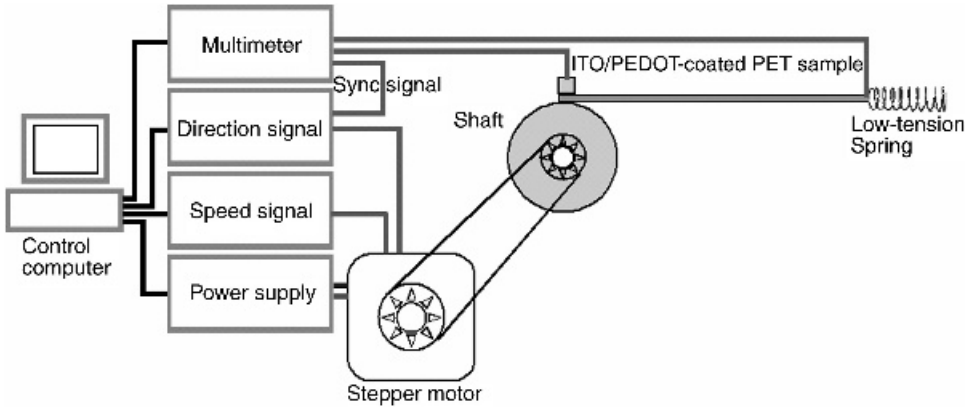


Figure 9.7 Schematic of custom-built apparatus to monitor resistance during cyclic mandrel bending

Petitioner Samsung Ex-1011, 0201

current and run current which determine the maximum torque generated by the motor during its stop and running stages. These settings are used to limit excess stress in the sample. The microstep resolution parameter specifies the number of steps per revolution for the motor, with a maximum resolution of 51 200 steps per revolution. Selecting a high resolution results in smooth and accurate motion but also requires synchronized high-fidelity control signals.

The control signals were generated by using Hewlet-Packard (HP) systems. Two HP 33120 15 MHz function/arbitrary waveform signal generators provide pulses to drive the step clock drive signal and the direction control signal. Any slight mismatch between these two signals would slowly shift the start point of the cycle. This is very significant, especially for long tests where even very small differences accumulate over a long period of time, rolling the sample completely in the forward or reverse direction. Hence the two signal generators were externally synchronized for perfect match, and burst mode was used to avoid any cumulative fractional pulse accumulation. The output signals were verified using an HP 54602B 150 MHz oscilloscope.

ITO-coated PET and PEDOT:PSS-coated PET samples were repeatedly loaded and unloaded using cyclic mandrel loading and the resistance was measured in situ. Figure 9.8 is a graph showing the increase in resistance as a function of cycles for ITO-coated PET and PEDOT:PSS. Data are shown for a 1.5 in mandrel. An initial increase in resistance is evident for both conductive materials but a gradual linear increase in resistance appears after the system reaches equilibrium only for ITO-coated systems. No significant increase is evident for PEDOT:PSS.

The increase in resistance for ITO-coated PET can be segregated into three regimes (Figure 9.9): (I) increase in resistance due to changes in sample dimension until equilibrium width is obtained (50–100 cycles); (II) gradual linear increase in resistance, possibly due to cracking of ITO (if the crack number increases but the strain does not, then the resistance is directly proportional to the number of cracks; and (III) catastrophic failure after 50 000 cycles due to severe cracking. This catastrophic failure at strains less than the critical strain in uniaxial tension limits the use of ITO for rollable displays.

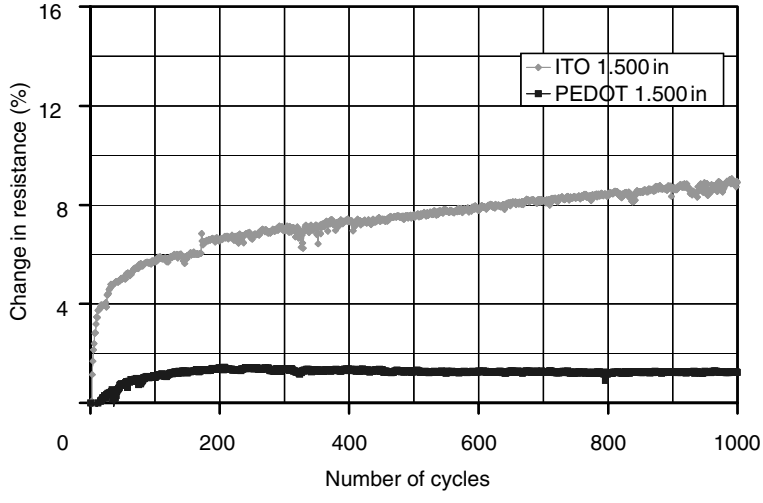


Figure 9.8 Resistance as a function of number of cycles for ITO (upper) and PEDOT:PSS (lower)

Petitioner Samsung Ex-1011, 0202

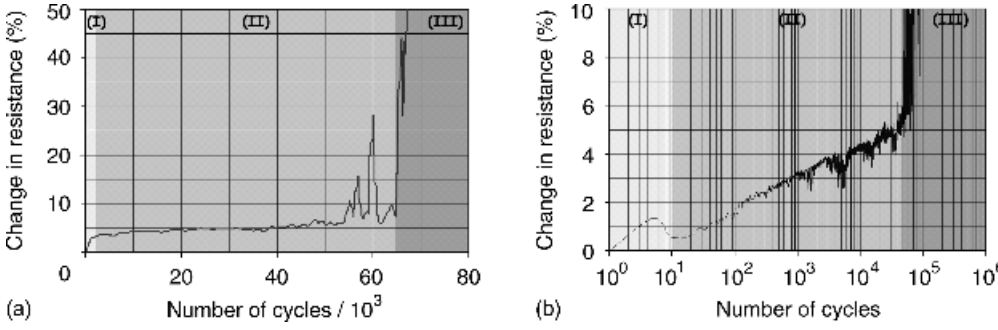


Figure 9.9 Fatigue test until catastrophic failure of ITO samples: linear scale (left) and logarithmic scale (right)

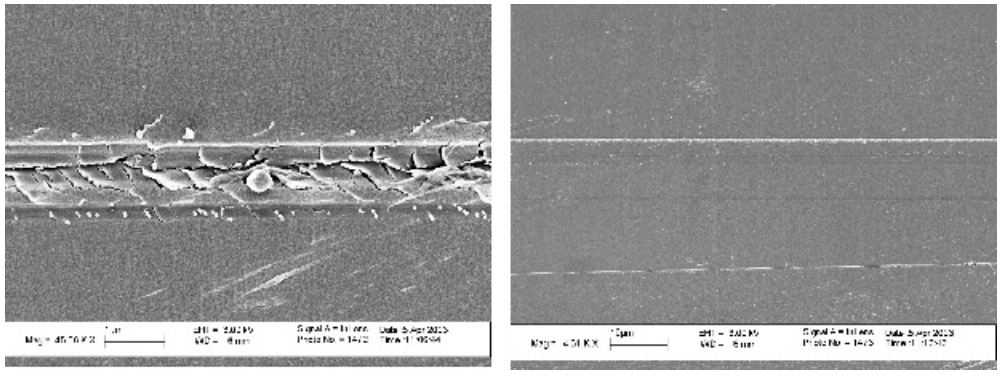


Figure 9.10 Scanning electron micrograph of ITO-coated PET substrate showing parallel cracks created after 100 000 cycles of fatigue test. Resolution 1 μm (left), 10 μm (right)

In order to analyze the morphological features of the cracks created, fracture surfaces of ITO were examined using a scanning electron microscope (SEM). SEM micrographs are shown in Figure 9.10, where fatigue cracks are clearly visible. The cracks are perpendicular to the loading direction and show the results of progressive damage. The micrographs show cracks produced after 100 000 cycles well into region III of the resistance change for ITO. No significant damage was observed in the PEDOT:PSS samples.

9.5 Conclusions

Even when the strain is below the cracking threshold, there are measurable changes in the ITO resistance. Cyclic loading of ITO-coated PET shows three regimes of resistance increase.: (I) an increase in resistance due to changes in sample dimension until equilibrium width is obtained (50–100 cycles); (II) a gradual linear increase in resistance possibly due to cracking of ITO (if the crack number increases but the strain does not, then the resistance is directly proportional to the number of cracks); and (III) a catastrophic failure after

Petitioner Samsung Ex-1011, 0203

50 000 cycles due to severe cracking. This could severely limit the use of ITO for rollable and flexible applications.

For PEDOT:PSS-coated PET the resistance does not increase significantly with increasing tensile strain and it is also less susceptible to damage from repeated bending (Figure 9.8). PEDOT:PSS appears to be an excellent choice for flexible rollable displays. However, continuing work in this area is still required to increase the conductivity and the thermal stability of PEDOT:PSS (Greczynski *et al.* 1999).

Developing an understanding of the degradation of conductivity in transparent conducting substrates is particularly important when considering flexible displays. This understanding and the development of test methodologies for the reliability of flexible displays and materials is essential to the field of flexible displays. We believe that determining the maximum allowable bend radius for cyclic loading of conducting substrates (and understanding the failure mechanisms) provides an important design parameter for rollable and flexible displays. We also believe that such measurements will be key for defining industry standards within this rapidly growing field.

References

Aziz, H., Popovic, Z., Tripp, C. P., Hu, N.-X., Hor, A.-M. and Xu, G. (1998) Degradation processes at the cathode/organic interface in organic light emitting devices with Mg:Ag cathodes. *Applied Physics Letters* **72**, 2642.

Becker, H., Heun, S., Treacher, K., Busing A., and Falcou, A. (2002) Materials and inks for full color PLED-displays. *SID Digest* **XXXIII**, 780–783.

Burrows, P. E., Bulovic, V., Forrest, S. R., Sapochak, L. S., McCarty, D. M. and Thompson M. E. (1994) Reliability and degradation of organic light emitting devices. *Applied Physics Letters* **65**, 2922–2924.

Burrows, P. E., Graff, G. L., Gross, M. E., Martin., P. M., Shi, M. K., Hall, M., Mast, E., Bonham, C., Bennett, W. and Sullivan, M. B. (2001) Ultra barrier flexible substrates for flat panel displays. *Displays* **22**, 65–69.

Cairns, D. R., Witte, R. P., Sparacin, D. K., Sachsman, S. M., Paine, D. C. and Crawford, G. P. (2000) Strain dependent electrical resistance of ITO on polymer substrates. *Applied Physics Letters* **76**, 1425–1427.

Cairns, D. R., Gorkhali, S. P., Esmailzadeh, S., Vedrine, J. and Crawford, G. P. (2003) Conformable displays based on polymer dispersed liquid crystal materials on flexible substrates. *Journal of the Society for Information Display* **11**, 289.

Chen, B. F., Hwang, J., Yu, G. P. and Huang, J. H. (1999) In situ observation of the cracking behavior of TiN coating on 304 stainless steel subjected to tensile strain. *Thin Solid Films* **352**, 173–178.

Chwang A. B. *et al.* (2003) Thin film encapsulated flexible organic electroluminescent displays. *Applied Physics Letters* **83**, 413–415.

Crawford, G. P. (2000) A bright new page in portable displays, *IEEE Spectrum* October, 40–46.

Drzaic, P., Comisket, B., Albert, J. D., Zhang, L., Loxley, A. and Feeney, R (1998) A printed and rollable bistable electronic display. *SID Digest* **XXIX**, 1131–1134.

Funamoto, T., Matsueda, Y., Yokoyama, O., Tsuda, A., Takeshita, H. and Miyashita, Y. (2002) A 130–ppi, full-color polymer OLED display fabricated using an ink-jet process. *SID Digest* **XXXIII**, 899–901.

Gardner, T. J. and Wenz, R. P. (1995) STN Alignment on rib-spaced plastic LCD substrate. *SID Digest* **XVI**, 695–698.

Gorkhali, S. J., Cairns, D. R. and Crawford, G. P. (2004) Reliability of transparent conducting substrates for rollable displays: A cyclic loading investigation. *Journal of the Society for Information Display* **12**, 45–49.

Petitioner Samsung Ex-1011, 0204

Greczynski, G., Kugler, T. and Salaneck, W. R. (1999) Characterization of the PEDOT-PSS system by means of X-ray and ultravilolet photoelectron spectroscopy. *Thin Solid Films* **354**, 12135.

Grove, M., Hayes, D., Antohe, B. and Cox, R. (2002) Array printheads for the ink jet fabrication of color polymer LEDs. *SID Digest* **XXXIII**, 627–630.

Gu, G., Burrows, P. E. and Forrest, S. R. (1997) Vacuum-deposited, nonpolymeric flexible organic light-emitting devices, US Patent 5,844,363.

Haskal, E.I., Buechel, M., Dijksman, J. F., Duineveld, P. C., Meulenkamp, E. A., Mutsaers, C. A. H. A., Sempel, A., Snijder, P., Vulto, S. I. E.. Van de Weijer, P. and de Winter, S. H. P. M. (2002) Ink jet printing of passive-matrix polymer light emitting displays. *SID Digest* **XXXIII**, 776–779.

Innocenzo, J. (2002) Roll to roll PLED process development. *SID Digest* **XXXIII**, 884–885.

Kawase, T., Newsome, C., Inoue, S., Saeki, T., Kawai, H., Kanbe, S., Shimoda, T., Sirringhaus, H., Mackenzie, D., Burns S. and Friend, R. (2002) Active-matrix operation of electrophoretic devices with inkjet-printed polymer thin film transistors. *SID Digest* **XXXIII**, 1017–1019.

Kim, J.-H., Vorflusev, V. and Kumar, S. (1999) Flexible displays prepared using phase-separated composite organic films of liquid crystals. *SID Digest* **XXX**, 880–883.

Kim, W. H. and Kafafi, Z. H. (2002) Flexible organic light emitting devices using conductive polymeric anodes. *SID Digest* **XXXIII**, 1090–1091.

Krasnov A. N. (2002) High-contrast organic light-emitting diodes on flexible substrates. *Applied Physics Letters* **80**, 3853–3855.

Lee, O.-J. and Lee K.-H. (2003) Fabrication of flexible field emitter arrays of carbon nanotubes using self-assembly monolayers. *Applied Physics Letters* **82**, 3770–3772.

Leterrier, Y., Boogh, L., Andersons, J. and Manson, J. A. E. (1997a) Adhesion of silicon oxide layers on poly(ethylene terephthalate). 1. Effect of substrate properties on coating's fragmentation process. *Journal of Polymer Science Part B* **35**, 1449–1461.

Leterrier, Y., Andersons, J., Pitton, Y. and Manson, J. A. E. (1997b) Adhesion of silicon oxide layers on poly(ethylene terephthalate). 2. Effect of coating thickness on adhesive and cohesive strengths. *Journal of Polymer Science Part B* **35**, 1463–1472.

Leterrier, Y., Medico L., Demarco F., Manson J. A. E., Betz U., Escola M. F., Olsson M. K. and Atamny F. (2004) Mechanical integrity of transparent conductive oxide films for flexible polymer-based displays. *Thin Solid Films* **460**, 156–166.

Lewis, B. G. and Paine, D. C. (2000) Applications and processing of transparent conducting oxides. *MRS Bulletin* **25**, 22–27.

Miyashita, S. (2002) Printing panels. *Information Display* **18**, 16–19.

Oversluizen, G., Klein, M., de Zwart, S., van Heusden, S. and Dekker, T. (2000) Discharge efficiency in plasma displays. *Applied Physics Letters* **77**, 948–950.

Ohring, M. (1992) *The Materials Science of Thin Films*, Academic Press, San Diego CA.

Penterman, R., Klink, S. I., de Konig, H., Nisato, G. and Broer, D. J. (2002) Single substrate lcds produced by photo-enforced stratification. *SID Digest* **XXXIII**, 1020–1023.

Podojil, G. M., David, D. J., Huang, X. Y., Miller, N. and Doane, J. W. (1998) Plastic VGA reflective cholesteric LCDs with dynamic drive. *SID Digest* **XXIX**, 51–54.

Rannou, P. and Nechtschein, M. (1999) Ageing of poly(3,4-ethylenedioxythiophene): kinetics of conductivity decay and lifespan. *Synthetic Metals* **101**, 474.

Rogers, J. A., Bao, Z, Baldwin, K., Dodabalapur, A., Crone, B., Raju, V. R., Kuck, V., Katz, H., Amundson, K., Ewing, J. and Drzaic, P. (2001) Paper-like electronic displays: large-area rubber-stamped plastic sheets of electronics and microencapsulated electrophoretic inks. *Proceedings of the National Academy of Science*, **98**, 4835–4840.

Sheraw, C. D., Zhou, L., Huang, J. R., Gundlack, D. J., Jackson, T. N., Kane, M. G., Hill, I. G., Hammond, M. S., Campi, J., Greening, B. K., Francl, J. and West J. W. (2002) Organic thin-film transistor-driven polymer dispersed liquid crystals. *Applied Physics Letters* **80**, 1088–1090.

Sheridon, N. K. (1999) The Gyricon ball display. *Journal of the Society for Information Display* **7**, 141–144.

Petitioner Samsung Ex-1011, 0205

Slikkerveer, P., Nisato, G., Kooyman, N., Cirkel P. and Bouten, P. (2002) A fully flexible, cholesteric lc matrix display. *SID Digest* **XXXIII**, 27–29.

Slikkerveer, P., Bouten, P., Cirkel, P., de Goede, J., Jagt, H., Kooyman, N., Nisato G., van Rijswijk, R. and Duineveld, P. (2004) A fully flexible colour display. *SID Digest* **XXXV**, 770–773.

Stephenson, S. W., Johnson, D. M. Kilburn, J. I. Mi, X.-D., Rankin, C. M. and Capurso, R. G. (2004) Development of a flexible electronic display using photographic technology. *SID Digest* **XXXV**, 774–777.

Wang, J. S., Sugimura, Y., Evans, A. G. and Tredway, W. K. (1998) The mechanical performance of DLC films on steel substrates. *Thin Solid Films* **325**, 163.

Wedding, C. A., Guy, J. W., Strbik, O. M., Wedding, D. K., Wenzlaff, R. P. and Olsen, W. W. (2004) Flexible AC plasma displays using plasma-spheres. *SID Digest* **XXXV**, 815–818.

West, J. L., Rouberol, M., Franci, J. J., Li, Y., Doane, J. W. and Pfeiffer, M. (1995) Flexible displays utilizing bistable, reflective cholesteric/polymer dispersions and polyester substrates. *Asia Display* **1995**, 55–58.

West J. L., Bodnar, V. H., Kim, Y. and Wonderly, H. (1999) Multi-color, cholesteric displays using plastic substrates. *Proceedings of the International Display Workshop* **1999**, 235–238.

Yanaka, M., Kato, Y., Tsukahara, Y. and Takeda, N. (1999) Effects of temperature on the multiple cracking progress of sub-micron thick glass films deposited on a polymer substrate. *Thin Solid Films* **355/6**, 337–342.

Petitioner Samsung Ex-1011, 0206

10

Optical and Functional Coatings for Flexible Displays

Matthew E. Sousa and Gregory P. Crawford

Division of Engineering, Brown University, Providence RI

10.1 Introduction

The convergence of many technologies, such as plastic substrates, conductive films, barrier layers, encapsulated electrodes, organic thin film transistors, and roll-to-roll processing is enabling the realization of lightweight, robust, flexible display technology. There has been much focus on the above technologies, but there has been less emphasis in the literature on passive optical films that may be required for certain flexible display configurations. In addition, roll-to-roll manufacturing is a real possibility for flexible display technologies; however, it would require any optical films used in the display to be compatible with the roll-to-roll manufacturing process.

In this chapter we review various optical film technologies that are potentially compatible with roll-to-roll manufacturing processes and may be useful for certain flexible display applications. The optical film technologies that exist today were not necessarily developed explicitly for flexible display applications, but nevertheless they can be adapted to and employed in flexible applications. We cover the following optical and functional film technologies: thin film polarizers and retarders, cholesteric color filters, photopolymerizable alignment layers and antireflective coatings. In addition, we have also included and reviewed the available mechanical data on these films.

Flexible Flat Panel Displays Edited by G. P. Crawford
© 2005 John Wiley & Sons, Ltd., ISBN 0-470-87048-6

Petitioner Samsung Ex-1011, 0208

10.2 Thin Film Polarizers

Polarizers are key components in almost all liquid crystal displays (LCDs). In general, a polarizer consists of a thin, dichroic sheet, which transmits one polarization component and absorbs the other component. The majority of sheet polarizers are synthesized by stretching films containing needle-like dichroic molecules (Yeh and Gu 1999). These polarizers are thermally stable up to 80 °C and function in the ordinary (O-type) mode (Bobrov *et al.* 2003). Typical sheet polarizers can be on the order of hundreds of micrometers thick. If used in flexible displays, these thick sheets can inhibit the overall bending and rolling of the plastic substrates; therefore it becomes necessary to find thin film polarizer solutions. Several types of thin film polarizer have been proposed. They include thin crystal film polarizers (Ignatov *et al.* 2001, 2002a, 2002b) and cholesteric films (Broer *et al*. 1995, 1999).

10.2.1 Thin Crystal Film Polarizers

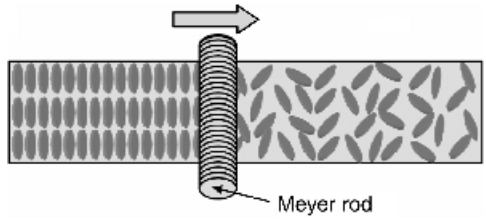
Thin crystal film polarizers have been developed by Optiva, Inc. for use in LCDs. These thin films consist of highly ordered lyotropic liquid crystal (LLC) coatings, which are formed by rod-like supramolecular assemblies of organic sulfonic acids. These materials include water-soluble modified organic blue, violet, and red dyes resulting from the sulfonation of indanthrone, dibenzimidazole, and naphthalenetetracarboxylic acid, respectively (Gvon *et al.* 1998). The total concentration of these materials in water varies from 3.0% to 21% (Dembo *et al.* 2001). These supramolecules have long, columnar structures with aspect ratios of greater than 100:1 resulting from interactions between the disk-shaped molecules (Lazarev *et al.* 2003). The resulting films have the properties of an extraordinary (E-type) polarizer (Yeh and Paukshto 1999), and it has been demonstrated that they can be used to improve the viewing angle of a twisted nematic LCD (Sergan and Kelly 2000).

Thin crystal film polarizers are fabricated from water-soluble conjugated polyaromatic compounds (Bobrov *et al.* 2003). When these materials are put into an aqueous solution, an LLC mesophase is formed. The resulting mesophases are formed by rod-like supramolecules containing flat, elliptical shaped molecules stacked face-to-face in such a way that the hydrophobic planar cores are stacked on top of one another in the core of the supramolecule and the hydrophilic peripheral groups are exposed to water (Dembo *et al.* 2001). Electrostatic interactions between the supramolecules prevent them from clumping. The LLC is then deposited onto a transparent substrate as a wet molecular film. The molecules are aligned upon application of a shear force using a standard coating technique such as Meyer rod, die slot and doctor blade (Ignatov *et al.* 2001, 2002b). The thickness of the wire on the Meyer rod controls the overall film thickness, typically between 300 and 500 nm. The preoriented LLC film is allowed to dry, leading to directional crystallization of the film as the water dries. Figure 10.1(a) is a schematic diagram of the Meyer rod coating process and Figure 10.1(b) shows indanthrone disulfonate, a typical discotic dye molecule.

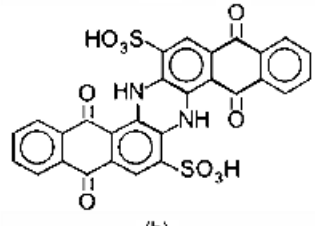
The molecular order parameter, S, of the film can be calculated from the transmittance spectra of the thin crystal film polarizers using the following expression (Bahadur 1998):

$$S = (D_{\perp} - D_{\parallel})/(D_{\perp} + 2D_{\parallel}), \tag{10.1}$$

Petitioner Samsung Ex-1011, 0209



(a)



(b)

Figure 10.1 (a) Schematic diagram of the Meyer rod coating technique used to produce thin crystal film polarizers. The directors of the molecules align in the direction of the shear force during the coating process. (b) Indanthrone disulfonate, a blue discotic dye used in the fabrication of thin crystal film polarizers

where $D_\perp$ and $D_\parallel$ are the absorption perpendicular and parallel to the polarizer axis. D can be calculated relative to the transmission T (Nazarov *et al.* 2001) using

$$D = -\log_{10} T \tag{10.2}$$

and

$$T = \sqrt{(H_0^2 - H_{90}^2)/2}, \tag{10.3}$$

where H_0 and H_{90} are the transmission of two parallel and two crossed polarizers, respectively. The order parameter increases substantially during the time that the coated material is allowed to rise and crystallize; sometimes the order parameter increased from 0.65 for the ordered liquid film to 0.90 after drying (Ignatov 2002b).

Optical microscopy shows that these materials appear to have birefringent textures when they are placed between crossed polarizers (Dembo *et al.* 2001). Dye solutions with dilute concentrations exhibit schlieren-like textures, which are characteristic of lyotropic nematic mesophases; higher-concentration solutions exhibit grainy textures that are characteristic of a more symmetrical mesophase (Fiske *et al.* 2002).

Thin crystal film polarizers are typically less than 500 nm thick, and they can be directly integrated onto plastic substrates for flexible displays. Thin crystal film polarizers can also be employed as in-cell polarizers (Bobrov *et al.* 2002). Being able to integrate thin film polarizers in the cell or the substrate itself can save 180–300 μm of thickness when compared to cases where conventional polarizer technology is used (Bobrov *et al.* 2003).

Petitioner Samsung Ex-1011, 0210

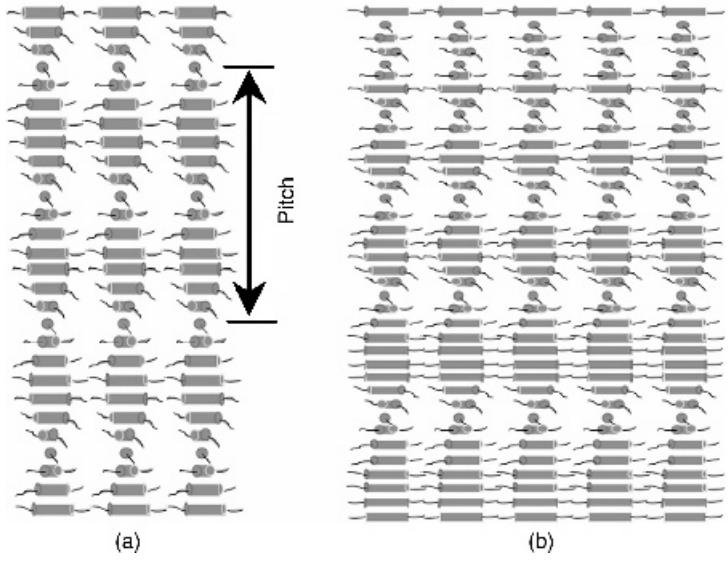


Figure 10.2 Schematic diagram of a chiral nematic liquid crystal. (a) A conventional chiral material; the pitch is defined as the length corresponding to one complete 360° rotation of the director. (b) A chiral material with a pitch gradient. Image courtesy of D. Broer, Philips

10.2.2 Cholesteric Film Polarizers

The cholesteric or chiral nematic liquid crystal phase can also be used to fabricate polarizers for LCDs. The structure of the cholesteric phase can be described as consisting of liquid crystal molecules with a chiral constituent. These molecules have statistically parallel directors; however, the irregularity of the constituent portion of the molecules causes a slight asymmetry. This creates a gradual rotation of the nematic director, producing the helical structure (Collings 1997) in Figure 10.2(a). The pitch of a cholesteric material is defined as the length, which corresponds to one complete 360° rotation of the director. See Chapter 17 for more information on the cholesteric liquid crystal phase.

Optical coatings fabricated using cholesteric materials can be used to polarize light by reflecting light of one polarization direction; however, these coatings only generate circularly polarized light and operate only within a narrow band of the visible spectrum (Lub *et al.* 2002). The relationship between the reflected wavelength, λ, and the pitch, p, of the cholesteric material can be defined as

$$\lambda = pn, \tag{10.4}$$

where n is the average index of refraction of the material. The peak reflection width of a material with a single pitch, $\Delta\lambda$, can be determined by

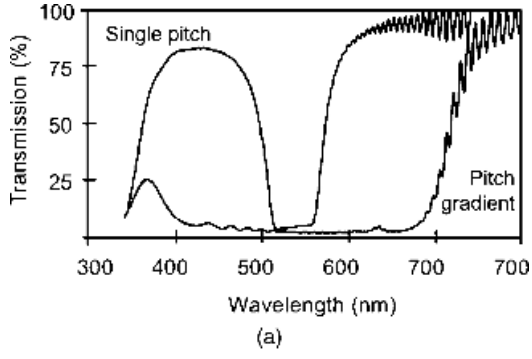
$$\Delta\lambda = p\,\Delta n, \tag{10.5}$$

Petitioner Samsung Ex-1011, 0211

where Δn is the birefringence of the material. In this reflection band, left-circularly polarized light is transmitted, and right-circularly polarized light is reflected by a right-handed helix. For a typical colorless material with a Δn of 0.2, the bandwidth of the reflected region is less than 75 nm (Broer *et al.* 1995). For use in the visible spectrum, this bandwidth needs to be expanded more than three times.

A solution to this narrow bandwidth problem is to create a cholesteric reactive mesogen film with a pitch gradient (Broer *et al.* 1995, 1999; Lub *et al.* 2002; Jiang *et al.* 2004) as depicted in Figure 10.2(b). Reactive mesogens are low molecular weight liquid crystal monomers that can form high molecular weight liquid crystalline polymeric structures (Broer *et al.* 1995). Using a pitch gradient has allowed the production of films with bandwidths of greater than 300 nm located between $\lambda_1 = p_1 n_o$and $\lambda_2 = p_2 n_e$ where p_1 and p_2 are the smallest and largest pitches, respectively. A plot of transmission versus wavelength of left-handed circularly polarized light for a single-pitch material and a material with a pitch gradient is shown in Figure 10.3(a).

The pitch gradient is fabricated by manipulating the kinetics of the photocuring reaction of a material set that includes a cholesteric compound, a nematic monoacrylate, a UV



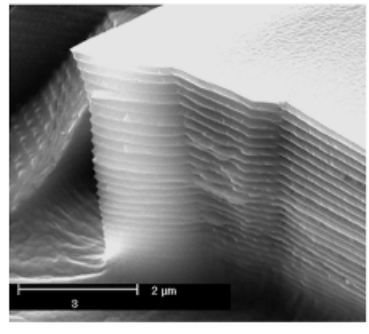


Figure 10.3 (a) Plot of transmission versus wavelength of left-handed circularly polarized light for a single-pitch cholesteric material and a cholesteric material with a pitch gradient. Use of a pitch gradient allows the fabrication of films that can reflect light over the complete range of visible wavelengths (Broer *et al.* 1999). (b) A scanning electron micrograph of a pitch gradient cholesteric network. The observed layers correspond to one-half the pitch and decrease in thickness from the top of the film to the bottom. Image courtesy of D. Broer, Philips

Petitioner Samsung Ex-1011, 0212

photoinitiator and a UV-absorbing dye. The use of the nematic monoacrylate is necessary to shift the wide reflection band of the cholesteric diacrylate into the visible region of the spectrum. The photoreaction takes place in such a way that the coating near the top surface of the film (closest to the UV lamp) contains more chiral material and has a shorter reflection wavelength than the bottom portion of the coating, which contains more of the nematic monoacrylate. This is possible since the cholesteric material is a diacrylate, which has two reactive sites per molecule, and is two times more likely to be incorporated into the polymer than the nematic monoacrylate, which has only a single reactive site. The addition of a UV-absorbing dye creates a gradient in the intensity of the UV light perpendicular to the surface of the coating. The result is that the polymerization occurs faster at the top of the film than at the bottom. The cholesteric diacrylate is consumed rapidly at the surface of the film, causing the formation of a concentration gradient across the film enriching the top layer with cholesteric material.

The resulting pitch gradient cholesteric networks are 15 μm thick, colorless, and reflect 50% of the light evenly over the visible spectrum. Left-handed circularly polarized light with a wavelength of greater than 400 nm is completely transmitted while only 2% of right-handed circularly polarized light is transmitted. A scanning electron micrograph of a pitch gradient cholesteric network is shown in Figure 10.3(b). Using these materials in an LCD improves the light yield by 40% by recycling the wrongly polarized light. It is possible to fabricate sheets of this material in a continuous coating process, which could be cut into sheets for use in LCDs, or adapted to a roll-to-roll fabrication process for use in flexible displays.

10.3 Thin Film Retarders

Retarders are optical elements that can change the polarization of an incident light wave by causing a predetermined amount of phase lag between two coherent polarization states (Hecht 2002). The resulting phase lag causes a change in the polarization state of the emerging beams. Typically, retarders are used to enhance the viewing angle of LCDs (Yeh and Gu 1999).

10.3.1 Thin Crystal Film Retarders

Thin crystal film retarders have been developed using dichroic dyes and substrate coating processes similar to those used for the thin crystal film polarizers described in the previous section (Lazarev and Paukshto 2000; Lazarev *et al.* 2001). TCF R003, a dichroic dye developed by Optiva, absorbs light over a range from 450–500 nm and is transparent over the rest of the spectrum. The resulting films fabricated from this material are highly anisotropic with a maximum retardation value $\Delta n = 0.85$ in the range of wavelengths 500–700 nm for a film thickness of 300 nm (Lazarev *et al.* 2001). A conventional retarder with the same retardation values would have a thickness of 200,000 nm (Ignatov *et al.* 2002a).

A water-based LLC material based on disodium chromoglycate (DSCG) can be coated and dried on substrates to form highly transparent retarders. Over a range of wavelengths from 400 to 700 nm there is a range of retardation of $\Delta n = 0.1$ to 0.13 (Ignatov *et al.* 2002a).

Petitioner Samsung Ex-1011, 0213

Thin crystal film retarders can be fabricated to provide a wide range of retardations and can be coated onto a variety of different substrates. The film thickness is much thinner than for a conventional retarder, allowing a reduction in the overall thickness of the display.

10.3.2 Reactive Mesogen Retarders

It has been demonstrated that chiral reactive mesogen films can be used as retarders (Broer *et al.* 1999) using a cholesteric network with a deformed helix in combination with the pitch gradient technique for creating cholesteric film polarizers (Section 10.2.2). The retardation property of the film can be used to transform the circularly polarized light generated by the cholesteric polarizer into linear polarized light (Broer *et al.* 1999).

Reactive mesogen quarter-wave plates were fabricated using a 60:40 mixture of a chiral liquid crystal diacrylate and a nematic monoacrylate. The deformation of the helix is accomplished by using a rod-like dichroic photoinitiator. A UV-absorbing dye is used to create a pitch gradient in the film. Linear polarized UV light is used to photopolymerize the film. The resulting films have optimum quarter-wave retardation at 500 nm. The retardation effect deviates at longer and shorter wavelengths (Broer *et al.* 1999).

In order to implement reactive mesogen retarders in flexible displays, it is necessary to understand how the mechanical properties of the films will affect their optical properties. Escuti *et al.* (2004) carried out an optomechanical study of ordered polymeric films fabricated from a photopolymerizable reactive mesogen material. The study included measuring the birefringence and dispersion of uniformly aligned films (≤ 10 μm thick) between glass substrates as well as measuring the birefringence of freestanding films (≤ 175 μm thick) under tensile stress applied at three orientations with respect to the nematic axis as shown in Figure 10.4(a) and (b). The setup used to measure the optomechanical performance of these films is shown in Figure 10.4(c). The study gives information on how these films perform under strain, which provides insight into their usefulness in flexible display configurations. The material used in this study was a 98:2 weight percent ratio of the liquid crystal diacrylate LC242 from BASF and the photoinitiator Darocur-1173 from Ciba. The thin films were prepared between glass substrates coated with rubbed polyimide and arranged in an antiparallel manner. The thicker films used for tensile tests were fabricated using a poly(ethylene terephthalate) (PET) dog-bone template coated with polyimide. The films were photocured in the UV and then detached from the PET templates for use in the tensile test.

The transmission of the film was found to depend on the strain applied, as shown by the following equation:

$$T = \frac{1}{2} T_0 \sin^2(2\theta) \sin^2\left(\frac{\pi d_0}{\lambda} \Delta n(\varepsilon)(1 - \nu\varepsilon)\right), \tag{10.6}$$

where T_0 is the unpolarized irradiance on the first polarizer, θ is the angle between the effective optical axis of the polymer film and the transmission axis of the polarizer, d_0 is the original film thickness, ε is the nominal strain, and ν is Poisson's ratio for the film. Lasers of two wavelengths were used in order to determine Δn and ν for the films.

Samples produced at room temperature had the highest values of birefringence ($\Delta n = 0.142$). This value decreased with increasing polymerization temperature due to a decrease in molecular order at the time of photopolymerization. The Young's modulus was measured for each film orientation, and the values were 0.81 GPa for parallel alignment,

Petitioner Samsung Ex-1011, 0214

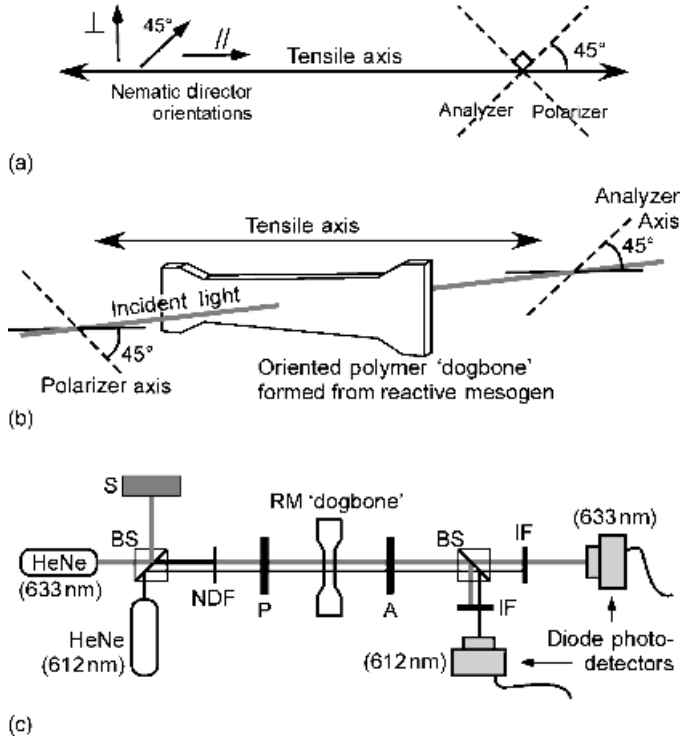


Figure 10.4 The optomechanical setup used for testing reactive mesogen retarder films. (a) The nematic director and crossed polarizer orientations. (b) The reactive mesogen orientation with respect to incident light and tensile axis. (c) The experimental setup: NDF = neutral density filter, BS = beam splitter, S = beamstop, P = polarizer, A = analyzer, IF = interference filter. Reproduced by the permission of American Institute of Physics

0.55 GPa for perpendicular alignment, and 0.68 GPa for 45° alignment with respect to the tensile axis. The parallel-aligned film failed at strains of $\varepsilon = 6$–8% but there was almost no change in the birefringence up to the critical failure. The film with perpendicular alignment failed at higher strains, $\varepsilon = 10$–12%, and there was a 1% decrease in the birefringence caused by local disorder in the polymer chains due to the applied stress. The film with 45° alignment showed no change in birefringence up to $\varepsilon = 10\%$.

The study indicated that there is little change in the birefringence of ordered polymer films when subjected to strains in the direction of molecular alignment, and there is minimal change in its birefringence when a film is subjected to strains perpendicular to the molecular alignment.

10.4 Color Filters

Color filers are an integral part of modern displays allowing for the production of full-color images. A wide variety of materials exist for use as color filters, including colored inks, dyed polyimide, and dyed gelatin, which is the most common (Yeh and Gu 1999). In order to

Petitioner Samsung Ex-1011, 0215

generate a full color image, three colors are needed: red, green, and blue. Typically in an LCD, each pixel is divided into a red, green, and blue subpixel. Assuming an even distribution of optical energy, each subpixel will transmit only one-third of the total optical energy (Yeh and Gu 1999). To increase the efficiency of a display, it would be ideal if the light reflected from a particular subpixel could be recycled for it to be transmitted by one of the remaining subpixels.

Cholesteric materials can also be used to fabricate color filters (Broer *et al.* 1999; van de Witte *et al.* 1999; Wegh and Broer 2004) using a pitch gradient similar to the process described in Section 10.2.2 (van Asslet *et al.* 2000; Lub *et al.* 2002). Displays using a cholesteric filter are typically used in reflective mode; however, they can also function in the transmissive mode. This allows for the fabrication of transflective displays, but a complementary color scheme is displayed in the transmissive mode (van Asslet *et al.* 2000).

In order to fabricate red, green, and blue filters in the same layer of film, the pitch of the cholesteric material must change locally within the layer (Lub *et al.* 2002). This can be achieved by using a combination of an isomerizable chiral compound and a copolymer made from the same isomerizable chiral compound and a nematic monomer. The chiral compound, before UV irradiation, is in the Z configuration and has a relatively high helical twisting power (HTP). The isomerized E configuration has an HTP of almost zero. The proper combination of the isomer and copolymer results in a material that reflects blue light. The reflected wavelength, λ, is governed by the following equation:

$$\lambda = n(\text{HTP} \times c)^{-1}, \tag{10.7}$$

where n is the index of refraction for the material and c is the concentration of the chiral component (Lub *et al.* 2002). During UV irradiation, the reflectivity gradually changes from blue to green to red as the helical twist relaxes. Using a pixelated grayscale mask, the three colors can be fabricated as a pixelated color filter for a reflective LCD in a single exposure step. Figure 10.5 is a schematic representation of the grayscale mask exposure.

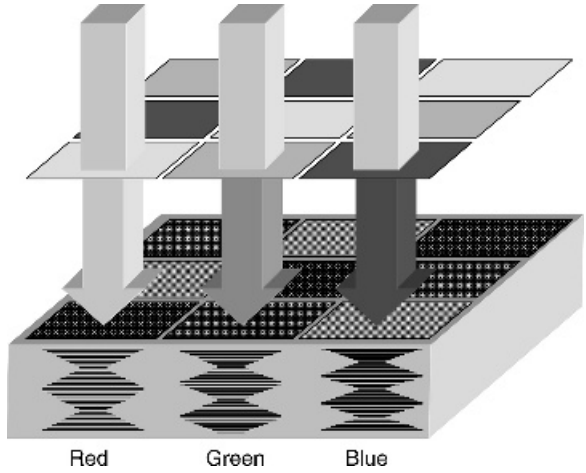


Figure 10.5 The single exposure step process used to fabricate color filters from cholesteric reactive mesogens

Petitioner Samsung Ex-1011, 0216

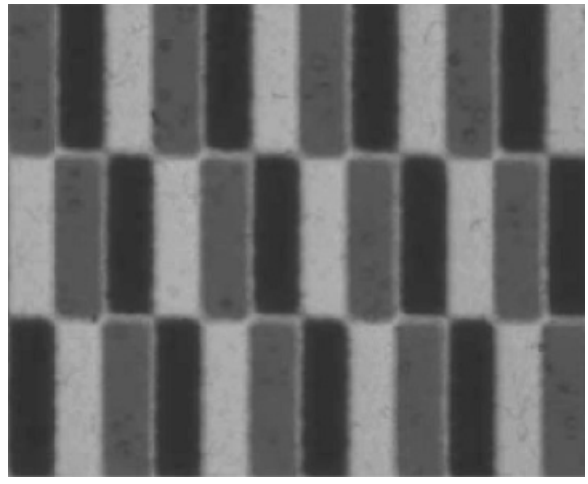


Figure 10.6 The color filters produced using the photoisomerizable cholesteric copolymer. Image courtesy of J. Lub and D. Broer, Philips

To achieve stability in the color filters, easily alignable reactive mesogens are used in conjunction with the photoisomerizable chiral compound. Using a reactive mesogen material makes it easier to align the film before UV curing, reducing the optical impurities of the polymer color filters. High degrees of crosslinking prevent any postisomerization from affecting the helix and increases the thermal stability of the colored film (Lub *et al.* 2002).

The fabrication of cholesteric color filters using the pitch gradient technique allows for the three different colors to be formed in the same layer by being able to locally adjust the pitch of the cholesteric material (Figure 10.6). The cholesteric color filter also provides a polarization function (Section 10.2.2) and a reflection function in the same layer, whereas three separate layers would be needed for absorption-based color filters in order to provide the same functionality (van de Witte *et al.* 1999). This method provides a simple, single-step process for fabricating color filters that could be employed by a reflection mode, flexible display.

10.5 Alignment Layers

Liquid crystals can be aligned with the long molecular axis parallel to the substrate (planar alignment) or with the long molecular axis perpendicular to the substrate (homeotropic alignment); see Collings (1997). Alignment layers are necessary at the liquid crystal–glass interface to induce order in the liquid crystal layer. Typically, the planar alignment layers used in twisted nematic and super twisted nematic displays are fabricated from polymer thin films that have been rubbed to create linear grooves in the polymer layer's surface (Yeh and Gu 1999). Surface interactions between the grooved polymer layer and the liquid crystal result in the alignment of the liquid crystal molecules in the direction of the grooves. There are several drawbacks to using the mechanical rubbing of polymer to create an alignment layer. The mechanical rubbing of the polymer can create debris, which can be left behind

Petitioner Samsung Ex-1011, 0217

and produce defects in the display. It is also not possible to create layers in which there are different localized azimuthal angles for the long axis of the liquid crystal molecules to align (Schadt *et al.* 1992, 1995).

10.5.1 Linear Polymerized Photopolymer Alignment Layers

Linear polymerized photopolymer (LPP) alignment layers can be used to overcome some of the problems associated with mechanically rubbed polymer alignment layers. Since there is no mechanical contact of a rubbing wheel with the surface layers, there is no creation of debris. Photomasks can be used to fabricate local areas with different angles of alignment. LPP alignment layers are fabricated by first spin coating a substrate with 2 wt% of poly(vinyl 4-methoxy-cinnamate) (PVMC) photopolymer dissolved in a 50/50 mixture of chlorobenzene and methylene chloride at 3000 rpm for 30 s. The substrates are then dried for 1 h at 90 °C. Following drying, the films are isotropically polymerized with 1 J/cm^2 of unpolarized UV light at $\lambda = 320$ nm to further increase the aligning stability of the final film. Final polymerization is done with 5 J/cm^2 of linear polarized UV light at $\lambda = 320$ nm (Schadt *et al.* 1992).

Tilt dislocations were seen when the resulting LPP films were incorporated into twisted nematic LCDs where both substrates are treated with LPP alignment layers. These were due to the lack of a molecular pretilt or the presence of splay dislocations. This problem can be overcome by using one LPP substrate and one substrate prepared using a conventional mechanically rubbed polymer with a pretilt angle of $\Theta \sim 3^\circ$ (Schadt *et al.* 1992).

10.5.2 Multidomain Linear Polymerized Photopolymer Alignment Layers

Multiple domains can be used in LCDs to reduce the angular dependence of the optical transmission and thus improve the viewing angle characteristics of the display (Yeh and Gu 1999). LPP alignment layers can easily be fabricated to create two and four domain systems (Schadt *et al.* 1996; Schadt and Seiberle 1997; Seiberle *et al.* 1999). A requirement of a multidomain system is the ability to generate and control a molecular pretilt (Scheffer and Nehring 1984); however, the PVMC LPP described above has a pretilt angle of $\Theta < 0.3^\circ$ (Schadt *et al.* 1996). By modifying the above LPP process, such that the liquid crystal alignment occurs within the plane of $\hat{\mathbf{E}}$ and $\hat{\mathbf{k}}$, tilt angles can be photoinduced over a range of $\Theta = 0$–90° by changing the angle of incidence of $\hat{\mathbf{k}}$ relative to the substrate $\Theta < 0.3^\circ$ (Schadt *et al.* 1996).

Multidomain systems can easily be created by fabricating an alignment layer on one substrate. Figure 10.7 depicts the fabrication of a dual-domain alignment layer. Using a photomask with the polarization direction of the incident UV light controlling the alignment direction of the liquid crystal molecules, the transparent regions of the mask control the alignment pattern. A molecular pretilt is obtained by rotating the substrate perpendicular to the incident direction of the incident UV light. The second substrate is uniaxially photoaligned, but fabricated with no pretilt in order to prevent reverse twist domains in the on-state (Hoffman *et al.* 1998). Polarization holography can also be used as a method to create LPP alignment layers with periodic and continuous boundary conditions (Eakin *et al.* 2004).

Petitioner Samsung Ex-1011, 0218

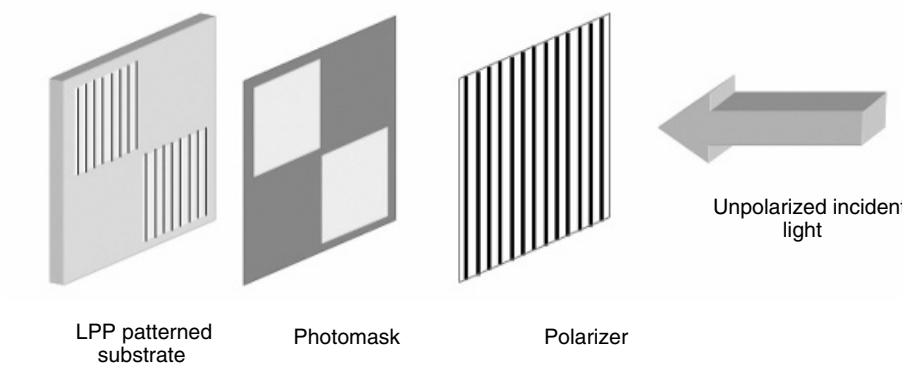


Figure 10.7 Schematic diagram of the fabrication process used for creating a multidomain LPP alignment layer

Crosslinking during the LPP process yields very stable optical films (Schadt *et al.* 1996). After 100 h of exposure to 120 °C temperatures, there is almost no change in the tilt bias (Schadt *et al.* 1997). Using the multidomain configurations, there is a great increase in LCD viewing angle characteristics when compared to displays fabricated with rubbed polymer substrates or single-domain LPP substrates. LPP materials can also be used in the fabrication of patterned interference filters, polarizers, optical retarders (Schadt *et al.* 1996), and antireflective coatings (Ibn-Elhaj and Schadt 2002).

10.6 Antireflective Coatings

Antireflective (AR) coatings are used to increase the transmission of light and decrease the glare of display substrates, thus increasing the contrast and brightness of the display. AR coatings can be made from either single- or multilayer films. Single-layer films only operate in a narrow range of wavelengths; multilayer films can be used to increase the range of wavelengths that the AR coating will work for. Unfortunately, these films can be quite difficult to fabricate and are very expensive. An alternative to complex and expensive films is the use of nanostructured surfaces that are able to act as AR coatings (Ibn-Elhaj and Schadt 2001; Theijs *et al.* 2004).

One approach to fabricating nanostructured AR films is to fabricate high-resolution thin film polymer topologies using photopolymerizable materials (Ibn-Elhaj and Schadt 2001). Monomer corrugation (MC) is a simple, low-cost method that can be applied to planar and nonplanar materials (Ibn-Elhaj and Schadt 2002). To fabricate these films, blends of liquid crystalline prepolymers and liquid crystal monomers are coated onto a substrate. The materials are chosen such that only the liquid crystalline prepolymers are photocrosslinkable. UV light is used to crosslink the prepolymer materials. Depending on the components of the MC mixture, the removal of the liquid crystal monomers results in nanopores that are anisotropic in shape and distribution in the solid polymer thin film (Ibn-Elhaj and Schadt 2001). Anisotropic pores can be fabricated by using an LPP layer (Section 10.5) under the MC layer in order to align the liquid crystalline components of the MC mixture before the crosslinking step (Ibn-Elhaj and Schadt 2001).

Petitioner Samsung Ex-1011, 0219

The resulting isotropic MC nanostructured films are efficient AR coatings for glass and plastic substrates. Poly(methyl methacyrlate) (PMMA) films coated with MC nanostructured films on both sides display a drastic reduction in reflectance. Over the entire visible spectrum, the photopic reflectance is 0.1% per MC coating (Ibn-Elhaj and Schadt 2002).

Another approach to creating nanostructured AR films is to create single-layer films using self-assembly and crosslinking of nanoparticles. Reactive nanoparticales are applied in a suspension in the presence of reactive dilutents using an organic solvent. The nanoparticles are made reactive by surface modification with reactive groups able to form polymer networks. The solvent is evaporated, and thermal or photochemical processes are used to crosslink the nanoparticles (Theijs *et al.* 2004).

The resulting coatings range in thickness from 100 to 200 nm. The thickness can be controlled to control the optical properties of the film. The transmission of the films is greater than 98%. An uncoated PET substrate has a reflectance that varies between 10 and 12% across the visible spectrum. For a PET substrate coated with a nanoparticle AR film, the reflectance is less than 2% over the visible spectrum with a minimum reflectance of 0.7% at 550 nm, which is a considerable improvement (Theijs *et al.* 2004).

10.7 Summary

Although many of the electro-optic configurations presented in this book do not require the optical films discussed in this chapter for operation, there are still those that do. These include twisted nematic and super twisted nematic display configurations that have been adapted for use with flexible substrates. In order to use these configurations in a flexible display, it is essential that all the layers of the display can be modified such that they can be bent or rolled without breaking down and causing any degradation of the overall image quality. An example is a flexible super twisted nematic flat panel display that has recently been reported. This display uses thin crystal film polarizers, liquid crystal polymer wave plates, color filters, and a flexible backlight (Slikkerveer *et al.* 2004). The flexible backlight can be the combination of a rigid sidelight and flexible polymeric waveguide or it can be a flexible inorganic electroluminescent panel (Slikkerveer *et al.* 2004).

A wide variety of optical thin film technology exits for use in conventional glass displays that could be used in flexible display configurations. Although very little mechanical data exist on these films, it is expected that the technologies discussed in this chapter will be functional in flexible display technology. Furthermore, many of the technologies discussed in this chapter can be coated onto substrates using methods that are consistent with roll-to-roll manufacturing.

References

Bahadur, B. (1998) Guest-host effect. In D. Demus, J. Goodby, G. W. Gray, H.-W. Spies and V. Vill, (eds.) *Handbook of Liquid Crystals*. Weinheim: Wiley-VCH, pp. 257–302.

Bobrov, Y., Fennel, L., Ganpule, T., Lazarev, P., Ohmura, S., Bae, H., Ishibashi, Y. and Yamashita, O. (2002) *Proceedings of the International Display Workshops* **9**, 405–408.

Bobrov, Y., Blinov, L., Ignatov, L., King, G., Lazarev, P., Nazarov, V., Ovchinnkova, N. and Remizov, S. (2003) Environmental and optical testing of thin crystal film polarizers. *Journal of the Society for Information Display* **11**, 63–70.

Petitioner Samsung Ex-1011, 0220

Broer, D. J., Lub, J. and Mol, G. N. (1995) Wide-band reflective polarizers from cholesteric polymer networks with a pitch gradient. *Nature* **378**, 467–469.

Broer, D. J, Mol, G. N., van Haaren, A. M. M. and Lub, J. (1999) Photo-induced diffusion in polymerizing chiral-nematic media. *Advanced Materials* **11**, 573–578.

Collings, P. J. (1997) *Introduction to Liquid Crystals*. London: Taylor & Francis.

Dembo, A., Ionov, A., Lazarev, P., Manko, A. and Nazarov, V. (2001) Lyotropic dye-water mesophases formed by rod-like supramolecules. *Molecular Materials* **14**, 275–290.

Eakin, J. N., Xie, Y., Pelcovits, R. A., Radcliffe, M. D. and Crawford, G. P. (2004) Zero voltage freedericksz transition in periodically aligned liquid crystals. *Applied Physics Letters* **85**, 1671–1673.

Escuti, M. J., Cairns, D. R. and Crawford, G. P. (2004) Optical-strain characteristics of anisotropic polymer films fabricated from a liquid crystal diacrylate. *Journal of Applied Physics* **95**, 2386–2390.

Fiske, T., Ignatov, L., Lazarev, P., Nazarov, V. and Paukshto, M. (2002) Molecular alignment in crystal polarizers and retarders. *Society for Information Display Digest of Technical Papers* **XXXIII**, 866–869.

Gvon, K. I., Bobrov, Y. A., Bykov, V. A., Ignatov, L. A., Ivanova, T. D., Popov, S. I., Shishkina, E. Y. and Vorozhtsov, G. N. (1998) Method and materials for thermostable and lightfast dichroic light polarizers, US Patent 5,739,296.

Hecht, E. (2002) *Optics*. Boston MA. Addison-Wesley.

Hoffman, E., Klausmann, H., Ginter, E., Knoll, P. M., Seiberle, H. and Schadt, M. (1998) Development of a dualdomain TFT-LCD by optical patterning. *Society for Information Display Digest of Technical Papers* **XXIX**, 734–737.

Ibn-Elhaj, M. and Schadt, M. (2001) Optical polymer thin films with isotropic and anisotropic nano-corrugated surface topologies. *Nature* **410**, 796–799.

Ibn-Elhaj, M. and Schadt, M. (2002) Photo-aligned nano- and micro-corrugated novel optical thin films for LCDs. *Society for Information Display Digest of Technical Papers* **XXXIII**, 1046–1049.

Ignatov, L., Lazarev, P., Ovchinnikova, N. and Paukshto, M., (2001) Thin crystal film optical components. *Proceedings of SPIE* **4459**, 148–154.

Ignatov, L. Y., Lazarev, P. I., Nazarov, V. V. and Ovchinnikova, N. A. (2002a) Thin crystal film polarizers and retarders. *Proceedings of SPIE* **4658**, 79–90.

Ignatov, L., Lazarev, P., Nazarov, V., Ovchinnikova, N. and Paukshto, M., (2002b) Molecular alignment in nano-film crystal polarizers and retarders. *Proceedings of SPIE* **4807**, 177–188.

Jiang, Y, Li, L., Hochbaun, A., Galabova, H., Wiley, R., and Faris, S. M. (2004) High-brightness color liquid crystal display panel employing light recycling there within, US Patent 6,831,720.

Lazarev, P. and Paukshto, M. (2000) Thin crystal film retarders. *Proceedings of the International Display Workshops, Materials and Components* **7**, 1159–1160.

Lazarev, P., Ovchinnikova, N. and Paukshto, M. (2001) Submicron thin retardation coating. *Society for Information Display Digest of Technical Papers* **XXXII**, 571–573.

Lazarev, P. I., Paukshto, M. V. and Sidorenko, E. N. (2003) Self-assembly optical components. *Proceedings of the 2003 Materials Research Society* **771**.

Lub, J., Broer, D. J. and van de Witte, P. (2002) Colourful photo-curable coatings for application in the electro-optical industry. *Progress in Organic Coatings* **45**, 211–217.

Nazarov, V., Ignatov, L. and Kienskaya, K. (2001) Electronic spectra of aqueous solutions and films made of liquid crystal ink for thin film polarizers. *Molecular Materials* **14**, 153–163.

Schadt, M. and Seiberle, H. (1997) Optical patterning of multidomain liquid crystal displays. *Society for Information Display Digest of Technical Papers* **XXVIII**, 397–400.

Schadt, M., Schmitt, K., Kozinkov, V. and Chigrinov, V. (1992) Surface-induced parallel alignment of liquid crystals by linear polymerized photopolymers. *Japanese Journal of Applied Physics* **31**, 2155–2164.

Petitioner Samsung Ex-1011, 0221

Schadt, M., Seiberle, H., Schuster, A. and Kelly, S. M. (1995) Photo-generation of linearly polymerized liquid crystal aligning layers comprising novel, integrated optically patterned retarders and color filters. *Japanese Journal of Applied Physics* **34**, 3240–3249.

Schadt, M., Seiberle, H. and Schuster, A. (1996) Optical patterning of multi-domain liquid-crystal diplays with wide viewing angles. *Nature* **381**, 212–215.

Scheffer, T. J. and Nehring, J. (1984) A new, highly multiplexable liquid crystal display. *Applied Physics Letters* **45** 1021–1023.

Seiberle, H., Schmitt, K. and Schadt, M. (1999) Multidomain LCDs and complex retarders generated by photo-alignment. *Proceedings of Eurodisplay.*

Sergan, T. and Kelly, J. (2000) Negative uniaxial films from lyotropic liquid crystalline material for liquid crystal display. *Liquid Crystals* **27**, 1481–1484.

Slikkerveer, P., Bouten, P., Cirkel, P., de Goede, J., Jagt, H., Kooyman, N., Nisato, G., van Rijswijk, R. and Duineveld, P. (2004) A fully flexible colour display. *Society for Information Display Digest of Technical Papers* **XXXV**, 770–773.

Theis, J., Currie, E., Meijers, G., Southwell, J. and Chander, C. (2004) High Peroformance single layer anti-reflective coatings via wet UV curing technology. *Society for Information Display Digest of Technical Papers* **XXXV**, 1174–1177.

Yeh, P. and Gu, C. (1999) *Optics of Liquid Crystal Displays*. New York: John Wiley & Sons, Inc.

Yeh, P. and Paukshto, M. (2001) Molecular crystalline thin-film E-polarizer. *Molecular Materials* **14**, 1–19.

van Asslet, R., van Rooij, R. A. W. and Broer, D. J. (2000) Birefringent color reflective liquid crystal displays using broadband cholesteric reflectors. *Society for Information Display Digest of Technical Papers* **XXXI**, 742–745.

van de Witte, P., Brehmer, M. and Lub, J. (1999) LCD components obtained by patterning of chiral nematic polymer layers. *Journal of Material Chemistry* **9**, 2087–2094.

Wegh, R. and Broer, D. J. (2004) Cholesteric color filter and method of manufacturing such, World Intellectual Property Organization, International Document Number WO 2004/044631 A1.

Petitioner Samsung Ex-1011, 0222

11

Patterning Techniques and Semiconductor Materials for Flexible Electronics

John A. Rogers[1] and Graciela Blanchet[2]

[1]University of Illinois at Urbana-Champaign and [2]DuPont Central Research

11.1 Introduction

Advances in materials and processing techniques for silicon electronics continue to drive improvements in the speed and performance of a wide range of devices for consumer electronics. More recent research efforts seek to develop unconventional materials and printing techniques for completely new types of electronic systems. This class of circuitry will be important (at least initially) not because of its potential for high speed, density, etc., but because it can be mechanically flexible, lightweight, durable and easy to print rapidly over large areas. These plastic circuits will form the foundations for novel devices – electronic paper, wearable computers or sensors, disposable wireless ID tags, etc. – that complement the types of systems that conventional electronics supports well (microprocessors, high-density RAM, etc.). This field is new (i.e. there are no entrenched technologies) and it has a strong materials content. As a result, there are considerable opportunities for innovation and basic scientific research into new types of electronic materials and methods for patterning them into large-area, low-cost circuits.

Flexible Flat Panel Displays Edited by G. P. Crawford
© 2005 John Wiley & Sons, Ltd., ISBN 0-470-87048-6

Petitioner Samsung Ex-1011, 0224

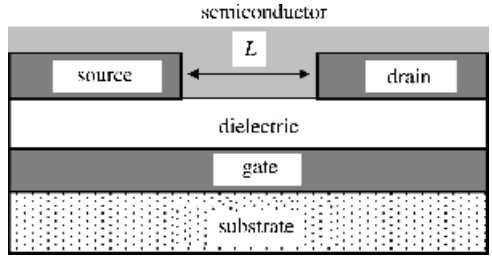


Figure 11.1 Schematic cross-sectional view of an organic thin film transistor. A semiconductor layer coats source and drain electrodes that are electrically isolated from a gate electrode by a dielectric layer. The separation between the electrodes defines the channel length, *L*

This chapter focuses on the fundamental element of complex active circuits: the thin film transistor (TFT). Figure 11.1 shows a cross-sectional view of a standard geometry for a TFT. The design includes a semiconducting layer that is electrically connected to source and drain electrodes. A thin insulating film (gate dielectric) isolates these electrodes and the semiconductor from an underlying gate electrode. The source and drain electrodes can be deposited on top of the semiconductor (top contact TFT), or the semiconductor can be deposited on top of them (bottom contact TFT; Figure 11.1). The region between the source and drain electrodes is known as the channel. The separation between these electrodes defines the channel length, *L*; their lengths define the channel width, *W*.

Modulating the voltage applied to the gate changes the conductance of the channel region by altering the electrical properties of the semiconductor near its interface with the gate dielectric. The magnitudes of the currents that flow when the gate voltage is adjusted to maximize (i.e. ''on''state) or minimize (i.e. ''off''state) the conductance, and the time required to switch between these two states often determine the utility of a transistor in a circuit. The TFT must produce enough ''on''current to activate or switch another part of a circuit but it must not generate ''off''currents that are large enough to cause unwanted switching. The ''on''current is typically measured in a regime where its magnitude is independent of the source/drain voltage. This saturation current can be related to other characteristics of the device in the following way (Sze 1985):

$$I_{sd} = \frac{W}{2L} C\mu \left(V_g - V_T\right)^2 = \frac{W}{2L} \frac{k\varepsilon_0}{t} \mu \left(V_g - V_T\right)^2, \tag{11.1}$$

where μ is the effective mobility of the semiconductor, k is the dielectric constant of the gate dielectric, t is its thickness and ε_0 is the permittivity of free space. V_g is the gate voltage and V_T is known as the threshold voltage. Transistors that have large ''on''currents possess some combination of large μ, high ε, small t, small L and/or large W. Limits on the overall physical size of a transistor for a particular application typically place an upper bound on W. The key properties therefore reduce to μ, t, ε and L. This chapter focuses on μ and L. It begins by describing some high-resolution printing techniques that enable small L and that are compatible with large-area plastic substrates. It then reviews the classes of organic semiconductors that have already been demonstrated for prototype flexible circuits. Data from single-crystal samples provide some insights into upper limits on the mobilities of TFT

Petitioner Samsung Ex-1011, 0225

formed with these classes of molecules. New types of organic and inorganic micro- and nanomaterials that can enable high-performance systems are also described. The chapter concludes with two examples of large-area prototype devices that have been built using these technologies.

11.2 Large-Area Patterning Techniques

High-resolution patterning methods for defining the separation between the source and drain electrodes are important since this dimension, L, influences current output (Kagan and Andry 2003) as well as the switching speed and other characteristics. Although photolithography, electron beam lithography and other conventional techniques have the required resolution, they are not well suited to flexible electronics because they are expensive and generally require multiple processing steps with resists, solvents and developers that can be difficult to use with plastic substrates. Inkjet printing and screen printing are promising nonphotolithographic methods that have been applied to organic transistors (Sirringhaus *et al.* 2000; Garnier *et al.* 1994). They both have the disadvantage, however, that high-resolution patterned wetting areas on the substrate are necessary to control the spread of the printed liquids at dimensions less than $\sim$50 μm. Precision polymer shadow masks represent a potentially attractive means for patterning evaporated materials with resolution of a few tens of microns (Baude *et al.* 2003). Registration and alignment of such masks could, however, be challenging for large areas. This chapter focuses on methods that offer micron resolution and which have been used to produce flexible circuits for working prototype systems. It includes two printing techniques that use high-resolution stamps – microcontact printing (Kumar and Whitesides 1993; Rogers *et al.* 1999) and nanotransfer printing (Loo *et al.* 2002c) – and one approach that uses thermal imaging with a scanned laser head (Blanchet *et al.* 2003). It also describes how these methods might be combined and matched to form a complete system for patterning all layers in practical devices.

11.2.1 Contact Printing with High-Resolution Stamps

Contact printing uses an element with surface relief (i.e. the stamp) to transfer material (i.e. the ink) to a substrate. Historically this approach has been used primarily to produce printed text or images with features that are 100 μm or larger in their minimum dimension. Its application to electronic systems that incorporate micron- or nanometer-sized features is much less well explored. The nature of the inks and their role in process steps after the printing define the classes of materials that can be patterned. The resolution is determined by the properties of the ink and its interaction with the stamp and/or substrate, the resolution of the stamp, and the conditions that convert the pattern of ink into a pattern of functional material.

The printing process can be separated into two parts: fabrication of the stamp and use of this stamp to pattern features defined by the relief on its surface (Xia *et al.* 1999). Often, stamps are produced by replication against a structure, known as the master, that has features of relief in the desired geometry. A single master can generate many stamps, each one of which can then be used many times for printing. As a result, the technique for producing the master does not need to be fast or low in cost. In a common approach, a lithographic method

Petitioner Samsung Ex-1011, 0226

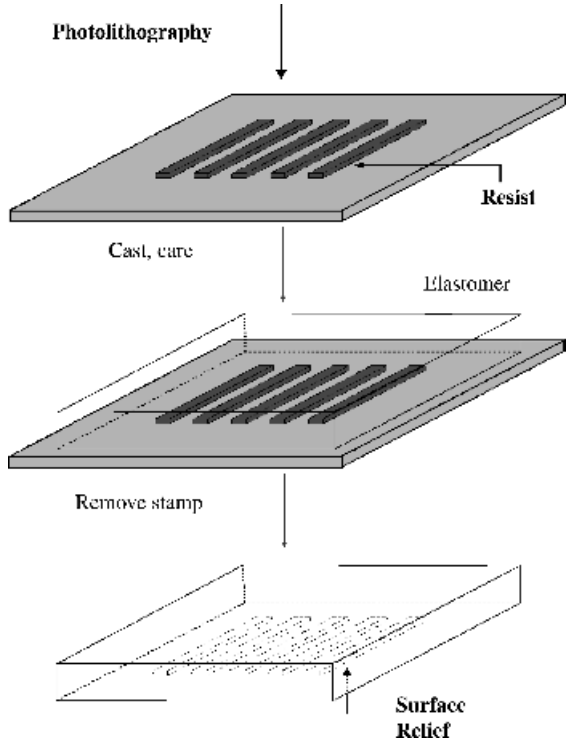


Figure 11.2 Casting and curing procedures for building high-resolution stamps. The first step involves patterning a layer of resist on a flat substrate to define a master. It is convenient to use a technique such as photolithography for this purpose. Casting, curing (thermally or optically) and then peeling the resulting polymer away from the master yields a stamp. Many stamps can be made with a single master and each stamp can be used many times. Reproduced by the permission of the American Institute of Physics

developed for the microelectronics industry defines the master. Casting a light- or heat-curable prepolymer against this master yields high-resolution stamps (Figure 11.2).

This replication process can have extremely high fidelity. Recent experimental evidence suggests that optimized materials and casting procedures enable stamps with relief features that have lateral dimensions of less than 5 nm (Hua *et al.* 2004). For feature sizes larger than $\sim$1–2 μm, contact and proximity mode photolithography are convenient tools for fabricating the master. Other techniques, such as direct write electron beam lithography and projection mode photolithography, must be used for features smaller than $\sim$2 μm. The circuit applications described in the following used masters with micron-sized features formed by contact or projection mode photolithography. Stamps designed to demonstrate resolution used masters formed by electron beam lithography.

Microcontact printing

Microcontact printing (μCP) uses high-resolution rubber stamps of poly(dimethylsiloxane) (PDMS) with inks (e.g. alkanethiols) that form self-assembled monolayers (SAMs) on the

Petitioner Samsung Ex-1011, 0227

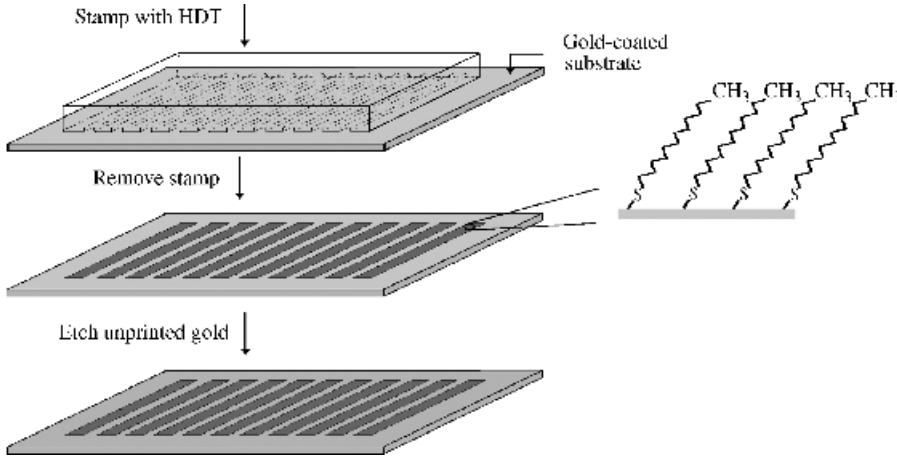


Figure 11.3 Steps for microcontact printing. The stamp is first inked with a solution of a material that is capable of forming a self-assembled monolayer (SAM) on the substrate that will be printed. In the case illustrated here, the ink is a millimolar concentration of hexadecanethiol (HDT) in ethanol. The substrate consists of a thin layer of Au on a flat support. Removing the stamp after a few seconds of contact leaves a patterned SAM of HDT on the surface of the Au film. The printed SAM can act as a resist for the aqueous wet etching of the exposed regions of the Au. The pattern of Au that results after etching and removal of the ink can be used to build devices of various types, including thin film transistors for flexible electronic systems. Reproduced by permission of the American Institute of Physics

surface (e.g. thin gold film) that is printed (Kumar and Whitesides 1993; Xia *et al.* 1999). These SAMs can serve as resists for etching material in the unprinted areas, as illustrated in Figure 11.3.

Figure 11.4 shows patterns of thin films of gold and silver generated in this manner. The typical edge resolution is ~50–100 nm; features with dimensions greater than ~200 nm can be generated easily. One of advantage of μCP is that it can form these high-resolution patterns over large areas on flexible plastic substrates, in a single patterning step (Rogers

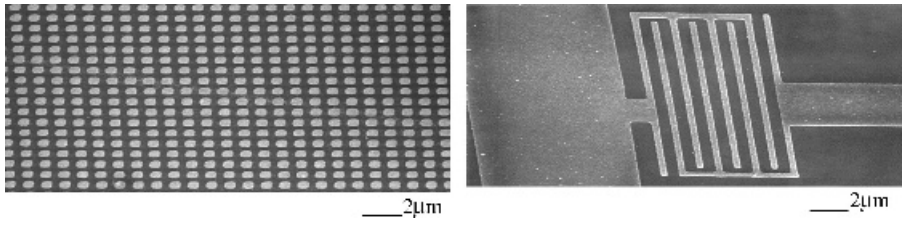


Figure 11.4 Scanning electron micrographs of structures formed by microcontact printing a self-assembled monolayer ink of hexadecanethiol onto a thin metal film of Au (left) and Ag (right) followed by wet etching of the unprinted areas. The left-hand image shows an array of Au (20 nm thick) dots with ~500 nm diameters. The right-hand image shows a printed structure of Ag (100 nm thick) in the geometry of interdigitated source and drain electrodes for a transistor in a simple inverter circuit. An edge resolution of ~100 nm can be achieved with this technique. Reproduced by permission of the American Institute of Physics

Petitioner Samsung Ex-1011, 0228

et al. 1999, 2001). Depositing an organic semiconductor on top of electrodes patterned by μCP can yield high-performance transistors with layouts like Figure 11.1 (Rogers *et al*. 1999).

When integrated with flexographic or related commercial printing systems, μCP has the potential to enable large-area patterning of flexible circuits at low cost. A significant challenge is that the elastomeric stamps tend to deform during the printing. This deformation can alter, in ways that are difficult to control, the precise alignment of features, thereby frustrating the type of multilevel registration that is required for circuit applications. There are at least two simple strategies to reduce these distortions: (i) eliminate significant mechanical manipulation of the stamp during printing (Rogers *et al.* 2001) and (ii) implement composite stamps that use PDMS layers bonded to high modulus supports (Rogers *et al.* 1998). The second approach has the advantage that it provides flexibility in the choice of means to perform the printing. Stamps that use a thin layer of PDMS on top of a sheet of polyimide, for example, reduce distortions significantly (Menard *et al.* 2004a); similar stamp designs that incorporate other different materials are also useful (Michel *et al.* 2001). The relatively high in-plane modulus of the polyimide reduces distortions that can prevent accurate registration. Its small thickness enables the stamp to be bent in a manner that facilitates printing. Detailed measurements on stamps that use $\sim$50 μm thick layers of PDMS on $\sim$50 μm thick polyimide substrates (Kapton, DuPont) show that distortions of less than 4 μm can be obtained over areas of up to 6 in $\times$ 6 in (Menard *et al.* 2004a). This value, which is more than a factor of 10 smaller than that previously reported by us for a single-component PDMS stamp used in an electronic paper application (Rogers *et al.* 2001), should satisfy many interesting applications in plastic electronics, such as reflective flexible displays.

Nanotransfer printing

Nanotransfer printing (nTP) is a more recent high-resolution printing technique (Loo *et al.* 2002c,2002d; Zaumseil *et al.* 2003b). It uses surface chemistries as interfacial glues and release layers (rather than inks) to control the transfer of solid material layers from relief features on a stamp to a substrate. This approach is purely additive (i.e. material is only deposited in locations where it is needed) and it can generate complex two- or three-dimensional structures in single or multiple layers with nanometer resolution. It has been explored mainly by our group and, in independent efforts, by groups at Princeton (Kim *et al.* 2002) and IBM/Zurich (Schmid *et al.* 2003). Elastomeric stamps similar to those of μCP, as well as stamps of hard, inorganic materials can be used. Depositing a thin layer of solid material onto the raised features of the stamp constitutes the inking step. Contacting this coated stamp with a substrate that supports a suitable surface chemistry results in covalent bonding between the coating and the substrate. If the surface of the stamp is treated such that the coating does not adhere well to it, then removing the stamp leaves a pattern with the geometry of the relief features. nTP can be used with SAMs and other surface chemistries for printing onto flexible or rigid substrates.

Figure 11.5 illustrates typical procedures. In this case, a vertical, collimated flux of Au forms a discontinuous coating on the surface of a high-resolution stamp. A self-assembled monolayer on the substrate provides exposed thiol groups that can bond to the Au coating when the stamp contacts the substrate. Figure 11.6 shows two printed patterns that have deep submicron and nanometer resolution. A PDMS stamp formed the pattern on the left

Petitioner Samsung Ex-1011, 0229

Publisher's Note:
Permission to reproduce this image online was not granted by the copyright holder. Readers are kindly requested to refer to the printed version of this chapter.

Figure 11.5 Schematic diagram of steps for nanotransfer printing. Depositing a layer of metal on the surface of a stamp, using a collimated flux normal to the stamp surface, yields a thin discontinuous coating on the raised and recessed regions. Contacting this coated stamp to a substrate that supports suitable surface chemical groups leads to covalent bonding between the metal and the substrate. In one example, self-assembled monolayers with exposed thiol groups allow printing of Au patterns on GaAs substrates. If the adhesion between the metal and the stamp is poor, then removing the stamp leaves a pattern in the geometry of the relief features on the substrate. Reprinted with permission from American Physical Society

(Zaumseil *et al.* 2003b); a hard stamp of GaAs, fabricated by electron beam lithography and etching, patterned the structure on the right (Loo *et al.* 2002d).

nTP offers much higher resolution than μCP, and it also provides some unique patterning capabilities (i.e. multilayer and three-dimensional structures can be fabricated). Its processing windows, however, are narrower than those of μCP (Menard *et al.* 2004b). There are at least three aspects that are important to achieving high fidelity with nTP: (i) the deposition

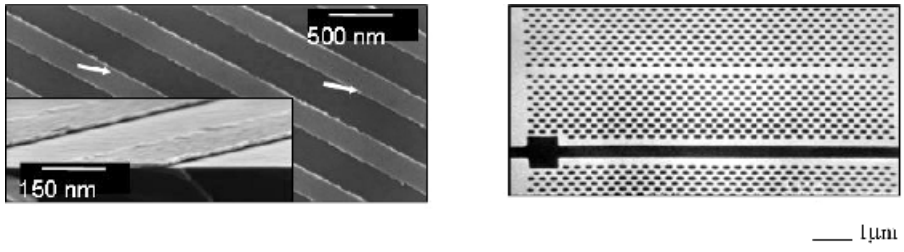


Figure 11.6 SEM images of patterns produced by nanotransfer printing. The left-hand image shows 300 nm lines of Au (20 nm thick) printed onto a GaAs wafer using a PDMS stamp. The slightly raised regions on the edges of the features are due to curved edges on the relief features of the stamps. The structure on the right consists of a bilayer of Au (20 nm)/Ti (5 nm) (white) in the geometry of a photonic band gap waveguide printed onto a sheet of plastic. Electron beam lithography and etching of a GaAs wafer produced the stamp that was used in this case. The stamp geometry limits the minimum feature size (∼70 nm) and the edge resolution (∼5–10 nm) in this case

Petitioner Samsung Ex-1011, 0230

procedures must be carefully controlled to avoid cracking or buckling of the metal films when PDMS stamps are used; (ii) PDMS stamps must be handled carefully before and during the printing to avoid surface strains that can damage the metal coatings; and (iii) the surface chemistry must provide a high density of bonding sites, and the stamps and substrates must come into uniform, intimate contact to allow efficient transfer. For the first issue, high deposition rates and surface treatments that facilitate wetting of the metals on the surfaces of the stamps are important. For the second, composite stamp designs that use rigid backings and relatively thin PDMS layers are helpful. These same stamps also prevent in-plane distortions that can frustrate multilevel registration. In the case of the third issue, suitable chemistries must be employed with substrates that present a low degree of roughness. With well-controlled procedures, patterns over large areas (several square centimeters) that are free of defects or cracks (as observed by high-resolution scanning electron and atomic force microscopy) can be produced (Menard *et al.* 2004b). We have demonstrated gold–gold cold welding, surface hydroxyl chemistries, and thiol-based SAMs for inducing the transfer (Loo *et al.* 2002a, 2002c, 2002d). In many cases, X-ray photoelectron spectroscopy (XPS) analysis shows that a residual, ultrathin layer of organic material can transfer with the metal film to the substrate when PDMS stamps are used (Menard *et al.* 2004b). This layer is of order of 1–4 nm thick, depending on the processing conditions. It can be removed using various dry or wet etching procedures (Menard *et al.* 2004b). As with μCP, the metal structures formed by nTP can be used in a variety of ways in flexible circuits. Their most compelling is to source and drain electrodes that define short channel lengths.

11.2.2 Thermal Transfer Printing

nTP and μCP have many attractive features, but they do not yet exist in the form of commercial tools. Thermal transfer printing, on the other hand, is an established technique that is already well developed for digital printing applications. Because suitable output engines are commercially available, thermal transfer may well be a suitable route for early commercialization of organic electronic devices (Blanchet *et al.* 2003). Figure 11.7 illustrates this approach. Patterning proceeds via the purely additive, selective dry transfer of a solid film from a donor sheet to a substrate. By removing the demanding solvent and etching compatibility requirements that are associated with most fabrication techniques, this approach expands considerably the range of usable materials. In addition, thermal printing maintains features desirable in large-scale manufacturing such as high speed, high resolution and the ability to perform multilayer registration.

The process begins by coating a donor substrate with a thin layer of material to be patterned and then placing this sheet against a flexible substrate onto which the circuit is to be printed. A 40 W, 780 nm infrared diode laser, split into 250 2.7 μm × 5 μm individually addressable spots, is focused through the donor base at a thin absorbing layer onto which is coated the material to be imaged. The efficient conversion of light to heat at this interface decomposes a thin layer of adjacent organics into gaseous products while somewhat softening the remaining film. The expansion of the gaseous decomposition products propels the thin conducting layer onto the receiver film. The desired conducting pattern is printed by rastering the laser beam, thereby selectively transferring the individual 5 μm × 2.7 μm pixels comprising the image from the donor layer onto the substrate. Since the beam is fully

Petitioner Samsung Ex-1011, 0231

Publisher's Note:
Permission to reproduce this image online was not granted by the copyright holder. Readers are kindly requested to refer to the printed version of this chapter.

Figure 11.7 Sequence for patterning structures by thermal transfer printing. A donor sheet that is coated with a layer of the material to be printed is laminated against a substrate. The inset shows the process by which local heating with a laser causes the transfer of some part of the material from the donor to the substrate. Repeating these steps of lamination, laser transfer printing, and removal gives an additive, dry multilayer route to flexible electronic circuits. Reprinted with permission from American Physical Society

addressable, any pattern can be formed. In addition, after printing a first layer, the donor film can be removed and another donor sheet whose top layer has a different functionality (i.e. dielectric) can be positioned and exposed in registry on top of the conducting layer. Multilayer electronic circuitry can be readily built in this fashion (Blanchet *et al.* 2003). Although a variety of conductors can be printed, we focus on a polymer system that consists of dinonylnaphthalene sulfonic acid doped polyaniline (DNNSA-PANI) mixed with several weight percent of single-walled carbon nanotubes (SWNT), which we call PANI/SWNT (Blanchet *et al.* 2003), and a silver-based conductive paste (Blanchet *et al.* 2003).

Figures 11.8 to 11.10 show some typical structures of these materials formed by thermal transfer printing. Figure 11.8 shows optical micrographs of the source/drain layer of a complementary logic gate (i.e. inverter). The left frame shows the inverter; the right frame presents a magnified view of the interdigitated source/drains. This layout is designed to balance the difference in mobilities between p- and n-type semiconductors in the circuit (Lefenfeld *et al.* 2003). Figure 11.9 illustrates the ability to print multiple layers of different

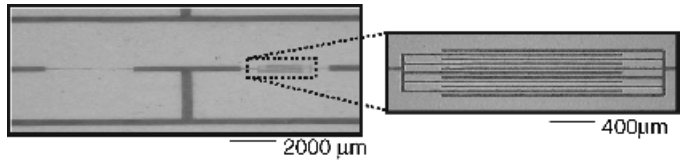


Figure 11.8 Optical micrographs of thermal transfer printed patterns of the doped conducting polymer PANI/SWNT. The left-hand image shows printed source and drain electrodes and interconnections for a complementary logic gate. The right-hand image shows a magnified view of interdigitated source and drain electrodes for the n-channel transistor of this simple circuit. Reprinted with permission from American Physical Society

Petitioner Samsung Ex-1011, 0232

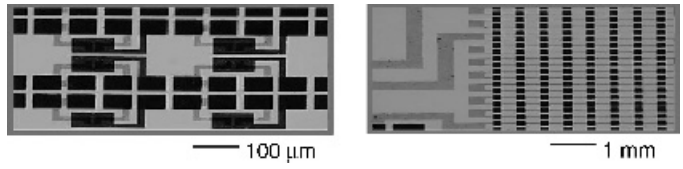


Figure 11.9 Optical micrographs of some patterns that consist of multiple thermal transfer printed layers of conducting films. The results illustrate multilayer printing with good registration

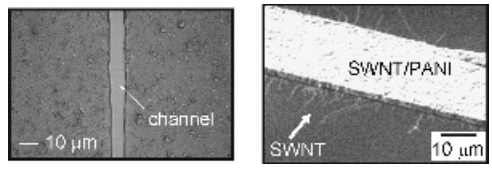


Figure 11.10 The left-hand image shows an optical micrograph of source and drain electrodes of a PANI/SWNT patterned by thermal transfer printing. This structure defines a transistor channel length of ~7 μm. The right-hand image is a scanning electron micrograph showing the edge of a printed line. Note the SWNTs that pull out at the edges of this structure. These tubes interact with semiconductors in the transistor channels. Reprinted with permission from Elsevier

conducting materials with good registration. The figure on the left shows serpentine patterns of 10 μm PANI/SWNT lines and 50 μm squares of the silver composite. An overprint of 50 μm squares of the PANI/SWNT is shown on the right. As illustrated by these examples, the pattern geometries are flexible. The edge resolution, which is of order 3 μm, is comparable to the size of the laser spot used for printing.

The PANI/SWNT forms an excellent material for the source and drain electrodes of organic transistors. Figure 11.10 shows a sub-10 μm channel fabricated by printing. The frame on the right illustrates the SWNTs that pull out at the edges of the printed lines (Lefenfeld *et al.* 2003). Depositing an organic semiconductor on top of such printed electrodes yields high-performance transistors with low contact resistances (Lefenfeld *et al.* 2003). The SWNTs may play a role in facilitating charge injection in this case. Note that these tubes might themselves form the basis of a semiconducting layer. This type of semiconductor nanomaterial is described in detail in the following section.

11.2.3 Combining Contact and Thermal Transfer Printing

Microcontact and nanotransfer printing are attractive because they provide simple and potentially low-cost routes to structures with dimensions deep into the submicron regime. Nanotransfer printing offers true nanometer resolution in an additive fashion that allows complex 3D and multilayer fabrication. For plastic electronics, both these techniques have the important ability to pattern high-resolution source and drain electrodes out of materials that are compatible with known organic semiconductors. This resolution enables channel lengths that are sufficiently small to produce transistors with large ''on'' currents even with the moderate to low mobilities that are available from organic semiconductors. Thermal

Petitioner Samsung Ex-1011, 0233

transfer printing has, by comparison to μCP and nTP, enormous flexibility in the materials that can be patterned. It can process large areas with good registration at high speed with commercial engines. It benefits from its all-dry and purely additive operation; it does not require etchants or solution routes for depositing or patterning the key materials. In addition, our vast experience in formulating materials for thermal imaging enables us to easily design formulations with widely different functionalities, readily balancing the adhesion between the layers that are sequentially transferred such that interfaces have intimate physical and electrical contact. Although current systems have a pixel size of 5 μm × 2.2 μm, which limits the resolution, systems with 2 μm × 2 μm pixels are in the process of being commercialized. For applications that demand sub-5 μm resolution, it may be possible to combine microcontact or nanotransfer printing with thermal transfer printing: high-resolution source and drain electrodes printed with μCP or nTP could be used with other components that are patterned by thermal transfer. These and other strategies that combine and match different patterning techniques may provide an attractive means for building plastic circuits.

11.3 Printable Semiconductors and Devices

Printing techniques such as those described in the previous sections must be combined with high-quality electronic materials to yield useful circuits. The semiconductor is an important and challenging component of the devices. Several classes of materials have been demonstrated for this purpose, including a range of organic, inorganic, and organic/inorganic hybrids (Kagan and Andry 2003). There are processing advantages, especially for large-area systems, in having materials that can be printed or cast from solution. Considerable research has focused on developing such materials, beginning with the first demonstration of a printed plastic transistor in 1994 (Garnier *et al.* 1994). Known organic semiconducting polymers and oligomers exhibit effective device mobilities (as measured in thin film transistors) of 0.1 to 1 $cm^2/V\,s$ (Kagan and Andry 2003). They also have other good properties such as the ability to support large ($> 10^5$) on/off current ratios. These characteristics are satisfactory for many applications, such as displays. They are inadequate, however, for high-speed signal processing or computing. Research therefore continues to focus on improving the properties of existing classes of materials and on understanding the drift in their properties during use. More recent work seeks to establish different materials that have performance competitive with conventional single-crystal silicon devices.

11.3.1 Conventional Organic Semiconductors

Conjugated polycyclic compounds of molecular weight < 1000, and polyheterocycles with much higher average molecular weight represent two classes of organic materials that offer performance suitable for realistic display applications.

Figure 11.11 shows the chemical structures of a few of these organic semiconductors. To achieve good performance in TFTs, it is necessary to prepare these materials in highly purified forms. In the case of polymers, control of regiochemistry, molecular weight distribution and end groups are also necessary to ensure the needed chain overlaps and orientation. Solution casting or low-temperature vacuum evaporation of these molecules onto printed electrodes (formed by nTP or μCP, for example) yields TFTs. It is also possible

Petitioner Samsung Ex-1011, 0234

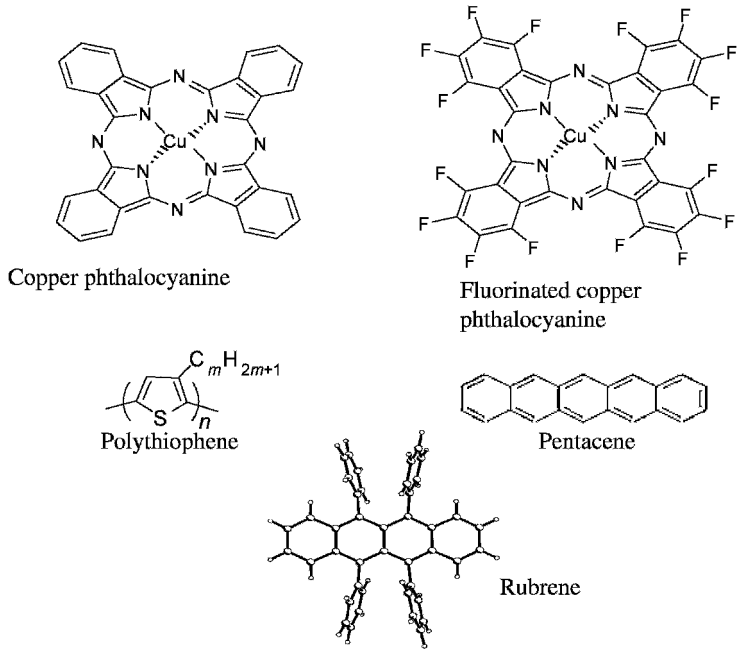


Figure 11.11 Chemical structures of some organic semiconductors. Thin films of these materials act as p-type materials in thin film transistors, except for the compound at the upper right, which exhibits n-type behavior

to print the electrode structures onto separate susbtrates and to build the TFTs by lamination against layers of the semiconductor. Good performance can be obtained with both of these procedures.

Figure 11.12 shows an optical micrograph (inset) and current–voltage characteristics (left frame) of a transistor that incorporates interdigitated source/drain electrodes of Au/Ti

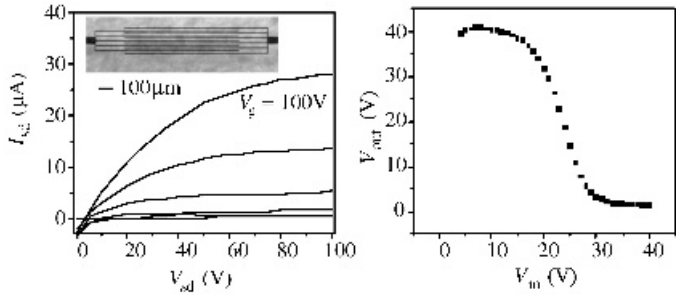


Figure 11.12 The left-hand image shows current–voltage characteristics of an n-channel transistor formed with electrodes patterned by nanotransfer printing. Laminating these electrodes against a substrate (PET) that supports an organic semiconductor (FCuPc), a gate dielectric, and a gate completes the device. The inset shows an optical micrograph of the interdigitated electrodes. The right-hand image shows the transfer characteristics of a complementary logic gate that uses this device and a similar one for the p-channel (pentacene) transistor

Petitioner Samsung Ex-1011, 0235

patterned by nTP on a substrate of PDMS ($\sim$20 μm)/poly(ethylene terephthalate) (250 μm) (Loo *et al.* 2002c). Laminating these electrode structures against a substrate that supports an organic semiconductor, gate dielectric (glass resin) and gate electrode (ITO) produces a TFT. This device uses the n-type organic semiconductor copper hexadecafluorophthalocyanine (FCuPc). The right frame of Figure 11.12 shows the transfer characteristics of a laminated complementary logic gate whose electrodes and connecting lines are defined by nTP. The p-channel transistor in this circuit uses pentacene for the semiconductor (Loo *et al.* 2002c). The effective mobility of these transistors and the behavior of the inverter are comparable to those of similar devices that use large-scale electrodes patterned by evaporation of metals through shadow masks. The pentacene devices exhibit mobilities as high as $\sim 1\ \mathrm{cm}^2/\mathrm{V\ s}$.

Reducing the channel length can improve the current output and switching speed. The high resolution of nTP enables channel lengths deep into the submicron range. Figure 11.13 shows, as an example, a scanning electron micrograph and current–voltage characteristics of a transistor with $L = 150$ nm. In this device, an Au-coated stamp is simply placed into contact with the semiconductor (pentacene) to form a top contact device (Zaumseil *et al.* 2003c).

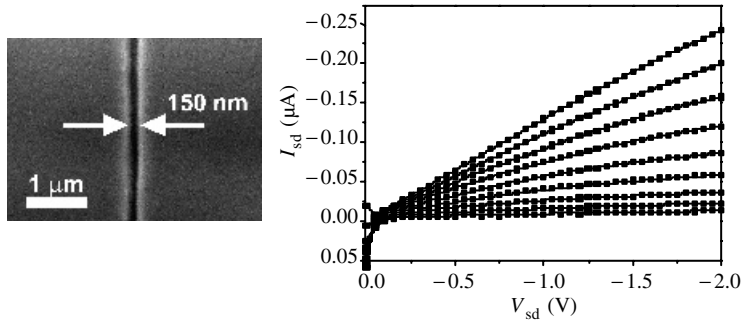


Figure 11.13 Current–voltage characteristics from a nanoscale organic transistor formed by contact of a metal-coated stamp against a thin film of the organic semiconductor pentacene. The gate voltage varies between +1.0 V and −2.2 V in steps of 0.4 V. The channel length is $\sim$150 nm. The image on the left shows a scanning electron micrograph of the separation between the source and drain electrodes on the stamp.

Analysis shows that its effective mobility is much lower than expected, based on measurements in TFTs that use similar materials with micron-scale channel lengths. Studies of channel length scaling of current output suggest that barriers at the metal–semiconductor contacts limit the performance for channel lengths of less than a few microns. As a result, improvements in the contacts will be needed to increase performance of devices with short channels. Contact engineering of these systems is in its infancy. Empirical observations suggest that laminated top contacts can show resistances lower than those formed by direct evaporation (Loo *et al.* 2002b; Zaumseil *et al.* 2003a). In the bottom contact configuration, thermal transfer printed electrodes of PANI/SWNT show much lower resistances than Au

Petitioner Samsung Ex-1011, 0236

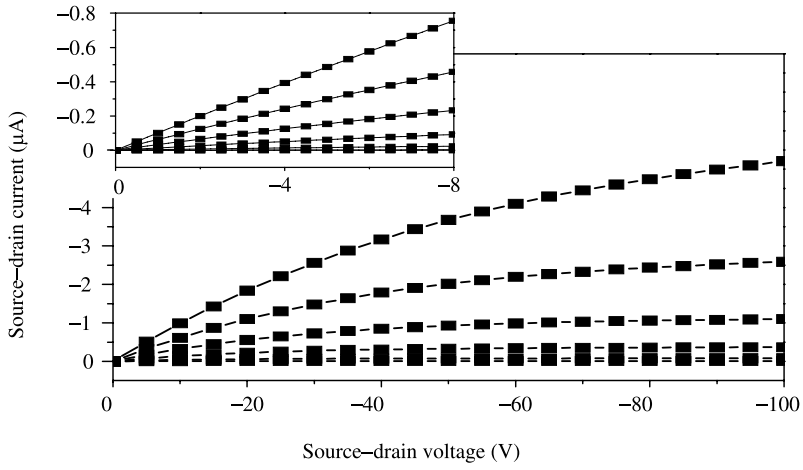


Figure 11.14 Current–voltage characteristics of an organic transistor that uses thermal transfer printed source and drain electrodes of PANI/SWNT. A thin (25 nm) film of pentacene deposited onto the electrodes provides the semiconductor. The gate voltage varies from 0 to −100 V in steps of −20 V. The channel length is 15 μm and the channel width is 0.5 mm. The inset shows the linear behavior of the device at small source–drain voltages. Reprinted with permission from American Chemical Society

electrodes (Lefenfeld *et al.* 2003). Figure 11.14 presents current–voltage characteristics obtained from a TFT that uses pentacene deposited onto prepatterned PANI/SWNT electrodes (Lefenfeld *et al.* 2003). The inset shows the highly linear response in the regime where the source/drain voltage is much lower than the gate voltage. This behavior, and the expected $1/L$ scaling of the device properties, are consistent with low resistance contacts. The fundamental causes for the good electrical behavior of these contacts are the subject of current study.

In addition to the channel length and the metal–semiconductor interface, transport in the organic itself is critically important to device performance. Although it is difficult to predict the upper limits in the mobilities of pentacene and related classes of organics, insights can be obtained from studies of highly pure single crystals.

Figure 11.15 presents characteristics of a well-controlled transistor formed from a bulk single crystal of the organic semiconductor rubrene (Sundar *et al.* 2004). This device was constructed in a completely noninvasive fashion by physical lamination of the crystal against an elastomeric element that provides source and drain electrodes, gate dielectric and gate electrode. The response shows highly idealized behavior, including nearly zero threshold voltages and mobilities independent of gate voltage. Device mobilities as high as 20 cm^2/V s have been observed at room temperature in these systems. This value is 10–100 times higher than those observed in the best organic TFTs. These data indicate, therefore, that substantial improvements in performance might be obtained by optimizing the growth conditions of the thin films. Nevertheless, even the single-crystal value of 20 cm^2/V s is relatively modest; it is more than a factor of 10 lower than the mobilitity of single-crystal silicon, and ∼100–1000 times lower than the mobility of semiconducting single-walled carbon nanotubes. This result suggests that upper limits in the mobilities of conventional organics might lie

Petitioner Samsung Ex-1011, 0237

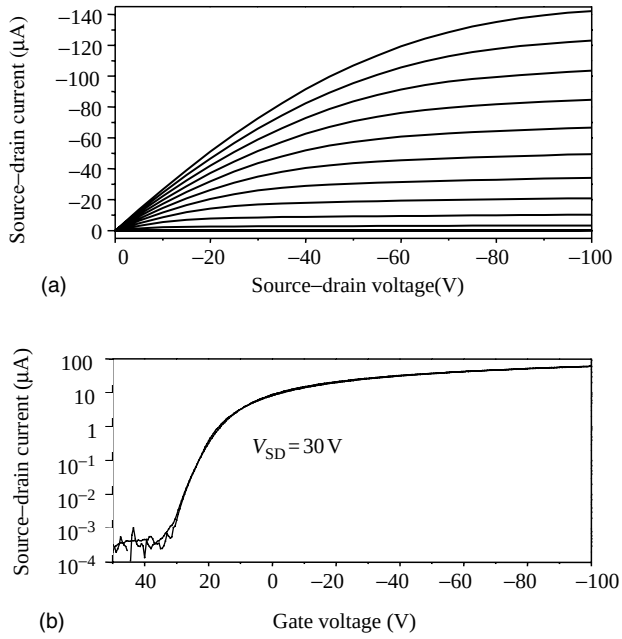


Figure 11.15 Current–voltage characteristics of a field effect transistor that uses a single crystal of the organic semiconductor rubrene. (a) Variation of current with source–drain voltage at several gate voltages. Typical p-type behavior is observed, with well-resolved linear and saturation current regimes. The channel is normally off and turns on at successively more negative gate voltage (from +20 to −100 V). (b) Transfer characteristics measured at $V_{SD} = 30$ V. On/off ratios are of order 10^5 and mobilities are as high as 20 cm^2/V s.

significantly below existing classes of materials, such as silicon and single-walled carbon nanotubes, as outlined in the following section.

11.3.2 New Printable Semiconductors for Flexible Circuits

Semiconducting single-walled carbon nanotubes are remarkable materials. Intrinsic tube mobilities, for example, have been observed to approach values as high as 80 000 cm^2/V s in single-tube devices at room temperature (Durkop *et al.* 2004; McEuen *et al.* 2002; Avouris 2002). Those properties suggest that a massively parallel array of SWNTs (SWNT arrays) that span the gap between source and drain electrodes could form an effective semiconductor film for transistors with performance (speed, current output, power efficiency, etc.) that is many orders of magnitude better than achievable with conventional organic semiconductors. Because the tubes can be dispersed in a variety of solvents, it is possible to cast them directly onto a range of different substrates, including plastics, at room temperature. Printing electrodes onto cast submonolayer films of these SWNTs can yield SWNT array transistors with good performance. Optimizing alignment and packing density, and achieving high intrinsic tube mobilities from solution-cast SWNT represent some challenges. In addition, metallic tubes must be removed from the channel to achieve high on/off ratios. The simplest

Petitioner Samsung Ex-1011, 0238

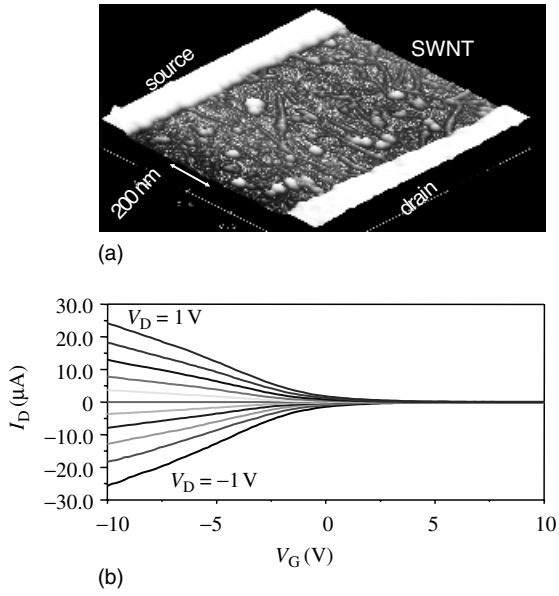


Figure 11.16 (a) An atomic force micrograph of the channel region of a thin film transistor that uses an array of SWNTs as the semiconductor. (b) Transfer characteristics of such a device

approach uses high source/drain voltages with the gate voltage adjusted to strongly turn off the semiconducting tubes in order to burn out the metallic tubes. Chemical and dielectrophoretic approaches for separation are also emerging from research activities at several laboratories (Strano *et al.* 2003; Zheng *et al.* 2003; Krupke *et al.* 2003). As a result, this separation problem does not appear to be a serious one for SWNT array TFTs.

Figure 11.16 shows an atomic force micrograph of an SWNT array device and some transfer characteristics obtained from it (Meitl *et al.* 2004; Zhou *et al.* 2004). This device uses solution-cast tubes synthesized using the well-known high-pressure carbon monoxide technique (Bronikowski *et al.* 2000; Alvarez *et al.* 2001). A zeroth-order approximation of the device behavior suggests that, after burnout, it operates similar to a conventional p-type TFT, with a mobility (computed using the physical width of the channel) of 0.1 to 1 $cm^2/V\,s$ and on/off ratios of $\sim 10^5$. Although these values are not high compared to those obtained with conventional organics, these early results suggest that high performance can be achieved by increasing the number of spanning tubes in the channel. Such an analysis assumes, of course, that operation of the devices is not dominated by contacts. Further study is required to obtain a better understanding of these and other issues.

The good performance and well-understood properties of silicon make it another potentially attractive material for flexible electronics. Most forms of silicon, other than amorphous, require high-temperature deposition and/or processing; they are therefore incompatible with many plastic substrates. Solution-deposited films of inorganic nanoparticle and nanowire semiconductors appear promising, although the device mobilities of reported devices are only in the range ~ 1–$3\ cm^2/V\,s$ (Ridley *et al.* 1999; Duan *et al.* 2003). We demonstrated recently that top-down fabrication techniques (i.e. lithography and anisotropic etching) can produce freestanding objects of high-quality single-crystal silicon

Petitioner Samsung Ex-1011, 0239

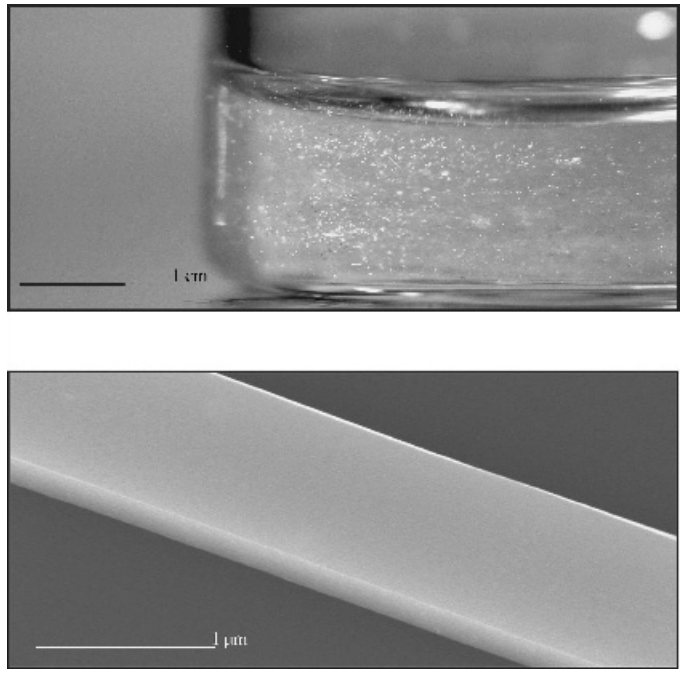


Figure 11.17 High-resolution images of transferred silicon wires and ribbons

with a wide range of geometries (Menard *et al.* 2004b). A large collection of such objects constitutes a type of material, which we call microstructured silicon (μs-Si), that can be used to form mechanically flexible thin film transistors that have excellent electrical properties (Ridley *et al.* 1999).

Figure 11.17 shows a suspension of silicon ribbons (several tens of millions) in ethanol, and a high-resolution scanning electron micrograph of a single ribbon to illustrate the extremely smooth surfaces that can be obtained. The lateral dimensions of these ribbons and other objects can be as small as 50 nm by using etch resists formed using nTP or other soft lithographic approaches.

Solution casting can deliver μs-Si to a range of different substrates, including plastics. Dry transfer printing provides another method to pattern this material.

Figure 11.18 shows high-resolution images of transferred silicon wires and ribbons. Figure 11.19 shows electrical properties of a TFT that uses a single silicon ribbon solution cast onto a substrate of SiO_2/Si. Analysis of the slope of the transfer characteristic shown in the right frame yields a mobility of $\sim$200 cm^2/V s (using the physical width of the channel, which in this case is equal to that of the ribbon).

The threshold voltages and the contact properties are very sensitive to the techniques for fabricating the μs-Si and for transferring it to the device substrate. The basic techniques, however, are compatible with the sorts of printing techniques described in the previous sections. This form of top-down microtechnology might represent an attractive route to high-performance flexible electronic systems.

Petitioner Samsung Ex-1011, 0240

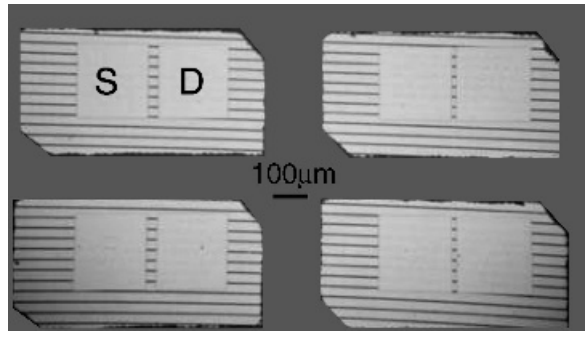


Figure 11.18 Optical image of a set of TFTs formed on a plastic substrate with aligned arrays of single crystal silicon ribbons as the semiconductor.

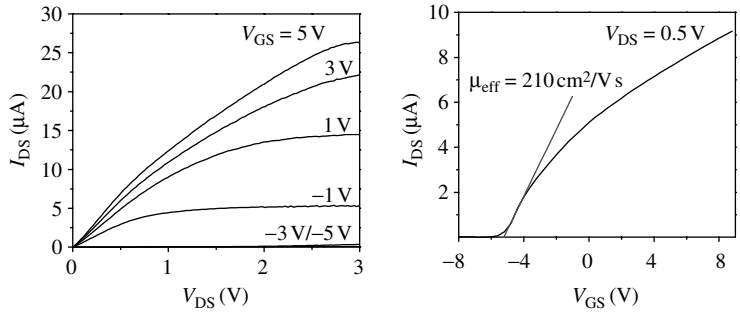


Figure 11.19 Electrical properties of a TFT that uses a single silicon ribbon solution cast onto a substrate of SiO_2/Si

11.4 Prototype Circuits and Systems

Not only can these printing techniques and semiconductor materials form individual transistors with good characteristics, but they can also be used for large-area circuits that have performance sufficient for interesting systems that might have some commercial value. Figure 11.20 shows images of a 6 in × 6 in plastic active matrix backplane circuit formed by microcontact printing using the materials and procedures described previously (Rogers *et al.* 2001). Pentacene serves as the semiconductor in this case. Glass resin films spin cast to thicknesses of ∼1 μm serve as gate dielectrics (Bao *et al.* 2002). The substrate consists of a 250 μm thick sheet of poly(ethylene terephthalate) (PET) with a thin (100 nm) coating of indium tin oxide (ITO) for the gate. The channel lengths for the drive transistors are ∼15 μm; the leads that connect the source and drain electrodes to the row and pixel electrodes are ∼15 μm wide. An image of a display, built by laminating this circuit against an unpatterned sheet of electronic ink, appears in Figure 11.21.

The high resolution of μCP is important to achieving the necessary performance (transistor current output and switching speed) for this application. The details of this

Petitioner Samsung Ex-1011, 0241

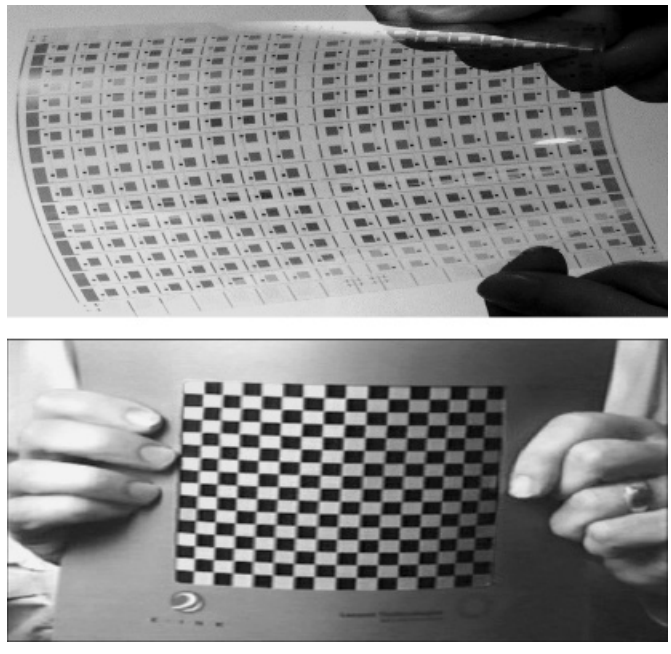


Figure 11.20 Mechanically flexible plastic active matrix circuit (top image) for an electronic paper-like display (bottom image). Microcontact printing defined the critical features in the organic transistors of this circuit

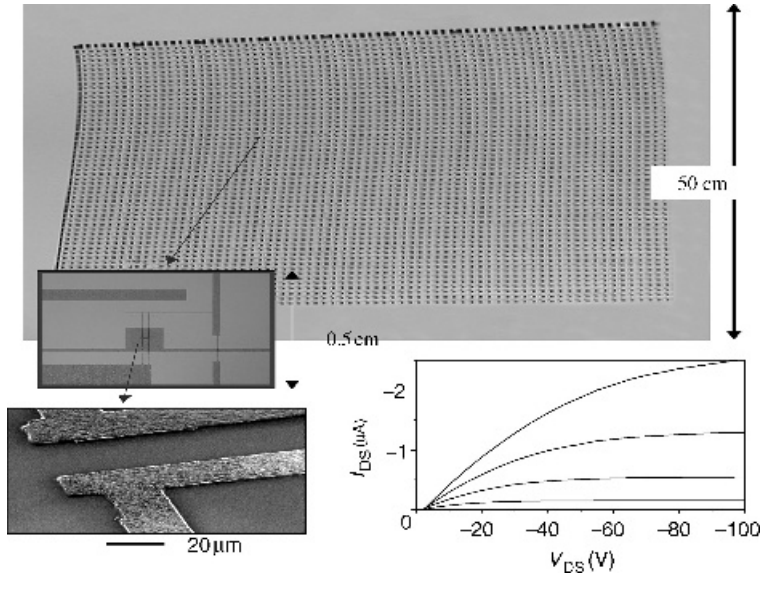


Figure 11.21 Active matrix backplane circuit formed by thermal transfer. A photograph of a 50 cm × 75 cm printed panel is shown at the top. The micrograph at the middle left illustrates a unit cell of the circuit. The scanning electron micrograph at the bottom left provides a high-resolution view of the source and drain electrodes and the channel region. The graph at the bottom right shows the electrical characteristic of one of the transistors in the large printed panel. The gate voltage varies from 0 to −100 V in −20 V steps

Petitioner Samsung Ex-1011, 0242

device can be found elsewhere (Rogers *et al.* 2001). Although the number and size of the pixels are not suitable for realistic applications, there are no inherent limitations in the printing techniques that prevent more pixels and higher resolution.

Figure 11.21 shows a backplane with a similar layout, but much larger in size. This circuit was formed using thermal transfer printing and lamination for all the layers of the circuit according to the procedures illustrated in Figure 11.4 followed by pentacene evaporation (Blanchet *et al.* 2003). First a PANI/SWNT donor and a flexible receiver are positioned and held in contact by vacuum. Gates were then printed by selectively transferring PANI/SWNT from a donor film onto a flexible receiver as previously described. The receiver was then removed for the lamination of a 1 μm methacrylate copolymer layer over the whole area and repositioned in registry for printing the source and drain layer. The backplane was completed by evaporation unpurified pentacene through a shadow mask. Although the printing system maintains a 2–5 μm registration when imaging via the transfer of sequential layers onto a fixed receiver, it lacks built-in registration once the receiver is removed. Registration was achieved by aligning the receiver onto preset orthogonal edges on a carrier sheet that could, in turn, be precisely located onto the drum of the printer. Even with this rudimentary approach, it was possible to achieve registration errors of less than 200 μm over the 4000 cm^2 area. The circuit contains 5000 transistors with 20 μm channels printed onto a 50 cm × 80 cm flexible substrate. Micrographs of a typical transistor are shown in the lower left-hand corner. The transfer characteristics of a typical transistor in the panel are also shown in the lower right.

11.5 Conclusions

This chapter provides an overview of some recent work in the areas of printing techniques and semiconductor materials for flexible circuits, with an emphasis on our own efforts. Working TFTs, simple logic gates, large-area circuits and flexible displays demonstrate the implementation of these technologies. Our description of this field is not, of course, comprehensive. Impressive work exists, for example, in the areas of imprinting (Behl *et al.* 2002), inkjet printing(Sirringhaus *et al.* 2000), precision shadow masking (Baude *et al.* 2003), and many other techniques for patterning circuits on plastic (Talghader *et al.* 1995). In addition, there are a range of semiconductors that have promise for flexible circuits, including amorphous silicon. It is also worth pointing out that pick-and-place or fluidic assembly (Talghader *et al.* 1995; Jacobs *et al.* 2002) of preformed silicon circuit elements onto plastic as well as the full transfer (Lee *et al.* 2003) of circuits from silicon wafers to flexible substrates represent alternative approaches to flexible circuits. The performance requirements and cost targets of the end application will ultimately determine the choice of technology. The broad variety of approaches and the interesting scientific issues that surround each of them make these areas exciting to research.

Acknowledgements

The work presented here represents efforts of a large number of researchers from Lucent Technologies, University of Illinois at Urbana-Champaign and DuPont.

Petitioner Samsung Ex-1011, 0243

References

Alvarez W. E., Kitiyanan B., Borgna A. and Resasco D. E. (2001) Synergism of Co and Mo in the catalytic production of single-wall carbon nanotubes by decomposition of CO. *Carbon* **39**, 547–58.

Avouris P. (2002) Molecular electronics with carbon nanotubes. *Accounts of Chemical Research* **35**, 1026–34.

Bao Z., Kuck V., Rogers J. A. and Paczkowski M. A. (2002) Silsesquioxane resins as high performance solution processable dielectric materials for organic transistor applications. *Advanced Functional Materials* **12**, 526–31.

Baude P. F., Ender D. A., Haase M. A., Kelley T. W., Muyres D. V. and Theiss S. D. (2003) Pentacene-based radio-frequency identification circuitry. *Applied Physics Letters* **82**, 3964–66.

Behl M., Seekamp J., Zankovych S., Torres C. M. S., Zentel R. and Ahopelto J. (2002) Towards plastic electronics: patterning semiconducting polymers by nanoimprint lithography. *Advanced Materials* **14**, 588–91.

Blanchet G., Loo Y.-L., Rogers J. A., Gao F. and Fincher C. (2003) Large area dry printing of organic transistors and circuits. *Applied Physics Letters* **82**, 463–65.

Bronikowski M. J., Bradley R. K., Nikolaev P., Willis P. A., Colbert D. T., Smith K. A. and Smalley R. E. (2000) Gas-phase method for large-scale production of single-walled carbon nanotubes. *Abstracts of Papers of the American Chemical Society* **219**, 421.

Duan X. F., Niu C. M., Sahi V., Chen J., Parce J. W., Empedocles S. and Goldman J. L. (2003) High-performance thin film transistors using semiconductor nanowires and nanoribbons. *Nature* **425**, 274–78.

Durkop T., Getty S. A., Cobas E. and Fuhrer M. S. (2004) Extraordinary mobility in semiconducting carbon nanotubes. *Nano Letters* **4**, 35–9.

Garnier F., Hajlaouir R., Yassar A. and Srivastava P. (1994) All-polymer field-effect transistor realized by printing techniques. *Science* **265**, 1684–86.

Hua F., Sun Y., Guar A., Meitl M. A., Bilhaut, L., Rotkina L., Wang J., Geil P., Shim M., Rogers J. A. and Shim A. (2004) Polymer imprint lithography with molecular-scale resolution. *Nano letters* **4**, 2467–2471.

Jacobs H. O., Tao A. R., Schwartz A., Gracias D. H. and Whitesides G. M. (2002) Fabrication of a cylindrical display by patterned assembly. *Science* **296**, 323–25.

Kagan, C. R. and Andry, P. (2003) *Thin Film Transistors, Marcel Dekker.*

Kim C., Shtein M. and Forrest S. R. (2002) Nanolithography based on patterned metal transfer and its application to organic electronic devices. *Applied Physics Letters* **80**, 4051–53.

Krupke R., Hennrich F., von Lohneysen H. and Kappes M. M. (2003) Separation of metallic from semiconducting single-walled carbon nanotubes. *Science* **301**, 344–47.

Kumar A. and Whitesides G. M. (1993) Features of gold having micrometer to centimeter can be formed through a combination of stamping with an elastomeric stamp and an alkanethiol ink followed by chemical etching. *Applied Physics Letters* **63**, 2002–4.

Lee Y., Li H. D. and Fonash S. J. (2003) High-performance poly-Si TIFTs on plastic substrates using a nano-structured separation layer approach. *IEEE Electron Device Letters* **24**, 19–21.

Lefenfeld M., Blanchet G. and Rogers J. A. (2003) High performance contacts in plastic transistors and logic gates that use printed electrodes of DNNSA-PANI doped with single-walled carbon nanotubes. *Advanced Materials* **15**, 1188–91.

Loo Y.-L., Hsu J. W. P., Willett R. L., Baldwin K. W., West K. W. and Rogers J. A. (2002a) High-resolution transfer printing on GaAs surfaces using alkane dithiol self-assembled monolayers. *Journal of Vacuum Science and Technology B* **20**, 2853–56.

Loo Y.-L., Someya T., Baldwin K. W., Ho P., Bao Z., Dodabalapur A., Katz H. E. and Rogers J. A. (2002b) Soft, conformable electrical contacts for organic transistors: high resolution circuits by lamination. *Proceedings of the National Academic Science USA* **99**, 10252–56.

Petitioner Samsung Ex-1011, 0244

Loo Y.-L., Willett R. W., Baldwin K. and Rogers J. A. (2002c) Additive, nanoscale patterning of metal films with a stamp and a surface chemistry mediated transfer process: applications in plastic electronics. *Applied Physics Letters* **81**, 562–64.

Loo Y.-L., Willett R. W., Baldwin K. and Rogers J. A. (2002d) Interfacial chemistries for nanoscale transfer printing, *Journal of the American Chemistry Society* **124**, 7654–55.

McEuen P. L., Fuhrer M. S. and Park H. K. (2002) Single-walled carbon nanotube electronics. *IEEE Transitions on Nanotechnology* **1**, 78–85.

Meitl, M. A., Zhou, Y. X. Gaur, A., Jeon, S., Usrey, M. L., Strano M. S. and Rogers, J. A (2004) *Nano Letters* **4**, 1643.

Menard E., Bilhaut L., Zamseil J. and Rogers J. A. (2004) Improved chemistries, thin film deposition techniques and stam design for nontransfer printing. *Langmuir* **20**, 6871–6878.

Menard E., Lee K., Young D. Y., Nuzzo R. and Rogers J. A. (2004b) A printable form of silicon for high performance flexible thin film transistors. *Applied Physics Letters*, submitted.

Michel B., Bernard A., Bietsch A., Delamarche E., Geissler M., Juncker D., Kind H., Renault J. P., Rothuizen H., Schmid H., Schmidt-Winkel P., Stutz R. and Wolf H. (2001) Printing meets lithography: soft approaches to high-resolution printing. *IBM Journal of Research and Development* **45**, 697–719.

Mirkin C. A. and Rogers J. A. (2001) Emerging methods for micro- and nanofabrication. *MRS Bulletin* **26**, 506–07.

Ridley B. A., Nivi B. and Jacobson J. M. (1999) All-inorganic field effect transistors fabricated by printing. *Science* **286**, 746–49.

Rogers J. A., Paul K. E. and Whitesides G. M. (1998) Quantifying distortions in soft lithography. *Journal of Vacuum Science and Technology B* **16**, 88–97.

Rogers J. A., Bao Z. and Makhija A. (1999) Non-photolithographic fabrication sequence suitable for reel-to-reel production of high performance organic transistors and circuits that incorporate them. *Advanced Materieals* **11**, 741–45.

Rogers J. A., Bao Z., Baldwin K., Dodabalapur A., Crone B., Raju V. R., Kuck V., Katz H. E., Amundson K., Ewing J. and Drzaic P. (2001) Paper-like electronic displays: large area, rubber stamped plastic sheets of electronics and electrophoretic inks. *Proceedings of the National Academy of Sciences USA* **98**, 4835–40.

Schmid H., Wolf H., Allenspach R., Riel H., Karg S., Michel B. and Delamarche E. (2003) Preparation of metallic films on elastomeric stamps and their application for contact processing and contact printing. *Advanced Functional Materials* **13**, 145–53.

Sirringhaus H., Kawase T., Friend R. H., Shimoda T., Inbasekaran M., W. M. and Woo E. P. (2000) High-resolution inkjet printing of all-polymer transistor circuits. *Science* **290**, 2123–26.

Strano M. S., Dyke C. A., Usrey M. L., Barone P. W., Allen M. J., Shan H. W., Kittrell C., Hauge R. H., Tour J. M. and Smalley R. E. (2003) Electronic structure control of single-walled carbon nanotube functionalization. *Science* **301**, 1519–22.

Sundar V. C., Zaumseil J., Podzorov V., Someya T., Gershenson M. and Rogers J. A. (2004) Elastomeric transistor stamps for reversible probing of charge transport in molecular crystals. *Science* **303,** 1644–46.

Sze S. (1985) *Semiconductor Devices: Physics and Technology*, John Wiley & Sons, Inc., New York.

Talghader J. J., Tu. J. K. and Smith J. S. (1995) Integration of fluidically self-assembled optoelectronic devices using a silicon-based process. *IEEE Photon Technology* **7**, 1321–23.

Xia Y., Rogers J. A., Paul K. E. and Whitesides G. M. (1999) Unconventional methods for fabricating and patterning nanostructures, *Chemical Reviews* **99**, 1823–48.

Zaumseil J., Baldwin K. and Rogers J. A. (2003a) Electrical characteristics of organic transistors formed by soft contact lamination. *Journal of Applied Physics* **93**, 6117–24.

Zaumseil J., Meitl M. A., Hsu J. W. P., Acharya B., Baldwin K. W., Loo Y.-L. and Rogers J. A. (2003b) Three-dimensional and multilayer nanostructures formed by nanotransfer printing. *Nano Letters* **3**, 1223–27.

Petitioner Samsung Ex-1011, 0245

Zaumseil J., Someya T., Baldwin K., Bao Z., Loo Y.-L. and Rogers J. A. (2003c) Nanoscale organic transistors formed by soft contact lamination and source/drain electrodes supported by high resolution rubber stamps. *Applied Physics Letters* **82**, 793–95.

Zheng M., Jagota A., Semke E. D., Diner B. A., McLean R. S., Lustig S. R., Richardson R. E. and Tassi N. G. (2003) DNA-assisted dispersion and separation of carbon nanotubes. *Nature Materials* **2**, 338–42.

Zhou, Y., Gaur, A., Hur, S.-H., Kocabas, C., Meitl, M., Shim, M. and Rogers, J.A. (2004) *Nano Letters* **4**, 2031.

Petitioner Samsung Ex-1011, 0246

12

Printed Organic Electronics

Raj B. Apte,[1] Robert A. Street,[1] Ana Claudia Arias,[1] Alberto Salleo,[1] Michael Chabinyc,[1] William S. Wong,[1] Beng S. Ong,[2] Yiliang Wu,[2] Ping Liu,[2] and Sandra Gardner[2]

[1]Electronic Materials Laboratory, Palo Alto Research Center and [2]Xerox Research Centre of Canada

12.1 Introduction

Organic thin film transistors (OTFTs) have received interest in recent years for their potential as a low-cost alternative to amorphous silicon thin film transistors (TFTs) for electronic applications (Dimitrakopoulos and Malenfont 2002; Katz *et al.* 2001). OTFT-based circuits are particularly suited for large-area devices, such as active matrix displays, where high switching speed is not required; they may also be attractive for low-cost microelectronic devices such as radio frequency identification (RFID) tags where the high cost of packaging silicon circuits becomes limiting. Production of low-cost OTFTs requires a shift from inorganic semiconductor processing paradigms – epitaxial wafers, photolithography, and vacuum deposition – to a new set of fabrication methods – roll-to-roll processing, print patterning, and solution-based deposition.

Rolled plastics allow the use of very-large substrates with superior scaling compared to large cut sheets. The flat panel industry has been increasing the lateral dimensions of glass substrates steadily – Gen 6 fabs are settling on $1.5 \times 1.8\ m^2$ glass substrates – but the cost of the associated vacuum machinery scales with area. Printers faced the challenge of ever-increasing substrate size and shifted from flat platens to cylinders in the first decades of the nineteenth century, more that 1200 years after the first printing press in China. The

Flexible Flat Panel Displays Edited by G. P. Crawford
© 2005 John Wiley & Sons, Ltd., ISBN 0-470-87048-6

Petitioner Samsung Ex-1011, 0248

immediate effect was a factor of 5 increase in the amount of newspaper that a single press could produce (Smith 1979; Steinberg 1956). One limit associated with plastic substrates is thermal budget, with the cost of the substrate increasing for plastics having higher temperature stability. A second limit is associated with outgassing: both the surface and bulk of a plastic substrate may outgas and disturb operation of high-vacuum deposition techniques. A third limit is the presence of surface roughness.

Much of the expense in fabricating circuits is associated with photolithography, because the equipment is expensive and because of the handling during the many process steps required to deposit, bake, expose develop, and strip the resist. Another limitation of photolithography arises from the use of flexible substrates with low dimensional stability. Stepping systems are able to register each reticle, and this is sufficient to fabricate circuits on glass. But for plastics which have lower dimensional stability the runout associated with a fixed reticle size increases, forcing a decrease in reticle size and an increase in the number of steps required by the stepper. Inkjet printing is a high-throughput technique that can register dynamically over large areas. It can be the basis for simplifying and rendering less costly the process of patterning thin films on rolled substrates.

Not all of the films needed to build a transistor need be solution deposited, but each one that can presents an opportunity to lower the cost of fabrication. One critical material is the channel semiconductor. Some high-performance organic semiconductors such as pentacene are vacuum deposited. Many workers have attempted to find methods of solution deposition of pentacene. Molecular semiconductor precursors are now able to be deposited and converted in situ to semiconducting films (Afzali *et al.* 2002). These methods require high temperatures, however, and may not be consistent with less expensive substrate material. Solution-deposited semiconductors, if they satisfy functional requirements, enable the lowest-cost OTFTs. A detailed discussion of structural features and molecular ordering of regioregular polythiophenes will cover the development of several polymers that we have tested.

In this chapter we will discuss the electrical requirements and performance characteristics of printed organic electronics and the development and properties of poly(dialkylquaterthiophene) (PQT), our semiconducting material. We will conclude by showing a 128×128 pixel, 75 dpi active matrix array.

12.2 System Requirements

This chapter focuses on the materials, device operation, and fabrication of OTFTs with emphasis on application to active matrix displays. This section will present some of the operational requirements of active matrix displays to frame the discussion. Active matrices for emissive devices, such as organic light-emitting diodes (OLEDs), generally require several transistors per pixel. In such a configuration, each transistor may have very different performance requirements, e.g. a high-transconductance transistor with good mobility and large width-to-length ratio and a control transistor with low leakage. OTFTs do not at present have enough transconductance to drive OLEDs, and this discussion will focus on nonemissive displays. The low mobility of polymers is suited to nonemissive displays because a large current is not required, e.g. liquid crystals, electrophoretics. Amorphous silicon with a mobility of about 0.5 $cm^2/V\,s$ is easily able to operate very large active matrix liquid crystal displays (AMLCDs) at video rates. The mobility of the best polymers is within an order of

Petitioner Samsung Ex-1011, 0249

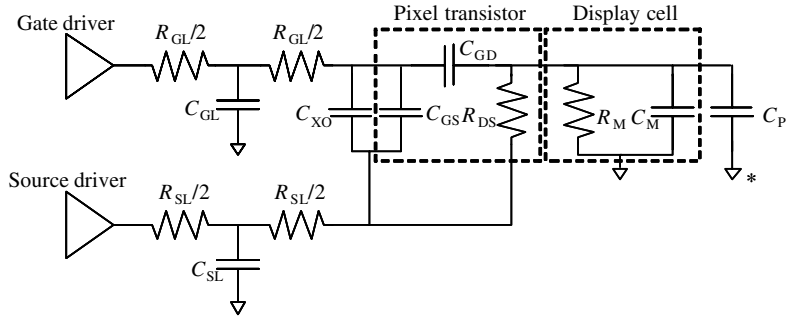


Figure 12.1 Equivalent circuit of a nonemissive active matrix display cell for an $m \times n$ (gate lines $\times$ source lines) array. The gate driver switches between two levels (on and off). The source driver may drive the source line to one of 256 or more levels. R_{GL} is the gate line resistance; C_{GL} is the gate line capacitance, which includes n gate and overlap capacitances distributed along its length. R_{SL} is the source line resistance; C_{SL} is the source line capacitance, which includes m gate–source and overlap capacitances distributed along its length. C_{XO} is the single-pixel overlap capacitance. The transistor is modeled by C_{GD}, the gate–drain capacitance; C_{GS}, the gate–source capacitance; and R_{DS}, the drain source resistance. The display cell is represented by a medium resistance, R_M, and a medium capacitance, C_M. Finally, any capacitance of the pixel to the adjacent gate driver is represented by C_P. (*) connects to the adjacent gate driver, represented as a virtual ground

magnitude of amorphous silicon. More important is the on-current to off-current ratio, which must exceed 10^6, and is also achieved by polymers.

Figure 12.1 shows a circuit model of an active matrix array. The array consists of m gate lines and n source lines, each connected to their respective drivers. The pixel itself is modeled as a gate–source capacitor, C_{GS}, a gate–drain capacitor, C_{GD}, and a resistance, R_{DS}. Given that gate drivers are often binary in operation, R_{DS} takes two values, R_{ON}, the one resistance, and R_{OFF}, the off resistance. The display medium is modeled as a pixel leakage resistance, R_M, and capacitance, C_M. Because the line capacitances are aggregates of many other pixels, they may be approximated by

$$\begin{aligned} C_{GL} &= n(C_{GS} + C_{GD} + C_{XO}), \\ C_{SL} &= m(C_{GS} + C_{XO}). \end{aligned} \tag{12.1}$$

Since C_{GS} is generally the same as C_{GD}, C_{GL} is just under double the capacitance of C_{SL}. Display timing suggests constraints on rise time and charging time, which in turn give us device parameters for OTFTs. For a standard display with frame time T, say 16 ms, the line time would be T/m. To insure that the display cell is charged with less that 1% error during this time, to the first order, we have

$$(R_{SL} + R_{ON})(C_P + C_M) \leq \frac{T}{5m}. \tag{12.2}$$

Charge retention during the frame time is a second constraint. In this case the leakage of the charge requires

$$\frac{R_{OFF}R_M}{R_{OFF} + R_M}(C_P + C_M) \geq 5T. \tag{12.3}$$

Petitioner Samsung Ex-1011, 0250

Two further constraints concern the rise times of signals on the gate and source lines themselves:

$$R_{GL}C_{GL} < \frac{T}{5m}, \qquad R_{SL}C_{SL} < \frac{T}{5m}. \tag{12.4}$$

Finally, most electro-optic media are significantly thicker than the gate dielectric, maybe 100 times. In this case the gate–drain capacitance C_{GD} may be much larger than the medium capacitance C_M and may also be nonuniform. Feedthrough charge, which is the loss in pixel charge when the gate switches off, will shift significantly the range of pixel charges produced by the source driver. To combat this problem, addition pixel capacitance, C_P, is added by extending the pixel electrode to overlap a previous gate line. To insure that the feedthrough charge is 10 times smaller than the signal charge, we require

$$10\Delta V_G\, C_{GD} \leq \Delta V_S(C_M + C_P). \tag{12.5}$$

Minimizing C_{GD} can increase channel resistance or disable transistor operation altogether (if the gate and drain do not overlap), so registration uniformity of the conductor layers is essential to limiting feedthrough. When overlap is less than 20 μm, then registration errors of a few microns can create nonuniformities in the feedthrough charge which will show up clearly in images. Increasing C_P presents no difficulty as long as R_{ON} is sufficiently low and there is space in the pixel.

For systems of order $m, n = 1000$ and pixel pitch of 400 μm the gate and source rise times need to be less than 3 μs. Since the line capacitances tend to be in picofarads, the line resistances will have to be less than 1 MΩ. Since there may well be 10^5 squares, at least 1 Ω/□ is needed for the line conductors. C_M is typically a fraction of a picofarad at most, while C_{GD} may be close to one picofarad. By careful layout, it is possible for C_P to exceed C_{GD} by a factor of 5 or more, which is barely enough to limit the feedthrough shift. For transistors with $\mu = 0.1\ \text{cm}^2/\text{V s}$, the ''on'' resistance may be 1–5 MΩ and the total capacitance on the drain may be several picofarads. This mobility is just enough to make the system work at video rates unless the gate–drain overlap can be reduced from the assumed 20 μm. For jet-printed transistors, $0.1\ \text{cm}^2/\text{V s}$ must be regarded as the necessary mobility. Finally, the ''off'' resistance may be in teraohms, which means the dominant leakage is likely to be through the medium, which must have a resistivity of 0.1 to 1 TΩ cm, assuming a 10 μm cell gap. It is clear from this discussion that making the channel length shorter is not as important as controlling layer-to-layer registration.

12.3 Transistor Requirements

Basic OTFT operation is similar to that of other field-effect transistors. A number of different analyses are possible (Muller and Kamins 1986), but we make the usual assumption that the gradual channel approximation applies, and that the channel is longer than the depletion

Petitioner Samsung Ex-1011, 0251

region that forms around the drain. The current, I_D, is related to the potential, $V(x)$, in the channel by

$$I_D = WC_G\mu(V_G - V_T - V(x))\frac{dV}{dx}, \tag{12.6}$$

where C_G is the total gate capacitance $C_G = C_{GD} + C_{GS}$, V_T is the threshold voltage, μ is the mobility and W the width. The integration yields the linear-regime TFT relation for $V_G - V_T > V_{DS}$:

$$I_D = \mu C_G \frac{W}{L}(V_G - V_T)V_{DS}. \tag{12.7}$$

Where $V_G - V_T < V_{DS}$ the transistor saturates and the current reaches a maximum value:

$$I_D = \mu C_G \frac{W}{2L}(V_G - V_T)^2. \tag{12.8}$$

Figure 12.2 shows the current–voltage (I–V) characteristics of an OTFT. In this case there is a good fit to the TFT model over the whole data range, and reliable parameters can be extracted. In many cases the fit to the model is poorer and reflects many possible complicating effects. Examples include contact resistance, short-channel effects and a field-dependent mobility. In addition, time-dependent changes due to bias stress or chemical degradation can complicate the analysis of I–V data. Without reliable models for all these effects, it becomes difficult or impossible to specify the active matrix driver waveforms.

A low OFET leakage current is important for active matrix arrays because it is essential to hold charge on the pixel of an image sensor or display between addressing frames. Polymer

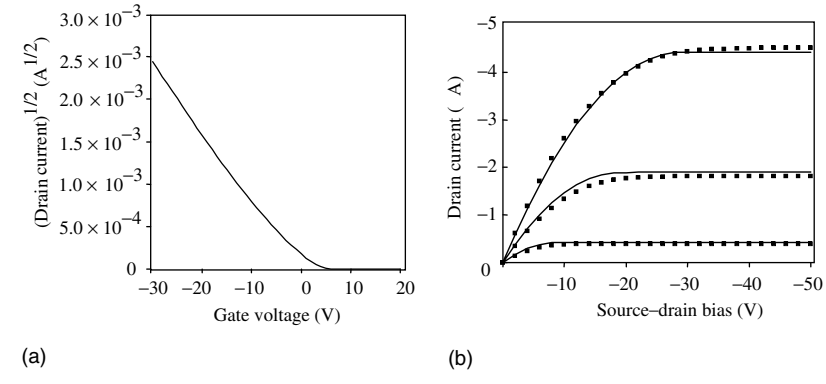


Figure 12.2 Current–voltage characteristics of OTFT on glass with PQT-12, $W = 200\,\mu m$ and $L = 50\,\mu m$. (a) Saturation regime for $V_{DS} = -30$ V. From this we can obtain $\mu = 0.07\,cm^2/V\,s$ and $V_T = -1$ V. (b) Output characteristics for $V_G = -10$, -20, -30 V (squares) and computed (line). Note that even for such a long transistor, some variation from the model is indicated by the current variation for high V_{DS}

Petitioner Samsung Ex-1011, 0252

semiconductors are generally only p-type and do not exhibit n-type channel conduction for positive $V_G - V_T$. This is partly due to the low n-type mobility in these materials, and partly because the high work function metals used as low-resistance p-type contacts are blocking for electrons. Because of the presence of defects and recombination centers, polymer OTFTs often work in accumulation mode.

The turn-on of the OTFT is described by the subthreshold slope, a measure of the steepness of the *I–V* characteristics near the threshold voltage. A slow turn-on is attributed to a broad distribution of localized states in the polymer semiconductor which arises from the structural disorder in the film. These localized states tend to reduce the mobility. There is still no agreed theoretical model to explain the transport in OFETs, and models based on hopping or multiple trapping are both applied. Both approaches relate the mobility to the density of states distribution of localized states in the band tail. Application of the multiple trapping model to PQT (Salleo *et al.* 2004) gives a good fit to the temperature dependence of the mobility consistent with an exponential band tail whose slope varies with the degree of structural order and is 30–50 meV.

To build reliable switch transistors and logic circuits requires accurate models of OTFT behavior. The effects of contact resistance, short channels, bulk conductivity, bias stress, and aging must all be included by the system designer. The following sections will review these effects.

12.3.1 Fabrication Methods

We use three different fabrication methods to test the *I–V* characteristics of transistors. For basic electrical testing to validate materials properties, devices are built on n-doped silicon wafers with a 100 nm thermal silicon oxide (SiO_2) dielectric layer. The SiO_2 surface is modified with a self-assembled monolayer of octyltrichlorosilane (OTS) (Salleo *et al.* 2002; Ong 2004a, 2004b). Both staggered and coplanar devices are fabricated. For staggered devices, the semiconductor layer ($\sim$20–50 nm) is deposited on the OTS-modified SiO_2 surface by spin coating a polymer solution (polymer ink) and vacuum drying. Subsequently, gold source and drain electrodes are deposited by vacuum evaporation through a shadow mask. For coplanar devices, polymer ink is coated on the OTS-modified surface after the patterning of gold electrodes on the substrate.

For testing device characteristics, including short-channel effects and environmental stability, polymer ink is spin coated on a glass die that is prefabricated using conventional lithographic techniques and treated with OTS. Contacts are gold, and the dielectric is PECVD oxynitride. PECVD is plasma-enhanced chemical vapor deposition.

For testing array devices, both glass plates and flexible plastic foils are used. Metal gate material is vacuum deposited and patterned using a jet printer. The dielectric is desposited by PECVD. Then the source/drain metal is deposited and patterned by jet printing. Finally, semiconducting ink is jetted into the channel regions. This is described in detail in Section 12.5.

12.3.2 Contact Resistance

Contact resistance can occur in any FET, but is particularly likely in OTFTs because doped polymer contacts cannot yet be deposited. Instead contacts are usually made with metals

Petitioner Samsung Ex-1011, 0253

which tend to form Schottky barriers impeding the flow of charge. High work function metals are needed to reduce the barrier, which is why gold and ITO are common metals for OTFTs. When the contact resistance is ohmic, it can be extracted by measuring the OTFT as a function of channel length. However, metal contacts are more likely to have a nonohmic, diode-like resistance. In this case the contact resistance is observed as curvature in the output characteristics near the origin.

The contact I–V characteristics can be analysed from the conventional FET model by integrating (12.6) along the channel except over the contact region of assumed length, d, which gives the following result (Street and Salleo 2002):

$$I_{\mathrm{D}} = C_{\mathrm{G}}\mu\frac{W}{L-d}\left[(V_{\mathrm{G}}-V_{\mathrm{T}})V_{\mathrm{D}} - V_{\mathrm{D}}^2/2 - \left\{(V_{\mathrm{G}}-V_{\mathrm{T}})V_{\mathrm{C}} - V_{\mathrm{C}}^2/2\right\}\right], \tag{12.9}$$

where V_{C} is the voltage across the source contact and the voltage drop at the drain is neglected for simplicity. The dependence of drain current on contact voltage is extracted by obtaining the function $I_{\mathrm{D}}(V_{\mathrm{C}})$ that fits the output characteristics. An example of the contact characteristics for an OFET made with poly(9,9′-dioctyl-fluorene-*co*-bithiophene) (F8T2) with coplanar contacts, is shown in Figure 12.3. $I_{\mathrm{D}}(V_{\mathrm{C}})$ does follow an approximate diode-type relation:

$$I_{\mathrm{D}} = I_{\mathrm{O}}\left(e^{V_{\mathrm{C}}/V_{\mathrm{O}}} - 1\right), \tag{12.10}$$

where $I_{\mathrm{O}} = 6\times10^{-9}$ A and $\mathrm{V_O} = 0.5$ V. In general, the staggered TFT geometry is less susceptible to high contact resistance than the coplanar geometry, because the effective area of the contact is larger, at least when there is overlap of the gate and source/drain contacts. However, it is also possible that the structure of the polymer film near the contact is different in the two cases.

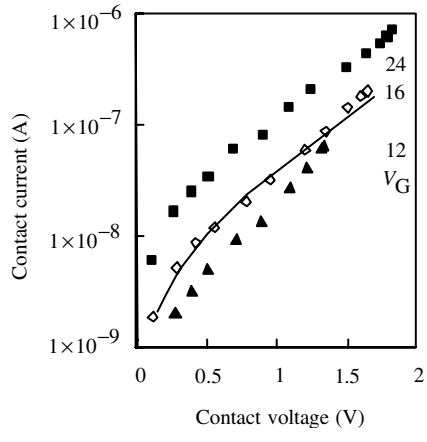


Figure 12.3 The dependence of drain current on contact voltage, $I_{\mathrm{D}}(V_{\mathrm{C}})$, obtained from a coplanar F8T2 OTFT and deduced from a fit to the output characteristics. The solid line is a fit to (12.10)

Petitioner Samsung Ex-1011, 0254

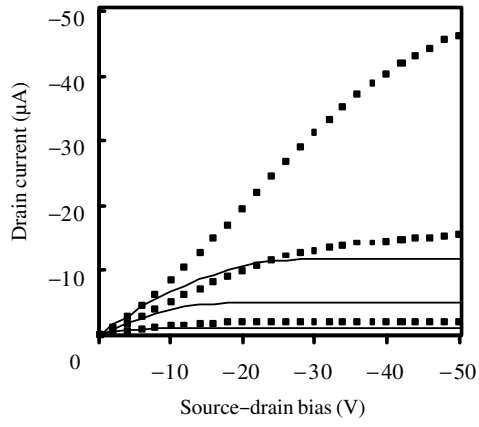


Figure 12.4 Device characteristics for a PQT-based OTFT with $L = 3\,\mu m$. Output characteristics are shows for $V_G = -10$, -20, and $-30\,V$ according to the transistor model (solid line) and measured (squares). Reproduced by permission of the American Institute of Physics

12.3.3 Short-Channel Effects

OTFT characteristics tend to deviate from the simple FET model as the channel length is shortened below about 10 μm. Explanations for the effects include channel length dependent mobility (Wang 2003), increasing effect of contact resistance (Meijer *et al.* 2003), and self-heating (Chabinyc *et al.* 2003). Figure 12.4 shows the output characteristics for a shortchannel PQT device. The extracted linear mobility is much smaller than the apparent saturation mobility; in fact, saturation is not observed.

The departure from saturation shows that the conventional FET model is not obeyed, and so parameters such as the mobility cannot be reliably extracted. When comparing different devices and materials, it is important to show the complete characteristic and cite a mobility only when linear and saturation mobility agree.

For the PQT data in Figure 12.4, the explanation for the lack of saturation in short-channel OFETs is the competition between channel and bulk current. When the OTFT is in saturation, the accumulation layer has few carriers near the drain, and the large voltage drop between the channel and the drain contact will allow a bulk current to flow. Charge breaks away from the channel some distance from the drain and the effective channel length is reduced. Chabinyc *et al.* (2003) showed that a model of space charge limited current flow in the film is consistent with the measured output characteristics.

12.3.4 Bias Stress and Chemical Stability

Bias stress is the change in the transistor characteristics as a result of a prolonged application of a gate bias, and is common in disordered materials. The effect is observed in most polymers (Street *et al.* 2003; Salleo and Street 2003). In Figure 12.5 the drain current is measured as a function of time under constant applied bias. Results are shown for PQT-12 and F8T2.

Petitioner Samsung Ex-1011, 0255

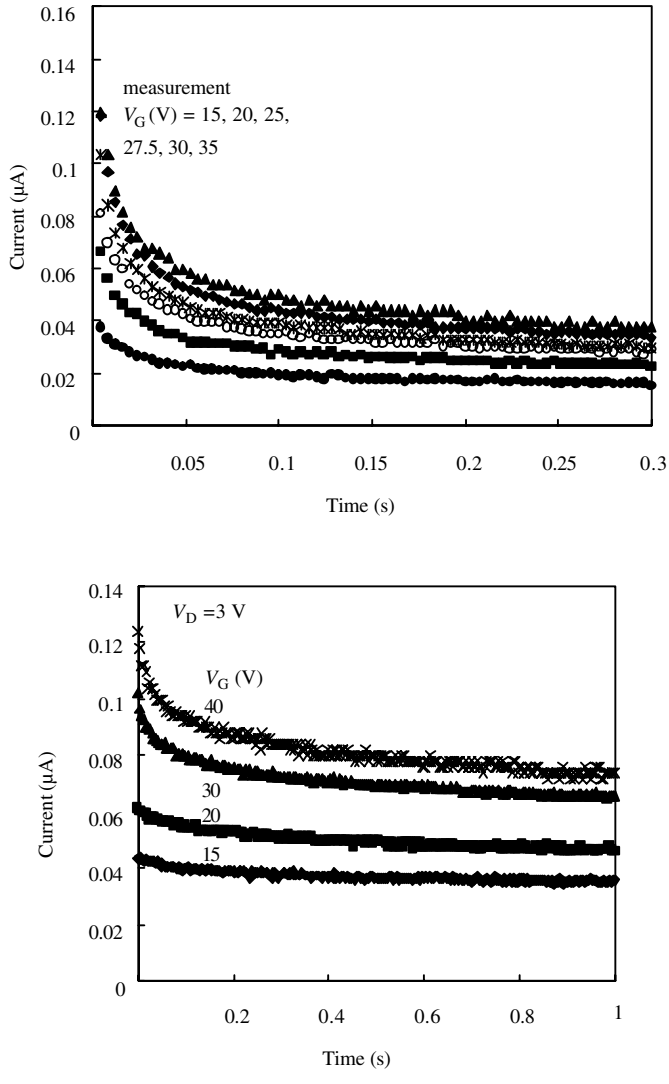


Figure 12.5 Bias stress in two polymer TFTs. Transistors are held with $V_G = 0$ V and constant V_D until stabilized. V_G is then raised quickly while I_D is monitored. Two semiconductors are compared: (a) F8T2 and (b) PQT (b). Reproduced by permission of the American Physical Society

The current decay is more pronounced at higher gate voltage and is larger in F8T2 than PQT. The hypothesis that carriers are being removed from the channel is supported by the strong shift in transfer characteristics shown in Figure 12.6. In these quasistatic measurements the gate voltage is ramped from 0 V. Once the final V_G has been reached, the gate is returned to zero for a second sweep. The shift in the F8T2 characteristic suggests that a substantial quantity of charge is being trapped in the channel. Although PQT does not show any hysteresis in TFT characteristics, the current decay displayed in Figure 12.5 indicates

Petitioner Samsung Ex-1011, 0256

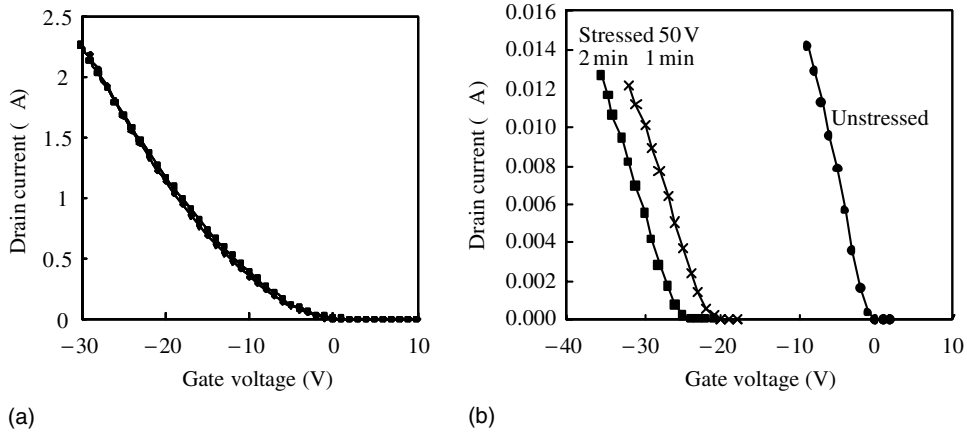


Figure 12.6 Bias stress in two polymer TFTs. Device transfer characteristics are measured (a) twice in succession for PQT and (b) three times under bias for F8T2

that bias stress occurs in this material as well. Charge trapping could be occurring in either the polymer semiconductor or in the gate dielectric. The evidence is strong that the effect is in the polymer, since it is independent of the gate dielectric material, and is so different in the two materials.

Figure 12.7 shows a linear relationship between dN_H/dt and N_H^2, where N_H is the concentration of holes in the channel. This relation suggests that hole pairs are trapped, and we have proposed that these are bipolaron pairs. The slow capture of hole pairs is attributed to the

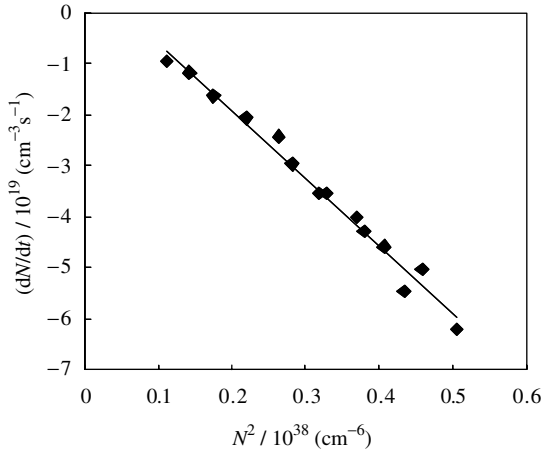


Figure 12.7 Bias stress data expressed as a function of channel carrier density for PQT. The linearity of the plot is the strongest evidence for holes forming stationary pairs and no longer participating in channel conduction. dN/dT measured at fixed time, $k = 1.3 \times 10^{-18}$ cm^2/s. Reproduced by permission of the American Physical Society

Petitioner Samsung Ex-1011, 0257

Coulomb repulsion between holes, which reduces their capture cross section. The different stress effects between F8T2 and PQT can be explained by the binding energy of the bipolarons. The trapped bipolarons in PQT have a small bindng energy and are released within a few seconds in the absence of a gate bias. The rapid reversal explains the lack of a long-lived threshold voltage shift in the transfer characteristics of this material. The bipolarons in F8T2 have larger binding energy, which increases the stability of the pair and causes a much larger threshold voltage shift. The formation of bipolarons probably depends on the local structural ordering of the polymer.

The chemical stability of OTFTs is a concern because polymers are knows to degrade in the presence of oxygen and water vapour, although the sensitivity varies for different materials. Figure 12.10(b) shows the OTFT transfer characteristics for a P3HT device as a function of exposure, and is typical of other materials. The mobility decreases, but the larger effects are in the subthreshold region. The subthreshold slope decreases and the leakage current increases. All three effects indicate a change in the distribution of localized states, although exactly how these are manifested is unknown. As discussed below, we have focused on designing materials with long-term chemical stability.

12.4 Organic Semiconductors

While field-effect properties in organic materials were first noted in 1960s (Heilmeier and Zanoni 1964), little progress had been made until two decades later when several organic semiconductor materials were demonstrated for OTFTs (Ebisawa *et al.* 1983; Tsumura *et al.* 1986; Horowitz *et al.* 1989). Since then great strides have been made in the semiconductor materials development for OTFTs. The highest mobility measured for an OTFT is higher than that of hydrogenated amorphous silicon (Kelley *et al.* 2003).

Table 12.1 summarizes the basic performance of OTFTs made from a variety of materials. The high-mobility characteristics are mostly obtained from vacuum-deposited materials

Table 12.1 Some p-channel organic semiconductors for OTFTs

Semiconductor	Mobility (cm^2/V s)	Deposition method	I_{on}/I_{off}	Reference
Copper phthalocyanine, CuPC	0.02	vacuum	10^5	Bao *et al.* (1997)
Pentacene	3.3	vacuum	10^6	Kelley *et al.* (2003)
α-Sexithiophene	0.03	vacuum	10^6	Dodabalapur *et al.* (1995)
α,ω-Dialkylsexithiophene	1.1	vacuum	10^4	Halik *et al.* (2003)
α,ω-Dialkylsexithiophene	0.01	solution	10^4	Katz *et al.* (1998) Garnier *et al.* (1998)
Poly(3,3‴-dialkylquaterthiophene), PQT	0.14	solution	10^7	Wu *et al.* (2004c)
Regiorandom poly(3-alkylthiophene), P3AT	0.046	solution	—	J. Wang and Gonsalves (1998)
Pentacene, from soluble precursor	0.42	solution	10^6	Afzali *et al.* (2002)
Poly(thienylene–vinylene) from soluble precursor, PTV	0.0015	solution	10^4	Huitema *et al.* (2001)
Poly(9,9′-dioctylfluorene-*co*-bithiophene), F8T2	0.02	solution	10^6	Sirringhaus *et al.* (2000)

Petitioner Samsung Ex-1011, 0258

possessing high structural order. The FET performance of solution-processed semiconductors, particularly those fabricated in air, is generally poorer. These results reflect the significance of semiconductor molecular ordering on FET performance.

An additional problem with solution-processed OTFTs is sensitivity to atmospheric oxygen and water, which degrades performance. An exception is the solution-processed pentacene precursor (Afzali *et al.* 2002). However, the reported current–voltage characteristics does not show good saturation, and a large threshold voltage and subthreshold swing were observed. An earlier Diels–Alder pentacene adduct approach had yielded much lower mobility (Brown *et al.* 1995, 1996). These results reveal the challenges and complexities that confront the development of low-temperature, solution-processed semiconductor materials for OTFTs.

The charge carrier transport in solution-deposited organic semiconductor systems is dominated by localized states (Horowitz 1998), therefore presence of proper structural order in the semiconductor is necessary to achieve high mobility (Sirringhaus *et al.* 1999). To enable fabrication of functionally useful OTFTs in air, the semiconductor material needs to possess sufficient air stability so that desirable FET characteristics can be maintained until encapsulation. Accordingly, two critical requirements on semiconductor materials need to be met: (i) self-assembly to form optimum structural order for charge transport, and (ii) sufficient air stability against adverse environmental effects, particularly p-doping by atmospheric oxygen. Most current solution-processable organic semiconductor compounds fail to simultaneously meet both of these requirements.

There are two classes of organic semiconductor materials for OTFTs: small molecules and polymers. Small molecular semiconductors generally possess better stability against degradative effects of environmental attacks by virtue of their higher crystallinity in the solid state, which shields and protects semiconductor molecules from exposure to atmospheric constituents. However, high-performance small molecular semiconductors such as pentacene often cannot be processed by solution techniques due to poor solubility and may require vacuum deposition. Some oligomeric small molecules such as short-chain alkyl-substituted oligothiophenes are soluble, but their solution-fabricated OTFTs provide poor performance (Katz *et al.* 2001), demonstrating the difficulties in forming properly structured channel layers from solution deposition. Similarly, soluble semiconductor polymers also suffer from their inability in establishing high structural domains for efficient charge transport. Those polymers which form highly structured films from solution do exhibit efficient charge transport, but tend to be sensitive to oxidative doping. Polymer OTFTs are processed in an inert atmosphere to deliver high mobility.

Both reversible and irreversible chemical effects degrade organic semiconductors. Further, quantifying the level of degradation is essential to understanding the challenges of encapsulation. For example, many organic light-emitting diode technologies need to be encapsulated by glass on the top and bottom sides of the device to have adequate lifetimes. Encapsulation and protection from light are likely to be required for any OTFT. But whether the device needs to be protected from oxygen (hard) or water (easier) and at what level will determine if the device is environmentally stable.

One solution-processed semiconductor polymer that displays excellent OTFT performance in an inert atmosphere is regioregular head-to-tail poly(3-alkylthiophene). The mobility and on/off ratio of regioregular head-to-tail poly(3-hexylthiophene), or

Petitioner Samsung Ex-1011, 0259

HT-P3HT, are 0.1 $cm^2/V\,s$ and 10^6, respectively, when processed and characterized in an inert atmosphere (Sirringhaus *et al.* 1999). However, HT-P3HT yielded poorer mobility and significantly lower on/off ratio when the devices were fabricated at ambient (Bao *et al.* 1996); FET characteristics degraded rapidly on exposure to air. The cause of performance degradation may be the fact that HT-P3HT assumes a highly delocalized coplanar conformation in a lamellar structural order in the solid state. All the thienylene moieties along the backbone of HT-P3HT are held in coplanarity by intermolecular side-chain alignment (McCullough *et al.* 1993; Yamamoto *et al.* 1998). While a lamellar structure of this type allows efficient charge transport by hopping, the highly delocalized π-conjugation system of HT-P3HT in the coplanar conformation may lead to an elevated highest occupied molecular orbital (HOMO) energy level, and a propensity to oxidative doping. Nonetheless, the fact that HT-P3HT is capable of exhibiting high mobility and on/off ratio in an inert atmosphere demonstrates the excellent self-organization and charge transport capabilities of this regioregular polythiophene system. These results suggest that a plausible approach to low-cost, high-performance OTFTs is possible if appropriate structural features can be incorporated into the conjugated polymer system to properly curtail its π-conjugation for air stability and FET functionality.

We present here our structural studies on regioregular polythiophene systems to demonstrate the structure–property principles for OTFT semiconductors. Our effort has culminated in the design of a unique polythiophene system that enables inkjet printing of high-performance OTFT circuits under ambient conditions.

12.4.1 High-Performance Polythiophene Designs

Our studies of regioregular polythiophenes are driven by the objective of achieving useful FET functionality with a semiconductor material that can be processed in solution under ambient conditions. Solution processing in an environment that does not require elimination of atmospheric oxygen is important to delivering the low-cost economic advantage of OTFTs. We believe this can be accomplished through proper deployment of the following structural design principles (Ong 2003, 2004a, 2004b): (i) sufficiently long alkyl side chains to provide solution processability; (ii) structural regularity to promote molecular organization (crystallization) in the solid state; and (iii) proper control on the extended π-conjugation of the polythiophene system to achieve an effective conjugation length that balances mobility and air stability. Of these design principles, the requirement to build stability against oxidative doping in a soluble semiconductor structure without compromising its FET properties is perhaps the most demanding.

The oxidative doping of conjugated polymers depends on their ionization potentials (IPs), i.e. their HOMO levels from vacuum, which depend on their effective π-conjugation lengths. For polythiophenes, coplanarity of the thienylene moieties along the polymer chain leads to extensive π-conjugation, thus a lower IP, and a greater propensity to be oxidatively doped by atmospheric oxygen. Deviations from coplanarity result in shorter effective π-conjugation lengths, higher IPs, and thus greater resistance to oxidative doping. However, an unduly short π-conjugation length suppresses the charge transport efficiency and leads to low mobility. Through our structural studies, we have found

Petitioner Samsung Ex-1011, 0260

that simple torsional deviations from coplanarity can be effectively utilized in tuning the π-conjugation system of polythiophenes to strike an optimum balance between oxidative stability and mobility.

12.4.2 Poly(dialkylterthiophene)

Regioregular poly(dialkylterthiophene) (PTT) compounds constitute interesting model compounds for the study of oxidative doping stability, self-assembly, and FET functionality. They can be readily prepared by $FeCl_3$-mediated oxidative polymerization of the corresponding dialkylterthiophene (Pomerantz *et al.* 1991; Niemi *et al.* 1992) or dehalogenative coupling reaction of dihalodialkylterthiophene (Chen *et al.* 1995). Although our work focuses on PQT, a review of the prior development of PTT reveals the importance of proper molecular ordering on polymer semiconductor performance.

Poly(3′,4′-alkylterthiophene), or 1, is prepared by $FeCl_3$-mediated oxidative coupling polymerization (Wang *et al.* 1994). 1 with a long alkyl side-chain such as 1a (1, R = n-$C_{10}H_{21}$) exhibits the ability to self-organize in the solid state as reflected by a bathochromatic shift in its UV-visible absorption spectra from solution to thin film (Figure 12.8(a)). Aggregation of 1a in a solution of (methylene chloride) was also observed when a nonsolvent (methanol) was added. The aggregation in solution and the structural ordering of 1a in its thin film caused by formation of a face-to-face π–π stacking order is schematically represented by Figure 12.8(b); no lamellar structural order of any nature similar to that of HT-P3HT could be detected by X-ray diffraction (XRD) studies.

OTFTs fabricated with 1a under ambient conditions show good FET characteristics (Figure 12.9). The extracted mobility from the saturated regime is 0.01 cm^2/V s and on/off ratio 10^5 (Ong 2004a). While these results are similar to those of HT-P3HT devices fabricated under ambient conditions, OTFTs using 1a show greater stability in air. Figure 12.10(a)

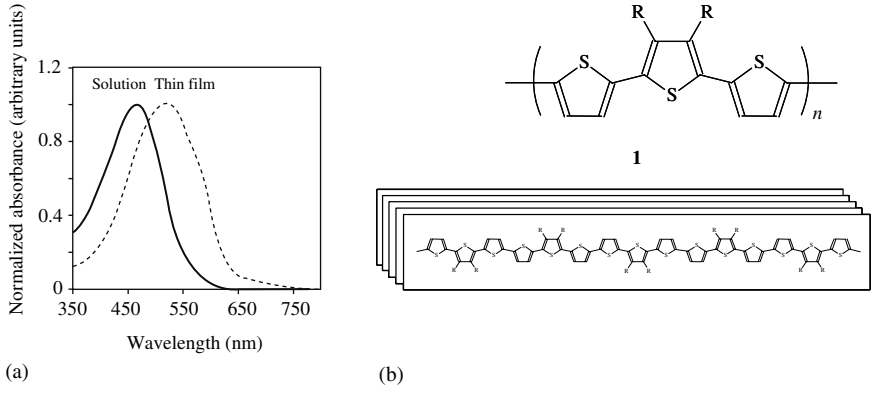


Figure 12.8 (a) Solution and thin film UV–visible spectra of 1a (1, R = n-$C_{10}H_{23}$) and (b) face-to-face π–π stacking order of 1

Petitioner Samsung Ex-1011, 0261

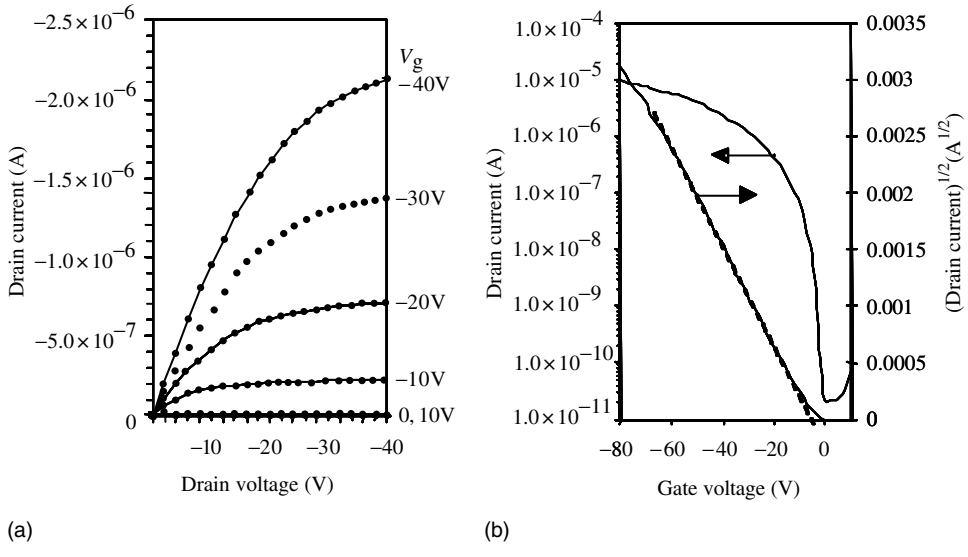


Figure 12.9 *I–V* characteristics of an exemplary 1a-OTFT with channel length (L) = 165 μm and channel width (W) = 5000 μm: (a) output curves at different gate voltages and (b) transfer curves at $V_D = -80$ V

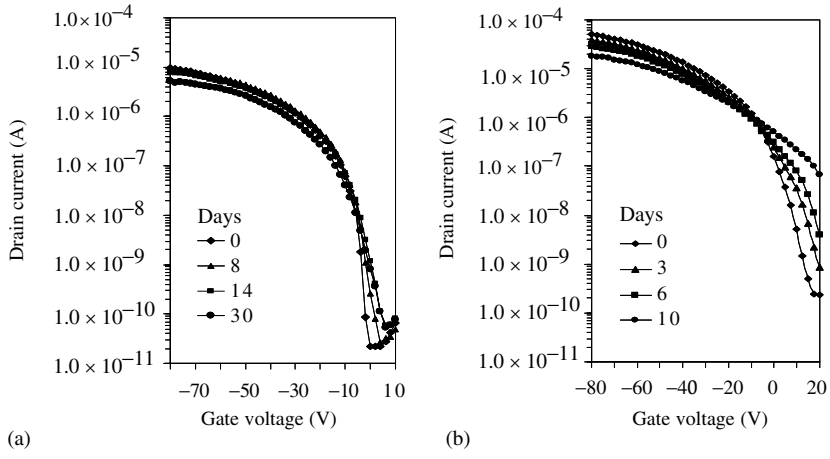
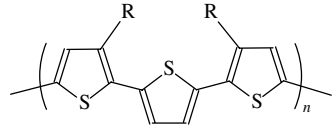


Figure 12.10 Transfer characteristics in the saturated regime of OTFTs (L = 165 μm; W = 5000 μm; $V_D = -80$ V) as a function of time: (a) 1a-OTFT; and (b) HT-P3HT-OTFT. The devices were stored in air in the dark at 30% relative humidity and characterized under ambient conditions and annealed before measurement

shows the *I–V* characteristics of 1a transistors stored in air in the dark for 30 days; Figure 12.10(b) shows the *I–V* characteristics of HT-P3HT transistors stored for 10 days. The degradation of the HT-P3HT devices is irreversible. The mobility of 1a is in part limited by its inability to form extended lamellar π-stacking structure similar to that of HT-P3HT. A three-dimensional lamellar π-stacking order of this nature should be far more efficient

Petitioner Samsung Ex-1011, 0262

than the two-dimensional π–π stacking structure (Figure 12.8(b)) in establishing extended structural domain order in the semiconductor channel layer.



2

Poly(3,3′′-alkylterthiophene), 2, is a regioisomer of 1, differing only in the regiochemistry of alkyl side chains. However, this ''spaced-out'' distribution of alkyl side chains along the backbone confers on 2 improved self-assembly. While 1 forms a face-to-face π–π stacking in the solid state, 2a (2, R = n-C_8H_{17}) readily crystallizes into a three-dimensional structure when cast from solution, a consequence of extensive side-chain interactions enabled by the spaced-out alkyl side-chain substitution pattern. 2a is prepared from monomer via an $FeCl_3$-mediated polymerization in chlorobenzene (Wu, *et al*., 2005) instead of chloroform (Gallazzi *et al.* 1993) to achieve well-defined, high molecular weight properties. The solution absorption spectrum of 2a shows a broad absorption at $\lambda_{max} \sim 470$ nm (Figure 12.11), typical of a twisted polythiophene conformation. But in thin films the absorption is singificantly red shifted and shows the appearance of vibronic splitting at $\lambda_{max} \sim 510$ nm (shoulder), 540 nm, and 583 nm (shoulder), manifesting a higher structural order than 1a in the solid state.

The XRD pattern of a thin film of 2a shows diffraction peaks at $2\theta = 5.8^\circ$ (100), 11.8° (200), and 17.8° (300), corresponding to an interlayer spacing of 15.1 Å. Transmission electron diffraction pattern of a freestanding thin film of 2a shows a peak at ~3.9 Å, corresponding to the face-to-face π–π stacking distance. The wider than usual π–π stacking distance of 3.9 Å is a reflection of the loosely packed lamellar π-stacking, which may be due

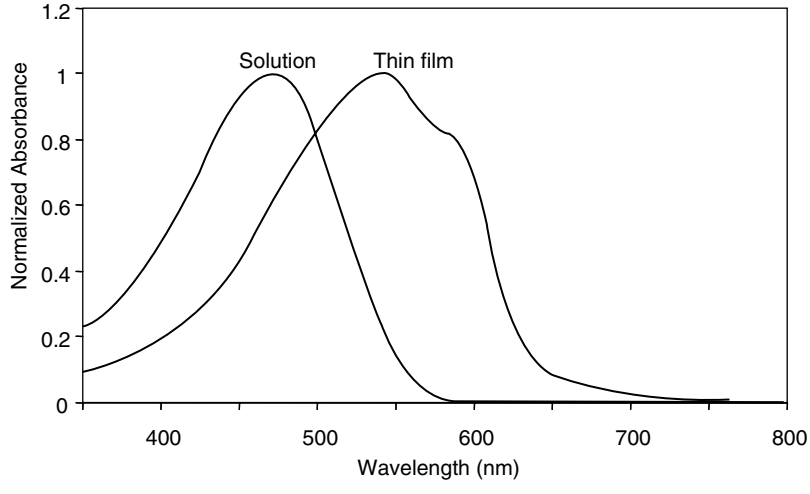


Figure 12.11 Absorption spectral properties of 2a (R = n-C_8H_{17}): dichlorobenzene solution shows an absorption at $\lambda_{max} = \sim 470$ nm, and thin film shows a abroad absorption with vibronic splitting at $\lambda_{max} = \sim 510$ nm (shoulder), 540 nm, and 583 nm (shoulder)

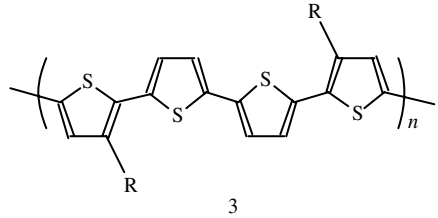
Petitioner Samsung Ex-1011, 0263

to the steric interference between the two octyl side chains on the same repeating units of 2a, twisting the substituted thienylene moieties slightly out of coplanarity and hindering the lamellar layers from packing closer together.

OTFTs fabricated with 2a as the channel semiconductor exhibit similar air stability and better FET characteristics than 1a, with an average mobility extracted from the saturated regime of $0.019\,cm^2/V\,s$ and on/off ratio of $> 10^5$. The lessons of molecular ordering for PTT carry over to our work on PQT. We envision a tightly packed lamellar π-stacking structure might lead to higher mobility.

12.4.3 Poly(dialkylquaterthiophene)

Regioregular polythiophene, poly(3,3‴-dialkyl-quaterthiophene), 3, is a solution-processed semiconductor with the ability to achieve high mobility under ambient fabrication conditions.



3

The alkyl side chains of PQT are regioregularly positioned along the backbone such that its repeating length is about 15.5 Å. The *d* spacing of the alkyl side chains oriented in the same direction in the extended coplanar conformation is approximately 12 Å, since the side chains are tilted at an angle of $\sim 50^\circ$ against the backbone. This 12 Å spacing together with a sufficiently long alkyl ($R \geq C_6$) enables 3 to organize more efficiently than 2 through intermolecular alternating side-chain interdigitation, which leads to the formation of a strongly held lamellar structure (Figure 12.12). Lamellar structures of this type were observed

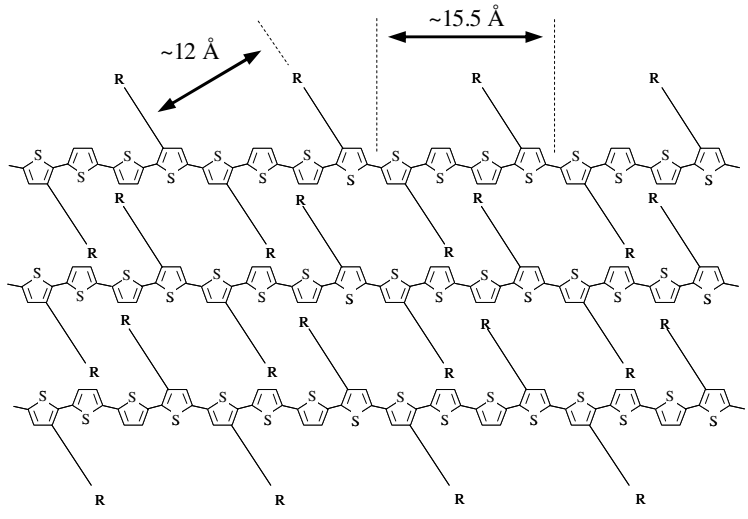


Figure 12.12 Schematic representation of lamellar structural order of PQT-3

Petitioner Samsung Ex-1011, 0264

in the oligomeric forms of 3 (Bäuerle *et al.* 1995). The presence of two unsubstituted thienylene moieties in the repeating units of PQT, which possess some rotational freedom and can deviate from coplanarity, reduces π-conjugation to provide the needed air stability. 3 is prepared by $FeCl_3$-mediated oxidative coupling polymerization and purified by extraction (Ong 2004b). The ionization potential of 3 is 0.1 eV higher than that of HT-P3HT, confirming its higher oxidative doping stability.

Differential scanning calorimetry of PQT-12, 3a (3, R = n-$C_{12}H_{25}$) shows liquid crystalline characteristics with two endotherms at ~120 °C and ~140 °C, corresponding respectively to the crystalline to liquid crystalline and liquid crystalline to isotropic phase transitions. XRD of an annealed thin film (145 °C) of PQT-12 shows diffraction peaks at $2\theta = 5.1°$ (100), 10.3° (200) and 15.4° (300) (Figure 12.13(a)), manifesting formation of lamellar

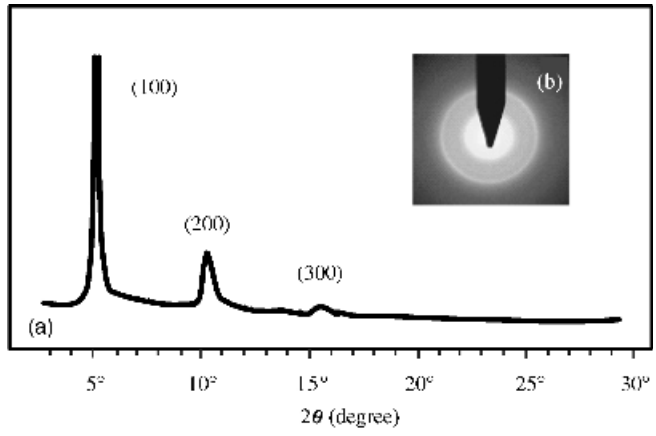


Figure 12.13 (a) XRD of an annealed thin film of PQT showing diffraction peaks at $2\theta = 5.1°$ (100), 10.3° (200) and 15.4° (300). (b) Transmission electron diffraction pattern of a freestanding film of PQT-12 on a carbon grid showing diffraction at 3.7 Å

π-stacking structures which are preferentially oriented with their lamellar axes normal to the substrate. Transmission electron diffraction analysis gave a π–π stacking of 3.7 Å (Figure 12.13(b)). PQT-12 organizes into a highly ordered lamellar π–π stacking structure whose orientation to the substrate could be manipulated through alignment layers, brushing, or SAMs. This is reminiscent of the self-assembly behaviours exhibited by regioregular poly(3-alkylthiophene)s (McCullough *et al.* 1993; Chen *et al.* 1995; Sirringhaus *et al.* 1999).

OTFTs fabricated with PQT-12 by spin coating a hot solution of PQT-12 in dichlorobenzene under ambient conditions, and annealed at 120–145 °C exhibit excellent FET performance. Output characteristics show no noticeable contact resistance and true saturation. The device switches on at 0 V, with a subthreshold swing of 1.5 V per decade (Figure 12.14). Mobility of up to 0.14 cm^2/V s, with an average value of 0.10 cm^2/V s, and on/off ratio of 10^7 were obtained. This ability to achieve high mobility and high on/off ratio in air attests to the good environmental stability of PQT-12. In addition, the mobility values extracted from the linear and saturated regimes are about the same, and both top- and bottom-contact devices perform similarly. Little or no hysteresis and bias stress effects were observed with these devices at and above room temperature.

Petitioner Samsung Ex-1011, 0265

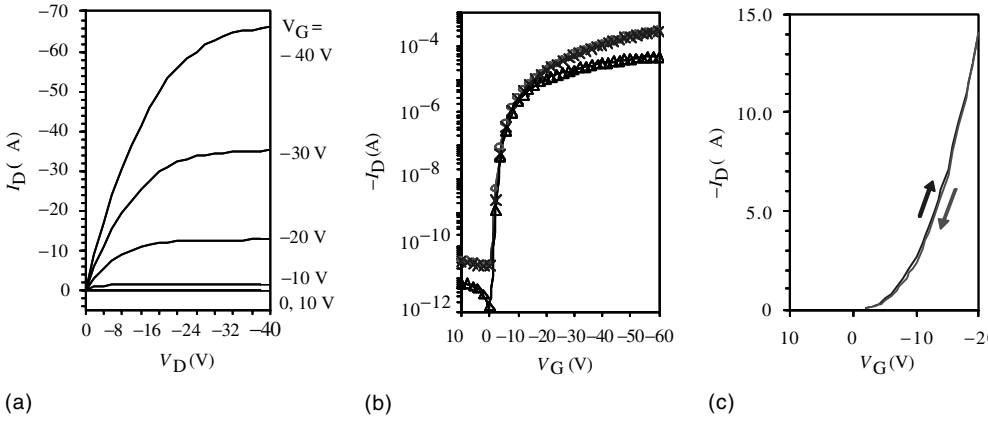


Figure 12.14 *I–V* characteristics of exemplary PQT-12 OTFTs with 90 μm channel length and 5000 μm channel width: (a) output curves at different gate voltages; (b) two transfer curves in the saturated regime scanned from positive to negative gate voltages (o and ×, $V_D = -60$ V) and the transfer curve in the linear regime (Δ, $V_D = -6$ V); (c) two transfer curves scanned in different directions between +10 V and −20 V

12.5 Digital Lithography

The manufacturing of OTFTs must place an emphasis on cost reduction though inexpensive processes, inexpensive substrates, and mass production. Both of the two principal target markets, displays and radio frequency tags, are extremely cost sensistive. Low-cost flexible substrates suffer from dimensional instability. To pattern circuits on an unstable substrate requires the abililty to register and modify the print pattern to accommodate changes in the substrate. Further, typical methods of polymer application, such as spin coating and lamination, result in a very large amount of wasted material and disposal issues. Inkjet printing is a high-throughput, low-waste process for patterning OTFTs that allows for registration correction on flexible substrates.

12.5.1 Subtractive Printing

Inkjet printing can be used to deposit resist materials that can then be used in place of photoresist for conventional TFT processes (Wong *et al.* 2002, 2003). First a subject material (eg, gold or SiO_2) is deposited everywhere. But instead of coating uniformly with photoresist and exposing through a reticle, the mask is jet printed directly onto the subject layer. The subject material is etched, and the mask is stripped. As shown in Figure 12.15, this process reduces the number of steps from six to four. For this purpose, Wong uses a wax-based ink that undergoes a phase change when jetted from a heated printhead. The amount of wax reflow that occurs before solidification can be adjusted by controlling the susbstrate's temperature. Phase-change ink, once deposited, functions as a mask to a variety of chemical etchants. Metallic conductors, glassy dielectrics, and large-area semiconductors (including amorphous silicon) may be patterned. Drop sizes from 20–40 μm are possible with industrially produced printheads. Because these heads we use exhibit superior directionality,

Petitioner Samsung Ex-1011, 0266

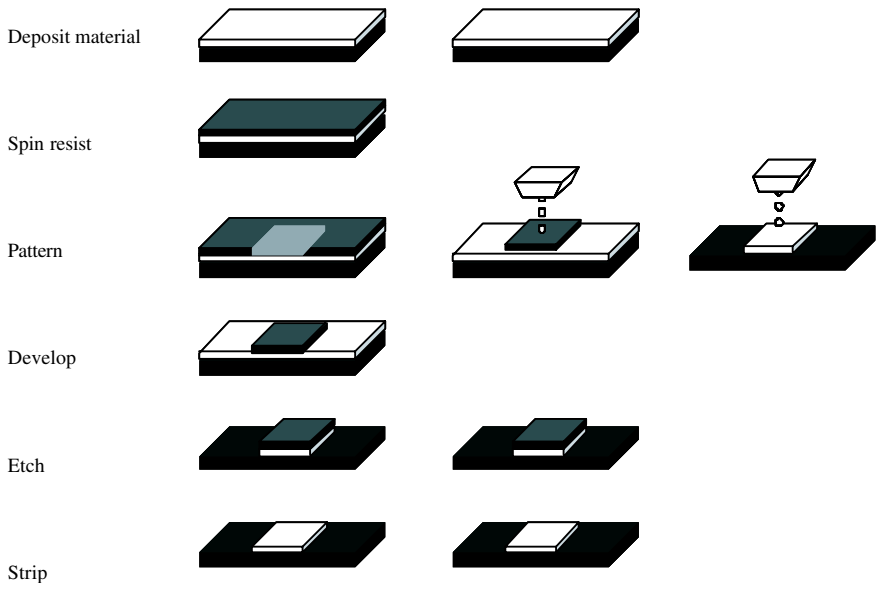


Figure 12.15 Advantages of printing organic electronics. The first column depicts a typical lithographic process. Subject material is deposited on the substrate. Photoresist is applied, exposed, and developed. The subject material is etched and the photoresist is stripped. The second column depicts a subtractive printing process. Subject material is deposited on the substrate. A mask is printed and the subject material is etched. The resist in then stripped. The third column depicts an additive printing process in which an ink carrying the subject material is printed only where necessary

features produced by gaps may be fabricated down to 5 μm. Wang and Bokor (2004) have built a custom printhead capable of printing line features below 10 μm in vacuum.

12.5.2 Additive Printing

Much simpler even than subtractive printing is additive printing, shown to the right of Figure 12 .15. The subject material is formulated into an ink and jetted just where necessary. The challenge in this case is threefold. First, some soluble or precursor form of the subject material must be synthesized. Second, a postprocess may be required to achieve optimum performance from the deposited material. The postprocess may be as simple as drying, or it may require annealing or UV exposure. Finally, the solvent and postprocess must not damage underlying layers.

Entirely jet-printed single OTFTs have been demonstrated (Paul *et al.* 2003) as well as 128×128 pixel arrays (Arias *et al.* 2004) using PQT as a semiconductor. In these arrays, the semiconductor is printed from a dispersion or solution. Through careful optimization, the printed transistors perform as well as spin-coated transistors on silicon or conventionally processed glass dice. Other layers, such as dielectric and metallization, are printed subtractively using printed wax resist. A vision system is used for layer-to-layer registration using printed fiducials.

Two printing systems are used, one to print additively the semiconductor and a second to print the wax resist. In this example the first step is to subtractively print the gate metal. This

Petitioner Samsung Ex-1011, 0267

step involves vapor deposition of the metal on the substrate, printing the wax mask, etching, and resist stripping. There are several promising approaches to printing additively the conductors. PEDOT may be used as a contact material but it does not exhibit enough conductivity for gate and source lines. Nanoparticle inks have demonstrated promise (Huang *et al.* 2003) but they may be rough. Vacuum-deposited metals are quite suitable and are currently used for bulk consumer and electrostatic control applications.

The second step is to print the dielectric. To achieve good quality surfaces for the molecular ordering of the semiconductor, the dielectric surface must be smooth and regular. A number of materials have been proposed and tried, but compatibility with the semiconductor is a challenge. Generally for additive printing, the ink used for subsequent layers must not contain solvents that allow swelling or interdiffusion of already deposited layers. Composing inks of suitable viscosity and compatibility is a major challenge for making transistors entirely without the use of nonprinting depositions. PECVD materials such as oxynitride are expensive to deposit but can have excellent electrical properties. Finally, source/drain metal is deposited and patterned.

Our prototype printer is capable of 40 μm drops with 5 μm registration over 100 mm substrates for the production of arrays, although it is capable of better performance over smaller areas. Figure 12.16 shows a portion of a 128 × 128 pixel array printed at 75 dpi,

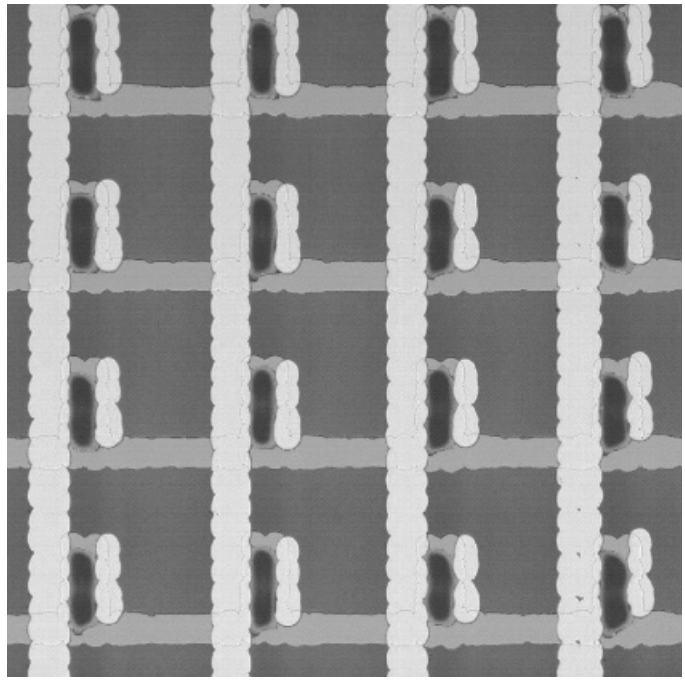


Figure 12.16 Portion of a 128 × 128 all-jet-printed OTFT array. An array pitch of 340 μm corresponds to a 75 dpi array. Gate lines run horizontally and source lines run vertically through the photomicrograph. The semiconductor, nanoPQT, is printed into the channel, where it wets the print-patterned gold source and drain. No pixel electrode or pixel capacitor is shown. The dielectric was deposited by PECVD

Petitioner Samsung Ex-1011, 0268

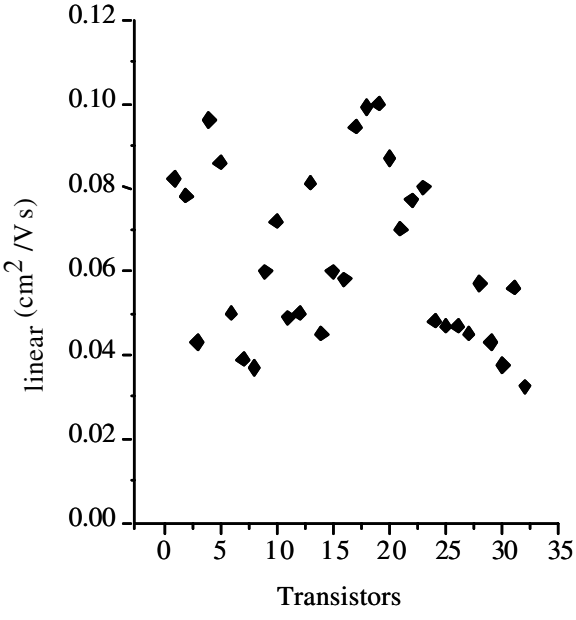


Figure 12.17 Uniformity of mobility across a printed array. Mean = 0.063 cm^2/V s, deviation = 0.021 cm^2/V s, linear regime $V_D = 1$ V

340 μm pitch. *I–V* characteristics were sampled across the array (Figure 12.17). This array was entirely patterned with printing on a glass substrate. The clear aperture, about 65%, is sufficient for backlit or reflective display media.

12.6 Prospects

In the nineteenth century, printing was revolutionized by switching from sheet to roll processing. Several of the necessary elements are in place for a similar revolution in large-area electronics. An electronic patterning technology is in place that is scalable and capable of very high throughput. Semiconducting ink is available for the transistor channels. Many other challenges remain, not the least of which is building production-ready tools and a complete materials suite consisting of a smooth, printable conductor technology with bulk metallic conductivity, a printable dielectric which presents an ordered surface to the semiconductor, further exploration of aging and encapsulation of PQT, and integration with display media.

Acknowledgements

The authors are indebted to Rene Lujan and Steve Ready of the Palo Alto Research Center for their invaluable contributions toward printed organic arrays and to Ni Zhao of McMaster University for obtaining transmission electron diffraction data.

Petitioner Samsung Ex-1011, 0269

References

Afzali, A., Dimitrakopoulos, C. D. and Breen, T. L. (2002) High-performance, solution-processed organic thin film transistors from a novel pentacene precursor. *Journal of the American Chemical Society* **124**, 8812–8813.

Arias, A. C., Ready, S. E., Lujan, R., Wong, W. S., Paul, K. E., Salleo, A., Chabinyc, M. L., Apte, R. B., Wu, Y., Liu, P., Ong, B. and Street, R.A. (2004) All jet-printed polymer thin film transistor active-matrix backplanes. *Applied Physics Letters* **96**, 2063–2070.

Bao, Z., Dodabalapur, A. and Lovinger, A. (1996) Soluble and processable regioregular poly-(3-hexylthiophene) for thin film field-effect transistor applications with high mobility. *Applied Physics Letters* **69**, 4108–4110.

Bao, Z., Lovinger, A. J. and Dodabalpur, A. (1997) Highly ordered vacuum-deposited thin films of metallophthalocyanines and their applications as field-effect transistors. *Advanced Materials* **9**, 42.

Bäuerle, P., Fischer, T., Bidlingmeier, B., Stabel, A. and Rabe, J. P. (1995) Synthesis, characterization, and scanning tunneling microscopy images of homogogues, isomerically pure oligo(alkylthiophenes). *Angewandte Chemie International Edition in English* **34**, 303–307.

Brown, A. R., Pomp, A., Hart, C. M., and de Leeuw, D. M. (1995) Logic gates made from polymer transistors and their use in ring oscillators. *Science* **270**, 972–974.

Brown, A. R., Pomp, A., de Leeuw, D. M., Klaassen, D. B. M., Havinga, E. E., Herwig, P. and Müllen, K. (1996) Precursor route pentacene metal-insulator-semiconductor field-effect transistors. *Journal of Applied Physics* **79**, 2136–2138.

Chabinyc, M. L., Lu, J.-P., Street, R. A., Wu, Y., Liu, P. and Ong, B. S. (2003) Short channel effects in regioregular poly(thiophene) thin film transistors. *Journal of Applied Physics* **96**, 2063–2070.

Chen, T., Wu, X. and Rieke, R. D. (1995) Regiocontrolled synthesis of poly(3-alkylthiophenes) mediated by Rieke zinc: their characterization and solid-state properties. *Journal of the American Chemical Society* **117**, 233–244.

Dimitrakopoulos, C. D. and Malenfant, P. R. L. (2002) Organic thin film transistors for large area electronics. *Advanced Materials* **14**, 99–117.

Dodabalapur, A., Tousi, L. and Katz, H. E. (1995) Organic transistors: two-dimensional transport and improved electrical characteristics. *Science* **268**, 270–271.

Ebisawa, F., Kurokawa, T. and Nara, S. (1983) Electrical properties of olyacetylene/polysiloxane interface. *Journal of Applied Physics* **54**, 3255–3259.

Gallazzi, M. C., Castellani, L., Martin, R. A. and Zerbi, G. (1993) Regiodefined substituted poly(2,5-thienylene)s. *Journal of Polymer Science Part A* **31**, 3339–3349.

Garnier, F., Hajlaoui, R., El Kassmi, A., Horowitz, G., Laigre, L. Porzio, W., Armanini, M. and Provasoli, F. (1998) Dihexylquaterthiophene, a two-dimensional liquid crystal-like organic semiconductor with high transport properties, *Chemistry of Materials* **11**, 3334–3339.

Halik, M., Klauk, H., Zschieschang, U., Schmid, G. Ponomarenko, S., Kirchemeyer, S. and Weber, W. (2003) Relationship between molecular structure and electrical performance of oligothiophene organic thin film transistors. *Advanced Materials* **15**, 917–922.

Heilmeier, G. H. and Zanoni, L. A. (1964) Surface studies of α-copper phthalocyanine films. *Journal of Physics and Chemistry of Solids* **25**, 603–611.

Horowitz, G. (1998) Organic field-effect transistors. *Advanced Materials* **10**, 365–377.

Horowitz, G., Fichou, D., Peng, X., Xu, Z. and Garnier, F. (1989) Alpha-sexithienyl: a p- and n-type dopable molecular semiconductor. *Solid State Communications* **72**, 385–388.

Huang, D., Liao, F., Molesa, S., Redinger, D. and Subramanian, V. (2003) Plastic-compatible low resistance printable gold nanoparticle conductors for flexible electronics. *Journal of the Electron Society* **150** (7), G412–G417.

Huitema, H. E. A., Gelinck, G. H., van der Putten, J. B. P. H, Kuijk, K. E, Hart, C. M, Cantatore, E, Herwig, P. T, van Breemen, A. J. J. M and de Leeuw, D. M. (2001). *Nature* **414**, 599.

Petitioner Samsung Ex-1011, 0270

Katz, H. E, Laquindanum, J. G. and Lovinger, A. J. (1998) Synthesis, solubility, and field-effect mobility of elongated and oxa-substituted dialkyl thiophene oligomers. Extension of ''polar intermediate'' synthetic strategy and solution deposition on transistor substrates. *Chemistry of Materials* **10**, 633–638.

Katz, H. E., Bao, Z. and Gilant, S. L. (2001) Synthetic chemistry for ultrapure, processable, and high-mobility organic transistor semiconductors. *Accounts of Chemical Research* **34**, 359–369.

Kelley, T. W., Boardman, L. D., Dunbar, T. D., Muyres, D. V., Pellerite, M. J. and Smith, T. P. (2003) High-performance OTFTs using surface-modified alumina dielectrics. *Journal of Physics and Chemistry B* **107**, 5877–5881.

McCullough, R. D., Tristram-Nagle, S., Williams, S. P., Lowe, R. D. and Jayaraman, M. (1993) Self-orienting head-to-tail poly(3-alkylthiophenes): new insights on structure-property relationships in conducting polymers. *Journal of American Chemistry Society* **115**, 4910–4911.

Meijer, E. J, Gelinck, G. H., van Veenendaal, E., Huisman, B.-H., de Leeuw, D. M. and Klapwijk, M. (2003) Scaling behavior and parasitic series resistance in disordered organic field-effect transistors. *Applied Physics Letters* **82**, 4576.

Muller, R. S. and Kamins, T. I., (1986) *Device Electronics for Integrated Circuits*, 2nd edn John Wiley & Sons, Inc., New York.

Niemi, V. M., Knuuttila, P., Österholm, J.-E. and Korvola, J. (1992) Polymerization of 3-alkylthiophenes with FeCl3. *Polymer* **33**, 1559–1562.

Ong, B. S., Wu, Y., Liu, P. and Gardner, S. (2003) Towards printed organic electronics: semiconductor materials design for plastic transistors. *Polymer Preproceedings* **44**, 321–322.

Ong, B. S., Wu, Y., Jiang, L., Liu, P. and Murti, K. (2004a) Polythiophene-based field-effect transistors with enhanced air stability. *Synthetic Metals,* **142**, 49–52.

Ong, B. S., Wu, Y., Liu. P. and Gardner, S. (2004b) High-performance semiconducting polythiophenes for organic thin-film transistors. *Journal of the American Chemical Society* **126**, 3378–3379.

Paul, K. E., Wong, W. S., Ready, S. E. and Street, R. A. (2003) Additive jet printing of polymer thin-film transistors. *Applied Physics Letters* **83**, 2070.

Pomerantz, M., Tseng, J. J., Zhu, H., Sproull, S. J., Reynolds, J. R., Uitz, R., Arnott, H. J. and Haider, M. I. (1991) Processable polymers and copolymers of 3-alkylthiophenes and their blends. *Synthetic Metals* **41**, 825–830.

Salleo, A., Chabinyc, M. L., Yang, M. S. and Street, R. A. (2002) Polymer thin-film transistors with chemically modified dielectric interfaces. *Applied Physics Letters* **81**, 4383.

Salleo, A. and Street, R. A. (2003) Light-induced bias stress reversal in polyfluorene thin-film transistors. *Journal of Applied Physics* **94**, 471.

Salleo, A., Chen, T. W., Volkel, A. R., Wu, Y., Liu, P. Ong, B.S. and Street, R.A. (2004) Intrinsic hole mobility and trapping in a regioregular poly(thiophene). *Physical Review B* **70**, 115311.

Sirringhaus, H., Brown, P. J., Friend, R. H., Nielen, M. M., Bechgaard, K., Langeveld-Voss, B. M. W., Spiering, A. J. H., Janssen, R. A. J., Meijer, E. W., Herwig, P. and de Leeuw, D. M. (1999) Two-dimensional charge transport in self-organized, high-mobility conjugated polymers. *Nature* **401**, 685–688.

Sirringhaus, H., Wilson, R. J., Friend, R. H., Inbasekaran, M., Wu, W., Woo, E. P., Grell, M. and Bradley, D. D. C. (2000) Mobility enhancement in conjugated polymer field-effect transistors through chain alignment in a liquid-crystalline phase. *Applied Physics Letters* **77**, 406.

Smith, A. (1979) *The Newspaper: An International History,* Thames and Hudson, London.

Steinberg, S. H. (1956) *Five Hundred Years of Printing*, 3rd edn, Viking Press, England.

Street, R. A., and Salleo, A. (2002) Contact effects in polymer transistors. *Applied Physics Letters* **81**, 2887.

Street, R. A., Salleo, A. and Chabinyc, M. L. (2003) Bipolaron mechanism for bias-stress effects in organic transistors, *Physical Review B* **68**, 085316.

Tsumura, A., Koezuka, H. and Ando, T. (1986) Macromolecular electronic devices:field-effect transistor with a polythiophene thin film. *Applied Physics Letters* **49**, 1210–1212.

Petitioner Samsung Ex-1011, 0271

Wang, C., Benz, M. E., LeGoff, E., Schindler, J. L., Allbritton-Thomas, J., Kannewurf, C. R. and Kanatzidis, M. G. (1994) Studies on conjugated polymers: preparation, spectroscopic, and charge-transfer properties of a new soluble polythiophene derivative: poly(3′4′-dibutyl-2,2′:5′2″-terthiophene), *Chemistry of Materials* **6**, 401.

Wang, G., Swensen, J., Moses, D. and Heeger, A. J. (2003) Increased mobility from regioregular poly-(3-hexylthiophene) field-effect transistors. *Journal of Applied Physics* **93**, 6137.

Wang, J. and Gonsalves, K. E. (1998) Synthesis of poly(p-ethyl phenol-*co*-4-hydroxythiophenol)/cds nanocomposites and their dispersion in polycarbonate. *MRS Fall Meeting Digest*, 372.

Wang, Y. and Bokor, J. (2004) Maskless lithography using drop-on-demand inkjet printing method. SPIE Microlithography, Santa Clara, CA, February 2004.

Wong, W. S., Ready, S., Matusiak, R., White, S. D., Lu, J.-P., Ho, J. and Street, R. A. (2002) Amorphous silicon thin-film transistors and arrays fabricated by jet printing. *Applied Physics Letters* **80**, 610.

Wong, W. S., Ready, S. E., Lu, J.-P. and Street, R. A. (2003) Hydrogenated amorphous silicon thin-film transistor arrays fabricated by digital lithography. *IEEE Electron Device Letters* **24**, 577–579.

Wu Y., Liu P., Gardner S. and Ong B. S. (2005) Poly (3,3″-dialkylterthiophene)s: Room-temperature, solution-processed, high-mobility semiconductors for organic thin-film transistors. *Chemistry of Materials* **17**, 221–223.

Yamamoto, T., Komarudin, D., Arai, M., Lee, B.-L., Suganuma, H., Asakawa, N., Inoue, Y., Kubota, K., Sasaki, S., Fukuda, T. and Matsuda, H. (1998) Extensive studies on stacking of poly(3-alkylthiophene-2,5-diyl)s and poly(4-alkylthiazole-2,5-diyl)s by optical spectroscopy, NMR analysis, light scattering analysis, and X-ray crystallography. *Journal of the American Chemical Society* 120, 2047–2058.

Petitioner Samsung Ex-1011, 0272

13

Rollable Active Matrix Displays with Organic Electronics

Edzer Huitema, Gerwin Gelinck, Erik van Veenendaal, Fred Touwslager, and Pieter van Lieshout

Philips Research Laboratories

13.1 Introduction

Flexible displays have the potential to replace part of the paper used today and are therefore a focus of the current display research. The advantages of flexible displays compared to their rigid counterparts are that they weight less, are more rugged and that they eventually could become truly rollable. These are important features for the mobile market. This chapter presents state-of-the-art rollable active matrix displays with organic electronics. This work is currently part of the ongoing effort of Polymer Vision to bring rollable active matrix displays to the market. Polymer Vision has been a venture inside the Philips Technology Incubator since 2003.

Section 13.2 is an overview of the current research and development in the field of flexible displays. Section 13.3 presents our organic electronics technology. Display design and processing are presented in Section 13.4, followed by the requirements on the organic pixel switches in Section 13.5 and the current performance of organic transistors in Section 13.6. A flexible QVGA display is demonstrated in Section 13.7 that can display 2-bit monochrome images. The generation of grey levels is possible due to a sufficiently high speed of the pixel switches that allows pulse width modulation with small enough pulse periods. Section 13.8

Flexible Flat Panel Displays Edited by G. P. Crawford
© 2005 John Wiley & Sons, Ltd., ISBN 0-470-87048-6

Petitioner Samsung Ex-1011, 0274

presents the current situation and our recent results on integrated row drivers for rollable active matrix displays. The advantages of integrated row drivers are the reduced number of connections from the display to the addressing hardware, the reduced footprint of the display and the cost reduction due to elimination of the row driver ICs. This new development has been enabled by the rapid progress in processing technology that made it possible to produce active matrix backplanes as well as electronic circuits using the same organic electronics technology (Gelinck *et al.* 2004).

13.2 Flexible Display Overview

Displays with flexible plastic substrates have already been demonstrated, but these are mainly direct drive and passive matrix displays based on liquid crystal (Park *et al.* 2000; Lueder 1999), polymer light-emitting diodes (Gustafsson *et al.* 1992) and electrophoretic ink (Liang *et al.* 2003). Direct drive displays can be used in simple applications, like signage, price tagging or smart cards. Passive matrix displays have the additional capability of displaying graphics and text. The limitations of passive matrix displays are the maximum resolution of a few hundred rows, the long image update time when used in combination with certain display effects (e.g. electrophoretics) and the lower image quality, due to crosstalk.

Active matrix displays differ from the aforementioned displays in that they have a switch incorporated in each pixel (Tsukada 2000). This removes the limitations encountered in passive matrix displays, but requires more sophisticated processing equipment to be used. The dominant pixel switch technology is the amorphous silicon thin film transistor (TFT) on glass (Tsukada 2000), although other technologies have also been used (Brody 1996; Kuijk 1991). Currently, rigid active matrix displays on glass are already widespread. However, flexible active matrix displays on plastic substrates are still in the research and development phase. Plastic active matrix backplanes have been made with amorphous silicon (Gleskova *et al.* 1999, Sandoe 1998, Polach *et al.* 2000) and with polycrystalline silicon as semiconductor (Young *et al.* 1997). Also complete plastic active matrix liquid crystal displays (LCDs) have been demonstrated using amorphous silicon diodes (Young *et al.* 1997), amorphous silicon TFTs (Okamoto *et al.* 2002) and by using a substrate transfer process with polycrystalline silicon TFTs (Inoue *et al.* 2002). Alternatively, the amorphous silicon process has been carried out on pliable steel foils, resulting in pliable electrophoretic displays (Chen *et al.* 2003).

In the nineties organic electronics, i.e. using an organic material as semiconductor, has emerged as a promising thin film technology for large-area integrated circuits (Voss 2000). The use of organic materials has a number of important advantages over conventional techniques using mainly inorganic materials, like amorphous silicon. The low process temperature, less than 200 °C (Gelinck *et al.* 2000), creates the possibility of using a wide range of plastic substrates instead of glass. Furthermore, the mechanical properties of organic materials are compatible with plastic substrates. This technology therefore opens the way to plastic displays that are truly rollable.

In recent years, field-effect mobilities comparable to amorphous silicon have been reported using a variety of organic semiconductors (Dimitrakopoulos and Malenfant 2002). One of the key goals is the integration of these organic transistors into functional electronic circuits. Small logic building blocks such as ring oscillators (Brown *et al.* 1995) and even more complex circuits such as code generators (Drury *et al.* 1998) have been made.

Petitioner Samsung Ex-1011, 0275



Figure 13.1 An image on a 64 × 64 display on glass driven by 4096 polymer TFTs, with solution-processed PTV as the semiconductor. An image containing 256 grey levels is shown; the display is refreshed at 50 Hz

The first active matrix display with an organic semiconductor was reported in 2000 (Philips 2000). The display (Huitema *et al.* 2001), shown in Figure 13.1, was processed on glass, used a solution-processed semiconductor, contained 4096 pixels and was able to show monochrome images. This was rapidly followed by the first active matrix displays with organic semiconductors on plastic substrates (Mach *et al.* 2001; Sheraw *et al.* 2002; Fujisaki *et al.* 2003; Gelinck *et al.* 2004). Lately, a flexible QVGA (quarter VGA) active matrix display with an organic semiconductor was reported (Huitema *et al.* 2003). Having a total of 76 800 pixels, this is the largest flexible display with organic transistors to date.

13.3 Organic Electronics Technology

The organic semiconductor can be applied in two fundamentally different ways: vapour deposition and solution processing. A vapour-deposited organic semiconductor generally yields higher thin film transistor performance. Solution processing is, however, preferred for high-volume, low-cost production. The deposition of soluble organic materials by, for instance, spinoating simplifies the display manufacturing process compared to the conventional chemical vapour deposition techniques, especially for large areas. Next to the deposition, solution processing opens a plethora of alternative patterning technologies such as printing (Blanchet and Rogers 2003; Huebler *et al.* 2002), stamping (Park *et al.* 2002), selective dewetting (Chabinyc *et al.* 2002), inkjet printing (Sirringhaus *et al.* 2000). Here the ultimate goal would be a low-cost roll-to-roll solution-based process. However, to fully exploit the mature production equipment used in the established active matrix liquid crystal display (AMLCD) industry, it is best to use standard photolithography techniques for patterning of the layers. This allows the use of a mature knowledge base to quickly move up the learning curve towards a fully industrialized process.

Petitioner Samsung Ex-1011, 0276

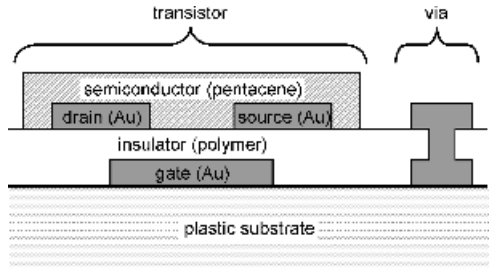


Figure 13.2 Cross section of a TFT and vertical interconnect (via)

Our TFT technology is based on a bottom-gate device architecture (Figure 13.2). This geometry is comparable to the inverted staggered-electrode structure that is commonly used for amorphous silicon TFTs (Tsukada 2000). The thin film transistors are processed on 150 mm diameter, 25 μm thin polyethylene naphthalate (PEN) films laminated on a removable support. The organic semiconductor and gate dielectric are processed from solution. Given the specifications of sheet conductivity of the column and row lines in the display, metallic electrodes are used (Huitema *et al.* 2003). Gate electrodes and first-level interconnect lines are made by patterning gold using photolithography techniques. The gate dielectric is a 350 nm thick photo-imageable polymer (polyvinylphenol) that is spin coated and subsequently exposed to UV light to define contact holes. Source and drain electrodes, pixel pad and second-level interconnect lines are defined in the second gold layer. On top of this stack, a 100 nm thick precursor pentacene film is spin coated. Synthesis of this precursor and the conversion procedure to pentacene are described elsewhere (Herwig and Müllen 1999). Next the semiconductor is patterned using a subtractive photolithography process (Kymissis *et al.* 2002). This finishes the fabrication of the TFT backplane and the row shift registers.

The key features of this technology are that first a thin flexible foil is glued onto a rigid support, then the functional layer stack is processed and finally the foil containing the microelectronic devices is delaminated from its support without degradation of the devices.

The rigid support can be reused. This allows the use of standard of-the-shelf patterning and deposition equipment. Typically, a registration better than 2.5 μm over a 150 mm wafer for a four-mask process is achieved. Integration of transistors over large areas with a relatively low overlap of 5 μm is possible. This allows the production of transistors with sufficiently small parasitic stray capacitances for active matrix displays and row driver circuits.

13.4 Display Design and Processing

The display contains 240 rows and 320 columns. The layout is shown in Figure 13.3. The pixel size is 300 μm × 300 μm, resulting in a display diagonal of 4.7 in. The TFT channel length (L) and width (W) are 5 μm and 140 μm, respectively. The rows of the display are processed on the gate metal level; the columns and the pixel pads are processed on the source/drain level. This results in a reflective active matrix display, with an optical aperture ratio of 79%. The pixel pads overlap the gate line of the preceding row, thus forming the storage capacitors in the usual way.

Petitioner Samsung Ex-1011, 0277

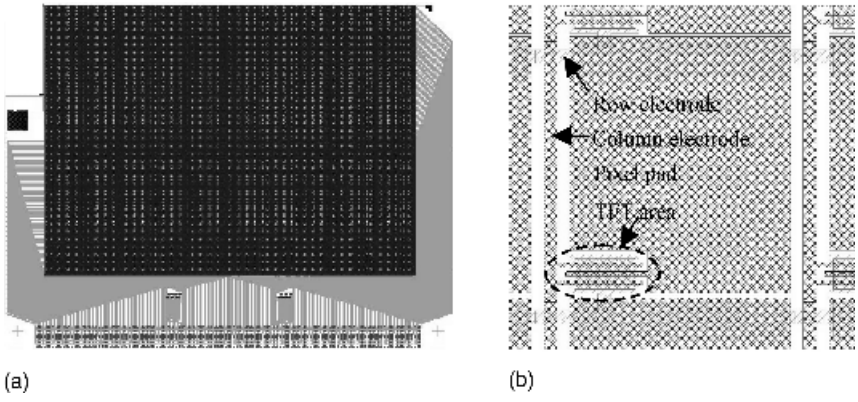


Figure 13.3 (a) Overview of the layout of the QVGA display and (b) a zoom-in on the pixel layout

After processing the backplanes, an electronic ink film is laminated onto the TFT backplane (Comiskey *et al.* 1998). This film consists of electrophoretic microcapsules in a polymer binder, coated onto a polyester/indium tin oxide sheet. Optical contrast is achieved by moving black and white submicron particles with opposite charge in a transparent fluid within a microcapsule. Depending on which submicron particles are closest to the viewer, light is scattered back (white state) or absorbed (black state). The electrophoretic effect is bistable – without any electric field the microcapsules keep their switching state. This greatly reduces the power consumption of the display.

13.5 Transistor Requirements

The equivalent circuit of one pixel is shown in Figure 13.4. The display is driven row by row. During one frame all the rows are sequentially selected by applying a voltage that switches the TFTs from the non-conducting state (positive voltage) to the conducting state

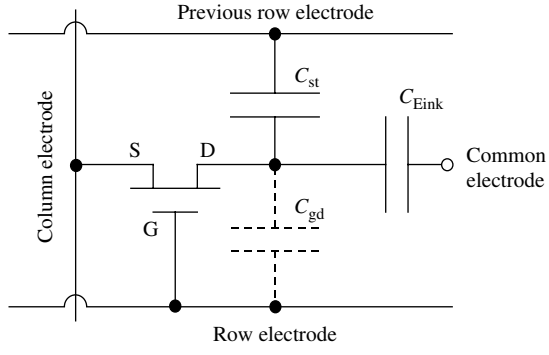


Figure 13.4 Equivalent circuit of one pixel. The source, drain, and gate of the TFT are indicated by S, D, G, respectively. The storage capacitor is C_{st}, the pixel capacitor is C_{Eink} and the parasitic gate–drain capacitance is C_{gd}

Petitioner Samsung Ex-1011, 0278

(negative voltage). During the row selection period, the pixel capacitors of the selected row are charged to the voltage supplied on the column electrodes. The pixel capacitance consists of the sum of the capacitors on the drain side of the TFT in Figure 13.4. During the remaining frame time (i.e. the hold time) the other rows are addressed. The TFTs are then in their non-conducting state and the charge on the pixel capacitors must be retained. Typical voltages that are used on the gate lines are -25 V during row selection and $+25$ V during the hold time. Typical column voltages are -15 V, 0 V and $+15$ V.

In order to change a pixel from a black to a white state, a pixel voltage of -15 V must be applied for about 600 ms. The reverse transition requires a pixel voltage of $+15$ V for the same period of time. The generation of grey levels is done by pulse width modulation, which requires shorter pulses to be supplied to the pixels. Therefore a frame rate of 50 Hz is used to drive our displays, thus enabling a minimum pulse period of 20 ms on the pixels. A frame rate of 50 Hz imposes restrictions on the minimum field-effect mobility and the maximum off-current of the TFTs, as will be discussed next.

In order to estimate the transistor requirements for our display, we use a transistor model (Detcheverry and Matters 2000) that includes a field-effect mobility which depends on the gate voltage:

$$\mu_{\mathrm{FE}} = \mu_0 \left(-V_{\mathrm{gs}} + V_{\mathrm{T}}\right)^{\gamma}, \tag{13.1}$$

where V_{T} is the threshold voltage. Parameter γ is a fit parameter that has a value close to 1 for the organic semiconductor and parameter μ_0 is equal to the mobility at $-V_{\mathrm{gs}} + V_{\mathrm{T}} = 1$ V. By combining (13.1) with the classical analytical Shockley expression for the drain current in a MOS transistor, the following expression for the drain current in the linear regime is derived:

$$I_{\mathrm{d}} = \frac{W}{L}\frac{\mu_0 C_{\mathrm{i}}}{(\gamma+2)}\left[\left(-V_{\mathrm{gs}} + V_{\mathrm{T}}\right)^{\gamma+2} - \left(-V_{\mathrm{gs}} + V_{\mathrm{T}} + V_{\mathrm{ds}}\right)^{\gamma+2}\right], \tag{13.2}$$

where C_{i} is the gate insulator capacitance per unit area.

13.5.1 Field-Effect Mobility Effects

The required field-effect mobility for our display can be determined by performing circuit simulations with the circuit shown in Figure 13.4. Parameter μ_0 in (13.1) is varied between simulations. The resulting mobility is determined at $V_{\mathrm{gs}} = -20$ V, with a value for parameter γ of (13.1). The transfer characteristics of the simulated transistor are shown in Figure 13.5(a). The on-current increases with increasing field-effect mobility. The off-current is taken sufficiently small in order to retain more than 99% of the charge during the hold time. The resulting charging behaviour of the pixel is shown in Figure 13.5(b). The vertical axis shows the average pixel voltage during one frame; the horizontal axis shows the frame number. For every value of the mobility, first a simulation of a pixel charging towards -15 V is performed for 10 frames followed by a simulation of a pixel charging towards $+15$ V during 10 frames. The gate voltage is -25 V during the line selection time and $+25$ V during the hold time.

Petitioner Samsung Ex-1011, 0279

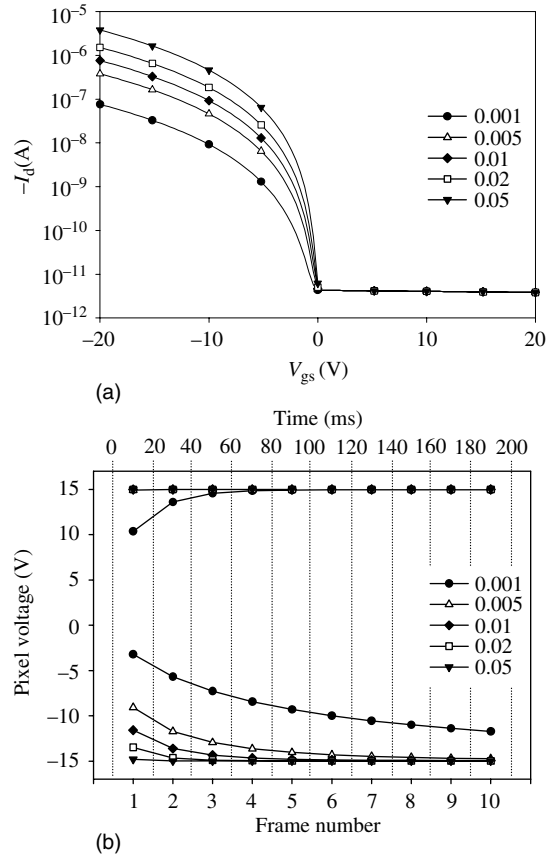


Figure 13.5 (a) Simulated transfer characteristics at five different values of parameter μ_0 in (13.1) for $V_{sd} = 20$ V. The key shows the resulting field-effect mobility (cm^2/V s) at $V_{sg} - V_T = 25$ V and parameter $\gamma = 1.1$. The leakage current was set to 3 pA. (b) Simulated charging behavior of a pixel with the same five values for the mobility. The vertical axis shows the pixel voltage, the horizontal axis the frame number. The simulated frame rate was 50 Hz

Charging to -15 V is slower than charging to $+15$ V due to the smaller value for the source–gate voltage. At a mobility of 0.001 cm^2/V s, charging to $+15$ V is incomplete during the first three frames, while charging to -15 V is incomplete for more than 10 frames. Incomplete charging of the pixels can lower the optical performance of our display in at least two different ways. The first is a decreased switching speed, due to the decreasing drift velocity of the electrophoretic particles with decreasing pixel voltage. The second is non-uniformity between pixels, as the sensitivity of the pixel voltage towards small differences in the mobility increases when pixel charging becomes incomplete.

At a mobility of 0.01 cm^2/V s, charging to $+15$ V is complete, while charging to -15 V results in a pixel voltage of -12 V during the first frame and -14.8 V after five frames. The average pixel voltage during the first five frames is -14 V, which is a charging ratio of 93%. As the smallest pulses supplied to the pixels are five frames or longer when generating images with four grey levels at a refresh rate of 50 Hz, the effect of incomplete charging

Petitioner Samsung Ex-1011, 0280

during the first frame is small. By comparing the average pixel voltage with the switching curves (not shown here) it was verified that it is possible to generate at least four grey levels with sufficient uniformity at a mobility of 0.01 cm^2/V s.

13.5.2 Leakage Current Effects

In Figure 13.6(a) the transfer characteristics of simulated transistors with different leakage currents are shown. The field-effect mobility is set to 0.05 cm^2/V s, the highest value used in Figure 13.6, which implies that charging of the pixels is complete in these simulations. The column voltage is set to 0 V during the hold time and +15 V and −15 V during the line selection period. In Figure 13.6(b) the simulated pixel voltage is shown. The vertical axis

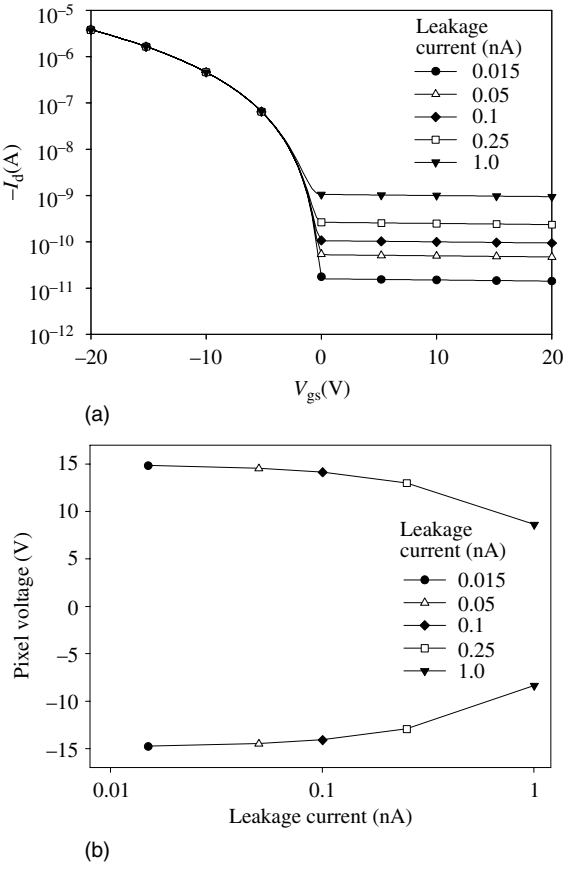


Figure 13.6 (a) Simulated transfer characteristics for $V_{sd} = 20$ V at five different values of the leakage current (A) shown in the key. The field-effect mobility was set to 0.05 cm^2/V s. (b) Simulated charging behavior of a pixel with the same five values for the leakage current. The vertical axis shows the pixel voltage, the horizontal axis the leakage current. The simulated frame rate was 50 Hz

Petitioner Samsung Ex-1011, 0281

shows the average pixel voltage during one frame and the horizontal axis the leakage current. At a leakage current of 1 nA, the average pixel voltage is only 60% of the voltage supplied on the column electrode. Optically this large leakage current negatively affects the switching speed of the electrophoretic particles and the image uniformity due to vertical crosstalk, i.e. the current leakage between the column electrode and the pixel during the hold time. When the leakage current is smaller than 50 pA, more than 97% of the charge on the pixel is retained during the hold time. This results in a voltage drop smaller than 0.5 V. By comparing the switching speed at 15 V with the switching speeds at 14.5 V (not shown here) it was verified that it is possible to generate at least four grey levels with sufficient uniformity at a leakage current of 50 pA. An even smaller leakage current further reduces the voltage drop and enables more grey levels.

13.6 Transistor Characteristics

The pixel TFT performance has been evaluated on a QVGA active matrix backplane. In total 380 devices in a number of random columns have been measured. In Figure 13.7 the transfer

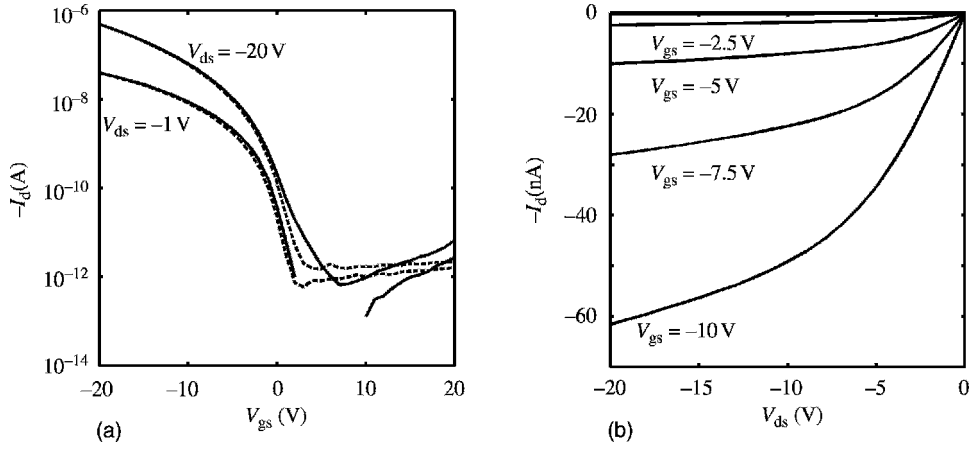


Figure 13.7 Characteristics of a pixel TFT with typical mobility 0.01 cm^2/V s: (a) transfer characteristics and (b) output characteristics

and output characteristics of a typical organic pixel TFT are shown. The field-effect mobility is 0.010 cm^2/V s (linear mobility extracted from the transfer characteristics for $V_{gs} = -20$ V and $V_{ds} = -1$ V), while the leakage current is a few picoamperes. When compared to the requirements, the transistor has sufficient on-current and an excellent off-current for driving the QVGA display at 50 Hz.

An impression of the uniformity of the active matrix backplane is given in Figure 13.8. Figure 13.8(a) shows the distribution of the mobility of the pixel TFTs. The average field-

Petitioner Samsung Ex-1011, 0282

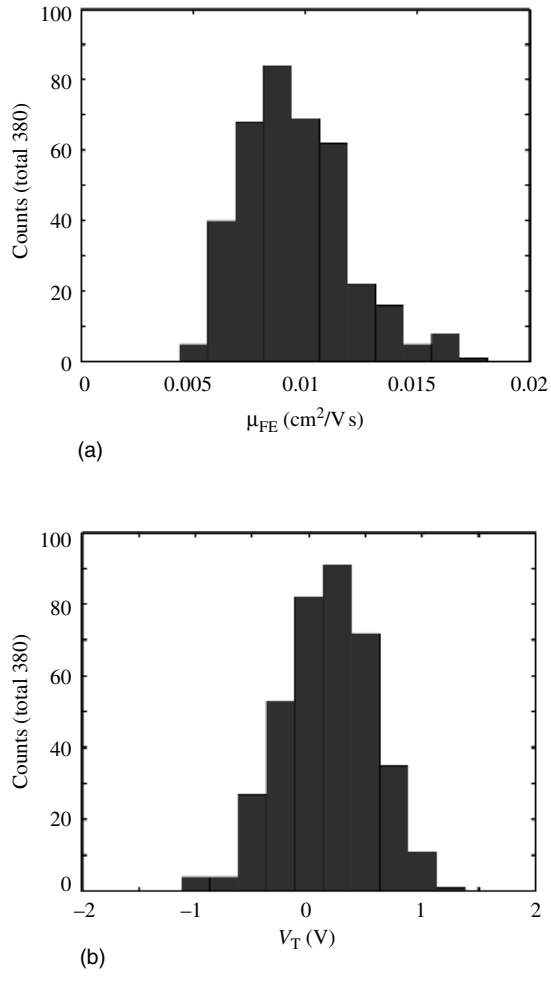


Figure 13.8 Impression of the uniformity of a QVGA active matrix backplane based on measurements of 380-pixel TFTs. (a) Distribution of the mobility, extracted from the transfer characteristics for $V_{gs} = -20$ V and $V_{ds} = -1$ V. (b) Distribution of the threshold voltage, obtained by fitting (13.1) to the transfer characteristics for $V_{ds} = -1$ V

effect mobility is 0.010 cm^2/V s with a standard deviation of 0.0024 cm^2/V s. The average on-current is $-1.0\,\mu$A, measured for $V_{gs} = -25$ V and $V_{ds} = -15$ V (typical for charging a pixel to -15 V). The average off-current is -5.7 pA, measured for $V_{gs} = +10$ V and $V_{ds} = -15$ V (typical for leakage of a pixel charged to $+15$ V). Hence our pixel TFTs have an on/off ratio exceeding 10^5. Figure 13.8(b) shows the distribution of the threshold voltage of the pixel TFTs. The threshold voltage of a TFT is obtained by fitting (13.1) to the transfer characteristics for $V_{ds} = -1$ V. The threshold voltage has a Gaussian-like distribution around 0.2 V with a small standard deviation of 0.4 V. The average value of the power parameter γ obtained in the same analysis is 1.1 (standard deviation 0.1).

Petitioner Samsung Ex-1011, 0283

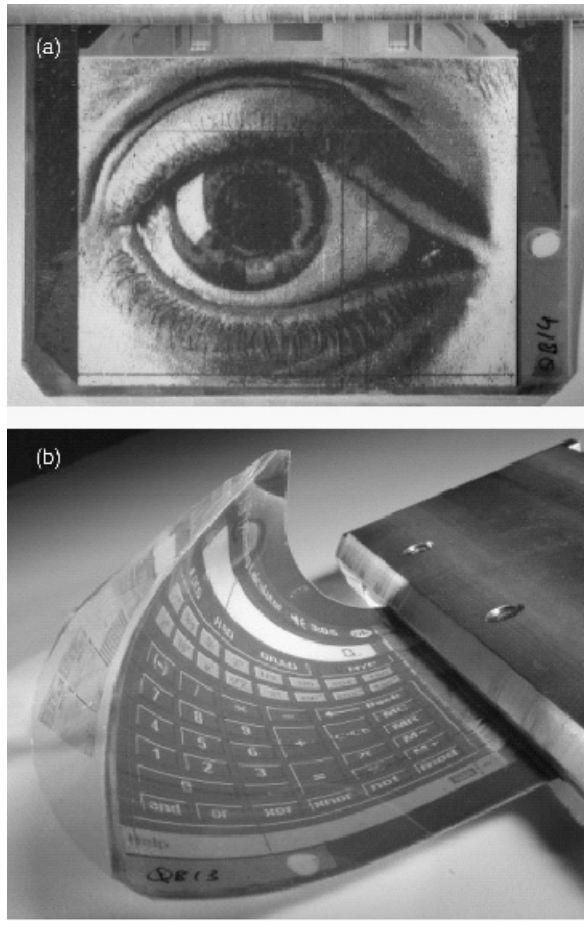


Figure 13.9 (a) A picture of the flexible QVGA active matrix display with organic TFTs, refreshed at 50 Hz. An image with four grey levels is displayed. (b) The same display in the bent state

13.7 Functional Displays

Pictures of a functional display are shown in Figure 13.9. The column electrodes are driven between -15 V and $+15$ V, while the row electrodes are driven at -25 V during the line selection time and 25 V during the hold time. The frame rate of the display is 50 Hz. Images containing four grey levels can be displayed. The switching time is 600 ms. Table 13.1 is a summary of the display specifications.

Three types of lifetime test have been performed on the displays; note that our displays do not incorporate any type of additional barrier layer. The displays have been bent 100 times to a radius of curvature of 2 cm. The display has been subjected to a 100 h operational lifetime test under a duty cycle of 10%. Both tests were passed without any apparent degradation in the optical contrast and without any additional line or pixel defects. During a shelf lifetime

Petitioner Samsung Ex-1011, 0284

Table 13.1 Specifications of the flexible QVGA display

Parameter	Value
Panel size	4.7 in (72 mm × 96 mm)
Resolution	320 × 240 (85dpi)
Number of pixels	76 800
Pixel size	300 μm × 300 μm
Display type	Electrophoretic (E Ink)
Number of gray levels	4
Frame rate	50 Hz
Image update time	600 ms
Aperture ratio	79%
Display thickness	300 μm
Display weight	7 g
Flexibility	A bending radius of ∼2 cm
TFT channel length	5 μm
TFT channel width	140 μm
Measured mobility	0.01 cm^2/V s
Measured on-current	1.0 μA
Measured off-current	6 pA
Measured threshold voltage	0.2 V

test of 2 months at ambient conditions, the field-effect mobility decreased by 30%. As the TFT current is linearly proportional to the mobility in (13.2), the TFT current is also reduced by 30%. The pixels will then be charged to the same voltage in 30% extra line selection time. This corresponds to exactly the same optical contrast at a 30% lower frame rate (38 Hz instead of 50 Hz). This trade-off is possible because our off-current is sufficiently low for this reduced frame rate.

13.8 Driver Integration

Figure 13.10(a) shows that to enable roll-up of the QVGA display, all connections should be on one side of the foil. For each individual row and column there is a contact to the external addressing hardware, resulting in almost 600 contacts in total for a QVGA display. The pitch of these contacts must be as small as 175 μm, resulting in a challenging contact problem for rollable displays. Furthermore, the area needed to route the interconnects from the contact area to the rows and columns in the active matrix is rather large, which is disadvantageous for the footprint of the display.

Shift registers, which can be used as row drivers, only need clock and data signals and supply lines. The number of connections between the shift register and the external addressing hardware is therefore only about 10 in total. The number of contacts to a complete QVGA display with integrated row drivers will be less than 400, resulting in higher

Petitioner Samsung Ex-1011, 0285

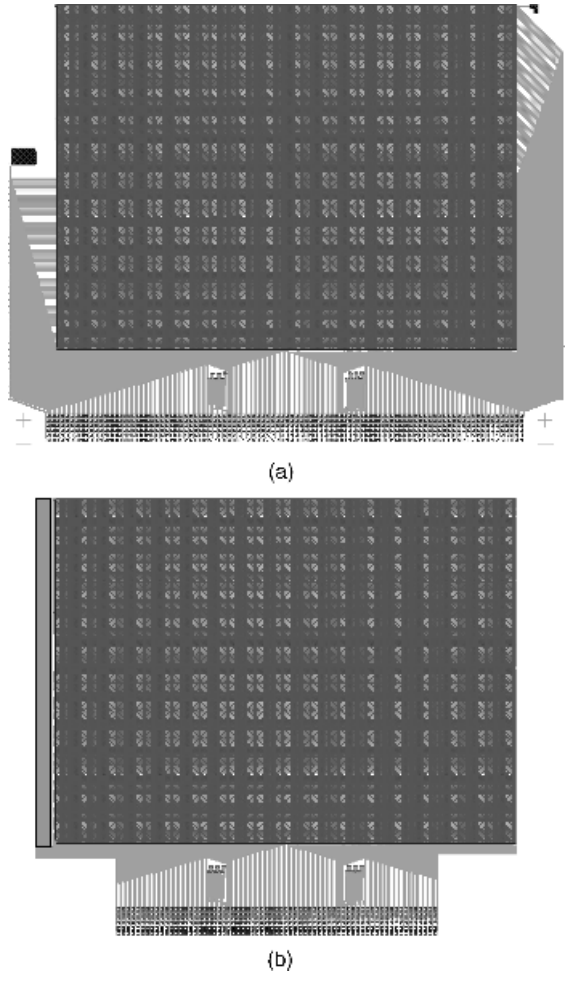


Figure 13.10 (a) Layout of the display without integrated drivers; (b) artist's impression of the display with integrated row driver

contact reliability. As the width of the circuitry is only a few millimetres, the footprint of the display will become smaller. Figure 13.10(b) gives an artist's impression of our current QVGA matrix, combined with shift registers. Both the reduced number of contacts and the decreased footprint are obvious from this figure.

Another advantage of driver integration is the decreased number of external drivers needed to operate a display. Also, the number of signals going to the internal drivers is decoupled from the actual number of rows present in the display. This simplifies the design of the external driving electronics and increases the flexibility of the driver platform.

As the chosen electrophoretic display effect is bistable, the row drivers are only operational during an image update. This is different from the commonly used LCD effects

Petitioner Samsung Ex-1011, 0286

that need to be driven continuously during use of the display. This makes the electrophoretic display effect ideal for integration of row drivers in organic electronics.

In a shift register, a selection pulse is shifted from one stage to the next at every clock pulse. The frame rate and the number of rows in the display determine the requirements for the clock frequency. As the image update time of the display is 600 ms, a frame rate of approximately 10 Hz is sufficient for black and white images. This enables e-reading applications. The corresponding minimal clock frequency of the shift register for our display is 2.4 kHz. For accurate rendering of grey levels, the frame rate, and thus the clock frequency of the row shift register, should be higher.

13.8.1 32-Stage Shift Registers

Results on static 32-stage shift registers were published recently (Gelinck *et al.* 2004). Figure 13.11 shows a photograph of a foil containing a display as well as one of the 32-stage shift register variants containing 18 TFTs per stage. The complete 32-stage shift register

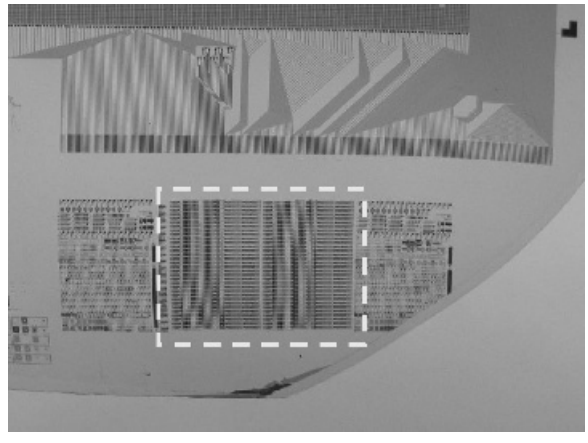


Figure 13.11 Photograph of a flexible foil, containing a QVGA display (near the top) and shift registers (inside the dashed rectangle)

contains 576 TFTs. The area per stage is 0.45 mm^2. The 32-stage shift register functions at a clock frequency of up to 5 kHz, corresponding to a maximum frame rate of 20 Hz for the QVGA display. Approximately 80% of the shift registers are fully functional up to the 32nd stage. Measurements have shown an operational lifetime exceeding 4 h at a clock frequency of 2.8 kHz and a supply voltage of 20 V (Figure 13.12).

As displays and shift registers are fabricated in the same technology, it is expected that results of shelf life tests and bending tests of displays are also valid for shift registers.

Petitioner Samsung Ex-1011, 0287

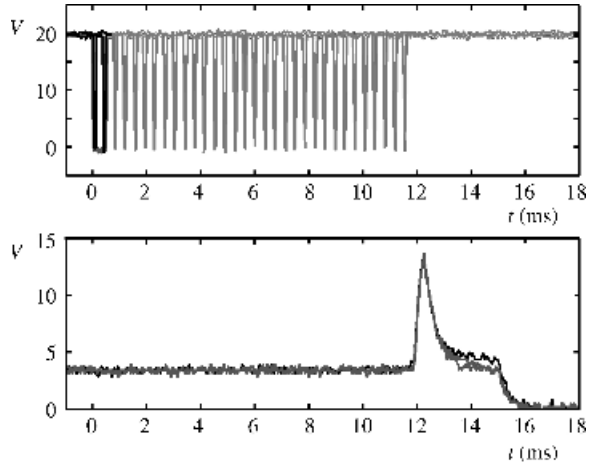


Figure 13.12 Measurement results of the 32-stage shift register: the top graph shows the clock pulses and the start pulse; the bottom graph shows the output pulse of the 32nd stage after 0, 2, and 4 h

13.8.2 120-Stage Shift Registers

Recently, shift registers have been made with 120 stages, half the number of rows of the QVGA display. The topology of the 120-stage shift register is similar to that of the 32-stage version. Figure 13.13 shows measurement results of the new shift register. The top graph shows the clock signal and the lower graphs shows the output waveform of every 20th output. The shift register functions at a clock frequency of up to 2 kHz, which corresponds to a frame rate of 8 Hz for our QVGA display.

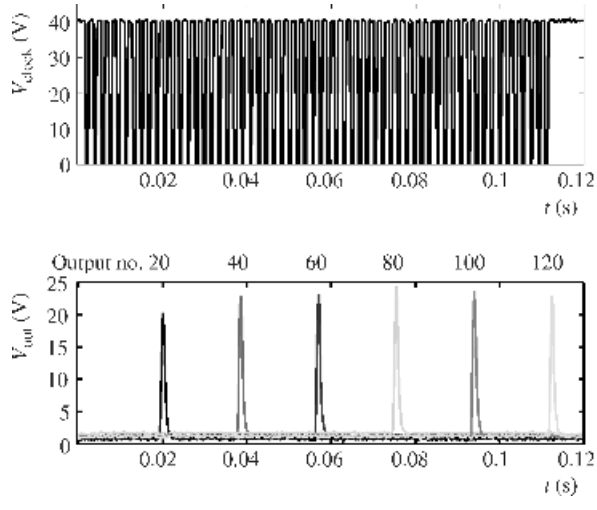


Figure 13.13 Measurement results of the 120-stage shift register, showing the clock pulses and the output pulses for every 20th stage

Petitioner Samsung Ex-1011, 0288

Table 13.2 Specifications of the 120-stage shift register

Parameter	Value
Size per stage ($w \times h$)	1800 μm × 300 μm
Area per stage	0.54 mm^2
Total area	65 mm^2
Max. clock frequency	2 kHz
Max. QVGA frame rate	8 Hz
Number of stages	120
TFTs per stage	18
Total number of TFTs	2130
Circuit yield	30%
Max. supply voltage	40 V
TFT channel length	5 μm

The yield for fully functioning 120-stage shift registers is approximately 30%, which is in line with the increment in area compared to the 32-stage shift registers. Extensive operational life tests will be performed in the near future. With a total of 2130 TFTs, this circuit is the largest functioning circuit in organic electronics reported to date.

Table 13.2 summarizes some key parameters of the 120-stage shift registers. Notice that, the vertical cell pitch of the shift register has been matched to the row pitch of the QVGA display for easy integration in the near future.

Acknowledgement

The authors thank the other members of the Polymer Vision team for their help in realizing the results described here. Dago de Leeuw and Eugenio Cantatore are acknowledged for their numerous contributions to the polymer electronics technology that was used to produce the results. Mark Hage is acknowledged for help with the display measurements and Siebe-Jan van der Hoef and Albert Geven for realizing the display addressing hardware and software. E Ink Corporation is thanked for supplying electrophoretic material and DuPont Teijin Films for supplying plastic substrates.

References

Blanchet, G. and Rogers, J. A. (2003) Printing techniques for plastic electronics. *Journal of Information Science and Technology* **47**, 296–303.

Brody, T. P. (1996) The birth and early childhood of active-matrix – a personal memoir. *Journal of the SID* **4**, 113–7.

Brown, A. R., Pomp, A., Hart, C. M. and de Leeuw, D. M. (1995) Logic gates made from polymer transistors and their use in ring oscillators. *Science* **270**, 972–4.

Chabinyc, M. L., Wong, W. S., Salleo, A., Paul, K. E. and Street, R. A. (2002) Organic polymeric thin-film transistors fabricated by selectrive dewetting. *Applied Physics Letters* **81**, 4260–2.

Petitioner Samsung Ex-1011, 0289

Chen, Y., Kazlas, J. A. P., Ritenour, A., Gates, H. and McCreary, M. (2003) Flexible active-matrix electronic ink display. *Nature* **423**, 136.

Comiskey, B., Albert, J. D., Yoshizawa, H. and Jacobson, J. (1998) An electrophoretic ink for all-printed reflective electronic displays. *Nature* **394**, 253–5.

Detcheverry, C. and Matters, M. (2000) Device simulation of all-polymer thin-film transistors. *Proceedings of ESSDERC*, 328–31.

Dimitrakopoulos, C. D. and Malenfant, P. R. L. (2002) Organic thin film transistors for large area electronics. *Advanced Materials* **14**, 99–117.

Drury, C. J., Mutsaers, C. M. J., Hart, C. M., Matters, M. and de Leeuw, D. M. (1998) Low-cost all-polymer integrated circuits. *Applied Physics Letters* **73**, 108–10.

Fujisaki, Y., Inoue, Y., Sato, H., Kurita, T., Tokito, S. and Fujikake, H. (2003) Organic TFT-driven liquid crystal cell with anodic-oxidised gate insulator and double protection layer. *IDW Digest*, 291–4.

Gelinck, G. H., Geuns, T. C. T. and de Leeuw, D. M. (2000) High-performance all-polymer integrated circuits. *Applied Physics Letters* **77**, 1487–9.

Gelinck, G. H., Huitema, H. E. A., van Veenendaal, E., Cantatore, E., Schrijnemakers, L., van der Putten, J. B. P. H., Geuns, T. C. T., Beenhakkers, M., Giesbers, B., Huisman, B.-H., Mena Benito, E., Touwslager, F. J., Marsman, A., van Rens, B. and de Leeuw, D. M. (2004) Flexible active-matrix displays and shift registers based on solution-processed organic transistors. *Nature Materials* **3**, 106–10.

Gleskova, H., Wagner, S. and Suo, Z. (1999) Failure resistance of amorphous silicon transistors under extreme in-plane strain. *Applied Physics Letters* **75**, 3011–3.

Gustafsson, G., Cao, Y., Treacy, G. M., Klavetter, F., Colaneri, N. and Heeger, A. J. (1992) Flexible light-emitting diodes made from soluble conducting polymers. *Nature* **357**, 477–9.

Herwig, P. T and Müllen, K. A. (1999) A soluble pentacene precursor: synthesis, solid-state conversion into pentacene and application in a field-effect transistor. *Advanced Materials* **11**, 480–3.

Huebler, A., Hahn, U., Beier, W., Lasch, N. and Fischer, T. (2002) High volume printing technologies for the production of polymer electronic structures. *IEEE Polytronic Conference*, 172–6.

Huitema, E., Gelinck, G., van der Putten, B., Cantatore, E., van Veenendaal, E., Schrijnemakers, L., Huisman, B.-H. and de Leeuw, D. (2003) Plastic transistors in active-matrix displays. *ISSCC Digest*, 380–1.

Huitema, H. E. A., Gelinck, G. H., van der Putten, J. B. P. H., Kuijk, K. E., Hart, C. M., Cantatore, E., Herwig, P. T., van Breemen, A. J. J. M. and de Leeuw, D. M. (2001) Plastic transistors in active-matrix displays. *Nature* **414**, 599.

Huitema, H. E. A., Gelinck, G. H., van Veenendaal, E., Cantatore, E., Touwslager, F. J., Schrijnemakers, L. R. R., van der Putten, J. B. P. H., Geuns, T. C. T., Beenhakkers, M. J., van Lieshout, P. J. G., Lafarre, R. W., de Leeuw, D. M. and van Rens, B. J. E. (2003) A flexible QVGA display with organic transistors. *IDW Digest*, 1663–4.

Inoue, S., Utsunomiya, S., Saeki, T. and Shimoda, T. (2002) Surface-free technology by laser annealing (SUFTLA) and its application to poly-Si TFT LCDs on plastic film with integrated drivers. *IEEE Transactions on Electron Devices* **49**, 1353–60.

Kuijk, K. E. (1991) A novel diode matrix for LC-TV displays. *SID Digest*, 401–8.

Kymissis, I., Dimtrakopolous, C. D. and Purushothaman, S. (2002) Patterning pentacene organic thin film transistors. *Journal of Vacuum Science and Technology B* **20**, 956.

Liang, R. C., Hou, J., Zang, H. M. and Chung, J. (2003) Passive matrix microcup electrophoretic displays. *IDMC Digest*, 351–4.

Lueder, E. (1999) Passive and MIM-driven LCDs with plastic substrates. *IDW Digest*, 215–8.

Mach, P., Rodriquez, S. J., Nortrup, R., Wiltzius, P. and Rogers, J. A. (2001) Monolithically integrated flexible display of polymer-dispersed liquid crystal driven by rubber-stamped organic thin-film transistors. *Applied Physics Letters* **78**, 3592–4.

Okamoto, M., Okada, Y., Ban, A., Oka, W., Matsuda, Y. and Shibahara, S. (2002) Development of a color reflective TFT-LCD using plastic substrates. *IDW Digest*, 315–8.

Petitioner Samsung Ex-1011, 0290

Park, S. K., Han, J. I., Kim, W. K. and Kwak, M. K. (2000) Development of 2-inch plastic-film STN-LCD with uniform cell gap. *SID Digest*, 514–7.

Park, S. K., Kim, Y. H., Han, J. I., Moon, D. G. and Kim, W. K. (2002) High performance polymer TFTs printed on a plastic substrate. *IEEE Transactions on Electron Devices* **49**, 2008–15.

Philips (2000) Philips Research develops the world's first display using polymeric semiconductors as pixel drivers, press release, September 2000, www.polymervision.com/.

Polach, S., Randler, M., Bahnmueller, F. and Lueder, E. (2000) A transmissive TN display addressed by a-Si:H TFTs on a plastic substrate. *IDW Digest*, 203–6.

Sandoe, J. N. (1998) AMLCD on plastic substrates. *SID Digest*, 293–6.

Sheraw, C. D., Zhou, L., Juang, J. R., Gundlach, D. J., Jackson, T. N., Kane, M. G., Hill, I. G., Hammond, M. S., Campi, J., Greening, B. K., Francl, J. and West, J. (2002) Organic thin-film transistor-driven polymer-dispersed liquid crystal displays on flexible polymeric substrates. *Applied Physics Letters* **80**, 1088–90.

Sirringhaus, H., Kawase, T., Friend, R. H., Shimoda, T., Binbasekaran, M., Wu, W. and Woo, E. P. (2000) High-resolution inkjet printing of all-polymer transistor circuits. *Science* **290**, 2123–6.

Tsukada, T. (2000) Active-matrix liquid-crystal displays. In *Technology and Applications of Amorphous Silicon*, R. A. Street (ed.), Springer, New York, pp. 7–93.

Voss, D. (2000) Cheap and cheerful circuits. *Nature* **407**, 442–4.

Young, N. D., Bunn, R. M., Wilks, R. W., McCulloch, D. J., Deane, S. C., Edwards, M. J., Harkin, G. and Pearson, A. D. (1997) Thin-film-transistor- and diode-addressed AMLCDs on polymer substrates. *Journal of the SID* **5**, 275–81.

Petitioner Samsung Ex-1011, 0291

14

Mechanics of TFT Technology on Flexible Substrates

Sigurd Wagner,[1] Helena Gleskova,[1] I-Chun Cheng,[1] James C. Sturm,[1] and Z. Suo[2]

[1]Department of Electrical Engineering, Princeton University and [2]Division of Engineering and Applied Sciences, Harvard University

14.1 Introduction

The effect of mechanical stress on amorphous silicon (a-Si) thin film transistors (TFTs) and material began to be studied in the mid 1980s (Jones 1985; Spear and Heintze 1986). Research with TFTs on flexible substrates dates back to 1967 (Brody 1996), and was revived when the commercially important a-Si TFTs were made in the mid 1990s on flexible substrates of glass (Gleskova *et al.* 1995), steel (Theiss and Wagner 1996) and organic polymers (Constant *et al.* 1994; Burns *et al.* 1997; Gleskova *et al.* 1998; Parsons *et al.* 1998; Sandoe 1998; Lueder *et al.* 1998; Bonse *et al.* 1998; Theiss *et al.* 1998). Flexible TFT backplanes are in industrial development (Young *et al.* 2003). Eventually they may be made by roll-to-roll processing (Wagner *et al.* 2000). Research on flexible TFT backplanes has been accompanied by studies of the effects of mechanical deformation on the TFTs. By now the basic experimental and theoretical information required for the manufacture and use of flexible TFT backplanes has been developed. We review it with some emphasis on TFTs made of rigid a-Si on compliant substrates of organic polymers.

Flexible Flat Panel Displays Edited by G. P. Crawford
© 2005 John Wiley & Sons, Ltd., ISBN 0-470-87048-6

Petitioner Samsung Ex-1011, 0292

14.2 Deformation of a TFT Backplane

A TFT backplane may be deformed by internally produced forces. These forces include stresses built in by film growth, by differential thermal expansion or contraction, and by the uptake or release of humidity. A backplane also may be deformed by an external force that bends it, shapes it conformally, or elastically stretches and relaxes it. We survey how mechanical stress may be applied to a TFT backplane and how it may develop in a TFT backplane.

14.2.1 Mechanical Stresses Introduced during Shaping

TFT backplanes are manufactured flat, to benefit from the tools that have been developed for planar semiconductor fabrication. Then the backplanes are strained to produce various shapes. Figure 14.1 illustrates the three types of electronic surfaces that are subsumed under the concept of ''flexible.'' Bending, flexing, or folding produces the cylinder illustrated in Figure 14.1(a). The strain experienced by the active devices may be small, particularly when the device is placed in the neutral plane. Figure 14.1(b) shows a spherical dome that is produced by out-of-plane deformation. This deformation may be large, may deform the surface permanently by plastic flow, and may not be uniform over the surface. Such shaped surfaces are called deformed, conformal, conformally shaped, or compliant. A third type of electronic surface is shaped in the same way but with the added property that it is elastic, as would be the sensor glove whose concept is shown in Figure 14.1(c). Present industrial development is focused on the bending of flexible TFT backplanes. A spherically shaped TFT circuit of the type shown in Figure 14.1(b) has been demonstrated (Hsu *et al.* 2002a), and an organic light-emitting diode (OLED) display has been made on a dome (Bhattacharya *et al.* 2004). Active electronic surfaces that can undergo large elastic deformation are only beginning to enter research (Lacour *et al.* 2003; Gray *et al.* 2004; Wagner *et al.* 2004). In this chapter we discuss bent and conformally shaped surfaces.

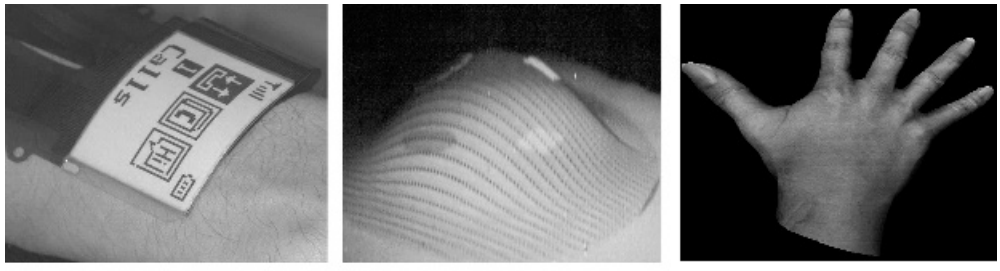


Figure 14.1 Types of deformation of electronic surfaces: (a) elastic bending, once or repeatedly, as for a wristband display (Chen, 2001); (b) conformal shaping by large, one-time, plastic deformation (Hsu 2000); (c) elastic electronic surfaces for large, repeated deformation (Lumelsky *et al.* 2001). In (b) and (c) the devices are placed on rigid islands that are integrated with a deformable substrate

Petitioner Samsung Ex-1011, 0293

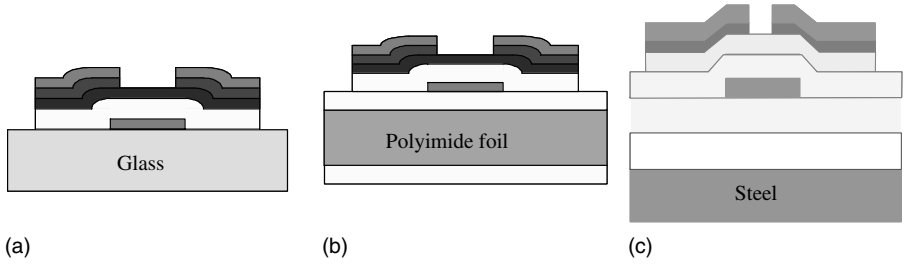


Figure 14.2 Schematic cross sections of back channel cut a-Si TFTs on (a) glass (Gleskova *et al.* 1996), (b) polyimide passivated on both sides with silicon nitride (Gleskova *et al.* 1998), (c) steel planarized with spin-on glass and then passivated with silicon nitride (Ma *et al.* 1997)

14.2.2 Mechanical Stresses Introduced during Fabrication

TFTs are built on substrates layer by layer. Typical layer sequences including substrate planarization and passivation are shown in Figure 14.2 for a back channel cut amorphous silicon (a-Si) TFT structure. Standard thickness ranges of flexible substrate thicknesses are glass 50–80 μm, organic polymers 50–200 μm, and steel 25–150 μm. Planarization and passivation layers are 0.2 to 1 μm thick, and the TFT is slightly less than 1 μm thick.

Even when a TFT backplane is designed to be flat, it experiences stress at many stages during manufacture and use. Built-in stress originates in films that are grown with out-of-equilibrium atoms that seek to move to low-energy, equilibrium, positions. Thermal and humidity stresses are caused by differences in thermal expansion and humidity coefficients between film and substrate, or between films.

The mechanics of TFT backplanes is understood most easily when device and passivation layers are approximated by a single homogeneous film that completely covers the substrate. This approximation, which simplifies analysis and modeling, does not do justice to layered and patterned devices, but is useful in the frequent absence of detailed information.

The stress σ, a force applied to an area, is the response to the strain ε:

$$\sigma = Y\varepsilon. \tag{14.1}$$

Y is the elastic modulus. σ and Y have the dimension of pressure and are stated in GPa. ε is dimensionless and frequently stated in percent.

The behavior of the film-on-substrate structure under stress depend strongly on the elastic modulus and thickness of the substrate Y_s, d_s and the elastic modulus and thickness of the film Y_f, d_f. Three different situations encountered are listed in Table 14.1. When $Y_f d_f \ll Y_s d_s$, the substrate dominates and the film complies with it, as a TFT does on a plate glass substrate or an OLED on steel. The stress in the substrate is small, and the film/substrate couple curves little or only slightly, even when the film is highly stressed. When $Y_f d_f \gg Y_s d_s$, the film dominates. This situation has not been encountered in displays but is being reached in electronic skins. A stiff film and a compliant substrate, like a-Si TFT film on an organic polymer foil, may have similar products of elastic modulus and thickness, $Y_f d_f \approx Y_s d_s$. Such equal strength of film and substrate gives rise to complicated mechanical

Petitioner Samsung Ex-1011, 0294

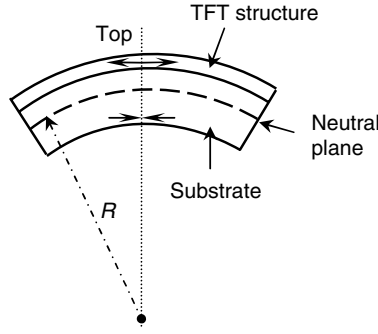


Figure 14.3 A film-on-foil structure bent to a cylindrical roll. When a TFT backplane of thickness d is rolled to a radius r, the thin film is put into a well-defined strain, which is tensile when the film is on the outside of the roll and compressive when the film is on the inside

Table 14.1 Device film/substrate combinations grouped by elastic moduli

	Thin film (small d_f)	
Thick substrate (large d_s)	Stiff (large Y_f)	Compliant (small Y_f)
Stiff (large Y_s)	Si TFT/glass	OLED/steel
Compliant (small Y_s)	ITO/polymer	OTFT/polymer

situations. The material with the high elastic modulus is called stiff and the material with the low elastic modulus is called compliant. In TFT backplanes, silicon device semiconductors, insulators and metals, and glass and steel substrates with Y ranging from $\sim$50 GPa to $\sim$200 GPa are stiff. Organic polymer substrates and organic semiconductors with $Y < 5$ GPa are compliant.

Structures of silicon TFT films on organic polymer substrates change their curvature throughout circuit fabrication. With this change in curvature comes a change in the size of the workpiece. A size change between mask levels, for example the gate level and the source/drain contact level in non-self aligned TFTs, causes misalignment between gate and source/drain. To prevent this misalignment the organic polymer (''plastic'') substrate may be bonded to a rigid carrier of glass or an oxidized silicon wafer. The adhesive used for bonding must withstand the TFT process temperatures and chemicals. If a thermoplastic adhesive is used, its glass temperature must be lower than the glass temperature of the plastic substrate. This use of an adhesive reduces the maximum process temperature from the value that the substrate itself would withstand. Peeling of the finished backplane from the carrier still requires force, which can break the TFTs. In our laboratory we have been working with freestanding substrates that are bonded temporarily only for photolithography.

Petitioner Samsung Ex-1011, 0295

For a quantitative understanding of the mechanics of a homogeneous stiff film on a compliant substrate, we summarize here the theoretical description of stress, strain and curvature induced by processing or by external force (Gleskova *et al.* 1998; Suo *et al.* 1999).

14.3 Stress, Strain and Curvature of a Film/Substrate Couple

The built-in stress σ_0 in a film arises from a mismatch strain ε_0, which is taken to be positive when it induces a tensile stress in the film. ε_0 is determined experimentally as a function of materials system and deposition condition. The thermal expansion mismatch strain ε_{th} is produced by a temperature change of ΔT and the difference in the thermal expansion coefficients of the film and the substrate, α_{f} and α_{s}. The total mismatch strain is the sum of the two contributions:

$$\varepsilon_{\text{M}} = \varepsilon_0 + (\alpha_{\text{f}} - \alpha_{\text{s}})\Delta T. \tag{14.2}$$

We assume that this strain is not relaxed by any inelastic process such as plastic deformation of the film or substrate. We now compare the mechanical behavior of a film on a stiff substrate to the behavior of a film on a compliant substrate (Suo *et al.* 1999).

14.3.1 Stiff Substrate

Because the substrate is stiff, the film must conform to it. A biaxial stress, σ_{f}, arises in the plane of the film, which relates to the mismatch strain as

$$\sigma_{\text{f}} = \varepsilon_{\text{M}} Y_{\text{f}}^*. \tag{14.3}$$

Here $Y_{\text{f}}^* = Y_{\text{f}}/(1-\nu_{\text{f}})$ is the biaxial elastic modulus of the film, where Y_{f} is Young's modulus and ν_{f} is Poisson's ratio. The stress in the substrate is much smaller than the stress in the film. The mismatch causes the substrate to bend. The radius of curvature R is given by the well-known Stoney formula (Timoshenko and Goodier 1970):

$$R = \frac{Y_{\text{s}}^* d_{\text{s}}^2}{6\sigma_{\text{f}} d_{\text{f}}}, \tag{14.4}$$

where d_{f} is the film thickness, d_{s} is the substrate thickness, and Y_{s}^* is the biaxial elastic modulus of the substrate. Because the substrate is stiff, the radius of curvature is very large. Determining the stress in the film by measuring this radius of curvature is an established practice.

Petitioner Samsung Ex-1011, 0296

14.3.2 Compliant Substrate

When a film is deposited on a thin, compliant substrate, the substrate also deforms considerably. Consequently, *the stress in the film is reduced*. In addition, the radius of curvature R can become very small. When during deposition we hold the substrate in a rigid frame, so that the substrate is flat, the stress in the film is given by

$$\sigma_f = \frac{\varepsilon_M Y_f^*}{1 + Y_f^* d_f / Y_s^* d_s}. \tag{14.5}$$

Stiff device films have much higher elastic moduli than the plastic substrate. Therefore the products $Y_f^* d_f$ and $Y_s^* d_s$ are comparable in magnitude. Consequently, the stress in the film deposited on the thin, compliant substrate is reduced by a factor of about 2 compared with a film on a stiff substrate. The stress in the film is no longer set by a rigid substrate, but now depends on the substrate thickness and elastic modulus. The stress in the substrate is given by

$$\sigma_s = -\sigma_f d_f / d_s. \tag{14.6}$$

This stress is still quite small compared to the stress in the film for a thickness ratio $d_f/d_s = 1/50$ (e. g., a 1 μm thick film on a 50 μm thick substrate).

One technique for flattening the substrate is to deposit films of the same thickness on both sides of the substrate, as shown in Figure 14.2(b). The above equations are still applicable, with d_f being the sum of the thicknesses of the two films.

When a film is deposited on a compliant substrate that is held in a frame, and the structure is then released from the frame, the substrate may bend substantially. Although the stresses in the film and the substrate are biaxial, the substrate bends into a roll with a radius of curvature

$$R = \frac{\left(\bar{Y}_s d_s^2 - \bar{Y}_f d_f^2\right)^2 + 4\bar{Y}_f \bar{Y}_s d_f d_s (d_f + d_s)^2}{6\varepsilon_{(1+\nu)} \bar{Y}_s d_f d_s (d_f + d_s)}. \tag{14.7}$$

Here $\bar{Y} = Y/(1-\nu^2)$ is the plane strain elastic modulus (Timoshenko and Goodier 1970). For a compliant substrate, Equation (14.7) must be used instead of the Stoney formula (14.4), for example, when calculating the mismatch strain from the experimentally determined radius of curvature. Figure 14.4 shows the normalized radius of curvature, calculated using (14.4) and (14.7), plotted as a function of the film-to-substrate thickness ratio. For inorganic semiconductors and metals on a glass substrate, $Y_f/Y_s \cong 1$ and the Stoney formula is a good approximation if $d_f/d_s \leq 1$. For an organic polymer substrate, $Y_f/Y_s \cong 100$ and the Stoney formula is useful only for $d_f/d_s \leq 0.001$. With typical thicknesses of plastic substrates of 50–200 μm, $d_f/d_s \cong 0.01$ and (14.7) must be used. Another important conclusion from Figure 14.4 is that even with a compliant substrate, theoretically there are two regimes when the film/substrate couple is flat, i.e., $R \to \infty$: (1) the film is much thinner than the substrate and therefore must comply with it, and (2) the film is much thicker than the substrate and therefore the substrate must comply with the film.

Petitioner Samsung Ex-1011, 0297

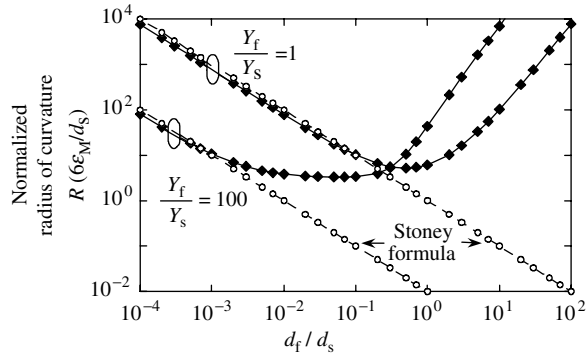


Figure 14.4 Normalized radius of curvature as a function of film/substrate thickness ratio. Two different substrate types are illustrated: glass or steel ($Y_f/Y_s \cong 1$) and organic polymer ($Y_f/Y_s \cong 100$). We assume that $\nu_f = \nu_s$. Full lines represent the exact solution of (14.7); dashed lines represent the approximation (14.4) for a thick, stiff substrate (Gleskova *et al.* 1998)

14.3.3 Bending by Externally Applied Moment

Let us analyze the strain in a blanket film deposited on a stiff foil substrate like steel or glass. Both fabrication process and externally applied bending moment cause strain in the film. We first consider the external bending moment. Figure 14.3 illustrates a sheet bent to a cylinder of radius R. The film and the substrate have thicknesses d_f and d_s and Young's moduli Y_f and Y_s. When the sheet is bent, the top surface is in tension and the bottom surface is in compression. One surface inside the sheet, known as the neutral surface, has no strain. The strain in the top surface ε_{top} equals the distance from the neutral surface divided by R. Typical silicon TFT materials and steel or glass have about the same Young's modulus. Consequently, the neutral surface is the mid-surface of the sheet, and the strain in the top surface is given by

$$\varepsilon_{top} = (d_f + d_s)/2R. \tag{14.8}$$

The minimum allowable radius of curvature scales linearly with the total thickness, assuming that the transistors fail upon reaching a critical value of strain.

Now let us look at the TFT film on a compliant substrate such as plastic. The film and the substrate have different elastic moduli ($Y_f > Y_s$), so that the neutral surface shifts from the mid-surface and toward the film. Consequently, the strain on the top surface is reduced, as given by

$$\varepsilon_{top} = \left(\frac{d_f + d_s}{2R}\right) \frac{1 + 2\eta + \chi\eta^2}{(1+\eta)(1+\chi\eta)}, \tag{14.9}$$

where $\eta = d_f/d_s$ and $\chi = Y_f + Y_s$. Figure 14.5 plots the normalized strain in the film versus d_f/d_s. Two kinds of substrate are compared: steel ($Y_f/Y_s \cong 1$) and plastic ($Y_f/Y_s \cong 100$). For given R and d_f/d_s, the compliant substrate can reduce the strain by as much as a factor of 5.

Petitioner Samsung Ex-1011, 0298

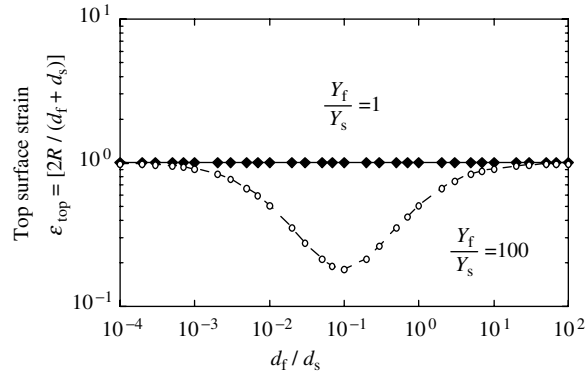


Figure 14.5 Normalized strain in the film as a function of film/substrate thickness ratio. Two types of substrate are illustrated: glass or steel ($Y_f/Y_s \cong 1$) and organic polymer ($Y_f/Y_s \cong 100$) (Suo *et al.* 1999)

The strain in a circuit is further reduced if it is placed in the neutral surface itself, sandwiched between the substrate and an encapsulation layer of suitable Young's modulus and thickness, Y_e and d_e. When the stiffness of the circuit proper is negligible, the circuit comes to lie in the neutral surface if

$$Y_s d_s^2 = Y_e d_e^2. \tag{14.10}$$

In this case, bending does not add any strain to the circuit. Consequently, the bending curvature is no longer limited by the failure strains of the transistor materials, but by those of the substrate and the encapsulation. When the substrate and encapsulation have low modulus and low thickness the whole structure can be bent to extremely small radii. Because a-Si TFTs can be made on substrates as thin as 3 μm (Ma and Wagner 1999), foldable TFT backplanes are possible.

To compare the data for a given strain ε between bending and stretching experiments, we calculate the strain ε under stretching from the load F measured with a load cell, using the following equation:

$$\varepsilon = \frac{F}{Y_f A_f + Y_s A_s},$$

where A_f and A_s are the cross-sectional areas of film and substrate. It assumes a linear relationship between stress and strain (elastic deformation), which in our experience is a reasonable assumption for a-Si TFTs on a polyimide substrate.

14.4 Effects of Mechanical Strain on a-Si TFTs

a-Si TFTs respond to increasing mechanical strain by elastic deformation followed by fracture (Ma *et al.* 1997; Gleskova *et al.* 1999). In measurements of TFTs on organic polymer substrates, we find transition regimes where the TFT fails but electrical function is restored

Petitioner Samsung Ex-1011, 0299

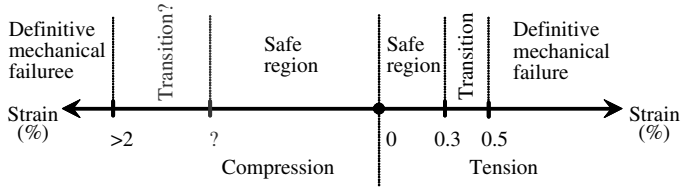


Figure 14.6 Summary of the response of a-Si TFTs to mechanical strain

when the strain is reduced (Gleskova 2002). This phenomenon, which can cause confusion in tests, is believed to result from the electrical opening and closing of a crack in the TFT channel. The safe regimes of elastic deformation and the regimes of temporary and definitive failure explored by experiments are illustrated in Figure 14.6.

Under elastic deformation up to fracture the transport properties of the TFT change reversibly (Gleskova *et al.* 1999; Gleskova 2003). The electron mobility is reduced by compressive strain and is raised by tensile strain as shown in Figure 14.7. These mobility changes correlate with a broadening or steepening of the conduction band tail in a-Si (Gleskova *et al.* 2002).

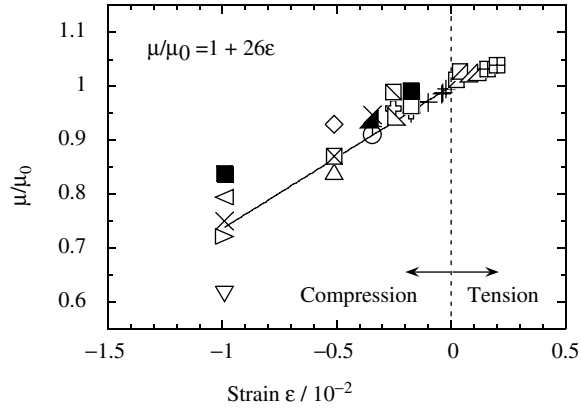


Figure 14.7 Electron mobility in a-Si TFTs plotted as a function of strain. Each symbol represents a different TFT. Empty and full symbols correspond to TFTs with the bending direction parallel and perpendicular to the source–drain current path, respectively. The linear fit is for TFTs with the bending direction parallel to the source–drain current path (Gleskova *et al.* 2002)

a-Si TFTs can be strained more in compression than in tension. The theory of fracture of stiff films on stiff substrates provides a guide to explaining this difference in critical (fracture) strains (Suo 2001). In tension the TFTs fail by crack propagation from pre-existing defects. In compression they fail by delamination followed by buckling and fracture. Fracture under tensile stress is illustrated in Figure 14.8(a), where a crack propagates from a pre-existing flaw. Equation (14.11) gives the condition for crack formation. The

Petitioner Samsung Ex-1011, 0300

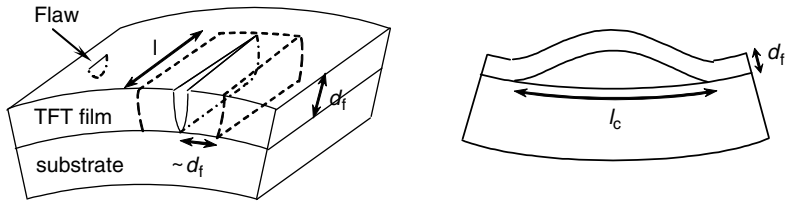


Figure 14.8 Failure mechanisms of a-Si TFT layers in (a) tension and (b) compression (Suo *et al.* 1999)

dimensionless constant χ depends on the elastic constants of the film and the substrate; it can be very large for a stiff film on a compliant substrate. Γ is the specific surface energy in the crack. However, (14.11) provides only a qualitative guide, because experiments with glassy materials show that cracks can propagate at a critical stress much higher than predicted by (14.11). It agrees qualitatively with the observation that films crack more easily as their thickness is built up.

$$2\chi\frac{(1-\nu_f)\sigma_f^2 d_f^2 l}{Y_f} > 2\Gamma l d_f. \tag{14.11}$$

Fracture under compressive stress, which is illustrated in Figure 14.8(b), occurs if the film debonds from the substrate. If the debonded area is sufficiently large, the film buckles and then fractures. The critical debonding length for buckling is given by

$$l_c = \frac{\pi d_f}{\sqrt{3(1-\nu_f^2)}}\sqrt{\frac{Y_f}{\sigma_f}}. \tag{14.12}$$

Estimates of critical debonding length for a-Si TFTs on Kapton polyimide show that $l_c = 10d_{film}$ for $Y_{film}/\sigma_{film} = 0.02$. Suppose we have a device film with $d_{film} = 1\,\mu m$, the critical debonding length is $l_c = 10\,\mu m$. In structures fabricated in a clean room this would be an unusually large defect. Therefore TFT/substrate structures are robust under compression. TFTs under compression have been observed to fracture if the substrate underneath first ruptures under the corresponding tensile strain that it experiences (Suo 2001; Kattamis 2004).

Cracking of device layers on polymer substrates can be suppressed by cutting the films into islands to expose the bare substrate. When TFT backplanes are going to be shaped to conformal surfaces, the TFTs must be placed on rigid device islands.

14.5 Shaping of TFT Backplanes by Plastic Deformation

The deformation of a TFT backplane from a flat surface to a conformal surface may require a large, tensile, plastic deformation. A flat disk can be shaped to a dome by applying gas pressure to one side of the disk as shown in Figure 14.9 (Hsu *et al.* 2000; Hsu *et al.* 2002b,

Petitioner Samsung Ex-1011, 0301

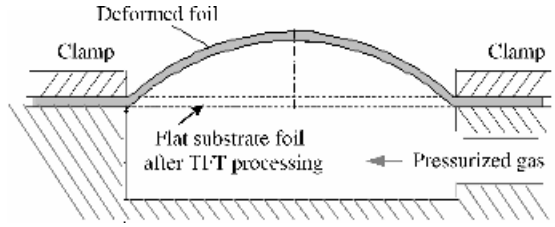


Figure 14.9 Apparatus for shaping a flat TFT backplane to a dome (Hsu *et al.* 2002b)

Hsu *et al.* 2004). Because the strain may easily exceed the critical fracture strain of a-Si TFTs of 0.3–0.5% shown in Figure 14.6, the TFTs are placed on rigid island platforms (Hsu *et al.* 2002 [2002a]). Rows of such islands can be seen in Figure 14.1(b). The size and thickness of islands that can withstand deformation to a given radius (or field of view) of the dome are determined by experiment. The island size is of the order of the substrate thickness.

The contour plot of Figure 14.10 shows the radial strain distribution in an organic polymer substrate around one rigid island. For the calculation by finite element modeling, a 0.5 μm thick silicon island with 100 μm diameter was placed in the center of a 200 μm diameter disk of a 50 μm thick Kapton E polyimide substrate (Hsu 2003). The substrate was stretched radially at its periphery to an average biaxial tension of 6%. Because the island is only 0.5 μm thick, its cross section is too thin to be seen in Figure 14.10. The strain in the island is the same as in the island/substrate interface. The strain in the substrate underneath the island is pinned to low values by the high elastic modulus of the island. Deep below the island, the strain increases and it is large in the exposed substrate surface.

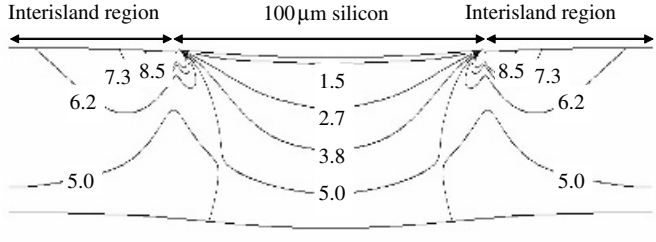


Figure 14.10 Contour plot of the radial strain (%) in a polyimide substrate with a round silicon island, after stretching. See text for details (Hsu 2003)

As long as the strain in the island is kept below its critical fracture strain, the island and the devices placed on it remain intact. However, islands and devices do exhibit secondary effects and we will discuss two of them: slip of the island edge and compressive buckling of the island. The strain concentration in the polymer substrate at the edge of the island, evident in Figure 14.10, can cause the island edge to slip on the substrate. Substrate newly exposed by this slip is visible in the scanning electron micrograph of Figure 14.11, which shows the edge of an SiN_x island on a Kapton E polyimide substrate (Bhattacharya 2003). The slip may

Petitioner Samsung Ex-1011, 0302

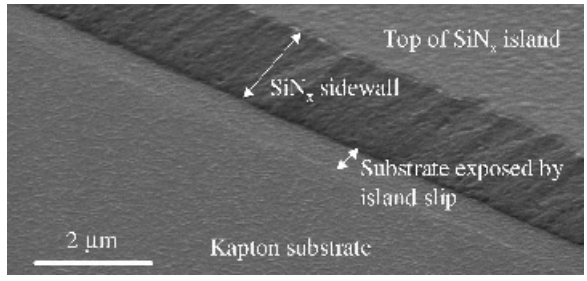


Figure 14.11 SEM micrograph of the edge of an SiN_x island on a polyimide foil after deformation of the foil to a dome. The substrate exposed by island slip is seen at the edge of the island (Bhattacharya 2003)

be accompanied by local delamination of the island at its perimeter. Both slip and delamination present challenges to the fabrication of electrically continuous interconnect.

When the force (pressure) that expands the substrate disk to the dome is released, the dome partly relaxes by elastic snap-back. This relaxation corresponds to the step from point 2 to point 3 shown in Figure 14.12. It puts the rigid islands in compression. The ensuing buckling of the islands has been observed by optical microscopy (Bhattacharya 2003) and atomic force microscopy (Salomon 2003), and the compressive strain is manifest in a reduced electron mobility of the a-Si TFTs that are fabricated on the islands (Hsu *et al.* 2004).

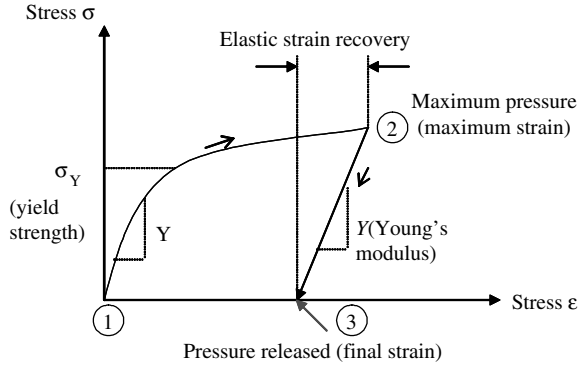


Figure 14.12 Stress–strain diagram illustrating the tensile shaping of a polymer substrate (step 1 to 2) followed by elastic snap-back (step 2 to 3) (Hsu *et al.* 2002b)

As illustrated by Figure 14.8(a), TFTs fail in tension by brittle fracture, which can be suppressed by passivation of the flaws on which cracks nucleate. Some evidence suggests that TFTs can be passivated by organic overlayers. Quantitative evidence for such passivation comes from recent work with islands of indium tin oxide (ITO), also a brittle material. Figure 14.13 shows the yield of intact square islands of 150 nm thick ITO on a 175 μm thick substrate of polyethylene terephthalate (PET). The islands are equispaced and cover 44% of the substrate. A 6 cm diameter disk covered with islands was deformed to a dome with 10 cm

Petitioner Samsung Ex-1011, 0303

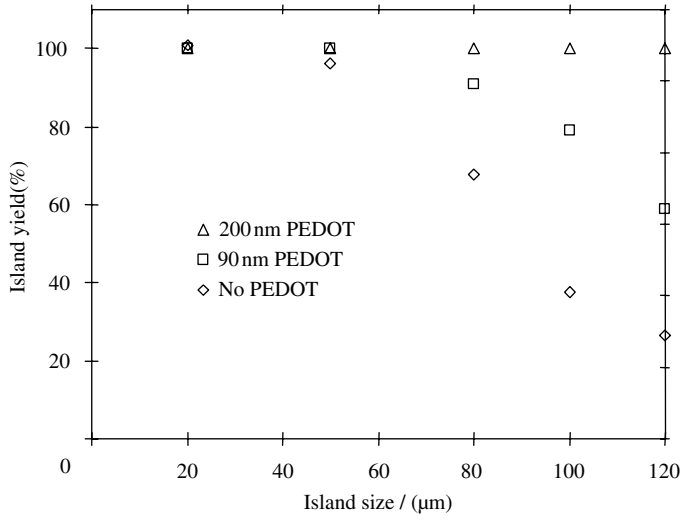


Figure 14.13 Yield of crack-free ITO islands on PET versus island size, without PEDOT cover and for two different thicknesses of PEDOT coverage (Bhattacharya *et al.* 2004)

radius of curvature, which produced an average strain of 1.6%. The yield of crack-free ITO islands is seen to decrease with increasing island size. The yield is raised noticeably when the entire surface is coated with a blanket organic overlayer, and more so when this overlayer is made thick. In this particular case the overlayer is of poly-3,4-ethylenedioxythiophene (PEDOT), but the effect has been observed with other organic overlayers as well (Bhattacharya *et al.* 2004).

14.6 Case Studies of Stiff TFT Films on Organic Polymer Substrates

We use three examples to illustrate the mechanics of stiff device films on compliant substrates: (1) evaluation of built-in stress in a device film, (2) control of mask overlay alignment by adjustment of this built-in stress, and (3) determination of electrical failure of TFTs after bending to progressively smaller radii of curvature.

14.6.1 Evaluating Built-in Stress in a Device Film

Film stress is extracted from the radius of curvature R using (14.7), instead of (14.4) for stiff samples. On sufficiently rigid samples, R can be measured with a surface profiler. In samples with low mechanical strength, the laser reflection technique can be used. Samples with low strength may bend under their own weight. Then R can be measured when the samples are stood on end as shown in Figure 14.14 (Cheng 2004b). If R is not uniform, an average must be estimated.

Petitioner Samsung Ex-1011, 0304

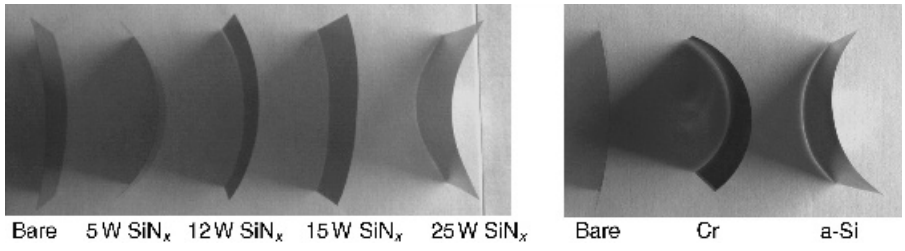


Figure 14.14 Stress-induced curvatures of (a) SiN_x films deposited at various deposition powers and (b) Cr and a-Si films, all on 51 μm thick Kapton E polyimide substrates. The 300–500 nm thick SiN_x and the 250 nm a-Si films were deposited at 150 °C; the thermally evaporated Cr film is 80 nm thick. The built-in stress in the SiN_x film can be adjusted by deposition power. The built-in stresses of Cr and a-Si:H films are tensile and compressive, respectively. The films are on the left-hand side of the substrates (Cheng 2004)

The net curvature produced in the samples $K = 1/R$, as in the samples of Figure 14.14, is the sum of the ''effective'' curvature introduced by processing and the curvature $K_0 = 1/R_0$ of the as-received, bare, substrate. (A sheet of polymer foil cut from a roll is usually curved.) Figure 14.15 plots values for the effective curvature $1/R - 1/R_0$ for samples with plasma-ehnaced chemical vapor deposition (PECVD) SiN_x films on Kapton E polyimide.

The sign of the radius of curvature R is defined as negative when films face outward (convex), because the film is in compression, i.e., $\varepsilon_f < 0$. R is positive when the film faces inward (concave) because the film is in tension, i.e., $\varepsilon_f > 0$. This sign definition is opposite to that in bending by an externally applied moment, because we are now dealing with an

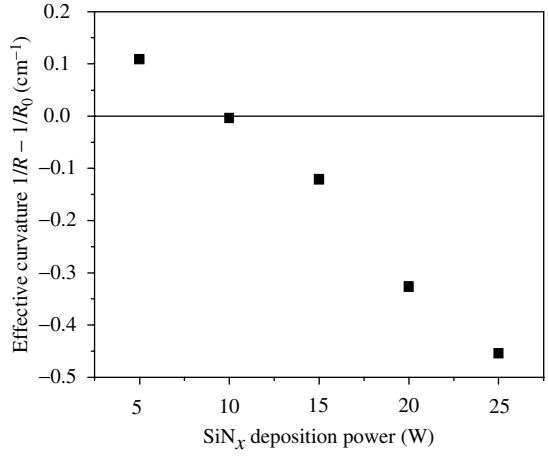


Figure 14.15 Effective curvature produced by PECVD deposition of 300 nm thick SiN_x at 150 °C on 51 μm thick Kapton E polyimide substrates. Substrates are preheated for 50 min in vacuum; radii are measured after 30 min cooling in vacuum, at room temperature and RH = 29% (Cheng 2004)

Petitioner Samsung Ex-1011, 0305

internally produced, film stress induced, curvature. The total mismatch strain ε_{M} is given by

$$\varepsilon_{\mathrm{M}} = \varepsilon_{\mathrm{th}} + \varepsilon_{\mathrm{ch}} + \varepsilon_0, \tag{14.13}$$

Where the thermal mismatch strain $\varepsilon_{\mathrm{th}}$ is given by

$$\varepsilon_{\mathrm{th}} = (\alpha_{\mathrm{f}} - \alpha_{\mathrm{s}}) \times (T_{\mathrm{dep}} - T_{\mathrm{room}}), \tag{14.15}$$

and the mismatch strain produced by moisture absorption $\varepsilon_{\mathrm{ch}}$, in a sample that was dried completely before vacuum processing and afterwards was brought into air for measuring R, is given by

$$\varepsilon_{\mathrm{ch}} = -(\beta_{\mathrm{f}} - \beta_{\mathrm{s}}) \times \ \%\,\mathrm{RH}. \tag{14.16}$$

We use the symbol β for the coefficient of humidity expansion, and %RH stands for percent of relative humidity. Table 14.2 shows the data used in the extraction of the built-in stress in SiN_x films on Kapton E foil substrates.

Now we are able to approximate the total mismatch strain ε_{M} from the measured radius of curvature R, using the tabulated material properties Y and ν, and the thicknesses d:

$$\varepsilon_M = \frac{\left(\bar{Y}_{\mathrm{s}} d_{\mathrm{s}}^2 - \bar{Y}_{\mathrm{f}} d_{\mathrm{f}}^2\right)^2 + 4\bar{Y}_{\mathrm{f}}\bar{Y}_{\mathrm{s}} d_{\mathrm{f}} d_{\mathrm{s}} (d_{\mathrm{f}} + d_{\mathrm{s}})^2}{6_{(1+\nu)}\bar{Y}_{\mathrm{s}} d_{\mathrm{f}} d_s (d_{\mathrm{f}} + d_{\mathrm{s}})} \left(\frac{1}{R} - \frac{1}{R_0}\right), \tag{14.17}$$

Equation (14.17) is identical to (14.7), except that we consider the radius of the substrate before film deposition, R_0.

Now we subtract from ε_{M} the thermal mismatch strain $\varepsilon_{\mathrm{th}}$ and the humidity expansion strain $\varepsilon_{\mathrm{ch}}$ (14.14). Left over is the built-in strain ε_0 produced by film growth as shown in Figure 14.16.

Table 14.2 Data used in extracting the built-in stress in SiN_x films on Kapton E foil substrates

	Kapton E	SiN_x deposited at 150 °C ($T_{\mathrm{dep}} - T_{\mathrm{room}} = 125$ °C)
Young's modulus (GPa)	$Y_{\mathrm{s}} = 5.3$	$Y_{\mathrm{f}} = 210$
Poisson's Ratio	$\nu_{\mathrm{s}} = 0.32$	$\nu_{\mathrm{f}} = 0.25$
Biaxial stress modulus (GPa)	$Y_{\mathrm{s}}^* = 7.8$	$Y_{\mathrm{f}}^* = 280$
Plane strain modulus (GPa)	$\bar{Y}_{\mathrm{s}} = 5.9$	$\bar{Y}_{\mathrm{f}} = 224$
Coefficient of thermal expansion (ppm/K)	$\alpha_{\mathrm{s}} = 16$	$\alpha_{\mathrm{f}} = 2.7$
Coefficient of humidity expansion (ppm/% RH)	$\beta_{\mathrm{s}} = 8$	$\beta_{\mathrm{f}} = 0$
Radius of curvature of substrate as received (cm)	$R_0 = 14.3$	$R_0 = 14.3$

Petitioner Samsung Ex-1011, 0306

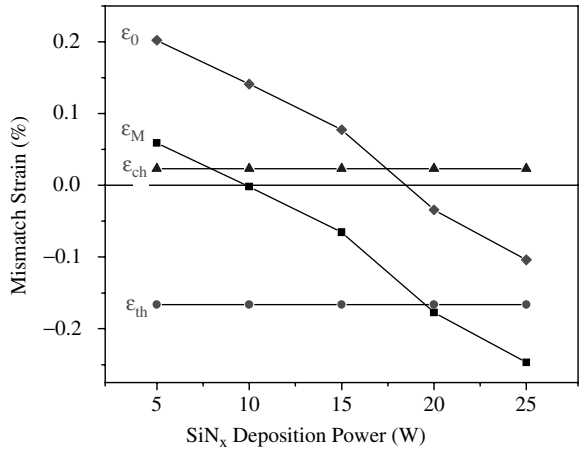


Figure 14.16 Mismatch strain components calculated or extracted for the samples of Figure 14.15. The horizontal line denotes zero strain. The film is under tension at positive strain and compression at negative strain. (Cheng, 2004a)

Next we calculate the built-in stress in the film after the deposition is completed while the sample is still held flat in a frame. Assuming that the built-in strain, ε_0, does not change during cooling and/or after releasing from the frame, the built-in stress in the film, σ_0^{f}, can be expressed by (14.18) and an example is shown in Figure 14.17.

$$\sigma_0^{\mathrm{f}} = \frac{Y_{\mathrm{f}}^* Y_{\mathrm{s}}^* d_{\mathrm{s}}}{Y_{\mathrm{f}}^* d_{\mathrm{f}} + Y_{\mathrm{s}}^* d_{\mathrm{s}}} \times \varepsilon_0 \tag{14.18}$$

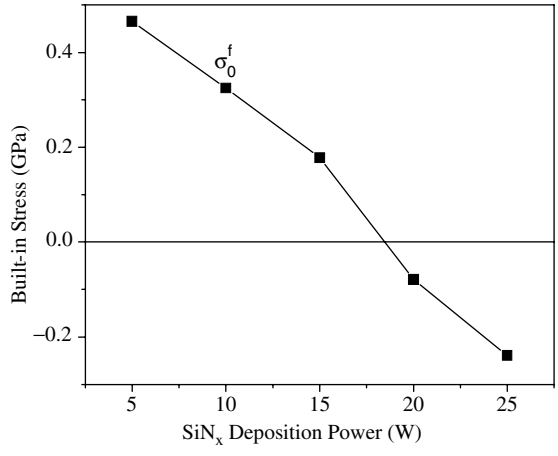


Figure 14.17 Built-in stress in the film when the sample is held in a frame. The stress is calculated or extracted for the samples of Figure 14.15. The horizontal line denotes zero stress. Positive stress stretches and negative stress compresses the film.

Petitioner Samsung Ex-1011, 0307

14.6.2 Controlling Mask Overlay Alignment by Adjusting Built-in Stress

Varying curvature corresponds to varying size of the flattened sample. Stress-induced curvature that varies during backplane fabrication causes misalignment in overlay registration. It is possible to improve the overlay registration by stress management in the device layers (Cheng 2004a).

TFTs were fabricated in the non-self-aligned, back channel etched geometry of Figure 14.2(b) on 2 mil (51 μm) thick, 70 mm × 70 mm square Kapton E polyimide substrates. The samples were carried as freestanding films through most of the process steps except photolithography, where they were temporarily bonded to glass by the surface tension of water. (Figure 14.16 shows that the uptake and release of water by the polyimide has a secondary effect compared to built-in and thermal stress.) We monitored the degree of misalignment between the first and second photolithography levels, i.e., the bottom gate and the source/drain. Their alignment is crucial to setting source/gate and gate/drain overlaps. At both levels we aligned to a mark at the center of the substrate, and measured the misalignment of four marks lying at the corners of a 52 mm × 52 mm square, with each mark close to a corner of the substrate.

Between the two photolithographic steps fell the deposition at 150°C of the silicon stack, composed of (i) 300 nm SiN_x gate dielectric, (ii) 200 nm i a-Si channel, (iii) 50 nm n^+ a-Si source/drain and (iv) Cr source/drain contact. To quantify the stress compensation, we kept all these layers the same except for intentionally varying the built-in stress in the gate SiN_x from tensile to compressive. This we did by tuning the deposition power from low to high, 5 W, 12 W, 25 W (22, 53, 111 mW/cm^2), which results in an effective stress in the film stack ranging from highly tensile to slightly tensile to slightly compressive (Figure 14.14). The corresponding overlay misalignment is illustrated by Figure 14.18. The sample is seen to shrink substantially with a 5 W gate SiN_x, shrink slightly at 12 W, and expand somewhat at 25 W. The TFT transfer characteristics of Figure 14.19 show that varying the deposition power has only a slight effect on electrical performance: I_{on} at $V_g = 25$V drops slightly as the tensile stress is reduced, in agreement with the mobility change shown in Figure 14.7.

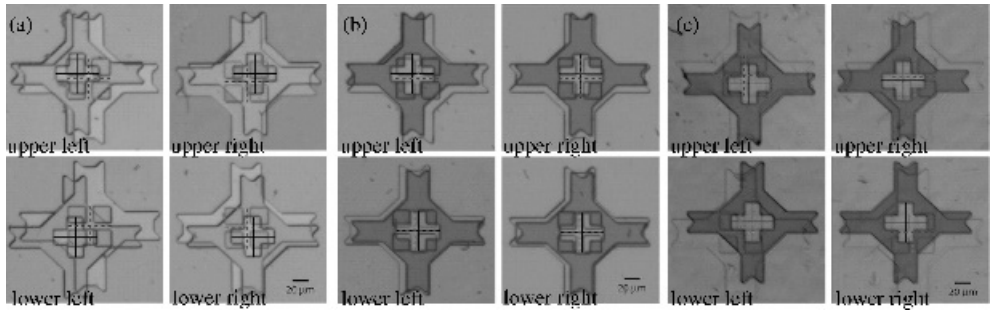


Figure 14.18 Overlay misalignment between the first, bottom gate, and second, source/drain, photolithography levels in back channel etched a-Si TFT process with (a) 5 W gate SiN_x, (b) 12 W gate SiN_x and (c) 25 W gate SiN_x. The frames lie 52 mm apart near the corners of the 70 mm square substrate. The dashed crosses mark the center at the gate mask level and the solid crosses the center at the source/drain mask levels. The sample is seen to shrink substantially with 5 W SiN_x, to shrink slightly with 12 W SiN_x, and to expand substantially with 25 W SiN_x (Cheng 2004)

Petitioner Samsung Ex-1011, 0308

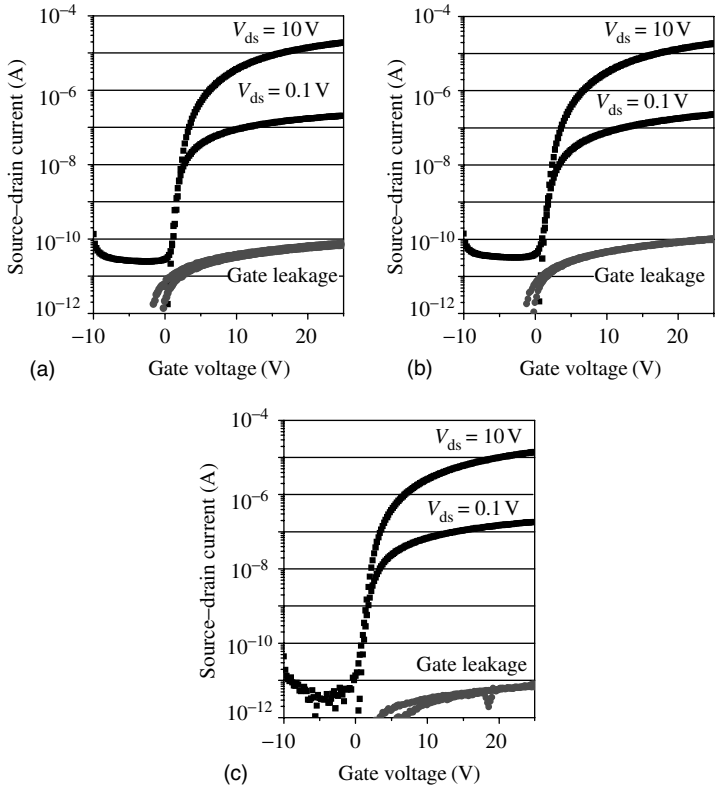


Figure 14.19 Transfer characteristics of the TFTs in Figure 14.17: (a) 5 W SiN_x, (b) 12 W SiN_x, (c) 25 W SiN_x. The TFT gates are 80 μm wide and 10 μm long (Cheng 2004)

Thus adjusting stress in the SiN_x layer is a realistic technique for controlling overlay alignment for a-Si TFT circuits on a compliant substrate.

14.6.3 Determining Electrical Failure of a-Si TFTs after Bending

Because elastic deformation has a small and reversible effect on the electrical performance of a-Si TFTs, the critical radius where the TFTs fracture may be all the information that is needed. The only mechanical test needed may be bending the backplane to progressively sharper radii, and in between measuring the TFT characteristics on the flattened substrate (Gleskova *et al.* 1999). We bent TFTs on Kapton substrates outward, top surface of Figure 14.3(b), or inward, bottom surface of Figure 14.3(b) (Gleskova *et al*. 1999). Single TFTs were bent to decreasing R, beginning with $R = 4$ mm down to $R = 0.5$ mm. The TFT was stressed for 1 min at each bending radius then released, flattened and remeasured. Figure 14.20 summarizes the effects of inward/compressive and outward/tensile bending on TFT performance. The upper graphs show the on-current I_{on}, the off-current I_{off}, and the gate leakage current I_{leak} as functions of the radius of curvature. The lower graphs show the threshold voltage V_T and the saturated electron mobility μ_n, calculated from the transfer

Petitioner Samsung Ex-1011, 0309

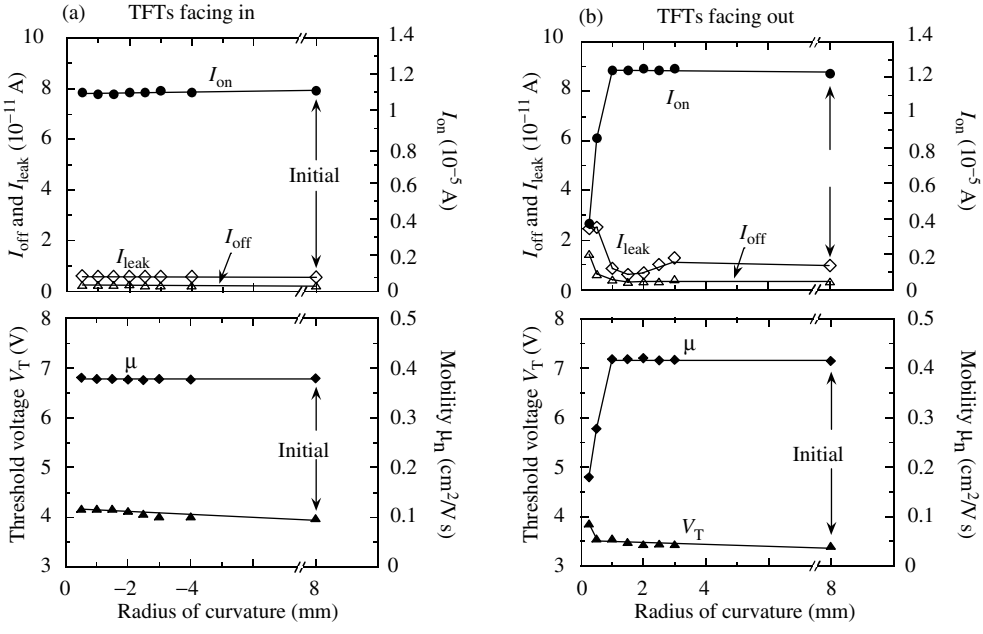


Figure 14.20 On-current, source–gate leakage current, off-current, electron mobility and threshold voltage in the saturation regime as functions of bending radius. I_{off} is the smallest source–drain current at $V_{ds} = 10\,V$, I_{on} is the source–drain current for $V_{ds} = 10\,V$ and the gate voltage $V_{gs} = 20\,V$, and I_{leak} is the source–gate current for $V_{ds} = 10\,V$ and $V_{gs} = 20\,V$. Outward bending R is defined positive, inward bending negative. The as-fabricated radius, before bending, was 8 mm. Differences between the ''initial'' characteristics reflect spread between as-fabricated TFTs (Gleskova *et al.* 1999)

characteristic at source–drain voltage $V_{ds} = 10V$. Differences between the ''initial'' characteristics reflect spread between as-fabricated TFTs.

Inward/compressive bending down to $R = 0.5$ mm, left column of Figure 14.19, shows that the TFT can be compressed by at least 2% without failing. In outward/tensile bending, right column of Figure 14.19, no substantial changes are observed down to $R = 1$ mm (0.5% strain). After bending to sharper radii some TFTs had failed. The electrical failure was caused by periodic cracks in the TFT island that run perpendicular to the bending direction.

14.7 Summary and Outlook

Research on flexible TFT backplanes remains focused on materials and processes for backplane fabrication. Initial exploration of the limits of bending and shaping made clear that TFT backplanes can be bent tightly and even folded. Work on backplane mechanics has now moved to design of materials and processes for film integrity, and control of substrate dimensions, during fabrication. Accurate control of substrate dimensions by mounting on temporary carriers for production on plates and eventually roll-to-roll is an important goal. Detailed experiments and theory on the mechanics of layered and patterned structures will

Petitioner Samsung Ex-1011, 0310

help design locally stable films and dimensions. Further layering and lamination of the TFT backplane to a finished product will raise mechanical issues that are similar to those encountered in backplane mechanics. Conformally shaped and elastomeric TFT backplanes will continue to provide demanding subjects for experimental and theoretical mechanics, the latter challenged by the need for providing simple if approximate analytical tools. The gradual introduction of organic electronics will expand the mechanical boundaries of TFT backplanes and undoubtedly will present new tasks to the researcher.

Many signals indicate that the mechanics of electronic surfaces will remain important and demanding for a long time to come: the rapid growth of the flat panel display industry; the growing number of techniques for fabricating thin film electronics by potentially inexpensive processes; the demonstration of new display, sensor, and actuator frontplane functions; and widespread interest in large screens, unbreakable and wearable electronics, e-textiles, and electronic skins.

References

Bhattacharya, R. (2003) Princeton University, unpublished work.

Bhattacharya, R., Wagner, S., Tung, Y.-J., Esler, J. and Hack, M. (2004) In *Conference Record of the 2004 IEEE International Electron Devices Meeting*. San Francisco, 13–15 December 2004, in press.

Bonse, M., Huang, J. R., Wronski, C. R. and Jackson, T. N. (1998) *IEDM Technical Digest*, pp. 253–256.

Brody, T. P. (1996) *Journal of the SID* **4**, 113–127.

Burns, S. G., Shanks, H., Constant, A., Gruber, C., Schmidt, D., Landin, A. and Olympie, F. (1997) *Proceedings of the Electrochemical Society* **96**(23), 382–390.

Cheng, I.-C. (2004) Princeton University, unpublished work.

Constant, A., Burns, S. G., Shanks, H., Gruber, C., Landin, A., Schmidt, D., Thielen, C., Olympie, F., Schumacher, T. and Cobbs, J. (1994) *Proceedings of the Electrochemical Society* **94**(35), 392–400.

Gleskova, H. (2003) Princeton University, unpublished work.

Gleskova, H., Wagner, S. and Shen, D. S. (1995) *IEEE Electron Device Letters* **16**, 418–420.

Gleskova, H., Ma, E. Y., Wagner, S. and Shen, D. S. (1996) In *Digest of Technical Papers for the 1996 Display Manufacturing Technical Conference*, SID, Santa Ana CA, San Jose CA, pp. 97–98.

Gleskova, H., Wagner, S. and Suo, Z. (1998) *Materials Research Society Symposium Proceedings* **508**, 73–78.

Gleskova, H., Wagner, S. and Suo, Z. (1999) *Applied Physics Letters* **75**, 3011–3013.

Gleskova, H., Wagner, S., Soboyejo, W. and Suo, Z. (2002) *Journal of Applied Physics* **92**, 6224–6229.

Gray, D. S., Tien, J. and Chen, C. S. (2004) *Advanced Materials*, **16**, 393–397.

Hsu, P.-H. I. (2003) Electrical Engineering, Princeton University, Ph.D. Thesis.

Hsu, P.-H. I., Huang, M., Wagner, S., Suo, Z. and Sturm, J. C. (2000) *Materials Research Society Symposium Proceedings* **621**, Q8.6.1–Q8.6.6.

Hsu, P.-H. I., Bhattacharya, R., Gleskova, H., Huang, M., Xi, Z., Suo, Z.,Wagner, S. and Sturm, J. C. (2002a) *Applied Physics Letters* **81**, 1723–1725.

Hsu, P.-H. I., Gleskova, H., Bhattacharya, R., Xi, Z., Suo, Z., Wagner, S. and Sturm, J. C. (2002b) Paper G1.8 presented at the Materials Research Society Spring 2002 Meeting, San Francisco CA.

Hsu, P.-H. I., Huang, M., Gleskova, H., Xi, Z., Suo, Z., Wagner, S. and Sturm, J. C. (2004) *IEEE Transactions on Electron Devices* **51**, 371–377.

Jones, B. L. (1985) *Journal of Non-Crystalline Solids* **77/78**, 1405–1408.

Kattamis, A. (2004) Princeton University, unpublished work.

Lacour, S. P., Wagner, S., Huang, Z. and Suo, Z. (2003) *Applied Physics Letters* **82**, 2404–2406.

Petitioner Samsung Ex-1011, 0311

Lueder, E., Muecke, M. and Polach, S. (1998) In *Proceedings of the 18th SID International Display Research Conference, Asia Display '98*, pp. 173–177.

Lumelsky, V., Shur, M. and Wagner, S. (2001) *IEEE Sensors Journal* **1**, 41–51.

Ma, E. Y. and Wagner, S. (1999) *Applied Physics Letters* **74**, 2661–2662.

Ma, E. Y., Theiss, S. D., Lu, M. H., Wu, C. C., Sturm, J. C. and Wagner, S. (1997) *IEDM Technical Digest*, pp. 535–538.

MacDonald, B. A., Rollins, K., Eveson, R., Rakos, K., Rustin, B. A. and Handa, M. (2003) *Materials Research Society Symposium Proceedings* **769**, H9.3.1–H9.3.8.

Parsons, G. N., Yang, C. S., Arthur, C. B., Klein, T. M. and Smith, L. (1998) *Materials Research Society Symposium Proceedings* **508**, 19–24.

Salomon, A. (2003) Electrical Engineering Princeton University, M. Eng. Thesis.

Sandoe, J. N. (1998) *Society for Information Display 1998 International Symposium Digest of Technical Papers*, SID, Santa Ana, CA, **29**, 293–296.

Spear, W. E. and Heintze, M. (1986) *Phiosophical Magazine B* **54**, 343–358.

Suo, Z. (2001) In *Encyclopedia of Materials: Science and Technology* 2nd Ed. London: Elsevier, pp. 3290–3296.

Suo, Z., Ma, E. Y., Gleskova, H. and Wagner, S. (1999) *Applied Physics Letters* **74**, 1177–1179.

Theiss, S. D. and Wagner, S. (1996) *IEEE Electron Device Letters* **17**, 578–580.

Theiss, S. D., Carey, P. G., Smith, P. M., Wickboldt, P., Sigmon, T. W., Tung, Y. J. and King, T.-J. (1998) In *Technical Digest of the IEEE 1998 International Electron Devices Meeting*, pp. 257–260.

Timoshenko, S. P. and Goodier, J. N. (1970) *Theory of Elasticity*: New York: McGraw-Hill.

Wagner, S., Gleskova, H., Sturm, J. C. and Suo, Z. (2000) In *Technology and Applications of Hydrogenated Amorphous Silicon* (ed. R.A. Street). Berlin: Springer, pp. 222–251.

Wagner, S., Lacour, S. P., Jones, J., Hsu, P.-H. I., Sturm, J. C., Li, T. and Suo, Z. (2004) *Physica E* **25**, 326–334.

Young, N. D., Trainor, M. J., Yoon, S.-Y., McCulloch, D. J., Wilks, R. W., Pearson, A., Godfrey, S., Green, P. W., Rosendall, S. and Hallworth, E. (2003) *Materials Research Society Symposium Proceedings* **769**, H2.1.1–H2.1.12.

Petitioner Samsung Ex-1011, 0312

15

OLED Displays on Plastic

Mark L. Hildner

DuPont Displays

15.1 Introduction

Organic light-emitting diode (OLED) technology has captured tremendous interest and has rapidly developed since the discovery of organic electroluminescence roughly 15 years ago. Commercial OLED displays on glass are now available and the industry is poised for substantial growth in the next few years. Much of the attention given to OLEDs is due to the performance advantages that it has over other types of flat panel display (FPD) technologies, including the industry dominant liquid crystal displays (LCDs). Recognized advantages include nearly Lambertian emission, which provides wider viewing angles than LCD; fast response times, which facilitate grayscale and video capabilities in active matrix applications; and low-voltage operation, which leads to low-cost components and low-profile packaging. Furthermore, the high efficiency of OLED materials makes OLED the lowest-power emissive FPD technology and offers the potential for lower power consumption than backlit LCDs.

An additional factor giving OLED technology impetus, perhaps to an extent equal to the performance advantages, is the perception that OLEDs are a natural choice for flexible displays. The very thin structure (the active layers are less than 1 μm), solid-state construction (there is no cell gap as in an LCD), and active material composition of an OLED are very suitable for flexibility. These characteristics, combined with the performance characteristics, have many thinking that OLED is the technology path to high-performance full-color flexible displays.

Flexible Flat Panel Displays Edited by G. P. Crawford
© 2005 John Wiley & Sons, Ltd., ISBN 0-470-87048-6

Petitioner Samsung Ex-1011, 0314

The two main types of OLED are based on small molecules and conjugated polymers. Small-molecule OLEDs (SMOLEDs) were first reported by Tang and VanSlyke (1987) and are typically thermally evaporated. Light emission from polymer OLEDs (PLEDs) was first reported by Burroughes *et al.* (1990), where a solution-processable precursor polymer was deposited by spin coating and then thermally converted at high temperature ($\geq 250\,^{\circ}\mathrm{C}$). Then Braun and Heeger (1991) were able to make a light-emitting device with a polymer that was soluble in its conjugated form, thus eliminating the need for high-temperature processing. Solution processing at low temperatures may revolutionize how displays are manufactured because it permits a number of process options (spin coating, inkjet printing, dipping, spraying, etc.) that are lower cost than vacuum deposition; it would replace much of the vacuum processing used in today's FPD fab; it can cover large areas; and it is well suited for roll-to-roll manufacturing, which may lead to further cost reduction from the current batch process. That is why this chapter will focus on conjugated polymer OLEDs.

A number of flexible materials are being explored as OLED substrates. The first flexible OLED display demonstration was on a transparent plastic substrate (Gustafsson *et al.* 1992). Plastic is a logical choice because its transparency allows much of the architecture of an OLED on glass to be used. Plastic is rugged, more so than regular glass; able to be accurately cut with a laser, allowing for irregular shapes with the only downside being some discoloration at the cutting site; and is already incorporated into roll-to-roll process technology, both in its own manufacture and current applications.

While flexibility may be the ultimate goal for OLED displays on plastic, there are significant opportunities that are less technologically demanding than a display that can be flexed or rolled up multiple times. A flat plastic OLED display is thin, lightweight, and rugged. These are significant attributes that may be taken advantage of in mobile applications. Plastic displays can be easily cut into a wide variety of nonrectangular shapes, and can be bent into a curved, but rigid, format. These characteristics allow greater freedom in product design. Even for these nonflexible display manifestations, there are significant development challenges to bringing a plastic OLED display to the marketplace.

After a brief introduction describing how a PLED display works, this chapter will present the challenges associated with two key technology developments that must take place. The first is to obtain a plastic substrate that can withstand processing and lead to a reliable and long-lived device. The second is to obtain an understanding of the manufacturing issues associated with a plastic substrate, and then to incorporate this understanding into device processing. The issues associated with making a passive matrix (PM) OLED will then be discussed, and finally, there will be a review of thin film transistor technologies that are appropriate for plastic active matrix (AM) backplanes.

15.2 PLED Basics

15.2.1 Conjugated Polymers

Conjugated polymers are characterized by alternating single and double or single and triple bonds (Heeger 2001). Overlapping of the p_z orbitals from the double or triple bonds along the polymer backbone leads to the formation of a delocalized π-bonding system. This gives rise to energy bands similar to those in an inorganic semiconductor. The occupied π-band, analogous to the valence band, is comprised of hole-transport states, and the highest

Petitioner Samsung Ex-1011, 0315

occupied molecular orbital (HOMO) is analogous to the valence band edge. The unoccupied π^*-band, analogous to the conduction band, is comprised of electron-transport states, and the lowest unoccupied molecular orbital (LUMO) is analogous to the conduction band edge. Despite this analogy, charge transport in conjugated polymers differs in a number of ways from that in inorganic semiconductors (Patel *et al.* 2002): intrinsic and extrinsic carriers are generally negligible and conduction is dominated by injected carriers; the polymer chains distort around the charge carrier so that the charged excitation is best described as a polaron (the charge plus the distortion); and the energy bands are inhomogeneously broadened due to the amorphous polymer structure and, therefore, transport is through hopping along or between polymer chains.

15.2.2 Light-Emitting Diodes

A conjugated polymer can emit light because it has an energy gap. Figure 15.1 shows three common light-emitting polymers: poly(*p*-phenylenevinylene) or PPV; poly[2-methoxy,

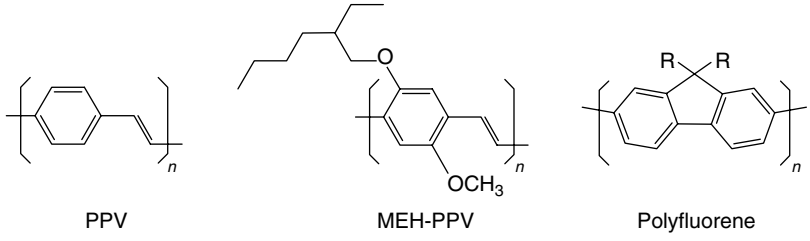


Figure 15.1 Example light-emitting conjugated polymers

5-(2′-ethyl-hexyloxy)-*p*-phenylenevinylene] or MEH-PPV; and polyfluorine. The basic polymer light-emitting device (a diode) consists of a light-emitting polymer (LEP) film of ∼100 nm sandwiched between an optically transparent anode, which sits on an optical quality glass or plastic substrate, and a metallic cathode. The anode is usually indium tin oxide (ITO), which has a high work function, whereas the cathode is typically a low work function metal such as Ca or Mg. When a bias greater than the difference between the anode and cathode work functions (the built-in potential) is applied as illustrated in the band diagram of Figure 15.2(a), electrons are injected from the cathode into the π^*-band, and holes are injected from the anode into the π-band. The injected charges (electron and hole type polarons) form bound polaron-excitons, i.e. neutral bipolarons bound by their Coulomb attraction and their shared distortion (Heeger 2001). Electroluminescence (EL) results from the radiative decay (electron–hole recombination) of these excitons. The device is a diode because application of a reverse bias prevents charge flow (there is no light emission). The energy gap and thus the emission color of the diode can be tuned by changing the length of the polymer molecule, by changing the structure of the polymer repeat unit, by making copolymers, and/or by making polymer blends (Braun *et al.* 1992; Berggren *et al.* 1994; Akcelrud 2003).

A number of factors influence the efficiency of this EL process (Patel *et al.* 2002). Barriers to injection result from the mismatches of the anode and cathode work functions with the HOMO and LUMO, respectively; this defines the need for a high work function anode and a

Petitioner Samsung Ex-1011, 0316

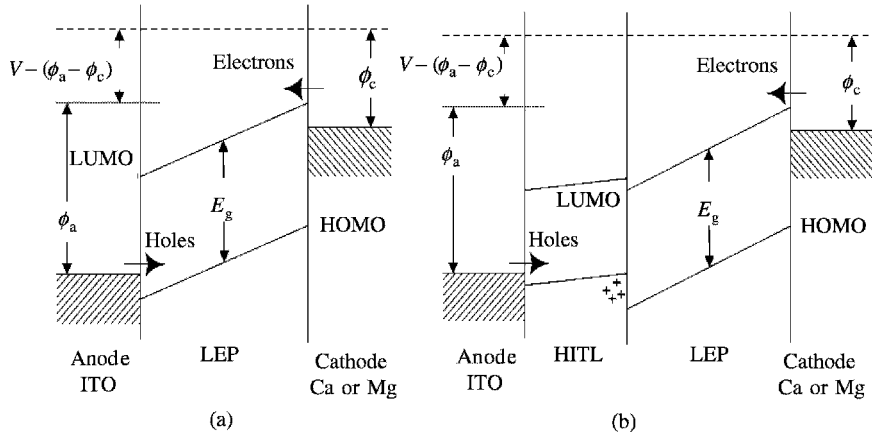


Figure 15.2 Illustrative band diagrams of (a) single-layer and (b) two-layer PLED diodes under a bias V with LEP energy gap E_g, cathode work function ϕ_c, and anode work function ϕ_a

low work function cathode. While exciton binding energies are high, not all excitons radiatively decay. Excitons can be in either a singlet or triplet state according to spin statistics. Spin conservation only allows radiative decay from the singlet state (fluorescence). Radiative decay can result from the triplet state (phosphorescence) if one of the spin states of the electron–hole pair were to flip, a process that can occur through interactions with impurities or defects; in general, however, phosphorescent emission is orders of magnitude smaller than fluorescent emission. If exciton formation is spin-independent, there is only one singlet state for every three triplet states, and the maximum efficiency obtainable is 25%. However, there are some polymer systems where exciton formation is spin-dependent and singlet fractions are as high as 60% (Wilson *et al.* 2001) – the efficiency could potentially be increased further by doping with phosphorescent dyes to significantly enhance the spin-flip process of, and thus the emission from, triplet states; this is a practice that has shown much success for SMOLEDs (Guo *et al.* 2000; Forrest *et al.* 2002). Not all singlet states will radiatively decay – some will decay via competitive nonradiative processes – and the fraction that do depends on the polymer and its purity.

Two other factors that can affect efficiency are preferential injection of one carrier over another and significant differences in the hole and electron mobilities. The hole mobility is typically much greater than the electron mobility, so in the single-layer device architecture, excitons will tend to form near the cathode where they nonradiatively decay due to image force interactions. To prevent this, it has become customary to insert a hole injection and transport layer (HITL) between the anode and the LEP, as shown in the band diagram of Figure 15.2(b) (Yang and Heeger 1994). The HITL serves a number of purposes: (1) it increases the likelihood of recombination in the LEP with the proper choice of HOMO and LUMO by blocking and localizing holes in the active layers of the device; (2) it can increase hole injection at the anode by lowering the barrier; (3) and it can reduce leakage current and the prospects for shorting by planarizing the rough, potentially spiked ITO surface (Brown *et al.* 1992; Heeger *et al.* 1994; Sheats *et al.* 1996; Patel *et al.* 2002). Polyethylene dioxythiophene/polystyrenesulfonate (PEDOT:PSS) and polyaniline (PANI) are two polymers commonly used for the HITL.

Petitioner Samsung Ex-1011, 0317

15.2.3 OLED Display Types

The pixels of a passive matrix OLED display (PMOLED) are created by patterning the anode into columns and the cathode into rows. Light is emitted from an individual pixel by addressing its corresponding row and column and applying a current-controlled forward bias that will provide the desired luminance. To create an image, each line is sequentially addressed and briefly illuminated (Sempel and Buchel 2002). The illumination must be extremely bright in order to obtain the desired overall display luminance and increases with the number of lines in the display (the peak luminance required is proportional to the product of the number of lines and the average luminance). This means that high currents and voltages are needed, which has a number of consequences. (1) The transparent anode (ITO) lines need to be bussed with metal to reduce significant power losses in the electrode lines. (2) Highly efficient polymers are needed to mitigate the other power dissipation factors in the display; this requirement is an order of magnitude greater for full-color displays because, compared to a pixel from a monochrome display of the same resolution, each color subpixel has one-third the area and will be addressed one-third of the time. (3) High-resolution and large-area PM displays are impractical because the power dissipation will be too large and the polymer emitters will degrade faster with the increased peak current demands. Compared to glass displays, the power issues are more acute for plastic displays: resistive losses are generally greater due to a greater resistance in the anode lines, and plastic substrates have a lower tolerance for the Joule heating from resistive losses. For these reasons, PMOLED displays on plastic are limited to a display size of $\sim$1.5 in (Innocenzo 2002).

Active matrix OLED displays (AMOLED), in which a thin film transistor (TFT) circuit is placed at each pixel, overcome many of the PMOLED problems. The TFT circuit provides a controlled current source with storage so that each pixel emits continuously. This drastically reduces the peak currents, which in turn significantly reduces power dissipation and the efficiency and lifetime demands on the polymer emitters. Current control also makes accurate grayscale achievable, which is difficult in PMOLED. A blanket cathode can also be used in an AMOLED, which eliminates many of the cathode patterning challenges associated with PMOLEDs.

15.3 Plastic Substrates for OLED

15.3.1 Substrate Requirements

The plastic substrate suitable for an OLED display must satisfy numerous requirements: high optical quality, which means few defects and high transmission ($>$ 85%) across the visible spectrum to let the light out; substrate smoothness in the nanometer range to prevent protrusions into subsequent barrier and device layers and to provide a surface that will promote high-quality deposition of subsequent films; the ability to withstand processing temperatures, which are expected to be at least 150 °C and possibly as high as 300 °C for AM displays; a good barrier to moisture and oxygen; good dimensional stability so that the various patterned device layers can be aligned; good resistance to any chemicals used in processing; and low water absorption to minimize the consequent dimensional changes and the exposure of the device to moisture.

Petitioner Samsung Ex-1011, 0318

Because there is no plastic film that meets or is likely to meet all of these requirements, there is a great deal of development work focused on obtaining a multilayer composite substrate that will. The approach is to start with an optical quality base film meeting the critical specifications – such as high transparency, high working temperature, and good dimensional stability – and add surface treatments for smoothing; coatings for scratch resistance and, if needed, for chemical resistance; and barrier layers.

15.3.2 Plastic Base Film

Even for the base film, commercially available films are not adequate and require process and/or recipe modification for improving smoothness, increasing working temperature, and/or stabilizing optical transmission (MacDonald 2004). Table 15.1 lists most of the potentially

Table 15.1 Plastic film candidate properties

Base polymer	PET	PEN	PC	PES	PAR	PCO	PI
A commercial name	Melinex	Teonex	Lexan	Sumalite	Arylite	Appear	Kapton
T_g (°C)	78	120	150	220	340	330	355
Transmission at 400–700 nm (%)	> 85	85	> 90	90	90	91.6	orange
CTE (ppm/°C)	15	13	60–70	54	53	74	30–60
CHE (ppm/% RH)		100					10
Water absorption (%)	0.14	0.14	0.4	1.4	0.4	0.03	1.8
Young's modulus (GPa)	5.3	6.1	1.7	2.2	2.9	1.9	2.5
Tensile strength (MPa)	225	275		83	100	50	231
WVTR (g/m^2 per day)	40	1.8		62	84	220	54
OTR (cc/m^2 per day	160	5.5		100	1500	580	388
Chemical resistance	good	good	issues	issues	issues	issues	good

suitable plastic films with their material properties that are relevant to making plastic OLED displays. The glass transition temperature, T_g, is used as a rule of thumb for the temperature extreme that the film can withstand without undergoing undesirable size changes (above this temperature the polymer molecules start to move and will usually rearrange themselves into a lower-energy structure because many of them are not at equilibrium below T_g). However, there are heat stabilization techniques that enable films to have a working temperature above T_g.

Taking polyethylene terephthalate (PET) as an example, with a T_g of 78 °C, it is not a good candidate for AMOLED. However, it has been used in a great deal of research because of its other properties (clarity, low coefficient of thermal expansion, good chemical resistance, and low water absorption) and the fact that it is the most readily available and economically reasonable film. This could be a viable candidate for PMOLED were it not for the unacceptable number of defects and the surface roughness of commercially available films (the payback for addressing these issues appears small given the availability of other films, most notably PEN).

Plate 15.1 shows some images of defects observed on commercial grade PET and the consequences they have on a single diode device: surface roughness can lead to poor image

Petitioner Samsung Ex-1011, 0319

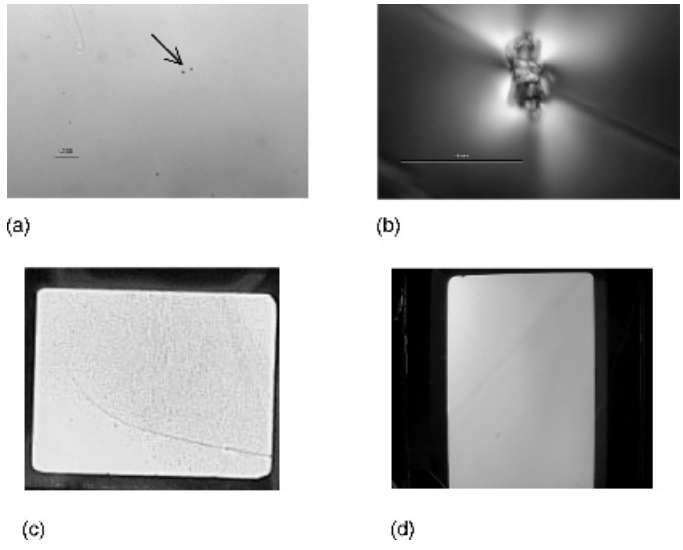


Plate 15.1 (a) Defects on commercially available optical grade PET; (b) magnification of defect; (c) display made with PET substrate having poor surface quality shows low output, grainy appearance, and line defect; (d) display made on PET substrate with improved surface quality has improved characteristics

quality in addition to creating a risk for device shorting. This points out that optical quality is not any easier to achieve than other plastic film requirements. The importance of the additional material properties will become clear in subsequent sections.

15.3.3 Barrier

OLED devices are extremely sensitive to moisture and oxygen. Emission can be easily quenched when organic light-emitting materials are exposed to water, and the highly reactive low work function cathodes can be easily corroded by moisture and oxygen. This means that the substrate must protect the device from the ingress of these materials. Glass substrates are essentially impermeable to moisture and oxygen, but plastic films provide little protection. A barrier structure must therefore be deposited onto the base film. There is currently no instrumental method to measure the ultra low permeation rates required for OLEDs, but an estimate for the water vapor transmission rate (WVTR) has been made by calculating the amount of water needed to oxidize the reactive cathode (Burrows *et al.* 2001). For operating lifetimes in excess of 10 000 h, it was determined that the barrier structure should limit the WVTR to about 10^{-6} g/m^2 per day. For similar lifetimes, oxygen transmission rate (OTR) requirements have been estimated to be somewhere between 10^{-3} and 10^{-5} cc/m^2 per day. These transmission rate requirements have made barrier development one of the biggest challenges in making OLED displays on plastic because the transmission rates of bare plastic films are six or more orders of magnitude greater than these values, and the most demanding requirements outside this arena are in the packaging industry, where the barrier structures provide only two to three orders of magnitude improvement at best (Chatham 1996).

Petitioner Samsung Ex-1011, 0320

The fact that the most sensitive commercially available systems that can measure WVTR and OTR have detection limits at 5×10^{-3} g/m^2 per day and 5×10^{-3} cc/m^2 per day, respectively, has presented the additional challenge of developing techniques to obtain the needed sensitivity. A method that is commonly used is the Ca test (Nisato *et al.* 2001). There are variations of this test, but they all involve observing the optical changes that a reactive metal layer undergoes as it oxidizes. An effort has been made to quantify this test and water vapor transmission rates for barrier films have been reported to be as low as 4×10^{-7} g/m^2 per day using this technique. The Ca test, however, cannot distinguish between moisture and oxygen permeation. Techniques that can make this distinction and that are truly quantitative are currently being pursued, and if they are successful, should accelerate the understanding and development of barrier structures (Dunkel 2004; Vogt 2004). In contrast, the Ca test has the benefit of being able to distinguish between bulk permeation and permeation through defects, which is evidenced by spots in the Ca film. This is important because the reduction in permeation through barrier films developed in the packaging industry – typically single-layer thin film oxides – has been shown to be limited by transport through defects such as pinholes, grain boundaries, and microcracks (Chatham 1996). For this reason, the current barrier development efforts are either directed at creating dense defect-free films (Pakbaz 2004; Snow 2004) or multilayer films that decouple the defects and create a long circuitous path for the diffusing species (Burrows *et al.* 2001; Rutherford 2004; Yan 2004).

15.3.4 Composite Substrate

Finally, the base film, appropriately chosen coatings, and barrier structure must be integrated into a mechanically stable composite substrate. While flexibility may ultimately place the strongest demands on mechanical integrity, the demands are still great even if the substrate is not incorporated into a flexed display. This is because the substrate must be able to withstand the temperature, humidity, chemical, and process conditions that it will be exposed to during device fabrication and device lifetime. Adhesion of the various layers is of particular concern and can be tested for each layer after being subjected to either ambient or accelerated conditions that simulate the anticipated exposure (O'Regan 2003).

Adhesion or peel tests can be performed using a standard tensile tester. A minimum adhesion or bond strength specification can be established based on an understanding of the process conditions and product environments the substrate is expected to experience. Samples can be tested as fabricated, after exposure to either thermal cycling or combined high temperature and humidity, or after outgassing in vacuum. Submersion in boiling water is a truly accelerated condition for testing survivability to moisture that provides quick turnaround for testing. Figure 15.3 shows 90° peel tests to determine if a series of surface treatments on top of Teonex Q65 PEN would provide a good surface for various barrier layers to adhere to (Hildner 2004). The tests are for samples as fabricated (or received) and for samples after being immersed in boiling water for 2 h. Each sample was cut into a 2.5 in $\times$ 4 in strip. Two pieces of 4.5 in $\times$ 0.5 in testing tape (3M 4905/Foil) were attached onto the center of the strip and the excess length of tape was folded over to make a tab. Care was taken to avoid wrinkles and excessive air pockets during tape attachment and then the strip was put through the heated rollers (75 °C) of a dry film laminator to remove all air pockets and set the tape. The back side of the strip was mounted onto a German rotating wheel fixture of an Instron peel tester with 1 in double-sided tape (1 in Permacel double-

Petitioner Samsung Ex-1011, 0321

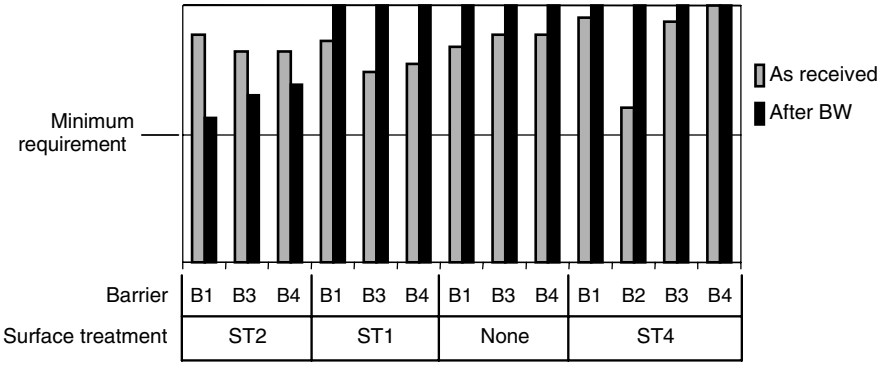


Figure 15.3 Adhesion of barrier layers on Teonex Q65 with various surface treatments; tests were performed on samples as received and after immersion in boiling water (BW)

sided adhesive tape from Anderson Distributors), and the tape tab was clamped to the constant 90° angle peel fixture of the Instron. The tape was then peeled a minimum length of 1.5 in at a speed of 2 in/min while the force required to peel the tape was monitored by the load weighting system of the Instron. For this test to be meaningful, the bond strength of the tape to the sample surface, S_{ts}, must be greater than the minimum specification. If this criterion is met, then the tape will either peel off when the load exceeds S_{ts} or earlier if one of the films or coatings in the sample has a weaker bond strength than S_{ts}. An examination of the tape surface is required to see if any sample coatings peeled off, and adhesion failure is noted only if peel-off is observed and that it occurred at a load below specification. Figure 15.3 shows that the surface treatments under investigation provide the needed adhesion properties. Interestingly, some samples required a greater load after boiling water; this is probably due to a change in the surface character of the sample, which in turn changed the tape adhesion properties to increase S_{ts}.

Adhesion remains a mechanical integrity concern when the substrate is flexed or bent. An additional concern during bending is the development of cracks in the coatings, particularly in the barrier as this will lead to increased permeability. Contributing to these failures are the internal stresses of the various layers, which will be introduced as the various materials – which have different thermal and mechanical properties – are processed together. One of the objectives in developing these composite substrates will therefore be to control these stresses. The critical strain – the strain above which a film will form a crack – of individual layers is another factor that will determine the mechanical reliability of the composite substrate and the extent to which it can bend. A considerable amount of study is being directed at developing testing methods for understanding these issues (Nisato 2004; Bouten 2002; Gorkhali *et al.* 2003).

15.4 Substrate Processing Issues

15.4.1 Processing Issues

Conventional photolithography is used to pattern many of the layers of PM and AM OLED displays on glass, and can be used on plastic as well, but the glass processes cannot be

Petitioner Samsung Ex-1011, 0322

directly transferred to plastic. Internal stresses will be present in the deposited films, and they will probably be of a different character from those on glass substrates because during deposition, which is usually at elevated temperature, the plastic will experience significant dimensional change. These stresses can have a sizable influence on the flatness of a plastic substrate and may also lead to film adhesion issues. Furthermore, in the remaining photolithography steps – these include coating, baking, exposing, developing, and stripping of photoresist, and etching of deposited films – the substrate will be exposed to heat and solvents, which will have a significant impact on the flatness and dimensional stability of the substrate. Another nontrivial issue is that current flat panel display tooling is designed for glass and is therefore not equipped to handle substrates that flex.

15.4.2 Film Stress

There will be stress in deposited films from the differences in thermal expansion between the substrate and film (thermal stress) and from the microstructure of the deposited film (intrinsic stress) (Thornton and Hoffman 1977; Leterrier 2003). When a deposition is performed at elevated temperature, the difference between the coefficient of thermal expansion (CTE) of the film and the CTE of the substrate will result in a different amount of contraction during cooling, imposing a compressive or tensile stress in the film. On plastic substrates, which have higher CTEs than most films of interest, this thermal stress is typically compressive. The intrinsic stress, on the other hand, is determined by the deposition process and is thus largely independent of substrate type and film thickness. The physical and chemical vapor deposition processes typically used for deposition are nonequilibrium in nature and will lead to a quenched disordered state in the film with an intrinsic internal stress that can be either tensile (resulting from attractive interactions across nanovoids) or compressive (as a result of high atomic density).

Internal stresses (both thermal and intrinsic) lead to curling of the substrate, a phenomenon that has been modeled extensively. According to the classic one-dimensional model of Stoney (1909), the radius of curvature of the coated film, R, is related to its internal stress, σ_i, by the expression

$$R = -\frac{E_s h_s^2}{6\sigma_i h_f}, \tag{15.1}$$

where E_s is the Young's modulus of the substrate and h_s and h_f are the thicknesses of the substrate and film, respectively. This curvature will be noticeable (very small R) if the internal stress is large enough (for compressive stress, the film is on the convex side of the curl). For a display substrate, such curling will make completion of subsequent processing steps difficult if not impossible. This illustrates, in part, the value of selecting a substrate with a low CTE and a high Young's modulus. The thermal stress, and thus the imposed amount of curling, is smaller for a small-CTE substrate because it is roughly proportional to the CTE mismatch between the substrate and film (Leterrier 2003). Furthermore, the radius of curvature resulting from all internal stresses will be smaller if the Young's modulus of the substrate is large. Once the substrate has been selected, however, the only option for reducing the radius of curvature is to control the intrinsic stress by tuning the film deposition parameters.

Petitioner Samsung Ex-1011, 0323

The internal stresses also play a role in controlling the adhesion and the coating strength of a film. The coating strength will be of particular concern if the display is to be flexed, and it depends on growth heterogeneities and surface flaws, which have been shown to be related to the surface morphology of the substrate.

In addition to introducing internal stress in a different manner from glass, the plastic substrate will outgas from heating during film deposition. This must either be accounted for and/or controlled or it may affect the chemistry of the film and lead to less than desirable performance characteristics.

15.4.3 Dimensional Stability

The dimensional stability of the substrate is of concern throughout the remaining photolithography steps because changes in size will affect the ability to align subsequently patterned layers and may also affect the mechanical integrity of deposited layers. During temperature cycling, the substrate will change size through two mechanisms: (1) intermolecular relaxation with increasing temperature; and (2) mobility of the polymer chains as the temperature approaches T_g (MacDonald 2004). The first mechanism is reflected in the CTE of the substrate, and if it is not suitably low, the deposited films may crack from repeated strain experienced during process thermal cycling. In the second mechanism, any stresses in the substrate have the opportunity to relax and the substrate will have a different size when it returns to room temperature. This shrinkage (or expansion) will have a compounding effect through the various heat cycles during fabrication and can become quite large unless the substrate stresses are significantly removed before the substrate is introduced into the process. The heat stabilization processes mentioned in Section 15.3.2 are used to remove these stresses and are being developed to provide substrates with sufficiently low shrinkage.

Plastic substrates will also change size on exposure to moisture (O'Regan 2003). Changes in substrate size will not only occur with exposure to photolithography chemistries, but will also result from changes in the relative humidity of the clean room, and gradual water absorption after the substrate has been baked in ovens. The first defense against these changes is selection of a substrate with low water absorption and low coefficient of hydroscopic expansion (CHE), which describes the amount the film expands as a function of relative humidity.

Appropriate substrate selection and heat stabilization techniques can significantly reduce the size changes, but they cannot eliminate them. Substrate movement, if not eliminated, has to be controlled. Once controlled and repeatable, artwork can be used to compensate if the movement is small enough. Controls include stabilizing clean room humidity and temperature, and substrate handling procedures that allow the substrate to reach equilibrium between processes. This requires a detailed understanding of how the substrate changes dimension throughout the process.

One way to assess the effects of various process steps on substrate size is to measure and track overlay registration. Overlay registration is the accuracy with which one patterned layer is aligned to a second patterned layer and can be assessed by microscope images of overlay targets, which are usually a variant of a box-in-box structure. Figure 15.4 shows the extent of misalignment that can occur through the patterning of ITO lines in a PMOLED. These are images from the photo-aligner, looking through the metal mask of the subsequent

Petitioner Samsung Ex-1011, 0324

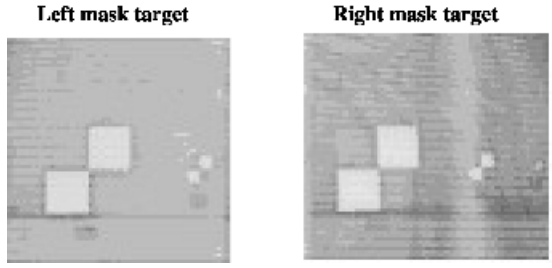


Figure 15.4 Metal layer photomask (bright squares) misaligned from the left-hand side of the device to the right-hand side by ~5 μm after ITO patterning (dark squares) on PET substrate without heat stabilization and dimensional controls; the substrate has shrunk during ITO patterning

metal bus layer, of a patterned ITO substrate before metal deposition. The metal mask target (bright squares) is aligned with the ITO patterned target (dark squares) on the left side of the device, and the overlay offset is measured by the amount of misalignment on the right side of the device. These images are for a PET substrate without heat stabilization and show an overlay misalignment from one side of the device to the other of ~5 μm – the substrate has shrunk after ITO patterning. On this same substrate the overlay offset is larger after the deposition and patterning of the metal layer. Figure 15.5 shows a ~25 μm offset in the horizontal direction of the image after these processes due to further shrinkage during metal deposition.

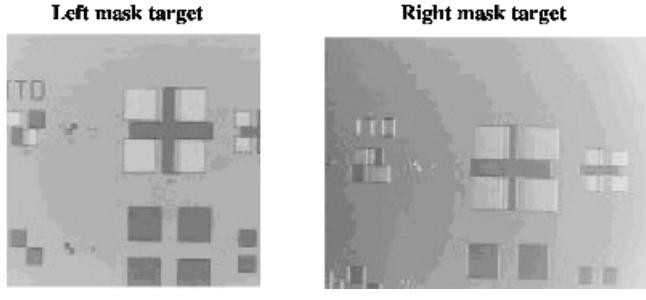


Figure 15.5 Metal deposition and patterning on the same substrate as in Figure 15.4 increases misalignment to ~25 μm

Another way to assess dimensional stability is to accurately measure substrate material dimensions and observe how they change through simulated process environment conditions such as relative humidity, temperature cycling, and climate equilibration. Figure 15.6 shows an eight-point measurement method that is used at DuPont Displays to track dimensional changes, and thus the shrinkage or expansion, of a polymer film in the machine and transverse directions. Figure 15.7 is a graph of such measurements for a biaxial polymer film sample that was subjected to a simulated photoresist hard bake and then allowed to

Petitioner Samsung Ex-1011, 0325

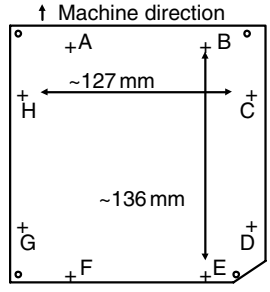


Figure 15.6 Eight-point measurement to assess dimensional change of a 6 in substrate

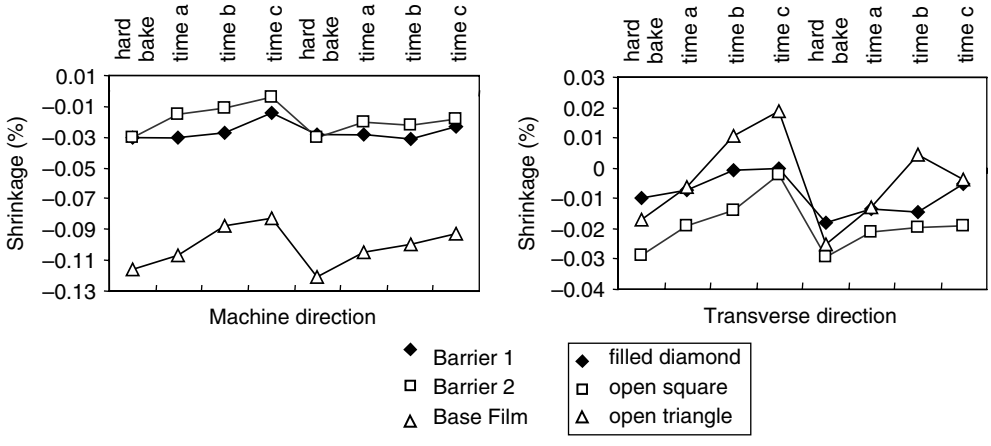


Figure 15.7 Substrate dimensional changes during process simulation

equilibrate in ambient conditions. The film is smaller after the bake, largely because the bake drives out much of the moisture in the film. As the film equilibrates with the ambient conditions, it absorbs moisture and expands. It is also evident that a barrier can promote dimensional stability; the initial shrinkage for the substrate without the barrier is much larger because it had a significantly larger amount of absorbed moisture to begin with. Because the film is biaxial, the dimensional stability is different in the machine and transverse directions; the film moves more in the machine direction.

If the amount of substrate movement during processing is sufficiently small and can be predicted, then compensation artwork can be used. In this approach, which is common in the printed circuit board industry, the masks for the various layers are designed to take substrate changes into account. The effectiveness of this technique is illustrated in Figure 15.8 where metal mask artwork, which included a 25 μm offset or runout from one side of the mask to the other, produced a well aligned metal layer on top of the same type of PET substrate used in Figure 15.5.

Petitioner Samsung Ex-1011, 0326

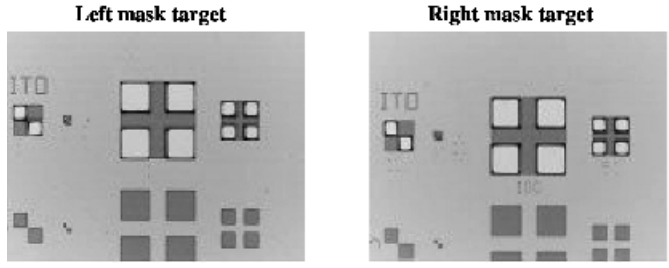


Figure 15.8 Alignment of metal layer achieved with compensation artwork

15.4.4 Substrate Fixturing

It is likely that the first displays will use batch processing where the polymer or composite film is cut into sheets (roll-to-roll fabrication of displays from beginning to end is many years away). Batch processing is used in current display manufacturing on glass, but the equipment is designed to handle a rigid substrate. This is particularly true for film deposition and photolithography steps. While one option may be to develop a new type of display factory, the approach most commonly being pursued is to render the substrate rigid in some fashion. An example of this kind of method is to laminate the substrate to a standard glass plate that acts as a carrier (Lemmi 2004). There are a number of challenges to this process. First the glue must withstand all processing, including wet processing, and allow the substrate to be easily removed at the end without being damaged. The substrate must also remain flat, which is an issue as it goes through numerous heat cycles. Regardless, there will be times in the process when the substrate film will be freestanding and be very difficult to handle if it doesn't have a certain amount of rigidity. It may be an advantage to trade off some flexibility in the display for some rigidity needed for manufacturing. This rigidity can be obtained by using thicker films and/or films with a relatively large Young's modulus.

15.5 Passive Matrix Display Fabrication

15.5.1 PMOLED Structure

A number of PMOLED structures appropriate for plastic have been proposed, and the cathode patterning step, because it must be performed on top of the LEP layer, is a significant differentiator. Conventional photolithography techniques are severely limited due to the sensitivity of the organic layer to moisture, oxygen, and solvents (Lidzey *et al.* 1996). However, a photolithography technique using conventional photoresist and metal dry etching has been developed (Pschenitzka *et al.* 2001). A simpler option is to deposit the cathode through a shadow mask, but this is not practical for high-resolution displays. To address this issue, another method is to integrate the shadow mask into the display architecture by placing a series of cathode separators (also called pillars, mushrooms, and ribs) onto the substrate before the organic materials are deposited (Hosokawa *et al.* 1997; Chang *et al.* 2001). The overhang of these structures then breaks up the continuity of the cathode layer and separates it into rows. These structures are usually made of photoresist and patterned by

Petitioner Samsung Ex-1011, 0327

conventional photolithography, although an alternative PECVD insulator process has been proposed (Py *et al.* 2000), which is unlikely to be a viable option for flexible displays.

An additional photoresist structure is often used on full-color displays. Active material deposition for a monochrome OLED is relatively straightforward, because it simply requires a blanket deposit of the OLED material. Making a full-color display by blanket coating individual red, green, and blue OLED materials is not practical, although it can be done (Wu *et al.* 1996). Schemes where a single emitter is blanket deposited and separate colors are obtained with color filters have been devised, but these are unattractive due to material waste and reduced power efficiency. Local patterning technologies where individual red, green, and blue OLED materials are placed in their respective subpixel locations are more attractive (Duineveld *et al.* 2002). Since different polymers are deposited into neighboring subpixels in these techniques, a photoresist bank or confinement structure is needed to prevent polymer solutions in neighboring subpixels from mixing.

The moisture and oxygen sensitivity of the device will also add some variability to the final structure because the device must be encapsulated after fabrication, and there are a number of architectural options for doing this.

The fabrication of an OLED onto a composite plastic barrier substrate can be subdivided into three parts. Substrate patterning is the first part and it consists of the following steps:

- deposit and pattern the transparent anode;
- deposit and pattern the metal bus lines;
- deposit and pattern any color confinement and/or cathode separating structures that may be used.

The polymer or active materials are then deposited as follows:

- apply HITL material;
- apply LEP material.

The device is then completed with these steps:

- deposit and, if needed, pattern the cathode;
- encapsulate the device.

15.5.2 Substrate Patterning

Anode deposition, patterning, and conditioning

ITO is the transparent anode of choice throughout the display industry (for LCDs and OLEDs on glass). ITO films suitable for OLED displays can be deposited onto plastic substrates, but serious issues arise when the desire is to make a display that will undergo either a significant amount of bend or repeated flexures because ITO is brittle. There are alternative, more flexible anodes being developed to overcome these issues (Arthur 2004), but these materials currently have inferior electrical performance, and there are expected to be a number of display applications where such bending conditions will not be experienced. Thus, ITO remains very useful in the making of plastic OLEDs.

Petitioner Samsung Ex-1011, 0328

The typical method of depositing ITO is magnetron sputtering, where deposition conditions are optimized to yield highly transparent, low-resistivity films. Films grown at low temperature are largely amorphous in character, which means that low resistivity ($\sim$1–3 $\times$ $10^{-4}\,\Omega$ cm) is typically obtained on glass by depositing at elevated temperatures ($>400\,^{\circ}$C) and subsequently annealing at even higher temperatures (Vink *et al.* 1995). This process is clearly unsuitable for plastic substrates. ITO has been deposited on a wide range of plastic substrates, but because of the lower process temperatures, these films have amorphous character and higher resistivities ($>5 \times 10^{-4}\,\Omega$ cm). The lower resistivity will lead to greater resistive losses than in a glass PMOLED, but it should be suitable for small PM displays as well as most AM applications. There are a number of processes being explored to provide lower resistivity; they include postdeposition laser annealing (Chung *et al.* 2002), pulsed laser deposition (Izumi *et al.* 2002), reactive evaporation (Ma *et al.* 1997), DC arc discharge ion plating (Niino *et al.* 2002), and sol-gel synthesis (Asakuma *et al.* 2003).

Plastic substrates are routinely coated by DC magnetron sputtering in a roll-to-roll process, and such processes are being adapted by barrier developers to supply rolls of ITO-coated barrier substrate composite films to display makers (Rutherford 2004). The film is then likely to be cut by laser into sheets. The substrate should then be cleaned by processes adapted from those used for glass in order to avoid either scratching the substrate or damaging the barrier structure. Photoresist is then applied and patterned through the bake, expose, and develop steps to protect the ITO lines that will remain after etch.

Wet etching is most commonly used in the LCD industry and for glass OLED displays (Lan *et al.* 1996). Standard ITO etchants are acidic and examples include HCl, HCl:HNO_2, and HBr. In wet etching, amorphous ITO and crystalline ITO can have significantly different etch rates. As a result, ITO on plastic will not only have a different etch rate than ITO on glass (which can be considered wholly crystalline in comparison), but it will also exhibit a variation of etch rates across the sample. This is because, while largely amorphous, it has some crystallinity, and the degree of crystallinity varies across the surface. This makes it difficult to completely etch away all of the unwanted ITO. The residual ITO can sometimes be hard to find because it can be too small an amount and too discontinuous to be detected by a conductivity measurement; but all of it must be removed because it may short the ITO and/or metal lines. Nonuniform etch rates can also lead to edge roughness in the ITO lines, which will lead to irregular pixel shapes and a distribution of pixel sizes. The residue and the nonuniform patterning issues can be successfully addressed with appropriate optimization of etch chemistry, time, and temperature.

Dry etching is another option. Unlike wet etching, which is isotropic, dry etching is anisotropic (Takabatake *et al.* 1995). In addition, the etch rates for amorphous and crystalline ITO are the same in dry etching. These are important characteristics that are getting much attention as LCD displays are being manufactured with higher resolutions and on larger substrate panels (Kuo 1998). Anisotropic etching and very smooth edges are needed for fine patterning, whereas residues become a greater yield issue for more closely spaced lines and larger panels. These are not likely to be issues for PMOLEDs, but may become a concern as AMOLEDs mature. Dry etching of ITO is a two-step process: reduction of the indium and tin oxides followed by the removal of In and Sn. Development has been hampered by slow etch rates as a result of kinetic limitations in the second step. However, high etch rates of desired selectivity have been obtained with HCl, Cl_2, and HBr through elevated temperature conditions (as high as 250 °C), but this points out that plastic substrates will add extra complexity to dry etch process development (Lee *et al.* 2001).

Petitioner Samsung Ex-1011, 0329

It is well established that the ITO surface as fabricated is not ideal for display performance (Wu *et al.* 1997). Contaminants are not only a potential cause for device failure, but can also lead to nonuniform ITO work functions and consequent nonuniform luminance across the display surface. Carbon-containing contaminants are common and are not sufficiently removed with simple cleaning processes such as ultrasonic cleaning in aqueous or organic solvents. Furthermore, as-fabricated ITO usually has a less than optimal work function that is strongly dependent on the method and conditions of deposition. Various surface treatments have been explored for ITO on glass with the objective of obtaining a smooth, carbon-free, uniformly high work function surface (J. S. Kim *et al.* 1998). The most effective include oxygen plasma, UV ozone, and heating in oxygen. Carbon is removed and high work function values are obtained in these processes. The oxygen not only reacts with the carbon to aid its removal, but also preserves and/or enhances the O/In ratio. There is evidence that the carbon removal and the oxygen concentration enhancement lead to the high work function (Sugiyama *et al.* 2000). Oxygen plasma and UV ozone treatments can be used for ITO on plastic or plastic composite substrates but processes optimized for glass substrates may not be directly transferable. Highly reactive radicals in a plasma may alter organic surfaces, therefore it is best to ensure that organic surfaces are protected by a dielectric layer if plasma treatment is used. Such a layer is likely to be present in the composite film because the top layer of all proposed barrier structures is a dielectric. Also, care must be taken in using UV ozone treatments because the energy and intensity of the UV radiation are such that bonds may be broken in organic films (either the plastic base film or any organic films that may be in the barrier) in the composite substrate.

Metal bus deposition and patterning

The metal bus lines must have a lower sheet resistance than the ITO lines, be environmentally stable, adhere well to the substrate, and exhibit etch selectivity compatible with the other materials exposed to the etch process. Again, the material that meets these conditions and/or the processes used to deposit and pattern it on glass are not likely to be suitable for plastic. Etch selectivity is a concern because of the transition to the plastic substrate and the different character of the ITO layer that the bus lines must make contact with. Adhesion to the substrate becomes an issue due to the increased CTE mismatch between the substrate and the metal layer. The ductility of the material becomes another factor to consider if the display is going to be flexed (Hur *et al.* 2002). The challenge is to identify the material with the desired performance characteristics (resistivity, ductility, and etch selectivity); choose an appropriate deposition technique; and optimize deposition and etch chemistry for film adhesion, conductivity, etch rate, and film stress.

Metals can either be deposited by thermal evaporation or sputtering. The stress in an evaporated film is usually not very significant. However, substrate heating can be an issue. In sputter deposition, heating is less of an issue, and although film stress can be high, it can be adjusted by the sputtering conditions (Thornton and Hoffman 1977). The initial energy of sputtered atoms (sputtering power), the target-to-substrate distance, and the sputtering gas pressure will strongly affect the film stress. These can also change the structural and electrical properties of the film as well.

It may not be possible to fulfill all of the mechanical and electrical properties with a single metal (Baeuerle *et al.* 1999). Multilayer stacks or alloys can be used to tune specific

Petitioner Samsung Ex-1011, 0330

properties. Multilayer stacks will add complexity to the etching process. The different metals may require different etchants, and the etch processes must be optimized to avoid undercut edges, which can result in metal peel-off.

Resist structures patterning

If used, the color confinement structures and/or the cathode separators are likely to be made of photoresist. The dimensional stability concerns here are the same as in the photoresist steps for the anode and metal layers. The working temperature of the substrate must be considered for the baking steps, dimensional changes through all steps must be understood, and processing must proceed with controls that take into account the dimensional changes.

15.5.3 Active Material Application

Monochrome display

In a monochrome PMOLED the HITL and the LEP are usually applied in successive spin coating processes. The chemistries of the two layers must be established so that the first layer does not redissolve when the second layer is deposited. The HITL is normally an aqueous dispersion of the conductive polymer, and the LEP is dissolved in an organic solvent. In each spin coating process, a puddle of polymer solution is dispensed onto the center of the substrate, which is spun at a high rate to spread it over the substrate. A thin film remains on the surface due to surface tension and its thickness depends on spin speed, solution concentration, and molecular weight. The film is then baked to remove the solvent. The uniformity of the film will have a significant impact on the visual appearance of the display. Two major concerns are the cleanliness of the substrate surface and how the coating material wets the surface. Wetting is of particular importance if the substrate has resist structures on it, because the coating must be able to flow easily into any deep topography. Surface treatments such as oxygen plasma or UV ozone are often used in spin coating processes to clean and improve the wettability of the substrate. They have potential use in this application, but they must be tuned to be compatible with the plastic composite substrate.

Full color display

There are a number of printing technologies that could be used for full-color displays such as screen, flexographic, and microcontact. The most promising is inkjet printing (IJP). In this process, drops of polymer solution are ejected from the nozzle of a piezoelectric printhead that is positioned directly over the targeted subpixel. The volume, placement, and spreading of the drops are critical factors for obtaining a process that makes uniformly bright, color-separated, and efficient displays (Haskal *et al.* 2002; MacPherson *et al.* 2003a, 2003b). Because the polymer solutions contain only a few percent solids in a given solvent volume, drop sizes that are tens of microns in diameter are typically deposited into subpixels that are only slightly wider. Drop placement accuracy of current inkjet printers is of order ± 10–15 μm, which means that displays of 80–130 ppi (pixels per inch) can be printed. Even with this level of accuracy, some drops will arrive at the edge of the subpixel, which partly

Petitioner Samsung Ex-1011, 0331

illustrates why a bank structure is used to separate neighboring emitter material. The bank structure presents a problem, however. Solution will adhere to the sidewalls and a nonuniform layer thickness will develop inside the subpixel, which will result in a nonuniform electric field in the emissive layer and nonuniform light emission within the subpixel. This is frequently addressed by treating the bank surface so it is nonwetting, with a CF_4 plasma treatment for example, (Kobayashi *et al.* 2000), but the trick is to keep the substrate wettable at the same time. The process of IJP OLEDs is not fully developed, and many of the issues are being worked out on glass substrates. Development on plastic is under way, however (Hildner 2004; Nisato 2004). The degree and importance of drop placement accuracy point out once again the value of obtaining control and an understanding of the dimensional changes of the plastic substrate; this is the only way IJP on plastic will be successful. Also, any surface treatments used in the process will have to be optimized for the plastic substrate.

15.5.4 Cathode and Encapsulation

Cathode deposition and patterning

The cathode is deposited by vacuum thermal evaporation through a shadow mask. In the absence of cathode separators, the shadow mask can be used to pattern the cathode lines and the control of substrate dimensions will come into play for proper alignment. However, cathode separators will allow deposition through a mask of order square inches and dimensional control will be less of an issue.

Because the low work function metal is highly reactive, exposure to the atmosphere will allow air and water to reach and attack the cathode/polymer interface. Because these areas will become inactive and appear as black spots when the device is operated, it is important that the device is kept in a dry, oxygen-free environment. The deposition chamber is therefore typically attached to a glove box in which the device can subsequently be encapsulated. In addition, a thick capping layer of a more stable metal, such as Al, is often used for added protection.

Encapsulation

The currently used encapsulation scheme for glass PMOLEDs is to create a can-like structure by attaching a lid with an active area perimeter epoxy seal. The encapsulation is performed inside the controlled environment of a glove box, and a desiccant is attached to the lid, or ceiling of the can, to capture any moisture and/or oxygen that manages to make its way into the can once the display is brought into atmospheric conditions. The lid is a rigid material such as glass or metal, and the can would double or triple the thickness of a plastic OLED, which is usually 0.3 mm or less without encapsulation. Metal lids might prove useful in some applications as they achieve ruggedness, but most plastic display applications will require either a thinner encapsulation scheme or one that is flexible. One possibility is to laminate a plastic barrier lid to the back of the device. Because no desiccant is used, one challenge in this method is to develop an epoxy that is sufficiently moisture and oxygen impermeable.

The ultimate goal is to use a thin film encapsulation (TFE) process, because this will provide more flexibility than a laminated lid. TFE has also been pursued for glass displays

Petitioner Samsung Ex-1011, 0332

because of the reduced profile and lower manufacturing cost. Current efforts are similar to those in barrier development, and are focused on either obtaining a dense, defect-free inorganic film or an inorganic–organic multilayer system (Chwang *et al.* 2003; Pakbaz 2004; H. Kim *et al.* 2003). The mechanical integrity of TFE layers is an issue even if the display is not going to be flexed. Again, adhesion is an issue because of the internal stresses that evolve from multiple layers of dissimilar materials being integrated into a single device. Conformality of the coating is an issue particular to a PMOLED that has cathode separators. While flexibility is being considered to some extent in current efforts, a TFE structure that provides sufficient barrier properties on glass displays has yet to be demonstrated. Once one is found, it should be easily transferable to flat plastic displays; the challenge may still remain, however, to develop a TFE system that facilitates flexing.

15.5.5 Device Operation

Plate 15.2(a) shows a PMOLED fabricated by DuPont Displays after it has been encapsulated. The row and column patterning was such that all the traces of each type are extended beyond the active area of the device and then merged into a single contact pad or shorting

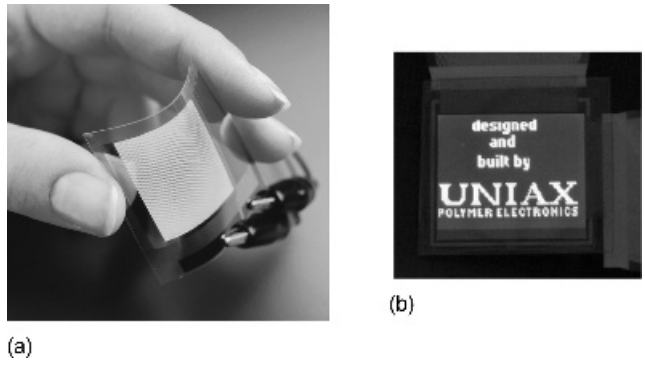


Plate 15.2 Passive matrix OLED displays on plastic with more than 6000 pixels made by DuPont Displays

bar. The display is lit up by a DC power supply connected across the two shorting bars. A final display is shown in Plate 15.2(b). The shorting bars have been trimmed off, flex cables have been bonded, and the display is being driven by an IC chip.

15.6 Active Matrix for OLED on Plastic

15.6.1 Structure

In a plastic AMOLED, an AM array is fabricated on the transparent plastic substrate. The AM array consists of patterned ITO and the TFT circuitry. The active materials can then be applied in the same manner as in a PMOLED. Following blanket cathode deposition, the

Petitioner Samsung Ex-1011, 0333

possible device encapsulation methods are also the same as in a PMOLED. TFT technology is the chief differentiator between AMOLED and PMOLED displays on plastic.

15.6.2 TFT Requirements

The object of the TFT circuit is to continuously run an OLED pixel throughout the frame period, and to do this in a manner that leads to uniform emission across the whole display for a given signal level. A minimum of two TFTs are needed for continuous operation and a uniform current level to every pixel is needed for display uniformity. Basic two-transistor circuits for n-channel and p-channel TFTs are shown in Figure 15.9(a) and (b) (Gu and

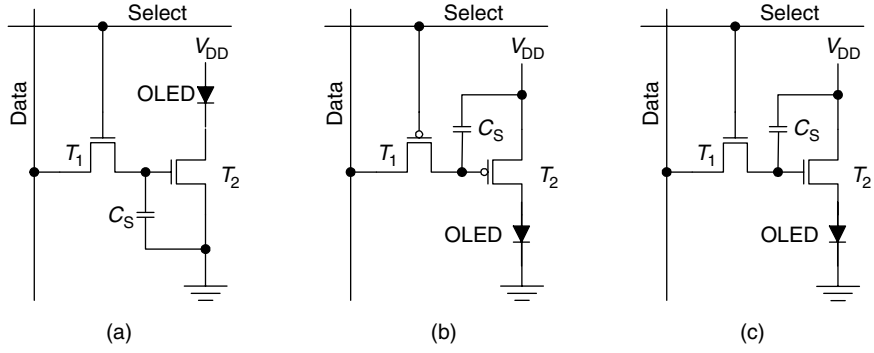


Figure 15.9 Basic 2-TFT circuits for AMOLED: (a) n-channel and (b) p-channel circuits with OLED on the drain side of the TFT; (c) n-channel TFT with OLED on the source side of the TFT, but with the TFT in contact with the OLED anode instead of the OLED cathode as in (a)

Forrest 1998; Sarma *et al.* 2003). The components are a select transistor, a drive transistor, which acts as the current source, and a storage capacitor. Row selection turns on the select transistor, T_1, which then transfers the data voltage from the column electrode to the gate of the drive transistor, T_2. T_1 is turned off leaving the data voltage on T_2 for the remainder of the frame period, and the storage capacitor, C_S, prevents discharge of the T_2 gate voltage. The result is continuous emission from the pixel during the frame period. The objective is to bias T_2 in saturation where it will act as a constant current source with a current, I_D, given by

$$I_D = \mu_{FET} C_d \frac{W}{2L} (V_{GS} - V_t)^2, \tag{15.2}$$

where μ_{FET} is the mobility, C_d is the capacitance of the gate dielectric, W is the channel width, L is the channel length, V_{GS} is the gate-to-source voltage, and V_t is the threshold voltage. This equation points out a major concern: the luminance across a display will be nonuniform if there are any pixel-to-pixel variations in μ_{FET} or V_t.

There is an additional nonuniformity concern. The n-channel and p-channel circuits of Figure 15.9 (a) and (b) are ideal because they place the OLED on the drain side of the TFT so that, for a given drive signal or gate voltage, V_{GS} is independent of the OLED voltage drop, V_{OLED}. However, the OLED cathode is in contact with the TFT in the n-channel circuit,

Petitioner Samsung Ex-1011, 0334

which implies a reverse build of the OLED. For plastic, which uses a forward build, the OLED must be placed on the source side of the TFT as in Figure 15.9(c). The problem here is that, for a given data or gate voltage, V_{GS} is dependent on V_{OLED}, and the circuit cannot provide a uniform current across the display if the OLED I–V characteristics vary. This makes p-channel TFT technology preferable to n-channel for OLED on plastic.

Because of the various nonuniformity issues, practical TFT circuits have more than two TFTs and a number of designs have been proposed (Hong *et al.* 2002; He *et al.* 2001; Akimoto *et al.* 2002; Stryahilev *et al.* 2002). These circuits essentially use current programming to compensate for the TFT and OLED variations. In these designs, the data input is a specified current instead of a voltage and the circuit acts to drive the OLED at the specified current level.

The path to display brightness is revealed in (15.2). The TFT will cover some of the pixel area, therefore obtaining the desired I_D by increasing the channel width has limitations. Short-channel effects limit the extent that the channel length can be shortened, and any increases in $V_{GS} - V_t$ result in more power consumption. Thus, efficiently obtained display brightness is achieved with high mobility (μ_{FET}).

There are minimum mobility requirements ($> 1\ \mathrm{cm}^2/\mathrm{V\,s}$) and these are imposed by the ability of the select transistor, T_1, to fully charge the storage capacitor, C_S, within the addressing period. T_1 must also exhibit a sufficiently high on/off ratio (or low leakage) lest the voltage in the storage capacitor drop appreciably between each frame refresh, and thus change the pixel brightness; the requirement is determined by the display's grayscale depth and will be of order 10^6 (Gu and Forrest 1998).

A number of TFT technologies have the potential to meet the display requirements for an AMOLED on plastic. Amorphous silicon (a-Si) and low-temperature polysilicon (LTPS) are established TFT technologies in the LCD industry. Their performance characteristics are suitable for AMOLED displays. These are typically processed at too high a temperature for plastic substrates, but there is a lot of progress in bringing the processing temperatures suitably low. Organic TFTs are made at low temperature and a high performance has been demonstrated, but the processing techniques are not yet manufacturable.

Amorphous silicon is the most common TFT used in AMLCDs, and is being incorporated into glass AMOLEDs. Mobilities are relatively low, thus TFT widths are relatively large, which limits the resolution of a-Si displays. Only n-channel a-Si TFTs have been realized; in conjunction with the low mobilities, this prohibits the integration of device drivers into the TFT circuit. Deposition processes for a-Si tend to generate uniform initial V_t values, which make the technology suitable for large substrates. However, the V_t of a-Si TFTs shift after prolonged use, but this problem is most acute at high operating voltages, so there are efforts to obtain emitters with lower operating voltages, which would ameliorate this problem.

Conventional a-Si is fabricated at 300–350 °C, the gate dielectric deposition temperature used to obtain low leakage current. However, high-quality gate dielectric layers have been obtained at 150 °C (Gleskova *et al.* 2001), and TFTs fabricated on a polyimide substrate using this process show the same performance characteristics as TFTs conventionally fabricated on glass (Forbes *et al.* 2002). A temperature of 150 °C is a reasonable temperature for heat-stabilized PEN, and the feasibility of this process on PEN has been demonstrated with the device in Plate 15.3. This is a 64×64, 80 ppi, monochrome display with a pixel pitch of 300 μm (Sarma *et al.* 2003).

Low-temperature polysilicon (LTPS) offers some significant performance advantages over a-Si, but with some drawbacks (Tam *et al.* 1999). With high mobilities, LTPS TFTs offer

Petitioner Samsung Ex-1011, 0335

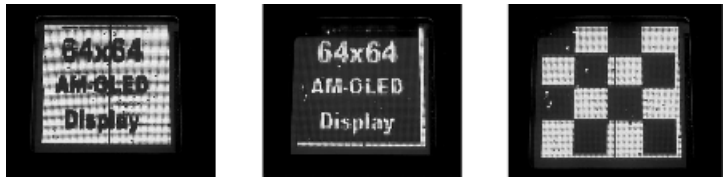


Plate 15.3 Active matrix OLED display on plastic: monochrome, 150 °C, a-Si TFT on heat-stabilized Teonex Q65 PEN, 64 × 64, 80 dpi

brighter and lower-power displays, and can be used in high-resolution displays because they cover a smaller fraction of the pixel area. Display driver integration is possible with LTPS because of the high mobilities and the fact that n- and p-channel TFTs are available. While long-term stability of V_t is good, V_t pixel-to-pixel uniformity is an issue.

Process temperatures for LTPS in the LCD industry are typically 450–600 °C (Ohkura *et al.* 2002), where amorphous silicon is deposited and then recrystallized by excimer laser. Ultra low temperature polysilicon (ULTPS) processes are being developed to bring the process temperature down to 150 °C (Theiss *et al.* 1998; Gosain *et al.* 2000). Both n-channel and p-channel TFTs with high mobilities and adequate threshold voltage have been made with ULTPS on glass, and with slightly lower but adequate mobilities on plastic; however, on/off ratios are of order 10^5 (Wickboldt *et al.* 2003; Lemmi 2004).

The best performing organic TFTs (OTFTs) to date have been fabricated with pentacene have shown the best performance to date. Mobilities greater than 3 cm^2/V s, near zero V_t, and on/off ratios larger than 10^8 have been demonstrated on vacuum-deposited pentacene OTFTs (Jackson 2003). An added attractiveness of OTFTs is that they have the potential to be solution processed, and in conjunction with solution-processed PLEDs they open up the opportunity for a fully printable display. Solution-processed OTFTs have shown mobilities up to 0.2 cm^2/V s (Jackson 2003). However, a dry patterning technique, which uses donor sheets containing thin films of active materials that are thermally transferred to the substrate, has produced pentacene TFTs with a mobility of 0.9 cm^2/V s, a threshold voltage of 14.9 V, and an on/off ratio of 3.6×10^7 (Firester 2004). The performance characteristics of OTFTs are thus approaching, and sometimes better than, those typically achieved with a-Si. Stability issues remain a concern, however, and a considerable amount of technology development is needed to make OTFTs manufacturable.

The search for a suitable TFT technology extends beyond a-Si, LTPS, and OTFT. Alternative inorganic TFT technologies with suitably low processing temperatures are being explored as well (Carcia *et al.* 2003). In addition, TFT transfer technologies, in which the TFTs are fabricated on a substrate that can withstand high processing temperatures and then transferred to the plastic substrate, offer another avenue for circumventing the high-temperature issues of Si processing; not only can traditional LTPS techniques be used (Asano and Kinoshita 2002; Utsunomiya *et al.* 2003), but so can those for single-crystal silicon, which has even higher mobilities (Shi *et al.* 2002).

15.7 Conclusion

With the appreciable focus on the various pieces of technology, there has been considerable progress in the development of plastic OLED displays. Monochrome PMOLEDs have been

Petitioner Samsung Ex-1011, 0336

demonstrated and plastic film development, if not already there, is on the verge of providing substrates suitable for PMOLEDs. However, barrier performance is limiting the lifetime of these devices and is the biggest hurdle for having a commercially viable product. While monochrome AMOLEDs have been demonstrated, applications are likely to be for full color, and full-color deposition processes are still being developed on glass. However, TFT technology presents the biggest hurdle for plastic AMOLED. TFT development is being aided by the drive to decrease TFT processing temperatures and the development of a number of plastic films covering a wide range of working temperatures. A final challenge that should not be overlooked, however, is the ability to make all processes manufacturable. Plastic presents a paradigm shift in manufacturing, and adapting to this may end up being the biggest hurdle in getting to the marketplace.

Acknowledgements

I acknowledge the contributions from the members of the DuPont Displays Plastic Displays Program in Santa Barbara and Research Triangle Park and the various collaborators from DuPont Teijin Films, Honeywell International, and Princeton University who have participated in the technology development and the fabrication of the technology demonstrations presented in this chapter.

References

Akcelrud, L. (2003) Electroluminescent polymers. *Progress in Polymer Science* **28**, 875–962.

Akimoto, H., Kageyama, H., Shimizu, Y., Awakura, H., Nishitani, S. and Sato, T. (2002) An innovative pixel-driving scheme for 64-level gray-scale full-color active matrix OLED displays. *SID International Symposium Digest of Technical Papers, Society for Information Display*, 21 May, Boston MA, pp. 972–5.

Arthur, D. (2004) Transparent electrodes and circuits from carbon nanotubes. *USDC's 3rd Annual Flexible Displays and Microelectronics Conference*, 10–12 Feb, Phoenix AZ.

Asakuma, N., Fukui, T., Toki, M. and Imai, H. (2003) Low-temperature synthesis of ITO thin films using an ultraviolet laser for conductive coating on organic polymer substrates. *Journal of Sol-Gel Science and Technology* **27**, 91–5.

Asano, A. and Kinoshita, T. (2002) Low-temperature polycrystalline-silicon TFT color LCD panel made of plastic substrates. *SID International Symposium Digest of Technical Papers, Society for Information Display*, 21 May, Boston MA, pp. 1196–9.

Baeuerle, R., Baumbach, J., Leuder, E. and Siegordner, J. (1999) A MIM driven display with colour filters on 2" diagonal plastic substrates. *SID International Symposium Digest of Technical Papers, Society for Information Display*, 18–20 May, San Jose CA, pp. 14–7.

Berggren, M., Inganas, O., Gustafsson, C., Rasmusson, J., Andersson, M. R., Hjertberg, T. and Wennerstrom, O. (1994) Light-emitting diodes with variable colours from polymer blends. *Nature* **372**, 444–6.

Bouten, P. C. P. (2002) Failure test for brittle conductive layers on flexible display substrates. *SID Proceedings of the International Display Research Conference, Society for Information Display*, 2–4 Oct, Nice, France, pp. 313–6.

Braun, D. and Heeger, A. J. (1991) Visible-light emission from semiconducting polymer diodes. *Applied Physics Letters* **58**, 1982–4.

Petitioner Samsung Ex-1011, 0337

Braun, D., Gustafsson, G., McBranch, D. and Heeger, A. J. (1992) Electroluminescence and electrical transport in poly(3-octylthiophene) diodes. *Journal of Applied Physics* **72**, 564–8.

Brown, A. R., Bradley, D. D. C., Burroughes, J. H., Friend, R. H., Greenham, N. C., Burn, P. L., Holmes, A. B. and Kraft, A. (1992) Poly(p-phenylenevinylene) light-emitting diodes: enhanced electroluminescent efficiency through charge carrier confinement. *Applied Physics Letters* **61**, 2793–5.

Burroughes, J. H., Bradley, D. D. C., Brown, A. R., Marks, R. N., Mackay, K., Friend, R. H., Burns, P. L. and Holmes, A. B. (1990) Light-emitting diodes based on conjugated polymers. *Nature* **347**, 539–541.

Burrows, P. E., Graff, G. L., Gross, M. E., Martin, P. M., Shi, M. K., Hall, M., Mast, E., Bonham, C., Bennett, W. and Sullivan, M. B. (2001) Ultra barrier flexible substrates for flat panel displays. *Displays* **22**, 65–9.

Carcia, P. F., McLean, R. S., Reilly, M. H. and Nunes, G. Jr (2003) Transparent ZnO thin-film transistor fabricated by rf magnetron sputtering. *Applied Physics Letters* **82**, 1117–9.

Chang, Y., Wei, M. K., Kuo, C. M., Sheih, S. J., Lee, J. H. and Chen, C. C. (2001) Manufacturing of passive matrix OLED-organic light emitting display. *SID International Symposium Digest of Technical Papers*. *Society for Information Display*, 5–7 Jun, San Jose CA, pp. 1040–3.

Chatham, H. (1996) Oxygen diffusion barrier properties of transparent oxide coatings on polymeric substrates. *Surface & Coatings Technology* **78**, 1–9.

Chung, W., Thompson, M. O., Wickboldt, P., Toet, D. and Carey, P. G. (2002) Crystallization of ultra-low temperature ITO by XeCl excimer laser annealing. *SID International Symposium Digest of Technical Papers, Society for Information Display*, 21 May, Boston MA, pp. 57–61.

Chwang, A. B., Rothman, M. A., Mao, S. Y., Hewitt, R. H., Weaver, M. S., Silvernail, J. A., Rajan, K., Hack, M., Brown, J. J., Xi, C., Moro, L., Krajewski, T. and Rutherford, N. (2003) Thin film encapsulated flexible organic electroluminescent displays. *Applied Physics Letters* **83**, 413–5.

Duineveld, P. C., de Kok, M. M., Buechel, M., Sempel, A. H., Mutsaers, K. A. H., van de Weijer, P., Camps, I. G. J., van den Biggelaar, T. J. M., Rubingh, J. E. and Haskal, E. I. (2002) Ink-jet printing of polymer light-emitting devices. *Proceedings of SPIE* **4464**, 59–67.

Dunkel, R. (2004) Method of measuring ultra-low WV permeation. *USDC's 3rd Annual Flexible Displays and Microelectronics Conference*, 10–12 Feb, Phoenix AZ.

Firester, A. H. (2004) Printed organic transistors on plastic for electronic displays and circuits. *USDC's 3rd Annual Flexible Displays and Microelectronics Conference*, 10–12 Feb, Phoenix AZ.

Forbes, C. E., Gelbman, A., Turner, C., Gleskova, H. and Wagner, S. (2002) A rugged conformable backplane fabricated with an a-Si:H TFT array on a polyimide substrate. *SID International Symposium Digest of Technical Papers*. *Society for Information Display*, 21 May, Boston MA, pp. 1200–3.

Forrest, S. R., Baldo, M. A., D Andrade, B., Kawamura, Y., Brown, J. J., Kwong, R., Yanagida, S. and Thompson, M. E. (2002) Electrophosphorescent organic light emitting devices. *SID International Symposium Digest of Technical Papers, Society for Information Display*, 21 May, Boston MA, pp. 1357–60.

Gleskova, H., Wagner, S., Gasparik, V. and Kovac, P. (2001) Low-temperature silicon nitride for thin-film electronics on polyimide foil substrates. *Applied Surface Science* **175**, 12–16.

Gorkhali, S., Cairns, D. R. and Crawford, G. P. (2003) Reliability of transparent conducting substrates for rollable displays: a cyclic loading investigation. *SID International Symposium Digest of Technical Papers*. *Society for Information Display*, 20–22 May, Baltimore MD, pp. 1332–6.

Gosain, D. P., Noguchi, T. and Usui, S. (2000) High mobility thin film transistors fabricated on a plastic substrate at a processing temperature of 110 degrees C. *Japanese Journal of Applied Physics, Part II* **39**, L179–81.

Gu, G. and Forrest, S. R. (1998) Design of flat-panel displays based on organic light-emitting devices. *Selected Topics in Quantum Electronics, IEEE Journal* **4**, 83–99.

Guo, T.-F., Chang, S.-C., Yang, Y. C., Kwong, R. and Thompson, M. (2000) Highly efficient electrophosphorescent polymer light-emitting devices. *Organic Electronics* **1**, 15–20.

Petitioner Samsung Ex-1011, 0338

Gustafsson, G., Cao, Y., Treacy, G. M., Klavetter, F., Colaneri, N. and Heeger, A. J. (1992) Flexible light-emitting diodes made from soluble conducting polymers. *Nature* **357**, 477–9.

Haskal, E. I., Buechel, M., Dijksman, J. F., Duineveld, P. C., Meulenkamp, E. A., Mutsaers, C. A. H. A., Sempel, A., Snijder, P., Vulto, S. I. E. and van de Weijer, P. (2002) Ink jet printing of passive-matrix polymer light emitting displays. *SID International Symposium Digest of Technical Papers*. *Society for Information Display*, 21 May, Boston, MA, pp. 776–9.

He, Y., Hattori, R. and Kanicki, J. (2001) Improved a-Si:H TFT pixel electrode circuits for active-matrix organic light emitting displays. *IEEE Transactions on Electron Devices* **48**, 1322–5.

Heeger, A. J. (2001) Semiconducting and metallic polymers: the fourth generation of polymeric materials. *Synthetic Metals* **125**, 23–42.

Heeger, A. J., Parker, I. D. and Yang, Y. (1994) Carrier injection into semiconducting polymers: Fowler–Nordheim field-emission tunnelling. *Synthetic Metals* **67**, 23–9.

Hildner, M. L. (2004) Plastic display program at DuPont Displays. *USDC's 3rd Annual Flexible Displays and Microelectronics Conference*, 10–12 Feb, Phoenix AZ.

Hong, Y., Kanicki, J. and Hattori, R. (2002) P-103: Novel poly-Si TFT pixel electrode circuits and current programmed active-matrix driving methods for AM-OLEDs. *SID International Symposium Digest of Technical Papers, Society for Information Display*, 21 May, Boston MA, pp. 618–21.

Hosokawa, C., Eida, M., Matsuura, M., Fukuoka, K., Nakamura, H. and Kusumoto, T. (1997) Organic multi-color electroluminescence display with fine pixels. *Synthetic Metals* **91**, 3–7.

Hur, J. H., Lee, C. B., Won, S. H. and Jang, J. (2002) A 2 inch a-Si:H TFT-LCD on plastic. *SID International Symposium Digest of Technical Papers, Society for Information Display*, 21 May, Boston MA, pp. 802–5.

Innocenzo, J. (2002) Roll to roll PLED process development. *SID International Symposium Digest of Technical Papers*. *Society for Information Display*, 21 May, Boston MA, pp. 884–5.

Izumi, H., Ishihara, T., Yoshioka, H. and Motoyama, M. (2002) Electrical properties of crystalline ITO films prepared at room temperature by pulsed laser deposition on plastic substrates. *Thin Solid Films* **411**, 32–5.

Jackson, T. N. (2003) Organic thin film transistors for flat panel display applications. *SID Proceedings of the International Display Research Conference*. *Society for Information Display*, 16–18 Sep, Phoenix AZ, pp. 58–60.

Kim, H., Kim, K. H., Koo, H. M., Kim, J. K., Ju, B. K., Do, L. M., Oh, M. H. and Jang, J. (2003) Passivation properties of inorganic films for flexible OLEDs (F-OLED). *SID International Symposium Digest of Technical Papers, Society for Information Display*, 20–22 May, Baltimore MD, pp. 554–8.

Kim, J. S., Granstrom, M., Friend, R. H., Johansson, N., Salaneck, W. R., Daik, R., Feast, W. J. and Cacialli, F. (1998) Indium tin oxide treatments for single- and double-layer polymeric light-emitting diodes: the relation between the anode physical, chemical, and morphological properties and the device performance. *Journal of Applied Physics* **84**, 6859–70.

Kobayashi, H., Kanbe, S., Seki, S., Kigchi, H., Kimura, M., Yudasaka, I., Miyashita, S., Shimoda, T., Towns, C. R., Burroughes, J. H. and Friend, R. H. (2000) A novel RGB multicolor light-emitting polymer display. *Synthetic Metals* **111/2**, 125–18.

Kuo, Y. (1998) Reactive ion etching of indium tin oxide by $SiCl_4$-based plasmas – substrate temperature effect. *Vacuum* **51**, 777–9.

Lan, J. H., Kanicki, J., Catalano, A., Keane, J., den Boer, W. and Gu, T. (1996) Patterning of transparent conducting oxide thin films by wet etching for a-Si:H TFT-LCDs. *Journal of Electronic Materials* **25**, 1806–17.

Lee, Y. J., Bae, J. W., Han, H. R., Kim, J. S. and Yeom, G. Y. (2001) Dry etching characteristics of ITO thin films deposited on plastic substrates. *Thin Solid Films* **383**, 281–3.

Lemmi, F. (2004) A manufacturable process for poly-Si TFT and active matrix displays on plastic substrates. *USDC's 3rd Annual Flexible Displays and Microelectronics Conference*, 10–12 Feb, Phoenix AZ.

Petitioner Samsung Ex-1011, 0339

Leterrier, Y. (2003) Durability of nanosized oxygen-barrier coatings on polymers – internal stresses. *Progress in Materials Science* **48**, 1–55.

Lidzey, D. G., Weaver, M. S., Bradley, D. D. C., Pate, M. A. and Fisher, T. A. (1996) Photoprocessed and micropatterned conjugated polymer LEDs. *Synthetic Metals* **82**, 141–8.

Ma, J., Li, S., Zhao, J. and Ma, H. (1997) Preparation and properties of indium tin oxide films deposited on polyester substrates by reactive evaporation. *Thin Solid Films* **307**, 200–2.

MacDonald, W. A. (2004) Engineered films for display technologies. *Journal of Materials Chemistry* **14**, 4–10.

MacPherson, C., Anzlowar, M., Innocenzo, J., Kolosov, D., Lehr, W., O'Regan, M., Sant, P., Stainer, M., Sysavat, S. and Venkatesh, S. (2003a) Development of full color passive PLED displays by inkjet printing. *SID International Symposium Digest of Technical Papers*. *Society for Information Display*, 20–22 May, Baltimore MD, pp. 1191–5.

MacPherson, C., Stainer, M., Yu, G. and O'Regan, M. (2003b) Fabricating full-color OLED displays using ink-jet printing. *Information Display* **19**, 16–20.

Niino, F., Hirasawa, H. and Kondo, K. (2002) Deposition of low-resistivity ITO on plastic substrates by DC arc-discharge ion plating. *Thin Solid Films* **411**, 28–31.

Nisato, G. (2004) Technologies for flexible PLED displays. *USDC's 3rd Annual Flexible Displays and Microelectronics Conference*, 10–12 Feb, Phoenix AZ.

Nisato, G., Bouten, P. C. P., Slikkerveer, P. J., Bennett, W. D., Graff, G. L., Rutherford, N. and Wiese, L. (2001) Evaluating high performance diffusion barriers: the calcium test. *SID Proceedings of the International Display Research Conference, Society for Information Display*, 16–19 Oct, Nagoya, Japan, pp. 1435–8.

Ohkura, M., Shimomura, S., Miyazawa, T., Itoga, T. and Shiba, T. (2002) 450 °C low-temperature poly-Si TFT fabrication process applicable to the display manufacturing using $730 \times 920\,\mathrm{mm}^2$ glass substrates. *Society for Information Display*, May 2002, Boston MA, pp. 146–149.

O'Regan, M. (2003) Plastic display program at Dupont Displays. *USDC's 2rd Annual Flexible Displays and Microelectronics Conference*, Phoenix AZ.

Pakbaz, H. (2004) Symmorphix. *USDC's 3rd Annual Flexible Displays and Microelectronics Conference*, 10–12 Feb, Phoenix AZ.

Patel, N. K., Cina, S. and Burroughes, J. H. (2002) High-efficiency organic light-emitting diodes. *Selected Topics in Quantum Electronics, IEEE Journal* **8**, 346–61.

Pschenitzka, F., Lu, M. H. and Sturm, J. C. (2001) P-48 patterning of OLED cathodes by metal dry etching. *SID International Symposium Digest of Technical Papers, Society for Information Display*, 5–7 Jun, San Jose CA, pp. 731–3.

Py, C., D'Iorio, M., Tao, Y., Stapledon, J. and Marshall, P. (2000) A passive matrix addressed organic electroluminescent display using a stack of insulators as row separators. *Synthetic Metals* **113**, 155–9.

Rutherford, N. (2004) Barix(tm) & Flexible Glass(tm). *USDC's 3rd Annual Flexible Displays and Microelectronics Conference*, 10–12 Feb, Phoenix AZ.

Sarma, K. R., Chanley, C., Dodd, S., Roush, J., Schmidt, J., Srdanov, G., Stevenson, M., Wessel, R., Innocenzo, J., Yu, G., O'Regan, M., MacDonald, W. A., Eveson, R., Long, K., Gleskova, H. *et al.* (2003) Active matrix OLED using 150 degree C a-Si TFT backplane built on flexible plastic substrate. *Proceedings of SPIE* **5080**, 180–91.

Sempel, A. and Buchel, M. (2002) Design aspects of low power polymer/OLED passive-matrix displays. *Organic Electronics* **3**, 89–92.

Sheats, J. R., Antoniadis, H., Hueschen, M., Leonard, W., Miller, J., Moon, R., Roitman, D. and Stocking, A. (1996) Organic electroluminescent devices. *Science* **273**, 884–8.

Shi, Y., Bernkopf, J., Herrmann, S., Hermanns, A. and Choquette, D. (2002) Polymer light-emitting diode displays driven by integrated nanoblock IC drivers. *SID International Symposium Digest of Technical Papers*. *Society for Information Display*, 21 May, Boston MA, 1092–5.

Snow, S. A. (2004) Silicon–carbon alloy films as protective barriers for OLED display applications. *USDC's 3rd Annual Flexible Displays and Microelectronics Conference*, 10–12 Feb, Phoenix AZ.

Petitioner Samsung Ex-1011, 0340

Stoney, G. G. (1909) The tension of metallic films deposited by electrolysis. *Proceedings of the Royal Society of London* **82**, 72.

Stryahilev, D., Sazonov, A. and Nathan, A. (2002) Amorphous silicon nitride deposited at 120 degree C for organic light emitting display-thin film transistor arrays on plastic substrates. *Journal of Vacuum Science and Technology* **20**, 1087–90.

Sugiyama, K., Ishii, H., Ouchi, Y. and Seki, K. (2000) Dependence of indium tin oxide work function on surface cleaning method as studied by ultraviolet and x-ray photoemission spectroscopies. *Journal of Applied Physics* **87**, 295–8.

Takabatake, M., Wakui, Y. and Konishi, N. (1995) Indium tin oxide dry-etching using HBr gas for thin-film-transistor liquid-crystal displays. *Journal of the Electrochemical Society* **142**, 2470–3.

Tam, S. W. B., Matsueda, Y., Maeda, H., Kimura, M., Shimoda, T. and Migliorato, P. (1999) Polysilicon TFT drivers for light emitting polymer displays. *SID International Display Workshops, Society for Information Display*, 1–3 Dec, Sendai, Japan, pp. 175–8.

Tang, C. W. and VanSlyke, S. A. (1987) Organic electroluminescent diodes. *Applied Physics Letters* **51**, 913–5.

Theiss, S. D., Carey, P. G., Smith, P. M., Wickboldt, P., Sigmon, T. W., Tung, Y. J. and King, T. J. (1998) Polysilicon thin film transistors fabricated at 100 degree C on a flexible plastic substrate. *Technical Digest of the International Electron Devices Meeting 1998*, 6–9 Dec, San Francisco CA, pp. 257–60.

Thornton, J. A. and Hoffman, D. W. (1977) Internal stresses in titanium, nickel, molybdenum, and tantalum films deposited by cylindrical magnetron sputtering. *Journal of Vacuum Science and Technology* **14**, 164–8.

Utsunomiya, S., Kamakura, T., Kasuga, M., Kimura, M., Miyazawa, W., Inoue, S. and Shimoda, T. (2003) Flexible color AM-OLED display fabricated using surface free technology by laser ablation/annealing (SUFTLA) and ink-jet printing technology. *SID International Symposium Digest of Technical Papers, Society for Information Display*, 20–22 May, Baltimore MD, pp. 864–7.

Vink, T. J., Walrave, W., Daams, J. L. C., Baarslag, P. C. and van den Meerakker, J. E. A. M. (1995) On the homogeneity of sputter-deposited ITO films. Part I: Stress and microstructure. *Thin Solid Films* **266**, 145–51.

Vogt, B. D. (2004) A reflectivity-based metrology to quantify moisture transport through barrier layers for OLED applications. *USDC's 3rd Annual Flexible Displays and Microelectronics Conference*, 10–12 Feb, Phoenix AZ.

Wickboldt, P., Smith, P., Lemmi, F., Sasagawa, T. and Lin, S. (2003) Progress on ultra-low temperature polysilicon (ULTPS) fabrication. *USDC's 2rd Annual Flexible Displays and Microelectronics Conference*, Phoenix AZ.

Wilson, J. S., Dhoot, A. S., Seeley, A. J. A. B., Khan, M. S., Kohler, A. and Friend, R. H. (2001) Spin-dependent exciton formation in conjugated compounds. *Nature* **413**, 828–31.

Wu, C. C., Sturm, J. C., Register, R. A. and Thompson, M. E. (1996) Integrated three-color organic light-emitting devices. *Applied Physics Letters* **69**, 3117–9.

Wu, C. C., Wu, C.I., Sturm, J. C. and Kahn, A. (1997) Surface modification of indium tin oxide by plasma treatment: an effective method to improve the efficiency, brightness, and reliability of organic light emitting devices. *Applied Physics Letters* **70**, 1348–50.

Yan, M. (2004) Lexan(r) film substrates for flexible flat panel devices. *USDC's 3rd Annual Flexible Displays and Microelectronics Conference*, 10–12 Feb, Phoenix AZ.

Yang, Y. and Heeger, A. J. (1994) Polyaniline as a transparent electrode for polymer light-emitting diodes: lower operating voltage and higher efficiency. *Applied Physics Letters* **64**, 1245–7.

Petitioner Samsung Ex-1011, 0341

16

Encapsulated Liquid Crystal Materials for Flexible Display Applications

Gregory P. Crawford

Division of Engineering, Brown University, Providence RI

16.1 Introduction

Dispersions of low molecular weight liquid crystals and polymers fit into a broad class of materials in which the concentration of polymer can be as large as 80% or as small as 2%, depending on the type of polymer used and the application. In their most celebrated form, the concentration of polymer is in the range 30–50% and the liquid crystal is separated out in the form of droplets or domains randomly distributed throughout the polymer binder (Drzaic 1995; Crawford *et al.* 1996). These materials are called polymer-dispersed liquid crystals (PDLCs) and have been evaluated for several electro-optical applications, including switchable windows, high-definition projection systems, large flat panel displays, light shutters for optical signal processing, etc. (Doane 1991; Drzaic 1995). In the case of low polymer concentrations, the polymer forms a network dispersed in the liquid crystal (Hikmet 1991; Crawford and Zumer 1996). One example involves cholesteric liquid crystals where the dispersed polymer locks in specific textures useful for bistable color reflective displays. Bistability is a much sought-after property of liquid crystalline materials, since it is particularly important for low power consumption devices (Yang and Crooker 1991). The amount of polymer

Flexible Flat Panel Displays Edited by G. P. Crawford
© 2005 John Wiley & Sons, Ltd., ISBN 0-470-87048-6

Petitioner Samsung Ex-1011, 0342

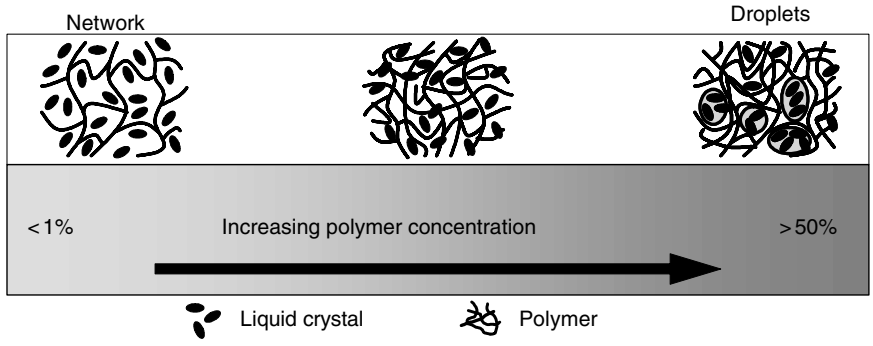


Figure 16.1 Schematic diagram of polymer morphology as a function of concentration

strongly drives the nature of the polymer morphology as qualitatively illustrated in Figure 16.1, where low concentrations of polymer result in a network morphology and higher concentrations of polymer result in domain or droplet structures. The type of polymer used and the polymer morphology strongly dictate the electro-optic properties of the display itself (Serbutoviez *et al.* 1996; Amundson *et al.* 1997; Muncha 2003; Yang *et al.* 2004).

For flexible display applications, encapsulation of the electro-optic material tends to be a prerequisite. Encapsulation is important in OLEDs (Chapter 15), cholesteric liquid crystals (Chapter 17), paintable liquid crystals (Chapter 18), electrophoretics (Chapter 19) and Gyricon materials (Chapter 20). This chapter covers encapsulated nematic liquid crystals. Chapter 17 gives an extensive treatment of encapsulated chiral liquid crystals.

16.2 History of Encapsulated Liquid Crystals

The idea of encapsulating liquid crystals to a nonplanar geometry is not a derivative of recent display technology, but dates back to the early 1900s. Although it is impossible to do this vast field justice in this chapter, it is worthwhile to review some of the highlights of the past 100 years to set the stage for our current understanding of encapsulated liquid crystals. Lehmann discovered liquid crystals suspended in an isotropic fluid form spherical inclusions and conform to a specific configuration that depends on the liquid crystal material and the angle at which the liquid crystal molecules are anchored to the encapsulated binder interface (Lehmann 1904). Lehmann studied birefringent textures with optical polarizing microscopy as a principal way of observing ordered structures. Lehmann further discussed the possibility of a volume defect in orientational order, occurring in the center of the droplet being transformed into two point defects as the droplet was squeezed between planar glass plates. He subsequently studied the dynamics of these unusual defects in the presence of a magnetic field for basic science reasons without further regard to potential applications.

It was not until the late 1960s that researchers revisited the notion of encapsulated liquid crystals. Chandrasekhar studied the problem of finding the equilibrium shape of a small particle with an emphasis on liquid crystalline materials (Chandrasekhar 1966). Dubois-Violette and Parodi applied elastic theory to nematic liquid crystal droplets suspended in a fluid binder to predict their stable configurations of the nematic director field (Dubois-Violette and Parodi 1969). Assuming an anisotropic surface energy, they were able to predict the stability of two configurations, the radial and bipolar structure, depending on whether the surface induces a

Petitioner Samsung Ex-1011, 0343

perpendicular or parallel orientation of the liquid crystal molecules at the surface boundary. They also treated the nature of point defects in the droplet, occurring in locations in the droplet where the elastic energy diverged. These theoretical studies were stimulated by the experiments of Meyer, who earlier observed point defects in the center and at opposite poles of nematic droplets dispersed in various isotropic fluids (Meyer 1969). Meyer extended his work on point defects and experimentally prepared circumstances that allowed for their detailed study (Meyer 1973). Candau and coworkers studied cholesteric liquid crystal materials in spherical droplets suspended in an isotropic fluid (Candau *et al.* 1973). The cholesteric droplets adopted a new spiral structure, unlike those earlier reported by Meyer in 1969 for ordinary nematic materials, when the radius of the droplet was much larger than the intrinsic pitch length of the cholesteric material. Press and Arrott applied elastic theory to nematic liquid crystal droplets with perpendicular anchoring conditions. They numerically derived twisted solutions to describe their unusual observation of a twisted star in the center of a radial droplet as viewed between crossed polarizers of an optical microscope (Press and Arrott 1974).

Also during the 1970s, a similar problem was being addressed in parallel concerning the nature of the ordering of a nematic liquid crystal confined to cylindrical environment (capillary tubes). It was theoretically predicted that the nematic director configuration within a cylindrical capillary tube with perpendicular surface boundary conditions was a pure radial configuration with a line disclination along the cylindrical axis (Dzyaloshinksii 1970). Cladis and Kleman used elastic theory to demonstrate that another configuration is stable for cylindrical tubes larger than 0.1 μm in diameter where the line disclination escapes into the third dimension along the cylinder axis; this structure, named the escaped-radial configuration, is continuous and involves no disclination or defect (Cladis and Kleman 1972). Optical observations by Williams *et al.* (1972), Meyer (1973), and Saupe (1973), verified the existence of the escaped-radial configuration. Cladis continued studying liquid crystals constrained to capillary tubes using a material with a smectic A phase. As the bend elastic constant (K_{33}) became large on approaching the smectic A phase, the escaped-radial configuration transformed into a planar-radial configuration (Cladis 1974). Researchers then attempted to study nematic liquid crystals constrained to capillary tubes when concentric parallel ordering is induced at the surface (Melzer and Nabarro 1977) to verify the stability of the escaped-twisted structure predicted earlier by Cladis and Kleman (1972). Furthering her work, Cladis and coworkers studied defect structures occurring in capillary tubes near the cholesteric–smectic A transition; they proposed that the cholesteric phase grows from the smectic A phase via a spiraling line disclination (Cladis *et al.* 1979).

The fundamental interest in confined liquid crystals reverted back to droplets in the early 1980s when a method of varying the surface boundary conditions was demonstrated (Volovik and Lavrentovich 1983). Volovik and Lavrentovich demonstrated that the dynamics of creation, annihilation, and transformation of topological defects (e.g. boojums, hedgehogs, and dislinations) in a closed system follow the predictions of the topological theory. Later the studies on defects were extended by investigating the defect lines that occur in cholesteric liquid crystal droplets (Kurik and Lavrentovich 1982).

In the 1980s, liquid crystals encapsulated to small volumes became more than just curious systems from the basic science perspective. Encapsulated liquid crystals showed great promise for light modulation devices, based on a concept introduced earlier by Hilsum (1976), in which a microporous filter (prefabricated encapsulating membrane) permeated with nematic liquid crystal of positive dielectric anisotropy ($\Delta n > 0$) is secured between conducting glass substrates (Craighead *et al.* 1982). The orientation of the liquid crystal

Petitioner Samsung Ex-1011, 0344

confined to the inclusions was manipulated by an external electric field to produce a variation in the refractive index. When the index of refraction of the microporous filter matched that of the liquid crystal, the composite medium was transparent (nonscattering); however, if the refractive indices were mismatched, the composite medium was translucent (scattering). This index matching/mismatching function controlled by an electric field was analogous to the index matching concept of Hilsum, who dispersed isotropic particles in a liquid crystal medium. The contrast ratio and the switching times of both devices were not impressive and these device concepts did not see extensive development for commercial display application.

Following the efforts of Hilsum (1976) and Craighead *et al.* (1982), two new types of encapsulated liquid crystal and polymers emerged in the mid 1980s. Doane *et al.* (1986) discovered a phase separation procedure to obtain dispersions of liquid crystal droplets inside a solid polymer binder. The name polymer-dispersed liquid crystals (PDLCs) was coined for these systems. Phase separation techniques gave the necessary control over droplet size and distribution to optimize PDLCs for light shutter applications. Polymer-dispersed liquid crystal materials are easily sandwiched between conducting glass plates. The spacing is controlled by spacers in the range 10–25 μm. The PDLC material strongly scatters light in the zero-field state. It can be switched to a transparent mode on application of a voltage. The transparent condition arises when the electric field is of sufficient strength to align the droplets such that their ordinary refractive index (n_o) matches that of the polymer (n_p), subsequently reducing the scattering power of the droplets (Figure 16.2). On removal of

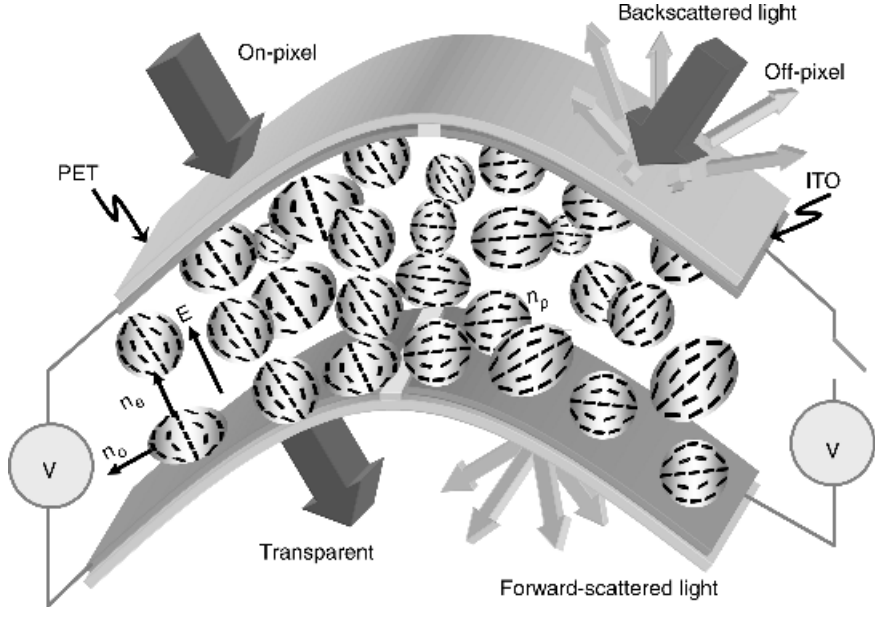


Figure 16.2 Operation of the PDLC in the transparent state (left pixel) and in the scattering state (right pixel). In the transparent state, a voltage is applied to the pixel, thereby aligning the liquid crystal within the droplet and creating an index matching condition where n_o matches n_p. In the scattering state, the symmetry axes of the droplets are randomly oriented, creating an index mismatch between droplets and the encapsulating matrix. Reproduced by the permission of the Society for Information Display

Petitioner Samsung Ex-1011, 0345

the voltage, the droplets return to their original scattering condition. Fergason (1985) reported a different encapsulation procedure to create micrometer-size liquid crystal capsules inside a rigid polymer binder. The material was prepared using a water-based emulsion and in the older literature it is often known as nematic curvilinear aligned phase (NCAP) (Drzaic 1986). As the field has matured, most researchers often use the acronym PDLC to describe encapsulated liquid crystals in droplet form. The light-modulating and reflective devices based on PDLC dispersions possess advantages over other liquid crystal technologies because they do not require alignment layers or polarizers, and large, meter-sized devices are relatively simple to fabricate. Because of their potential, there were a flurry of publications that addressed the underlying physics of liquid crystals confined in spherical containers (Golemme *et al.* 1988a, 1988b; Erdmann *et al.* 1990; Ondris-Crawford *et al.* 1991; Ambrozic *et al.* 1997; Amundson and Srivasarao 1998; Amundson 1998).

Margerum and coworkers invented new ways in which PDLCs could be formed (Margerum *et al.* 1990). By carrying out the photopolymerization process with structured light (e.g. an interference pattern or masking techniques) they demonstrated that the liquid crystal droplets could be patterned in a polymer film making way for diffractive and reflective devices which are electrically addressable. Other groups reported patterned PDLCs using holographic methods in the literature (Sutherland *et al.* 1993; Tanaka *et al.* 1994), which furthered research on this new version of PDLCs (which became known as holographic PDLCs or HPDLCs). Holographic PDLCs, when operated in the reflection mode, offer a brilliant Bragg reflection and relatively narrow bandwidth, which is why they were evaluated for reflective color display applications (Date 1995; Crawford *et al.* 1996).

The versatility and simplicity of PDLC materials further led researchers to test the feasibility of embedding chiral nematic and ferroelectric materials into spherical and elliptical droplets. Crooker and Yang (1990) first demonstrated that chiral nematics are suitable for applications in colored electro-optic displays. For materials with negative dielectric anisotropy ($\Delta\varepsilon < 0$) and sufficiently short pitch length, they showed that it is possible to induce a texture showing bright selective reflection by applying electric fields. Kitzerow *et al.* (1992) revealed that the alignments of ferroelectric and antiferroelectric liquid crystals in droplets can be controlled by mechanical shear during the polymerization process, and they demonstrated bistability (Molsen and Kitzerow 1994) much like that in surface-stabilized ferroelectric liquid crystals (Clark and Lagerwall 1980). They demonstrated helical unwinding, leading to the rotation of the optic axis in the plane perpendicular to the electric field with switching times of $\sim$100 μs. Zyryanov *et al.* (1993) also revealed electro-optic data for ferroelectric PDLCs. Lee *et al.* (1994) presented a model for understanding the electro-optic switching in ferroelectric PDLCs. Mang *et al.* (1992) studied the layer structure of ferroelectric liquid crystals in glass capillary arrays with X-ray diffraction, and Aliev and Kelly (1994) studied the dynamics, structure, and phase transitions of ferroelectrics confined to porous glass matrices.

In the late 1980s and early 1990s, as PDLC materials were being investigated by a number of groups, a new school of thought began to emerge. Rather than creating liquid crystal drops or domains embedded in a polymer matrix, researchers began to investigate the dispersion of very low concentration polymer networks in a liquid crystal binder. Mariani *et al.* (1986) showed that a liquid crystal could be used as an ordering medium for a polymer network. Subsequently, dispersions consisting of low concentrations of polymer for display applications were then reported by Hikmet (1990), who prepared a light shutter for polarized light by dissolving and then polymerizing suitable monomers in a homogeneous aligned nematic liquid crystal. The composite material was polarization sensitive and operated in the reverse

Petitioner Samsung Ex-1011, 0346

mode as compared to conventional PDLCs, such that the film was transparent in zero voltage and transformed to a scattering state for one component of the polarization when a voltage was applied across the electrodes. Yang and coworkers found alternative applications of ordered polymer networks to stabilize and modify the cholesteric liquid crystal materials. They developed two display alternatives (Yang *et al.* 1992): (1) a haze-free light shutter for unpolarized light and (2) a bistable reflective mode display. By using cholesteric liquid crystals, they demonstrated modes that mimic a conventional PDLC (normal mode) and one that works in the reverse mode that were not polarization selective, and in addition, they showed a bistable display using cholesteric liquid crystals that reflect in the visible (Yang *et al.* 1996). The potential of polymer networks in display applications pushed researchers to better understand the role of the fragile networks of the crosslinked polymers that create unusual electro-optic effects not observable in the bulk liquid crystal (Hikmet and Zwerver 1991; Stannarius *et al.* 1991; Jakli *et al.* 1992, 1994; Crawford *et al.* 1994, 1995; Crawford and Zumer 1996).

The interest in encapsulated liquid crystals for electro-optic applications was largely responsible for driving the field of confined liquid crystals. Many basic science papers which study very fundamental aspects of confined liquid crystals often reference a PDLC paper in the introduction as a motivating factor. There has been a lot of basic work in systems where liquid crystals are backfilled into a prefabricated matrix, which includes polymer matrices with submicrometer cylindrical cavities (Crawford *et al.* 1991, 1992), alumina matrices with submicrometer cylindrical channels (Crawford *et al.* 1993, 1996; Jin *et al.* 2003), aerogel matrices (Bellini *et al.* 1992; Wu *et al.* 1992; Clark *et al.* 1993; Kralj *et al.* 1993; Maritan *et al.* 1994; Rappaport *et al.* 1996), porous glass materials (Aliev and Breganov 1989; Iannacchione *et al.* 1993, 1996), and Aerosil matrices (Kreuzer and Eidenschink 1996, Ramazanoglu *et al.* 2004; Jin and Finotello 2004; Anoardo *et al.* 2004).

The field of encapsulated liquid crystals has burgeoned over the past 25 years. Fortunately there is a large fundamental science base to help explain the underlying physics and chemistry. Unfortunately, many device applications using encapsulated liquid crystals never enjoyed commercial success for a number of reasons. One of the biggest factors hindering their penetration into the commercial market was their high driving voltages as compared to conventional liquid crystal devices. The high driving voltage is largely attributed to the high surface-to-volume ratio brought about by the encapsulation. However, as we enter into a new era in the development of flexible displays, encapsulation is vital. For example, encapsulation is used in organic light-emitting diodes (Chapter 15), electrophoretic devices (Chapter 16), cholesteric liquid crystals (Chapter 17), paintable displays (Chapter 18) and Gyricon (Chapter 20). Encapsulation, which is done for different reasons in the gamut of technologies being considered for flexible display applications, is a common underlying theme for display materials being developed for flexible display applications.

16.3 Encapsulation Techniques

Figure 16.3 shows the principal ways in which dispersions of liquid crystals and polymer are prepared; they include phase separation (West 1988), emulsion-based processes (Fergason 1985; Drzaic 1995; Amimori *et al.* 2003), and permeation (Craighead 1982; Liang and Tseng 2003). The underlying process of phase separation is well described by West (1988). In the most common embodiment, a liquid crystal and photoreactive monomer forms a

Petitioner Samsung Ex-1011, 0347

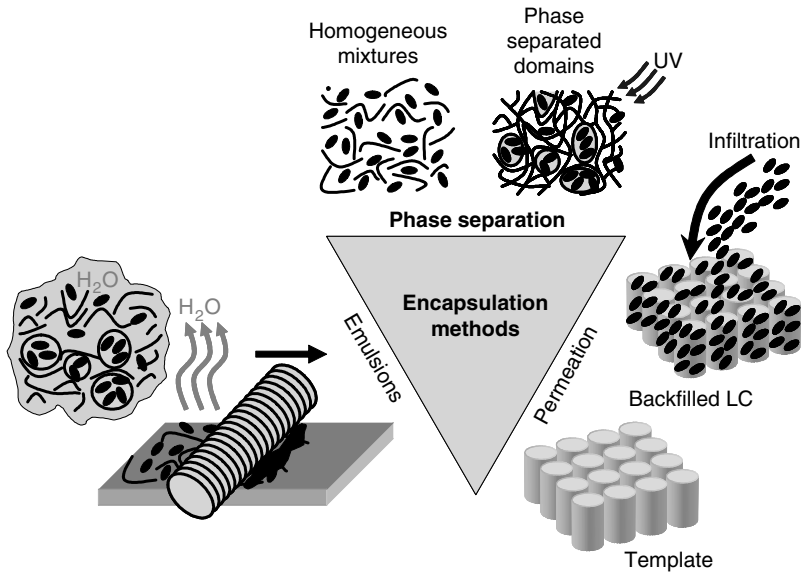


Figure 16.3 Schematic diagram of the various encapsulation methods to achieve confinement of liquid crystals for flexible display applications

homogeneous mixture, which is subsequently exposed to ultraviolet light to initiate photopolymerization (Serbutoviez *et al.* 1996). As polymerization proceeds, the liquid crystal phase separates out into domains. The domain size and shape are locked in by the polymerization. There has also been interest in curing PDLC materials with electron beam techniques (Maschke *et al.* 2004). Using the emulsion process, a liquid crystal and polymer are dispersed in an aqueous water environment. The polymer is typically soluble in water (e.g. polyvinyl alcohol). The emulsion can then be coated on a substrate using a Meyer bar or knife blade (Amimori *et al.* 2003). As the water evaporates from the thin layer, a thin polymer film forms which is responsible for encapsulating the liquid crystal droplets. The final approach is the permeation technique. A prefabricated matrix or template is infiltrated with a liquid crystal. First implemented by Craighead *et al.* (1982), there have been many basic physics studies on liquid crystals confined to a prefabricated matrix (Crawford *et al.* 1992). Most recently, a new type of prefabricated polymer matrix has been disclosed (Liang and Tseng 2003). The prefabricated matrix is known as Microcup and the porous substrate is manufactured using roll-to-roll processing (Liang *et al.* 2003).

16.4 Conformed Polymer-Dispersed Liquid Crystals

This section presents work on conformable polymer dispersed liquid crystals (C-PDLCs) to create a display device that is permanently conformed after manufacture as illustrated in Figure 16.2. A PDLC film is manufactured on indium tin oxide (ITO) coated polyester (PET) substrates and the display is subsequently conformed above the glass transition temperature (T_g) to relieve the stress introduced by the conformation process. This work is directed at applications where the display is conformed through its usable life.

Petitioner Samsung Ex-1011, 0348

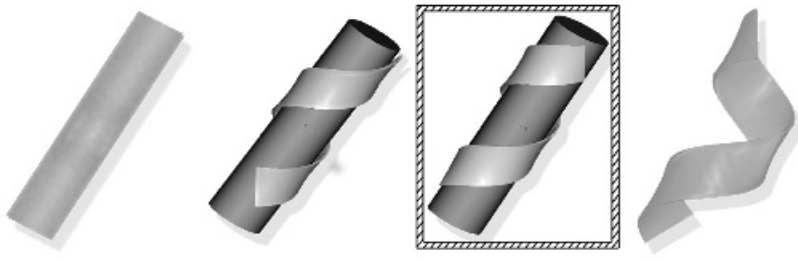


Figure 16.4 The four steps used to created a conformal PDLC. The box in step 3 represents the oven. Reproduced by the permission of the Society for Information Display

To create a conformed PDLC using the phase separation process, a commercial mixture of the reactive monomer (PN393) and liquid crystal (TL205) was used to create the electro-optic medium (both components are commercially available from EM Industries). This material was processed on 1 in $\times$ 5 in PET/ITO substrates using 10 μm spacers, vacuum pressed, and then photopolymerized with an ultraviolet blanket exposure process. The PET/ITO substrates are commercially available from Southwall. The PDLC display was prepared using standard processing techniques. After fabrication, the PDLC sample was wrapped around a 1 in. hollow pipe to create a spiral or it was interlaced between two pipes to create a sine wave deformation as shown in Figure 16.4. While conformed to this configuration, the sample was inserted in the oven at 90 °C (above the glass transition temperature T_g of the PET substrate) for 1 h. The oven in Figure 16.4 is represented as a box. The configuration was then removed and allowed to cool down to room temperature, where the template (pipe) was removed and the PDLC indefinitely retained the shape of the template.

Figure 16.5 shows photographs of actual conformable PDLC. All samples were conformed at room temperature, processed at 90 °C for 1 h and then cooled down to room temperature. In Figure 16.5(a) the conformal nature of one sheet of PET/ITO is demonstrated without any display medium. The control sample (unconformed) is shown in Figure 16.5(b) in the off (left) and on states (right). Figure 16.5(c) and (d) show conformed samples in the off and on states with helical and wave-like deformations. It is clear from Figure 16.5 that the conformal nature of the display is permanently captured and that the PDLC material is still switchable even after the fabrication process.

We have evaluated the electro-optic performance at room temperature before and after the conformal process. The transmission–voltage curve is presented in Figure 16.6 for an ITO/PET sample that was conformed around a 2 in pipe. The results are very interesting for several reasons. There are a few obvious features that can be easily seen in Figure 16.6: (1) lower threshold voltage for deformed displays; (2) significantly less hysteresis for the undeformed sample; and (3) lower contrast for the deformed sample. First, the conformed display has a lower threshold voltage, $V_{th} = \sim 60$ V, as compared to the threshold voltage of the unconformed sample, $V_{th} = \sim 75$ V.

The same sample, measured before heating and deformation and then again after, is used to obtain the data in Figure 16.5(a). Second, the hysteresis is much smaller for the conformed

Petitioner Samsung Ex-1011, 0349

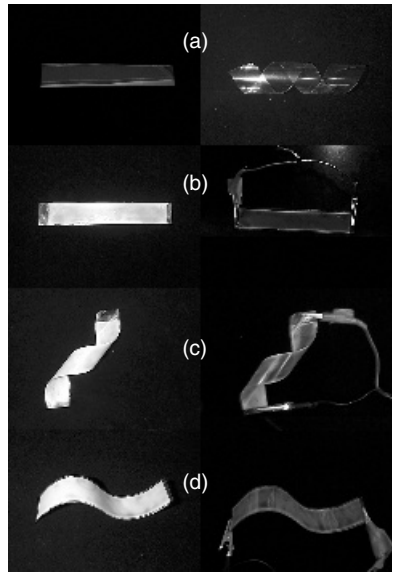


Figure 16.5 Actual conformed PDLC samples in the off (left) and on (right) states: (a) an ITO/PET substrate, (b) a control PDLC (nonconformed), (c, d) a spiral and wavy conformed PDLC sample. Reproduced by the permission of the Society for Information Display

sample at 50% transmission, $\Delta V_{50} = 1.4$ V, as compared to the unconformed sample, $\Delta V_{50} = 4.4$ V. The contrast ratio decreases in the conformed sample. Using a HeNe laser and a silicon detector (diameter = 1 mm) positioned 10 cm away from the PDLC sample, the contrast ratio is ~300:1 for the undeformed samples and ~20:1 for the conformed sample. We believe that the strain introduced by conforming the display can bias the droplet director configuration to some extent and enable it to switch at lower voltages, which would also explain the reduced hysteresis, and the less desirable feature of lowering the contrast. In principle, the PDLC would be in the neutral plane, but the heat treatment certainly alters the stress distribution.

To successfully implement the conformal process for a workable display, the PET/ITO substrates are crucial. In order to demonstrate the concept of stress relaxation, an experiment was performed where the PET substrate was loaded to 8% strain and then the temperature was raised above T_g as shown in Figure 16.6(b). It is clear in Figure 16.6(b) that the stress in the substrate significantly relaxes over time. This demonstrates that stress relaxation occurs during the conforming process (Gorkhali *et al.* 2003).

16.5 Holographic Polymer-Dispersed Liquid Crystals

Holographically formed polymer-dispersed liquid crystals (H-PDLCs) are a variation of conventional PDLCs (Crawford and Zumer 1996). Instead of a UV blanket exposure, PDLC materials are photopolymerized in the presence of an interference pattern of two plane waves (Sutherland *et al.* 1994). There are many material formulations which can be used to create H-PDLCs (Sutherland *et al.* 1993; De Sarkar *et al.* 2002; 2003; Natarajan *et al.* 2003). Through

Petitioner Samsung Ex-1011, 0350

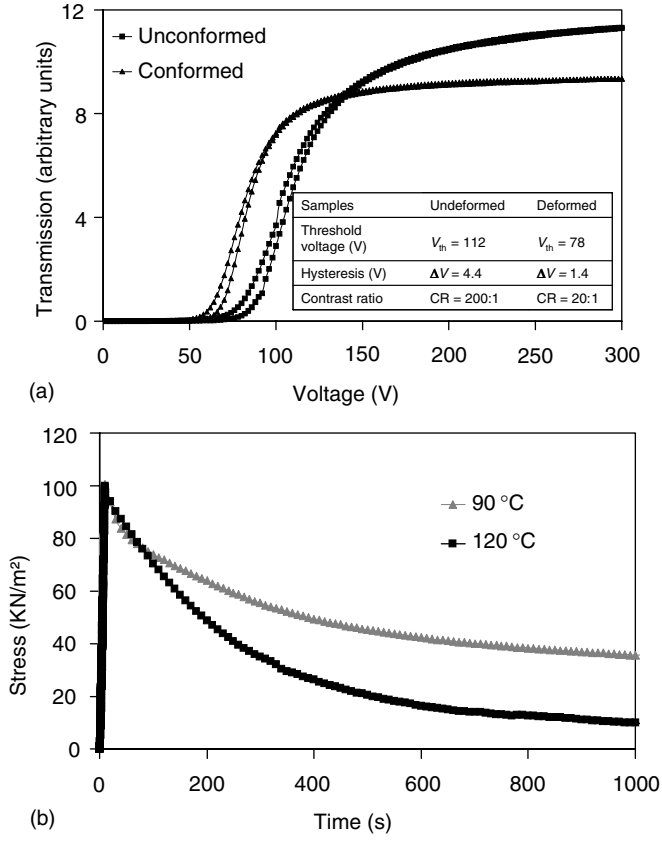


Figure 16.6 (a) Transmission–voltage curve for the conformed PDLC and (b) stress relaxation curve for PET/ITO. Reproduced by the permission of the Society for Information Display

a diffusion/counterdiffusion process during exposure, the interference pattern is permanently recorded and a periodic structure consisting of alterating polymer-rich and LC-rich layers is created as shown in Figure 16.7 (Bowley and Crawford 2000). The periodic structure of H-PDLCs offer unique Bragg reflection properties, which can be turned on and off by applying an electric field. H-PDLCs have been considered for various applications (Crawford 2003; Pogue *et al.* 2000), but we will only discuss their potential in reflective display applications in this section (Tanaka *et al.* 1995; 1999; Date *et al.* 1995; 1998; Crawford *et al.* 1996).

Tanaka and coworkers first recognized the potential of H-PDLC materials in reflective display applications and reported reflection mode Bragg gratings formed holographically (Tanaka *et al.* 1995). If the grating pitch is in the range 150–220 nm, a very narrow band of visible light (∼20–30 nm) can be selectively reflected from the H-PDLCs since there is an index mismatch between the LC-rich planes and the polymer-rich planes, as shown in Figure 16.7(a). Much as in PDLC displays (Figure 16.2), these H-PDLC Bragg gratings can be turned off by an external field, as shown in Figure 16.7(b). H-PDLCs can be tailored to reflective red, green, or blue; it depends on the exposure conditions used to define the pitch.

Petitioner Samsung Ex-1011, 0351

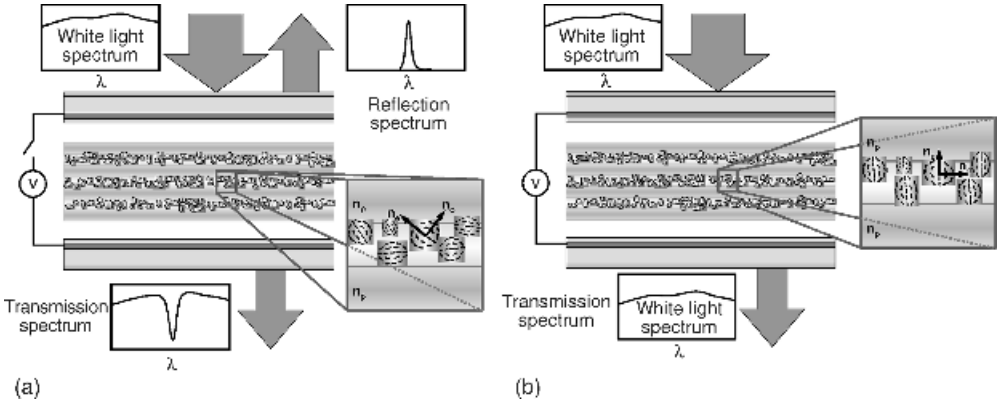


Figure 16.7 Schematic diagram of the H-PDLC display in (a) reflecting and (b) transmissive states

Due to their high color purity and ease of formation, H-PDLCs have been proposed for full-color reflective display applications (Crawford *et al.* 1996). Since there is minimal overlap between the spectral power distribution functions, a broad color gamut is also possible as shown in Figure 16.8(a). Three primary colors (red, green, and blue) can be fabricated using different wavelength lasers (Tanaka *et al.* 1995) or even using one laser (Date *et al.* 1995). Figure 16.8(a) shows the reflectance spectra of three H-PDLC filters and Figure 16.8(b) shows their corresponding chromaticity coordinates. As is evident in Figure 16.8(b), if glare is present then the H-PDLC has a suppressed color gamut. This is expected since the reflection from the holographic planes coincides with the glare from the top substrates. To alleviate this problem to obtain a larger color gamut as shown in Figure 16.8(b), glare can be suppressed by orienting the holographic planes at a slight angle so that they are not parallel with the substrate plane (Yuan *et al.* 1999).

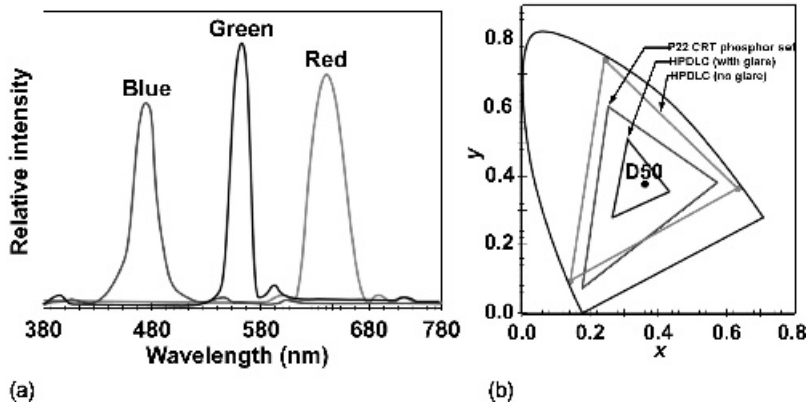


Figure 16.8 (a) The spectral reflectance of an RGB H-PDLC stack and (b) its corresponding chromaticity coordinates compared to a conventional CRT. Reproduced by the permission of the Society for Information Display

Petitioner Samsung Ex-1011, 0352

There have been two outstanding issues associated with H-PDLCs that have probably hindered their use in reflective display applications. First, the driving voltages of H-PDLCs is often well above 100 V since the droplets are so small. Since the droplets are constrained to the Bragg planes, their size tends to be less than 150 μm if visible reflections are desired. Second, H-PDLCs are Bragg reflectors so their viewing angle is very narrow. Some progress has been made toward remedying these issues. By introducing long hydrocarbon chain surfactants into the H-PDLC mixtures (Yuan *et al.* 1999), the drive voltages can be decreased to values less than 100 V, as shown in Figure 16.9(a). It is hypothesized that the surfactant lowers the surface anchoring energy between the liquid crystal and the polymer droplet wall, thereby reducing the drive voltage. To broaden the viewing angle, one can insert a diffusion film in front of one of the laser beams during exposure. This results in holographic planes that are ''fractured,'' which gives rise to reflections over a larger viewing volume, as shown in Figure 16.9(b) (Escuti *et al.* 2000). In addition, by forming droplets using a multi-dimensional interference pattern (Escuti *et al.* 2002), the reflectance versus voltage curve becomes steeper, so they can have a higher number of multiplexed lines (Alt and Pleshko 1974). With further improvements on the drive voltage and viewing angle, H-PDLCs may be future candidates for flexible and reflective full-color displays.

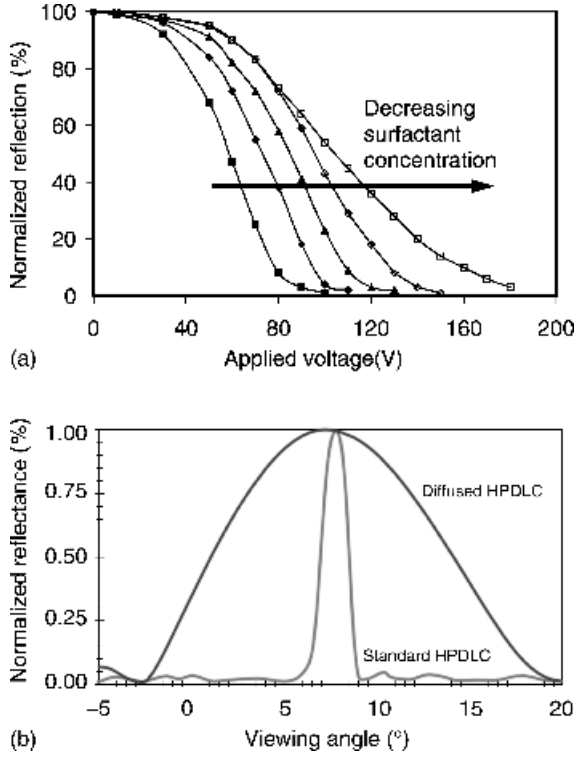


Figure 16.9 (a) Reflectance versus voltage of an H-PDLC that has been doped with a surfactant to lower its drive voltage and (b) a comparison of the viewing angle for a standard H-PDLC and one that has been fabricated using a diffusion plate during exposure. Reproduced by the permission of the Society for Information Display

Petitioner Samsung Ex-1011, 0353

16.6 Prefabricated Templates Impregnated with Liquid Crystal

The use of prefabricated templates filled with liquid crystal dates back to the early 1980s (Craighead *et al.* 1982). The primary reason that they were not commercialized was their poor contrast; however, the underlying principle is still sound. A new type of template is currently under development and is known as Microcup (Liang and Tseng 2003). Using a roll-to-roll process, small cylindrical holes can be created in a polymer film, as shown in Figure 16.10.

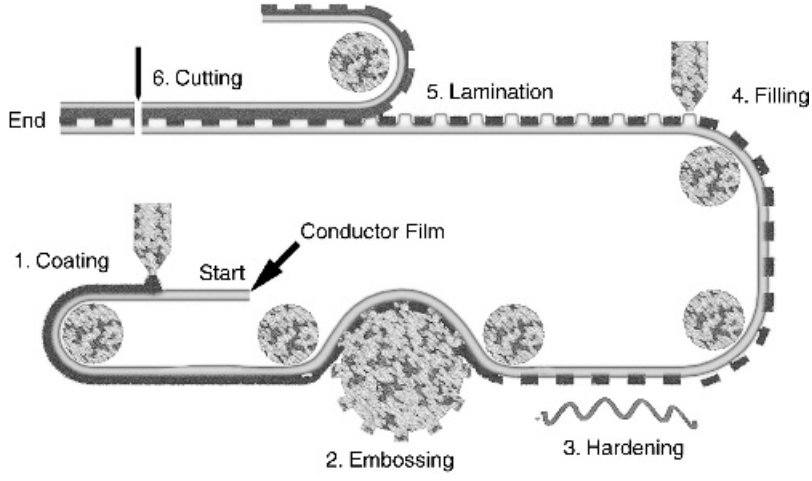


Figure 16.10 Schematic diagrams of roll-to-roll processing for Microcup LCD manufacturing where a polymer template is made through embossing and subsequently hardened before liquid crystal filling. Adapted from Liang and Tseng (2000)

The Microcup substrate process involves coating a UV-curable polymer composition on a conducting substrate (e.g. ITO/PET) followed by embossing and hardening of the polymer, as shown in Figure 16.10. As with PDLCs, the liquid crystal that is filled into the cups has its ordinary index of refraction matched to the Microcup matrix. After filling, the Microcups are sealed and laminated with a second conducting film. The liquid crystal Microcups have been reported to switch at threshold voltages around 3 V and they clear around 10 V (Liang and Tseng 2003).

16.7 Summary

Various types of nematic liquid crystal polymer dispersions were presented in this chapter, ranging from conventional PDLCs and holographic PDLCs, to backfilled polymer templates. It is almost a foregone conclusion that liquid crystals will be confined or stabilized in some form when implemented in flexible display configurations. When encapsulated in a polymer binder, the PDLCs can be manufactured and conformed with a high-temperature

Petitioner Samsung Ex-1011, 0354

process for applications needing a curved display. H-PDLCs have many advantages for full-color applications but they still have a relatively high driving voltage. The use of prefabricated polymer templates that are backfilled with liquid crystal appears to be very attractive for flexible display applications, since the roll-to-roll process has already been established.

References

Aliev, F. M. and Breganov, M. N. (1989) Electric polarization and dynamics of molecular motion of polar liquid crystals in micropores and macropores. *Zhurnal Eksperimentalnoi I Teoreticheskoi Fiziki* **95**, 122–138 (*Soviet Physics JETP* **68**, 70–79).

Aliev, F. M. and Kelly, J. (1994) Dynamics, structure, and phase transitions in ferroelectric liquid crystal confined in a porous matrix. *Ferroelectrics* **151**, 263–268.

Alt, P. M. and Pleshko, P. (1974) Scanning limitations of liquid crystal displays. *IEEE Transactions on Electron Devices* **ED-21**, 146–155.

Ambrozic, M., Formoso, P., Golemme, A. and Zumer, S. (1997) Anchoring and droplet deformation in polymer dispersed liquid crystals: NMR study in an electric field. *Physical Review E* **56**, 1825–1832.

Amimori, I., Priezjev, N. V., Pelcovits, R. A. and Crawford, G. P. (2003) Optomechanical properties of stretched polymer dispersed liquid crystal films for scattering polarizer applications. *Journal of Applied Physics* **93**, 3248–3252.

Amundson, K. R. (1998) Imprinting of nematic order at surfaces created by polymerization-induced phase separation. *Physical Review E* **58**, 3273–3279.

Amundson, K. R. and Srinivasarao, M. (1998) Liquid-crystal-anchoring transitions at surfaces created by polymerization-induced phase separation. *Physical Review E* **58**(2), R1211–R1214.

Amundson, K., van Blaaderen, A. and Wiltzius, P. (1997) Morphology and electro-optic properties of polymer-dispersed liquid-crystal films. *Physical Review E* **55**, 1646–1654.

Anoardo, E., Grinberg, F., Vilfan, M. and Kimmich, R. (2004) Proton spin-lattice relaxation in a liquid crystal-aerosil complex above the bulk isotropization temperature. *Chemical Physics* **297**, 99–110.

Bellini, T., Clark, N. A., Muzny, C. D., Wu, L., Garland, C. W., Schaefer, D. W. and Oliver, B. J. (1992) Phase behavior of the liquid crystal 8CB in silica aerogel. *Physical Review Letters* **69**, 788–791.

Bowley, C. C. and Crawford, G. P. (2000) Diffusion kinetics of formation of holographic polymer-dispersed liquid crystal display materials. *Applied Physics Letters* **76**, 2235–2237.

Candau, S., LeRoy, P. and Debeauvais, F. (1973) Magnetic field effects in nematic and cholesteric droplets suspended in an isotropic liquid. *Molecular Crystals and Liquid Crystals* **23**, 283–297.

Chandrasekhar, S. (1966) Surface tension of liquid crystals. *Molecular Crystals* **2**, 71–80.

Cladis, P. E. (1974) Study of the nematic and smectic A phases of an N-p-cyanobenzylidene-p-n-octyloxyaniline in tubes. *Philosophical Magazine* **29**, 641–663.

Cladis, P. E. and Kleman, M. (1972) Nonsingular disclinations of strength $S = +1$ in nematics. *Journal de Physique* **33**, 59–598.

Cladis, P. E., White, A. E. and Brinkman, W. F. (1979) Non-singular defect structures near the smectic A transition. *Journal de Physique* **40**, 325–335.

Clark, N. A., and Lagerwall, S. T. (1980) Submicrosecond bistable electro-optic switching in liquid crystals. *Applied Physics Letters* **36**, 899–901.

Clark, N. A., Bellini, T., Malzbender, R. M., Thomas, B. N, Rappaport, A. G., Muzny, C. D., Schaefer, D. W. and Hrubesh, L. (1993) X-ray scattering study of smectic ordering in a silica aerogel. *Physical Review Letters* **71**, 3505–3508.

Craighead, H. G., Cheng, J. and Hackwood, S. (1982) New display based on electrically induced index matching in an inhomogeneous medium. *Applied Physics Letters* **40**, 22–24.

Petitioner Samsung Ex-1011, 0355

Crawford, G. P. (2003) Electrically switchable Bragg gratings. *Optics and Photonics News* **14**, 54–59.
Crawford, G. P. and Zumer, S. (eds) (1996) *Liquid Crystals in Complex Geometries Formed by Polymer and Porous Networks*, Taylor & Francis, London.
Crawford, G. P., Vilfan, M., Doane, J. W. and Vilfan, I. (1991) Escaped-radial nematic configurations in submicrometer-size cylindrical cavities–deuterium NMR study. *Physical Review A* **43**, 835–842.
Crawford, G. P., Allender, D. W. and Doane, J. W. (1992) Surface elastic and molecular anchoring properties of nematic liquid crystals. *Physical Review A* **45**, 8693–8708.
Crawford, G. P., Ondris-Crawford, R. J., Zumer, S. and Doane, J. W. (1993) Anchoring and orientational wetting transitions of confined liquid crystals. *Physical Review Letters* **70**, 1838–1841.
Crawford, G. P., Polak, R. D., Scharkowski, A., Chien, L.-C, Zumer, S. and Doane, J. W. (1994) Nematic director-fields captured in polymer networks confined to spherical droplets. *Journal of Applied Physics* **75**, 1968–1971.
Crawford, G. P., Scharkowski, A., Fung, Y. K., Zumer, S. and Doane, J. W. (1995) Internal surface orientational order and distribution of a polymer network in a liquid crystal. *Physical Review E* **52**, R1273–R1276.
Crawford, G. P., Fiske T. G. and Silverstein, L. D. (1996) Reflective color LCDs based on H-PDLC and PSCT technologies. *SID Digest of Technical Papers* **XXVII**, 99–102.
Crooker, P. P. and Yang, D. K. (1990) Polymer-dispersed chiral liquid crystal color display. *Applied Physics Letters* **57**, 2529–2531.
Date, M., Naito, N., Tanaka, K., Kato, K. and Sakai, K. (1995) Three-primary-color holographic polymer dispersed liquid crystal (HPDLC) for reflective displays. *Proceedings of the 15th International Display Research Conference* **15**, 603–606.
Date, M., Takeuchi, Y., Tanaka, K. and Kato, K. (1998) Reflectivity improvement in holographic polymer dispersed liquid crystal (HPDLC) reflective display devices by controlling alignment. *IEICE Transactions on Electronics* **E81C**, 1685–1690.
De Sarkar, M., Qi, J. and Crawford, G. P. (2002) Influence of partial matrix fluorination on morphology and performance of HPDLC transmission gratings. *Polymer,* **43**, 7335–7344.
De Sarkar, M., Gill, N. L., Whitehead, J. B. and Crawford, G. P. (2003) Effect of monomer functionality on the morphology and performance of the holographic transmission gratings recorded on polymer dispersed liquid crystals. *Macromolecules* **36**, 630–638.
Doane, J. W. (1991) Polymer-dispersed liquid crystals: boojums at work. *MRS Bulletin* **16**, 22–28.
Doane, J. W., Vaz, N. A., Wu, B. G. and Žumer, S. (1986) Field controlled light scattering from nematic microdroplets. *Applied Physics Letters* **48**, 269–271.
Drzaic, P. (1995) *Liquid Crystal Dispersions,* World Scientific, River Edge NJ.
Drzaic, P. S. (1986) Polymer-dispersed nematic liquid crystal for large area displays and light valves. *Journal of Applied Physics* **60**, 2142–2148.
Dubois-Violette, E. and Parodi, O. (1969) Emulsions nematiques: effets de champ magnetiques et effets piezo-electriques. *Journal de Physique Colloque* **30**, C4-57 to C4-64.
Dzyaloshinskii, E. (1970) Theory of disclinations in liquid crystals. *Zhurnal Eksperimentalnoi I Teoreticheskoi Fiziki* **58,** 1443–1452 (*Soviet Physics JETP* **31**, 773–777).
Erdmann, J. H., Zumer, S. and Doane, J. W. (1990) Configuration transition in nematic liquid crystals confined to a small spherical cavity. *Physical Review Letters* **64**, 1907–1910.
Escuti, M. J., Kossyrev, P., Crawford, G. P., Fiske, T. G., Colegrove, J. and Silverstein, L. D. (2000) Expanded viewing-angle reflection from diffuse holographic-polymer dispersed liquid crystal films. *Applied Physics Letters* **77**, 4262–4264.
Escuti, M. J. and Crawford, G. P. (2002) Tailoring morphology in holographic-polymer dispersed liquid crystals for reflective display applications. *SID Digest of Technical Papers* **XXXIII**, 550–553.
Fergason, J. L. (1985) Polymer encapsulated nematic liquid crystals for display and light control applications. *SID Digest of Technical Papers* **XVI**, 68–71.
Golemme, A., Zumer, S., Doane, J. W. and Neubert, M. E. (1988a) Deuterium NMR of polymer-dispersed liquid crystals. *Physical Review A* **37**, 559–569.

Petitioner Samsung Ex-1011, 0356

Golemme, A., Zumer, S., Allender, D. W. and Doane, J. W. (1988b) Continuous nematic-isotropic transition in sub-micrometer-size liquid-crystal droplets. *Physical Review Letters* **61**, 2937–2940.

Gorkhali, S., Cairns, D. R. and Crawford, G. P. (2003) Reliability of transparent conducting substrates for rollable displays: a cyclic loading investigation. *SID Digest of Technical Papers* **XXXIV**, 1332–1335.

Hikmet, R. A. M. (1990) Electrically induced light scattering from anisotropic gels. *Journal of Applied Physics* **68**, 4406–4412.

Hikmet, R. A. M. (1991) Anisotropic gels and plasticized networks formed by liquid crystal molecules. *Liquid Crystals* **9**, 405–416.

Hikmet, R. A. M. and Zwerver, B. H. (1991) Dielectric relaxation of liquid crystal molecules in anisotropic confinements. *Liquid Crystals* **10**, 835–847.

Hilsum, C. (1976) Electrooptic device, UK Patent 1,442,360.

Iannacchione, G. S., Crawford, G. P., Zumer, S., Doane, J. W. and Finotello, D. (1993) Randomly constrained orientational order in porous glass. *Physical Review Letters* **71**, 2595–2598.

Iannacchione, G. S., Crawford, G. P., Qian, S. and Doane, J. W. (1996) Nematic ordering in highly restrictive Vycor glass. *Physical Review E* **53**, 2402–2411.

Jakli, A., Kim, D. R., Chien, L. -C. and Saupe, A. (1992) Effect of a polymer network on the alignment and rotational viscosity of a nematic liquid crystal. *Journal of Applied Physics* **72**, 3161–3164.

Jakli, A., Bata, L., Fodor-Csorba, K., Rosta, L. and Noirez, L. (1994) Structure of polymer networks dispersed in liquid crystals: small angle neutron scattering study. *Liquid Crystals* **17**, 227–234.

Jin, T. and Finotello, D. (2004) Controlling disorder in liquid crystal aerosil dispersions. *Physical Review E* **69**(4), article 041704.

Jin, T., Crawford, G. P., Crawford, R. J., Zumer, S. and Finotello, D. (2003) Surface ordering transitions at a liquid crystal-solid interface about the isotropic smectic-A transition. *Physical Review Letters* **90**, 015504-1 to 015504-4.

Kitzerow, H. -S., Molsen, H. and Heppke, G. (1992) Linear electro-optic effects in polymer-dispersed ferroelectric liquid crystal. *Applied Physics Letters* **60**, 3093–3095.

Kralj, S., Lahajnar, G., Zidansek, A., Vrbancic-Kopac, N., Vilfan, M., Blinc, R. and Kosec, M. (1993) Deuterium NMR of a 5CB liquid crystal confined in silica aerogel matrix. *Physical Review E.* **48**, 340–349.

Kreuzer, M. and Eidenschink, R. (1996) Filled nematics. In *Liquid Crystals in Complex Geometries Formed by Polymer and Porous Networks*. Crawford, G. P. and Zumer, S. (eds), Taylor & Francis, London.

Kurik, M. V. and Lavrentovich, O. D. (1982) Negative–positive monopole transitions in cholesteric liquid crystals. *Pis'ma Zhurnal Eksperimentalnoi I Teoreticheskoi Fiziki* **35**, 362–365 (*Soviet Physics JETP Lett.* **35**, 444–447).

Lee, K. P., Suh, S.-W. and Lee, S. -D. (1994) Fast linear electro-optical switching properties of polymer-dispersed ferroelectric liquid crystals. *Applied Physics Letters* **64**, 718–720.

Lehmann, O. (1904) Die Hauptstatze der Lehre von den Flussigen Kristallen. In *Flussige Kristalle*, Engelmann, Leipzig.

Liang, R. C. and Tseng, S. (2003) Microcup LCD: a new type of dispersed LCD by a roll-to-roll manufacturing process. *Proceedings of the International Display Manufacturing Conference* **3**, 351–354.

Liang, R. C., Hou, J., Chung, J., Wang, X., Pereira, C. and Chen, Y. (2003) Microcup active and passive matrix electrophoretic displays by a roll-to-roll manufacturing processes, *SID Digest of Technical Papers* **XXXIV**, 838–841.

Mang, J. T., Sakamoto, K. and Kumar, S. (1992) Smectic layer orientation in confined geometries. *Molecular Crystals and Liquid Crystals* **223**, 133–142.

Margerum, J. D., Lackner, A. M., Ramos, E., Smith, G. W., Vaz, N. A., Kohler, J. L. and Allison, C. R. (1990) Polymer dispersed liquid crystal film devices, and a method of forming the same. US Patent 4,938,568.

Petitioner Samsung Ex-1011, 0357

Mariani, P., Samori, B., Angeloni, A. S. and Ferruti, P. (1986) Polymerization of bisacrylic monomers within a liquid crystalline smectic B solvent. *Liquid Crystals* **1**, 327.

Maritan, A., Cieplak, M., Bellini, T. and Banavar, J. R. (1994) Nematic–isotropic transition in porous media. *Physical Review Letters* **72**, 4113–4116.

Maschke, U., Coqueret, X., Vendamme, R., Pakula, T. and Benmouna, M. (2004) Properties of electron beam cured reverse mode PDLC films. *Molecular Crystals and Liquid Crystals* **413**, 2157–2163.

Melzer, D. and Nabarro, F. R. N. (1977) Optical studies of a nematic liquid crystal with circumferential surface orientation in a capillary, *Philosophical Magazine* **35**, 901–906.

Meyer, R. B. (1969) Piezoelectric effects in liquid crystals. *Physical Review Letters* **22**, 918–921.

Meyer, R. B. (1973) On the existence of even-indexed disclination *s* in nematic liquid crystals. *Philosophical Magazine* **27**, 405–424.

Molsen, H. and Kitzerow, H. S. (1994) Bistability in polymer-dispersed ferroelectric liquid-crystals. *Journal of Applied Physics* **75**(2), 710–716.

Muncha, M. (2003) Polymer as an important component of blends and composites with liquid crystals. *Progress in Polymer Science* **28**, 837–873.

Natarajan, L. V., Shepherd, C. K., Brandelik, D. M., Sutherland, R. L., Chandra, S., Tondiglia, V. P., Tomlin, D. and Bunning, T. J. (2003) Switchable holographic polymer-dispersed liquid crystal reflection gratings based on thiol-ene photopolymerization. *Chemistry of Materials* **15**, 2477–2484.

Ondris-Crawford, R. J., Boyko, E. P., Wagner, B. G., Erdmann, J. H., Zumer, S. and Doane, J. W. (1991) Microscope textures of nematic droplets in polymer-dispersed liquid crystals. *Journal of Applied Physics* **69**, 6380–6386.

Pogue, R. T., Sutherland, R. L., Schmitt, M. G., Natarajan L. V. Siwecki, S. A., Tondiglia, V. P. and Bunning, T. J. (2000) Electrically switchable Bragg gratings from liquid crystal/polymer composites. *Applied Spectroscopy* **54**(1), 12A–28A.

Press, M. J. and Arrott, A. S. (1974) Theory and experiment on configurations with cylindrical symmetry in liquid crystal droplets. *Physical Review Letters* **33**, 403–406.

Rappaport, A. G., Clark, N. A., Thomas, B. N. and Bellini, T. (1996) X-ray scattering as a probe of smectic a liquid crystal ordering in silica aerogels. In *Liquid Crystals in Complex Geometries Formed by Polymer and Porous Networks*, Crawford, G. P. and Zumer, S. (eds), Taylor & Francis, London.

Saupe, A. (1973) Disclinations and properties of the directorfield in nematic and cholesteric liquid crystals. *Molecular Crystals and Liquid Crystals* **21**, 211–238.

Serbutoviez, C., Kloosterboer, J. G., Boots, H. M. J. and Touwslager, F. J. (1996) Polymerization-induced phase separation 2. Morphology of polymer-dispersed liquid crystal thin films, *Macromolecules* **29**, 7690–7698.

Stannarius, R., Crawford, G. P., Chien, L.-C. and Doane, J. W. (1991) Nematic director orientation in a liquid crystal dispersed polymer: a DNMR approach. *Journal of Applied Physics* **70** 135–143.

Sutherland, R. L., Natarajan, L. V., Tondiglia, V. P. and Bunning, T. J. (1993) Bragg gratings in an acrylate polymer consisting of periodic polymer-dispersed liquid-crystal planes. *Chemistry of Materials* **5**, 1533–1538.

Sutherland, R. L., Tondiglia, V. P., Natarajan, L. V., Bunning, T. J. and Adams, W. W. (1994) Electrically switchable volume gratings in polymer-dispersed liquid crystals. *Applied Physics Letters* **64**, 1074–1076.

Tanaka, K., Kato, K., Date, M. and Sakai, S. (1995) Optimization of holographic PDLC for reflective color display applications. *SID Digest of Technical Papers* **XXVI**, 267–270.

Tanaka, K., Kato, K. Tsuru, S. and Sakai, S. (1994) Holographically formed liquid-crystal/polymer device for reflective color display. *SID Journal* **2**, 37–41.

Tanaka, K., Kato, K. and Date, M. (1999) Fabrication of holographic polymer dispersed liquid crystal (HPDLC) with high reflection efficiency. *Japanese. Journal of Applied Physics* **38**, L277–L278.

Volovik, G. E. and Lavrentovich, O. D. (1983) Topological dynamics of defects: boojums in nematic droplets,.*Zhurnal Eksperimentalnoi I Teoreticheskoi Fiziki* **85**, 1997–2010 (*Soviet Physics JETP* **58**, 1159–1166).

Petitioner Samsung Ex-1011, 0358

West, J. L. (1988) Phase separation of liquid crystals in polymers. *Molecular Crystals and Liquid Crystals* **157**, 427–441.

Williams, C. E., Pieranski, P. and Cladis, P. E. (1972) Nonsingular $S = +1$ screw disclination lines in nematics. *Physical Review Letters* **29**, 90–92.

Wu, X., Goldburg, W. I., Liu, M. X. and Xue, J. Z. (1992) Slow dynamics of isotropic-nematic phase transition in silica gels. *Physical Review Letters* **69**, 470–473.

Yang, D. K. and Crooker, P. P. (1991) Field-induced textures of polymer-dispersed chiral liquid crystal microdroplets. *Liquid Crystals* **9**, 245–251.

Yang, D. K., Chien, L. -C. and Doane, J. W. (1992) Cholesteric liquid crystal/polymer dispersions for haze-free light shutters. *Applied Physics Letters* **60**, 3102–3104.

Yang, D. K., Fung, Y. K., and Chien, L. C. (1996) Polymer stabilized textures: materials and applications, Chapter 5 in *Liquid Crystals in Complex Geometries*, Gregory P. Crawford and Slobodan Zumer (eds), Taylor & Francis, London.

Yang, D. K., Lin, J. P., Li, T., Lin, S. L. and Tian, X. H. (2004) Effect of external electrical field on phase behavior and morphology development of polymer dispersed liquid crystal. *European Polymer Journal* **40**, 1823–1832.

Yuan, H., Hu, G., Fiske, T., Lewis, A., Gunther, J. E., Silverstein, L. D., Bowley, C., Crawford, G. P., Chien, L.-C. and Kelly, J. R. (1998) High efficiency color reflective displays with extended viewing angle. *Proceedings of the 18th International Display Research Conference, Asia Display*, 1136–1138.

Yuan, H., Colegrove, J. J., Hu, G., Fiske, T. G., Lewis, A., Gunther, J. E., Silverstein, L. D., Bowley, C. C., Crawford, G. P., Chien, L.-C. and Kelly J. R. (1999) HPDLC color reflective displays, *Proceedings of SPIE* **3690**, 196–206.

Zyryanov, V. Y., Smorgon, S. L. and Shabanov, V. F. (1993) Electrooptics of polymer-dispersed ferroelectrics. *Ferroelectrics* **143**, 271.

Petitioner Samsung Ex-1011, 0359

17

Cholesteric Liquid Crystals for Flexible Displays

J. William Doane and Asad Khan

Kent Displays, Inc.

17.1 Introduction

Bistable cholesteric reflective displays as described in this chapter were first introduced in 1991 (Yang *et al*. 1991). Since that time, there have been numerous contributions to the technology to develop drive schemes, introduce full color, create black and white (Huang and Doane 2002) as well as fabricate it on plastic substrates (Hashimoto *et al*. 1998; Podojil *et al*. 1998).Since these displays could use existing LCD manufacturing lines and drive chips, commercial display products were soon introduced into the marketplace (Khan *et al*. 2004b); some are shown in Figure 17.1(a).

New products on glass continue to be developed and marketed. One of the most exciting is the electronic book Sigma Book recently announced by Panasonic (Figure 17.1(b)). Being a bistable technology, it is made for such handheld devices as the electronic book because of its extremely low power consumption, wide viewing angle and readability in sunlight and low-level room light.

A problem faced by all new developing display technologies, particularly those manufactured on glass substrates, is that the market is already satisfied to a large extent by the STN, TN and active matrix TN displays. In fact, it is these technologies that enabled most handheld devices that we see on the market today. Nearly everyone has a handheld device such as a cellphone, PDA, handheld instrument or game that would not be possible without

Flexible Flat Panel Displays Edited by G. P. Crawford
© 2005 John Wiley & Sons, Ltd., ISBN 0-470-87048-6

Petitioner Samsung Ex-1011, 0360

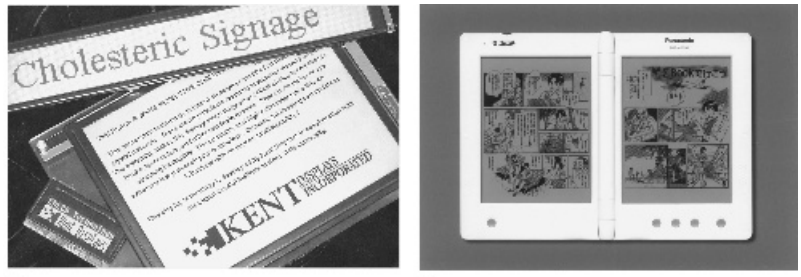


Figure 17.1 (a) Various reflective cholesteric display products on rigid glass substrates: wide 12.1 in sign-type display (blue/white), large 9.4 in ebook-type display (black/white) and small 2.3 in instrumentation-type display (green/black) of Kent Displays, Inc. (b) The electronic book Sigma Book by Matsushita/Panasonic with two cholesteric reflective displays. Part (b) reproduced by the permission of Panasonic

these LCDs. What improvements, at such a low cost, can be made to compete with this? Battery lifetime is an issue with nearly every handheld device. A large contribution to the power consumption in TN/STN devices is the refreshing power to maintain an image on the screen. If an image is refreshed at 30 Hz, this can be a substantial power waste if the image is fixed or unchanging for several seconds, minutes or hours as is the case in many handheld devices. Another issue is reflective brightness and contrast. Most handheld devices are viewed in daylight or room light. Today's technologies are marginal at best for being read without a backlight or not being washed out in bright sunlight. Limited by polarizers, color filters, and other factors, TN/STNs suffer considerable light loss reducing light reflectivity. An obvious missing factor in today's display market is the lack of display technologies on flexible substrates. As outlined in the introduction of this book, there is a need for such devices. Furthermore, there is the potential that such flexible devices could be manufactured at lower cost on web manufacturing lines.

These are the principal driving forces behind the development of flexible bistable cholesteric reflective displays. The issues for flexible cholesteric displays lie primarily in the development of cholesteric, electrode and other display materials that can be coated or printed. In the case of cholesteric materials, an attractive solution to printing or coating is the development of droplet dispersions. Droplet dispersions of liquid crystals are not new; however, droplets that can be suitably switched to retain their bistability, and yet exhibit the desired reflective brightness and contrast, are just now being developed. In addition to all this, the materials and processes should be able to use existing coating and printing technology as well as to take advantage, where possible, of drive and other electronics already developed for the display technology. This chapter covers some of approaches to these issues.

17.2 Basic Properties of Cholesteric Displays

Fundamentally, cholesteric liquid crystals are of interest in that they can be tailored to Bragg reflect light at a preselected wavelength and bandwidth (Crawford 2000; Huang and Doane 2002). The feature comes about because these materials posses a helical structure in which

Petitioner Samsung Ex-1011, 0361

the liquid crystal director twists around a helical axis. The distance over which the director rotates 360° is called the pitch and is denoted by *P*. The reflection band of a cholesteric liquid crystal is located at the wavelength, $\lambda_o = 0.5(n_e + n_o)$ and has the bandwidth, $\Delta\lambda = (n_e - n_o)P$, usually about 80 nm, where n_e and n_o are the extraordinary and ordinary refractive indices of the liquid crystal, respectively (Doane *et al*. 1994). In a cholesteric liquid crystalline material where the helical axes are perfectly aligned, the reflected light is circularly polarized with the same handedness as the helical structure of the liquid crystal.

In the confinement of a display cell, the cholesteric material can be electrically switched to either one of two stable textures, planar or focal conic (Figure 17.2). In the planar texture, the helical axis is oriented perpendicular to the display substrate to Bragg reflect light in a selected wavelength band. Incident unpolarized light will be decomposed into two circularly polarized components of opposite handedness; one of the components will be reflected and the other will pass through. For cholesteric materials with a positive dielectric anisotropy, a low-voltage pulse applied to electrodes on the substrates will change the orientation of the helical axis to an orientation preponderantly parallel to the substrates having a focal conic texture. There are usually numerous defects in this structure that are not illustrated in Figure 17.2 (Wu and Yang 2001) The focal conic texture can also be made very stable and is transparent to all wavelengths. Defects in this texture weakly scatter light. It is desirable to have a focal conic state where the defects are minimized to keep the scattering effect to a minimum.

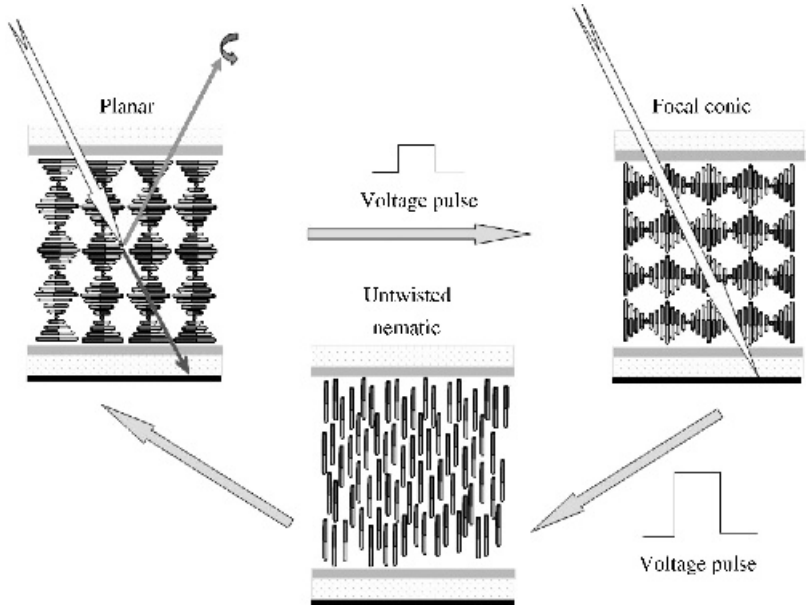


Figure 17.2 Textures of a bistable cholesteric material in a display cell. A small voltage pulse drives the material to a stable transparent focal conic texture whereas a large voltage pulse drives the material through an unstable homeotropic texture to a stable color-reflecting planar texture

Petitioner Samsung Ex-1011, 0362

A higher-voltage pulse applied to the electrodes will untwist the cholesteric material to form a metastable homeotropic texture that will immediately relax to the stable planar state following removal of the pulse.

17.2.1 Cholesteric Domains

In the realization of flexible cholesteric displays, an important property is the domain structure of the planar and the focal states (Doane *et al*. 1994). The domains can vary from submicron to many microns in size depending on the confinement of the cholesteric material. In a typical display cell with rigid substrates, the size of the domains depends on the treatment of the substrate surfaces and the spacing between them (St John *et al*. 1995). In the case of cholesteric droplet dispersions for flexible substrates, the domain texture depends on the size and shape of the droplet as well as the material compositions of the encapsulant and cholesteric liquid crystal.

Before discussing the features of the encapsulated materials, it is instructive to understand domain formation and electro-optical response in the more controlled environment of a cholesteric liquid crystal between two rigid substrates. Figure 17.3 shows microscope photos

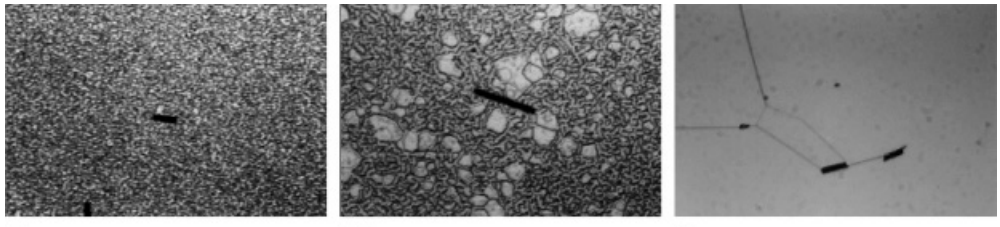


Figure 17.3 Microscope texture photographs of the planar texture with differently prepared substrates to create different domain sizes (the spacer in each photo is 5 μm wide): (a) small domains, less than 5 μm in diameter; (b) mixture of domain sizes from ∼5 to 50 μm; (c) large domains ∼100 μm and larger. Reproduced by the permission of the Society for Information Display

of the domain structures obtained under different substrate treatments (Khan *et al*. 2001). The three photos show domain sizes varying from about 1 μm wide in the first photo to larger that 100 μm in the last photo.

The origin of the domains is itself an interesting topic. They are created by the cholesteric material when it is switched into the reflective texture (Wu and Yang 2001); however, they will vanish in a short period of time if they are not stabilized somehow, either with a surface treatment of the substrates or using the droplet structure of a microencapsulated cholesteric. This feature was not well understood until recently when the system was modeled by Professor Bos and his students at Kent State University (Anderson *et al*. 2001). They found that a complex sequence of texture transitions creates this unusual effect. In the case of rigid substrates, the final stabilized domain texture can be controlled by the degree of homogeneity of the surface alignment layer. The domain structure in droplet dispersions is controlled by droplet, size shape, distribution, and encapsulant material (see later).

Petitioner Samsung Ex-1011, 0363

17.2.2 Display Brightness and View Angle

Increasing the density of domains increases the viewing angle of the display under typical lighting conditions. Each domain has a slightly different orientation for the helical axis and, as such, exhibits a different Bragg angle to the incident light. Consequently, in a collection of domains there exists a distribution in the orientation of the helical axis, hence a distribution in Bragg angles broadening viewing angle. The domain texture and resulting defects in the cholesteric structure further create a light-scattering effect, which increases with the domain density. The net effect provides a reflectance that can be made diffuse and nearly Lambertian, giving it the appearance of printed paper. This is a highly desirable property for a device such as an electronic book.

It is therefore the distribution of helical axes and the defect structure that is controlled to increase the brightness while maintaining a good viewing angle. A balance is obtained between domain size, density and distribution. Figure 17.4 shows a plot of brightness versus wavelength for a planar texture with two different domain sizes. The reflectance is more rounded and the peak is lower for a high density of small domains.

Increasing the brightness by increasing domain size can have a large impact on the viewing angle. A perfect planar texture can reflect 50% of the incident light; however, the reflection is completely specular and therefore appears more like a mirror. The viewing angle is therefore poor unless the ambient lighting conditions are perfectly diffuse. This is rarely the case (Khan *et al.* 2000). On the other hand, displays with small domains are excellent diffuse

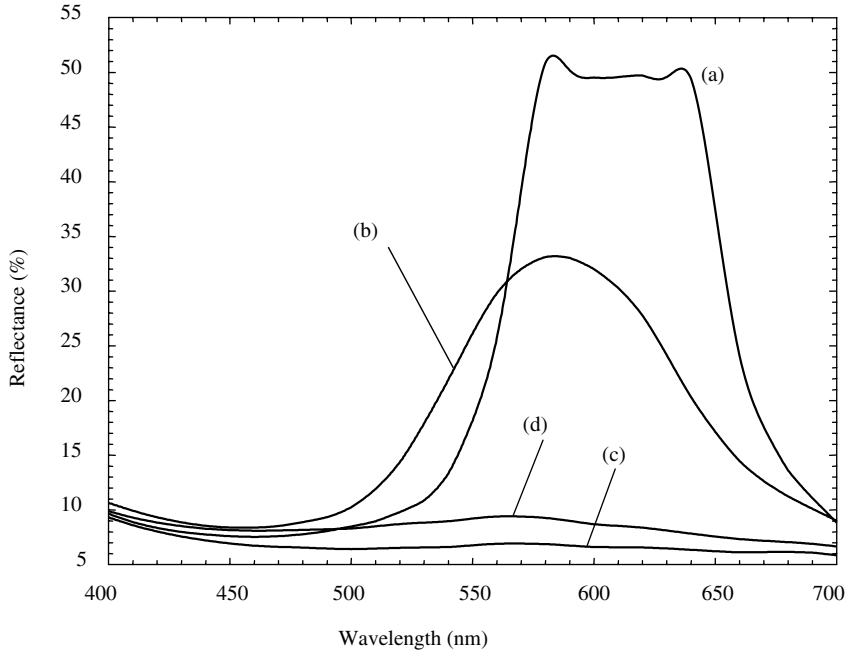


Figure 17.4 Reflection spectra for (a) large domain, near perfect planar texture such as in Figure 17. 2(c); (b) small, high-density domain texture such as in Figure 17.2(a); (c, d), focal conic states for large and small domains, respectively

Petitioner Samsung Ex-1011, 0364

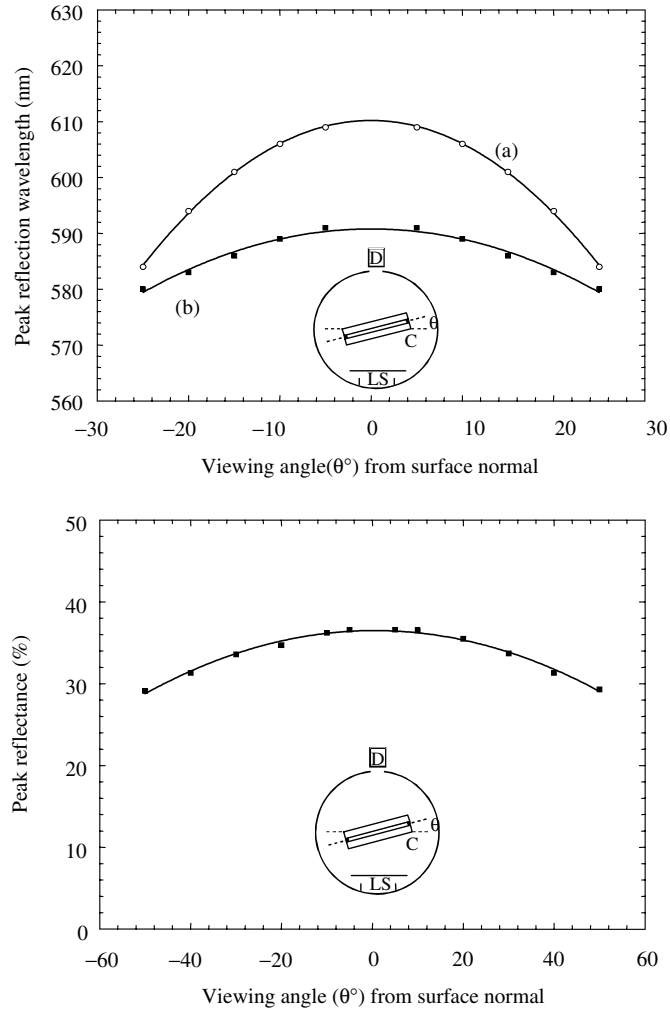


Figure 17.5 The upper figure shows the effect of domain size on color shift with (a) the change in the peak wavelength for a large domain texture and (b) a small domain texture. The lower figure shows reflectance versus view angle. The measurements were made under diffuse lighting conditions

reflectors, giving them a very wide viewing angle (Figure 17.5). The goal, therefore, is to optimize the domain structure to offer high brightness, good viewing angle, and high contrast. Since the cholesteric display is a Bragg-reflective technology, it is somewhat surprising that the color shift can be made so small and, in fact, negligible.

17.2.3 Degree of Circular Polarization and Brightness

The planar cholesteric state will Bragg reflect circularly polarized light of one handedness in a narrow spectral bandwidth. The reflected light is completely circularly polarized in

Petitioner Samsung Ex-1011, 0365

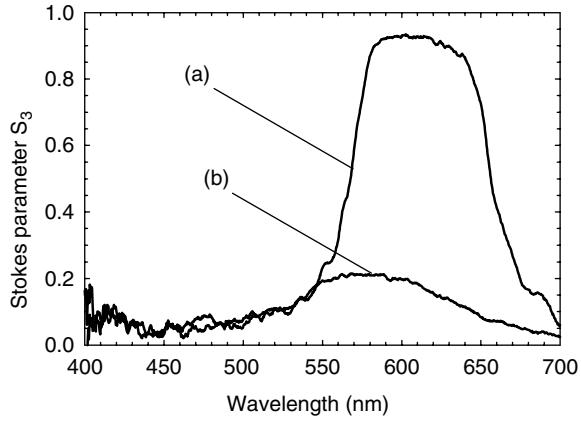


Figure 17.6 S_3 as a function of wavelength for (a) the large domain structure of Figure 17.3(c) and (b) the small, high-density domain structure of Figure 17.3(a). Reproduced by the permission of the Society for Information Display

the narrow reflection band for perfect single-domain planar textures. This, however, is not the case in stabilized planar textures that have a large number of domains and defects. The distribution and scattering from the defects reduce the degree of circularly polarized light reflected from the texture.

A measure of the degree of circular polarization of light is the third Stokes parameter, S_3. This parameter makes up the vertical axis on the Poincaré sphere. The range of the parameter is $-1 \leq S_3 \leq +1$. Values of $+1$ and -1 indicate purely right- and left-handed circularly polarized light, respectively. Figure 17.6 compares S_3 for reflected light from large and small domains as a function of wavelength. It shows that nearly all the reflected light is circularly polarized for large domains, whereas the value of S_3 is significantly reduced for small domains, where only about 20% of the reflected light is circularly polarized.

A display that reflects more than 50% and up to about 80% of the incident light is made by stacking displays cells of left- and right-hand twist (Khan *et al*. 2001). In order to achieve both brightness and wide viewing angle, the upper and lower cells may have different domain sizes. Figure 17.7 shows the reflectivity of a stacked cell with a left-handed twisted cholesteric layer on top of a right-handed twisted layer with a different preparation of domains sizes. High brightness of 75% reflectivity is achieved when the lower layer consists of large domains (as in Figure 17.3(c)) and the upper layer consists of mixed size domains (Figure 17.3(b)). Mixed domain sizes in the upper layer provide a wide viewing angle. The brightness of a stacked left/right system is not significantly enhanced, however, if both of the cells have small domains such that the value of S_3 is small in both cells (Figure 17.6(b)).

17.2.4 Effect of Cell Thickness: Brightness versus Contrast

The display cell has to be thick enough to reflect all the incident light of the appropriate handedness; however, if cholesteric material is too thick, light scattering from the focal conic state will degrade the contrast. Therefore the optimum should be sought in the display

Petitioner Samsung Ex-1011, 0366

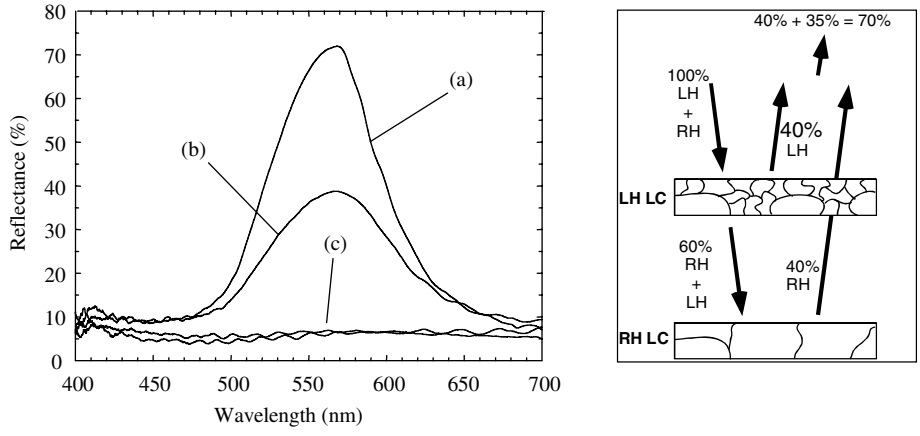


Figure 17.7 Comparison of reflectivity from a stacked display cell with layers of opposite twist. (a) High brightness is achieved when the layers possess large domains structures yielding high S_3 values, as illustrated on the right. (b) Both layers possess small domains which yield small S_3 values. (c) Reflectivity from the focal conic state of both stacked cells arrangements

performance. Figure 17.8(a) shows a theoretical plot of the reflectivity versus thickness (Doane *et al*. 1994) for a large domain structure. With small domains the optimum cell gap needs to be larger. A typical cell gap is about 5 μm.

The display contrast is primarily controlled by the transparency of the focal conic state, which is governed the degree of light scattering exhibited by the focal conic texture. Reducing the density of defects and increasing the size of the focal conic domains will minimize the light scattering. Light scattering from the focal conic texture increases as the cell increases in thickness. If the cell gap becomes too thick, the light scattering begins to degrade (Figure 17.8). In a rigid glass display cell, the treatment of the alignment layer on the glass substrate surface is the standard procedure used to reduce the focal conic scattering and increase the contrast. In encapsulated cholesteric materials, the light scattering and resulting contrast are controlled by the size and shape of the droplets as well as the alignment characteristics of the encapsulant material (see later). The contrast of the display can be improved by designing the display cell so that the black, light-absorbing backplane is as close as possible to the cholesteric material. For single-layer displays, contrast values of 20:1 are readily achieved. The added layers in a multicolor display, particularly those not adjacent to the backplane, contribute extra haze that reduces the contrast with the black background.

17.2.5 Drive Voltage Threshold and Multiplexing

An important feature of cholesteric displays is that the bistability comes with a voltage threshold. This threshold is important in that it avoids the need of an active matrix where a transistor switch is required at each pixel site (Yuan 1996). A reflective display with unlimited resolution is constructed with a simple passive matrix whereby the voltage thresholds allow a low-cost multiplexed driving scheme to address the display. The thresholds are

Petitioner Samsung Ex-1011, 0367

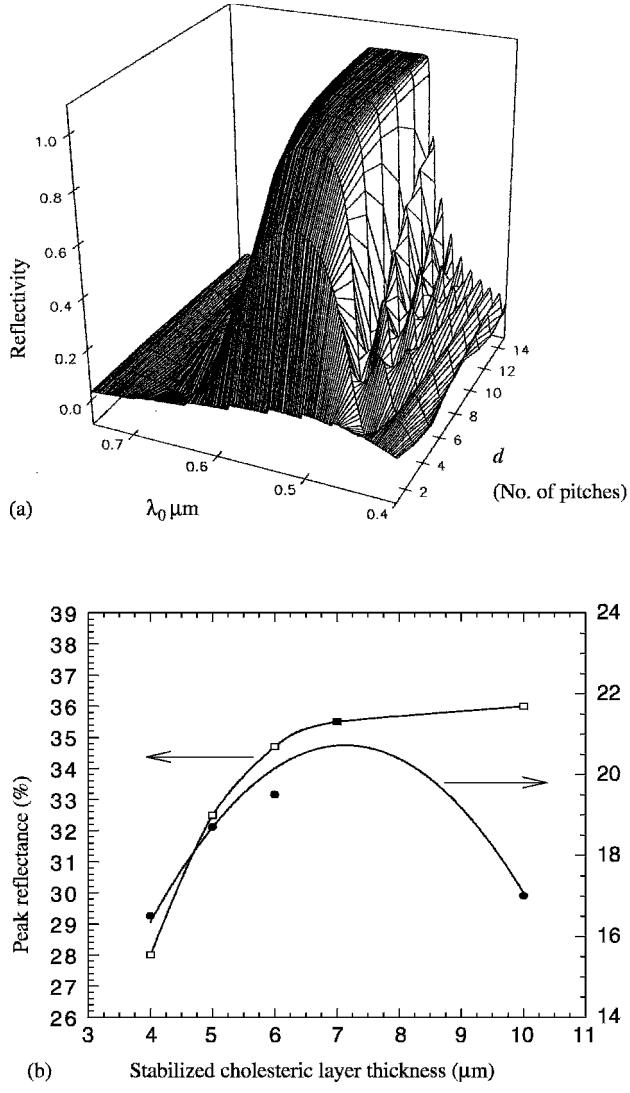


Figure 17.8 (a) Calculated reflection spectra versus cell thickness, d, in units of pitch length, p_0, where $np_0 = 0.54$, $\Delta n = 0.23$, and $n = 1.63$. (b) Experimental plot of reflectance and the contrast versus cell gap thickness for a cholesteric material of $\Delta n = 0.26$, $\Delta\varepsilon = +16.8$ and for substrates that have been treated for small micrometer-sized domains. The measurements were made at room temperature with a 250 Hz pulse of width 100 ms. Part (a) reproduced by the permission of the Society for Information Display

Petitioner Samsung Ex-1011, 0368

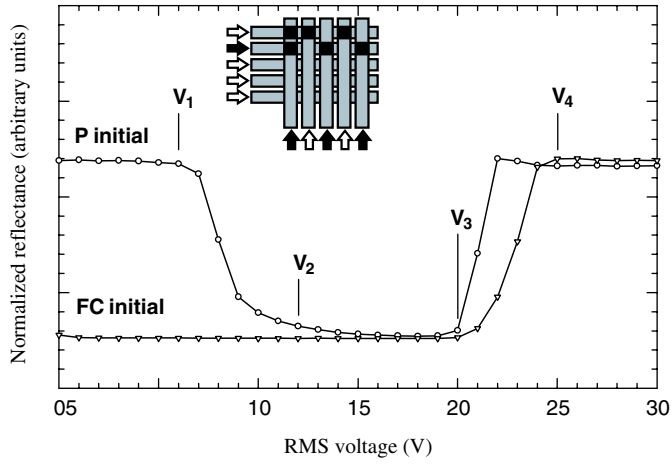


Figure 17.9 Electro-optic response curve of a cholesteric display driven by a voltage pulse, *V,* with a 250 Hz pulse 100 ms wide in a display with a cell gap of 5 μm. The cholesteric material was reflective in the yellow and formulated with a nematic liquid crystal of $\Delta n = 0.22$ and $\Delta\varepsilon = +31.4$. The voltages V_1, V_3, and V_4 are the thresholds important for multiplexing a high- resolution display for passive addressing as illustrated in the inset

seen in the voltage response curve of Figure 17.9. A voltage pulse drives the cholesteric material between planar and focal conic states. If the material is initially in the planar texture, a low-voltage pulse drives the material from the planar state to the focal conic state after reaching a threshold, V_1.

Above V_1 there is a grayscale region where the reflectivity of the display cell begins to diminish, since some of the domains in the display cell or pixel switch to the focal conic state before others. At some voltage, all the domains in the pixel are switched to the focal conic state. Note that the domain texture of the cholesteric material also plays a role in the grayscale capability of a cholesteric display and that this gray scale is reproducible and stable. An image with gray levels is just as stable as one without. It is this grayscale capability that allows a full-color reflective display. At high pulse voltages greater than V_4, the material is switched from the focal conic state to the planar state.

Fundamentally, two drive voltages, V_P and V_{FC}, are required to drive the material to either the planar state or the focal conic state, respectively. Voltage V_P is applied to turn a pixel to the bright state in the selected row and is subject to the constraint that $V_P \geq V_4$. V_{FC} is the voltage applied to turn a pixel to the dark state in the selected row and is subject to the constraint that $V_{FC} \leq V_3$. Note that V_3 and V_4 are selected using a suitable criterion of what constitutes ''dark'' or ''bright'' reflectance, respectively. The voltage seen by nonselect rows, V_{NS}, follows the relation $V_{NS} \leq V_1$. If we take a drive scheme where, $V_{NS} = (V_P - V_{FC})/2$, we can multiplex an indefinite number of rows without crosstalk as long as $(V_4 - V_3)/2 \leq V_1$. The values of V_1 through V_4 are affected by uneven cell spacing, nonuniform cells, and variations in drive waveforms due to ITO resistance and cell capacitance, and temperature gradients across the display. There is a dynamic range of voltages that provides the ability

Petitioner Samsung Ex-1011, 0369

of the display to tolerate variations in V_3 and V_4 while still producing a quality image (Khan *et al*. 2004a).

17.3 Drive Schemes, Chips and Circuitry

The Bragg-reflective texture and the light-scattering texture are stable but, more importantly, they can be switched with an electric field pulse either wholly or partially from one texture to the other with thresholds in the field response curve that allow a high-resolution matrix configuration to be multiplexed. Several driving schemes for the passive matrix have been developed over the years (Rybalochka *et al*. 2000; Roosendaal, *et al*. 2001; Huang *et al*. 1998a). The simplest is the conventional drive (Yuan 1996). For rapid paging, there is the dynamic drive (Huang *et al.* 1995); for video appearance, the cumulative drive (Huang *et al.* 2000) can be used, particularly for small displays.

17.3.1 Conventional Drive

The conventional scheme (Yuan 1996) is currently used on most products. It is not size or resolution limited, but addressing speed is currently about 5 ms per line at room temperature when used with 40 V STN drive chips. The availability and compatibility of low-cost STN drive chips allowed early entry of cholesteric displays into the market. These chips, however, are not optimally designed for bistable displays and their cost is higher than necessary as they were not designed for driving bistable displays. Many of the row and column outputs are often not used and they are size-specific. Furthermore, in a cholesteric display, a driver may be configured to function simultaneously as a column driver and a row driver. New display driver designs can further accommodate all three drive schemes: conventional, dynamic, and cumulative. Until chips specifically designed for cholesteric displays are available, the STN chips offer a solution for some types of display.

17.3.2 Dynamic Drive

Dynamic drive schemes (Huang *et al.* 1995; 1996; Miller *et al.* 2003) are substantially faster and are dramatically faster at low temperatures (Figure 17.10). Taking advantage of a fast transient texture unique to cholesteric materials, the select time of a row can be as short as 50 μs.

The choice of driving technique for cholesteric displays depends on the resolution of the display as well as the intended application. It is possible that more than one drive scheme is employed for a single system in order to optimize driving at different temperatures. An example is the use of the dynamic drive scheme for room temperature and colder conditions and the use of the conventional drive scheme for higher temperatures.

Although STN chips have implemented this drive scheme (Ruth *et al.* 1997), they are not practical for use in products. Kent has developed a low-cost chip specific to this drive scheme. The chip will also accommodate the cumulative drive scheme; however, on a passive matrix, the cumulative drive is limited to small displays with fewer than 16 rows For video on a large display, an active matrix is required (Nahm *et al.* 1998)

Petitioner Samsung Ex-1011, 0370

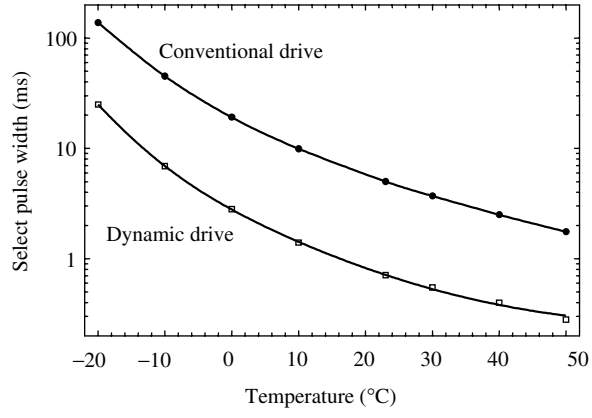


Figure 17.10 Update rates as indicated by the select pulse width for the conventional drive scheme versus the dynamic drive scheme. The difference is quite dramatic at low temperature. Reproduced by the permission of the Society for Information Display

17.3.3 Cumulative Drive

The cumulative drive scheme was developed to show video on small or low-resolution displays but is useful in larger, higher-resolution displays to eliminate the erasing sequence and paging appearance (black line) observed with the conventional and dynamic drive sequences (Huang *et al.* 2000). It works on the principle that a driving pulse can have a cumulative effect when partially driving a pixel to either the planar or focal conic state. Voltage pulses are repeatedly applied to the pixel, with each pulse driving more domains in the pixel into the desired state.

17.3.4 Active Matrix Drive

A careful study of passive matrix driving methods shows the majority of power is consumed in the nonselect rows by the data voltage. To further reduce the power, an active matrix with an ''update when changed'' drive method is required. This method could also significantly improve the response speed and remove the scan line important for mainstream applications such as laptops and PDAs.

17.4 Power Consumption

One of the most attractive features of bistable cholesteric displays is their very low power consumption. Bistable memory with grayscale means that the display does not have to be powered until the image has changed and, with the appropriate circuitry, only those parts of the image that change need to be powered. In many applications, this saves as much or more power than the elimination of a backlight.

The major contribution to power consumption is the charging of the pixel electrodes when the drive voltage is applied. The power required for changing the state or texture of the

Petitioner Samsung Ex-1011, 0371

cholesteric material is miniscule in comparison. The average power for updating a cholesteric display is calculated by summing the power on the select and nonselect rows. For a typical display cell, the power required for the select row is $\sim 2\,\mathrm{mW/cm^2}$. The power consumed by the nonselect row depends on the drive scheme. In a unipolar drive, the power consumed by the nonselect rows can be comparable to the select row power for high-resolution displays but is significantly reduced by a bipolar drive scheme and reduced to zero with an active matrix.

It is instructive to compare the power consumption of various display technologies and driving schemes in terms of the energy saving measured in battery lifetime. Considering power consumption alone, emissive-type and backlit-type displays rank the highest, demanding the largest batteries and/or most frequent recharge intervals. The displays we see on laptop computers and many instruments are of this type. With displays of e-book size, the power consumption to generate the light is, at the very least, 1000 mW. This value can be used for the power to run backlights as well as for the ELs, OLEDs, etc. For the power consumed by the e-book, we need to add to this value the power requirement for the control electronics (about 1500 mW). This translates into a battery usage time of only a few hours, which is not considered to be an acceptable time between battery recharges (or replacement) for convenient use of an e-book.

In addition to the backlight problem, nearly all flat panel displays in today's marketplace are of the refresh type. This results in a continual power usage that may be far more than the backlight depending on usage, as illustrated in Table 17.1, where, the battery lifetimes are compared for various technologies for a VGA resolution of 6.3 in diagonal size for a specific battery size.

Table 17.1 Energy consumption for an ebook in terms of the operating time between battery recharges for different display technologies. The operating times are listed for a 5.4 Wh battery, a size expected for a 2.0 lb ebook with a 6.3 in diagonal display

	Time (h) between recharges for reading time per page of		
	1 min	2 min	5 min
Backlit STN	2	2	2
Reflective STN	18	18	18
Reflective cholesteric	270	540	1350
active matrix	640	1280	3200

To appreciate this energy saving, let us consider that, on average, we spend one minute of time reading a page. This translates into a battery operating time of more than one month for 12 hours per day book usage. This is now well within reason for e-book operation.

17.5 Full Color

There are two approaches to full-color cholesteric reflective displays: cell stacking (Hashimoto *et al.* 1998; Huang *et al.* 1998b) and color patterning of pixels (Chien *et al.* 1995). In a stacked display, a red (R), a green (G), and a blue (B) reflecting display cell are stacked upon

Petitioner Samsung Ex-1011, 0372

each other. The reflecting colors from each display cell additively mix to create the desired color. Since each color can have gray levels, a full-color display is possible. For a reflective display, cell stacking is desired from the point of view that it is three times as bright. This is because the entire area of the display is effective in reflecting all colors. This is not so for a display cell in which each pixel is broken up into an RGB pattern. In the patterned cell, only one-third of the area is available for reflecting a particular color, making it one-third as bright.

17.5.1 Stacked Color Displays

RGB stacked full-color reflective cholesteric displays have been made on glass substrates (Huang *et al.* 1998b) and plastic substrates (Okada *et al.* 1997; Khan *et al.* 2004b). The largest stacked cholesteric display to date is made by Minolta (Hashimoto *et al.* 1998), which successfully fabricated an A4 size, 2048 × 1440 pixel, 180 dpi, full-color display (Figure 17.11). The display was made on plastic polyethersuflfone (PES) substrates. Resin supports (black inner gap supports in Figure 17.11) were made of hot-melt materials and formed regularly on the plastic substrates using screen printing methods (Hashimoto *et al.* 1998). Spacers were used to control the cell gap spacing. Heat and pressure were applied and the supports served to adhere the substrates together as well as maintain cell gaps

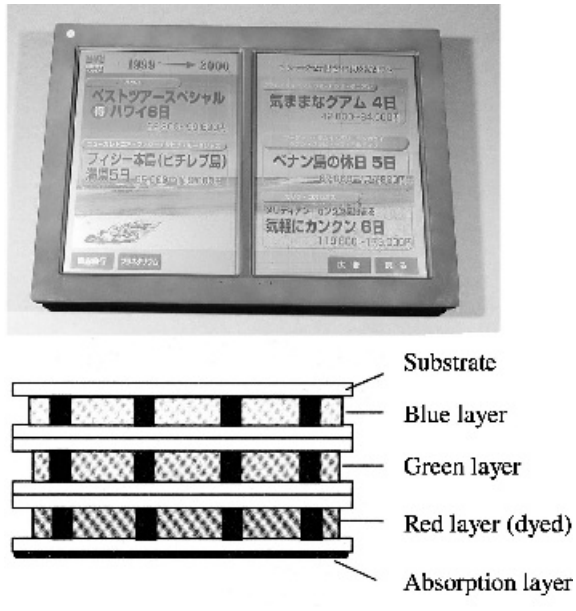


Figure 17.11 Two A4 size, 2048 × 1440 pixel, 180 dpi cholesteric reflective display by Minolta on plastic substrates in RGB color in a stacked configuration for full-color operation. Photo reproduced by the permission of Minolta (Kiyofumi Hashimoto). Diagram reproduced by the permission of the Society for Information Display

Petitioner Samsung Ex-1011, 0373

and make the device more rugged against pressure and bending. To the knowledge of these authors, it is the largest, high-resolution, color reflective display ever made on flexible plastic substrates to date. Full-color displays on plastic substrates were also made by Kent Displays; however, only having a 6.3 in diagonal, VGA resolution and 4096 colors (Khan *et al.* 2004b).

17.5.2 Color Patterning

Full-color images in cholesteric reflective displays can be achieved by patterning RGB reflective pixels on the same substrate. Although they can only be one-third as bright as stacked RGB cells, they can have the advantage of being simpler to construct, requiring only two substrates, and they possess fewer electronic interconnects. In an active matrix driven display, they may be the only solution to full reflective color.

One procedure for patterning the cholesteric materials is using tunable chiral materials where the chirality can be photochemically altered by exposing the cell to UV light (Chien *et al.* 1995). A color pattern is achieved through photolithography. Although such patterning methods have been demonstrated, there is no report in the literature of a manufactured display.

17.5.3 Black and White

The bandwidth, $\Delta\lambda$, of the reflected light of a cholesteric display is limited by the birefringence of the liquid crystalline material to about 100 nm. This is not broad enough to reflect white light if one only incorporates a single layer of cholesteric material. The distribution of the Bragg-reflective angles caused by a distribution in the orientation of the domains can broaden the peak. For displays on rigid substrates, surface treatments are not enough to sufficiently broaden the domain distribution. Polymer networks, however, have been shown to be effective (Khan *et al.* 2002; Miller *et al*. 2003). Likewise, droplet dispersions containing spherical droplets have shown wide domain distributions.

17.6 Droplet Dispersions for Flexible Displays

The key to flexible reflective displays from cholesteric materials is to formulate them in the form of droplet dispersions. Cholesteric materials confined to droplets are necessary to, first of all, maintain the bistable states when the material is flexed. The confinement prevents the cholesteric liquid crystal from flowing and erasing the focal conic state. Droplet dispersions tend to be very rugged in that an image on the display can be insensitive to pressure and flexing or bending of the substrates. A second important reason for droplet dispersions is that the materials can be coated or printed on the substrate. The fabrication of a flexible display by web processing requires this feature. A third important need for droplet dispersions is that they are self-sealing. The cholesteric liquid crystal is confined to the droplets and cannot flow out of the cell. There is no need for seals around the edges of a display cell as is typical in most other liquid crystal display technologies.

Petitioner Samsung Ex-1011, 0374

As it turns out, there are numerous ways to make droplet dispersions of cholesteric liquid crystal materials. In fact, before the time of liquid crystal displays, cholesteric liquid crystals were used as temperature sensors, and microencapsulation procedures were developed to produce them (Sage 1991). These procedures typically involved the use of emulsions where the liquid crystalline materials were blended with a waterborne material (Drzaic 1995). These same types of procedure will work on dispersions for displays. More recently, phase separation procedures have been developed for polymer-dispersed liquid crystals (PDLCs) and can also be used for cholesteric materials (Doane 1990). Cholesteric droplets for bistable displays generally need to be larger than the liquid crystal droplets used on light-scattering PDLC displays. Phase separation and emulsion techniques differ in the ways the droplets are made and processed. In the phase separation method, the droplets are formed after the material is coated or printed; in the emulsion method, the droplets are created before coating or printing.

17.6.1 Emulsification

The emulsification method for making droplet dispersions can have several advantages:

- Droplet dispersions from emulsions may contain a higher percentage of cholesteric material. This is because the polymer walls tend to be very rugged, even when the concentration of the polymer is only 12–15% with over 80% of the dispersion being liquid crystal.
- In the emulsion method, it is easy to obtain oblate-shaped droplets for high reflectivity of the planar texture and low scattering of the focal conic texture. The droplets are flattened to oblate structures during the evaporation process after coating. This happens since as the films dry, they shrink in a direction perpendicular to the film.
- Means to make uniform-sized cholesteric droplets have been demonstrated. Additives have been added to the emulsion (Stephenson *et al.* 2000) to create uniform droplets (see later). Monodisperse emulsions have been demonstrated with an extrusion process (Umbanhowar *et al.* 2000).

The most common emulsification procedure involves a liquid crystal being dispersed in an aqueous bath containing a water-soluble binder material such as deionized gelatin, polyvinyl alcohol (PVA), or latex. Water acts as a solvent and dissolves the polymer to form a viscous solution. This aqueous solution does not dissolve the liquid crystal, and they phase separate. When this system is stirred by a propeller blade at a sufficiently high speed, the micron-sized liquid crystal droplets are formed. Smaller liquid crystal droplets form at higher stirring speeds (Drzaic 1995). The molecular weight of the water-soluble polymer is also a factor affecting the droplet size. Larger droplets form with lower molecular weight polymer (Drzaic 1990). After the droplets are formed, the emulsion is coated onto a substrate and the water is allowed to evaporate. Small amounts of surfactants may be added to reduce the surface tension between the polymer/liquid crystal interface or the polymer/air interface. Crosslinking additives can strengthen the polymer walls of the dispersion. There are many different emulsification procedures (Sage 1991).

Petitioner Samsung Ex-1011, 0375

17.6.2 Droplet Morphology

There are some general statements one can make about the cholesteric droplet morphology. With regard to size, it appears that the diameter should be larger than about 2–3 μm and perhaps, after flattening, as large as 30–50 μm for two reasons. First, droplets that are too small tend to scatter too much light. Light scattering results from a mismatch of the refractive indices between the droplets or the droplet and the encapsulant. As the dimensions of the droplet approach the wavelength of light, light scattering becomes more prominent. A second and more important reason is that too small a droplet, particularly if the droplet is spherical, will tend to destabilize the planar texture. The shape of the droplet is also a significant factor for bistable function as well as reflective brightness and contrast. A nonspherical, preferably flattened structure appears to assist the planar texture and provide a brighter reflectivity as well as a larger S_3 value.

Droplet size uniformity can be an issue. The usual emulsification methods tend to make a broad distribution in droplet sizes. Recently, workers at Kodak (Stephenson *et al.* 2000; Stephenson 2004) demonstrated near-monodisperse droplet sizes using limited coalescence materials and unique processing methods. Taking advantage of this development, they were able to study the effects of droplet size on optical performance. They coated a dark layer directly adjacent to the emulsion to reduce scattering effects. To do this, they used methods of the photographic industry to simultaneously coat the dark layer and the emulsion (Figure 17.12). Droplet dispersions were coated and the optical response measured versus droplet size, with the results shown in Figure 17.12. Notice that if one takes care to reduce scattering effects, the size distribution is not as critical. Also, the dark layer in direct contact with the emulsion greatly improves the contrast by darkening the focal conic texture.

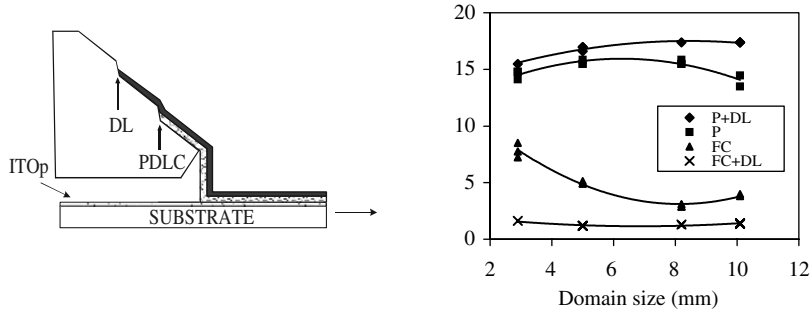


Figure 17.12 (Left) Diagram of the Kodak photographic coating process for laying down multiple coats with a dark coat, DL, coated on top of the cholesteric droplet dispersion. (Right) Droplet size versus reflectance for Kodak emulsion coatings with and without the dark layer overcoat. Reproduced by the permission of the Society for Information Display

17.6.3 Phase Separation

Phase separation is a process that involves mixing the cholesteric liquid crystalline material with a prepolymer (monomeric) solution then polymerizing under suitable conditions to

Petitioner Samsung Ex-1011, 0376

form the droplets. Polymerization, hence droplet formation, occurs after the material mixture has been coated. There are basically three types of polymerization techniques (Doane 1990) that can be used depending on the polymer (or monomer): (1) thermally induced phase separation (TIPS); (2) polymerization-induced phase separation (PIPS); and (3) solvent-induced phase separation (SIPS).

The preferred method is usually PIPS, starting with a homogeneous mixture of a prepolymer (monomer) and a liquid crystal usually at room temperature. As the monomers are polymerized, the number of possible configurations of the monomers decreases and therefore the mixing entropy decreases. When the degree of polymerization reaches a critical value, the liquid crystal phase separates from the polymer. The polymerization can be thermally initiated or photoinitiated; photoinitiation is the most manageable in controlling droplet size. In photopolymerization, monomers such as those with acrylate or methyacrylate end groups are often used. Some photoinitiators are needed and often a crosslinking agent is added to the mixture. On absorbing a photon, the photoinitiator becomes a free radical, which reacts with the acrylate group and results in an opened double bond. The opened double bond reacts with another acrylate group. The chain reaction propagates until the opened double bond reacts with another opened double bond or another free radical, and then the polymerization stops. In sample preparation, the mixture is printed or coated then cured under UV light. Smaller droplets are formed under more intense UV light; however, droplet size is often best controlled by the functionality of the system affected by the additive concentration.

In thermally induced phase separation (TIPS), the system is a binary mixture of a liquid crystal and a thermoplastic (polymer). As the temperature is lowered, the mixing entropy becomes smaller, and the liquid crystal phase separates to form droplets in order to reduce the total free energy. The droplet size can be controlled by the cooling rate, with smaller droplets being formed at faster cooling rates. TIPS can be advantageous in controlling droplet size, because cooling rates are easily adjusted. There are many thermoplastic polymers that can be used for this process. Some examples are PMMA (polymethyl methacrylate), which provides a tangential anchoring condition and PIMB (polyisobutyl methacrylate) which provides a perpendicular anchoring condition.

In the SIPS method, the initial material is a mixture of a liquid crystal and a thermoplastic dissolved in a common solvent. As the solvent evaporates, the mixing interaction energy increases. At a sufficiently low concentration of the solvent, the system phase separates to reduce the mixing interaction energy. The droplet size of the liquid crystal depends on the solvent evaporation rate, with smaller droplets obtained at faster evaporation rates. In practice the SIPS method is rarely used, because it is difficult to control the solvent evaporation rate.

A droplet dispersion of a cholesteric material formed by phase separation is shown in the microphotograph of Figure 17.13 (Lu 1995; Yang *et al.* 2003). A mixture consisting of 20% thermoplastic, poly(vinyl butyral), and 80% cholesteric liquid crystal was made and coated at an elevated temperature then cooled at a controlled rate. The reflectivity from the planar and focal conic textures is shown in Figure 17.13. Not only is the reflectivity very good for these materials, but also there is little scattering from the focal conic texture to achieve excellent contrast. These materials were also demonstrated to be very insensitive to pressure and bending of the substrate.

Notice that the droplets formed by the TIPS process are fairly uniform in size and, in this case, have a diameter of $\sim$40 μm, substantially larger than the thickness of the cell forcing

Petitioner Samsung Ex-1011, 0377

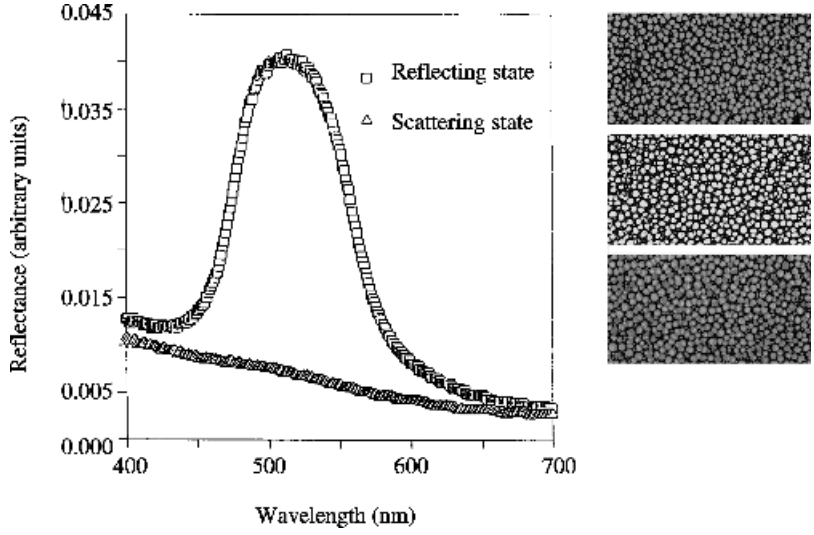


Figure 17.13 Microscope photographs of cholesteric droplet dispersions with three different Bragg-reflective colors and the reflection spectra of the yellow droplet in the planar reflective texture and nonreflective focal conic texture

the droplets to be disk-shaped. This flattened or ellipsoidal droplet morphology is important in achieving the desired domain texture. The domain texture of the cholesteric droplets in the planar and focal conic textures can be seen in Figure 17.14 for a dispersion made with the TIPS process. Two different focal conic textures are seen where one is electrically switched (small domains in the droplets) and the other obtained by thermal cooling (large domains

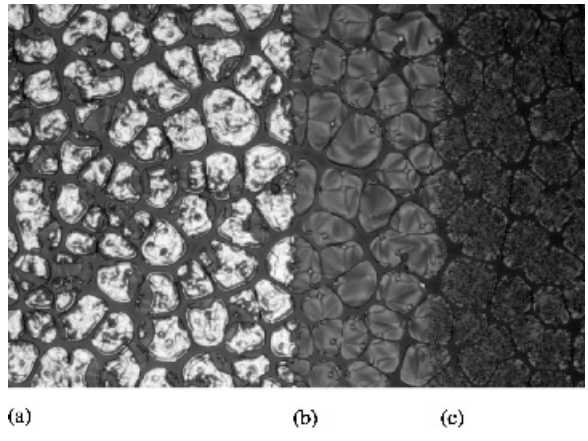


Figure 17.14 Domain textures in cholesteric droplets where the microscope photo is of a display cell that overlaps two pixels and the area between. The pixel on the left was electrically switched to the planar texture whereas the pixel on the far right was switched to the focal conic texture. The area between the cells has no electrode and could not be electrically switched; however, it was thermally cooled into the focal conic state. Note that droplets at the electrode edge have both textures

Petitioner Samsung Ex-1011, 0378

in the dropets). It is clearly seen in the microscope photo that an individual droplet can be divided such that part of the droplet is in the planar and the other in the focal conic. This feature is also important for grayscale.

17.7 Toward Flexible Displays

Droplet dispersions are important for flexible displays using coating and printing processes, but there are many other issues that need to be solved for producing them. These include such things as: the availability of a flexible transparent conductor that can be printed or easily patterned by web processing; providing interconnects to the drive electronics that are robust and unobtrusive; the design of web processes that can accommodate a variety of material layers that include electrodes, insulation layers, planarization layers, hardcoats, and a variety of other things that make up the display.

17.7.1 Displays from Emulsions

Most advanced in the manufacture of flexible cholesteric displays is Kodak (Stephenson 2004). It has reported impressive displays made by coating and printing methods used in the photographic industry. Starting with a plastic substrate containing a patterned ITO transparent conductor, a 250 nm insulation layer of dried gelatin is coated (gel washed) over the ITO followed by a coating of the droplet dispersion and dark layer. Opaque conducting electrodes could then be screen printed using polymer thick film inks typically used in microelectronic fabrication. Figure 17.15 shows one such display film made by photographic coating and printing methods. Kodak has demonstrated a variety of different flexible displays to include 1.0 mm pitch passive matrix displays having 64 rows and 96 columns processed on a 100 mm wide coating down on the center of the web. Figure 17.15 shows a seven-segment display and a conventional credit card with an attached display to create a display card.

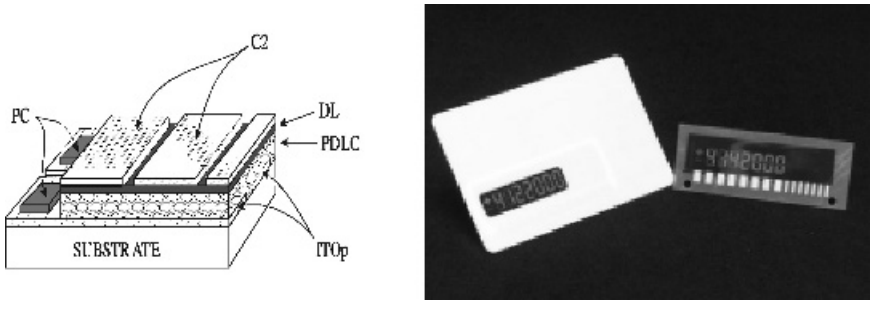


Figure 17.15 (Left) Diagram of the layers in a flexible cholesteric display developed by Kodak using photographic methods showing the backplane conductors (C2), dark layer (DL), and droplet dispersion (PDLC). (Right) A seven-segment cholesteric display fabricated with photographic methods for credit card applications. Reproduced by the permission of the Society for Information Display

Petitioner Samsung Ex-1011, 0379

17.7.2 Displays from PIPS Processes

Kent Displays, Inc. has been successful in producing prototypes of flexible cholesteric displays using droplet dispersions made from phase separations processes where the droplets are formed on the substrate after the polymeric solution is coated on the substrate. Figure 17.16 shows a 12-pixel cholesteric display on flexible polycarbonate substrates with

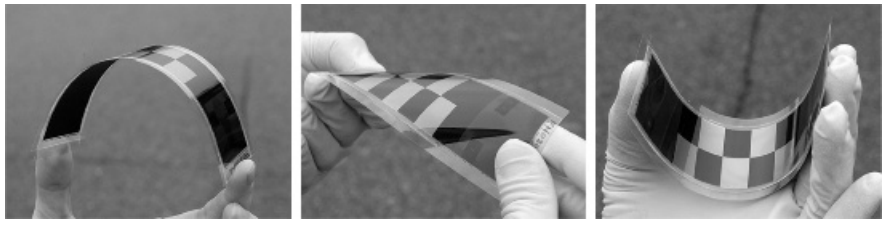


Figure 17.16 Photograph of a flexible bistable cholesteric reflective display on polycarbonate substrates with a droplet dispersion prepared by the PIPS process taken in broad daylight

patterned ITO electrodes (Schneider *et al.* 2005). It was made by coating a substrate with a solution of monomer/cholesteric liquid crystal in a ratio of ∼20/80 by weight, to which a small amount of crosslinking material was added along with spacers. An upper substrate was then laminated and the material polymerized with UV light. The resulting contrast, brightness, and viewing angle are excellent, as seen in Figure 17.16, and it is insensitive to flexing by pressure placed on the display.

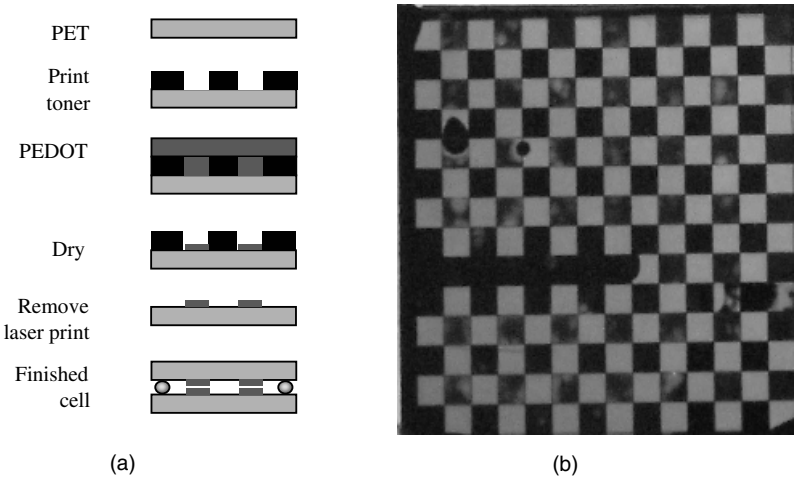


Figure 17.17 (a) The steps in patterning conducting polymer, PEDOT, electrodes with a standard office printer. (b) Cholesteric reflective display passive matrix demonstration fabricated with conducting polymer electrodes using this method

Petitioner Samsung Ex-1011, 0380

17.7.3 Conducting Polymer Electrodes

Another material development important for flexible displays is the transparent conductor. Most promising are materials such as conducting polymers (Fritz *et al.* 1999) and carbon nanotubes (Arthur 2004). For cholesteric displays, conducting polymers have already been developed with display use in mind. Researchers at Agfa in Belgium have developed some excellent materials with good conductivity-to-transparency ratios and formulations for coating on various materials. A nice thing about conducting polymers is that not only can they be printed, they can also be patterned in so many different ways.

Kent Displays and Professor MacDiarmid at the University of Pennsylvania have made cholesteric displays where the rows and columns of a matrix are patterned with a standard office copier. In this method, a PET sheet of plastic was loaded in a standard laser printer photocopier and the negative of the desired image of the rows or columns photocopied onto the PET. The conducting polymer PEDOT was then coated, which adhered in places where there was no printed toner. After the PEDOT dried, the toner was removed, leaving a substrate with patterned electrodes. Sandwiching cholesteric material between the electrodes then provided a simple display where the pixels were electrically driven to a checkerboard pattern (Figure 17.17).

17.8 Conclusions

Cholesteric materials have all the characteristics required for low-cost flexible displays. The substrates or outer protective coatings can be low-cost birefringent materials without the need of demanding gas and water barriers. They do not require an active backplane for a display of high resolution. As a flexible display technology they can feature a wide range of uses, particularly on handheld devices where long battery lifetimes are required. Bistability and reflectivity of cholesteric materials provide the characteristics required to minimize power consumption to its lowest level. The materials are also developed to provide full-color reflectivity and wide temperature ranges. Full-color, high-resolution cholesteric displays on plastic substrates were demonstrated as early as 1998, but flexible cholesteric displays will not reach the marketplace until the materials are better adapted to coating and printing processes suitable for manufacturing.

References

Anderson, J. E., Watson, P. and Bos, P. J. (2001) Study of the relaxation in cholesteric liquid crystals after reduction of an electric field. *Liquid Crystals* **28**, 945.

Arthur, D. J. (2004) Transparent electrodes and circuits from carbon nanotubes. *Proceedings of the USDC Displays and Microelectronics Conference* 2004, Phoenix AZ.

Chien, L.-C., Muller, U., Nabor, N.-F. and Doane, J. W. (1995) Multi-color reflective cholesteric displays. *SID Digest* **1998**, 169–71.

Crawford, G. (2000) A bright new page in portable displays. *IEEE Spectrum* **40**.

Doane, J. W. (1990) Chapter 14 in *Liquid Crystals: Applications and Uses* (ed. B. Bahadur), World Scientific, Singapore.

Doane, J. W., St John, W. D., Lu, Z. J. and Yang, D.-K. (1994) Stabilized and modified cholesteric liquid crystals for reflective displays. *Proceedings of the IDRC* 1994, Monterey CA, pp. 65–8.

Petitioner Samsung Ex-1011, 0381

Drzaic, P. (1990) *Proceedings of the SPIE Liquid Crystal Displays and Applications* **1257**, 29–36.

Drzaic, P. (1995) *Liquid Crystal Dispersions*, World Scientific, Singapore.

Fritz, W., Wonderly, H., Smith., S., Kim, Y., Chonko, J., Doane, J. W., Shashidhar, R., O'Ferrall, C. E. and Cuttino, D. (1999) Advances in ChLCD devices using plastic substrates with conducting polymer, *Proceedings of the SPIE Liquid Crystal Displays and Applications* **3635**, 114–9.

Hashimoto, K., Okada, M., Nishiguchi, K., Masazumi, N., Yamakawa, E. and Taniguchi, T. (1998) Reflective color display using cholesteric liquid crystals. *SID Digest* **1998**, 897–900.

Huang, X. Y. and Doane, J. W. (2002) Recent advances in cholesteric displays, *Information Display* **18/2**, 14–17.

Huang, X. Y., Yang, D.-K., Bos, P. and Doane, J. W. (1995) Dynamic drive for bistable reflective cholesteric displays: A rapid addressing scheme. *Journal of the SID* **3/4**, 165–8.

Huang, X. Y., Stefanov, M., Yang, D.-K. and Doane, J. W. (1996) High-performance dynamic drive scheme for bistable reflective cholesteric displays. *SID Digest* **1996**, 359–62.

Huang, X. Y., Miller, N., Khan, A., Davis, D., Doane, J. W. and Yang, D. K. (1998a) Gray scale of bistable reflective cholesteric displays. *SID Digest* **1998**, 810–3.

Huang, X. Y., Khan, A., Davis, D., Jones, C., Miller, N. and Doane, J. W. (1998b) Full color reflective cholesteric liquid crystal display. *Proceedings of Asia Display* **98**, 883–6.

Huang, X. Y., Khan, A., Miller, N., Jones, C. and Doane, J. W. (2000) Cumulative drive for bistable reflective cholesteric displays. *SID Digest* **2000**, 30–3.

Khan, A., Huang, X.-Y., Miller, N., Jones, C. and Doane, J. W. (2000) Color in Stacked Reflective Cholesteric Displays. *Proceedings of the 20th International Display Research Conference*, Palm Beach, 245–8.

Khan, A., Huang, X. Y., Armbruster, R., Nicholson, F., Miller, N., Wall, B. and Doane, J. W. (2001) Super high brightness reflective cholesteric display. *SID Digest* **2001**, 460–3.

Khan, A., Miller, N., Nicholson, F., Armbruster, R., Doane, J. W., Wang, D. and Yang, D.-K. (2002) Dynamically driven polymer stabilized blank and white cholesteric liquid crystal display. *Proceedings of the IDW* 20002, Hiroshima, pp. 1349–52.

Khan, A., Miller, N., Ernst, T., Marhefka, D., Huang, X. Y. and Doane, J. W. (2004a) Novel drive techniques and temperature compensation mechanisms in reflective cholesteric displays. *SID Digest* **2004**, forthcoming.

Khan, A., Huang, X. Y. and Doane, J. W. (2004b) Low power cholesteric LCD and electronic book. *Proceedings of the SPIE Defence and Securities Symposium*, Orlando FL, forthcoming.

Lu, Z.-J. (1995) *Reflective Cholesteric Liquid Crystal displays*, PhD dissertation, Kent State University.

Miller, N., Huang, X. Y., Armbruster, R., Nicholson, F., Pfeifer, J., Ernst, T, Khan, A., Haga, S., Kamata, T., Fukuda, K. and Takami, M. (2003) Ultra low power black and white cholesteric display with COG and solar array. *SID Digest* **2003**, 1446–9.

Nahm, J. Y., Goda, T., Min, B. H., Chou, T. K., Kanicki, J., Huang, X. Y., Miller, N., Sergan, V., Bos, P. and Doane, J. W. (1998) Amphorphous silicon thin film transistor active matrix reflective cholesteric liquid crystal display. *Asia Display* **98**, 979–82.

Okada, M., Hatano, T. and Hashimoto, K. (1997) Reflective multicolor display using cholesteric liquid crystals. *SID Digest* **1997**, 1019–22.

Podojil, G. M., Davis, D. J., Huang, X. Y., Miller, N. and Doane, J. W. (1998) Plastic VGA reflective cholesteric LCD's with dynamic drive. *SID Digest* **1998**, 51–4.

Roosendaal, S. J., Hage, L. M., Kuijk, D. E., Schlangen, L. J. M. and van Haaren, J. A. M. M. (2001) Fast addressing of cholesteric texture liquid crystal display. *SID Digest* **2001**, 1268–71.

Ruth, J., Hewitt, R. and Bos, P. (1997) Low cost dynamic drive scheme for reflective bistable cholesteric liquid crystal displays. *Proceedings of Flat Panel Displays* **1997**, Detroit MI, pp. 89–93.

Rybalochka, A., Sorokin,V., Valyukh, S., Sorokin, A. and Nazarenko, V. (2000) Dynamic drive scheme for fast addressing of cholesteric displays. *SID Digest* **2000**, 818–21.

Sage, I. (1991) Chapter 20 in *Liquid Crystals: Applications and Uses 3* (ed. B. Bahadur), World Scientific, Singapore.

Petitioner Samsung Ex-1011, 0382

Schneider, T., Nicholson, F., Chien, L. C. and Khan, A. (2005) forthcoming.

St John, W. D., Lu, Z. J. and Doane, J. W. (1995) Characterization of reflective cholesteric liquid crystal displays. *Journal of Applied Physics* **78**, 5253–5.

Stephenson, S. (2004) Development of flexible displays using photographic technology. *SID Digest* **2004**, 774–7.

Stephenson, S., Boettcher, J. and Giachero, D. (2000) US Patent **6**,423,368 B1.

Umbanhowar, P. B., Prasad, V. and Weitz, D. A. (2000) Monodisperse emulsion generation via drop break off in a coflowing stream. *Langmuir* **16**, 347–51.

Wu, S. T. and Yang, D.-K. (2001) *Reflective Liquid Crystal Displays*, John Wiley & Son Inc., New York.

Yang, D.-K., Chien, L. C. and Doane, J. W. (1991) Cholesteric liquid crystal/polymer gel dispersion bistable at zero field, *Proceedings of the 1991 International Display Research Conference*, 49–52.

Yang, D-K., Lu, Z. J., Chien, L. C. and Doane, J. W. (2003) Bistable polymer dispersed cholesteric reflective displays. *SID Digest* **2003**, 959–61.

Yuan, H. (1996) Bistable reflective cholesteric displays, Chapter 12 in *Liquid Crystals in Complex Geometries*, G. P. Crawford and S. Zumer (eds), Taylor & Francis, London.

Petitioner Samsung Ex-1011, 0383

18

Paintable LCDs: Single-Substrate LCDs Produced by Photoenforced Stratification

Roel Penterman, Stephen I. Klink, Joost P. A. Vogels, Edzer A. Huitema, Henk de Koning, and Dirk J. Broer

Philips Research Laboratories

18.1 Introduction

Liquid crystal displays (LCDs) make up most of the displays that have been integrated in everyday commodities ranging from watches and pocket calculators to more sophisticated electronic products like mobile phones, personal digital assistants (PDAs), computer monitors, television sets and car navigation systems. The reason why LCDs are so widely used is that the display is thin and has a low power consumption; the electro-optical effect is simple and well understood. However, the constraint of flat device surfaces, as imposed by their glass substrates, sometimes hinders further integration of LCDs into new product ranges or product designs. Another limitation, basically caused by fabrication methods and related substrate handling, is their restriction to rectangular shapes. LCDs are presently being made by accurately coupling two glass substrates, the substrates previously being provided with transparent electrodes such as indium tin oxide (ITO), orientation layers and other layers such as color filters, planarization layers and a black matrix (Morozumi 1990). Previously applied spacers keep the two plates at a distance of several microns while they are adhered

Flexible Flat Panel Displays Edited by G. P. Crawford
© 2005 John Wiley & Sons, Ltd., ISBN 0-470-87048-6

Petitioner Samsung Ex-1011, 0384

together. The formed cells are then filled with a liquid crystal (LC) mixture under vacuum. Subsequently the cell is divided into a number of smaller cells using the so-called scribe-and-brake method. Although it is a very efficient method, the shape of the resulting cells can only be rectangular. The throughput time can be shortened considerably by applying the one-drop-fill technique (Kamiya *et al.* 2001). In this technique an exact amount of LC droplets are dispensed on one of the substrates, after which the two substrates are accurately coupled in vacuum. These batchwise processes for cell making and filling are laborious and time-consuming, hence expensive. In addition, the application of two substrates adds unnecessarily to substrate costs and display thickness.

Our revolutionary concept of paintable LCDs represents a new LCD manufacturing technology by which an LCD is made by the sequential coating (painting) and UV curing of a stack of tailored organic layers. The key process that enables layer stacking is the formation of a thin polymer-covered LC layer and is called photoenforced stratification (PES). It comprises a two-step photopolymerization-induced phase separation of an LC blend and a polymer precursor. Since the paintable LCD technology is based on a sequence of simple coating processes, the manufacturing process is relatively simple and fast, and can be applied to rigid glass substrates as well as nonrectangular flexible substrates, such as polyester or polycarbonate. The display thickness of the resulting devices is dominated by one substrate instead of two, hence gives ultra-thin, conformable and potentially truly flexible displays.

18.2 Photoenforced Stratification

The basis for the technology is a directionally controlled polymerization-induced phase separation of a composite material consisting of an LC blend and a polymer-forming material. Many reports have appeared on random polymerization-induced phase separations to produce polymer-dispersed LCDs (Vaz *et al.* 1987; Doane *et al.* 1986; Hirai *et al.* 1990) and liquid crystal cells containing polymer networks (Hikmet 1999). Directionally controlled phase separations have been used to reduce the cell gap in situ (Vorflusev and Kumar 1999) or to produce holographic gratings (Bowley *et al.* 1999) and other electro-optical shutters of complex geometries (Yamada *et al.* 1995). Normally these processes are carried out in glass or plastic cell configurations where interfacial properties may enhance the formation of layers at the predestined surfaces (Vorflusev and Kumar 1999) Polymerization-induced phase separation may be the result of the increasing fraction of large molecules during polymerization (size-induced phase separation), the difference in the Flory–Huggins interaction parameter between the monomer and the liquid crystal material and the polymer and the liquid crystal material, and the elasticity of the polymer network.

In this study we have realized the formation of phase-separated LC and polymer layers by the photopolymerization of a thin film (tens of microns) coated on a single substrate. Directionality with respect to photoinduced diffusion has been achieved by doping the film with an absorbing compound that provides a UV intensity gradient in the z-direction over the layer's cross section (Broer *et al.* 1995; Qian *et al.* 2000). This absorbing compound has reactive groups so it is assured that on polymerization and phase separation the compound becomes incorporated in the polymer top coat and does not stay behind in the LC layer. The processing sequence is illustrated in Figure 18.1. A film-forming technique such as the doctor blade technique is used to apply a thin ''wet'' film of about 25 μm of the composite material. The film is subsequently exposed to ultraviolet light in a nitrogen

Petitioner Samsung Ex-1011, 0385

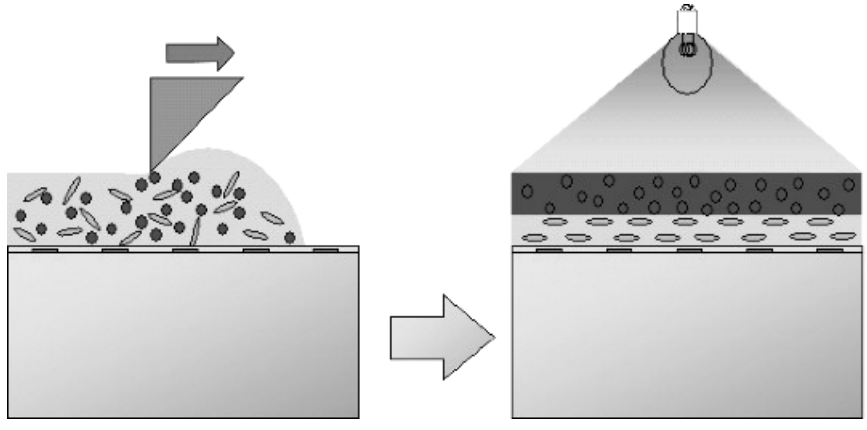


Figure 18.1 Schematic representation of the stratification process. The separation of a coated film into two discrete layers as the result of a photopolymerization-induced phase separation in the vertical direction. The formed LC layer at the bottom can be switched, by in-plane electrical fields, for example. On top of the polymer cover, the other necessary optical layers (e.g. polarizer, reflector) can be stacked

atmosphere. The presence of a compound in the film, which absorbs at the wavelengths of the UV irradiation, induces a UV intensity gradient across the film thickness. As a result, the photopolymerization predominantly takes place where the UV intensity is the highest, i.e. near the film surface that is directed towards the UV source. The local consumption and consequent depletion of monomers induces diffusion of monomers from the bottom of the layer towards the surface and a concomitant diffusion of LC molecules in the reverse direction. At the moment of the phase separation, pure LC droplets start to grow at the bottom of the film. The polymerization conditions (e.g. intensity, temperature) must be chosen such that coalescence of the LC droplets can take place, which results in the desired continuous LC layer with a hard polymer film on top. This last step, where the phase separation is controlled to form a layered structure, is called stratification.

18.3 Experimental Procedures

The experiments were carried out with a 50/50 (wt/wt) mixture of the liquid crystal blend E7 (Merck) and a methacrylate-based polymer-forming material. The chemical structures of the compounds are shown in Figure 18.2.

The methacrylate mixture of isobornylmethacrylate (Aldrich) and stilbene dimethacrylate (synthesized in-house) has been chosen such that the monomers dissolve in the LC, but phase separate during polymerization. Moreover, isobornyl methacrylate was selected as the main component as it combines properties like high solubility and low viscosity before polymerization, high diffusion rates and controlled phase separation during polymerization and rigidity after polymerization. For instance the glass transition temperature of pure poly-(isobornyl methacrylate) is 225 °C. The stilbene dimethacrylate compound was designed and synthesized in our laboratories and it combines two features. Firstly, it has an intense

Petitioner Samsung Ex-1011, 0386

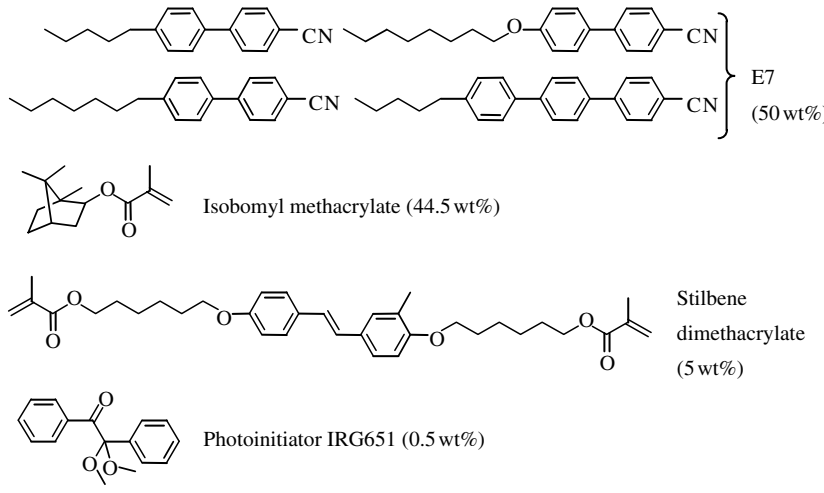


Figure 18.2 The structures of the liquid crystal blend E7 and the reactive monomers isobornyl methacrylate and stilbene dimethacrylate, as well as the photoinitiator Irgacure 651. The relative amounts of the compounds in the coating mixture are shown in parentheses

absorption band in the ultraviolet part of the spectrum that largely overlaps the absorption spectrum of the photoinitiator Irgacure 651 (Figure 18.3(a)). Therefore this absorber and photoinitiator are an ideal combination for our purposes. Secondly, it provides the crosslinks between the poly(isobornyl methacrylate) chains, which is a further driving force for the polymerization-induced phase separation process (Boots *et al.* 1996). The mixture that has

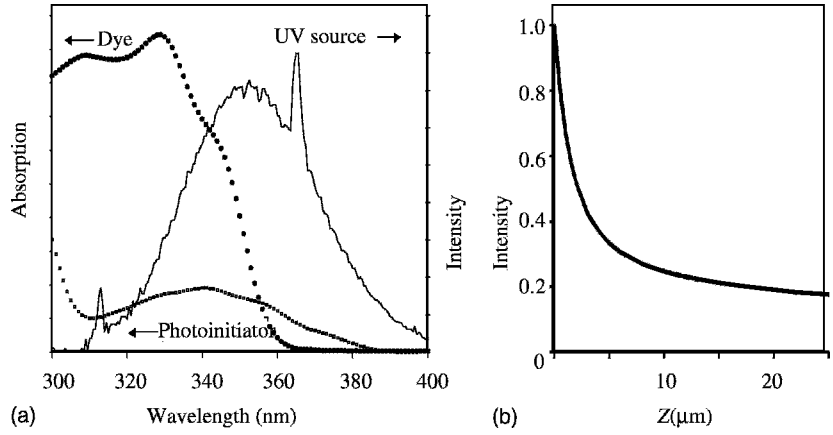


Figure 18.3 (a) The spectrum of the UV source used in the experiments and the absorption spectra of the stilbene dimethacrylate compound and the photoinitiator. In acetonitrile the extinction coefficient of the stilbene dimethacrylate compound is 25 0000 $M^{-1}cm^{-1}$ at 340 nm. Light above 370 nm is not absorbed by the stilbene dimethacrylate, so a small part of the UV light emitted by the UV source can penetrate the whole layer. (b) A typical gradient calculated for a 25 μm film at the onset of irradiation

Petitioner Samsung Ex-1011, 0387

been used in the process consisted of 50 wt% E7, 5 wt% stilbene dimethacrylate, 44.5 wt% isobornyl methacrylate and 0.5 wt% photoinitiator Irgacure 651 (Ciba Specialty Chemicals). We have used a variety of substrates to manufacture the displays. Most commonly we used ITO-coated glass or an engineered ITO-coated polycarbonate foil, where the ITO is structured into interdigitated electrodes by lithography. To align the liquid crystals after their phase separation, we applied a thin film of polyimide on the substrate that was subsequently rubbed in a unidirectional way with a velvet cloth. The thin film of the E7/reactive monomer blend was coated using the doctor blade technique. The distance between the knife and the substrate was adjusted to result in a wet film thickness of 25 μm. We conducted the photopolymerization in a nitrogen atmosphere since oxygen inhibits the radical polymerization of methacrylates. The intensity gradient over the film at the onset of irradiation could be estimated based on the emission spectrum of the UV source, in Figure 18.3(a), the intensity gradient at the onset of irradiation can be calculated (Figure 18.3 (b)).

18.4 Single UV Exposure

To study the stratification of the liquid crystal under unconfined conditions, a 25 μm film of the E7/reactive monomer mixture was applied on a polyimide-covered glass substrate and subsequently exposed to UV light. At the moment of phase separation, pure LC droplets start to grow on the polyimide alignment layer at the bottom of the film. The appearance of the birefringent LC droplets on the alignment layer was followed in time with a modified polarization microscope. The four snapshots of the LC droplets in Figures 18.4(a) to(d) illustrate that the principle of a directional phase separation works, but they also show that under these unconfined conditions the droplets do not fully coalesce into a continuous flat LC layer.

At the moment of phase separation, small pure LC droplets start to grow at the bottom of the film (Figure 18.4(a)). These droplets grow (Figure 18.4(b) and (c)) and many of them may coalesce, forming even bigger droplets. But on further polymerization the polymer cover becomes more and more rigid, which prevents the droplets from coalescing into a continuous layer (Figure 18.4(d) and (e)). Changing the polymerization conditions (temperature and irradiation intensity) did not improve the uniformity of the LC layer.

18.5 Two-Step UV Exposure

For good optical performance of our paintable LCDs, the resulting layers should be much more uniform. Our strategy has been to induce this uniformity by confining the nucleation, growth and coalescence of the LC droplets to small boxes. This has been realized by performing the photoenforced stratification in a two-step UV exposure procedure. In the first step, the E7/reactive monomer film was exposed through a mask with high-intensity light of wavelengths larger than 360 nm. These wavelengths are outside the absorption region of the stilbene dimethacrylate, but still at wavelengths where the photoinitiator has enough absorption for its photodissociation . Therefore the light can penetrate the layer all the way to the bottom and polymerization is initiated over the whole layer thickness. This results in the

Petitioner Samsung Ex-1011, 0388

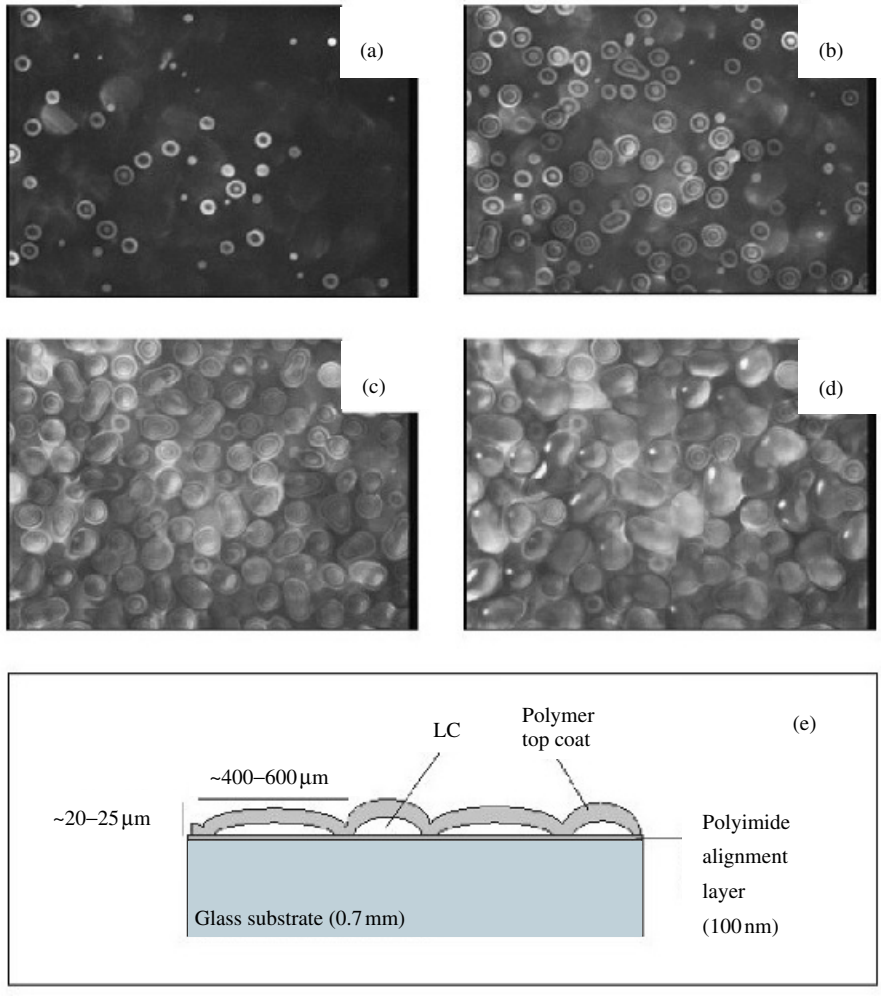


Figure 18.4 (a–d) Four stages of the polymerization-enforced stratification of the thin E7/reactive monomer film seen from the top. (e) Schematic cross section of the stratified layer; the dimensions are not to scale. The droplets do not coalesce into a continuous and flat LC layer

formation of polymer walls in the exposed areas, which form a grid of 500 µm × 500 µm boxes (Figure 18.5(a)). The surface profile of the film after the formation of the polymer walls is visualized with the aid of interferometric microscopy (Figure 18.5(b)). Due to diffusion of monomeric material into the irradiated areas, the polymer walls are a few microns higher than the rest of the film.

In a subsequent processing step, the unexposed areas were cured by a flood exposure with a second UV source. The emission spectrum of this UV lamp is shown in Figure 18.3(a). The absorption spectrum of the stilbene dimethacrylate partly overlaps with the emission

Petitioner Samsung Ex-1011, 0389

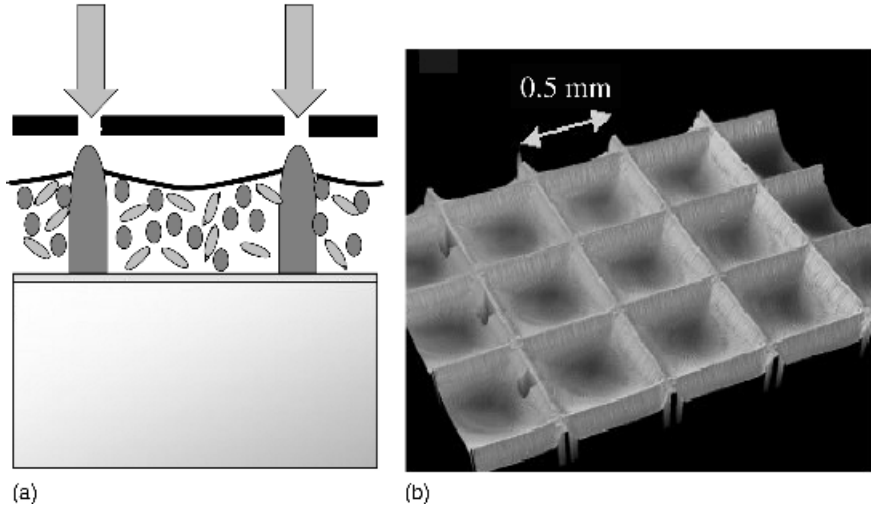


Figure 18.5 The two-step UV exposure to produce paintable LCDs. (a) Formation of the polymer walls. Local consumption of monomers induces a diffusion of monomers towards the exposed areas. (b) The resulting height variations could be observed with the aid of interferometric microscopy

spectrum of the lamp, creating the effective intensity gradient in the direction orthogonal to the film surface. The lamp intensity of the second exposure source must be well chosen to enable fast polymerization but simultaneously to allow sufficient monomer diffusion during the polymerization process.

During the second exposure step, i.e. the stratification step, the LC droplets within each box coalesce into continuous domains, confined by the polymer walls formed during the first exposure (Figure 18.6(a) to (d)). Apparently the interfacial thermodynamics of these confined volumes of material give preference to the formation of fully stratified layers. The whole process has led to the formation of polymer boxes filled with pure liquid crystal underneath a thin polymer cover. Besides confining the nucleation and growth, the polymer walls also serve a different purpose. Since the polymer top coat and the substrate are now mechanically coupled in regular fashion, we have obtained a stable device that can withstand lateral forces. The boxes in Figure 18.6(a) to (d) are of order 0.5 mm $\times$ 0.5 mm and 15 μm high, the walls are about 100 μm wide, and the polymer cover is about 10 μm thick. The surface profile of the film after the stratification step is shown in Figure 18.6(e). It clearly shows that the polymer cover between the polymer walls is dome-shaped. The LC was chosen to follow a planar director profile imposed by the alignment layer at the bottom. With the aid of the modified polarization microscope, the colors from birefringence of the growing and coalescing droplets can be visualized. Since the LC follows a planar orientation, it is possible to derive the developing thickness of the droplets during the polymerization process and the variation in thickness of the LC domains in the end result. By analyzing Figure 18.6(d) and 6(e), a schematic cross section can be deduced, as shown in Figure 18.6(f).

Petitioner Samsung Ex-1011, 0390

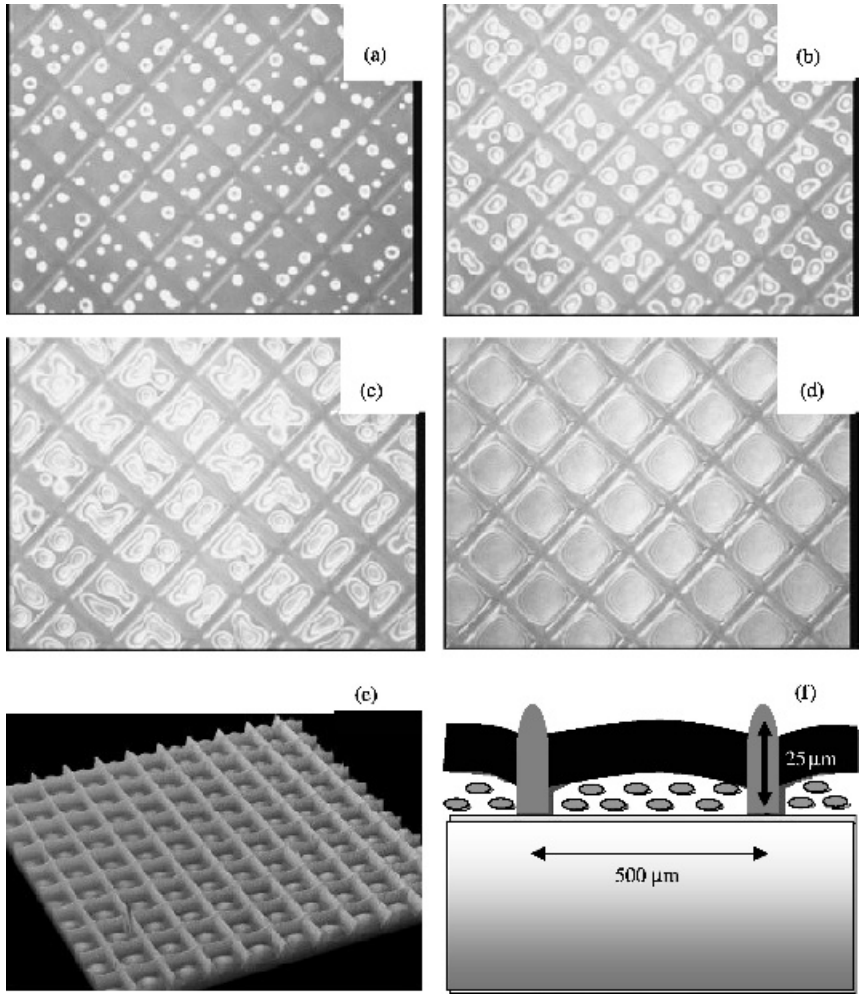


Figure 18.6 (a–d) Four stages of the polymerization-enforced stratification that has been localized in boxes due to the presence of the polymer walls: (a) nucleation at the start of the phase separation, (b, c) coalescence of LC droplets, (d) end result, within each box a (small) continuous LC layer is formed. After observation with optical microscopy (d) and interferometric microscopy (e), a schematic cross section (f) can be deduced

18.6 Paintable Displays

A paintable LCD has been made on a substrate provided with interdigitated electrodes below the polyimide alignment layer. The electrodes are separated with a spacing of 9 μm and the electrode pitch is 18 μm. The LC layers in the individual boxes can now be switched by in-plane electrical fields. When a field is applied over the interdigitated electrodes on the substrate, the LC molecules switch in the plane of the film (Kiefer *et al.* 1992; Oh-e *et al.* 1995). The in-plane switching liquid crystal effect combines fast switching ($\tau_{on} = 5$ ms

Petitioner Samsung Ex-1011, 0391

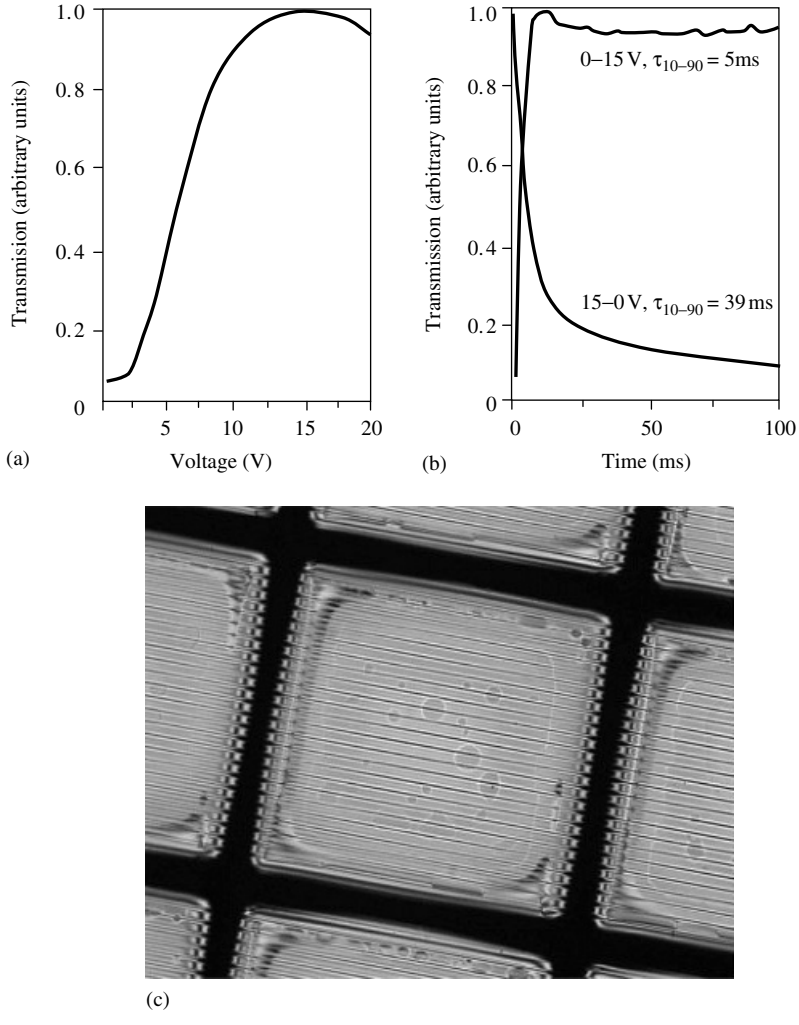


Figure 18.7 The electro-optical characteristics of the paintable LCD between crossed polars (normally black mode). (a) The transmission voltage curve and (b) the switching curves. The LC (E7) is driven by in-plane switching. The interdigitated electrode structure has a pitch of 18 μm and a spacing of 9 μm. (c) The microscope picture of a pixel driven in the on-state clearly shows that the LC is partially switched. Above the electrodes, the pixel stays dark. Obviously the isotropic walls stay dark as well

and $\tau_{\text{off}} = 40$ ms) with a contrast on the order of 1:20, sufficient for many applications. The contrast is of order 1:20, sufficient for many applications. The transmission–voltage curve and the response times are shown in Figure 18.7(a) and (b). Figure 18.7(c) shows a close-up of a pixel driven in the on-state.

To avoid an uneven top surface because of the surface profile generated during the wall formation step (Figure 18.6(e)), the paintable LCD was coated with a planarization layer. Thereto a 20 μm layer of tripropylene glycol diacrylate was deposited on top of the top coat with the aid of a doctor blade and subsequently photopolymerized. We selected the top coat

Petitioner Samsung Ex-1011, 0392

material on a set of properties. Firstly, it should not affect the stratified polymer by swelling or monomer diffusion. Secondly, it should be mechanically and chemically stable to resist further processing and add to the robustness of the display. Applying the polarizers finishes the LCD. In one of the various designs, we applied a so-called TCF polarizer on top of the planarization layer by shear orientation of a sulfonated perylene dye doctor bladed from a water solution (Bobrov *et al.* 2000). After UV ozone treatment of the planarizing poly-(tripropylene glycol diacrylate), the water-based solution of the dichroic dyes wets perfectly. After evaporation of the water, a 600 nm thick polarizer is formed. Figure 18.8 is a photograph of the display produced by the two-step stratification process and additional coating processes. Polarized light from the backlight/polarizer combination is transmitted by the stack at the location where the LC is addressed by an electric field.



Figure 18.8 A photograph of an LCD produced by the PES process. The paintable LCD has been provided with a coatable polarizer. It was operated in the transmissive mode (normally black) by using a backlight/polarizer combination. The Philips logo was activated by direct addressing

18.7 Improved Paintable LCD Technology

The process described so far yield stable displays when applied on relatively rigid substrates. However, we experienced some hurdles in the development towards cost-effective displays based on plastic substrates. When the paintable displays based on plastic substrates were bent over small radii, e.g. of order 20 mm or less, the stresses became too high and led to local delamination of the polymer walls from the bottom substrate, resulting in display

Petitioner Samsung Ex-1011, 0393

failure. Moreover, the two-step UV exposure process, which contains a lithographic UV step, is somewhat difficult to combine with high-volume mass production techniques such as reel-to-reel manufacturing of displays. A big step towards the industrialization of the paintable LCD technology is therefore the introduction of an offset printing step into the process as a replacement for the first lithographic UV step. As a result, the number of UV exposure steps to form LC-filled capsules, the heart of the paintable LCD, can be reduced to one. The direction of the phase separation perpendicular to the substrate is insured by the presence of the UV absorber; controlling the direction of the phase separation in the lateral direction parallel to the substrate is insured by a local modification of the alignment layer. Via an offset printing step, the alignment layer is locally modified with an adhesion promoter (Figure 18.9(a)). By its very nature, the printing step only modifies the selected areas and does not alter or damage the alignment properties of the layer in the unmodified areas. The adhesion promoter contains functional groups that can react with the forming polymer during polymerization.

After coating the modified alignment layer with the LC/prepolymer mixture (Figure 18.9(c)), a single UV exposure directly yields the structures depicted in Figure 18.9(d). Not only does this surface modification simplify the production process, it also enhances the robustness of the displays. Indeed, when a thin 120 μm polymer foil was used as the substrate, the stack could be bent to a curvature radius of less than 10 mm without delamination of the polymer walls.

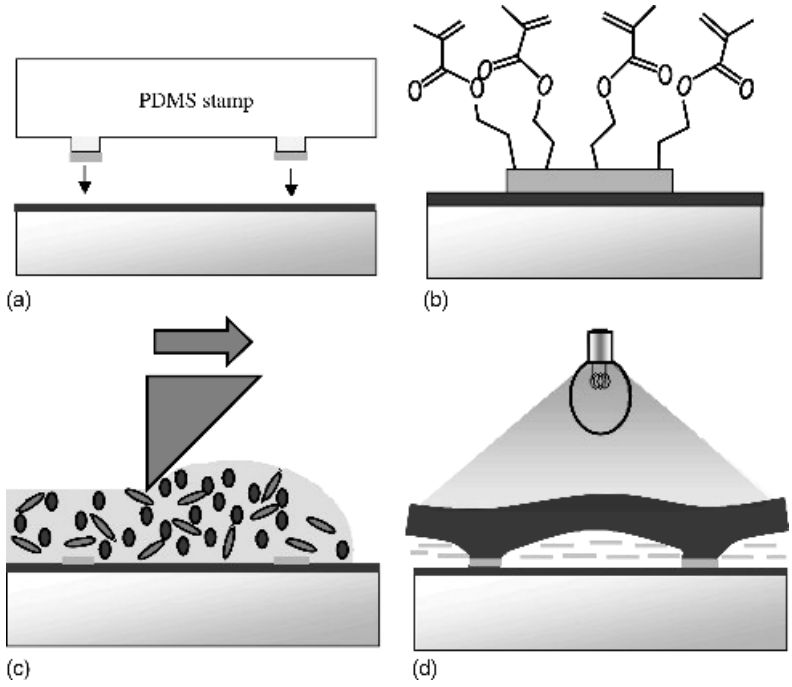


Figure 18.9 Via offset printing. (a) The alignment layer is locally modified with an adhesion promoter. (b) The adhesion promoter contains functional groups that can react with the forming polymer during polymerization. (c) After coating the modified alignment layer with the LC/prepolymer mixture, there is a single UV exposure step. (d) The UV exposure creates the LC-filled polymer boxes

Petitioner Samsung Ex-1011, 0394

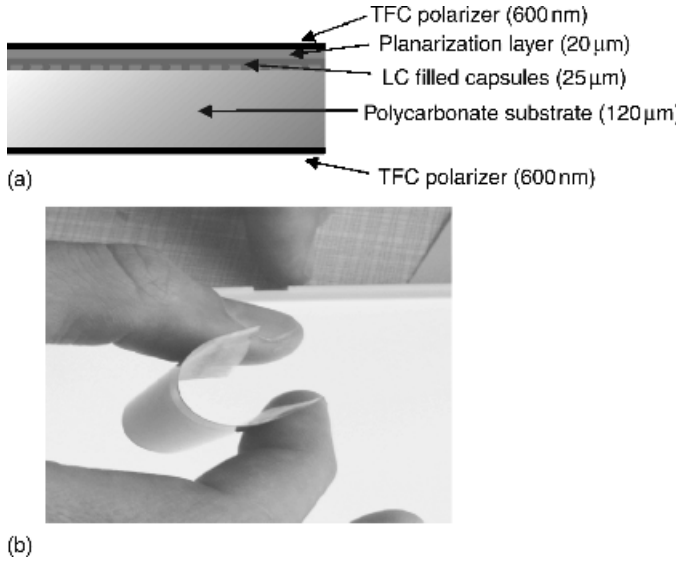


Figure 18.10 (a) Schematic representation of a stack of layers including coatable TCF polarizers. (b) Photograph of a paintable LCD bent to a curvature radius of less than 1 cm. The total thickness of this ultra-thin and flexible LCD is less than 170 μm

An example of a paintable LCD that provides flexibility and robustness has the following display design. A 120 μm thick engineered polycarbonate foil has been provided with interdigitated electrodes. An alignment layer is coated on the electrode structure and modified by the offset printing procedure as described above. After coating with LC/prepolymer mixture and the single-step formation of the polymer top layer, an additional UV-curable acrylate coating was deposited for planarization. The display is finished by application of the polarizers (Figure 18.10(a)). Applying coatable TCF polarizers results in flexible displays that are ultra thin. Figure 18.10(b) shows a paintable LCD with two coated polarizers. The resulting LCD is less than 170 μm thick, dominated by the thickness of the substrate film, and can be bent to a curvature radius of 10 mm. Rather than using coated polarizers, it is also an option to laminate sheet polarizers onto the paintable LCD (Figure 18.11).

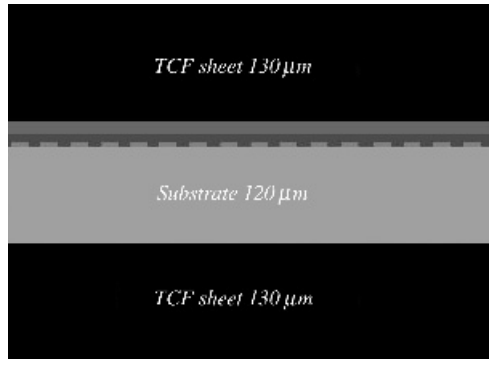


Figure 18.11 Schematic representation of the stack of layers including two TCF sheets

Petitioner Samsung Ex-1011, 0395



Figure 18.12 Photograph of an addressed paintable LCD. The Philips logo was activated by direct addressing of the in-plane switching electrodes. The total thickness of this paintable LCD with two TCF sheets is about 430 μm

The general advantage is that the contrast of the display is improved, but at the expense of display thickness and display flexibility. The preferred method will depend on the demands of the application. Figure 18.12 shows a paintable LCD provided with two sheet polarizers (TCF-coated sheets) having a thickness of 130 μm each. The resulting LCD is about 430 μm thick and is still robust and flexible.

18.8 Conclusion

This chapter presented the new photoenforced stratification technique (PES) to manufacture paintable LCDs. Pixel sizes and optical and switching characteristics compatible with display and shutter applications were demonstrated using this technique. A big step towards the industrialization of the paintable LCD technology is the introduction of an offset printing step into the process. This leads to devices with improved mechanical robustness and potentially enables the production of free form factor displays on a variety of substrates with high-speed reel-to-reel production processes.

Acknowledgements

The authors are indebted to Dr J. Lub (Philips Research Laboratories, Eindhoven, Netherlands) for the synthesis of the stilbene dimethacrylate compound and his participation in the discussions.

Petitioner Samsung Ex-1011, 0396

References

Bobrov, Y. A., Cobb, C., Lazarev, P., Bos, P., Bryant, D. and Wonderly, H. (2000) Lyotropic thin film polarizers. *SID 2000 International Symposium Digest of Technical Papers*, 1102–5.

Boots, H. M. J., Kloosterboer, J. G., Serbutoviez, C. and Touwslager, F. J. (1996) Polymerization-induced phase separation I. Conversion-phase diagrams. *Macromolecules* **29**, 7683–89.

Bowley, C. C., Yuan, H. and Crawford, G. P. (1999) Morphology of holographically-formed polymer dispersed liquid crystals (H-PDLC), *Molecular Crystals and Liquid Crystals Technology Section A* **331**, 2069–76.

Broer, D. J., Lub, J. and Mol, G. N. (1995) Wide-band reflective polarizers from cholesteric polymer networks with a pitch gradient. *Nature* **378**, 467–69.

Doane, J. W., Vaz, N. A., Wu, B. G. and Zumer, S. (1986) Field controlled light scattering from nematic microdroplets. *Applied Physics Letters* **48**, 269–71.

Hikmet, R. A. M. (1999) Anisotropic networks and gels formed by photopolymerisation in the ferroelectric state. *Journal of Materials Chemistry* **9**, 1921–32.

Hirai, Y., Niama, S., Kumain, H. and Gunjima, T. (1990) Phase diagram and phase separation in LC/prepolymer mixture. *Proceedings of SPIE* **1257**, 2–8.

Kamiya, H., Tajima, K., Toriumi, K., Terada, K., Inoue, H., Yokoue, Y., Shimizu, N., Kobahashi, T., Odahara, S., Hougham, S., Cai, C., Glownia, J. H., von Gutfiel, R. J., John, R. and Lien, S. C. A. (2001) Development of one drop fill technology for AM-LCDs. *SID 2001 International Symposium Digest of Technical Papers*, 1354–57.

Kiefer, R., Weber, B., Windscheid, F. and Baur, G. (1992) In-plane switching of nematic liquid crystals. *Proceedings of 12th IDRC, Japan Display 1992*, pp. 547–50.

Morozumi, S. (1990) Materials and assembling process of LCDs. In *Liquid Crystals: Applications and Uses*, Vol. 1 (ed. B. Bahadur), World Scientific, London, pp. 181–94.

Oh-e, M., Ohta, M., Aratani, S. and Kondo, K. (1995) Principles and characteristics of electro-optical behaviour with in-plane switching mode. *Proceedings of Asia Display 1995*, pp. 577–80.

Qian, T., Kim, J. H., Kumar, S. and Taylor, P. L. (2000) Phase-separated composite films: experiment and theory. *Physical Review E* **61**, 4007–10.

Vaz, N. A., Smith, G. W. and Montgomery, G. P. (1987) A light control film composed of liquid crystal droplets in a UV-curable polymer. *Molecular Crystals and Liquid Crystals* **146**, 1–15.

Vorflusev, V. and Kumar, S. (1999) Phase-separated composite films for liquid crystal displays. *Science* **283**, 1903–5.

Yamada, N., Kohzaki, S., Funada, F. and Awane, K. (1995) Axially symmetric aligned microcell (ASM) mode: electro-optical characteristics or new display mode with excellent wide viewing angle. *Journal of Society Information Display* **3**, 155–58.

Petitioner Samsung Ex-1011, 0397

19

Electrophoretic Imaging Films for Electronic Paper Displays

Karl Amundson

E Ink Corporation

19.1 Introduction

Historically, ink on paper has been a very successful display medium. It is bright, has a high contrast for easy readability, and its thinness and flexibility offer convenience for storage and portability. Further, it is the dominant material used for long-term storage of information. An electronic paper display seeks to incorporate many of these attributes: high brightness and contrast with full viewing angle, thinness and flexibility, and low power consumption, all into an electronically updateable display. Such a display would be especially advantageous in portable electronic devices where long battery life and high readability in a variety of lighting conditions are valued.

Several components are crucial players in determining the final performance of a display: the imaging film, the substrate material as well as the electronic structures used for the backplane and frontplane, and driver electronics. This chapter focuses on electrophoretic imaging films and their incorporation into flat panel displays. We will explore the appeal of electrophoretic imaging films for electronic paper displays, and examine several electrophoretic imaging films being developed for emerging applications. Prototypical flexible displays that incorporate electrophoretic imaging films will also be discussed.

Flexible Flat Panel Displays Edited by G. P. Crawford
© 2005 John Wiley & Sons, Ltd., ISBN 0-470-87048-6

Petitioner Samsung Ex-1011, 0398

Electronic displays can be divided into two broad classes based on their lighting source: emissive and nonemissive displays. Emissive displays emit light, and examples include cathode ray tube (CRT), backlit liquid crystal (LC), plasma, electroluminescent and light-emitting diode (LED) displays. These displays perform very well in dark conditions but tend to ''wash out'' in very bright conditions, such as under direct sunlight, where reflection of ambient light matches or exceeds light emission from the display. In nonemissive displays, the imaging layer acts as a light valve, and the film's reflectivity or transmissivity can be modulated electronically. Examples include the nonbacklit liquid crystal films, electrochromic films, and most particle-based films. There are crossover films as well. For example, transflective liquid crystal displays can operate either in backlit (emissive) or nonbacklit (nonemissive or reflective) mode. For portable devices, a passive display with wide angles of viewability combined with a front light for readability in dark conditions is an attractive option.

For use in portable devices, low power consumption is important for long battery life. Nonemissive displays draw less power than emissive displays, which require significant power to generate their own light. Further, nonemissive displays that exhibit image stability offer additional power savings because they need to draw power only to change an image but not to maintain it. For applications such as electronic books, where images are updated only occasionally, the power savings can be considerable. For these reasons, there is much interest in developing reflective, image-stable display films with wide viewability for portable display applications.

Twisted nematic (TN) and super twisted nematic (STN) displays are currently the most well-established flat panel display technology. While backlit versions offer high brightness, nonbacklit TN and STN displays do not exhibit high brightness, because they use polarizers that absorb about two-thirds of the incoming light. High-gain reflectors have been employed to achieve high brightness in TN displays over a limited range of viewing and illumination angles, but at the cost of significantly reduced contrast and brightness at other illumination and viewing angles. Because these films are monostable the display must be continuously refreshed in order to maintain an image.

Imaging films based upon switchable scattering, and especially bistable ones, are attractive candidates for bright, low-power displays. Scattering and diffracting films do not require polarizers, so they offer the potential of high brightness and readability in a variety of lighting conditions, and bistability can lead to low power consumption.

19.2 Scattering Imaging Films for Displays

Flat panel displays that are based on scattering or diffraction offer the potential for higher brightness than their twisted nematic counterparts because they do not require polarizers to achieve their optical contrast. There are several examples of electric field switchable scattering films made using liquid crystals and composites of liquid crystals and polymers; these are discussed in Chapters 14 and 15. Particle-based films include the Gyricon display, discussed in Chapter 20, and electrophoretic films discussed here. The fundamental visual appeal of particle-based displays is their ability to strongly backscatter light to give a bold, ink-on-paper appearance. Examining the factors that give rise to strong scattering will provide a basis for a better understanding.

Petitioner Samsung Ex-1011, 0399

Let us begin with an expression for light scattering from a hetergeneous, nonabsorbing material. In the single scattering limit, the amplitude of scattered light, A_{sc}, can be expressed simply in the first Born approximation (Born and Wolf 1980; Jackson 1999):

$$A_{sc}(\mathbf{k}') = \frac{k^2}{4\pi}\frac{1}{r}\int d\mathbf{r}\frac{\delta\varepsilon(\mathbf{r})}{\langle\varepsilon\rangle}\,\mathbf{D}_0\exp(i(\mathbf{k}-\mathbf{k}')\cdot\mathbf{r}), \tag{19.1}$$

where $\mathbf{k}$ and $\mathbf{k}'$ are the wave vectors of the incoming and scattered light, respectively, $\mathbf{D}_0$ is the electric displacement vector of the incoming light, r is the distance from the scattering source, and $\mathbf{r}$ the position vector. $<\varepsilon>$ is the average dielectric constant and $\delta\varepsilon(\mathbf{r})$ is the spatially varying part of the refractive index that causes scattering. The dielectric constant here is the value at the wavelength of light, more commonly expressed through the refractive index, which is the square root of the dielectric constant. The integration is over the volume of the scattering film. The intensity of scattered light is the square norm of this amplitude, which means that, for a given structure of the refractive index variation, the scattering intensity scales with the square of the dielectric constant variation, and for small variations this too scales as the square of refractive index variations:

$$I_{sc} \propto (\delta n(\mathbf{r}))^2. \tag{19.2}$$

These formulas are only valid for small refractive index variations and single scattering. Thus they are not valid for display films exhibiting large refractive index variations and where multiple scattering is significant. However, they do show the more than linear (in this case quadratic) dependence of the scattered light intensity on the refractive index variations causing single scattering events. These are the constituent events for backscattering in films that use multiple scattering to achieve high reflectivity. Equation (19.1) also shows that strong scattering requires structure, namely variations in the refractive index, must be on the order of the wavelength of light.

From these considerations, one can see how particle-based imaging films enable very bright reflective displays. For scattering films that employ liquid crystals, the switchable part of the scattering is bounded by the birefringence of the liquid crystal, which is typically on the order of 0.2, and at best $\sim$0.3. For particle-based films, the scattering arises from the contrast between particles and their surrounding medium. For titania particles in a simple oil, the refractive index contrast can be on the order of 1.2. This means that, for similar scattering object size and structure, particle-based films can attain on the order of 10–40 times stronger backscatterering than an LC-based film with similar structure. Such particles are available or can be made with sizes on the order of the wavelength of light, a second prerequisite for strong scattering.

It is noteworthy that the cholesteric imaging film escapes the backscattering limitation imposed by the birefringence of its liquid crystal by forming a periodic texture that gives a very large structure factor over a finite wavelength range (Chapter 15). In this case, light is brought back to the viewer through diffraction instead of scattering, resulting in bright, iridescent colors.

The strong backscattering capability of particle-based films, and their resultant bold, ink-on-paper appearance inspired efforts to develop electrophoretic films in the 1970s and 1980s.

Petitioner Samsung Ex-1011, 0400

Although no commercially viable efforts were developed during this time, the current proliferation of portable devices requiring displays that are highly readable in a variety of lighting conditions has focused considerable attention on electrophoretic films as a strong candidate. The following sections discuss the early development of electrophoretic films, look at the various electrophoretic films currently being developed, and review examples of flexible electrophoretic displays.

19.3 Electrophoresis and Electrophoretic Imaging

Electrophoresis is the translation of charged objects in a fluid in response to an electric field. The first example of the use of electrophoresis for creating an image was reported by Metcalfe and Wright (1956). In this early device, a plate containing charge in the form of a desired image is immersed in a fluid containing a colloidal suspension of the opposite charge. The oppositely charged colloid is electrically attracted to the plate, then chemically fixed to the plate to form a visible image. Early instances of displays using electrophoresis to create reversible images were reported by Evans *et al*. (1971) and Ota *et al* (1973) and reviewed by Dalisa (1977).

The typical electrophoretic display film construction consisted of a suspending dyed fluid containing charged pigment particles, in a thin film between a front electrode and a backplane containing a series of pixel electrodes (Figure 19.1), and were typically driven with tens to hundreds of volts.

Optical contrast is gained by pulling the charged pigment particles to the front or back surfaces of the film. By applying a voltage to a backplane electrode with a sign matching that of the pigment charge, the pigment is electrostatically driven to the front of the display. That region of the display then appears bright because the pigment scatters light back before the light passes through much of the dyed fluid. By applying the opposite voltage to the

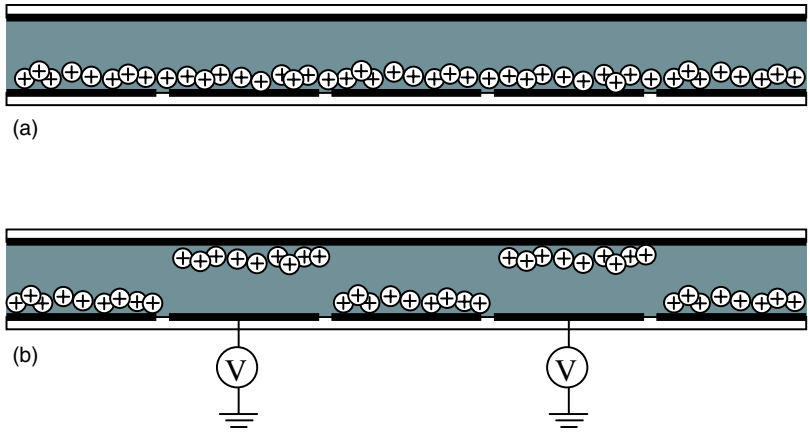


Figure 19.1 A thin electrophoretic film in cross section containing white scattering pigment particles in a dyed fluid. (a) The display appears dark or colored (viewer is above the display) because the pigment is behind the dyed fluid. (b) A voltage is applied to two pixels, driving the pigment over those pixels to the front of the display. These pixels appear white because the pigment is in front of the dyed fluid

Petitioner Samsung Ex-1011, 0401

backplane electrode, the particles are pulled back away from the viewer. In this case, light passes through the dyed fluid before and after being scattered by the pigment, and all or part of the visible spectrum is absorbed to give a black or colored state. The particle pack, or layer of particles, in the white state gives Lambertian scattering, imparting a bright white state at all or nearly all viewing and illumination angles. One is not limited to switching between a white state and a colored or dark state. By suitable choice of pigment and dye colors, one can switch between any pair of colors.

19.3.1 Electrophoretic Switching Speed

The switching speed of this type of electrophoretic film can be understood, at least approximately, from some elementary considerations. In an electric field, a charged particle in a fluid moves in response to an applied field **E** with a velocity **v** relative to the surrounding fluid. The proportionality constant, μ, is called the electrophoretic mobility:

$$\mathbf{v} = \mu \mathbf{E}. \tag{19.3}$$

For discussions of electrophoretic phenomena, see for example Morrison and Ross (2002) or Probstein (1994). Smoluchowski first developed an expression for the electrophoretic mobility:

$$\mu = \frac{\zeta \varepsilon}{\eta}, \tag{19.4}$$

where ε and η are the dielectric constant and viscosity of the surrounding fluid, respectively, and ζ, the so-called zeta potential, is the electrostatic potential at the shear plane around the particle. The zeta potential can be expressed approximately as

$$\zeta = \frac{q\lambda_D}{\varepsilon}, \tag{19.5}$$

where q is the charge on the particle and λ_D is the Debye length. The switching time can be approximated as the cell gap, h, divided by the electrophoretic particle speed, v:

$$t_{\text{switch}} \approx \frac{h}{v} = \frac{h}{\mu E} = \frac{h^2}{\mu V} \tag{19.6}$$

for a drive voltage V. These equations show how particle and fluid properties are important for fast switching. For example, a high particle charge and low fluid viscosity contribute to a high electrophoretic mobility, which can lead to fast switching. Outside of particle and fluid properties, (19.6) shows the importance of the cell gap and voltage on switching speed. In most practical applications, the voltage is limited by available electronics and cost. The quadratic dependence of the switching speed on cell gap means that reducing the cell gap is an important part of increasing switching speed. Cell gaps of electrophoretic films tend to be in the range 10–100 μm, and switching speeds tend to be tens to hundreds of milliseconds

Petitioner Samsung Ex-1011, 0402

with driving voltages of 5–100 V. Because of their distinct electrode configuration, the equation for switching speed is quite different for the in-plane electrophoretic films discussed later in this chapter.

19.3.2 Image Stability and Waveforms

Numerous efforts have been undertaken to develop electrophoretic films that exhibit image stability (whereby the image does not need to be refreshed except when the image is to be updated). Figure 19.2 shows examples of waveforms for driving (a) a twisted nematic film and (b) an image-stable electrophoretic film and between two optical states. The twisted

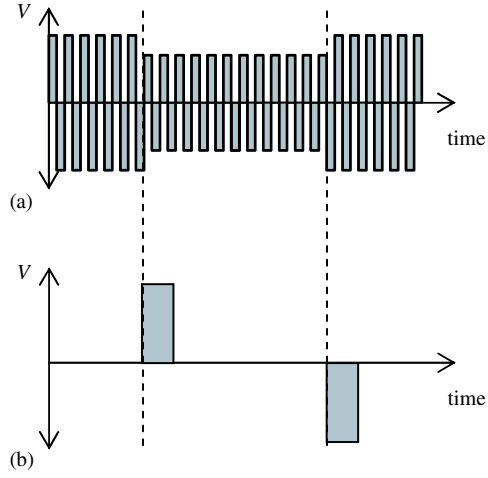


Figure 19.2 Representation of drive voltages required to achieve an image sequence where one begins in one optical state, transitions to another optical state, then goes back to the original optical state. (a) A sample waveform for a twisted nematic display and (b) a sample waveform for an image-stable electrophoretic display

nematic film requires continuous addressing. To change the optical state, the amplitude of the sign-alternating voltage is changed. For an image-stable electrophoretic film, the applied voltage is zero while the image is maintained. A voltage is applied only to change the image. In the example of Figure 19.2(a) a positive voltage is applied for a finite time to effect a change in the graytone of a pixel, and later a voltage impulse of the opposite sign is applied to change the graytone back to the original value. For displays that are updated only occasionally, the power consumption of a display employing an image-stable imaging film can be extremely low.

19.3.3 Integration of Films into Displays

In the 1970s a number of methods for driving electrophoretic films were pursued. Direct drive addressing is the most straightforward scheme. It employs a backplane tiled with pixel

Petitioner Samsung Ex-1011, 0403

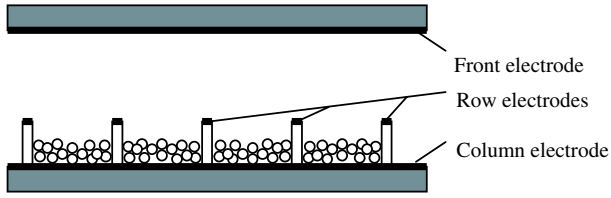


Figure 19.3 Control grid structure for driving electrophoretic films. The pigment is trapped in potential wells because of a voltage difference between the row electrode and column electrode

electrodes, with each pixel directly tied to the display controller through a conductive lead (Ota *et al*. 1977). The controller applies appropriate voltages to update each pixel's optical state. Direct drive displays are only practical and economical when the number of pixels is relatively small. For moderate to large information content, the direct connection to each pixel becomes spatially impractical and expensive; some type of matrix addressing is necessary.

One matrix addressing scheme uses a control grid like the one illustrated in Figure 19.3. The control grid design employs a third ''row'' electrode spatially set forward from the ''column'' electrode on the backplane. Pigment can be trapped behind the row electrodes by maintaining the appropriately signed voltage difference between the row and column electrode. Changing the row electrode voltage relative to the column electrode releases the pigment particles so they can move to the front electrode under the appropriate column electrode voltage relative to the front plane voltage (Singer and Dalisa 1977; Murau 1984). By sequentially addressing row electrodes and choosing appropriate column electrodes for that row, the entire display is addressed.

Electrophoretic films with a significant threshold voltage allow passive matrix addressing of an unlimited number of display rows. In passive matrix addressing, a pixel is defined by the crossing of a row electrode on the backplane and a column electrode on the frontplane, as illustrated in Figure 19.4. Passive addressing offers a very simple electrical construction of the display backplane compared to an active matrix display. To address a pixel, a partial addressing voltage is applied to the corresponding row and the complementary part of the addressing voltage to the corresponding column electrode. Other pixels in the row and column experience only a partial addressing voltage. If these partial addressing voltages are below the threshold voltage, image artifacts due to crosstalk are avoided.

For the control grid and passive matrix schemes, the display is addressed a line at a time, and the image update time is the time to address a single pixel times the number of rows in the display (Ota *et al*. 1977, 1975; Lewis *et al*. 1977). For an imaging layer with 100 ms intrinsic response time, a 200-row display will require 20 s to update. These displays are most appropriate where the image update time is not a critical issue, such as quasistatic signage. For applications where a reasonably fast update time is important, a multiplex scheme combined with an extremely fast electrophoretic film may be sufficient; alternatively an active matrix scheme where all pixels are updated simultaneously is required.

An active matrix display offers an image update speed as fast as for a single pixel, at the cost of requiring thin film transistor fabrication on the backplane. The low crosstalk voltages on an active matrix backplane make it compatible with electrophoretic films with no or low threshold voltages. An active matrix backplane is illustrated schematically in Figure 19.5. A thin film transistor (TFT) at each pixel acts as a nonlinear element that makes row-by-row

Petitioner Samsung Ex-1011, 0404

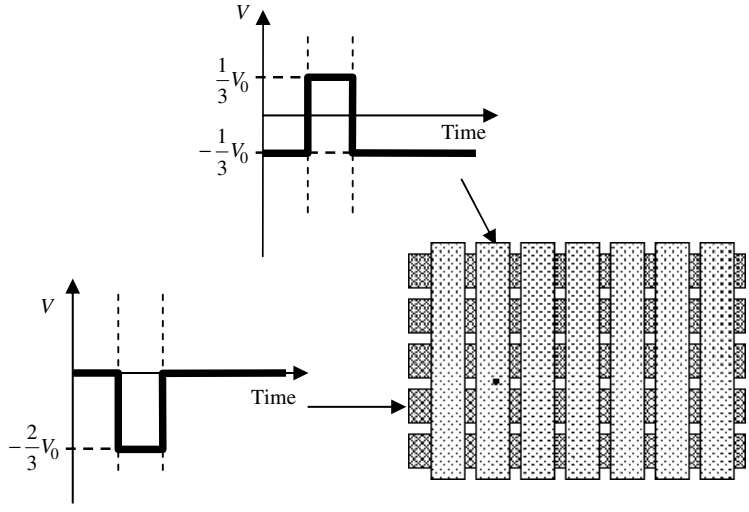


Figure 19.4 A passive matrix addressing scheme. The pixels are defined by row electrodes on one substrate and column electrodes running in the orthogonal direction on the other substrate. Example voltage curves used to address the pixel marked by an asterisk with voltage V_0 are also shown. In this scheme, other pixels in the display experience crosstalk voltages as large as one-third of the addressing voltage

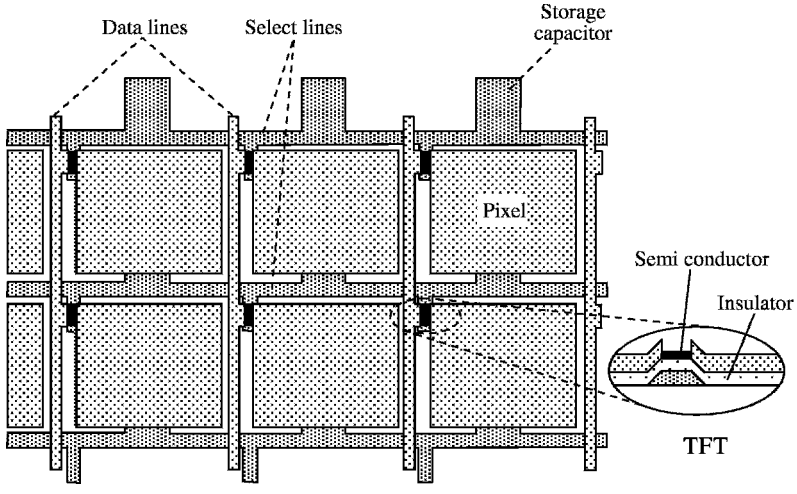


Figure 19.5 One type of active matrix backplane. The horizontal select (row) lines control whether the thin film transistor (TFT) is in depletion (insulating) or accumulation (conducting). Data (column or source) lines run vertically and bring voltages to the pixel electrodes. In this example, storage capacitors are formed by extending the select line from the previous row beneath the pixel electrode. In other variants, separate horizontal conductor lines form the storage capacitors

Petitioner Samsung Ex-1011, 0405

addressing possible. A row electrode brings the TFTs in that row into conduction, allowing voltages from the data lines to be transferred to the pixels in that row. Repeating this process for each row allows addressing of the entire display. A number of active matrix, electrophoretic displays have been developed, several of which will be reviewed in this chapter. Other novel addressing schemes include electrostatic addressing using a mechanical ionic writing head or a stylus (Chiang *et al*. 1979; Shiwa and Moshino 1988; Yamaguchi *et al*. 1991) that deposits charge on an electrophoretic sheet in regions where the pigment is to be addressed, and photoaddressing using a photoconductive layer (Blazo 1982).

19.3.4 Failure Modes and Their Remedies

Electrophoretic displays being developed in the 1970s were in competition with twisted nematic display development for flat panel display applications. History tells the story of the development and dominance of twisted nematic displays. Several failure modes hindered the development of electrophoretic displays for commercial success:

- sticking of particles to each other and on electrode surfaces;
- discoloration of dyes;
- migration of particles to electrode edges;
- floating or settling of particles.

Particle sticking can be eliminated by protection of the particle surfaces, for example, by grafting polymers on the particle surfaces. The polymer corona on particle surfaces must impose steric repulsion sufficient to guard against particles coming in contact and sticking through van der Waals attraction. Dye stability can be improved by using dyes stable under exposure to visible light and an ultraviolet-blocking front sheet. The problem of dye instability is completely avoided by using a dual-particle formulation in a clear fluid or an in-plane switching design.

The remaining primary failure modes result from lateral migration of the pigment. During a switching event, charged pigment particles move from one electrode to the other. This action requires displacing fluid, which must move in the reverse direction to the particles. This counterflow can result in roll cell flow, very much like the Rayleigh–Bernard roll cell instabilities induced by heating a thin film of fluid between two substrates from below, whereby the hot underlying fluid and the cold overlayer are driven by buoyancy to exchange places. These roll cells have a lateral extent on the order of the film thickness. In the case of electrophoretic films, the associated flow field leads to a nonuniform pigment distribution on the front surface with a length scale on the order of the film thickness.

There were additional recognized failure modes related to lateral migration. Particles can migrate to the edges of electrodes by a dielectrophoretic force. The induced electric dipole of the pigment particles is attracted to regions of high field, like an electrode edge where the electric field gathers most strongly. Finally, if the particles are not neutrally buoyant, when the display is held sideways, the particles can settle to one side of the display, rendering it nonfunctional.

All of these last three failure modes can be eliminated or reduced by restricting the extent of lateral migration to subcritical length scales. Early reports (Hopper and Novotny 1979;

Petitioner Samsung Ex-1011, 0406

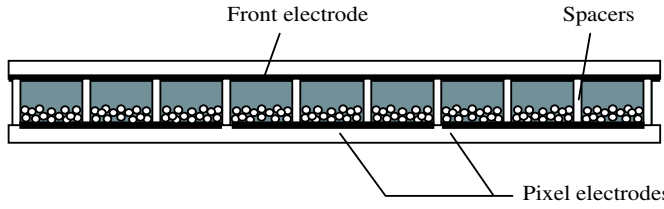


Figure 19.6 A series of ribs extending across the display limit lateral migration of pigment

Blazo, 1982) described the photopatterning of a photoresist layer to form a periodic rib structure that compartmentalizes the electrophoretic material and blocks lateral migration (Figure 19.6). Currently, a variety of electrophoretic displays are being developed, and all compartmentalize the electrophoretic fluid. These displays can be differentiated, among other things, by how the lateral migration is restricted. Several of these efforts are reviewed in the next section.

19.4 Current Electrophoretic Display Development Efforts

The recent proliferation of portable electronic devices with electronic displays has fueled a renewed interest in displays that consume low power, are easily readable in a variety of lighting conditions, and are thin, lightweight and rugged. Several initiatives are being pursued using electrophoretic technologies to address the needs of these and other applications. This section reviews several of these efforts.

19.4.1 Microencapsulated Electrophoretic Displays

Microencapsulated electrophoretic display films have been developed by E Ink Corporation (Comiskey *et al*. 1998) and independently at the NOK Corporation, and continued at the Seiko-Epson Corporation (Kawai and Kanae 1999). Instead of filling preexisting microcellular structures with an electrophoretic fluid, the electrophoretic fluid is microencapsulated and the microcapsules are coated onto a front electrode along with a polymeric binder. Microencapsulation restricts lateral migration of pigment particles. An adhesive layer is coated over the layer of microcapsules to facilitate attachment to a backplane. By adjusting the capsule wall mechanical properties and thickness, one can bestow sufficient capsule malleability so that the microspheres pack not as rigid spheres, but as a tightly packed array of deformed microspheres. A coating of a monolayer of rigid spheres would leave significant interstitial regions that would not participate in electro-optic switching, but the tight packing of deformed spheres gives almost complete coverage of active switching area (Figure 19.7), resulting in an increased optical dynamic range. Early microencapsulated electrophoretic films produced by E Ink had response times on the order of 1 s when driven at several hundred volts. Improvements in electrophoretic mobilities, and especially reduction in film thickness (Section 19.3) enabled by a dual-particle formulation, resulted in faster response at lower voltages. Current research formulations have been demonstrated by an E Ink electrophoretic film to have a black-to-white update time of less than 50 ms at 15 V drive

Petitioner Samsung Ex-1011, 0407

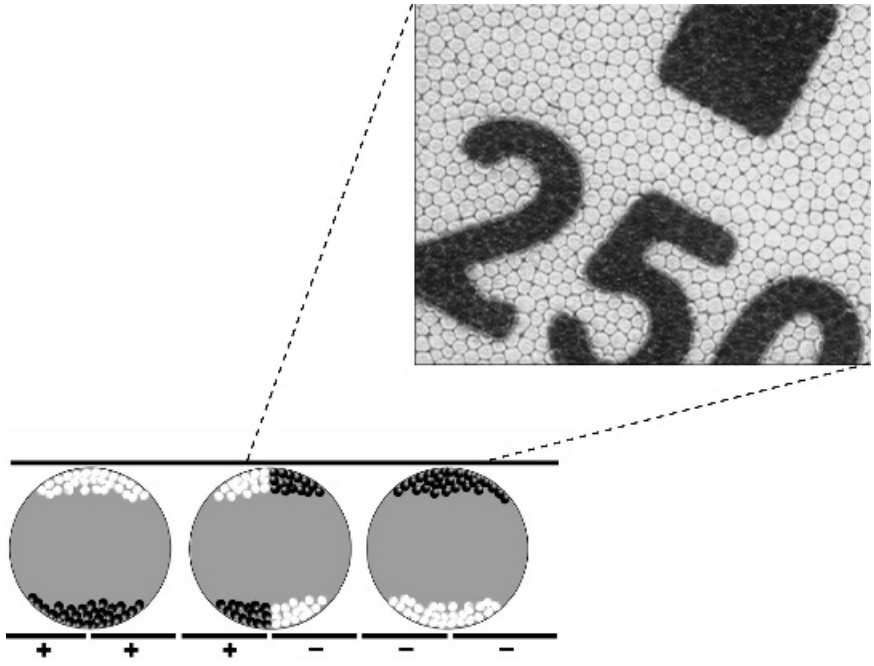


Figure 19.7 Microencapsulated electrophoretic display film from the E Ink Corporation. A side view schematic is shown along with a microscopic image of a display film

(Whitesides *et al*. 2004). Dark state reflectivities are in the range 2–4%; white state reflectivities for commercial films are in the range 35–40% and for research films they are over 50%.

Particle–dye and dual-particle electrophoretic display films

E Ink's first microencapsulated electrophoretic films had a particle–dye formulation. The bright state was achieved with white scattering particles and the dark state with a dye in the electrophoretic fluid. More recent electrophoretic films made at the E Ink Corporation have a dual-particle formulation, where the dark or colored state is achieved not by use of a dye, but by a second adsorbing pigment, as illustrated in Figure 19.8. The dual-particle system, although somewhat more complex to formulate, facilitates an improvement in display contrast.

In the particle–dye system, light is scattered off multiple pigment particles to achieve the bright state, during which light passes through dyed fluid in the interstices between the pigment particles. This has the effect of darkening or tinting the white state with the color of the dye (Figure 19.8(a)). This undesirable tinting can be reduced by decreasing the dye concentration, but then the dark state, achieved by moving the pigment to the back of the display, is not as dark. One could improve the dark state instead by increasing the cell gap. However, increasing the cell gap decreases the response speed of the display. The particle–dye electrophoretic films suffer from a threefold reciprocity constraint between the quality of the bright state, the quality of the dark state, and the response speed.

Petitioner Samsung Ex-1011, 0408

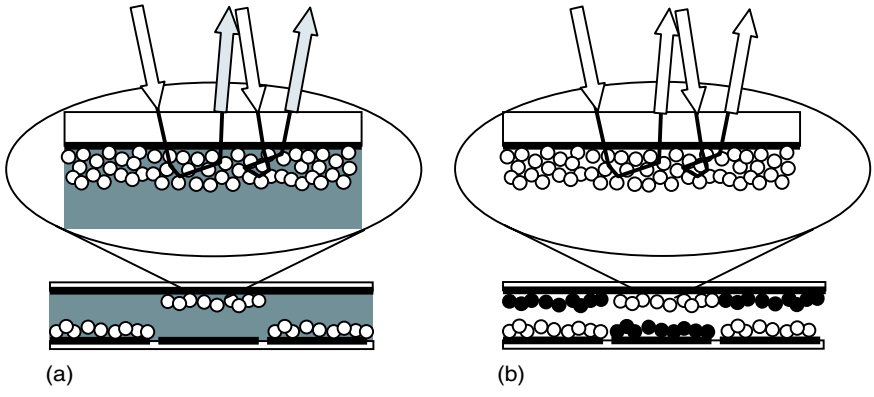


Figure 19.8 Light reflectance of (a) particle–dye and (b) dual-particle electrophoretic films in the white state. Interstitial dye in the particle–dye formulation taints the reflected light

A dual-particle system, on the other hand, offers a white state untainted by interstitial dye, as long as all the colored or black pigment is pulled to the back of the display cell. Using a dual-particle electrophoretic formulation, one escapes the reciprocity constraint just described for the dye-based electrophoretic films.

Graytones in E Ink imaging films are achieved by partial addressing between the black and white states, a method common to many electrophoretic displays. The graytones are persistent, so a grayscale display needs to be addressed only to change the image. A number of black and white and grayscale display prototypes have been demonstrated. The earliest integration of E Ink's microencapsulated electrophoretic film into an active-matrix display was reported in 2001 (Kazlas *et al* 2001; Ritter 2001). Figure 19.9 shows the first consumer application of a high-resolution electronic paper display module using E Ink's electrophoretic display material in a reading device made by the Sony Corporation launched in Japan in April 2004. The display cell consists of a frontplane laminate, comprised of the microencapsulated electrophoretic ink coated onto a plastic front sheet with a conductive



Figure 19.9 Sony Corporation's LIBRIe electronic reader with E Ink's microencapsulated electrophoretic imaging film in a display module made by Royal Philips Electronics

Petitioner Samsung Ex-1011, 0409

indium tin oxide (ITO) electrode, attached to a 167 ppi (pixel per inch) a-Si active matrix, glass backplane. A protective front sheet provides mechanical protection to the display cell. This display cell exhibits 2-bit grayscale, and the display is addressed only to update the image.

Color microencapsulated electrophoretic displays

Electrophoretic displays can readily be designed to switch between two colors by choosing appropriate pairs of pigments or a pigment and dye. For example, by combining a yellow pigment with a blue dye or second pigment that is blue and with the opposite charge, one can switch between yellow and blue optical states.

There are several proposed schemes for achieving full color. One is to use at least three combinations of two-color electrophoretic fluids in a subpixellated scheme to form various combinations of red, green, and blue. Most such schemes would require patterning of subpixels with distinct electrophoretic formulation to render the distinct colors. Arguably the simplest approach to full color is to combine an external color filter over a black and white electrophoretic film. Color display prototypes using E Ink's electrophoretic films in conjunction with a color filter made by Toppan Printing Company have been demonstrated. (Duthaler *et al*. 2001, 2002). The color filter consisted of alternating red, green, and blue stripes registered to subpixels of the backplane. To express red, for instance, the white pigment under the red subpixel is brought to the front, and black pigment is brought to the front under the green and blue subpixels (Figure 19.10). Figure 19.11 shows the reflectance and color coordinates as a function of illumination angle in a direct drive display that exhibited 3-bit color. A later version made using an 80 ppi (240 ppi subpixel resolution) active matrix display and controller electronics made at Royal Philips Electronics exhibited 3-bit color originally (Duthaler *et al*. 2002) and later 12-bit color. In each figure, a comparison is made to a state-of-the-art, twisted nematic liquid crystal display constructed with a high-gain reflector to optimize performance at particular illumination and viewing angles. As shown in Figures 19.10 and 19.11, the reflectance and saturation of the electrophoretic display

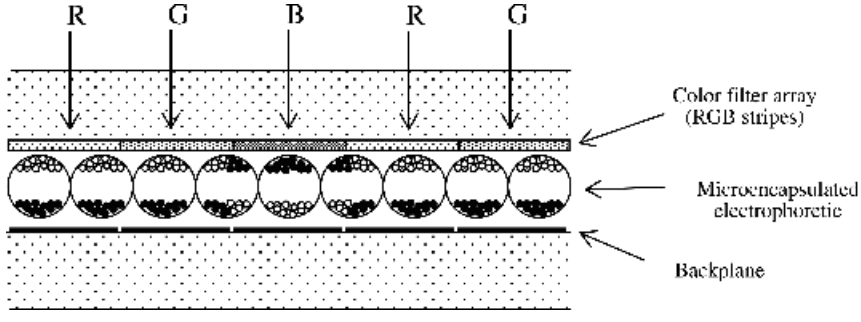


Figure 19.10 Schematic representation of a full-color microencapsulated electrophoretic film. On the front sheet, a color filter with red, green, and blue stripes is registered to subpixels on the backplane. Three subpixels constitute a full-color pixel. The three subpixels on the left form a pixel, and the particle configuration gives a yellow color. This is because light is back-reflected through the red and green stripes, and light passing through the blue stripe is absorbed

Petitioner Samsung Ex-1011, 0410

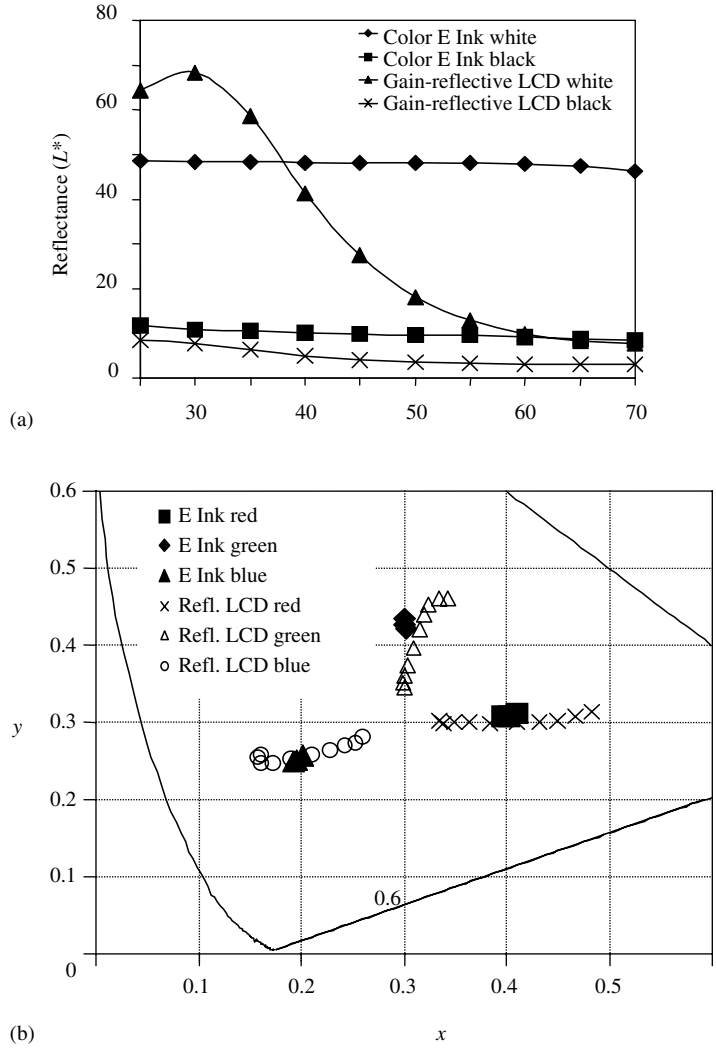


Figure 19.11 (a) Reflectivity and (b) color coordinates of a reflective E Ink electrophoretic color display and a commercial reflective color twisted nematic display as a function of illumination angle. The white and dark states of the E Ink display are insensitive to illumination angle, as are the color and saturation of red, green, and blue states

prototypes are not as strong as those for the liquid crystal display at its optimum illumination angle; however, the saturation and reflectance of the electrophoretic display are almost independent of angle, while the liquid crystal display film performance drops off sharply at illumination or viewing angles significantly away from the optimal angles.

Another pathway to full-color electrophoretic displays by stacking three imaging films over each other has also been proposed. This is possible using the in-plane-switching electrophoretic display in Section 19.4.3 because these films can be switched to a transparent state.

Petitioner Samsung Ex-1011, 0411

Microcellular electrophoretic display films

In the late 1970s and early 1980s, microcellular electrophoretic films were constructed by creating a square grid of rib structures using photoresists and photodefining (Hopper and Novotny 1979; Blazo 1982) in order to limit lateral particle migration. SiPix Corporation has recently developed a roll-to-roll manufacturing process for creating microcellular electrophoretic films (Liang *et al*. 2002, 2003) that can be attached to backplane electronics. The microcup structures are formed, filled, and sealed in one continuous process. A radiation-curable polymer is coated onto a front substrate with a transparent electrode. The film is pressed against an embossing wheel that imposes the rib pattern into this deformable polymer layer, after which the polymer layer is cured. The cells formed by the matrix of ribs are then filled with an electrophoretic fluid containing pigment particles and dye (Figure 19.12). An overcoat is then applied to this film to seal the electrophoretic fluid in the cells. This overcoat can be formed by polymerizing a monomer dissolved into the electrophoretic fluid; polymerization of this monomer forms a polymeric phase that floats to the surface of the electrophoretic film, where it forms a complete overlayer. Alternatively, a polymer overcoat is coated over the electrophoretic fluid in the cells. This overcoat serves as an adhesive layer or an additional adhesive layer is applied to the film to facilitate lamination onto a backplane.

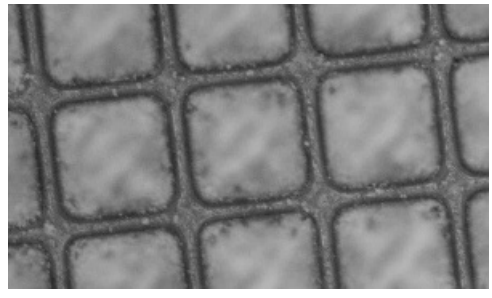


Figure 19.12 A Microcup electrophoretic film constructed with an embossed rib pattern and cells filled with an electrophoretic fluid, then sealed with an overcoat. Courtesy of SiPix

SiPix has demonstrated direct drive, active matrix, and passive matrix prototypes. As described in Section 19.3, passive matrix drive requires a threshold voltage. SiPix reports a 5–50 V threshold voltage built into electrophoretic films used for passive matrix applications (Liang *et al*. 2003). Passive addressing requires no active electrical elements on the backplane, so the manufacturing cost of the display is lower than for an active matrix counterpart and can simplify the transfer to flexible substrates, but the display must be addressed a row at a time, so the update time is given by the product of the native update time of the imaging layer and the number of rows in the display.

19.4.2 Microcellular Air-Gap Electrophoretic Displays

A collaboration between the Bridgestone Corporation and the Department of Electrical Engineering at Kyushu University in Japan has produced microcellular, air-gap

Petitioner Samsung Ex-1011, 0412

electrophoretic displays (Hattori *et al*. 2003). Replacing the fluid of the electrophoretic medium by air offers a great increase in response speed. The speed of an electrophoretic display is, roughly speaking, proportional to the electrophoretic mobility of the pigment particles, and the mobility is inversely proportional to the viscosity of the fluid through which the particles travel, as shown in (19.4). Noting that the viscosity of air is approximately 0.02 cP and the viscosity of simple fluids is typically on the order of 1 cP, one can expect on the order a hundredfold increase in speed for similar pigment charging, film geometry, and voltage.

Producing an air-based electrophoretic film poses new challenges over their liquid-based counterparts. Particle charging in fluids is understood to varying degrees. Charging in aqueous media by ionization of surface species is a well-developed practice. Charging in nonaqueous media is more complex, but has been achieved through micellization of dissociating ions. In air, these liquid-based mechanisms are not available. A second challenge is to avoid particles sticking to each other or on surfaces. Van der Waals and image charge forces are much stronger in a gas medium than a liquid medium, because of the strong contrast between the solid objects and gas, and the low dielectric constant of the surrounding medium. Collaborators at Bridgestone and Kyushu University created what they call ''liquid powder'' to reduce these problems of particle sticking. Figure 19.13 shows a demonstration of the liquid powder. A powder poured from a spout onto a plate forms a pile, with a characteristic angle of repose that is an indicator of the tendency of particles to associate (Figure 19.13(b)). The liquid powder, poured in the same manner (Figure 19.13(a)), exhibits a nearly zero angle of repose, indicating a much reduced tendency for the particles to associate. A mixture of black and white ''liquid powder'' pigment is poured into microcells on a bottom substrate. This bottom substrate has appropriate driving electronics and a rib structure that forms the microcells, as shown in Figure 19.14(a). A top substrate with transparent conductors is attached to the microcell plate to form the electrophoretic cell. The first prototype displays reported by this group exhibit a high voltage threshold, allowing the films to be multiplex addressed at 70–100 V. The response of the film is very fast, with about 0.2 ms switching time at 70–V drive. (To use standard display driving electronics, these voltages would need to be notably reduced.) Given this fast switching speed, even a multiplex-addressed display with over a hundred rows can be addressed relatively fast. The 160×160 pixel multiplex-addressed display prototype in Figure 19.14(b)) has a 67 ms

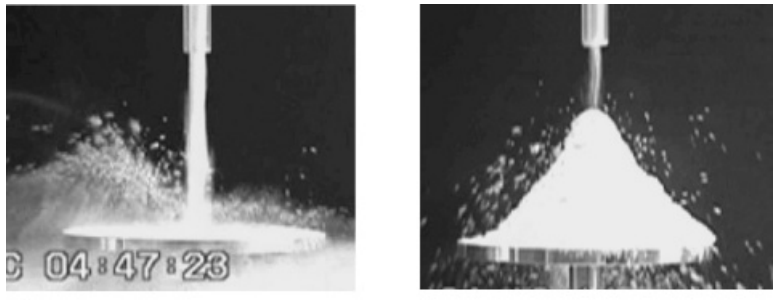


Figure 19.13 (a) Liquid powder made by Bridgestone and (b) an ordinary powder poured onto a platform. The liquid powder does not form a pile in this experiment, and an ordinary powder does. Reproduced with permission of the Society for Information Display

Petitioner Samsung Ex-1011, 0413

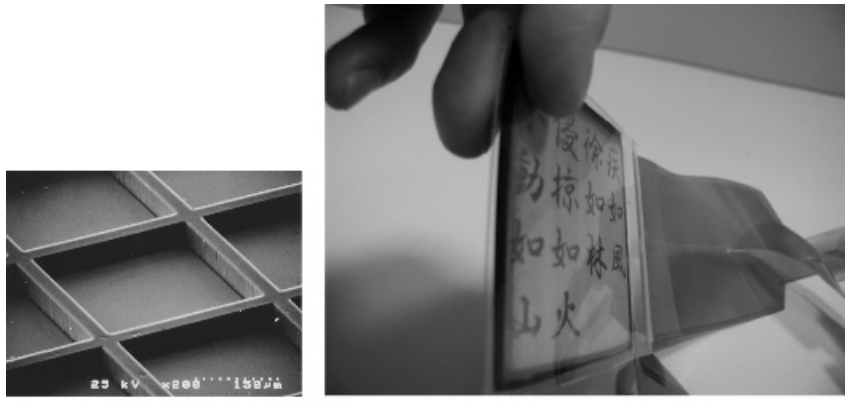


Figure 19.14 (a) Microscope image of the rib structure on a substrate used to make the air-gap electrophoretic film. (b) A 160 × 160 passive matrix display made on a plastic substrate by Bridgestone and Kyushu University. Part (a) reproduced by the permission of the Society for Information Display

update time. Grayscale addressing for these displays by partial addressing has also been reported (Hattori *et al*. 2003).

19.4.3 In-plane Electrophoretic Displays

Electrophoretic materials can also be addressed with in-plane electric fields (Swanson *et al*. 2000). The electrophoretic display film developed by Canon, Inc. is distinct from all other electrophoretic films discussed in this chapter in that optical contrast is achieved not by vertical movement of pigment toward or away from the frontplane, but by lateral, ''in-plane'' movement of pigment toward or away from a collecting electrode. There are no white scattering pigment particles in the imaging layer; instead, the white state derives from a fixed white scatterer behind the electrophoretic film, and a dark state from covering this scatterer with light-absorbing pigment. Each pixel has a ''displaying electrode'' under the electrophoretic fluid, and a collecting electrode that covers a small fraction of the pixel area. Holding the collecting electrode at zero volts, the displaying electrode can be brought to the opposite sign voltage as the charge on the pigment particles, causing the particles to disperse across the pixel to achieve a dark or colored state. Reversing the sign of the displaying electrode causes the pigment to be gathered near the collecting electrodes, exposing the back white reflector (Figure 19.15).

An earlier configuration utilized stripe-like collecting electrodes passing over the displaying electrode (Kishi *et al*. 2000). The frequently spaced collecting electrodes had stronger electric fields for faster response, but gave lower aperture ratios (the fraction of the pixel area not covered by the collecting electrodes). For example, for a 200 ppi display, Canon reported a 72% aperture ratio using this stripe electrode design. Embedding the collecting electrode inside the spacer between the electrodes, as shown in Figure 19.15, improves the aperture ratio. For example, a 200 ppi display with this design has a 92% aperture ratio. Placing the collecting electrodes in the spacers between the electrodes also reduces interpixel crosstalk (Matsuda *et al*. 2002; Ukigaya *et al*. 2003). Interpixel crosstalk manifests itself as a

Petitioner Samsung Ex-1011, 0414

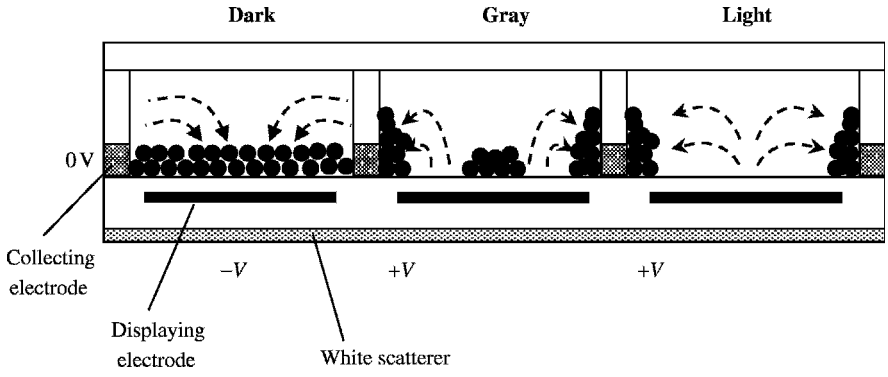


Figure 19.15 Cross section of one of Canon's in-plane electrophoretic films. Pixels are separated by vertical supports, and a collecting electrode is built into the supports and held at zero volts. A display electrode under every pixel drives the black pigment over the display surface to achieve a dark state or toward the collecting electrode to expose the white scatterer below. The left-hand pixel is driven dark, the middle pixel to a midtone, and the right-hand pixel to white reproduced by the permission of the Society for Information Display

modification of the pigment distribution in one pixel caused by the voltage on a neighboring pixel, leading to residual image artifacts. Increasing the height of the collecting electrode from 0.05 to 10 μm further reduces pixel crosstalk and improves the field distribution across the pixel (Ukigaya *et al*. 2003).

As with other electrophoretic films, grayscale is achieved by partial addressing, that is, by using a shorter or lower-voltage pulse than necessary to drive the display to the white state (Matsuda *et al*. 2002). Particles near the edge of the pixel are drawn to the collecting electrode rapidly because of the stronger electric fields near the edges of the pixels. The electric field near the center of the pixel is weaker, so the pigment there is drawn to the collecting electrode more slowly. By partial addressing, these pigment particles are left behind, to give a partially obscured backscatterer, and a graytone is achieved, as shown in Figure 19.16. Figure 19.16 shows a prototype active matrix electrophoretic display created at Canon, Inc (Ukigaya *et al*. 2003). This display has a 260 ppi resolution and is 5.32 cm × 5.32 cm. The high resolution was enabled using the 10 μm high collecting electrode design just mentioned. Canon reports an update time of under 1 s at 5 V drive, and a stable image at zero power.

In-plane-switched electrophoretic imaging layers offer the prospect of full-color pixels by stacking three display layers in front of the white backscatterer, and by using pigments that absorb one color and transmit the others. Full-color pixels offer greater brightness compared to the common design where each pixel is composed of a red, green, and blue subpixel. In the latter case, the brightness is reduced to one-third the brightness of a single pixel by separation into three subpixels. For example, rendering a red image requires that the associated green and blue subpixels are switched to black. Full-color pixels would allow the entire pixel to be red in this example, and in theory the brightness could be tripled. The cost of fabricating a triple-stacked display, however, is certainly considerably more than for fabricating a single-imaging-layer display. Another challenge is potential parallax, because the three layers must be vertically offset from each other.

Petitioner Samsung Ex-1011, 0415

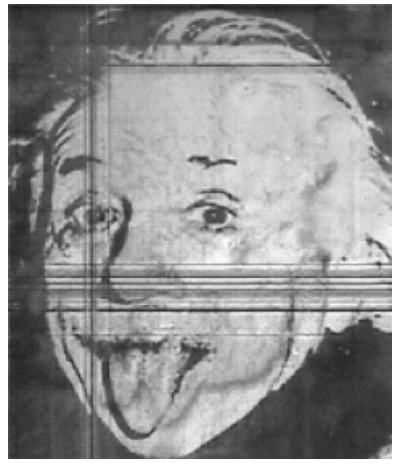


Figure 19.16 Active matrix, 260 ppi, 5.32 cm × 5.32 cm grayscale display prototype using Canon's in-plane electrophoretic film. Reproduced with permission of the Society for Information Display

19.5 Flexible and Conformable EPID Displays

Electrophoretic films are attractive candidates for incorporation into flexible displays and have attracted much interest recently. The strong optical contrast at all or nearly all viewing and illumination angles exhibited by electrophoretic films is an important attribute for a conformable or flexible display, by its nature viewed at a variety of viewing and illumination angles. Most electrophoretic film designs do not require a transparent rear substrate, so they are compatible with opaque backplanes constructed on, for example, metal foil. Since the optical contrast is not based on light polarization, the front substrate does not have to be birefringent free, thus allowing numerous polymeric front sheet constructions. Also, the solid structure between the front and rear substrates maintains the cell gap during deformation of the display.

Flexible, direct drive, electrophoretic displays were reported as early as 1998 (Comiskey *et al*. 1998) and flexible, microencapsulated, electrophoretic displays on Mylar plastic substrates were sold commercially by the E Ink Corporation beginning in 2001. Other groups have also demonstrated direct drive, flexible, electrophoretic displays (Kishi *et al*. 2000; Liang *et al*. 2002). Several active matrix, flexible prototype displays using E Ink's microencapsulated electrophoretic films have been constructed. The first of these, arising from a collaboration between Lucent Technologies, Bell Laboratories, and E Ink in 2001, represented a convergence of several new technologies: rubber-stamped monolayer resist patterning and thin film transistors based on organic semiconductors for fabrication of the active matrix backplane, and microencapsulated electrophoretic ink, in what was claimed to be the world's first flexible electronic paper display (Amundson *et al*. 2001). The construction of the backplane is described in Chapter 10. Microencapsulated electrophoretic ink was coated on an ITO-coated poly(ethylene terephthalate) flexible sheet of thickness between 100 and 200 μm, and this sheet was laminated to a via sheet in contact with the active matrix array (Rogers *et al*. 2001). An image of the display is shown in Figure 10.20. The coarse

Petitioner Samsung Ex-1011, 0416



(a) (b)

Figure 19.17 Thin, conformable, active matrix displays made using E Ink's electrophoretic film on an a-Si active matrix backplane fabricated on passivated steel foil. (a) The 300 μm thickness is shown and (b) a curved display. Reproduced by the permission of the Society for Information Display

pixel pitch was chosen to allow for a high yield in this laboratory-constructed, 16 × 16 pixel prototype. Based on the line, space, and registration rules for the backplane design and the thin film transistor performance, a display with several hundred rows could arguably be realized with the technology used to create this demonstration display.

E Ink produced conformable, active-matrix displays on steel foil in 2001 and 2002 (Chen *et al*. 2001; Kazlas *et al*. 2002; Au *et al*. 2002). Standard photolithographic processes for fabrication of a-Si active matrix backplanes were transferred from glass substrates to passivated steel foil to provide conformability while maintaining stability at the high temperatures required for the silicon base processes. The pixel transistors had a bottom-gate structure and an 8 μm channel length. Various displays were created; those with the highest resolution were 96 ppi, 240 × 160 pixel, 3.1 in diagonal displays (Figure 19.17(a)). These displays were constructed on 250 μm thick, passivated steel foil. The E Ink frontplane laminate on a plastic front sheet was attached to the backplane to yield a display cell with a total thickness of 300 μm. These displays were repeatedly curved down to a radius of ∼1.5 cm without signs of degradation in performance (Figure 19.17(b)) (Kazlas *et al*. 2002).

Recently, microencapsulated electrophoretic imaging films from E Ink have been integrated with flexible plastic, active-matrix backplanes to create high-resolution flexible displays. In one effort, these imaging films were integrated with active-matrix backplanes made by Royal Philips Electronics. The backplanes were constructed on plastic substrates and employ organic semiconductors. Prototypes from this effort include fully-functional, flexible, QVGA (240 × 320 pixel) active-matrix displays with five-inch diagonals. This effort is described in more detail in Chapter 16.

E Ink's microencapsulated electrophoretic films were also integrated with active-matrix backplanes made by Plastic Logic Limited. The backplanes were constructed on plastic using additive solution processing and direct write techniques based upon printing and also employ organic semiconductors. An example of an all-plastic, flexible display prototype is shown in Figure 19.18. These displays have been curved down to a radius of curvature below two centimeters without degradtion in performance.

Petitioner Samsung Ex-1011, 0417

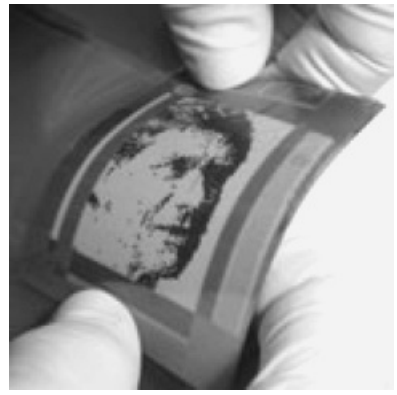


Figure 19.18 All-plastic display made using a microencapsulated electrophoretic imaging film from E Ink and an active-matrix backplane made by Plastic Logic. Courtesy of Plastic Logic Limited

These several display prototypes demonstrate the convergence of several new technical achievements into working flexible display devices. These early demonstrations of flexible displays provide learning experiences on basic integration issues, and show promise for further progress toward commercial flexible displays. Numerous important technical issues will require attention before a successful commercial product is realized, such as stability and lifetime of the display components, methods of encapsulating the display cell, interconnection and driver technology for a flexible display, reproducible manufacturability, and cost. Realizing a fully flexible active matrix display does have its challenges, but electrophoretic imaging films show great promise in making it a reality.

References

Amundson, K., Ewing, J., Kazlas, P., McCarthy, R., Albert, J. D., Zehner, R., Drzaic, P., Rogers, J., Bao, Z. and Baldwin, K. (2001) Flexible, active-matrix display constructed using a microencapsulated material and an organic-semiconductor-based backplane. *SID Digest* **2001**, 160–163.

Au, J., Chen, Y., Ritenour, A., Kazlas, P. and Gates, H. (2002) Ultra-thin 3.1-in. active-matrix electronic ink display for mobile devices. *IDW Proceedings* **2002**, 223–226.

Blazo, S. F. (1982) High resolution electrophoretic display with photoconductor addressing. *SID Digest* **1982**, 92–93.

Born, M. and Wolf, E. (1980) *Principles of Optics*, 6th edn, Pergamon Press, New York, Ch. 8.

Chen, Y., Denis, K., Kazlas, P. and Drzaic, P. (2001) A conformable electronic ink display using a foil-based a-Si TFT array. *SID Digest* **2001**, 157–159.

Chiang, A., Curry, D. and Zarzycki, M. (1979) A stylus writable electrophoretic display device. *SID Digest* **1979**, 44–45.

Comiskey, B., Albert, J. D., Yoshizawa, H. and Jacobson, J. (1998) An electrophoretic ink for all-printed reflective electronic displays. *Nature* **394**, 253–255.

Dalisa, A. L. (1977) Electrophoretic display technology. *Transactions on Electron Devices* **24**(7), 827–834.

Duthaler, G., Davis, M., Pratt, E., Gray, C. and Suzuki, K. (2001) Paper-like color displays using electrophoretic ink and color filters. *IDW Proceedings* **2001**, 473–476.

Petitioner Samsung Ex-1011, 0418

Duthaler, G., Au, J., Davis, M., Gates, H., Hone, B., Knaian, A., Pratt, E., Suzuki, K., Yoshida, S. and Ueda, M. (2002) Active-matrix color displays using electrophoretic ink and color filters. *SID Digest* **2002**, 1374–1377.

Evans, P. F., Lees, H., Maltz, M. and Dailey, J. (1971) Color display devices, U. S. Patent 3,612,758.

Hattori, R., Yamada, S., Masuda, Y. and Nihei, N. (2003) Novel type of bistable reflective display using quick response liquid powder. *SID Digest* **2003**, 846–849.

Hopper, M. A. and Novotny, V. (1979) An electrophoretic display, its properties, model, and addressing. *IEEE Transactions on Electron Devices* **26**(8), 1148–1151.

Jackson, J. D. (1999) *Classical Electrodynamics*, 3rd edn, John Wiley & Sons, Inc., New York, Ch. 10.

Kawai, H. and Kanae, N. (1999) Microencapsulated electrophoretic rewritable sheet. *SID Digest* **1999**, 1102–1105.

Kazlas, P., Au, J., Geramita, K., Gates, H., Steiner, M., Honeyman, C., Drzaic, P., Schleupen, K., Wisnieff, B., Horton, R. and John, R. (2001) 12. 1" SVGA microencapsulated electrophoretic active matrix display for information appliances. *SID Digest* **2001**, 152–155.

Kazlas, P., Ritenour, A., Au, J., Chen, Y., Goodman, J., Paolini, R. and Gates, H. (2002) Card-size active matrix electronic ink display. *Proceedings of Euro Display*, pp. 259–262.

Kishi, E., Matsuda, Y., Uno, Y., Ogawa, A., Goden, T., Ukigaya, N., Nakanishi, M., Ikeda, T., Matsuda, H. and Eguchi, K. (2000) Development of in-plane EPD. *SID Digest* **2000**, 24–27.

Lewis, J. C., Garner, G. M., Blunt, R. T. and Carter, F (1977). Gravitational, inter-particle and particle-electrode forces in the electrophoretic display. *Proceedings of SID* **18**(3/4), 235–242.

Liang, R. C., Hou, J. and Zang, H. (2002) Microcup electrophoretic displays by roll-to-roll manufacturing processes, *IDW Proceedings* **2002**, 1337–1340.

Liang, R. C., Hou, J., Zang, H., Chung, J. and Tseng, S. (2003) Microcup displays: electronic paper by roll-to-roll manufacturing processes. *Journal of the Society for Information Display* **11**(4), 621–628.

Matsuda, Y., Kishi, E., Goden, T., Ogawa, A., Ukigaya, N., Uno, Y., Ishige, K., Ikeda, T. and Matsuda, H. (2002) Newly designed, high resolution, active-matrix addressing in-plane EPD. *International Display Workshop Proceedings*, pp. 1341–1344.

Metcalfe, K. A. and Wright, R. J. (1956) Fine grain development in xerography. *Journal of Scientific Instruments* **33**, 194–195.

Morrison, I. and Ross, S. (2002) *Colloidal Dispersions: Suspensions, Emulsions, and Foams*, John Wiley & Sons, Inc., New York.

Murau, P. (1984) Characteristics of an X-Y addressed electrophoretic image display (EPID). *SID Digest* **1984**, 141.

Ota, I., Ohnishi, J. and Yoshiyama, M. (1973) Electrophoretic image display (EPD) panel. *Proceedings of IEEE* **61**, 832–836.

Ota, I., Sato, T., Tanka, S., Yamagami, T. and Takeda, H. (1975) Electrophoretic Display Devices. *Laser 75 Optoelectronics Conference Proceedings*, pp. 145–148.

Ota, I., Tsukamoto, M. and Ohtsuka, T. (1977) Developments in electrophoretic displays. *Proceedings of the Society for Information Display* **18**(3/4), 243–254.

Probstein, R. F. (1994) *Physicochemical Hydrodynamics: An Introduction*, 2nd edn, John Wiley & Sons, Inc., New York.

Ritter, J. (2001) Active-matrix electrophoretic displays. *Proceedings of the 21st International Display Research Conference*, pp. 343–346.

Rogers, J., Bao, Z., Baldwin, K., Dodabalapur, A., Crone, B., Raju, V. R., Kuck, V., Katz, H., Amundson, K., Ewing, J. and Drzaic, P. (2001) Paper-like electronic displays: large-area rubber-stamped plastic sheets of electronic and microencapsulated electrophoretic inks. *Proceedings of the Natural Academy of Science*, 4835–4840.

Singer, B. and Dalisa, A. L. (1977) An X-Y addressable electrophoretic display. *Proceedings of the Society for Information Display* **18**(3/4), 255–266.

Shiwa, S. and Hoshino, Y. (1988) Electrophoretic display method using ionographic technology. *SID Digest* **1988**, 61–62.

Petitioner Samsung Ex-1011, 0419

Swanson, S.A., Hart, M.W., and Gordon, J.G. (2000) High performance electrophoretic displays. *Proceedings of the Society for Information Display* **31**, 29–32.

Ukigaya, N., Endo, T., Matsuda, H., Goden, T., Ishige, K., Takagi, S. Nakanishi, N., Kishi, E., Ikeda, T. and Matsuda, H. (2003) Active matrix addressing in-plane EPD with a collecting electrode embedded in a spacer. *International Display Research Conference Proceedings*, pp. 107–110.

Yamaguchi, M., Matsuoka, H. and Matsuzawa, J. (1991) Equivalent circuit of ion projection-driven electrophoretic display. *IEICE Transactions E* **74**(12), 4152–4156.

Whitesides, T., Walls, M., Paolini, R., Sohn, S., Gates, H., McCreary, M. and Jacobson, J. (2004) *SID Digest* **2004**, 133–135.

Petitioner Samsung Ex-1011, 0420

20

Gyricon Materials for Flexible Displays

Nicholas Sheridon

Gyricon, LLC

20.1 Introduction

The Gyricon media (Sheridon and Berkovitz 1977; Sheridon *et al.* 1997) is a flexible rubber sheet. Like paper, the image on its diffusely reflecting surface is read by the modulation of reflected ambient light. This image can be seen over a wide range of angles and can be stored for long periods without the continued use of power.

A display made with Gyricon media consists of the rubber sheet situated between a pair of electroded windows. When an electrical voltage is applied across an area of the windows, the rubber sheet will turn white; when the opposite polarity voltage is applied, that area of the sheet will turn black (or another color). When the voltage is removed, the color of that area is retained. No backlight is needed to view an image on the rubber sheet. The Gyricon display only consumes power when forming an image, and this is of a very low level.

The Gyricon rubber sheet is 0.4 mm thick, robust and highly flexible. It can be made in large sheets, many feet in dimensions. Because media thickness uniformity is not critical, these large sheets can be economically made into large displays. Subject to the flexibility of the addressing system, a Gyricon display with plastic windows can be rolled up for easy transportation and storage.

Flexible Flat Panel Displays Edited by G. P. Crawford
© 2005 John Wiley & Sons, Ltd., ISBN 0-470-87048-6

Petitioner Samsung Ex-1011, 0422

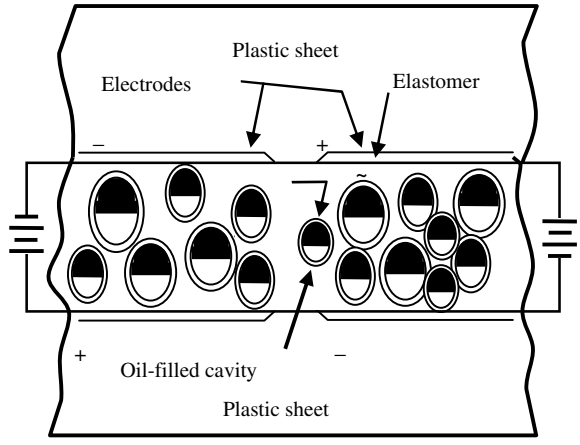


Figure 20.1 The Gyricon display consists of spherical beads, with optically contrasting hemispheres, dispersed in a transparent rubber sheet. A spherical cavity around each bead is filled with oil

The Gyricon display consists of spherical beads, with optically contrasting hemispheres, dispersed in a transparent rubber sheet. This is illustrated in Figure 20.1. A spherical cavity around each bead is filled with oil, allowing it to rotate in response to an electric field. One field polarity will cause hemispheres of a first color to face a viewing window, reversing the field polarity will allow the hemispheres of the second color to be seen. These bead orientations will persist after the field is removed, allowing long-term image storage.

The beads used in Gyricon displays are typically 100 μm in diameter and their coloration comes from the use of pigments. There are about a quarter of a million beads per square inch. Incident light is strongly scattered, in a Lambertian distribution, much like paper.

The first commercial applications of Gyricon technology are in retail signage and message boards. Longer-term applications are expected to include large-area signs, electronic newspaper and book readers and displays for handheld electronics.

20.2 Electro-Optical Response

The Gyricon beads are contained in individual spherical cavities in the rubber sheet. The cavity diameter is typically 25% larger than the bead diameter. The oil that fills the cavity is clear and dielectric. A photomicrograph of the edge of a Gyricon sheet (same aspect as Figure 20.1) is shown in Figure 20.2. The beads are called bichromal because they consist of two colors. Associated with each color is an electric charge; one hemisphere has a different magnitude of charge than the other, or a different polarity. Each bead has a dipole moment that is proportional to the charge difference between the two hemispheres. It also has a monopole moment that is proportional to the net charge on the bead. Both are important to the electro-optical behavior of the bead.

A single bead in its cavity is illustrated in Figure 20.3. Initially, the bead is adhered to the bottom of the cavity, with its white side facing up. As the electric field is applied, both the monopole and the dipole moments of the bead are acted upon. Rotation of the bead is initially prevented by the adhesion of the bead to the cavity wall. However, the field acts on the

Petitioner Samsung Ex-1011, 0423

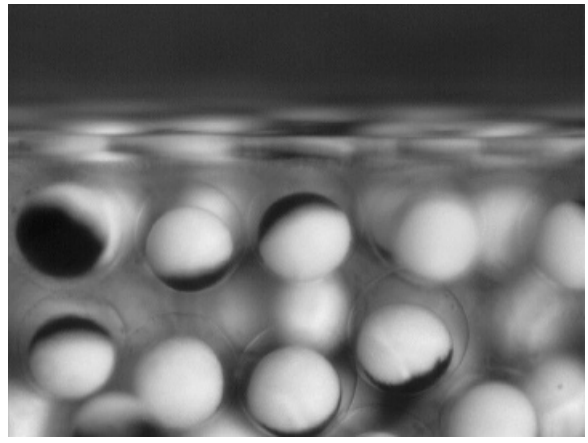


Figure 20.2 A photomicrograph of the edge of a Gyricon sheet having the same aspect as Figure 20.1

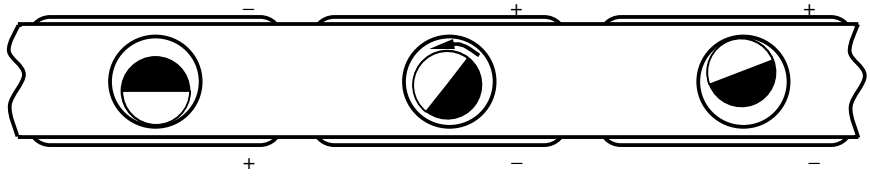


Figure 20.3 Dipole and monopole charges are associated with the Gyricon bead. On application of a field, the bead traverses the cavity and rotates. On reaching the wall it adheres

monopole moment of the bead, pulling it away from its adhesion to the cavity wall. Once this has happened, the dipole moment of the bead causes the bead to rotate, as the bead crosses the cavity. Maximum contrast is obtained if the bead rotates a full 180° as it crosses the cavity. Grayscale is obtained if the rotation of the bead is less than 180°. The bead never rotates more than 180°, because the oil/bead system is critically damped and momentum is effectively not conserved.

Using an integrating sphere photometer to measure the light reflected from an area of the Gyricon surface, the curve in Figure 20.4 is obtained. Here the relative reflectance of the surface is measured against an applied voltage across the rubber sheet. This is for a Gyricon display with black and white beads and the black hemispheres of the beads are initially toward the viewing window. As the voltage is increased, nothing happens until a significant number of the beads break loose from their cavity wall adhesions and move across the cavity, rotating as they go. The slope of this curve is partly due to the statistical distribution of monopole charges associated with the beads. Beads with low monopole charge require a larger external voltage to break their adhesion with their cavity walls. Hence more and more beads are able to rotate as the voltage increases. Augmenting this is the observation that bead rotation is not complete at low fields, but as the field is increased, the rotation reaches 180° and the reflectance plateaus.

Petitioner Samsung Ex-1011, 0424

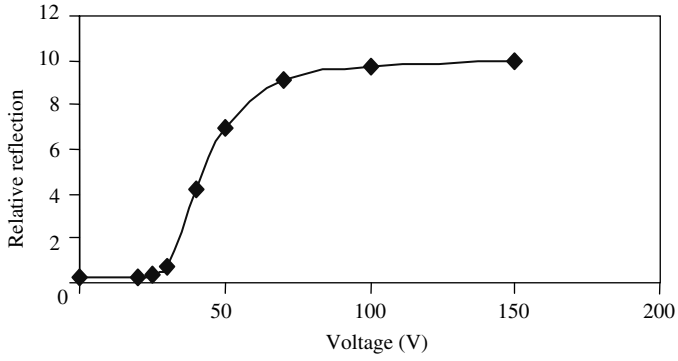


Figure 20.4 Diffuse reflection of light from the Gyricon as a function of an applied electrical voltage

The viscous drag associated with the motion of the bead across its cavity limits the response speed of the Gyricon. The applied voltage, the chemistry of the bead and the diameter of the bead also control this speed. The continued application of voltage after the bead has reached the wall controls the short-term bead adhesion. For current applications the switching rate is usually about 0.5 Hz. However, this is not a fundamental limitation and Figure 20.5 shows measured bead rotation times for bichromal beads made from two experimental pigments with three different diameters. Notice that bead rotation times of less than 3 ms can be obtained at under 100 V.

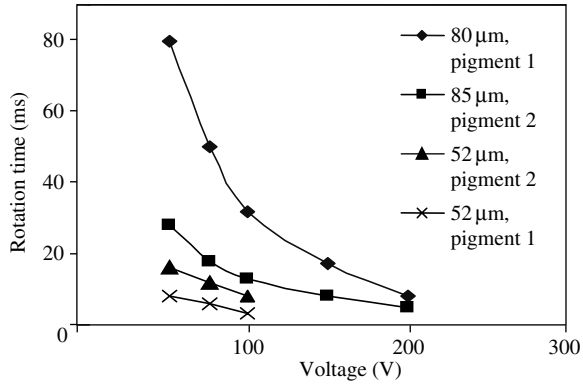


Figure 20.5 High bead rotation rates have been obtained with some experimental materials

20.3 Image Storage

The image storage characteristics of the Gyricon display make it ideally suited for flexible display applications (Pham *et al.* 2002). The tenacity of image storage increases with the duration of image storage. Thus, images are easily formed and erased for normal display applications, but long-term image storage for applications like electronic newspapers and

Petitioner Samsung Ex-1011, 0425

electronic books is highly durable. Image storage is controlled by adhesion of the bead to the elastomer cavity walls.

The image storage is controlled by adhesion of the bead to the cavity wall. The actual behavior of the bead during this process depends on the polarity of the switching field.

Generally, the bead has a positive monopole and the black side of the bead is positive, the white side negative. If we assume for the moment that the Gyricon sheet is in a horizontal position, when we turn the beads from black side facing the viewing window to white side facing the viewing window the beads will move from the tops of the cavities, rotating to show their white sides as they drop to the cavity bottoms. They will stay in this position if the display is not further addressed. If we next switch the beads from white sides facing the viewing window to black sides facing the viewing window, we do this with a negative voltage on the viewing window and the beads move from the bottoms of the cavities to the tops, rotating as they move.

The beads have a specific gravity about 25% larger than that of the cavity oil. They will stay adhered to the tops of their cavities for times on the order of a minute after the addressing voltage is removed, depending on the magnitude of the addressing voltage, the monopole charge associated with the bead and other bead characteristics. They will then drop to the bottoms of their cavities. There is very little rotation of the beads during this drop and thus very little loss of contrast. When the beads reach the bottoms of their cavities they are pulled into the cavity walls by gravity.

If the display is in a vertical position during addressing, the beads will slide down the cavity wall to the bottom of the cavity, again with little rotation or loss of contrast.

Adhesion of the bead to the cavity wall is believed to have several causes. We can first mention van der Waals forces that generally cause small objects to stick to one another. These are probably small in comparison with other forces.

More important is the hydraulic trap created by a spherical bead settling into a soft spherical cavity. As the bead is pulled into the cavity wall by gravity or by the external electric field acting on the monopole charge associated with the bead, the oil between the bead and the wall is forced out. Careful study shows that there is more than point contact between the bead and the elastomer surface. Because it is soft and sticky, the elastomer conforms to a significant fraction of the bead surface. Continued force on this interface forces out increased oil. To subsequently release the bead from the cavity wall requires flowing oil into the very thin space between the bead and the conformed elastomer wall. This process takes time and sustained force. For long-term image storage the beads are all at the bottoms of their cavities and are forced into their cavity walls by gravity.

The third bead adhesion force that is believed to be important derives from the electrical double layer at the interface between the bichromal bead and the cavity oil. Colloid chemistry tells us that this double layer consists of charges fixed to the surface of the bead, with an equal number of opposite sign ionic charges contained in a diffuse cloud in the oil close to the surface. All dielectric surfaces immersed in dielectric oil develop such a double layer. As the bichromal bead nestles into the soft elastomer of the cavity wall socket, the oil that is forced out carries with it a portion of the cloud of diffuse charges, leaving the charged bead partially unshielded. This charge is now attracted to its image charge in the addressing electrodes, pulling the bead into even tighter contact with the cavity wall. This force will persist until oppositely charged ions can diffuse through the elastomer to shield the bead charges. This is a short-lived force and is partly responsible for the initial adhesion of the beads to the cavity walls.

Petitioner Samsung Ex-1011, 0426

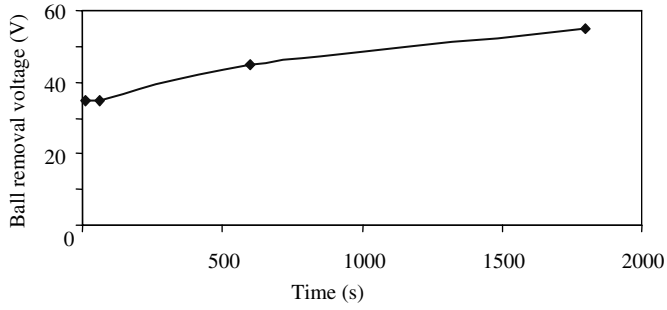


Figure 20.6 The threshold voltage for removal of a bichromal bead from wall adhesion increases with residence time on the wall

As these models imply the force required to remove the bead from the cavity wall in a given time increases with the amount of time the bead clings to the cavity wall. And this is confirmed in practice. Effectively, it creates an increase in the threshold voltage. Figure 20.6 is a graph of measured bead removal (threshold) voltages required to remove a bead from its adhesion to the bottom of a cavity wall as a function of the time the bead is in contact with the wall. Notice that adhesion increases with time.

20.4 Brightness and Contrast

The whiteness of a surface viewed in reflected light is the result of light scattering by transparent particles or fibers having small dimensions and significant refractive index differences from the medium they are immersed in.

Ambient light reaching the surface of the Gyricon display is diffusely reflected in the same way that ambient light is diffusely reflected from the surface of paper. The white hemispheres of the Gyricon beads contain a high density of titanium dioxide pigment. This has a refractive index of 2.7, compared to the refractive index of 1.51 for the polyethylene they are dispersed in. The refractive index difference is 1.19. The pigment particles are about 0.3 μm in diameter, a size selected by the pigment manufacturer to exhibit a high level of light scattering and thus whiteness in paint. By comparison, the whiteness of paper is due to scattering of light from the cellulose fibers in air, a refractive index difference with air of 0.53. As these numbers suggest, titanium dioxide dispersed in polyethylene can be brighter that a sheet of plain paper.

White light incident normally on a sheet of paper, or other diffusely reflecting surface, scatters light throughout a solid cone, with the intensity of scattered light decreasing linearly with the cosine of the angle to the normal of the paper surface (Lambert's law) (Born and Wolf 1970). Figure 20.7 plots the measured light intensity scattered by the Gyricon display in the white state, divided by the cosine of the angle of scattering. The relative straightness of the curve indicates that Gyricon is a good Lambertian scatterer. Like paper, the Gyricon display can be read over a wide angle.

We define the brightness of the Gyricon display in the same way it is defined for paper and we use photometers with integrating sphere sensors to measure this. Brightness is the percentage of incident light that is diffusely reflected from the surface of the Gyricon sheet

Petitioner Samsung Ex-1011, 0427

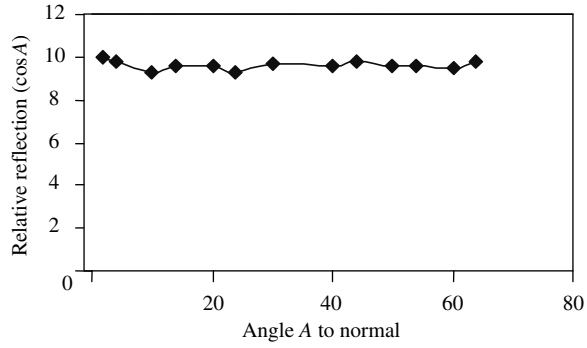


Figure 20.7 The ratio of diffuse angular reflection to the cosine of the angle is nearly a straight line, indicating Lambertian (or paper-like) scattering

when the beads are oriented with the white hemispheres of the beads facing the viewing window. Contrast is the intensity ratio of light diffusely reflected from the surface in the white state to the light in the dark state.

Figure 20.8 is a photomicrograph of a Gyricon sheet with its beads oriented in the white state. Notice that the beads in the layer closest to the viewing window are quite bright. The spaces between these beads are very gray in comparison. A closer look at these gray areas reveals that they are comprised of beads in the second and third layers beneath this first layer. Despite the brightness of the first layer of beads, these latter beads create a significant area of low brightness in the display, resulting in a display surface that is less bright than these outer-layer beads when viewed without a microscope. This photomicrograph was taken with diffuse, oblique illumination in order to simulate the kind of lighting conditions the display sees in actual use.

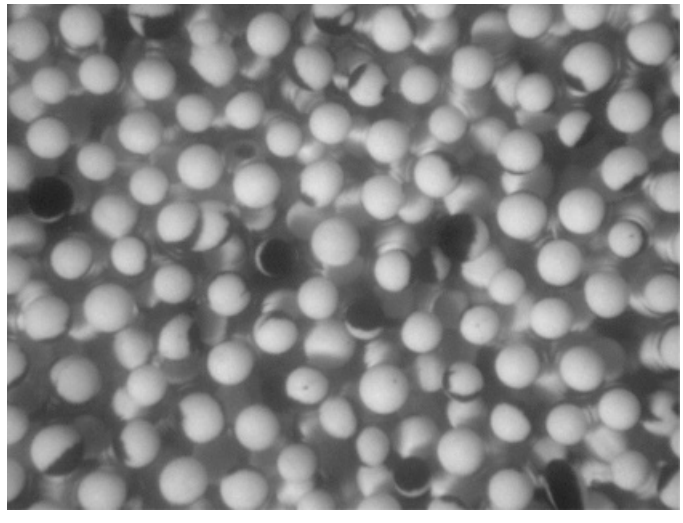


Figure 20.8 A photomicrograph of an obliquely illuminated Gyricon sheet. The dark spaces between beads are seen to be lower-level beads that receive less illumination

Petitioner Samsung Ex-1011, 0428

The low brightness contribution of lower layers of beads is primarily due to two effects. The lower layers of beads reside in the shadow of the upper layer of beads, thus less light reaches them and they reflect less light to the viewer. Exacerbating this effect, the black hemispheres of the first layer of beads lie directly above the white hemispheres of the second layer of beads, so much of the light reflected from the surfaces of the second layer of beads that reaches these black hemispheres is efficiently absorbed and is not available to illuminate the white surfaces of other beads. The net result is that little light is reflected to an observer from the second and third layers of beads, and thus spaces between the beads in the first layer look dark. Since a viewer sees an integration of light from all beads, the spaces between first-layer beads seriously degrade the brightness of the display.

Clearly, higher display brightness can be obtained by packing a higher density of beads into the first layer. This has been confirmed experimentally.

Further limiting the density of beads in the outermost layer of the Gyricon is the swelling of the elastomer during the cavity formation process. It is desirable to minimize this swelling. This can be done by a judicious choice of plasticizing liquids and elastomers.

A laboratory process has been developed for packing beads tightly into two layers, resulting in substantially brighter Gyricon displays. Figure 20.9 shows a photomicrograph of the

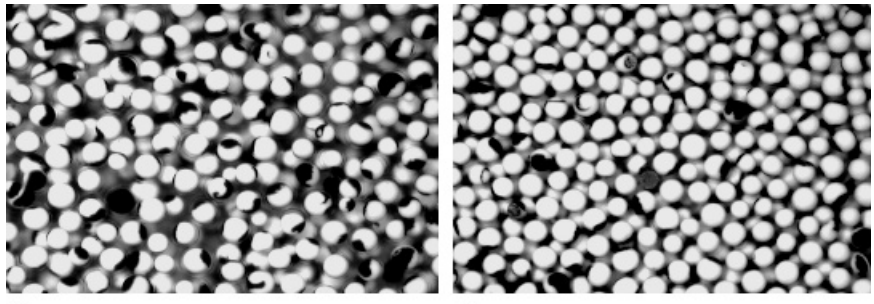


Figure 20.9 Photomicrographs of two Gyricon sheets: (a) a standard sheet and (b) a sheet that has been bead packed and swollen 19% rather than 25%

surface of a Gyricon display made using this bead-packing process in combination with a lower-swell elastomer (19% instead of 25%). This is compared with the surface of a Gyricon display made without packing and without a low-swell elastomer. Notice that the first layer of beads now occupies a substantially larger fraction of the display surface area. This results in higher display brightness, as shown in Figure 20.10, where the brightness of a packed display is compared to the brightness of a nonpacked display. The increase in display contrast is shown by the graph in Figure 20.11. For the same beads that give a brightness of 22% and a contrast ratio of 9 with standard processes, bead packing and lower swelling produce a brightness of 26% and a contrast ratio of 11.

Other factors that control brightness and contrast in the Gyricon include bead quality, degree of rotation, and the fraction of beads that rotate. The degree of rotation is controlled by the relation of the monopole and dipole charges associated with the bichromal beads. The dipole must be sufficiently strong to obtain complete rotation while the monopole pulls the bead across the cavity. In a high-quality display, more than 99% of the beads rotate 180°.

Petitioner Samsung Ex-1011, 0429

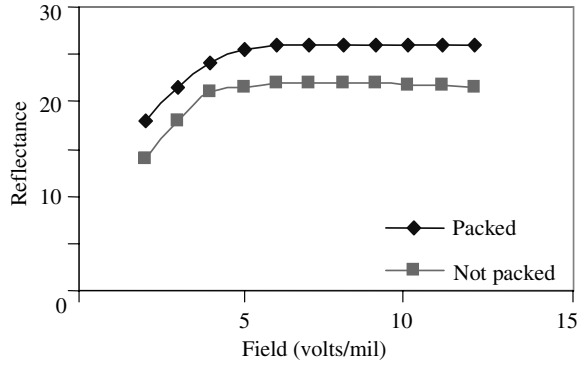


Figure 20.10 A higher density of (packed) beads in the top layer increases the brightness of the Gyricon display

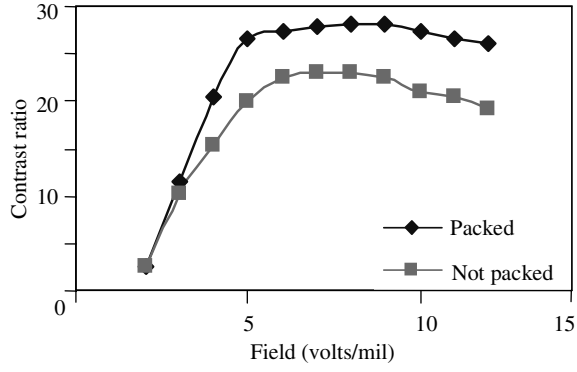


Figure 20.11 A higher density of beads packed into the first layer also improves the contrast

20.5 Addressing Methods

All methods currently used to address Gyricon displays can be considered forms of active matrix addressing. The Gyricon display is an extremely high-impedance device and current draw during switching is limited to that associated with the device capacitance. Currently, 80 V is required to switch devices. The high-impedance aspect allows some unique forms of address.

Despite the fact that the Gyricon is bistable and there is a threshold voltage associated with removal of Gyricon beads from adhesion to their cavity walls, the Gyricon in its present manufacture is not suitable for passive addressing. The reason for this is primarily due to the wide statistical distribution of charge associated with the individual beads. That is, individual beads show very suitable threshold behavior, but ensembles of beads do not.

High-voltage integrated circuit drivers mounted on the back side of a printed circuit board have been used to provide an active matrix addressing system for a Gyricon display (Preas *et al.* 1998).

Petitioner Samsung Ex-1011, 0430

Active matrix addressing of Gyricon displays using organic transistor arrays was demonstrated at the May 2003 meeting of the Society for Information Display, held in Boston, as part of a collaboration with Plastic Logic Ltd. Organic transistor arrays offer the prospect of lower costs and display flexibility.

20.5.1 Multiple Fixed-Image Addressing with Printed Circuit Boards

Very low-cost but high-resolution addressing of displays has been studied by Preas and Davis (2002). They point out that a 12 in $\times$ 12 in square display operating at 200 pixels per inch resolution requires 5 760 000 pixel drivers with active matrix addressing. If one is willing to reduce the number of separate, high-resolution images that can be exhibited on a display, to view a single one of these images at a time, and to build these images into the display at the time of manufacture, then this number can be greatly reduced. Preas describes a two-dimensional array of addressing electrodes, each of a suitable size and shape so it can be used in forming any one of the n images. (These shapes are determined by a computer program.) He shows that the maximum number of address drivers needed to separately present any one of n full-frame images is 2^n, whatever the complexity or resolution of the images. Shaped electrodes of this sort can be readily produced on a flexible printed circuit board This approach, called multifixed image, finds practical implementation in retail signs, where a limited number of general messages are needed.

Multilayer printed circuit boards provide a means of addressing large-area sheets of Gyricon media. These boards can be rigid or flexible. Gyricon LLC's Synchro Sign Message Board is an example of this approach (Figure 20.12). This is a 15 in $\times$ 16.7 in display that

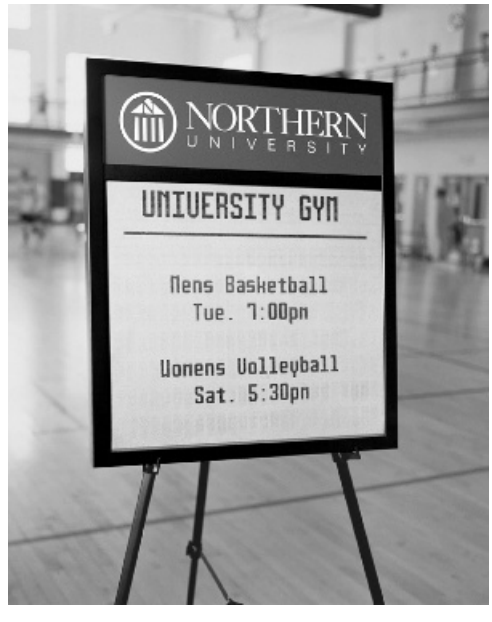


Figure 20.12 The Message Board uses a printed circuit board to provide electrodes for addressing. Courtesy Gyricon LLC, all rights reserved

Petitioner Samsung Ex-1011, 0431

presents 8 lines of wirelessly transmitted text, using up to 194 characters. Each character is created by an electrode array having shaped segments and capable of creating any alphanumeric within a set font.

The Gyricon properties that enable large displays like the Synchro Sign Message Board include a low sensitivity to thickness variations in the media, the ability to produce large-area rubber Gyricon sheets, and the fact that no power is expended to continuously display an image, only to change an image. (The saturation of reflection above a characteristic voltage, shown in Figure 20.4, implies uniform response above a characteristic field and therefore a lack of sensitivity to media thickness variations above a sufficient voltage.)

20.5.2 Linear Electrode Array (Stylus Wand) Addressing

Of particular value for low-cost addressing of flexible displays is stylus wand (linear electrode array) scanning (Sheridon 1995; Howard *et al.* 1998). Here a linear array of pixel-sized electrodes is moved across the surface of a flexible Gyricon display, depositing image-wise charge on a two-dimensional array of subpixel-sized, transparent, conducting islands on the outer surface of the Gyricon display viewing window. This results in a two-dimensional charge pattern that image-wise addresses the Gyricon display.

Figure 20.13 shows a section of a stylus wand linear electrode array being used to deposit image-wise charge on a two-dimensional subpixel island array. As the stylus wand is scanned across the islanded surface of a Gyricon display, the individual electrodes of the stylus wand make contact with the islands, depositing charge and raising the island potentials to those of the stylus electrodes. This image-wise array of charge causes an image-wise response of the Gyricon. In a stylus wand, the gap between adjacent electrodes should be larger than the island dimensions, to prevent shorting of adjacent stylus array electrodes. The width of the stylus array electrodes should cover several islands to obtain smooth lines.

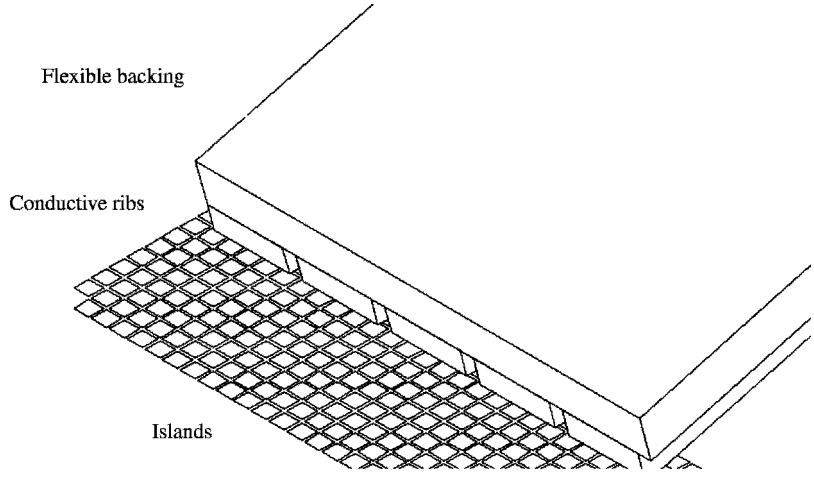


Figure 20.13 A section of a stylus wand linear electrode array for depositing image-wise charge on the islanded surface of a Gyricon display

Petitioner Samsung Ex-1011, 0432



Figure 20.14 Handheld stylus wand printer, depositing image-wise charge on the islanded plastic surface of an electronic paper sheet

This type of addressing works well because of the very high impedance and the bistable behavior of the Gyricon display. Charge deposited on the islands is retained long enough to reorient the bichromal beads before it is lost to a very low level of surface electrical conductivity. The reoriented beads are adhered to their cavity walls and store the image. Erasure in this system is accomplished by passing the same stylus wand across the surface, depositing a uniform voltage distribution.

The stylus wand can be a handheld instrument, like the mock-up in Figure 20.14. It can also be incorporated as part of a personal document reader, visualized in Figure 20.15. Here a sheet of Gyricon electric paper is rolled up inside the tube, using a spring mechanism (like a window shade).

As the sheet is pulled out of the tube it is contacted by a linear electrode array that deposits image-wise charge on the conductive, transparent islands formed on the surface of the sheet. Allowing the sheet to retract into the tube will enable the electrode array to remove image-wise charge from the last image. Again pulling it out of the tube will write the next page of information.

The tube form factor can also be used in conjunction with flexible organic transistor array backplanes, allowing new images to be presented without retracting the sheet for each page of information and providing a convenient storage container for the Gyricon sheet. Such a document reader, with a simple user interface, will enable downloading of e-mail and other documents from cellphone and satellite networks.



Figure 20.15 Simulated personal document reader. As the electronic paper sheet is pulled out through the slot in the cylinder sidewall, a linear electrode array prints an image

Petitioner Samsung Ex-1011, 0433

20.6 Fabrication

Gyricon beads are made from pigmented polyethylene. These beads are called bichromal because their two hemispheres have different (contrasting) colors. Any color pigments can be used to make Gyricon beads and about six different color combinations have been successfully demonstrated at this time. The beads are generally 40–106 μm in diameter; the smaller beads are used for higher-resolution devices. Beads with an average size of 100 μm have a measured resolution of about 100 dpi (dots per inch). Beads with an average diameter of 50 μm have a resolution of 200 dpi. This resolution corresponds to about 4 beads per pixel.

The Gyricon beads are made using a spinning disk. Molten, pigmented polyethylene of one color is pumped onto one side of the disk; molten, pigmented polyethylene of a contrasting color is pumped onto the opposite side of the spinning disk. These liquids wet the disk surfaces and flow to the edge of the disk under the influence of centrifugal force. At the edge of the disk, the two liquids join and experience a Taylor instability (Taylor 1950). Within the viscosity and flow rate parameters we work in, the Taylor instability produces a number of jets, about 32 per inch of disk edge. Spinning disks, wetted on one surface, have long been used to manufacture fine particles (Fraser and Eisenklam 1956).

The production of bichromal beads using the spinning disk is based on the observation that a bichromal cylindrical jet, created by combining equal semicircular cross sections of white and black liquid, for example, will form bichromal spheres when it becomes unstable. The spinning disk provides a large number of such jets under nonclogging conditions.

Figure 20.16 shows a photomicrograph of the edge of a spinning disk during bead making. It was taken with a video camera and the illumination of a pulsed LED light source. The disk was spinning at about 3000 rpm. The jets are highly stable, being continuously fed off the edge of the disk at one end and breaking up into bichromal spheres at the other. There is little



Figure 20.16 Flash-illuminated video image of a spinning disk showing the Taylor instability. The Taylor instability generates jets that become bichromal beads in the Gyricon bead generation equipment

Petitioner Samsung Ex-1011, 0434

mixing of the white and black liquids in the jets because of the short times involved. At their distal ends, the jets are about 50 μm in diameter.

The bichromal beads produced by the jets are highly spherical, due to of the surface tension of the molten polyethylene. They are rapidly cooled as they fly through the air and solidify before they reach solid surfaces.

The beads are sorted by size and dispersed into a liquid elastomer precursor. The precursor is extruded into a thin sheet, about 325 μm thick, and cured with heat to an elastomeric solid. This elastomer is next soaked in plasticizing oil. The oil is imbibed by the elastomer and causes the elastomer to swell by about 25%. The beads do not swell, so a vacuum cavity opens up around each bead. After a few minutes this cavity fills with oil. This is a stable and generally irreversible condition, unless the plasticizing oil evaporates.

The choice of plasticizer is determined by the desired display properties. Lower-viscosity oils allow faster bead rotation and thus faster image switching. Low-viscosity oils also have higher vapor pressures, so the Gyricon sheet must be carefully sealed when they are used. The plasticizing oil must be a good dielectric.

Silicone elastomers are generally used to fabricate Gyricon sheets. These elastomers have high optical clarity, excellent resistance to aging and ultraviolet light and very good electrical properties. They are easily swollen by plasticizers to produce cavities around the beads.

20.7 Conclusions

Gyricon media is well suited for use in flexible displays. As a rubber sheet, it is inherently highly flexible. The low sensitivity of the Gyricon display to thickness variations allows such configurations as rolling up the display. The very low power required to form the image, the ambient light readout of the image, and image storage without power expenditure enable practical battery-powered operation.

The high impedance of the Gyricon enables stylus wand addressing of a flexible display format. The compatibility of the Gyricon with organic transistor backplanes has been demonstrated; these backplanes are expected to be inexpensive and flexible.

The optical properties of the Gyricon are similar to those of paper, making it attractive for future flexible display applications such as book and newspaper readers.

References

Born, M. and Wolf, E. (1970) *Principles of Optics*, 4th edn, Pergamon Press.

Fraser, R. P. and Eisenklam, P. (1956) Liquid atomisation and the drop size of sprays. *Transactions of the Institution of Chemical Engineers* **34**, 294–319.

Howard, M. E., Richley, E. A., Sprague, R. and Sheridon, N. K. (1998) Gyricon electric paper. *Journal of the Society for Information Display* **6**(4), 215–217.

Pham, T, Sheridon, N. K. and Sprague, R. (2002) Electro-optical characteristics of the Gyricon display. *Society for Information Display 2002 International Symposium, Digest of Technical Papers* **33**(1), 119–121.

Preas, B. and Davis, H. (2002) Low cost, low power displays for retail signs. *Society for Information Display 2002 International Symposium, Digest of Technical Papers* **33**, no. 1.

Petitioner Samsung Ex-1011, 0435

Preas, B, Vest, F., Richley, E. A. and Sheridon, N. K. (1998) A large area, tiled gyricon display. *Society for Information Display 1998 International Symposium, Digest of Technical Papers* **29**, 211–214.

Sheridon, N. K. (1995) Writing system including paper-like digitally addressed media and addressing device therefore, US Patent 5,389,945, February 14, 1995.

Sheridon, N. K. and Berkovitz, M. A. (1977) The gyricon, a rotating ball display. *Proceedings of the Society for Information Display* **18**.

Sheridon, N. K., Richley, E. A., Mikkelsen, J. C., Tsuda, D., Crowley, J. M., Oraha, K. A., Howard, M. E., Rodkin, M. A., Swidler, R. and Sprague, R.(1997) The Gyricon, a rotating ball display. *Conference Record of the 1997 IDRC, Society for Information Display.*

Taylor, G. (1950) The instability of liquid surfaces when accelerated in a direction perpendicular to their planes. *Proceedings of the Royal Society A* **201**, 192–196.

Petitioner Samsung Ex-1011, 0436

21

Roll-to-Roll Manufacturing of Flexible Displays

Abbie Gregg, Lara York, and Mark Strnad

Abbie Gregg, Inc.

21.1 Background

The current method of producing display panels, circuit boards and other electronic devices is a batch process: one component at a time. Roll-to-roll manufacturing of microelectronics would be a revolutionary advancement in process capability. Once this process methodology has matured, it will allow for

- continuous production of fine-featured thin film devices;
- huge reduction in capital cost;
- dramatic reduction in device cost;
- lightweight, thin, and durable appliances;
- devices on demand, so no component supply chain.

To make these electronic devices, the films must be patterned. Sometimes this can be done just like newspapers – by printing the material in the desired pattern. For most semiconductors today, it is necessary to deposit the film and then pattern it with conventional lithography

Flexible Flat Panel Displays Edited by G. P. Crawford
© 2005 John Wiley & Sons, Ltd., ISBN 0-470-87048-6

Petitioner Samsung Ex-1011, 0438

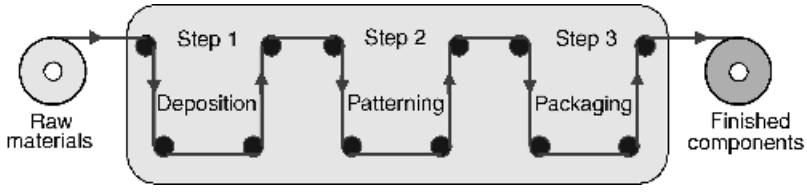


Figure 21.1 Roll-to-roll manufacturing

(in which a pattern is defined by photographic processing of a polymer masking layer that serves as a mask while the exposed areas are chemically etched into the desired pattern). These processes, which are routinely used to make integrated circuits on silicon wafers or glass plates, can all be adapted to polymer webs (Figure 21.1). The result is a much less expensive process, and products that are light, thin, rugged, and flexible (characteristics not shared by their silicon or glass counterparts).

As a result, there has been a surge of interest and activity in developing display devices based on plastic substrates to enable thin, lightweight, flexible, and durable displays. One significant factor of a flexible plastic substrate is also in the potential to provide economic benefits in display manufacturing. Using web processing for the manufacture of plastic display backplanes promises not only less capital investment in the long term, but it will also substantially reduce manufacturing costs. As the development of emerging display technologies such as OLED and PLED advance, display devices based on plastic substrates have become possible and the motivation to implement a roll-to-roll manufacturing process has become very attractive.

It is challenging to manufacture displays based on plastic substrates using a roll-to-roll process. The primary difficulty is display backplane manufacturing, in which electronics are fabricated on a plastic substrate with precision, accuracy, and high yield. For active matrix backplanes, this will be a semiconductor process whereby thin film transistors (TFT) are fabricated on the substrates.

The current practice is to manufacture such backplanes on glass plates in a batch mode. There are many challenges to move these processes from a glass substrate to a web processing platform. Even manufacturing the backplanes on glass and then transferring the devices to a roll-to-roll web is under investigation. Whatever methods are chosen, roll-to-toll processing of displays requires major innovations in machine design, process recipes, and system integration.

21.1.1 Some Challenges

- *Custom-built tools*: this new technology results in a demand for some tools that will have to be custom-built for single manufacturing lines. Thus, there exist few standard, qualified roll-to-roll tools that the display industry can order off the shelf. Even web material-handling equipment is not fully developed for the required defect levels, alignment, and web material stability.

Petitioner Samsung Ex-1011, 0439

- *Defect inspection*: inspection tools currently exist for plastic roll-to-roll processing, but they have been built for industries concerned with much larger defects, and they do not offer the level of cleanliness required for typical display manufacturing.
- *Thermal processing*: web materials such as PET can not tolerate extremes in thermal process cycling.
- *Resolution and registration*: roll-to-roll photolithography and etch processing tools currently exist but they are not capable of 2 μm processing.

21.2 Objective

This chapter reports on quantifying the current technical capabilities (and some projections of possible near-future processes that may allow manufacturing) for roll-to-roll processing of flexible microelectronics, specifically displays. It considers realistic goals for bringing roll-to-roll technology to the next level of process improvement and cost reduction. The technical capabilities to be considered include processes, tools, facilities, and costs for a backplane scenario and a postprocess application scenario:

- process types and their associated capabilities in terms of device dimensions, temperature requirements, throughput rate, and layer-to-layer registration;
- roll-to-roll tool and handling characteristics important to meet process and production criteria;
- tool and equipment types with reasonably established flexible substrate and roll-to-roll capabilities, and their estimated prices;
- possible factory layouts and tool groupings for flexible substrate processing, using roll-to-roll processes where possible;
- estimated cleanliness in terms of clean class and local minienvironments needed for processing;
- estimated cost to create a roll-to-roll factory for flexible displays with the parameters described above;
- estimated cost in dollars per square foot of a product, produced using roll-to-roll manufacturing;
- discussion of unresolved technical issues, operational problems and other obstacles that affect roll-to-roll processing.

21.3 Device Scenario

The product example used in this chapter is a standard PDA display with a size of 3.25 in × 3.25 in (82.55 mm × 82.55 mm).

Petitioner Samsung Ex-1011, 0440

In general, product design considerations include product size, product cost target, minimum feature size, use of layered substrates or single substrates with added films, quantity of devices that are to be produced with the same tooling.

Minimum feature size is driven by the resolution and color requirements of the display. Tooling can refer to masks and any other mechanical items that may be dedicated for a given product type.

Using a base substrate material of known parameters, e.g. enhanced PET (1000 ft roll by 24 in) and a proposed display size of 3.25 in $\times$ 3.25 in (PDA type), one can develop a cost and capacity model to determine the

- individual product cost per square foot,
- factory cost estimates,
- equipment cost,
- labor cost,
- clean room space/cost required by clean class.

In considering the product scenarios identified above, one must complete the following tasks to define a roll-to-roll manufacturing line and model the costs:

1. Determine the process flows.
2. Document any assumptions.
3. Research and identify capable tools.
4. Run a variety of demand scenarios.
5. Calculate the space requirements.
6. Determine the cost to create a roll-to-roll factory.
7. Determine the cost in dollars per square foot of product and compare it to market requirements.
8. Discuss any unresolved technical issues.
9. Determine the cost-driving processes and establish a plan to reduce costs.

21.4 Product Design

Strawman device designs were needed to define the process steps. Sample flows have been studied. More information is obtainable at www.flexics.com

21.4.1 Process and Tool Tables

Process and associated tool tables such as Table 21.1 must be established to identify the following items.

Petitioner Samsung Ex-1011, 0441

Table 21.1 Active matrix process (sample section)

Step	Operation	Tool	Tool action
100	Staging area	Stage	Stage
130	Web punch and clean	Clean, aqueous web	Unwind, punch, aqueous web cleaner, unpatterned inspect, wind
140	Vacuum dep dielectric barrier layer and cure	PECVD, microwave	Unwind, microwave PECVD, rewind
150	Sputter dep gate 1 metal	Sputter, DC magnetron	Unwind, DC magnetron sputter, rewind
160	Clean, coat and Cure	Roll coat	Unwind, dip, spray rinse, dry, roll coat, heat, dry, rewind
170	Align and expose	Exposure, step and repeat	Unwind, step and repeat exposure, rewind
180	Develop, etch (gate metal), strip the photoresist then dry with air knives with extra clean rinse	Develop, etch, strip line	Unwind, conveyorized DES system + extra clean rinse, dry system for reel-to-reel transport, inspect, wind
190	Silicon nitride, amorphous polysilicon, N+ dopant	PECVD deposit	Unwind, PECVD deposit, rewind
200	Poly-Si anneal	Laser	Unwind, rewind
205	Clean, coat and cure	Roll coat	Unwind, dip, spray rinse, dry, roll coat, heat, dry, rewind
210	Align and expose	Exposure, step and repeat	Unwind, step and repeat exposure, rewind
215	Develop, rinse and dry with air knives	Develop	Unwind, conveyorized develop system + rinse, dry system for reel to reel transport, inspect, rewind

Step

Step number, as used in the model, flowchart and on the layout. Operation, as used in the model process flow, is the basic description of what is happening within that process.

Tool

Abbreviated tool name, as the tool is known in the model (recipe list and process flow) and on the layout. Most of the tools start with a roll delivered to an unwind step and end with a step to wind the roll back up after the process is completed. In some cases the basic tool may be linked to another basic tool without a rewind step.

Tool Action

Tool action describes all the actions taken by that tool, including wind, inspection, and clean and other steps. This chart provides a good way to comprehend the details of what the tool is

Petitioner Samsung Ex-1011, 0442

doing at each step. This also indicates which steps are done as continuous web processes, and which are separated due to throughput rates, process environment, tool vendor differences, etc.

21.5 Tools

Upon review of the processes and requirements, actual roll-to-roll processing tools were surveyed. The Association of Industrial Metallizers, Coaters and Laminators (AIMCAL) conference for web-based vacuum coating is one of the best trade organization conferences addressing roll-to-roll processing of all types of products. Custom- and home-built integration of various processes into a continuous web process tool have been done in food packaging, touch screen manufacturing, and glare reduction screen manufacturing. In some cases, machine integrators have played a key role in grouping several disparate processes into a web-based tool. Additionally, the tool actions are grouped together to provide tools of a realistic size, throughput, and common process environment. Temperature, cleanliness, humidity, yellow light, and clean class are a few of the parameters to consider for the roll-to-roll tool groupings. Table 21.2 shows a sample table.

21.5.1 Tools for Roll-to-Roll Processing

Here are some roll-to-roll processing tools that were available during the period 2001–2004.

Cleaner, aqueous web

The ECD Ovonic 1-73 has been built by ECD (Energy Conversion Devices of Troy, MI) to clean continuous webs of stainless steel for solar cell applications and for some plastic web cleaning processes. It uses parts and modules common to, and proven by ECD, over several years on its solar cell applications. The tool is large and expensive.

A mechanical alignment hole punch can be incorporated into this cleaner before the actual cleaning. These holes can provide mechanical prealignment for many web process tools. Prealignment is followed by fine optical alignment to the lithography pattern, if necessary.

Clean, corona

The Enercon Treater Station Model TL Max 11PV-100 is a well-known cleaning tool in the plastic web processing industry. This tool is commonly added to various types of flexible substrate tools, such as screen printers and laminators.

Plasma, clean, reactive Ion Etch, and PECVD

The Ovonic 4-24 is one of ECD's very long web processing tools for making solar cells on stainless steel and polymer substrates. ECD's three decades of experience includes continuous webs of stainless steel and plastic. It has done work on PECVD applications (oxides, nitrides, amorphous silicon, and others) as well as plasma etch. It can provide

Petitioner Samsung Ex-1011, 0443

Table 21.2 Tool, manufacturer and model number sample table

Tool	Generic operation	Tool action	Manufacturer	Model number
Clean, corona	Mechanical and UV ozone clean	Unwind, tacky roller, corona treating system, wind	Enercon Teknek Northfield (integrator)	TL Max Series
Clean, plasma	Plasma clean	Unwind, plasma clean, wind	ECD APS Applied Films	Ovonic 4-24
Clean, ultrasonic	Ultrasonic clean	Unwind, Conveyerized ultrasonic clean + rinse and dry system, inspect, wind	Schmid Dalux Northfield Automation (integrator) Dark Field (inspection)	1270 series CF Serises
Cleaner, aqueous web	Web punched, and clean	Unwind, punch, aqueous web cleaner, unpatterned inspect, wind	ECD Schmid Dalux Northfield Automation (integrator) Dark Field (inspection)	Ovonic 1-73 1270 Series D:CF Series SC300HR
Develop, etch, strip line	Develop, etch, strip the photoresist then dry with air knives with extra clean	Unwind, conveyerized DES system + extra clean rinse, dry system for reel-to-reel transport, inspect, wind	Schmid Dalux Northfield Automation (integrator) Dark Field (inspection)	1270 Series D:CF Series SC300HR
Die punch 1	Free contacts	Die punch top sheet, pull off excess	Plastimach	RP28-2
Die punch 2	Cut sheets Into individual devices	Die punch device out of bottom sheet	Plastimach	RP28-2
Die punch 3	Cut shorting bars	Die punch cut of shorting bars	Plastimach	RP28-2
Evaporate, cathode	Thermal evap cathode	Thermal evap, receive interface, reorient roll, evaporate cathode, interface with encapsulation	ULVAC Von Ardenne Unaxis, CHA, Tokki	ECH Series
Exposure, proximity	Align and expose	Unwind, proximity exposure, wind	Perkin Elmer Automatech	Proforma 3000
Exposure, step and repeat	Align and expose	Unwind, step and repeat exposure, wind	Ushio Azores	UX-5040SC

Petitioner Samsung Ex-1011, 0444

inductively coupled plasma and sophisticated reactive ion etch (RIE) systems as well as simple systems. RF and microwave plasmas to enhance deposition rate or etch rate are also available. Tools are very large systems, for multiple 3 ft webs over 2000 ft long. Plasma Equipment Vendors March Instruments and Advanced Plasma Systems merged in October 2002. They have been suppliers of plasma cleaning systems for the printed circuit board industry and have experience with large substrates, and some with web cleaning for other applications. These tools are likely to be less expensive for the simpler plasma cleaning process before encapsulation. However, they would not be capable of sophisticated dry etching or RIE. Applied Films has also incorporated plasma cleaning modules into its deposition systems.

21.5.2 Develop, Etch, Strip

Dalux D: CF series

For these tools we looked at equipment being used by the printed circuit board industry (using the 18 in $\times$ 24 in form factor), especially for high-density interconnect with fine line pitch. Dalux has produced tools for fine line pitch and flexible substrates. It is also experienced with high-throughput inline continuous processing. It had built a very clean Develop Etch and Strip system for a large display product and is familiar with clean room tools. It has excellent ability to provide matched throughput and good uniformity for most wet processes by modifying bath length, temperature, spray patterns, and chemistry. Its use of cleaning and filtering techniques in liquids and air dryers is also very strong. It is a US company with some ties to Taiwan and China. This tool will also require an integrator to add on the roll-to-roll processing features, and to add on an inspection module, which we have selected to place after the final clean.

Schmid

Schmid is a German company with a background in printed circuit board processing and is also eager to participate in the fine line flexible circuit and flexible display industry. Its tools are similar in cleanliness to Dalux, and have some good technical features to minimize web contact on the device side, while using conveyor-type motion. It has worked with roll-to-roll integrators, such as Northfield Automation. Its tool would also require an inspection module to be mounted at the end.

These tools are in use at various flex circuit and touch screen manufacturing locations. There are also home-built versions of these tools, and other printed circuit board wet process tool vendors. Most process results seem to exceed expectations for line width and defect control, if the selectivity of the etchant is adequate.

21.6 Device Inspection

There are several inspection companies working to provide web-based high-resolution patterned and unpatterned inspection systems. Three of them are Darkfield Technologies, Integral Vision and V Technology.

Petitioner Samsung Ex-1011, 0445

21.6.1 Darkfield Technologies

Technical partnerships/development skills have been supplemented by Germany's Jenoptik. Dark Field Technologies is confident it can provide multiple pattern and unpatterned inspection systems. It has over 300 roll-to-roll coated plastic film inspection systems installed. Its systems use a telemetric optics system comprised of laser scanners, receivers, and cameras. Off-the-shelf systems for unpatterned webs include Model SC750.

For scale-up, a scanner is required that can deliver 4000 scans per second (2.4 m/min line speed). Additional hardware and software development are also required to support the data rates.

Alternate vendors Integral Vision (SharpEy tool) of Michigan and V Technology (Flex Scan tool) of Ontario have also made inspection tools for roll-to-roll processing. Speed varies by web size, number of points inspected, and resolution required for the inspection. Both V Tech and Integral Vision are able to compare a standard (CAD) pattern to a pattern on a moving substrate. Also, both can categorize defects based on preset class definitions for data collection or analysis. Figure 21.2 shows tools for roll-to-roll processing.

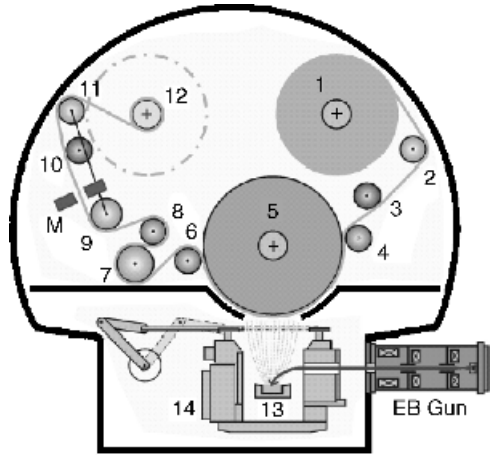


Figure 21.2 Tools for roll-to-roll processing: (1) unwinder, (2, 9, 11) guide rolls, (3, 10) spreader roller, (5) coating drum, (4, 6, 8) tension measurement roller, (6, 8) measurement roller, (7) tension isolation roller, (12) rewinder, (13) crucible, (14) magnetic trap, (M) optical measurement

If inspection of gross and fine pattern defects is required, multiple camera sizes or types may be required. Vendors have less experience with defects smaller than 10 μm, but probably have adequate capability that could be improved. They use cameras for data capture, and multiple cameras can be used. Ability to calibrate and see (transparent) ITO has been verified for these tools. Data storage and analysis is a critical point for all these tools. If the tool could be set up to match the process web speed, when the process reaches production levels, throughput of the inspection would not be a problem.

21.6.2 Batch Web Coater for EB Deposition

CHA Industries has a working roll-to-roll system, capable of processing multilayers. Versions of this system (the Mark 50 Web/Roll coater) can perform both sputtering and

Petitioner Samsung Ex-1011, 0446

evaporation on a web. The use of masks during the deposition process is an additional feature needed for OLED evaporation at this time.

21.7 Die Punch for Alignment and Registration

Die punches from Plastimach would be integrated by an integrator such as Northfield Automation, who would supply the alignment control and the wind, unwind, and tension control for these punch steps. Alignment can be optical or mechanical, via the prepunched holes in the PET. This technology is well developed for high-volume, high-speed web manufacturing for the skin packaging and vacuum forming industries.

21.8 Evaporator: Thermal Cathode for LEP Device

Ulvac is an international corporation that designs, manufacturers and markets equipment and materials for industrial application of vacuum technology. It has extensive experience with evaporation systems for use in the flat panel display industry, and specific experience with light-emitting polymer (LEP) cathode evaporation. Another vendor for evaporator tools is Von Ardenne Anlagentechnik GmbH. It has non-ebeam versions of this large-scale evaporator for large-scale, high-throughput web coatings.

21.9 Evaporators: OLED

Kodak, Sanyo, and Ulvac have collaborated in developing a linear source deposition tool that can be used to facilitate increased substrate size and roll-to-roll processing. It reveals that Kodak has found that using an extended linear evaporation source in a single direction will demonstrate film nonuniformity of less than 5% over a 300 mm $\times$ 400 mm substrate. The source is operated by establishing the deposition rate in a position remote from the substrate and scanning the source under the substrate. Uniformity along the x-axis is achieved by maintaining both a constant source emission rate as the source is scanned and a controlled scan rate. The organic material (Alq3) is placed in a quartz boat and heated by a bias (bottom) and primary top heater. The article also revealed that Ulvac is now developing the linear source tool for use on next-generation substrates (550 mm $\times$ 670 mm).

Ulvac is the strongest in discrete substrate processing, with a strong presence in semiconductors, disc drives, and FPDs. It also produces web-based vacuum systems for other applications. It has been involved in joint development of OLED and PLED systems with materials manufacturers for several years. It has provided expertise in the areas of shadow masking for precise patterns and OLED evaporation control, as well as interfaces to encapsulation systems. The Satella product has been serving this market. Ulvac has also been working on roll-to-roll and flexible substrate processing for OLEDs. It was confident it could produce an inline, multiple-chamber evaporation system for web processing.

Petitioner Samsung Ex-1011, 0447

21.10 Exposure: Proximity

The Perkin Elmer Performa 3000 was previously used in the high-density interconnect and flexible printed circuit board industry. It is a very clean tool that does a rollout, position, align, expose, index, and wind with interleaf (to protect pattern). It is a proximity printer and it can take flexible or glass masks. The tool has a class 100 or better interior environment. The resolution is continuing to improve, now about 25 μm down to 12 μm with proper resist conditions. The layer-to-layer registration or alignment accuracy can be as good as 2 μm, and is automated with CCD cameras, ultrasonic edge guide, and automatic clamp and pull-hitched assembly advance. It has processed substrates up to 21 in × 27 in (535 mm × 685 mm) on the standard tool. However, lamp uniformity is better (±8%) at sizes below 20 in × 24 in (510 mm × 610 mm). Perkin Elmer provides its own wind and unwind capability and indexing modules for all web handling, but will also work with other material-handling vendors. Due to the indexing of images in sheet-like groups, and the sensitive environment this tool needs in terms of temperature, humidity, and cleanliness, it is not usually coupled with a coater or a developer system. Coaters are typically faster and dirtier; developers have too much moisture and are also not as clean.

An alternate tool is the Ushio proximity exposure system for roll-to-roll substrates UX 3000SR that has resolution to 9 μm lines and spaces, and automatic alignment to 2 μm. The limit of the web size for this tool is currently about 250 mm.

Another alternate is the Automatech Proximity Exposure system, which is similar to the Perkin Elmer, although the resolution may not be quite as good, more like 25–35 μm minimum line or space. Registration too is probably not as tight for this tool.

21.11 Exposure: Step and Repeat

The Ushio UX-5258 step and repeat exposure machine will need to be modified for roll-to-roll processing. Ushio already provides tools for roll-to-roll processing for the high-density interconnect market. However, the current roll-to-roll stepper and proximity tools have widely varying resolution, at about 5–12 μm, depending on the web width. The best resolution available in 2002, for web width of 24 in, is 6 μm for use with liquid positive photoresist. Depending on the contraction and expansion behavior of PET, the overlay accuracy is expected to be 5 μm. If vendors can meet only a 5 μm overlay (registration), it will not be sufficient for the proposed active matrix process and device, even with 6 μm lines. The registration needs to be within about 1/4 of the smallest line to be sure that patterns coincide. For a 6 μm line, this is about 1.5 μm. For a 2 μm line, about 0.5 μm registration would be required. Ushio is working on high-density interconnect applications in this range for large, nonflat substrates, but is cautious about committing to a production tool.

Ushio believes it will not be a problem to achieve its best resolution and registration with a photoresist thicknesses of 1–3 μm, applied by a roller-coater. The lens on the UX-5258 has a diameter of 200 mm. This 141 mm × 141 mm exposure area is a problem for even a PDA device. Compare the 141 mm × 141 mm field size (square exposure area) on the reticle to a PDA device size: 82.5 mm plus borders. One cannot fit a device exactly into this size, nor can a 2 × 2 array fit, which would be 165 mm × 165 mm, so that would require stitching of a device together, which is not as easy to do. Therefore it is critical that the tool accommodates

Petitioner Samsung Ex-1011, 0448

a field size of about 170 mm × 170 mm for a PDA device or the throughput will be very, very slow: 1 exposure shot per device (35 per sheet), rather than 4 devices per exposure shot. If the tool field size can meet the 170 mm × 170 mm shot, 4 devices at once or about 12 shots are needed per sheet of 18 in × 24 in, or 35 displays (this also depends on the layout of the displays).

Active matrix devices need 2–4 μm resolution and 1 μm registration.

Azores and others are working on a stitcher-type tool for flexible display exposure in this performance range.

Typically a stitcher-type tool is necessary but slow for larger devices like laptop screens. It is likely that Canon or Nikon can make something for this application and a web-handling integrator would work with them to develop a roll-to-roll tool.

21.12 Inkjet Deposition

It appears that Seiko-Epson, MicroFab, and Litrex are working on inkjet color deposition systems and processes.

21.12.1 Litrex 140L Inkjet System

The Litrex inkjet printing system is currently under development and is part of a US Display Consortium (USDC) project to develop a suitable machine and process for inkjet printing.

Current inkjet systems are not capable of roll-to-roll processing.

A cure oven and integration will be required for the web handling and curing of inkjet-printed PLED, or organic TFT. The cure time for OLED materials is currently 1 h but will be reduced to minutes by further development work. All colors must be deposited in an inert atmosphere before curing. The buffer layer, however, must be deposited and cured first. Gruenberg and Systronic have experience with curing flexible substrates, and the associated web handling is commonly done during low-temperature bakes.

A multihead inkjet deposition tool (9 up) can be used to speed up the throughput of a roll-to-roll scenario.

21.13 Lamination

21.13.1 Preco 2430 P

US-based Preco has good lamination products. Its tools tend to be large and not particularly clean. It has quoted lamination for display industry applications and has built some clean tools. Preco has experience with removal and rewinding of matrices from substrates after windows have been punched out. This type of system would be used to apply the ''mask'' through which the encapsulant would be deposited onto the device. Preco's roll-handling experience is for very long and heavy rolls up to 38 in (965 mm) wide.

Petitioner Samsung Ex-1011, 0449

21.13.2 Schmid CSL 4000

The Schmid CSL 4000 is a standard laminator provided for the printed circuit board industry to laminate fine laminates. It is moderately clean and very well proven, with hundreds in the field. Schmid has demonstrated lab tests and experiments for display companies wishing to use the CSL 4000 for laminating two PET sheets together with clean, sensitive materials in between. If any further integration of roll-to-roll handling needs to be done, it has worked with Northfield Automation and others.

21.14 Laser Processing

Laser makers work with a web-handling integrator and provide their controls and laser. Similar systems with a laser, highly controlled moving optical table grade stage, roll-to-roll handling, and minienvironment have been integrated by a company in Minnesota and Creo in Canada. Lasers may be used for thin film annealing or for actual cutting or separating of polymer substrates. Laser processes have low throughput, so multiple-head lasers would typically be needed.

21.15 Roll Coater: Photoresist

21.15.1 Toray Model 1-2

Model 1-2 is a roller photoresist coat and bake system from the Japanese vendor Toray. Toray has a series of tools for photolithography processing for high-density interconnect and TAB tape that have been scaled up for display or other flex substrate patterning. TAB is tape automated bonding. These tools roller coat liquid photoresist to a thickness of 2–5 μm at a rate of up to 2 m/min (6 ft/min). There may be a pretreatment cleaning section with dry or wet precleaning and drying prior to the resist coat section. The drying can be forced convection with high-efficiency particulate air (HEPA) filters and possibly infrared assist. At least five to six zone controllers are required with a cooldown section. The resist pump is remote and automatic. The coating roller is typically hard chrome-plated stainless steel. Various dancers and unwind/rewind control are provided to manage tension in the web.

21.15.2 Systronic RC 4000

The RC 4000 is a roller photoresist coat and bake system from the German vendor Systronic. Systronic has done a lot of excellent liquid resist application and baking systems for the flexible circuit and printed board industry. Its ovens are known as well controlled with very good cooldown control. Systronic has its own handling system or can work with an integration vendor such as Northfield Automation or ECD.

Both of these photoresist roll coat systems can be used with an automatic interleaf unwind and rewind to remove and insert the slip sheet material for resist-coated roll protection. Photoresist is soft and easily damaged by particles and scratches. The interleaf option is also available on the align/expose tools. Roller coating is one of the fastest roll-to-roll processes. It is typically followed by align and expose, one of the slowest.

Petitioner Samsung Ex-1011, 0450

21.16 Screen Printer

21.16.1 Preco

Preco has a wind, screen print, UV cure and wind system. Screen printing on a web is tricky due to the need for distortion control. Screens by nature tend to distort the image the moment squeegee pressure is applied. Preco boasts that its AutoCentric image alignment system addresses this distortion issue. Regardless of the web width or the image length, Preco believes that its AutoCentric system will assure proper placement on the screen and along the path of the web. This technique has been used successfully to apply touch screen patterns and epoxy seal coatings for display manufacturing. Dorn is another screen print vendor.

The minimum geometries that these types of screen printing tools can create are 2–3 mm lines and spaces, with positional tolerance of about 250 μm (10 mil). This should be adequate for printing the epoxy sealant for the laminated encapsulant.

21.17 Oven for Low-Temperature Curing

21.17.1 Gruenberg Model 4/MM6H100.83M

A conveyor oven can be used in a curing process. A first partial cure by UV light immediately after application and a final heat cure provide the mechanical stability. An inert atmosphere can be provided, and the unload end can be in a class 1000 clean room.

Systronic is a likely alternate vendor for this type of specialized conveyor-type clean cure oven.

21.18 Sputtering

ECD, Arcotronics, Von Ardene and Applied Films have built very long web processing tools for the solar cell industry for the past three decades. Their experience includes continuous webs of stainless steel and plastic. They have done work in cleaning, as well as in reactive

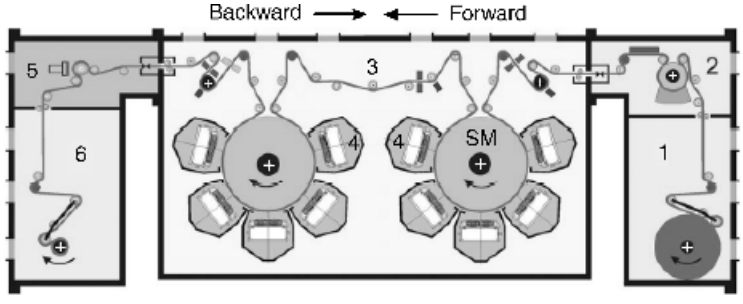


Figure 21.3 Web-based coater: (1) unwinder chamber, (2) pretreatment chamber, (3) intermediate chamber, (4) sputter compartment, (5) marking chamber, (6) rewinder chamber, (●) seven driven rollers including winders, (●) six tension measurement rollers, (●) nine spreader rollers, (SM) speed master. Courtesy of Von Ardenne Anlagentechnik GmbH

Petitioner Samsung Ex-1011, 0451

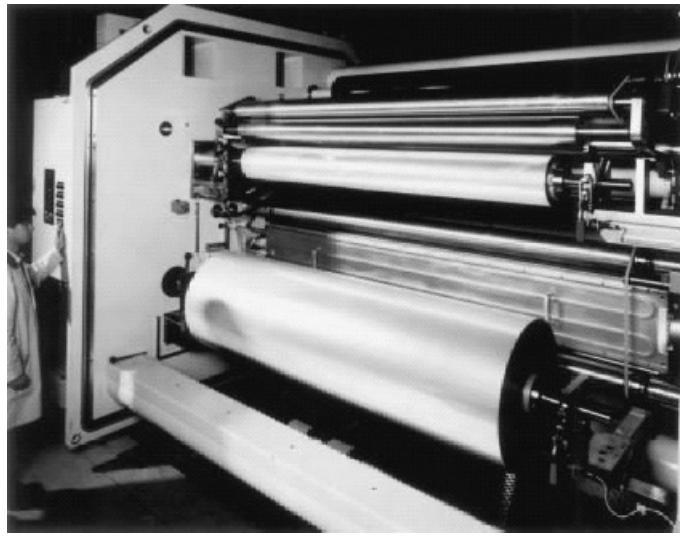


Figure 21.4 A DC magnetron substrate pretreatment system. Reproduced, with permission, from a conference presentation at AIMCAL, March 2, 2001

and nonreactive sputtering of metal and conductive oxide films. These tools are large and expensive. Proprietary features developed by ECD include circular targets and multiweb simultaneous processing (up to three webs within one tool).

Arcotronics and Von Ardenne have a strong presence in large, web-based vacuum coaters (Figure 21.3). Both have the ability to build clean tools. Applied Films has experience with most of the metals required for displays and with ITO. These tools typically have cooled drums around which the PET web is wound for cooling while it is processed. Figure 21.4 shows a substrate pretreatment system.

21.19 Materials Discussion

Materials for flexible displays will be a major focus. Significant cost reductions from glass displays are expected. Today's flexible substrates still have physical properties that prevent them from ideal suitability for a roll-to-roll display process, including temperature sensitivity, mechanical distortion, and permeability. Stainless steel, another flexible substrate option, lacks transparency.

21.19.1 PET Substrate

The PET material can only withstand temperatures up to 128 °C. This presents a challenge at several of the deposition steps. The evaporation and sputtering tool manufacturers have resolved this thermal excursion limitation through the use of cooled drums that cool the web during these short thermal exposures. Tool manufacturers report that this process has been successful in protecting the materials, but materials development will be required. It is well known that PET is a material with inadequate thermal budget.

Petitioner Samsung Ex-1011, 0452

21.20 Thermal Budget for Plastic Substrates

The use of plastic substrates creates special problems in active matrix displays. The standard TFT fabrication techniques using either amorphous silicon or polysilicon require temperatures above those that can be tolerated by most polymers. In addition, the coefficient of thermal expansion of plastics is usually much higher than that of silicon, so heating leads to considerable mechanical stress. These problems are particularly severe for the poly-Si TFTs that will be needed for high-performance OLEDs. Placing the drivers on the TFT substrate adds another level of complexity to the process, the thermal budget, and the device model. However, this may be an appealing addition to the process to reduce driver and TAB costs, which are typically half the price of a display.

21.21 Interleaf or Slip Sheet

The interleaf or slip sheet is commonly used in web-based processing to keep the processed roll from sticking to itself on rewinding. This is valuable at steps such as roller resist coat, align and expose, and develop (if not immediately followed by wet etching). These sheets can eliminate various types of defects. They can be disposable or reusable films or sheets and are often ribbed. Some are supplied by Ripco.

21.22 Materials List

Refer to Table 21.3.

Table 21.3 Materials, listed in alphabetic order, from left to right

7 mil PET	Evap electron source	Masks
Aluminum target	Evap green LE source	Oxide etch gas
Blades	Evap red LE source	Oxygen
Buffer solution	Flat board probe	PECVD source gas
Cathode evap Ca source	Flex with barrier	Photoresist
Cathode evap Li source	Free contacts die	PLED ink
Developer	Hole source	Shadow masks
Die blades	Inkjet head	Silicon etch gas
Epoxy and screens	Innerconnect target	Staging slip sheets
Etchant	ITO target	Stripper
Evap blue LE source	Mask sheet	Tacky rollers

21.23 Processing Issues

21.23.1 Moisture and Oxygen Resistance

The sensitivity of active organic materials to oxygen and water requires that the washing or rinsing, commonly used in TFT and OLED manufacturing, be followed by long or yet to be defined drying cycles, such that all traces of this water are removed.

Petitioner Samsung Ex-1011, 0453

However, moisture and oxygen barrier coatings can be deposited at the start of process for the active and passive substrate. PET or another polymer with an overcoat possessing moisture and oxygen resistance is expected to be a procurable material in the near future.

Another encapsulation process for OLEDs or PLEDs is direct deposition of the moisture and oxygen barrier film onto the OLED or PLED device. This process is under development and has not been proven, although several large US and Japanese companies are working on it.

21.23.2 Cleanliness and Particles

The very small thickness of OLED layers means that particulate control may have to be much more thorough.

21.23.3 Defects and Yield

Inspection points should be placed to collect information on the substrate and devices during processing, but the yield loss is not known until the postsingulation process steps. That is, a ''bad'' device cannot be cut out of the substrate during processing. However, it may be possible to program align/exposure devices to ''skip'' device patterns that are already known to be defective. Meanwhile, inspection data collected can be fed back upstream to stop processes or prevent them from adding defects to new devices.

A trade-off in matching etch speed to develop and strip speed is needed to keep the substrates moving at a consistent rate in the develop, etch, strip (DES) equipment. Etch speed trade-offs include temperature; concentration of etchant, spray or bath; and length of etchant spray module or tank.

Roll-to-roll processing is appropriate for high-volume production. The industrial design parameters related to roll-to-roll processing of flexible displays and microelectronics have been modeled to help set realistic goals to bring roll-to-roll technology to the required level of process improvement and cost reduction. A sample device scenario and roll-to-roll manufacturing methods were modeled for

- active matrix and/or passive matrix,
- small molecule OLED (OLED) and/or polymer OLED (PLED),
- lamination encapsulation and/or masked deposition encapsulation.

Modeling of a low-temperature polysilicon TFT transfer process was not explored, but would follow a similar evaluation, picking up the manufacturing flow during the transfer process to plastic.

21.24 Material Handling in Roll-to-Roll Processing

Material handling in roll-to-roll processing is critical and different from sheet processing. The ability to deal with flexible substrates on long rolls has been perfected by the solar cell, food packaging, and adhesive label industries. Tape automated bonding (TAB) and high-

Petitioner Samsung Ex-1011, 0454

density interconnect (HDI) substrates are also areas where roll-to-roll electronic devices are produced, although mostly on narrower webs. These industries draw heavily on the printed circuit board industry for their tool types, although fine line patterning has brought semiconductor and FPD grade exposure tools into the mix. Larger webs are already in use for flexible antiglare and touch screen ''cover layers'' placed on televisions, CRTs, and flat panel displays.[1] Figures 21.5 to 21.8 show examples of web-handling equipment.



Figure 21.5 Web handling: Northfield Automation's continuous process unwind/rewind with automatic tension control

21.24.1 Lift Cart

The staging area for the rolls of PET consists of an A-frame rack that will allow for three rolls to be stored on independent support bars. Staging racks will allow for the lift cart to access each roll without any manual lifting of the rolls of PET. For example, the roller coating process has two lift carts, one for each end of the process. The lift cart will allow the operator to transfer the roll of PET onto the cantilevered material shaft of the unwind system and also allow for easy removal of the roll of PET from the cantilevered material shaft of the rewind system.

[1] Energy Conversion Devices (ECD), Northfield Automation, and Toray all provided valuable input in these areas, based on their expertise in the areas of solar cells, adhesive labeling, and TAB/HDI. All have also done some work in display, transparent conductor, or fine line patterning. Descriptions and photographs of tools supplied for roll-to-roll processing are courtesy of Mark Wegner of Northfield Automation.

Petitioner Samsung Ex-1011, 0455



Figure 21.6 Web handling: Northfield Automation's unwind/rewind for develop, etch, strip (DES)

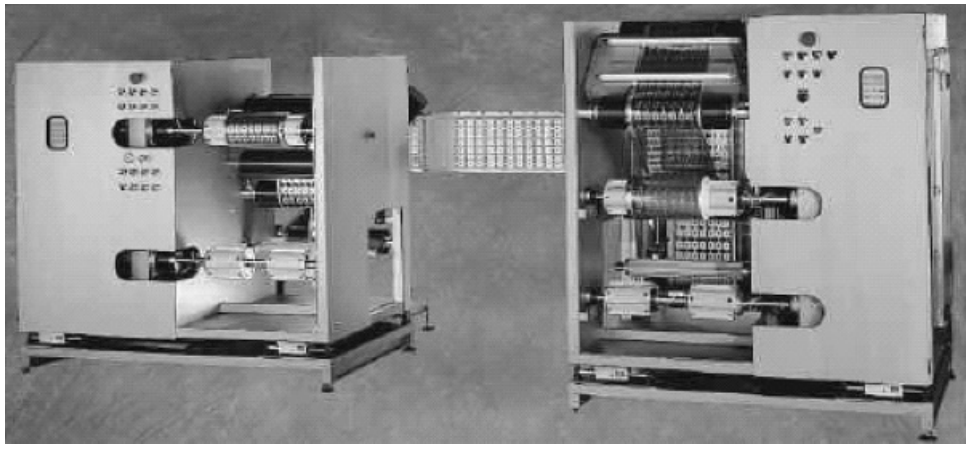


Figure 21.7 Web handling: Northfield Automation's vertical process unwind/rewind with accumulation and tension control

21.24.2 Leader Material

Each process will have a roll of leader material that will be used to purge the process when not in operation. This material allows for the process to be prethreaded from the unwind system through the tool and onto the rewind system. This roll of leader material will stay

Petitioner Samsung Ex-1011, 0456

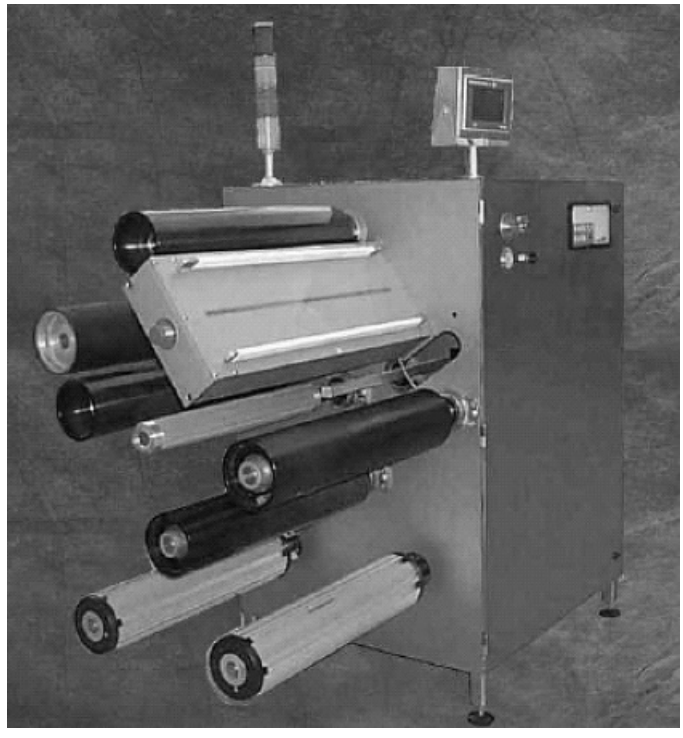


Figure 21.8 Web handling: Northfield Automation offers options such as dual material shafts, dual interleaf, and accumulation

with the process for reuse and allows for a higher yield with the production material. The operator will be able to load the roll of leader material when the last production roll is running. The same material should be able to be reused.

21.24.3 Loading New Rolls of Material

Here is the sequence of operations for loading a new roll of material:

1. The roll of PET will be loaded onto the material shaft of the unwind system with the lift cart.
2. The operator will then position the roll on the material shaft and activate the air chuck to secure the roll.
3. The leading end of the roll of PET is then placed on the splicing station.
4. The operator activates the clamping bar to hold the material until the taped splice is complete.
5. The end of the PET material is then taped with the end of the leader material that is already threaded throughout the process line.
6. The clamps are released and processing can begin.

Petitioner Samsung Ex-1011, 0457

The unwind and wind systems both have two material shafts and accumulation. This allows for continuous material feed or processing with material edge guidance and closed-loop tension during roll changes. The unwind system guides the material relative to the coater and the rewind system guides the material relative to the rewind material shaft for optimal roll windup. The unwind system can include a noncontact web cleaner, corona treatment system, and two vacuum rollers. The vacuum rollers control the web when the coating roller is opened, to allow for the splice to be advanced without damaging the roller. The rewind system has the option of including interleaf into the roll of substrate.

21.24.4 Resist Coater

The coating process is continuous and does not stop when a new roll is loaded. The coater cannot be stopped due to the process cleanliness required. Stopping the roller coater will require a complete clean of the machine. Proper splicing is very critical for this process. It requires air knives in the oven to support the web throughout the oven.

21.24.5 Web Edge in Photoresist Process

The estimated border at the edge that will be clear of resist may affect handling and the ability to keep the tools clean. when allowing for a variance in the web edge due to slitting, possible wavy edge variance, the capability of the ultrasonic edge sensors, and possible minimal resist bleed, allow for 1 mm edge clearance on each side.

21.24.6 Cleanliness

Additional HEPA filters with horizontal flow might have to be considered in the rewind stations when they are in a class 1000 environment. Class 100 is probably necessary for most processing zones.

21.24.7 Throughput of Handling Equipment

Throughput limitation should not be imposed by the handling. The handling equipment should be able to support a run rate of 6 ft/min throughout. The mid-process value will be the throughput limitation for each process.

21.24.8 Tension Control

There is concern that the PET should not be subjected to too much tension during exposure (Figure 21.9), due to the risk of distorting the pattern and causing inability to align. The substrate should be under a minimal and repeatable tension. A tension isolation zone is created at exposing with the vacuum roller advance on the outbound side of exposing (Figure 21.10). The leader optimizes the starting alignment of the production material while

Petitioner Samsung Ex-1011, 0458

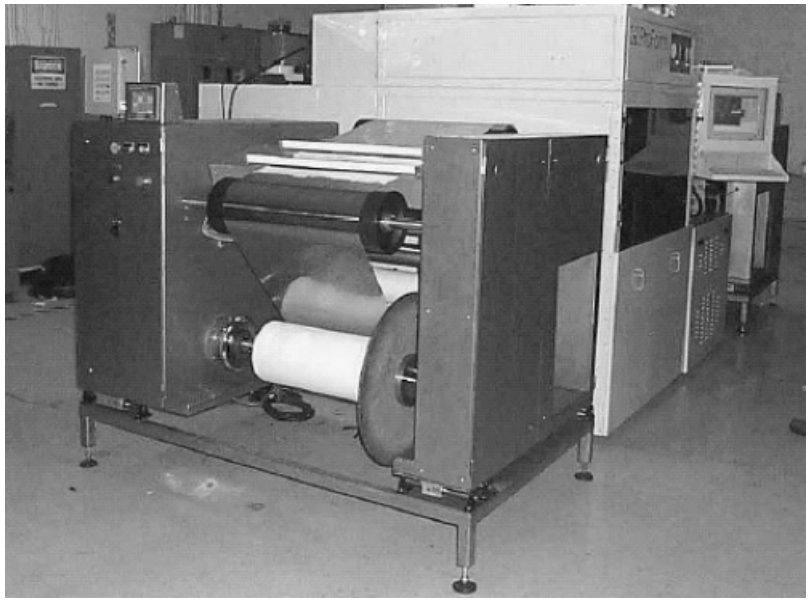


Figure 21.9 A Perkin Elmer exposer running 28 in wide 17 mil stainless steel

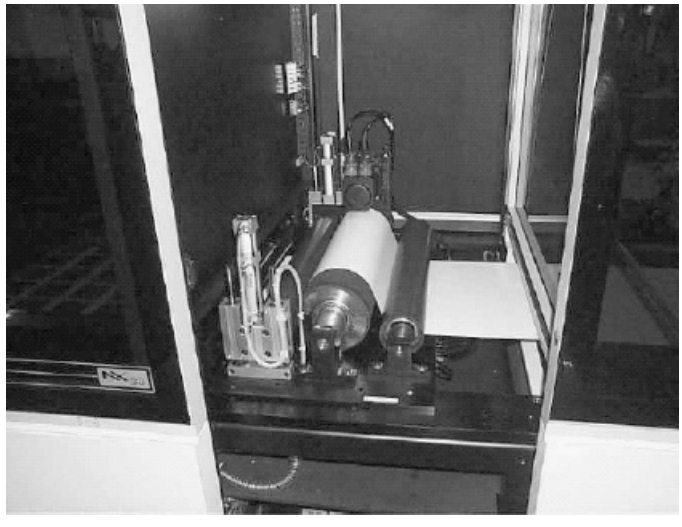


Figure 21.10 A web advance mechanism integrated into an Olec exposer

maintaining a controlled tension. Processors would lose control of the material if advancing a loose end of the roll, or trying to stabilize the first progression of the roll. The leader is therefore used to purge the line but still maintain a threaded process for faster startup and full production material utilization. Taping of the substrate and leader is currently a manual process.

Petitioner Samsung Ex-1011, 0459

21.24.9 Intermittent Processing and Alignment

If the process is intermittent, the unwind and rewind systems have only one cantilevered material shaft. Both systems in this case (such as align and exposure) have a horizontal dancer-accumulator for a rapid advance between exposures. The dancers utilize an ultra low friction and inertia design for nearly constant tension applied to the web even under start-stop conditions. The low-inertia dancer design allows for the index time to be minimized, which increases the throughput of the process. Both the unwind and rewind systems can include ultrasonic material edge guidance capability. The unwind system guides the material relative to the tool alignment and the rewind system guides the material relative to the material shaft for optimal roll windup. A servo-driven vacuum roller will precisely advance the material through the intermittent process tool (such as the exposure system) and allow for the square punch to be placed relative to the image during alignment, for downstream image registration. The registration punch at web initial clean eliminates the need for a vision system to register to the image at noncritical downstream processes. More critical alignment steps can use the optical system, which aligns to an optical alignment mark created during the photolithography process. This has been done on other applications and is the most cost-effective approach for downstream process registration. Figure 21.11 shows unwind/rewind for an ESI laser drill and Figure 21.12 shows dual rewind with inline slitting.

21.24.10 Punch

A line punch is mounted relative to the tool advance system. It is a single punch that is fixed based on the advance. A table punch process could allow for utilization of multiple holes. The punched hole will be able to hold ± 0.004 in accuracy in the material direction. The punched hole is just used for identification of the leading edge of the image for such steps as screening, stencil, and lamination. Vision registration systems can be used at stencil and screening to register to the edge of the material, as well as at exposing. This eliminates the stackup of tolerances when registering to something else. The punch is planned to be near the edge of the web. The die-cutting punch press will be designed to allow the slugs to be drawn out at the bottom of the die-set using a vacuum. The die construction will be relieved on the surface to allow for minimal contact with the ITO surface. The material will then be advanced through a web cleaner before the rewind system to remove particulates and then rolling up the PET.

21.24.11 Roll-to-Roll Optical Alignment

The material edge guidance system will be placed at the front of the tool. This will allow for accurate web edge alignment to the die. The tool can have a built-in fiber-optic sensor for detection of the square punched holes. Leading-edge detection with the fiber, along with the active edge alignment, will allow for proper registration of the image within the tool. The alignment accuracy in the y-axis (the transverse or cross-web direction) is ± 0.006 in. The alignment accuracy in the x-axis (the material or web-path direction) is ± 0.006 in for optical alignment, as of 2003.

Petitioner Samsung Ex-1011, 0460

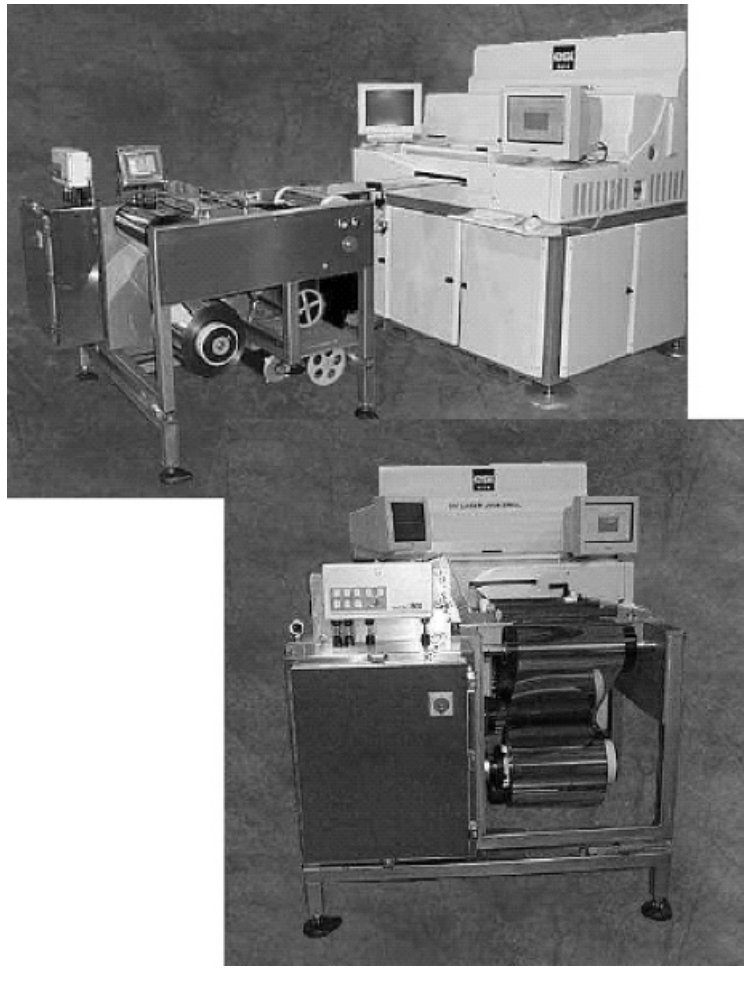


Figure 21.11 Unwind/rewind for an ESI laser drill, designed for web accelerations of g

The web edge alignment is performed with the ultrasonic edge guidance system that presents the material to the die at the stated y-axis accuracy. The fiber-optic sensor is used to stop the web advance when the sensor detects the punched hole in the material. The web advance will be a two-step advance. The majority of the progression can be a rapid advance, with the final part being a search mode for the fiber-optic sensor to detect the leading edge of the punched hole in the web. If required, a CCD camera system can be used with the patterned alignment mark to execute the fine alignment.

21.24.12 Price of Interleaf Handling

The unwind system and the rewind system have the option of interleaf handling (at the time of printing this was an additional $7000 not included in the typical price).

Petitioner Samsung Ex-1011, 0461



Figure 21.12 Dual rewind with inline slitting (28 in web to two 12 in webs)

21.24.13 Corrosion Prevention: Wet Process

The systems themselves should be powder coated to protect against corrosion, and the rollers made of hardcoated anodized aluminum. Exhaust is recommended throughout the wet process and associated material-handling systems as we have seen some significantly corroded wet process roll-to-roll systems

21.24.14 Lamination with Prepunched Windows

The laminator will be able to laminate the webs with prepunched windows in them. Northfield Automation, Preco, and others have extensive experience with handling thin substrate webs having empty windows. They have handled rolls of material with punched out circuits and also PET with windows from food packaging and labeling processes.

Petitioner Samsung Ex-1011, 0462

21.24.15 Integration of Vision Systems for Alignment

A vision registration system can be used to align the screen-printed adhesive or the windows in the web, or at other various steps. The vision registration system will identify the material edge and the punch locations to determine the positions from nominal and send this feedback to the tool to adjust for proper positioning. The web will be edge aligned using the same edge as was used at exposing to place the image. This, along with the square punch for leading-edge detection, will allow for proper registration of the subsequent pattern.

The sensor is a fixed point that continually monitors and reacts to the web edge. This creates a line reference for one edge. With control of the web, only one punched hole is necessary for the leading-edge detection.

Unwind/wind modules should be standardized for commonality of spare parts, etc. If possible, one automation vendor should be specified for all tools in a factory. This is similar to the Standard Mechanical Interface (SMIF) concept used in semiconductor wafer manufacturing.

Minienvironments with vertical or horizontal flow or inert environments (in the form of glove boxes) have been provided along with standard wind/unwind modules by companies such as ECD and VAC. Figure 21.13 was provided by Vin Cannella of ECD.

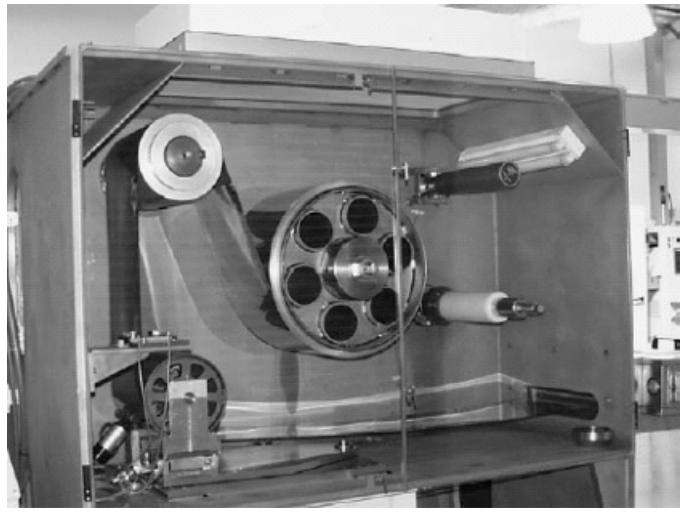


Figure 21.13 Minienvironment web payoff station for a roll-to-roll aqueous washer

21.24.16 Minienvironment Enclosures

Payoff and take-up stations are class 100 (or better), with HEPA filters supplying vertical laminar airflow, and ionizer bars to eliminate static problems common to unrolling and rolling plastic webs. Enclosures take air from the surrounding environment (assumed class 10 000 or better) and return the air to the same environment.[2]

[2]This section is a discussion of critical requirements in web handling. The source is ''Web Handling for Laminating and Coating Processes: How to Improve the Bottom Line,'' presented at the AIMCAL Conference, October 2002, by Jim Ward, vice president of engineering, at Martin Automatic, Inc.

Petitioner Samsung Ex-1011, 0463

21.24.17 Web Handling

The printing, coating, and laminating industries have one common theme: web handling.

Web handling rule 1

The single most important step that one can take to fixing web problems is to avoid them in the first place. Specify material characteristics and qualify suppliers. Stock roll and web variations come from

- caliper variation,
- modulus of elasticity,
- camber,
- wound-in tension,
- sidewall quality.

Web handling rule 2

The lowest-priced material is rarely the best value. Waste and delay from poor quality materials can dramatically increase production costs. Major web-handling components are

- unwinding systems,
- tensioning systems,
- web transport systems,
- web guiding systems.

Unwinding systems have these main functions:

- unwind a roll of material from the outside diameter through to the core;
- deliver the web flat, without wrinkles or folds;
- keep the web within the required tension limitations.

For winding, a lay-on roller, which can ''iron out'' air before entering the roll, allows winding tension to be lowered on a center winder.[3] The tools of winding are tension, nip pressure, torque (mnemonic TNT).

Flying splice systems are needed for long, multiple-tool roll-to-roll processes. Splicing takes place with the web running at its full machine speed. Key features include speed match, bump-and-cut transfer, and adhesive overlap splices.

[3]Adapted from ''Reasons to Rebuild Unwinds & Winders,'' presented at the AIMCAL Conference, October 2002, by Richard Greer of Faustel, Inc.

Petitioner Samsung Ex-1011, 0464

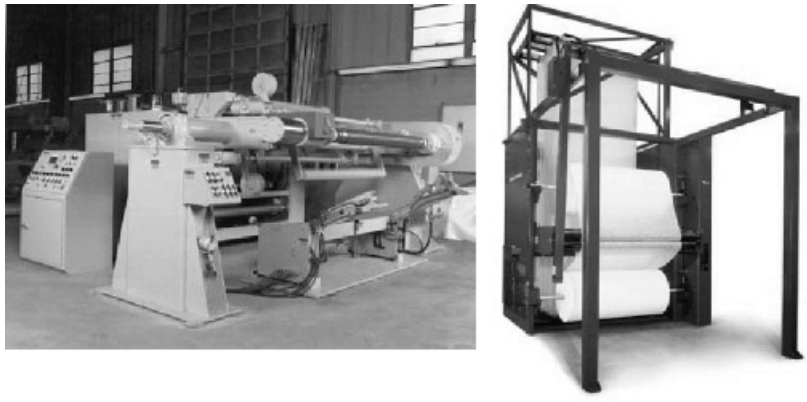


Figure 21.14 High-speed roll-to-roll process line

A zero-speed system has an accumulator system which allows both rolls to be stopped at time of splice. Multiple-splice types can be used, such as adhesive overlap splice, taped butt splice, heat seal overlap splice, and heat seal butt splice.

Splicing is important for production efficiency. A real-world example is splicing in a high-speed roll-to-roll process line (Figure 21.14) for a multiweb laminator with three splicers. It has full 24 h per day operation, 7 days per week, operating 52 weeks per year with 95% uptime and $1500 per hour operating cost. Each roll of material lasts one hour. How many splices per year?

$$\text{Number of splices} = 3\,\text{splicers} \times 1\text{splice per hour} \times 24\,\text{h} \times 7\,\text{days} \times 52\,\text{wks} \times 95\%\,\text{uptime} = 24\,897$$

21.24.18 Tension Control Systems

Tension control systems have two principal components: tension transducers and dancer systems. Here are some points about tension transducers.

- They sense and correct tension.
- There is virtually no web storage.
- Accuracy is a function of frequency response for a closed-loop control system.
- They may not be suitable for out-of-round rolls.
- They need to be tuned to the specific material characteristics.
- Drives and brakes are critical.

And here are some points about dancer systems:

- They set and maintain tension.
- They provide web accumulation control.

Petitioner Samsung Ex-1011, 0465

- Accuracy depends on
- inertial relationships,
- friction,
- geometry,
- pneumatic hysteresis.

So what is the optimum tension for my process? It is the lowest tension at which your material will track straight through the process without wrinkling or folding.

21.24.19 Web Transport Systems

Web transport systems include idler rollers and a true steering guide system (Figure 21.15). Here are some observations about idler rollers:

- Inertia is only important during speed changes.
- Bearing friction has a much greater effect on tension and web transport.
- Roller profiles are critical to remove wrinkles.
- Alignment is critical.

And here are some observations about the true steering guide system:

- The web guide carriage must pivot about the centerline of the incoming web.
- Lead in and distances must be based on material modulus of elasticity.

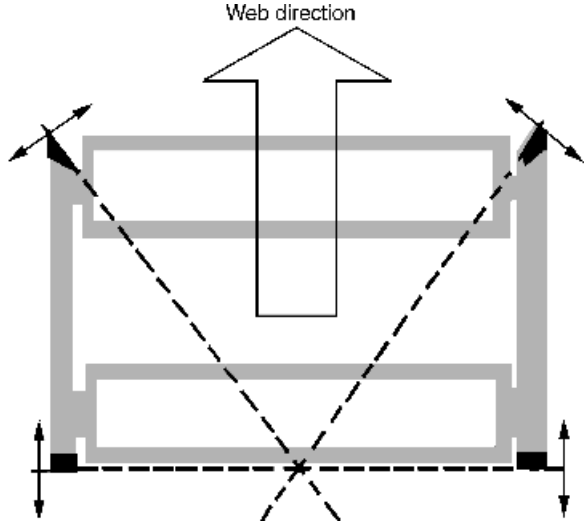


Figure 21.15 Steering guide systems

Petitioner Samsung Ex-1011, 0466

- Lead in and lead out must be parallel.
- Span determines correction.

21.24.20 Advanced Roll-to-Roll Processing

Vendors of advanced roll-to-roll material-handling equipment (Figure 21.16) are working to these goals:



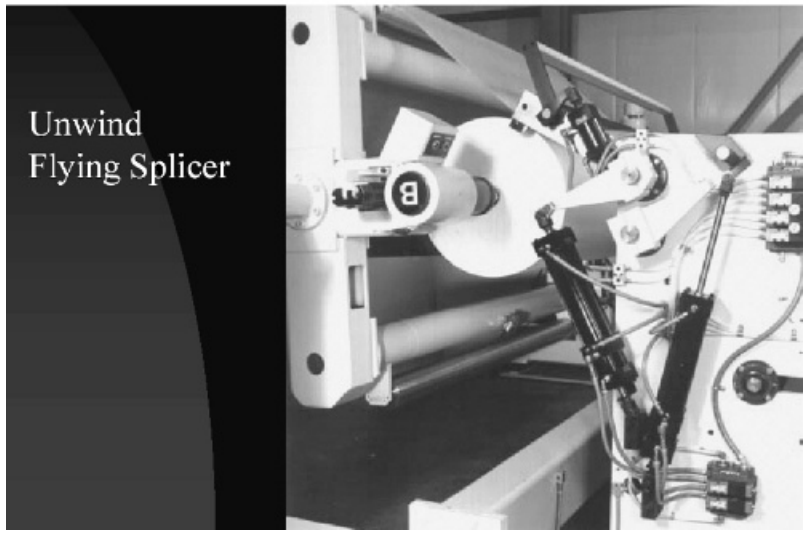


Figure 21.16 Decreasing waste and increasing productivity: web accumulator for ''zero-speed'' splicing

Petitioner Samsung Ex-1011, 0467

- Automatic splicers should deliver high reliability and constant tension.
- The substrate is consistent and flat.
- The splices are good enough that you can sell them to your customer.
- Splice as close to the core as possible so as to process as much of the material in the roll as possible.
- Web path idlers spin easily and they stop wrinkles from forming.
- The web guide delivers the web on center without edge deformation.

21.25 Results from the Cost Model

The author used the Abbie Gregg, Inc. Jupiter cost model to examine the effects of using different flows to create 3.25 in $\times$ 3.25 in displays. The processing tools to be considered are a combination of industry standard and developmental tools.

21.25.1 Glossary of Modelling Terms

- *Cost per square foot*: the typical output of a production cost model. It is the sum of several amortized capital and annual cost categories divided by good square feet of web produced per year.
- *Fitup costs*: the costs associated with installing a tool in the fab, performing tool hookup and certification, etc. The fitup costs are estimated as a percentage of the capital tool cost for each tool.
- *Operational utilization factor*: this factor is an estimate of how much available production time is actually utilized as production time.
- *Process yield*: The overall yield of the entire process. The detail for the models in this report are is Section 21.25.2.
- *Process step yield*: the yield associated with each step in the process. Normally these yields will vary from tool to tool, and from process to process on a given tool. Since we are dealing with continuous web processing, all yield loss is taken at the last test step, after the rolls have been singulated into individual devices.
- *Throughput*: the production capacity of the tool is measured in time (minutes) to process one batch (2000 ft^2 of web). Note that 2000 ft^2 is one 1000 ft roll (1000 ft $\times$ 2 ft). The throughput time includes setup, load, process, and unload times.
- *Tool uptime*: the percentage of time the tool is available for processing (i.e. the tool is not down, under repair, or in preventative maintenance).

The cost model provides the user with many inputs to create a custom factory. Here are some of the main inputs and values that were chosen for this model:

- Device size: individual device is 3.25 in $\times$ 3.25 in

Petitioner Samsung Ex-1011, 0468

- Substrate size: 18 in × 24 in
- Volume: in square feet of web desired for weekly output
- Batch size: 2000 ft^2 (purchase 1000 ft × 24 in roll = 2000 ft^2); there are 666.66 substrate equivalents in a roll/batch, hence there are 23 334 devices in a batch (one roll)
- Shift structure: 4 shifts, 7 day a week, 24 hours a day
- Cost: calculated per square foot of clean room by classification
- Salaries: by job classification
- Depreciation rates: equipment over 5 years, facilities over 20 years
- Flows: as described in Section 21.25.3
- Tools: as defined by cost, size, throughput and uptime
- Robots: required for web wind and unwind.

21.25.2 Yields

Since we are dealing with continuous web processing, all yield loss is taken at the last test step, after the rolls have been singulated into individual devices (Table 21.4).

The cost model is designed to give the user a quick way to analyze any changes that are made to the inputs. The main outputs of the model include total cost per square foot, equipment, material, facility, labor, overhead, headcount, and facility size.

Table 21.4 Yields table

Start-up		Mature product	
Used for $< 5000\ ft^2$/wk		Used for $\geq 5000\ ft^2$/wk	
Yield assumptions		Yield assumptions	
Inspection	97.0%	Inspection	99.4%
Test, TFT	85.0%	Test,TFT	97.0%
Test, passive	90.0%	Test, Passive	98.0%
Test, active	90.0%	Test, Active	97.0%
InkJet dep	95.0%	Ink Jet Dep	98.5%
OLED evap	95.0%	OLED Evap	98.5%
Resulting product yield		Resulting product yield	
Active	70.8%	Active	93.4%
Passive	82.1%	Passive	96.2%
PLED	95.0%	PLED	98.5%
OLED	95.0%	OLED	98.5%
Lam	87.3%	Lam	96.4%
Dep	87.3%	Dep	96.4%
Cumulative yields		Cumulative yields	
Passive start-up	68.1%	Passive mature	91.4%
Active start-up	58.7%	Active mature	88.9%

Petitioner Samsung Ex-1011, 0469

Table 21.5 USDC cost per square foot in dollars

Square feet per week	2000	6000	10 000	14 000	20 000	40 000	70 000	100 000
Devices per week	23 332	69 996	116 660	163 324	233 320	466 640	816 620	1166 600
Active PLED Lam	367.25							62.26
Active OLED Lam	386.35							74.94
Active PLED Dep	373.73							62.39
Active OLED Dep	392.06	155.84	113.26	101.31	88.40	80.83	75.29	75.04
Passive PLED Lam	244.91	90.79	61.11	48.65	40.31	36.47	35.47	34.23
Passive OLED Lam	258.09							46.44
Passive PLED Dep	250.76							34.32
Passive OLED Dep	264.72							46.56

21.25.3 Cost Results

The cost per square foot is shown from minimum volume (one roll per week) to a maximum of 100 000 ft^2 per week. The two flows shown in detail in Table 21.5 were chosen because they resulted in the minimum and maximum cost per square foot. The results are plotted in Figure 21.17.

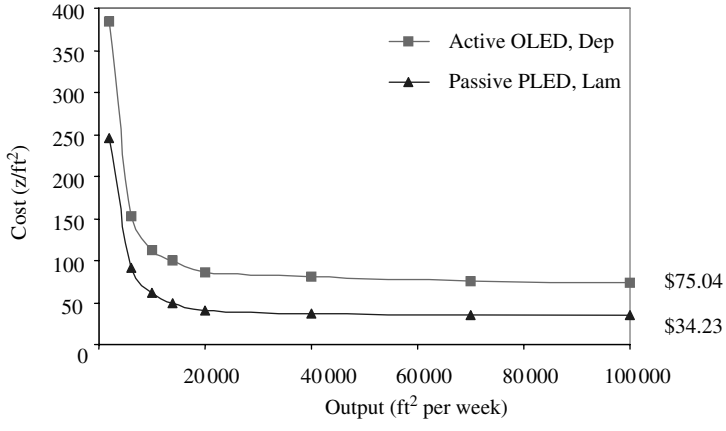


Figure 21.17 USDC results

21.25.4 Cost Components

Table 21.6 shows the the breakdown of the cost components at a run rate of 100 000 ft^2 per week.

Note that the TFT (active backplane) product costs using glass substrates, were $77.92 per square foot. In this study, the roll-to-roll backplane (active matrix) is $45.35, a difference of $32.57. Even with the most complex flow, this represents a significant cost reduction for roll-to-roll plastic substrate processing.

Petitioner Samsung Ex-1011, 0470

Table 21.6 Cost per square foot

	Cost ($)			
Component	Flow 4		Flow 5	
Backplane	Active	45.93	Passive	18.19
LED	OLED	25.31	PLED	12.45
Encapsulate	Dep	3.79	Lam	3.59
	Total	75.04	Total	34.23

21.25.5 Cost by Category

Table 21.7 shows that materials and equipment are the two dominant cost factors in these models. These figures are shown as a pie chart in Figure 21.18.

Table 21.7 Cost by category (percentage of whole cost)

Category	Active, OLED, Dep	Passive, PLED, Lam
Materials	55.5%	43.3%
Equipment	25.9%	31.6%
Overhead	8.5%	11.9%
Direct labor	6.1%	7.0%
Direct facilities	4.0%	6.2%

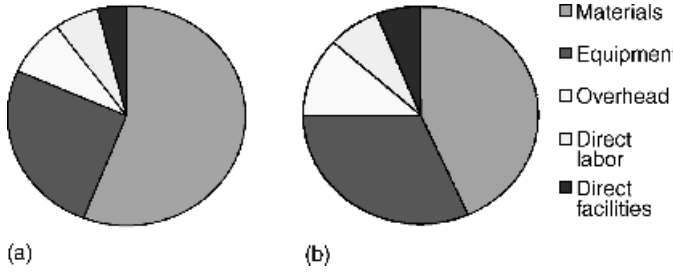


Figure 21.18 Cost by category

21.25.6 Factory Size Issues

The areas (all located in expensive clean space) required for maneuvering roll transport lift carts throughout the factory limits how close the tools can be placed to each other.

Petitioner Samsung Ex-1011, 0471

21.25.7 Tool Spacing Limitations

Typical semiconductor tools have an area space factor of 1.3. A typical tool has a footprint of 100 ft^2. This means the tool and the area necessary to access it require 130 ft^2. These tools can be placed very close together and the aisle between them can be 6 ft wide or less. This allows more than adequate room for operator and product movement.

Continuous web processing equipment has an area space factor of 1.75. This equipment is much larger. A typical tool is 784 ft^2. The access area required around the tool is also much larger. The maneuvering of the lift carts causes aisles to be 15 ft wide with 11 ft of space between tools. This means the tool and the area necessary to access it require 1372 ft^2. This space requirement can be reduced with future improvements in the lift carts.

21.25.8 Minimum Realistic Capital Investment

Have a look at Tables 21.8 and 21.9. The Passive, PLED, Lam product scenario is attractive because the initial capital investment is about $100million. This is much less than a comparable LCD fab today. This investment can produce approximately 8.5 million PDA devices a year.

Table 21.8 The minimum investment for the Active, OLED, Dep flow

Output (ft^2 per week)	10 000
Cost of facilities ($)	63 268 230
Cost of equipment ($)	115 906 874
Total cost of equipment and facilities ($)	179 175 104

Table 21.9 The minimum investment for the Passive, PLED, Lam flow

Output (ft^2 per week)	14 000
Cost of facilities ($)	49 672 018
Cost of equipment ($)	68 319 832
Total cost of equipment and facilities ($)	117 991 850

21.25.9 Summary of Results

The AGI Jupiter cost model was used on scenarios for continuous web processing of flexible displays. Here is a brief summary of the findings:

- Of the eight flows presented, the Active, OLED, Dep combination was the most expensive. The cost will be $75.04 at 100 000 ft^2 out put per week.

Petitioner Samsung Ex-1011, 0472

- The Passive, PLED, Lam flow was the least expensive. The cost will be $34.23 at 100 000 ft^2 out put per week.
- At high volume, the cost of a TFT (active backplane) on PET will be $45.93. A similar product on glass would cost about $77.92.
- A basic Passive, PLED, Lam factory can be built for a capital investment of $117million and will support 8.5million PDA devices per year.
- Materials and equipment comprise 75% of the product cost.
- The OLED evaporation is a major cost factor for equipment and materials.
- The alignment and etch processes offer many opportunities for throughput and yield enhancement.
- The lift carts, used for moving the rolls between tools, have a major impact on the layout. The maneuvering space they require needs to be reduced.
- Yields will also require immediate attention, and they have a large effect on cost.
- Labor costs have a low impact on the overall product cost.

21.25.10 Obstacles, Technical Issues, and Concerns

- *Emerging technology*: web processing for displays is an emerging technology. Prices, capacities, space requirements, and throughputs are constantly changing.
- *high material cost*: web processing is a new technology. High material costs and potential waste need to be analyzed. This is an area for much opportunity. OLED materials are especially dominant costs in the model.
- *Tools*: several tools are very large and very expensive. As the industry matures, these factors could change quite significantly. Merging roll-to-roll process knowledge and clean, fine line patterning is just beginning. Companies with few accomplishments in flexible microelectronics and display processing, but active in similar industries, have a lot to offer.
- *Yield*: a quick learning curve will be required to make this technology competitive. Hiring good engineering talent will need to be a priority. Capturing and using inspection data will also be critical.
- *Photolithography and etch*: these are critical process areas. The evolution of cost-effective steppers is needed for active matrix processing on flexible substrates in roll format. The development of stable dry etch processes will be required as geometries are reduced.
- *Core LED processes*: OLED evaporation and PLED application with inkjet are in their early stages of manufacturability. Both fundamental throughput of the process itself across a ''large'' substrate, and flexible substrate handling are challenges that no tool vendor has met up to now.

Petitioner Samsung Ex-1011, 0473

Bibliography

Carmody, M. (2003) *Flexible Microelectronics & Roll to Roll Processing Study*, USDC. FlexICs Website PolySilcon: TFT on plastic technology; polysilcon thin film transistors fabricated at 100 degrees C on a flexible plastic substrate.
FPD Technology Development Report (Q3,2002) Ink Jet Printing, para 3.3.
FPD Technology Development Report (Q3,2002) Linear Evaporation Tool.
Hough, S. (2003) *Flexible Microelectronics & Roll to Roll Processing Study*, USDC.
Innocenzo, J. (2003) *Flexible Microelectronics & Roll to Roll Processing Study*, USDC.
Lang, C. (2003) *Flexible Microelectronics & Roll to Roll Processing Study*, USDC.
Mahon, J. (2003) *Flexible Microelectronics & Roll to Roll Processing Study*, USDC.
Pinnel, R. (2003) *Flexible Microelectronics & Roll to Roll Processing Study*, USDC.
Praino, R. Jr (2003) *Flexible Microelectronics & Roll to Roll Processing Study*, USDC.
Slikkeveer, P. (2003) *Flexible Microelectronics & Roll to Roll Processing Study*, USDC.
Thompson, M. (2003) *Flexible Microelectronics & Roll to Roll Processing Study*, USDC.
Walker, K. (2003) *Flexible Microelectronics & Roll to Roll Processing Study*, USDC.
Wickboldt, P. (2003) *Flexible Microelectronics & Roll to Roll Processing Study*, USDC.

Petitioner Samsung Ex-1011, 0474

22

High-Resolution Full-Color Flexible TFT LCDs Based on Amorphous Silicon

Jin Jang,[1] Sung Hwan Won,[1] Bo Sung Kim,[2] Mun Pyo Hong,[2] and Kyu Ha Chung[2]

[1]Department of Information Display, Kyunghee University and [2]Samsung Electronics Co., Ltd

22.1 Introduction

Hydrogenated amorphous silicon (a-Si:H) thin film transistors (TFTs) have been widely used as switching devices in large-area electronics such as AMLCDs, imagers, X-ray detectors, etc. Recently, a portable communication system has been spotlighted, creating an increasing interest in display devices on plastic substrates that are flexible, unbreakable, foldable, and lightweight (Gleskova *et al*. 2001a). However, because of the thermal stress due to the difference in coefficient of thermal expansion (CTE) between the plastic and inorganic layers (a-Si:H, SiN_x), the substrate is bent considerably or the inorganic film deposited on plastic can be peeled off from the substrate (Gleskova *et al*. 2000).

Table 22.1 shows the CTEs of display materials. The organic materials like PES (polyethersulfone) and BCB (benzocyclobutene) have a CTE roughly 10 times that of inorganic materials such as SiN_x and glass. The CTEs of glass, PES, BCB, SiN_x, Si and Al are 4, 53, 43, 1.5, 3.4 and 23.5 ($\times 10^{-6}$ °C^{-1}), respectively.

Flexible Flat Panel Displays Edited by G. P. Crawford
© 2005 John Wiley & Sons, Ltd., ISBN 0-470-87048-6

Petitioner Samsung Ex-1011, 0476

Table 22.1 Coefficients of thermal expansion of the materials used for plastic display.

Material	CTE/10^{-6} (°C)	Reference
Glass	4	www.dilatometer.co.kr
PES	53	www.matweb.com
BCB	43	www.matweb.com
SiN_x	1.5	Retajczyk and Sinha (1980)
Si	3.4	http://microsensor.kyungpook.ac.kr
Cr	6.5	Murarka (1993)
Au	14	Murarka (1993)
Mo	5	Murarka (1993)
Al	24	Murarka (1993)

The fabrication of devices on plastic should be done at low temperatures because of the low heat resistance of plastic. Then the properties of the a-Si:H and SiN_x films for TFTs deposited at low temperatures are worse than those deposited at conventional process temperature (∼250–350 °C) on glass (Sazonov *et al*. 2000). He and/or H_2 dilution can be used to improve the material properties of the films deposited at low temperatures (< 150 °C) (He *et al*. 2000). Besides, there is considerable shrinkage and elongation by gas permeation through the plastic (Benmalek *et al*. 1995). Table 22.2 shows the characteristics of various plastics commercially available.

PI (polyimide) has the highest substrate temperature (T_s) and lowest CTE among the plastic materials shown in Table 22.2, so it is the best material for reflective display or for top-emission organic light emission display on plastic. Note that PI is coloured (www.matweb.com). Among transparent plastics, PES has the T_s, higher than 200 °C, and is therefore used in the TFT process for transmissive displays. We used PES because of its relatively high T_s and high transmittance. Polyarylate has high T_s but it also has high CTE compared with PI.

Table 22.2 Characteristics of the plastics for displays.

	UTS (MPa)	E (GPa)	T_s (°C)	CTE (ppm/K)	ε	ρ (Ω cm)	Color	Chemical resistance: Acetone	Chemical resistance: Acid
PET	55	2.5–3.0	76.5	79.2	3	2×10^{15}	Transparent	X	O
PC	52–72	2.1–2.4	150	70.2	3	7.3×10^{16}	Transparent	X	O
PES	83–100	2.4–8.6	228	49.1	3.8	2.9×10^{16}	Transparent	X	O
PEN	275	6.1	200	23		2×10^{17}	Transparent	X	O
PI	221	2.8	385	20	3.5	1.5×10^{17}	Colored	X	O
Polyarylate	100	2.9	330	50	2.6	1.0×10^{16}	Transparent	X	O
Glass*	—	73	620	5	5.7		Transparent	O	O

Notes: UTS = ultimate tensile strength. E = Young's modulus, CTE = coefficient of thermal expansion, ε = dielectric constant, X = bad, O = good.

*The glass is Corning 1737.

Petitioner Samsung Ex-1011, 0477

The CTE is an important issue for the TFT array process because of the thermal stress after cooling down to room temperature following film deposition.

We used the PES film with gas barriers on both sides to reduce gas permeation through the plastic and protect it from chemical attack during the TFT process. To reduce the gas permeation ratio, inorganic materials such as silicon nitride and silicon oxynitride are suitable compared to the organic layer for gas barrier. Therefore silicon nitride is frequently used as a gas barrier for the TFT LCD on plastic (Gleskova *et al*. 2001b). Ta_2O_5 is also a suitable material for the gas barrier (Polach *et al*. 1999). The requirement on the gas permission ratio for organic light emission display ($< 10^{-6}$ g/m^2 per day) is much lower than for TFT LCDs ($< 10^{-2}$ g/m^2 per day); see Burrows *et al*. (2000).

The deposition of TFT layers is usually carried out at elevated temperatures, for example 150 °C on plastic substrates. In this case the plastic is bent after the sample has cooled down to room temperature. Therefore it is difficult to carry out photolithography using the conventional photomasks for TFT arrays on glass. In our previous work, we introduced the concept of island formation before carrying out the conventional photolithography process (Hur *et al*. 2002). The plastic becomes flat after island formation.

The a-Si:H TFTs used in manufacturing an LCD on glass are fabricated at a temperature of ∼300 °C, the optimum temperature for depositing high-quality a-Si:H and silicon nitride (SiN_x). On plastic the substrate temperature should be as low as possible, so the growth of high-quality a-Si:H and SiN_x is important for high-performance TFTs. Hydrogen and/or helium dilution are used for the low-temperature deposition of these materials (Parsons 2000). Gas pressure, RF power, and gas flow rate are the other important variables.

Table 22.3 summarizes the literature giving performances of a-Si:H TFTs on plastic. Sazonov *et al*. (2002) used PI substrate at a maximum process temperature of 120 °C using an etch stopper (ES) TFT. Note that most of the LCDs are made with the back-channel etched (BCE) structure, because of its simplicity. This means that the number of masks when using the BCE TFT array is smaller than when using the ES TFT array. Sazonov *et al.* reported the field-effect mobility, subthreshold slope, and threshold voltage of an a-Si:H TFT as 0.7–0.8 cm^2/V s, 0.5 V/decade, and 4 V, respectively Gleskova *et. al*. (2001) also used PI substrate at a maximum process temperature of 150 °C (Won *et al*. 2004) used a BCE type and achieved a field-effect mobility of 0.45 cm^2/V s and a threshold voltage of 3 V. On the

Table 22.3 Published characteristics of a-Si:H TFTs on plastics

Maker	Plastic type	Process temp. (°C)	TFT type	Performance	References
Waterloo University	PI	120	ES	$\mu = 0.7$–0.8 cm^2/V s $V_{th} = 4$–5 V SS = 0.5 V/dec.	Sazonve *et al.* (2002)
Princeton University	PI	150	BCE	$\mu = 0.45$ cm^2/V s $V_{th} = 3$ V SS = 0.5 V/dec.	Gleskova *et al.* (2001)
Kyung Hee University	PES	150	BCE	$\mu = 0.4$ cm^2/V s $V_{th} = 0.7$ V SS = 0.82 V/dec.	Won *et al.* (2004)
Sharp Corp.	PI	220	BCE	$\mu = 0.3$ cm^2/V s $V_{th} = 2$ V	Okada *et al.* (2002)

Petitioner Samsung Ex-1011, 0478

other hand, Okada *et al*. (2002) used PI substrate at a maximum process temperature of 220 °C using the BCE type and they achieved a field-effect mobility of 0.3 cm^2/Vs and a threshold voltage of 3 V.

22.2 Effect of He Dilution on SiN_x Deposition

To have high-performance TFTs at low temperatures, the deposition conditions for the TFT layers of SiN_x, a-Si:H and n^+ a-Si:H should be optimized. It is not easy to optimize these layers completely, because there are many deposition parameters such as flow rate, gas pressure, and RF power. We added He for the low-temperature deposition of undoped a-Si:H and n^+ a-Si:H, as shown in Table 22.5. The RF power given in this table was also achieved by optimization. With the fixed values for the RF power, SiH_4 flow rate and NH_3 flow rate shown in this table, we varied the He flow rate for the deposition of SiN_x for a-Si:H TFTs. The TFT was made on a glass substrate at 150 °C. This is the optimization process, which was done on glass rather than on plastic. We used the BCE-type TFT (Yang *et al*. 1998). The SiN_x is normally used as the gate insulator for a-Si:H TFT. It requires high breakdown voltage and low defect density. For low-temperature deposition of SiN_x, He or H_2 dilution is mainly used for improving the electrical properties of the film (He *et al*. 2000). In this work we used He dilution.

Figure 22.1 shows the *I–V* characteristics of SiN_x deposited using He flow rates of 50–200 sccm (standard cubic centimeters per minute) at a substrate temperature of 150 °C. Its breakdown field is higher than 3 MV/cm and its leakage currents are less than 10^{-9} A/cm^2, making it suitable as a gate insulator for TFT. Therefore we conclude that the *I–V* characteristics of the SiN_x deposited at 150° C show no significant differences between the films deposited using various He flow rates.

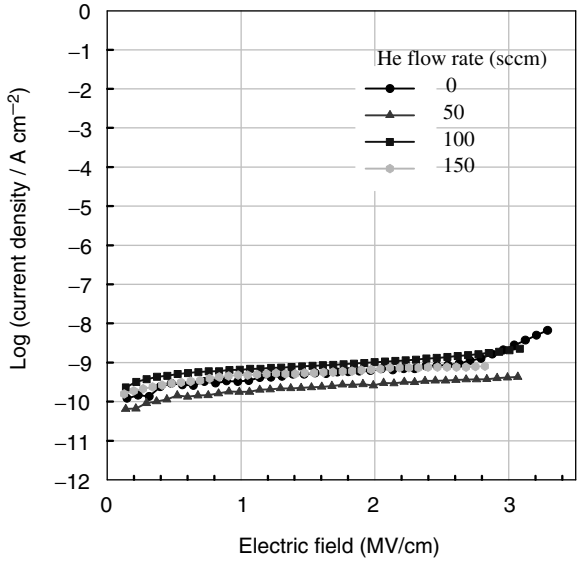


Figure 22.1 *I–V* characteristics of the SiN_x films deposited at 150 °C with different He flow rates

Petitioner Samsung Ex-1011, 0479

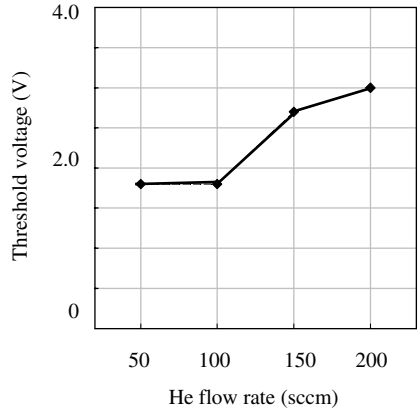


Figure 22.2 Threshold voltages of the a-Si:H TFTs fabricated on glass with the SiN_x deposited at different He dilution

Figure 22.2 shows the variation of threshold voltage of a-Si:H TFTs fabricated on glass with the SiN_x deposited at different He dilutions. The threshold voltage increases with He flow rate when the He flow rate is higher than 100 sccm. This indicates that the surface of SiN_x is damaged by excessive He ions when the flow rate is 150 or 200 sccm. This induces the increase in the interface state density between a-Si:H and SiN_x.

Figure 22.3 shows the field-effect mobility of a-Si:H TFTs fabricated using various He flow rates. There is little change in the field-effect mobility even though there is an increase in the threshold voltage at 150 and 200 sccm.

Figure 22.4 shows the transfer characteristics of a-Si:H TFTs on glass for SiN_x deposited using an He flow rate of 200 sccm. The on/off ratio is higher than 10^7 and the leakage current in the off-state and the gate leakage current through the gate insulator are less than 1 pA. Therefore this performance is suitable for the TFT LCD.

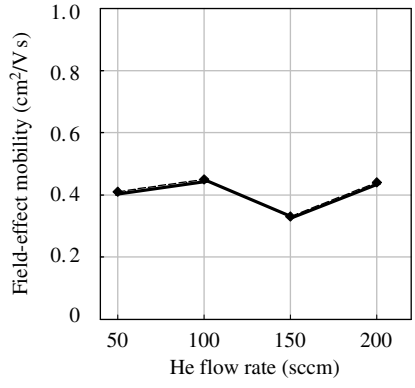


Figure 22.3 Field-effect mobility of the a-Si:H TFTs fabricated under different He flow rates for SiN_x deposition

Petitioner Samsung Ex-1011, 0480

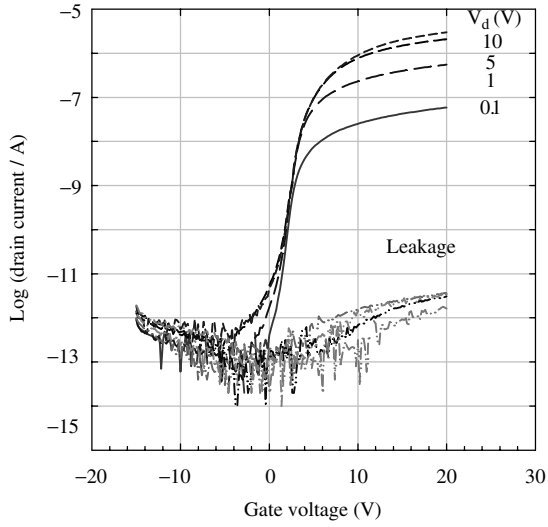


Figure 22.4 Transfer characteristics of the a-Si:H TFT where the SiN_x was deposited at an He flow rate of 200 sccm (standard cubic centimeters per minute)

22.3 a-Si:H TFT on Plastic with an Organic Gate Insulator

Bending of a plastic substrate and peeling of film from the substrate are the major issues for displays on plastic with amorphous silicon. The plastic is bent after depositions of a-Si:H and SiN_x at elevated temperature, hence the array process is impossible. Therefore, relatively thick SiN_x layers are deposited on both sides of the plastic. Then the SiN_x can endure the internal stress created by the difference in the CTEs of plastic and SiN_x.

Another method was proposed by our group to make a flat substrate with the TFT layers on plastic. The TFT area is a small portion of the pixel design and the inorganic layers n^+ a-Si:H/a-Si:H/SiN_x are needed only for the TFT area, not the whole pixel area. Therefore we made one island in one pixel at the TFT region. The plastic with numerous islands of n^+ a-Si:H/a-Si:H/SiN_x in the TFT regions is flat, so the conventional photolithographic process is possible.

Figure 22.5(a) shows a cross-sectional view of a conventional a-Si:H TFT. The 500 nm SiN_x layer was deposited on both sides of the PES before the a-Si:H TFT process. This is to

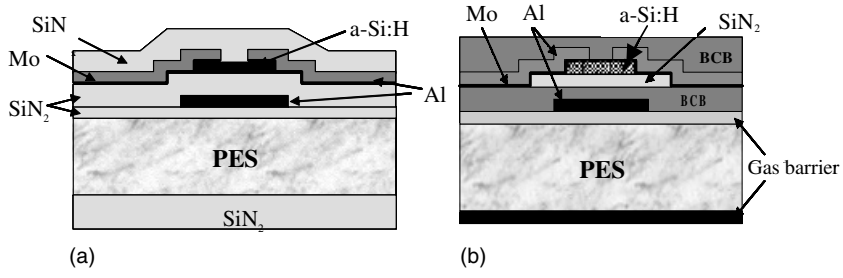


Figure 22.5 (a) A cross-sectional view of an a-Si:H TFT with SiN_x gate insulator and (b) an a-Si:H TFT with SiN_x/BCB gate insulator

Petitioner Samsung Ex-1011, 0481

protect the plastic from thermal expansion and vapor permeation. The SiN_x was deposited at 150 °C after annealing for 2 days at 180 °C to remove the vapor in the PES. The layers are also gas barriers to protect the PES against gas permeation from outside.

Figure 22.5(b) shows a cross-sectional view of an inverted staggered BCE a-Si:H TFT adopting a BCB as the first gate insulator for active matrix display on plastic. The ratio of channel width (W) to length (L) of a TFT was 16 μm /4 μm and Al was used for the bus lines (Jang and Lim 1999; Polach *et al*. 1999).

The BCB was coated by spin coating, cured in N_2 atmosphere at 180 °C, then cured in a vacuum oven at 180 °C. Triple layers of SiN_x (50 nm), a-Si:H (200 nm), and n^+ a-Si:H (50 nm) were consecutively deposited on the BCB at the substrate temperature of 150 °C by PECVD. Then the inorganic layers were patterned by a wet etch process. This causes the elongated substrate to return to its original form. Then active islands were defined by a wet etch process. Mo (50 nm) and then Al (300 nm) layers were consecutively deposited using magnetron RF sputtering and patterned for source/drain contacts. Next the n^+ a-Si:H layer on the back channel was etched. The BCB layer was also used as the passivation layer for the a-Si:H TFT. Onlt a thin SiN_x layer was used to reduce the interface state density between the a-Si:H and the gate insulator. A thin Mo layer was inserted to enhance the adhesion to the substrate.

Using an SiN_x single layer as a gate insulator for an a-Si:H TFT on plastic has the disadvantage of microcrack generation in the inorganic layer, especially in SiN_x films, because the plastic substrate with a thick inorganic material on both sides of it has a high internal stress. The other method is to pattern inorganic layers (a-Si:H, n^+ a-Si:H, SiN_x) in order to release the global stress between the plastic and the inorganic layers. This has the disadvantage of using an additional photomask step to pattern the inorganic layers, but it has the advantage of relaxing the global stress, producing a stress-free active layer in the TFT. Thin films may peel on bending, but this can be eliminated by forming islands of inorganic layers (Hur *et al*. 2002).

Figure 22.6 shows the transfer characteristic of an a-Si:H TFT on PES using only SiN_x as a gate insulator. The off-state currents and gate leakage currents are around 10^{-12} A and

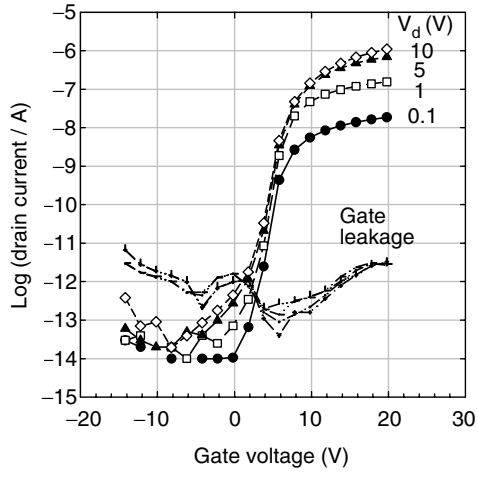


Figure 22.6 Transfer characteristic of an a-Si:H TFT on PES with SiN_x gate insulator

Petitioner Samsung Ex-1011, 0482

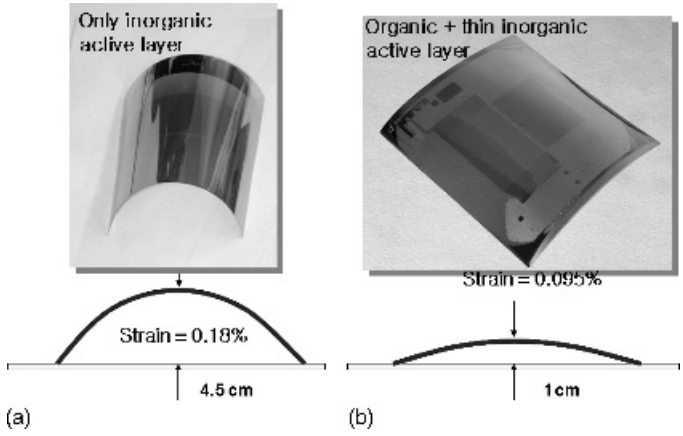


Figure 22.7 The shape of PES after deposition of TFT layers

therefore are higher than that of conventional TFTs on glass (10^{-13} A). This appears to result from the internal stress in the a-Si:H and SiN_x layers due to the thermal stress between SiN_x and PES. The PES substrate is elongated at the deposition temperature of 150 °C and shrinks when it is cooled down to room temperature. The SiN_x layer on the PES is stressed because of the difference in the CTEs of SiN_x and PES. The stress can generate a microcrack in the SiN_x film so that the gate leakage current can be unstable and high compared to the TFT on glass. TFT performance on glass is shown in Figures 22.2 through 22.4.

Figure 22.7 shows the shape of PES after depositing an active layer on the plastic substrate. The strain at room temperature was calculated from the bending of the sample after deposition of n^+a-Si:H, a-Si:H, and SiN_x on PES and also after deposition of n^+a-Si:H, a-Si:H, and SiN_x on BCB/PES at 150 °C. Both cases have the gate patterns on the PES substrate. The strain was 0.0018 (0.18%) for a single-layer SiN_x gate insulator and 9.49×10^{-4} (0.0949%) for a double-layer gate insulator. The strain on the top surface (a-Si:H) of a 200 μm thick PES substrate is given by

$$\varepsilon_{\text{top}} = \left(\frac{d_f + d_s}{2R}\right) \frac{1 + 2\eta + x\eta^2}{(1+\eta)(1+x\eta)} \quad \text{with} \quad \eta = d_f/d_s \ \text{ and } \ x = Y_f/Y_s. \tag{22.1}$$

Here d_f and d_s are the film and substrate thicknesses, respectively; Y_f and Y_s are the Young's moduli of the film and substrate, respectively (Suo *et al.* 1999).

The internal stress is also reduced by thinning the SiN_x layer. This means that the strain can be significantly reduced by using an organic gate insulator of BCB. Note that the CTE of BCB is $43 \times 10^{-6}\,°C^{-1}$, similar to PES ($53 \times 10^{-6}\,°C^{-1}$) rather than SiN_x ($1.5 \times 10^{-6}\,°C^{-1}$). Figure 22.8 shows the transfer characteristic of an a-Si:H TFT on plastic using BCB as the first gate insulator; the on/off current ratio is higher than 10^7. The leakage current through the gate insulator is less than 10^{-13} A. This low current results from the double-layer gate insulator and planarization of the gate insulator. The thin (50 nm) layer of SiN_x can be used without giving high internal stress; this is because the BCB layer plays a major role as a gate insulator. A thin SiN_x layer was just used to improve the interface between the a-Si:H and the gate insulator. Note that the SiN_x and a-Si:H interface is being used to manufacture a-Si:H TFT arrays because of its low interface state density. The use of BCB and thin SiN_x as a gate

Petitioner Samsung Ex-1011, 0483

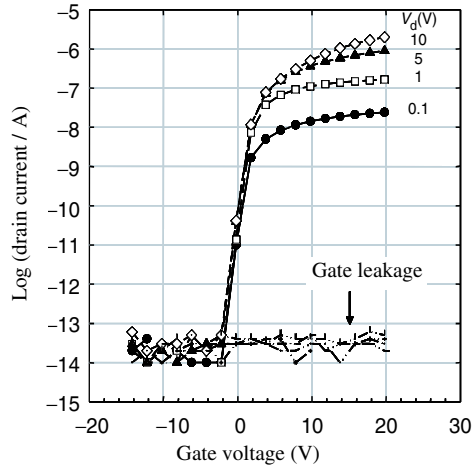


Figure 22.8 Transfer characteristic of an a-Si:H TFT on PES with SiN_x/BCB gate insulator

insulator can reduce the leakage current because of lower thermal and internal stresses. The dielectric constant of BCB is 2.7, low compared to the value for SiN_x (Mills *et al.* 1997). However, a BCB layer was able to play a sufficient role as a gate insulator because of its high resistivity (Mills *et al.* 1997). This results in a low threshold voltage of the TFT and low gate leakage current. Note that the off-state leakage current is less than 10^{-13} A.

Figure 22.9 plots the square root of drain current (I_d) as function of gate voltage (V_g) for the a-Si:H TFTs on plastic, measured with gate and drain electrodes connected together to obtain the field-effect mobility (μ) and threshold voltage (V_0) in the saturation region using the relation

$$I_d = \frac{CW\mu}{2L}\left(V_g - V_0\right)^2, \tag{22.2}$$

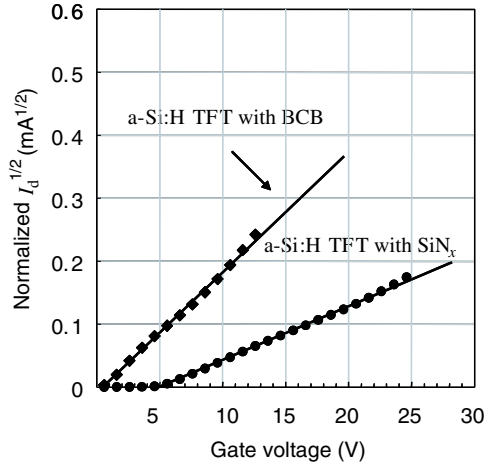


Figure 22.9 Square root of drain current plotted as a function of gate voltage to compare the field-effect mobility and threshold voltage between the a-Si:H TFTs with and without an organic gate insulator

Petitioner Samsung Ex-1011, 0484

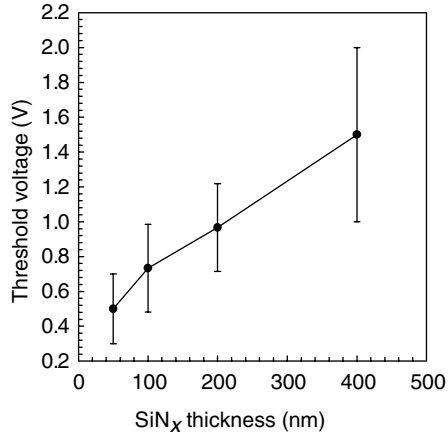


Figure 22.10 Threshold voltage of the a-Si:H TFTs on PES as a function of SiN_x thickness

where C is the capacitance of the gate insulator with a BCB dielectric constant of 2.7 (Kagan and Andry 2003).

The field-effect mobility and the threshold voltage of the TFT with an SiN_x gate insulator are 0.3 cm^2/V s and 5 V, respectively. However, the a-Si:H TFT with BCB gate insulator has a field-effect mobility of 0.4 cm^2/Vs and a threshold voltage of 0.7 V. The TFT with an SiN_x gate insulator has a higher threshold voltage and a lower field-effect mobility compared to the TFT with a BCB gate insulator. The TFT with an SiN_x gate insulator has high internal stress caused by the difference in CTE between organic and inorganic layers. The internal stress seems to reduce the field-effect mobility and to increase the threshold voltage (Glescova and Wagner 1999).

Figure 22.10 shows the threshold voltage of the a-Si:H TFTs on PES as a function of SiN_x thickness. It decreases from 1.5 V to 0.3 V when the SiN_x thickness deceases from 400 nm to 50 nm. The reduction in the threshold voltage is related to the charge traps in the SiN_x. Note that the threshold voltage of an a-Si:H TFT decreases with decreasing SiN_x thickness.

22.4 Fabrication of an a-Si:H TFT Array on Plastic

The bus line metals are exposed to high stress during the PECVD process at $\sim$150 °C because the CTE of organic material is generally about five times higher than that of most metals. The ductility of the bus line metal is important for the electronic device on plastic substrate. To avoid cracks in the bus lines, the chosen metal must have a high ductility characterized by Young's modulus. Note that Al has the lowest modulus. Therefore Al is mostly used for the bus lines of plastic displays.

Table 22.4 shows the Young's modulus and yield point for various metals. The Young's modulus valves in kN/mm^2 for Al, Ti, Ta, Cr, and Mo are 70, 107, 180, 248, and 334, respectively. The yield point indicates the reversible deformability of material. From Table 22.4, Al seems to be the most promising (Polach *et al.* 1999).

Figure 22.11 shows the fabrication procedure of an inverted staggered BCE a-Si:H TFT array using an organic layer as the first gate insulator for a plastic TFT LCD. To avoid

Petitioner Samsung Ex-1011, 0485

Table 22.4 The Young's modulus and yield point for the metals used for TFT LCDs

Metal	Young's modulus (kN/mm^2)	Yield point (kN/mm^2)
Al	70	13–22
Ti	107	137
Ta	180	
Cr	248	422
Mo	334	

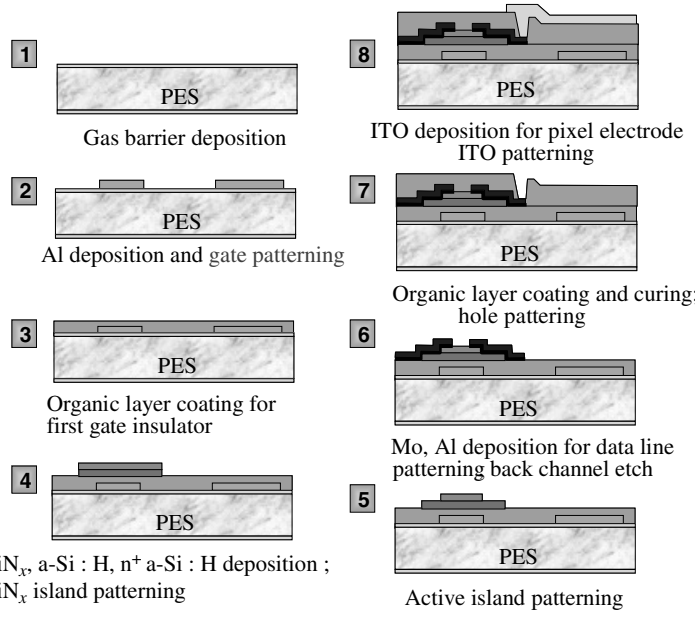


Figure 22.11 Fabrication procedure of an inverted staggered BCE a-Si:H TFT with organic layer as the first gate insulator for a plastic TFT LCD

irreversible shrinkage during the film deposition and to remove the contamination in the chamber, the PES substrates were preannealed at 180 °C for 2 days. Al for the gate lines was deposited by magnetron RF sputtering and then patterned for gate lines and storage capacitor electrodes (first mask in Figure. 22.11, item 2). BCB was coated and then cured at 180 °C. Triple layers of SiN_x (50 nm), a-Si:H (200 nm) and n^+ a-Si:H (50 nm) were consecutively deposited at the substrate temperature of 150 °C by PECVD. Then the inorganic layers were patterned by a wet etch process (second mask in Figure. 22.11, item 4). This causes the elongated substrate to return to its original size. Next active islands were defined by a wet etch process (third mask in Figure. 22.11, item 5). Metal layers were consecutively deposited by magnetron RF sputtering then patterned for data lines and TFT source/drain. The n^+ a-Si:H layer on the back channel was etched by a wet etch process (fourth mask in Figure. 22.11, item 6). We used an organic layer for the passivation layer of the a-Si:H TFT array. Acryl or BCB can be used for the organic passivation layer.

Petitioner Samsung Ex-1011, 0486

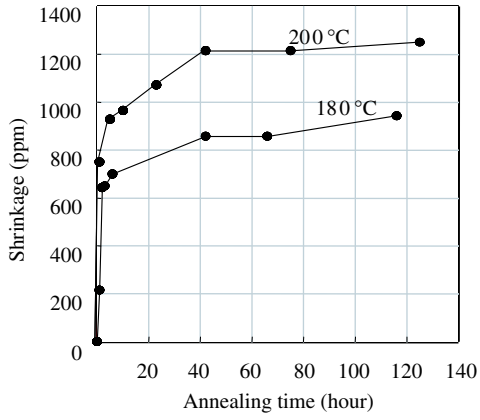


Figure 22.12 Shrinkage of a PES during the annealing process at 180 and 200 °C

Contact holes were formed by a plasma etch process (fifth mask in Figure 22.11). Then an IZO layer for pixel electrodes was deposited by magnetron RF sputtering and defined for pixel electrodes by a wet etch process (sixth mask in Figure. 22.11, item 8). Note that IZO is better than ITO to reduce the reaction between the TCO and Al.

The significant difficulty in the fabrication of TFT arrays on a plastic substrate is a dimensional change during the TFT process. Dimensional changes result from thermal stress as well as through shrinkage due to outgassing from the plastic. Figure 22.12 shows the shrinkage of a PES substrate during the annealing process at 180 and 200 °C, respectively. The changes mostly arise within a few minutes and then tend to saturate. Initial shrinkage is related to the initial fast desorption of water vapour and/or gas, and the results are from the outgassing of volatile molecules from the PES films. The shrinkage is ∼1000 ppm for the PES. To reduce additional shrinkage during the process, we preannealed PES in an oven at a temperature of 180 °C for 50 h, which is higher than the deposition temperature of a-Si:H and SiN_x by PECVD.

Figure 22.13 shows the elongation during each process step for the a-Si:H TFT array on PES using BCB as the first gate insulator. Size deformation does not exist except during the PECVD process. The elongation during the PECVD process disappears after forming the islands. The islands of inorganic layers were designed to have their margin based on thermal

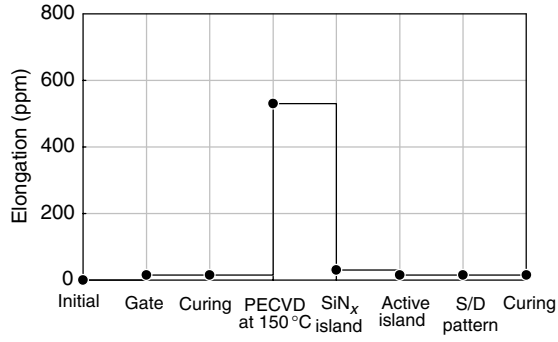


Figure 22.13 Elongation of the substrate during the TFT process step for an a-Si:H TFT on PES with BCB as the first gate insulator

Petitioner Samsung Ex-1011, 0487

Table 22.5 Summary of TFT LCDs on plastic using an a-Si:H TFT

Maker	Display type		Specification
Sharp		4 in plastic TFT LCD (based on a-Si)	Display type: reflective color Resolution: 240 × 240 (85 ppi) Pixel number: 172 800 Pixel size: 100 μm × 300 μm Aperture ratio: 92%
KHU		2.2 in plastic TFT LCD (based on a-Si)	Display type: transmissive Resolution: 128 × 160 (93 ppi) Pixel number: 61 440 Pixel size: 276 × 92 Aperture ratio: 48%

elongation. However, the reversible size deformation appears when the fabrication process is not carried out continuously. Note that the sample kept in a vacuum has no size deformation. This indicates that the origin of size deformation is gas absorption into the plastic substrate (Polach *et al.* 1999). Therefore, when the process is intermitted, the sample should be kept in a vacuum or an N_2 environment.

22.5 a-Si:H TFT LCD on Plastic

Color TFT LCDs with a-Si:H TFT switching on plastic were reported by Sharp and our group (Won *et al.* 2003). In addition to the low-temperature TFT array process, the cell and color filter should be made at low temperatures. The conventional cell process temperature is ∼200 °C, but the plastic process should be carried out at less than 150°C.

Table 22.5 summarizes the color TFT LCDs on plastic developed using a-Si:H switching devices. Sharp fabricated a reflective color a-Si:H TFT LCD on PI. The aperture ratio of this display is 92%, almost the same as for a conventional reflective LCD using glass substrates (Okada *et al.* 2002). On the other hand, our group fabricated a transmissive color a-Si:H TFT LCD on PES. Using two 0.2 mm plastic films for the TFT and color filter plates, the weight of the panel is about 20% of conventional TFT LCDs on glass substrates.

22.5.1 Color Filter on Plastic

Figure 22.14 shows the structure of a color filter (C/F) substrate. PES is coated with 100 nm thick black matrix (BM). The BM prevents any light leakage and protects the TFT from stray light. Conventional Cr/CrO_x BM can not be used for a plastic display because of its high stress on plastic. Al was used in our work. RGB color materials are coated in between the Al BM. The R material was spin coated with ∼1.2 μm and cured at 180 °C then patterned. The same procedure is carried out to make G and B color filters. Then a protecting film, or

Petitioner Samsung Ex-1011, 0488

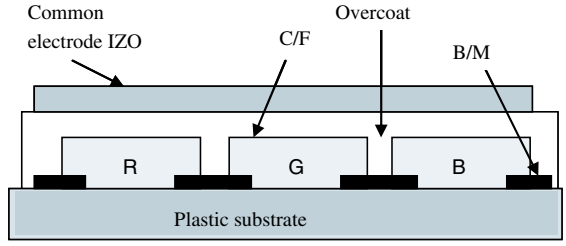


Figure 22.14 A cross-sectional view of a color filter on plastic

overcoat, is deposited. The protective film makes the C/F substrate surface flat by reducing the steps between the RGB and the BM. Finally, a common electrode IZO film is deposited. The optical transmission of RGB color filters relative to white light is approximately 25%.

22.5.2 LC Cell

Spacer

There are two kinds of spacer materials for TFT LCD on glass. One is rigid glass fiber or micro pearl. The other is a post spacer using resin. We used a soft ball spacer. This is soft and can therefore change its shape and thickness under pressure, hence it does not damage the plastic substrate. With increasing spacer density on the color filter substrate, the cell gap uniformity can be improved. However, the high-density spacer can degrade the display quality, especially the contrast ratio. The typical spacer density is 70 per square millimeter on glass, but we used 100 per square millimeter on the PES.

The sealant, mostly rectangular in shape, can be formed either by screen printing (Figure 22.15(a)) or by dispenser drawing (Figure 22.15 (b)). Screen printing offers better production throughput because the patterns are formed by one silk screen printing. On the other hand, the substrate can be contaminated during the printing because the silk screen touches the substrate directly and the screen can damage the substrate. Therefore the screen printing requires a high degree of contamination control. The dispenser method avoids the contamination problem, but in mass production, in which many LCD cells are cut out from a large mother glass, the dispenser method has lower throughput than the screen printing method (Yamazaki *et al.* 1996). We selected a dispenser method to make plastic LCDs.

After seal printing, we aligned the color filter and TFT substrates then solidified the sealant under 0.1 kg/cm^2 for 3 h at 150 °C. We injected LC into the cell by a conventional vacuum injection technique at a base pressure of 10^{-2} torr.

22.5.3 Driver IC Bonding and Driving

Figure 22.16 shows the tape bonding to the LCD conducting lines with a tape carrier package (TCP) on the TFT array substrate using an anisotropic conducting film (ACF)

Petitioner Samsung Ex-1011, 0489

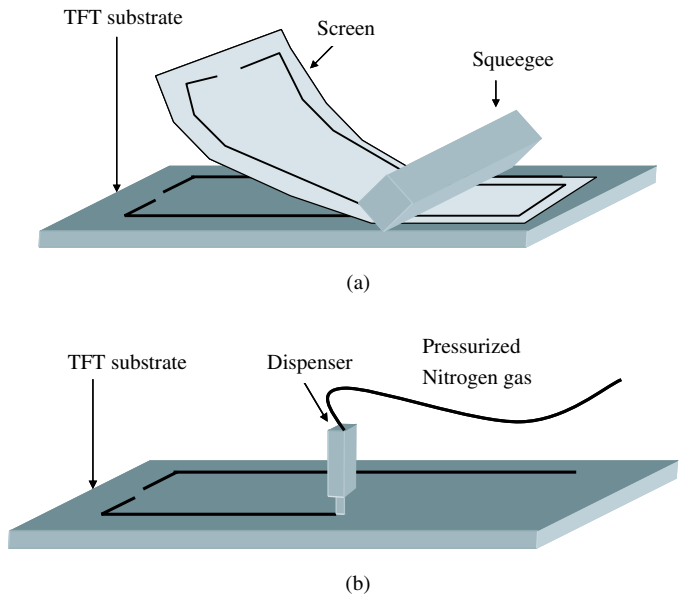


Figure 22.15 Seal formation by (a) screen printing and (b) dispensing

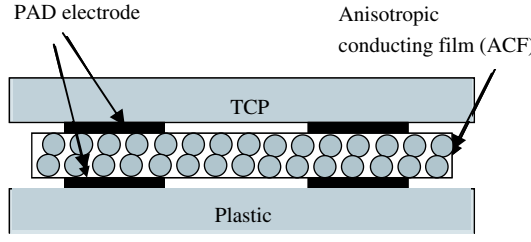


Figure 22.16 Connecting a TCP to a TFT array on plastic using an ACF

(Yamazaki *et al.* 1996). When subjected to pressure bonding, only the two conducting lines become connected. Chip-on-glass (COG) is not easy when the substrate is plastic, so we used tap bonding. However, chip-on-plastic (COP) should be developed to make plastic LCDs for mobile applications such as mobile phones, personal digital assistants (PDAs) and digital still cameras (DSCs).

References

Benmalek, M. and Dunlop, H. M. (1995) Inorganic coatings on polymers. *Surface and Coating Technology* **76 / 77**, 821–826.

Burrows, P. E., Graff, G. L., Gross, M. E., Martin, P. M., Hall, M., Mast, E., Bonham, C., Bennett, W., Michalskib, L., Weaverb, M., Brownb, J. J., Fogarty, co and Sapochakc, L. S. (2000) Gas permeation and lifetime tests on polymer-based barrier coatings. *SPIE Annual Meeting*, San Diego CA, pp. 1–9.

Petitioner Samsung Ex-1011, 0490

Glescova, H. and Wagner, S. (1999) Amorphous silicon thin-film transistors on compliant polyimide foil substrates. *IEEE Electron Device Letters* **20**, 473–475.

Gleskova, H. and Wagner, S. (2001a) Low-temperature silicon nitride for thin-film electronics on polyimide foil substrates. *Applied Surface Science* **175/176**, 12–16.

Gleskova, H. and Wagner, S. (2001b) a-Si:H TFTs on polyimided foil: electrical performance under mechanical strain. *IDW* **2001**, 331–334.

Gleskova, H., Wagner, S. and Suo, Z. (2000) a-Si:H thin film transistors after very high strain. *Journal of Non-Crystalline Solids* **266/269**, 1320–1324.

He, S., Nishiki, H., Hartzell, J. and Nakata, Y. (2000) Low temperature PECVD a-Si:H TFT for plastic substrate. *SID Digest* **2000**, 278–281.

Hur, J. H., Lee, C. B., Won, S. H. and Jang, J. (2002) A 2 inch a-Si:H TFT-LCD on plastic. *SID Digest* **2002**, 802–805.

Jang, J. and Lim, B. C. (1999) a-Si:H TFTs with planarized gate insulator. *SID Digest* **1999**, 728–731.

Kagan, C. R. and Andry, P. (2003) *Thin-Film Transistors*, Marcel Dekker, New York, pp. 38–43.

Mills, M. E., Townsend, P., Castillo, D., Martin, S. and Achen, A. (1997) Benzocyclobutene (DVS-BCB) polymer as an interlayer dielectric (ILD) material, *Microelectronic Engineering* **33**, 327–334.

Murarka, S. P. (1993) *Metallization*, Butterworth Heinemann.

Okada, Y., Ban, A., Okamoto, M., Oka, W., Matsuda, Y. and Shibahara, S. (2002) A 4-inch reflective color TFT-LCD using a plastic substrate. *SID Digest* **2002**, 1204–1207.

Parsons, G. N. (2000) Surface reactions in very low temperature ($< 150\ ^{\circ}C$) hydrogenated amorphous silicon deposition and applications to thin film transistors. *Journal of Non-Crystalline Solids* **266/269**, 23–30.

Polach, S., Hrst, D., Maier, G., Kallfass, T. and Lueder, E. (1999) Matrix of light sensors addressed by a-Si:H TFTs on a flexible plastic substrate. *SPIE Proceedings* **3649**, 31–39.

Retajczyk, T. F. Jr and Sinha, A. K. (1980) Elastic stiffness and thermal expansion coefficients of various refractory silicides and silicon nitride films. *Thin Solid Films* **70**, 241–247.

Sazonov, A., Nayhan, A., Striakhilev, D. (2000) Materials optimization for thin film transistors fabricated at low temperature on plastic substrate. *Journal of Non-Crystalline Solids* **266/269**, 1329–1334.

Sazonve, A., Stryahilev, D. and Nathan, A. (2002) Low temperature a-Si:H TFT on plastic films: materials and fabrication aspects, *International Conference on Microelectronics*, pp. 525–528.

Suo, Z., Ma, E. Y., Gleskova, H. and Wagner, S. (1999) Mechanics of rollable and foldable film-on-foil electronics, *Applied Physics Letters* **75**, 1177–1179.

Won, S. H., Lee, C. B., Nam, H. C., Chung, J. K., Jang, J., Hong, M. P., Kim, B. S., Lee, Y. U., Yang S. H., Huh, J. M. and Chung, K. H. (2003) A high-resolution full color TFT-LCD on transparent plastic. *SID Digest* **2003**, 992–995.

Won, S. H., Hur, J. H., Lee, C. B., Nam, H. C., Chung, J. K. and Jang, J. (2004) Hydrogenated amorphous silicon thin-film transistor on plastic with an organic gate insulator. *IEEE Electron Device Letters* **25**, 132–134.

Yamazaki, T., Kawakami, H. and Hori, H. (1996) Color TFT liquid crystal display, SEMI Standard FPD Technology Group, California, pp. 245–250.

Yang, C. S., Read, W. W., Arthur, C., Srinivasan, E. and Parsons, G. N. (1998) Self-aligned gate and source drain contacts in inverted-staggered a-Si:H thin-film transistors fabricated using selective area silicon PECVD. *IEEE Electron Device Letters* **19**, 180–182.

Petitioner Samsung Ex-1011, 0491

23

All-Plastic Color TFT LCDs Based on Low-Temperature Poly-Si

Akihiko Asano

Sony Corporation

23.1 Introduction

A low-temperature polycrystalline silicon (LTPS) thin film transistor (TFT) has advantages for mobile applications because it can integrate circuits such as gate drivers and D/A converters on an LCD panel. This leads to a reduction in the number of input/output terminals that are formed on the sides of the LCD panel. In addition, fine dot pitch, as narrow as 40 μm for example, can be achieved owing to the higher driving capability of LTPS TFTs than of amorphous silicon (a-Si) TFTs.

These advantages are ascribed to the following features of LTPS:

- The electron mobility of LTPS is higher than that of a-Si by two orders of magnitude; the channel size of the switching TFTs in each pixel can be typically several tens of square microns.
- The CMOS circuitry is possible since on-currents of the p- and n- channel TFTs balance within a factor of 2.

Flexible Flat Panel Displays Edited by G. P. Crawford
© 2005 John Wiley & Sons, Ltd., ISBN 0-470-87048-6

Petitioner Samsung Ex-1011, 0492

On the other hand, a plastic substrate (Smith *et al.* 1997; Gosain *et al.* 2000; Utsunomiya *et al.* 2000, 2001; Asano and Kinoshita 2002, 2003; Okada *et al.* 2002; Kim *et al.* 2003) meets the specifications needed for mobile applications such as PDAs or cellular phones, because plastic material can reduce a device thickness and weight significantly. The relative density of plastic is typically half that of glass. For example, the weight of a 0.4 mm thick plastic panel (total thickness of two 0.2 mm thick plastic substrates) measures only one-fifth that of a 1.0 mm thick glass panel. In addition, plastic does not break easily even if the thickness is less than 0.2 mm; it can improve the shock resistance of devices.

Since a plastic LTPS TFT LCD would be the best solution for mobile applications, various efforts have been made to realize LTPS-based TFTs (Smith *et al.* 1997; Gosain *et al.* 2000) and circuits (Utsunomiya *et al.* 2000) on plastic, and a plastic LCD panel (Utsunomiya *et al.* 2001; Asano and Kinoshita 2002). The biggest problem is that plastic has much lower stability against temperature than glass; transparent noncrystalline engineering plastics such as polycarbonate and polyethelsulfone have upper temperature limits between 200 and 300 °C. Even under the upper limit, since the thermal expansion coefficient is typically above 50 ppm/K, a temperature rise of 100 °C results in thermal expansion of more than 0.5%. In addition, the expansion and shrinkage generally have hysteresis under heat cycles. These deformations cause misalignment or cracking of device patterns made of materials that exhibit much less thermal expansion.

As shown in Figure 23.1, there are two approaches to plastic LTPS TFT LCD. The most straightforward approach is to replace a glass substrate by a plastic and reduce the maximum process temperature to 100–150 °C; this is called a *direct approach*. However, it has not achieved circuit operation to date. The most difficult problems would be deposition of the gate insulating layer for the MOS transistor and hydrogen diffusion to the polycrystalline layer at low temperatures which plastics can endure. In addition, photolithography for fine device patterns on a plastic substrate is generally difficult, since the plastic substrate can irreversibly expand or shrink, possibly nonuniformly from position to position in the substrate, when it goes through the LTPS process with heat cycles and chemical treatments.

The other approach is to prepare a device layer in a routine LTPS TFT process on a glass substrate, then to transfer it onto a plastic substrate; this is called a *transfer approach*. It has three advantages:

- TFTs are prepared without reducing the process temperature, which gives no change in TFT performance. This results in no change in circuit and device designs.

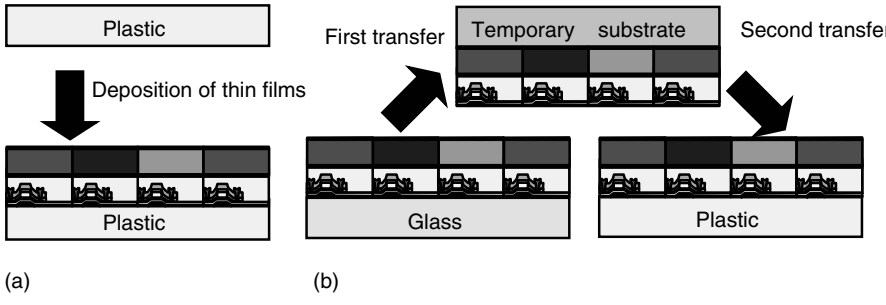


Figure 23.1 Preparing LTPS TFTs on a plastic substrate: (a) a direct process and (b) a transfer process

Petitioner Samsung Ex-1011, 0493

- There are less severe requirements on the properties and quality of the plastic material.
- The transfer process can be retrofitted to the present LTPS mass production processes.

However, it was once believed to be difficult to take a thin film several microns thick and possessing internal stress and micropatterns then transfer it from a glass substrate onto a plastic substrate without creating any defects on the TFT layer.

We have developed a process in which we can transfer a thin TFT layer from a conventional glass substrate, 350 mm × 300 mm in size, onto a plastic substrate of the same size without creating any major defects on TFT arrays. This chapter reviews our transfer process as well as the LTPS TFT process on glass substrate. It also presents the change of LTPS TFT performance on bending the substrate. Finally it shows the display performance in the flat and bent states.

23.2 Overview of the Process

23.2.1 TFT Device Process

The bottom-gate TFT device layer was prepared in an LTPS process on a 0.7 mm thick glass substrate, as described below. Here a new structure of on-panel color filter has been developed to realize the plastic color LCD, in which the color filter is formed on the TFT side. A post spacer is also introduced to ensure a uniform spacer distribution at higher spacer density compared with glass LCDs.

The bottom-gate LTPS TFT process is as follows:

(A1) The gate pattern is formed in the sequence metal sputtering, photolithography, and reactive ion etching.

(A2) A gate insulating layer and an a-Si layer are deposited using plasma-enhanced chemical vapor deposition (PECVD).

(A3) The a-Si layer is crystallized in a XeCl (308 nm) excimer laser annealing (ELA) process.

(A4) A stopper SiO_2 layer is deposited with PECVD and is pattered to protect the TFT channel region against ion implantation.

(A5) There is ion doping and/or implantation to the TFT source, drain, and other resistant regions.

(A6) Interlayer deposition by PECVD is followed by contact-hole boring with photolithography and etching.

For a transmissive LCD, skip to process A9.

(A7) Light-scattering micropatterns are formed with photoresist on each pixel by using photolithography then a thermal reflow process.

(A8) Reflective metal such as silver or aluminum is sputtered and then patterned to a pixel size with photolithography and etching.

Petitioner Samsung Ex-1011, 0494

(A9) RGB color filters with contact holes are formed by photolithography.

(A10) For a transmissive LCD, the planarizing layer is formed with photoresist. Then contact holes are formed with photolithography.

(A11) Transparent pixel electrodes are formed in the sequence sputtering, photolithography, and etching.

(A12) Post spacers are formed with photoresist coating and photolithography.

23.2.2 *Transfer Process*

The transfer process (Asano and Kinoshita 2002) is summarized in Figure 23.2:

(B1) The stopper layer is deposited against etching in hydrofluoric acid on a glass substrate.

(B2) A barrier layer is deposited against impurities and etching solution for the stopper layer that appeared in process B1. The thickness can be less than 1 μm.

(B3) Then the device layer is formed in the bottom-gate LTPS TFT process, as described above.

(B4) Glue to the temporary second substrate with removable, non-water-soluble glue (a). The glue has to sustain the thin film device layer after etching off the glass substrate (process B5), otherwise the thin film breaks and peels off at the end of the etching in hydrofluoric acid.

(B5) Etching off the glass substrate in hydrofluoric acid at room temperature (b). This takes two or three hours. Then the etching stopper is also removed in a different

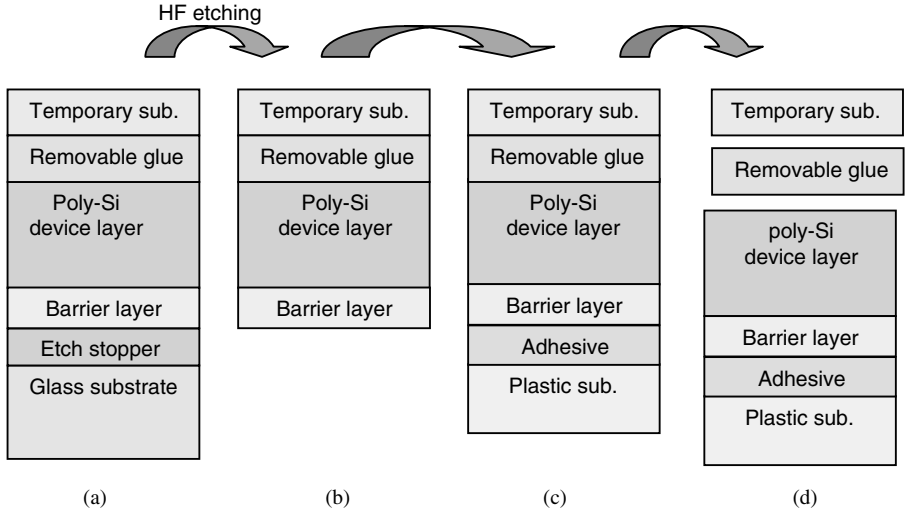


Figure 23.2 Flow diagram of the transfer process to transfer a thin film device layer from a glass substrate onto a plastic substrate

Petitioner Samsung Ex-1011, 0495

etching solution. At this stage, the thin film has been transferred onto the temporary second substrate with the bottom side of the TFT layer facing outside.

(B6) Sticking the transparent plastic substrate on the back surface of the device layer with a permanent, transparent adhesive (c)

(B7) Detaching the temporary second substrate (d). It was one of the most difficult problems in the development of the transfer process to find a solution that can provide good sticking in process B4 and detachability in this process. Note that the transfer has been completed with the original thin film surface facing outside.

This transfer method leaves no significant damage to the device layer, as confirmed by the TFT and display performances shown below. Compared with the direct process, the necessity of surface flatness of the plastic substrate is greatly relieved, since the adhesive layer acts as a buffer layer in between the substrate and the device layer. We believe that the transfer process can also transfer a-Si TFT arrays, color filters, and probably whatever is formed on glass.

23.2.3 Cell Process

The liquid crystal cells are processed in the substrate size 350 mm $\times$ 300 mm. To avoid the camber of panels in the cell process and also with the ambient temperature and humidity variations, the same plastic should be used for the TFT and the counter substrates.

First, the counter substrate is prepared as follows: an indium tin oxide (ITO) layer is deposited with sputtering. Next a polyimide (PI) layer is coated, baked, and rubbed to introduce an alignment to the liquid crystal. Markers can be formed for alignment to the TFT substrate.

A seal pattern is drawn or printed with liquid resin on one of the two substrates, i.e. the TFT or counter substrate. Next the substrates are pressed together under an appropriate alignment. After the seal is hardened by UV irradiation, the substrates are cut to the size of each panel with a laser beam or a mechanical blade.

Injection of liquid crystal into the cell is performed using a similar process as for conventional glass cells. It is characteristic of flexible panels that the cell has to be controlled so that it does not expand in a vacuum chamber. If the cell can blow up, the pressure of the residual air inside the cell decreases to balance the ambient pressure in the chamber, therefore the speed of exhausting air from inside the cell gets very slow, and sometimes the cell cannot be sufficiently exhausted. Finally, the injection beak is filled up with liquid resin and then hardened by UV irradiation.

23.3 Results of the Transfer Process

23.3.1 Transferred Device Pattern

Figure 23.3 shows microscope images of the transferred device layer on a plastic substrate in a pixel and a driver area for a transmissive LCD. The dot size is 63.5 μm $\times$ 95 μm. We find no cracking of the polycrystalline silicon and insulating layers, metal wiring, and ITO pixel

Petitioner Samsung Ex-1011, 0496

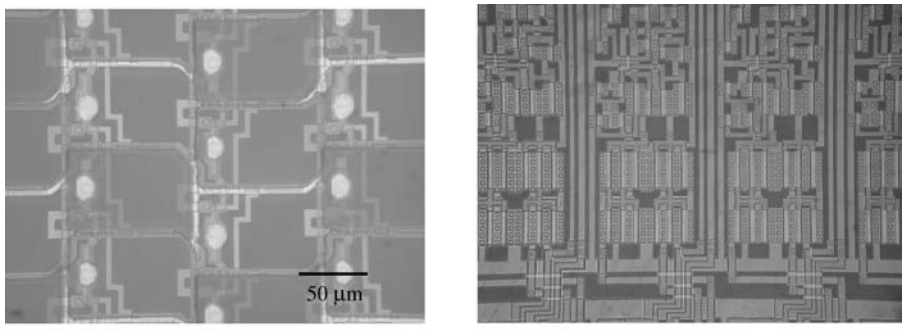


Figure 23.3 Optical microscope images of the transferred device layer patterns on a plastic substrate: (a) a pixel area and (b) a driver area

electrode. We did not change any dimensions such as thickness and patterns of device layers to be transferred, which means their dimensions are exactly the same as for the conventional device on a glass substrate. The process we have presented can transfer the thin layer, several microns thick, onto a 300 mm × 350 mm plastic substrate like printing. Figure 23.4 shows the flexible LTPS TFT on a 300 mm × 350 mm and 0.2 mm thick plastic substrate with nine dies for 3.8 in. diagonal LCDs. Color filters and post spacers have been formed on the TFT substrate.

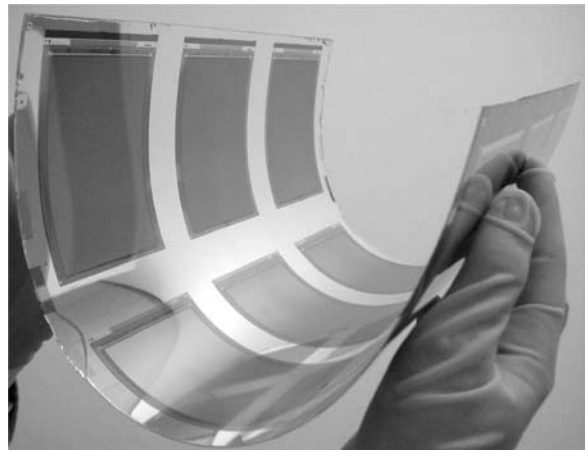


Figure 23.4 A flexible LTPS TFT on a 300 mm × 350 mm and 0.2 mm thick plastic substrate with nine dies for 3.8 inch diagonal LCDs. Color filters and post spacers have been formed on the TFT substrate. The radius of curvature is about 75 mm. Reproduced by permission of SID

23.3.2 *Influence on TFT Characteristics*

Figure 23.5 shows a set of typical transfer characteristics for TFTs before (on glass) and after (on plastic) the transfer process. The channel is 20 μm wide and 7 μm long. We see no

Petitioner Samsung Ex-1011, 0497

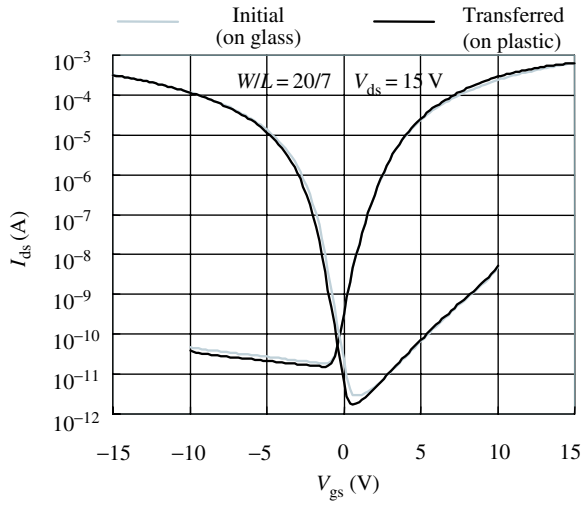


Figure 23.5 A set of typical transfer characteristics of TFTs: grey tint is before the transfer process (on glass) and solid black is after the transfer process (on plastic). Reproduced by permission of SID

significant change between them, which suggests no significant damage to the device layer during the transfer process.

Next the change in the minimum driving voltage was investigated for the scanning and data drivers that are integrated on the panel. Figure 23.6 shows the change in the minimum driving voltage, which is defined as the minimum drain voltage for the drivers to operate. The circuits were integrated on the 1.5 in. transmissive LCD (Section 23.5.1). The operation of the drivers was judged by watching to see if the output pulse from the last stage of the driver followed the starting pulse fed to the initial stage of the driver. The data driver was

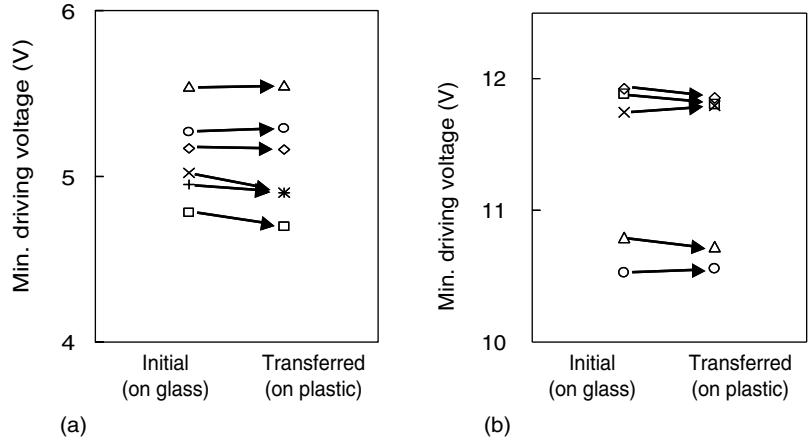


Figure 23.6 The change in the minimum driving voltage for (a) scanning and (b) data drivers on a 1.5 in transmissive LCD before and after the transfer process

Petitioner Samsung Ex-1011, 0498

driven at 1.5 MHz, and the scanning driver was driven at 8.3 kHz. Since the operating frequency was much higher for the horizontal data drivers than that for vertical scanning drivers, the minimum voltage was higher for the data drivers. There was no significant change by the transfer process.

23.4 Changes in TFT Characteristics with Substrate Bending

Before considering display performance, let us look at the fundamental behavior of LTPS TFTs on a flexible substrate; TFT performance was measured on a plastic substrate with substrate bending.

The TFT samples for the bending experiment were prepared on 188 μm thick polyethylene terephthalate (PET) films using the transfer process. The TFT channel is again 20 μm wide and 7 μm long. The sample TFTs have rather large terminal pads of 2 mm × 3 mm to ensure electrical connection to the TFT electrodes through thin wires connected to the pads.

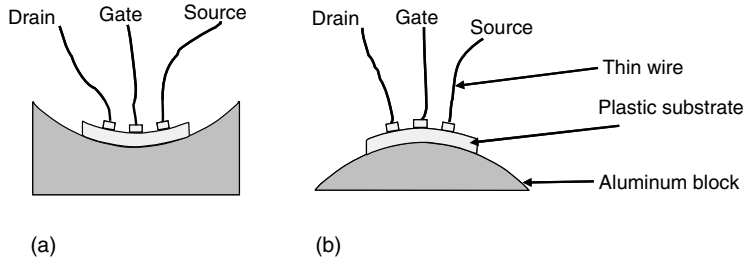


Figure 23.7 Sample configurations for measuring TFT characteristics with substrate bending: (a) compressive and (b) tensile

Figure 23.7 shows the sample configurations for measurement of the TFT characteristic with substrate bending. As shown in the figure, TFT samples were placed on the surface of aluminum blocks with various curvatures in order to bend the sample with known curvature, and the TFT characteristics were measured through thin probing wires. The bending configurations were arranged parallel to the drain–source current direction, as shown in Figure 23.7. Since the channel area is very small, bending the substrate results in a simple compressive or tensile stress in one direction in the polycrystalline silicon layer.

If the substrate is bent, the polycrystalline silicon layer is strained in proportion to the radius of curvature. The strain is a function of the radius and the thicknesses and Young's moduli of the film and the substrate. It can be calculated as follows (Suo *et al.* 1999):

$$\varepsilon_{\text{top}} = \frac{d_{\text{f}} + d_{\text{s}}}{2R}\left[\frac{1 + 2\eta + \chi\eta^2}{(1+\eta)(1+\eta\chi)}\right]$$

with

$$\chi = Y_{\text{f}}/Y_{\text{s}}$$

Petitioner Samsung Ex-1011, 0499

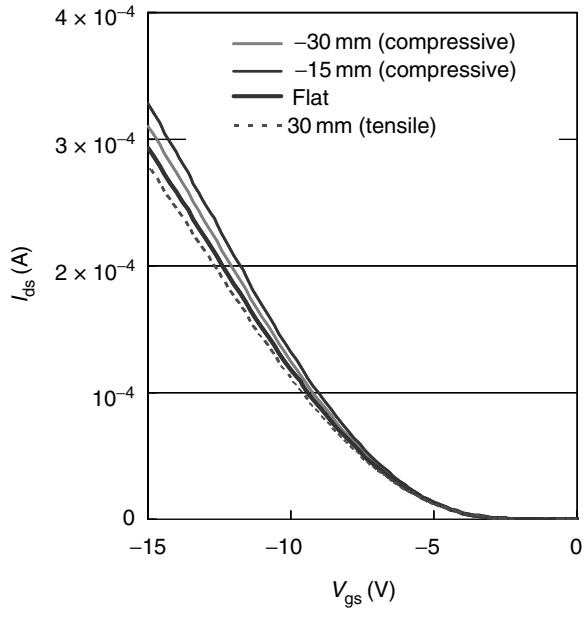


Figure 23.8 Plots of p-channel TFT performance (I_{ds} versus V_{gs}) at various curvatures

and

$$\eta = d_f / d_s.$$

ε_{top} is the strain of the top, i.e. in polycrystalline silicon, R is the radius of curvature, d_s and d_f are the thicknesses of substrate and thin film, respectively, Y_s and Y_f are the Young's moduli of substrate and thin film, respectively.

For example, a radius of curvature of 15 mm causes a strain of 0.75%. Note that mechanical destruction sometimes determined the maximum strain.

Figure 23.8 shows I_{ds}–V_{gs} curves for the p-channel TFT under various curvatures, where I_{ds} is the drain current and V_{gs} is the gate voltage. The vertical axis is on a linear scale to show the change in I_{ds} with bending.

Figure 23.9 shows the change in on-current defined as the drain current under the drain and gate voltages of 10 V and 15 V, respectively, with substrate bending in the sequence flat, 125 mm, 75 mm, and 30 mm radii, then flat again. The on-current decreases under tensile stress, but the initial TFT performance can be retrieved after substrate bending.

Figure 23.10 summarizes the bending test for several TFTs on plastic substrates and shows the change in on-current as functions of the strain in the polycrystalline silicon layer and radius of curvature. The positive side is tensile and the negative side is compressive. The vertical axis is a change in on-current from the flat state. The on-current changes in proportion to the strain; the on-current of the p-channel TFT increases by 12% under the compressive strain of 0.75%. Opposite changes in on-currents of n- and p-channel TFTs are observed; the on-current of p-channel increases under the compressive strain, whereas the on-current of n-channel increases under the tensile strain. These changes can change the balance between the p- and n- channel TFTs in CMOS circuitry; a greater margin in circuit design is needed for a flexible device.

Petitioner Samsung Ex-1011, 0500

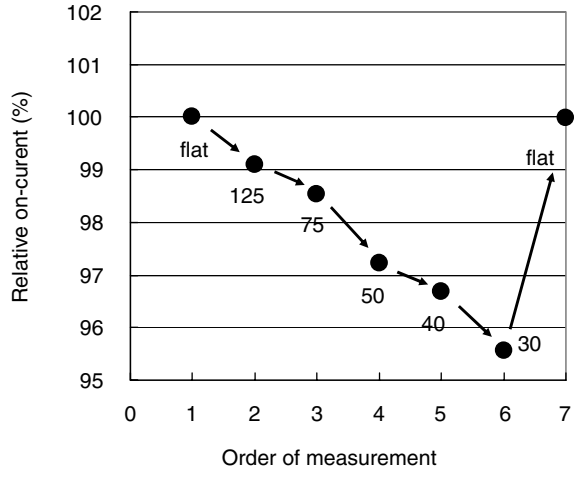


Figure 23.9 The change in on-current with substrate bending for a p-channel TFT. The radius of curvature (mm) is shown

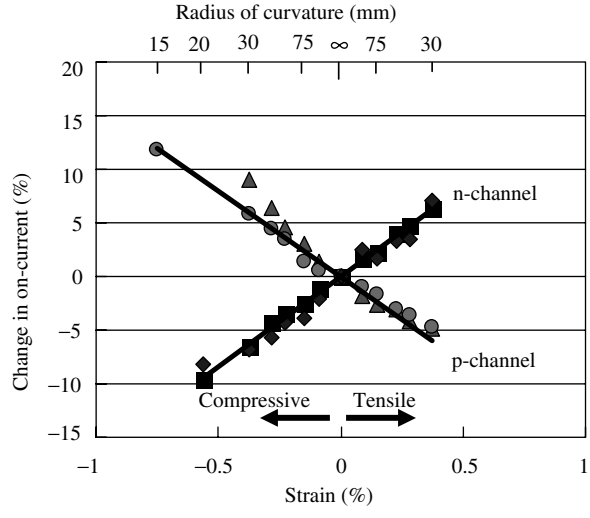


Figure 23.10 The change in on-current as a function of the strain in the polycrystalline silicon layer and as a function of the radius of curvature. Reproduced by permission of SID

The origin of the change in on-current by strain is investigated in terms of carrier mobility. Figure 23.11 shows the change in electron and hole mobilities as functions of the strain in the polycrystalline silicon layer. The drain voltage was 1 V.

The mobility changes in proportion to the strain; the mobility of the p-channel TFT increases by 16% under the compressive strain of 0.75%. In addition, opposite changes in n- and p-channel mobilities are observed. This behavior implies that the change in on-current

Petitioner Samsung Ex-1011, 0501

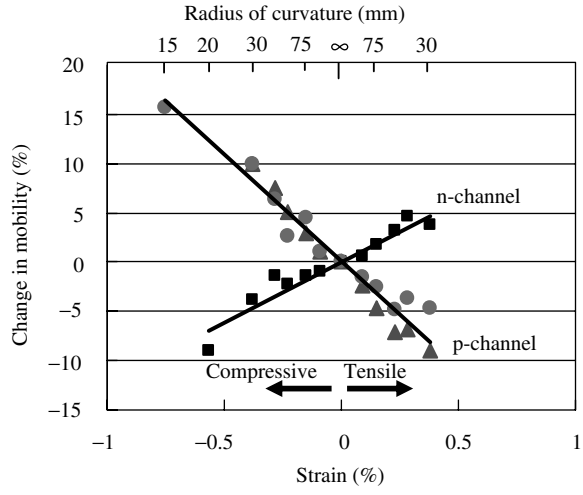


Figure 23.11 The change in electron and hole mobilities as functions of the strain in the polycrystalline silicon layer. Reproduced by permission of SID

is mainly ascribed to the change in mobility. We guess the mechanism of the change in mobility is the same as that of single-crystal strained silicon.

23.5 Display Properties of Plastic LCDs

23.5.1 Specification and Structure

Two types of LCDs, i.e. transmissive and reflective, have been developed with the plastic substrate. The thickness of each plastic substrate is 0.2 mm; the panel thickness is only 0.4 mm.

The specification of the transmissive LCD, which is compatible with a panel for digital still cameras, is 1.5 in. diagonal size, 490 (horizontal) × 240 (vertical), i.e. 117 600 dots in display area in delta-alignment, full-color analog dot-sequential drive, 1.5 MHz clock frequency, 12 V drive voltage, and scanning and data drivers and level shifters integrated on the panel.

The specifications of the reflective LCD, which is compatible with a panel for a PDA, is 3.8 in. diagonal, 320 × RGB(H) × 240(V), i.e. 230 400 dots in vertical stripe arrangement with built-in peripheral driving circuitry such as scanning and data drivers, and 4-bit digital-to-analog converters integrated on the panel. The plastic panel operates under the same driving voltage as for a glass panel, i.e. 9 V.

The structures of the panels are shown in Figures 23.12 and 23.13. The feature is color filters formed on the TFT substrate. For the transmissive LCD shown in Figure 23.12, it is located under the planarizing layer. For the reflective LCD, it is located in between the reflection metal layer and the transparent pixel electrode. This on-panel color filter relieves the alignment accuracy; if the color filter were located on the counter substrate, it would be difficult to align the pixels on the TFT substrate with the color filters on the counter

Petitioner Samsung Ex-1011, 0502

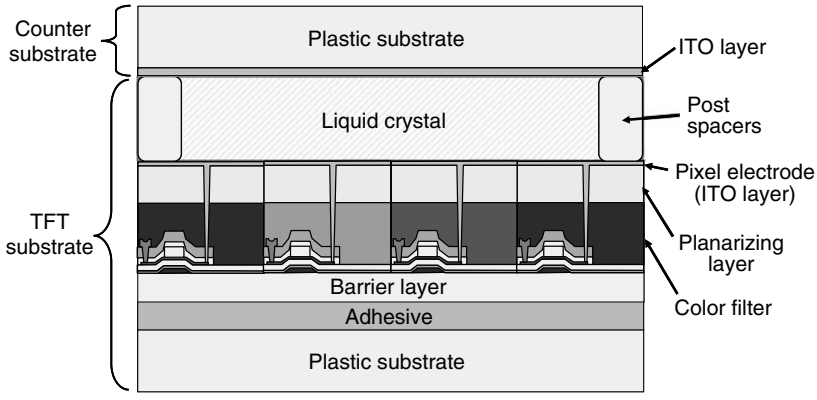


Figure 23.12 Structure of a transmissive color plastic LCD. Polyimide layers are abbreviated

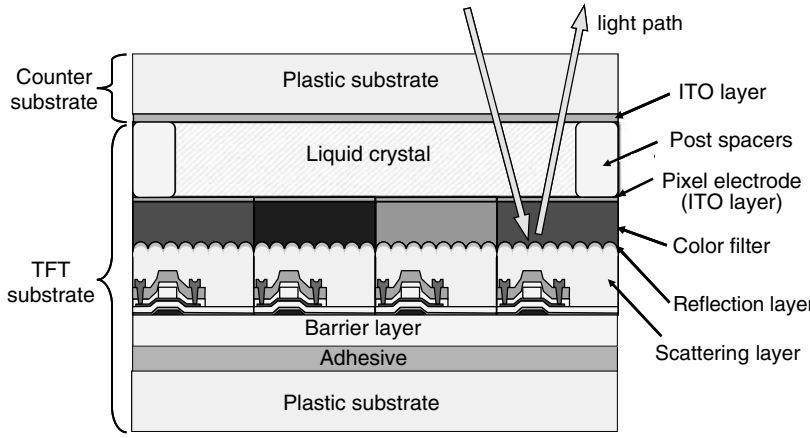


Figure 23.13 Structure of a reflective color plastic LCD. Polyimide layers and contact holes are abbreviated

substrate, since the substrates can expand and shrink differently from position to position in each substrate.

In addition, we could avoid the difficulty of preparing color filters on a plastic substrate. The counter substrate does not need the transfer process because only the ITO and the alignment polyimide layers are necessary on the counter substrate, which can be directly deposited on the plastic substrate.

23.5.2 *Display Performance*

Figure 23.14 shows an image displayed on the plastic transmissive color TFT LCD. This 1.5 in. diagonal panel weighs only 0.5 g. The much lower damage caused by the transfer

Petitioner Samsung Ex-1011, 0503



Figure 23.14 An image displayed on the plastic transmissive color LTPS TFT LCD. This 1.5 in. diagonal panel weighs only 0.5 g

process is confirmed by the image quality; we see only a few point defects. Of course, when displaying motion pictures, we see no difference in performance between plastic and conventional glass LCDs.

23.5.3 Displayed Image on Curved LCD

Figure 23.15 shows the image on the plastic reflective color TFT LCD. This 3.8 in. diagonal panel weighs only 3 g. It was taken with a polarizer plate in front of the 3.8 in. panel.

Figure 23.16 shows the displayed image on the same panel being bent. The radius of curvature is about 75 mm. This radius is, to our knowledge, the smallest reported for TFT LCDs. Since the amount of electric wiring for the LTPS LCD is much smaller than that for the a-Si LCD and only one side of the panel is occupied by electric wiring, the plastic LTPS LCD is easier to bend than the a-Si LCD. Using the post spacers formed by photolithography, which are immobile even if the panel is bent, the cell gap remains practically unchanged throughout the panel, even in the bent state. In addition, the flat-top shape of the post spacers reduces the cracking force to the ITO layer on the counter substrate.

23.6 Problems to Solve

Although the transfer process described here alleviates the necessity of severe thermal properties for a plastic substrate, there remains the problem of a difference in the thermal expansion coefficients between the substrate and the device layer. The upper limit of ambient temperature for the plastic LCD is at most 60–80 °C if the thermal expansion coefficient of the plastic substrates is 50–70 ppm/K. The development of a plastic material with lower

Petitioner Samsung Ex-1011, 0504



Figure 23.15 An image displayed on the 3.8 in. plastic reflective color LTPS TFT LCD. This panel weighs only 3 g



Figure 23.16 Displayed image on curved reflective color TFT LCD. The radius of curvature is about 75 mm

Petitioner Samsung Ex-1011, 0505

thermal expansion is essential to the realization of a practical plastic TFT LCD. We deduce that the thermal expansion coefficient has to be decreased to 10–15 ppm/K in the temperature range below 100–120 °C, which corresponds to the upper limit of ambient temperature.

Next reliability must be established. A major mode is that the pixel voltage decays in the period of one field if the ambient water vapor diffuses to the liquid crystal. We expect that a technology for the barrier layer on plastic substrate against water vapor will certainly attain an adequate performance in the near future.

23.7 Summaries and Future Prospect

We have demonstrated transmissive and reflective plastic LTPS TFT color LCDs that are prepared with our original transfer process. The reflective LCD of only 3 g displays 320 × 240 pixels in both flat and bent states. Considering the features of low thickness, light weight, and shock resistance plus the compatibilities in device design and production with conventional glass LCDs, we believe that once the plastic TFT LCD appears for mobile applications, it will rapidly prevail over the glass LCDs.

Incidentally, a plastic LCD sacrifices the inherent flexibility of a plastic substrate, since it has a structure of two substrates glued together with a seal typically 1 mm wide. The structure limits the bending of the panels, since the bending stress is concentrated on the seal and the panel finally breaks at the seal. In the future, we expect that the transfer process will be applied to an ultra thin display of plastic OLEDs comprising a single sheet of substrate.

Acknowledgements

The author is grateful to Mr Tomoatsu Kinoshita for being a codeveloper of the plastic LCD based on the transfer process, from the beginning of the project. He also acknowledges all the members of the LTPS TFT LCD pilot line for their skilful operations.

References

Asano, A. and Kinoshita, T. (2002) Low-temperature polycrystalline-silicon TFT color LCD panel made of plastic substrates. *SID Digest* **2002**, 1196–1199.

Asano, A. and Kinoshita, T. (2003) A plastic 3.8-in. low-temperature polycrystalline silicon TFT color LCD panel. *SID Digest* **2003**, 988–991.

Gosain, D. P., Noguchi, T. and Usui, S. (2000) High mobility thin film transistors fabricated on a plastic substrate at a processing temperature of 110 °C. *Japanese Journal of Applied Physics* **39**, L179–L181.

Kim, Y. H., Park, S. K., Moon, D. G., Han, J. I., Kim, I. H. and Jang, J. (2003) Fabrication of polycrystalline silicon thin films on plastic substrates for flexible active-matrix displays. *Proceedings of Asia Display/IDW* **2003**, 395–398.

Okada, Y., Ban, A., Okamoto, M., Oka, W., Matsuda, Y. and Shibahara, S. (2002) A 4-inch reflective color TFT-LCD using a plastic substrate. *SID Digest* **2002**, 1204–1207.

Smith, P. M., Carey, P. G. and Sigmon, T. W. (1997) Excimer laser crystallization and doping of silicon films on plastic substrates. *Applied Physics Letters* **70**, 342–344.

Petitioner Samsung Ex-1011, 0506

Suo, Z., Ma, E. Y., Gleskova, H. and Wagner, S. (1999) Mechanics of rollable and foldable film-on-foil electronics, *Applied Physics Letters* **74**, 1177–1179.

Utsunomiya, S., Inoue, S. and Shimoda, T. (2000) Low temperature poly-Si TFTs on plastic substrate using surface free technology by laser ablation/annealing. *SID Digest* **2000**, 916–919.

Utsunomiya, S., Saeki, T., Inoue, S. and Shimoda, T. (2001) Low temperature poly-Si TFT LCD transferred onto plastic substrate using surface free technology by laser ablation/annealing. *Proceedings of Asia Display/IDW* **2001**, 339–342.

Petitioner Samsung Ex-1011, 0507

24

TFT Transfer Technology

Sumio Utsunomiya, Satoshi Inoue, and Tatsuya Shimoda

Seiko Epson Corporation

24.1 Introduction

The flexible display belongs to the category of flat panel displays (FPDs). In place of a glass substrate, a thin flexible substrate, usually a plastic film, is used to fabricate the flexible display device. Various kinds of flexible displays, such as liquid crystal displays (LCDs) (Okada *et al.* 2002; Slikkerveer *et al.* 2002), electrophoretic displays (EPDs) (Ritter 2001) and organic light-emitting diode (OLED) displays (Sugimoto 2001), have been developed by researchers in recent years.

The FPD is mainly composed of a display imaging component and a circuit backplane that drives the display element. Over the history of FPD development, improvements in the display driving circuit have played an important role. The problems of a passive matrix display in the early days were the crosstalk or the flickers, but they were almost completely eliminated by the emergence of an active matrix driving circuit, in which an active element such as a thin film transistor (TFT) and a metal–insulator–metal thin film diode (MIM TFD) is arranged in every pixel. The good image quality of today's LCDs is greatly indebted to the active matrix display circuit. In the OLED display, several TFTs are necessary in the OLED pixel driving circuit to achieve a uniform and bright image (Dawson *et al.* 1998; Goh *et al.* 2001, 2003; Wang *et al.* 2001; Kimura *et al.* 2000; Mizukami *et al.* 2000; Sasaoka *et al.* 2001; Tsujimura *et al.* 2003).

Flexible Flat Panel Displays Edited by G. P. Crawford
© 2005 John Wiley & Sons, Ltd., ISBN 0-470-87048-6

Petitioner Samsung Ex-1011, 0508

Another advantage of manufacturing the active elements on the display backplane came from the development of polycrystalline silicon TFTs (poly-Si TFTs). Since the carrier mobility of a poly-Si TFT is much higher than an amorphous silicon TFT (a-Si TFT), it is possible to fabricate a complementary metal–oxide semiconductor (CMOS) circuit using the poly-Si TFT. Therefore a display driver circuit composed of CMOS TFTs can be integrated around the display area. The driver circuit integration is helpful to reduce the number of interconnections between the display device and the peripheral driver ICs. This is very important for flexible displays because having a lot of interconnections around the display area obstructs the flexibility of the complete display device, even though the backplane itself is flexible enough. TFT circuits similar to poly-Si TFT are necessary to realize a high-quality and fully flexible display device.

Manufacturing of the active elements such as the MIM TFD, the a-Si TFT and the poly-Si TFT (Young *et al.* 1997; Baeuerle *et al.* 1999; Serikawa *et al.* 1989; McCormick *et al.* 1997; Sandoe 1998; Klauk *et al.* 1999; Gosain *et al.* 2000) has been investigated. Most of the research work points to the problem of fabricating the active elements directly on the flexible plastic film. Because the heat resistance of the plastic film is much lower than for the conventional glass substrate, the maximum process temperature should be drastically reduced usually below 150 °C. However, the active elements fabricated at a low temperature tend to have a lower performance than those fabricated at high temperature, because high temperature is sometimes essential to achieve a pure and defectless material. Another difficulty of the direct fabrication process is the dimensional instability of the plastic films, because the plastic films can easily expand or shrink due to the temperature variation or moisture absorption. Figure 24.1 plots the thermal expansion and the humidity expansion for typical plastic materials where the material length is 100 mm. When the temperature changes by 1 °C and the humidity changes by 1%, the length changes by several micrometers. Thus the precise mask alignment during conventional photolithography is extremely difficult. (For example, the precision limit for 2μm is indicated in the figure.)

In order to circumvent such difficulties due to the nature of the plastic materials, a transfer process has been developed (Shimoda and Inoue 1999; Utsunomiya 2002; Utsunomiya *et al.*

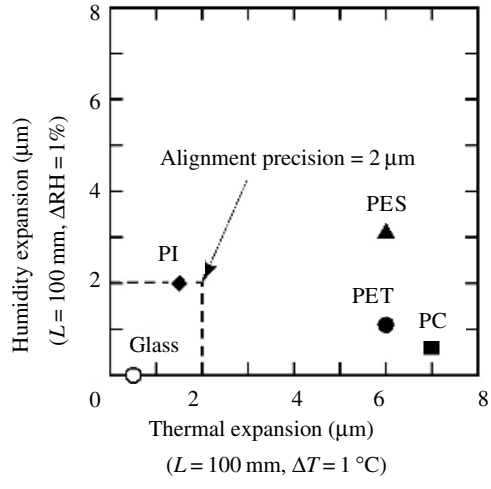


Figure 24.1 Dimensional instability of typical plastic materials

Petitioner Samsung Ex-1011, 0509

2000, 2001, 2002a, 2002b, 2003; Inoue *et al.* 2003). In this method, a high-performance and finely patterned TFT device is fabricated on a quartz or glass substrate using a conventional low-temperature poly-Si TFT (LTPS TFT) process. Then the TFT device is lifted off the original glass substrate, and attached again on the final plastic film. Therefore good TFT performance as conventional LTPS TFT is expected even on the plastic film unless the TFT characteristics degrade during the transfer process. The transfer process relies particularly on a laser irradiation technique that is favored for its high process throughput. This technique was named SUFTLA– surface free technology by laser ablation/annealing.

24.2 TFT Transfer Process Sequence

The TFT transfer process is usually completed after two transfer steps. The TFT layer is transferred from an original substrate to a temporary substrate during the first transfer step, and it is transferred from the temporary substrate to a final substrate during the second transfer step. This process sequence gives us the situation that the exposed surface of the TFT layer after transfer is the same as the exposed surface before transfer, and that only the substrate is exchanged from the original glass substrate to the final plastic film.

Figure 24.2 shows the schematic illustrations of the TFT transfer process sequence. At the beginning, a 100 nm thick a-Si thin film is deposited by chemical vapor deposition (CVD) on the original glass substrate (Figure 24.2(a)). This a-Si thin film works as a sacrificial layer during the first transfer step. Then a CMOS poly-Si TFT device is fabricated on the a-Si sacrificial layer by using a conventional low-temperature poly-Si (LTPS) TFT process in which the maximum temperature is less than 425 °C (Figure 24.2(b)). Fine circuit design

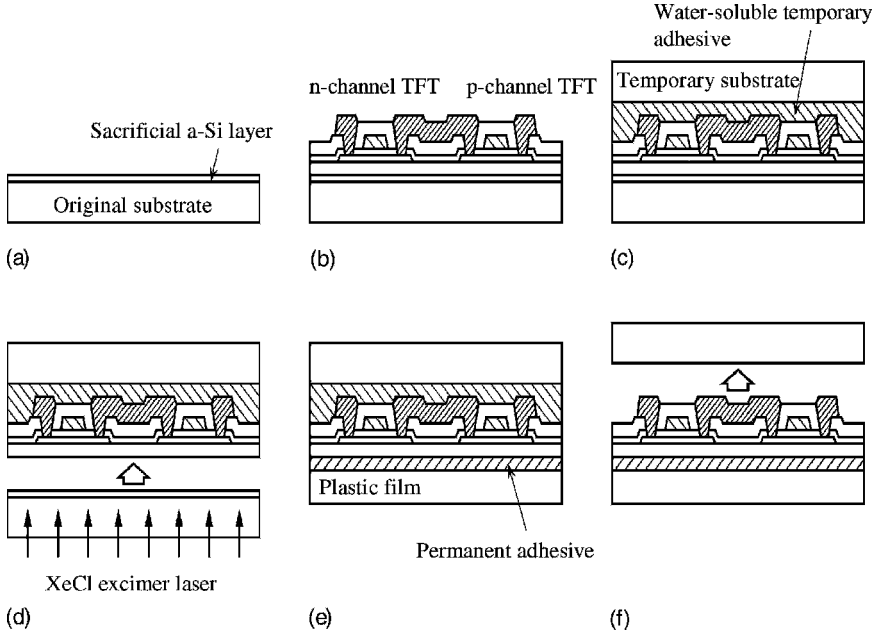


Figure 24.2 Schematic diagram of the TFT transfer process sequence

Petitioner Samsung Ex-1011, 0510

rules of the conventional LTPS TFT process can then be achieved, because TFT fabrication is carried out on the rigid glass substrate.

Next the surface of the TFT device layer is glued on the temporary glass substrate using a water-soluble temporary adhesive that is cured by UV irradiation (Figure 24.2(c)). Then the sacrificial a-Si layer is irradiated by an XeCl excimer laser (wavelength 308 nm) from the backside of the original glass substrate (Figure 24.2(d)). The sacrificial a-Si layer is irradiated by the incident excimer laser through the original glass substrate, and the a-Si layer is melted and recrystallized by abrupt heating due to the absorption of the laser energy. During the excimer laser irradiation, hydrogen atoms contained in the CVD-deposited a-Si layer are released at the interface between the sacrificial a-Si layer and the TFT layer. This phenomenon reduces the adhesion force at this interface, and results in easy separation of the TFT device from the original substrate at this interface, as shown in Figure 24.2(d). The sacrificial layer remaining on the original substrate can be etched off by being exposed to CF_4/O_2 plasma, and the original substrate can be reused.

During the laser irradiation step, the TFT device is not directly damaged by the incident excimer laser because the incident laser is completely absorbed by the sacrificial a-Si layer. Figure 24.3 shows the light absorption coefficient of silicon thin films as a function of the wavelength of the incident light. The light absorption coefficient of the silicon thin films for light of wavelength 308 nm is 1.8×10^{-1} nm^{-1}, which means that the incident XeCl excimer laser is completely absorbed in only 5.6 nm thick silicon thin film. Therefore the 100 nm thick sacrificial a-Si layer is enough to prevent direct incidence of the excimer laser to the TFT device layer.

After the TFT device is transferred onto the temporary substrate, the backside of the TFT device is glued onto the final substrate using permanent adhesive (Figure 24.2(e)). A flexible plastic film is usually used as the final substrate. Then the sample is soaked in water to dissolve the temporary adhesive, and the temporary substrate is spontaneously removed from the TFT device that is bonded onto the flexible final substrate (Figure 24.2(f)).

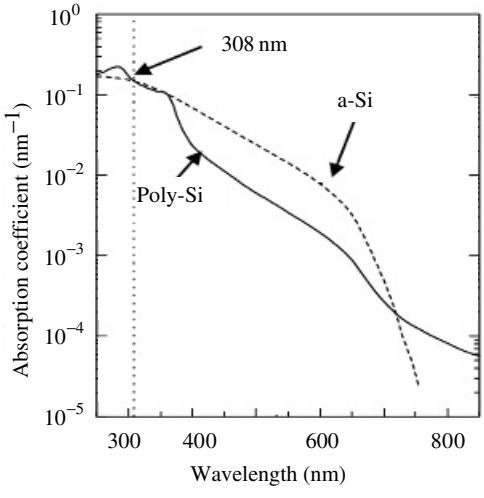


Figure 24.3 Light absorption coefficients of silicon films as a function of wavelength for the incident light

Petitioner Samsung Ex-1011, 0511

24.3 Transfer Mechanism

The TFT transfer mechanism is mainly due to the release of hydrogen atoms contained in the sacrificial a-Si layer during excimer laser irradiation (Sameshima 1996). The hydrogen is considered to have originated from monosilane (SiH_4) or disilane (Si_2H_6) gases, which are the ingredients of silicon thin films deposited by CVD. In this chapter we show some experimental data that support this theory.

In order to clarify the transfer mechanism, a simplified test piece was prepared (Figure 24.4). A 100 nm thick SiO_2 thin film, a 100 nm thick a-Si thin film and a 500 nm

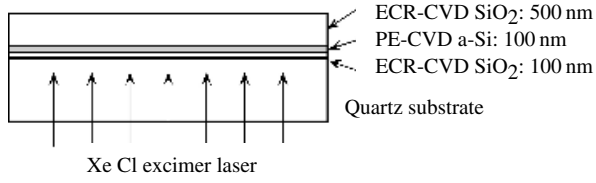


Figure 24.4 Cross-sectional structure of a test piece

thick SiO_2 thin film were deposited on a quartz substrate in a sequential manner. The SiO_2 thin film and the a-Si thin film were deposited by electron cyclotron resonance CVD (ECR CVD) and plasma-enhanced CVD (PECVD), respectively. After the thin film deposition, the specimen was heated at 450 °C for 1 h in order to simulate the thermal history during LTPS TFT fabrication. Then an XeCl excimer laser was used to irradiate the backside of the quartz substrate at an energy density of 300 mJ cm^{-2}, and the properties of the sacrificial silicon layer were evaluated, comparing them with and without laser irradiation.

Figure 24.5 shows the results of the thermal desorption spectroscopy (TDS) analysis, giving the quantity of hydrogen gas released from the sacrificial silicon layer at the elevated temperature. The cap SiO_2 layer was removed before the TDS analysis. The difference between with and without laser irradiation is clearly shown in peak intensity at 850 °C; in contrast, intensity levels of hydrogen below 500 °C are almost the same with and without

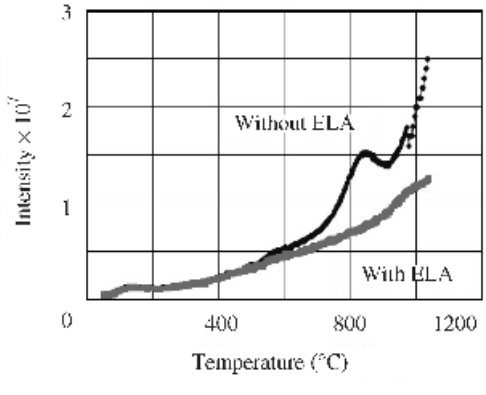


Figure 24.5 TDS analysis for hydrogen contained in the sacrificial silicon layer

Petitioner Samsung Ex-1011, 0512

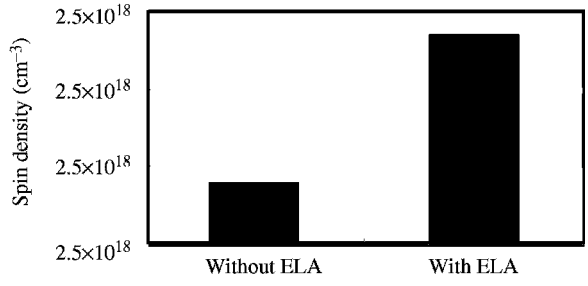


Figure 24.6 ESR analysis for the sacrificial silicon layer

laser irradiation. The results support the facts that hydrogen stays in the sacrificial silicon layer even after thermal history during LTPS TFT fabrication, and that the remaining hydrogen is released from the sacrificial silicon layer during melting and recrystallization due to the laser irradiation.

Figure 24.6 shows electron spin resonance (ESR) data obtained from the specimens with and without laser irradiation. It shows that the spin density of the sacrificial silicon layer is almost doubled by the laser irradiation. In addition, the observed g values were 2.005, which indicates that the observed defects were the dangling bonds in the silicon layer. It is predicted that hydrogen atoms, which were bonded with silicon atoms before laser irradiation, were released from the sacrificial silicon layer and the dangling bonds were produced in the silicon layer.

These results clearly show that hydrogen contained in the sacrificial silicon layer is released due to the excimer laser irradiation. The next question is where the released hydrogen goes. Because the sacrificial silicon layer is put between the original substrate and the TFT layer, it is supposed that the released hydrogen is concentrated at the interface. Some microscopic observations revealed the morphological transition of the interface by the laser irradiation. Figure 24.7 shows a cross-sectional TEM image of the sacrificial silicon

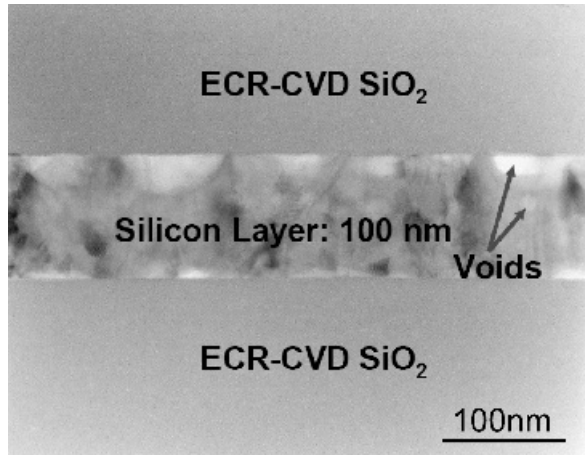
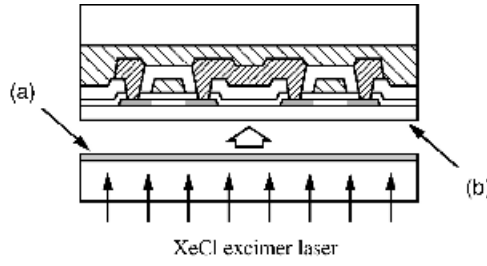


Figure 24.7 Cross-sectional TEM image of the sacrificial silicon layer after laser irradiation

Petitioner Samsung Ex-1011, 0513



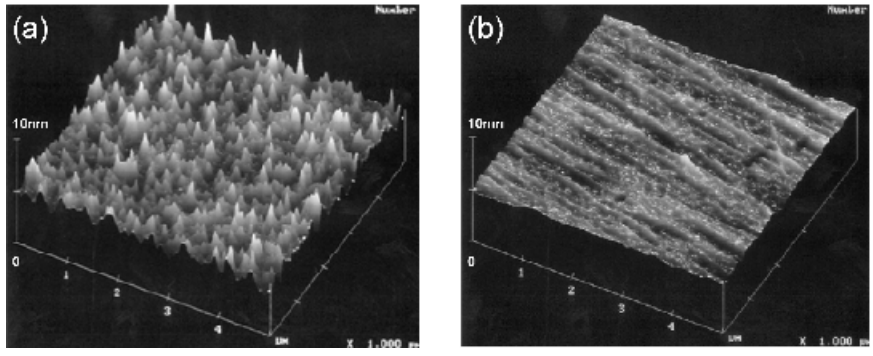


Figure 24.8 AFM images of the surface of (a) the sacrificial silicon layer and (b) the TFT underlayer of SiO_2 after transfer

layer after the laser irradiation. Numerous voids are observed at the interface between the sacrificial silicon layer and the SiO_2 layer. The surface morphology of the sacrificial layer was also observed by atomic force microscopy (AFM), as shown in Figure 24.8, after the TFT device was separated from the original substrate. The average surface roughness (R_a) of the sacrificial layer (a) was 0.56 nm, conceivably caused by the void formation in Figure 24.7. Meanwhile the surface roughness of the TFT backside (b) remained as smooth as 0.27 nm even after transfer.

To summarize the experimental results, the transfer mechanism of the SUFTLA process is qualitatively explained as follows. The sacrificial silicon layer is melted and recrystallized by the laser irradiation, and hydrogen contained in the sacrificial silicon layer is released. The evaporation pressure breaks the chemical bonding between the sacrificial layer and the SiO_2 layer of the TFT backside and then the voids are formed at the interface. The void formation reduces the contacting area, which reduces the adhesive force at the interface.

24.4 TFT Performance

The key issue of the SUFTLA technology is whether the TFT device transferred on the flexible plastic film performs as well as conventional LTPS TFT fabricated on the glass substrate. Figure 24.9 shows the transfer characteristics of the TFT measured on the glass substrate before transfer and on the polyethersulfone (PES) film after transfer. No characteristic degradation was observed due to the transfer process. Some characteristic

Petitioner Samsung Ex-1011, 0514

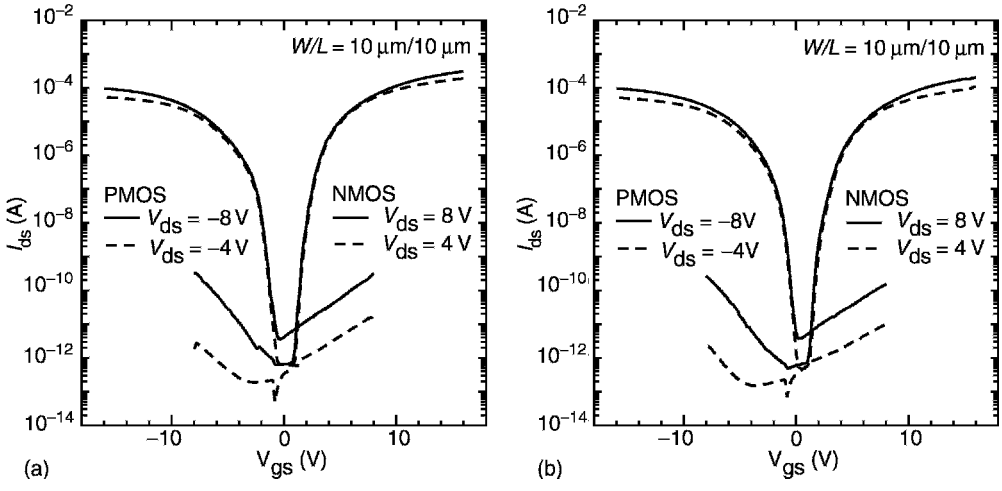


Figure 24.9 Transfer characteristics of the TFTs measured (a) before and (b) after transfer

parameters were calculated from the data measured on the PES film at a constant source–drain voltage (V_{ds}) of $\pm$ 8 V. For n-channel TFTs, we calculated the saturation mobility (μ_{sat}) as 124 $cm^2V^{-1}s^{-1}$, the threshold voltage (V_{th}) as 3.85 V and the subthreshold swing (s) as 0.20 V/decade. For p-channel TFTs, we calculated μ_{sat} as 63 $cm^2V^{-1}s^{-1}$, V_{th} as -2.36 V and s as 0.27 V/decade. These results support the fact that the TFT transferred on the plastic film by SUFTLA technology performs as well as a conventional LTPS TFT fabricated on the glass substrate. Having proved the individual TFT performance on the plastic film, we examined the operation of a basic circuit. Figure 24.10(a) shows an output waveform observed for a 15-stage ring oscillator transferred on the PES substrate, and Figure 24.10(b) shows its maximum operating frequency as a function of applied driving voltage. The output oscillation frequency at a driving voltage of 7 V was 1.2 MHz, which corresponds to a 27 ns

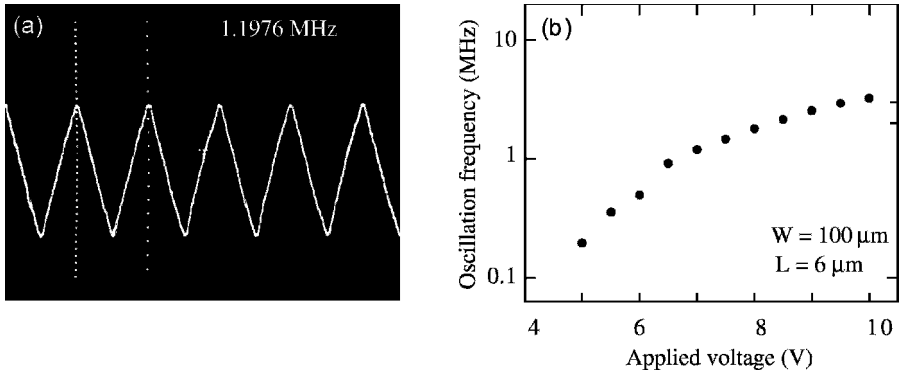


Figure 24.10 Operation of the 15-stage ring oscillator measured after transfer to the PES film: (a) output waveform and (b) the maximum operative frequency as a function of the applied voltage

Petitioner Samsung Ex-1011, 0515

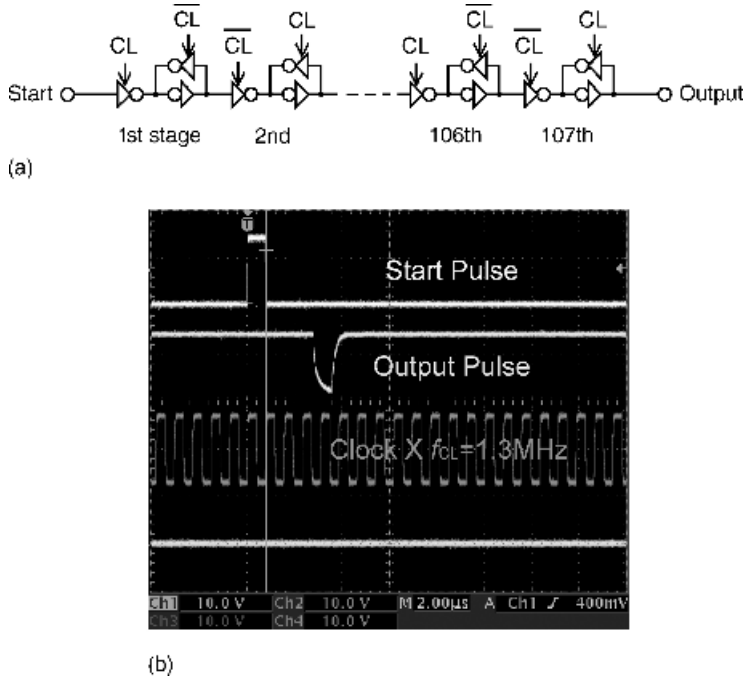


Figure 24.11 The operation of the 107-stage static shift register measured after transfer onto the PES film: (a) the circuit diagram and (b) the waveforms during operation

delay time for each stage. The oscillation frequency over 3 MHz was also observed when a 10 V driving voltage was applied.

Furthermore, the operation of a more practical circuit was also examined. Figure 24.11 shows the operation of a 107-stage static shift register, which was also measured after transfer. The static shift register is widely applied to an integrated driver circuit for active matrix display devices in order to select a data line or a scanning line in sequential manner. Figure 24.11(a) shows the circuit diagram of the shift register. When the start pulse is input to the first stage, the pulse passes through the register series with a delay time corresponding to the clock frequency. In Figure 24.11(b) the output pulse was successfully observed at the final stage of the shift register in correct timing when a clock frequency of 1.3 MHz and a driving voltage of 7 V were applied. It proves that all the transistors composing the shift register are working, even after transfer onto the plastic film.

It was experimentally confirmed from these results that the SUFTLA TFT device has enough potential to be applied to practical electronic devices.

24.5 Applications

24.5.1 SUFTLA TFT LCD

Having demonstrated the usability of the SUFTLA technology in our experiments, we tried to fabricate a real display device on the plastic film. The first trial was performed on a 0.4 in diagonal TFT LCD (Utsunomiya *et al.* 2001).

Petitioner Samsung Ex-1011, 0516

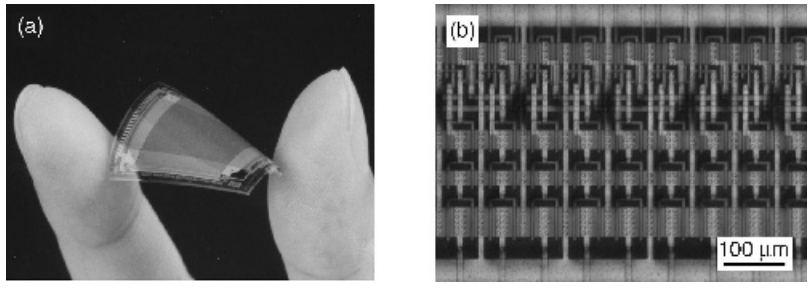


Figure 24.12 (a) The appearance and (b) the micrograph of the TFT LCD circuit transferred onto the plastic film

Table 24.1 Specifications of the SUFTLA TFT LCD displays.

Diagonal	0.7 in
Pixel number	428 × 238
Pixel pitch	34 μm × 46 μm
Driving scheme	Analog, point at a time
Frame frequency	60 Hz
Driving voltage	12 V
Data driver	
107-stage static shift register × 4 series	
Clock frequency	1.3 MHz
Scanning driver	
(119-stage static shift register + 238 NAND gates) × 2 series	
Clock frequency	4 kHz

Figure 24.12(a) shows the appearance of the SUFTLA TFT LCD circuit transferred onto a plastic film, and Figure 24.12(b) shows the micrograph of its driver circuit. Even though the chip size was as small as 25 mm × 21 mm, all of the display circuit was successfully transferred onto the plastic substrate without any mechanical damage. The specifications of the SUFTLA TFT LCD are summarized in Table 24.1. It has a 0.7 in diagonal display area with 428 × 238 pixels in it. The data driver circuit and the scanning driver circuit were integrated around the display area. The data driver consisted of a 107-stage static shift register, which was typically designed to drive at 1.3 MHz clock frequency and 12 V driving voltage. The scanning driver consisted of a 119-stage static shift register and 238 NAND gates. Both have a very basic and simple structure for the integrated driver circuit using a CMOS LTPS TFT.

The LCD assembly carried out by a conventional method after the TFT circuit was transferred onto the plastic film, as shown in Figure 24.13. A plastic film, with a sputter-deposited indium tin oxide (ITO) electrode was used as a counter substrate. The liquid crystal alignment layer of polyimide was formed on the counter substrate and the TFT circuit substrate, and a main seal was printed on the counter substrate by screen printing. After the gap spacer was dispersed on the counter substrate, the coated surfaces of the two substrates were presented to each other. Then liquid crystal was injected in the gap between the substrates, and the main seal opening was sealed with UV-curable adhesive. Finally, the flexible printed circuit (FPC) was bonded onto the circuit substrate with anisotropic conductive film (ACF).

Petitioner Samsung Ex-1011, 0517

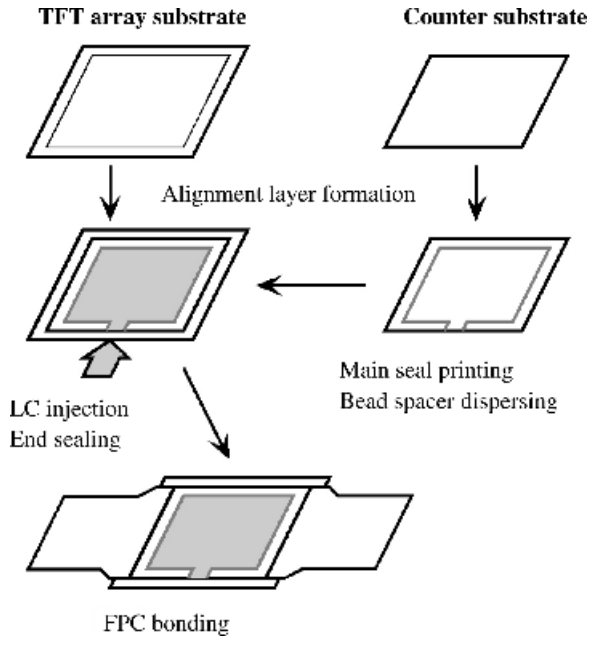


Figure 24.13 TFT LCD assembly process

Figure 24.14 shows a display image sample of the all-plastic substrate TFT LCD. The observed image was not so clear, but it proved that the TFT circuits, including integrated CMOS TFT driver circuits, worked even after transfer by the SUFTLA process.

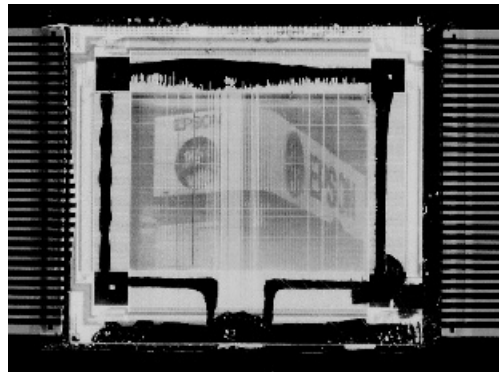


Figure 24.14 The display image sample of the all-plastic substrate SUFTLA TFT LCD

24.5.2 SUFTLA TFT OLED

In Section 24.5.1 the LCD was fabricated as a trial device to show the feasibility of the SUFTLA technology. But the LCD presents some difficulties for flexible display fabrication. Because several substrates, such as a polarizing film, a color filter and a backlight, are

Petitioner Samsung Ex-1011, 0518

needed to make a complete display module, the module becomes totally thick and hard to bend. The reflective LCD with color-filter-on-TFT structure, which was demonstrated by Asano *et al.* (2002, 2003) was a reasonable example to realize a flexible LCD device, because the backlight and the polarizing film on the backside are not necessarily unlike a transmission-type LCD.

On the other hand, the OLED display is expected to be one of the ideal systems for flexible display devices, because all the display components are thin solid films and they can be assembled on a single thin substrate. And the OLED display has the potential to reproduce a clear moving picture. This is the reason why we tried to fabricate the OLED display on the plastic film by using the SUFTLA technology.

The specifications of the TFT OLED display device are summarized in Table 24.2. It has a 5.3 cm diagonal display area, in which 200 × 150 pixels are arranged. The TFT circuit also

Table 24.2 Specifications of the SUFTLA TFT OLED display

Diagonal	5.3 cm (2.1 in)	
Pixel number	200 × 150	
Pixel pitch	211.5 μm (120 ppi)	
Subpixel pitch	70.5 μm	
Driving scheme	Digital, line at a time	
Typical driving conditions		
Clock frequency	Signal driver	333 kHz
	Scanning driver	5 kHz
Driving voltage	Signal driver	6.0–8.0 V
	Scanning driver	6.0–8.0 V
	OLED	5.0–8.0 V

includes the peripheral integrated drivers around the display area. The driver circuits drive the pixels in area ratio, grayscale, digital line at a time mode.

The scanning driver includes a 150-stage static shift register, which was designed to operate at 5 kHz clock frequency. A scanning line is selected by the scanning driver, and the signal driver applies the digital signals into the pixel circuits connected to the selected scanning line. The signal driver includes a 50-stage static shift register, which was designed to operate at 333 kHz clock frequency. The signal driver also has two sets of latch circuits in order to store the input signal data sets for the next scanning line. Figure 24.15 shows the block diagram. Figure 24.16 shows the pixel circuit layout. Each pixel consists of nine subpixels, which are controlled to be completely in the on-state or completely in the off-state. Three subpixels are allotted to each primary color (red, green and blue). Therefore 64 colors are reproduced by controlling the number of subpixels in the on-state.

The OLED display assembly was carried out after the TFT device was transferred onto the plastic film by the SUFTLA process. The OLED materials were patterned using an inkjet printing technique (Shimoda *et al.* 1999). Figure 24.17 shows a cross section of the pixel circuit. The pixel structure consists of an ITO anode electrode, a pixel-opening window and a pixel separator. A 3,4-polyethylenedioxythiopnene-polystyrenesulfonate (PEDOT-PSS), which works as a hole injection layer, and the OLED materials were inkjet printed at the appropriate position on the device surface. Before pattering, the surface of the pixel separator was treated so that it would repel the ink droplets, whereas a hydrophilic surface was

Petitioner Samsung Ex-1011, 0519

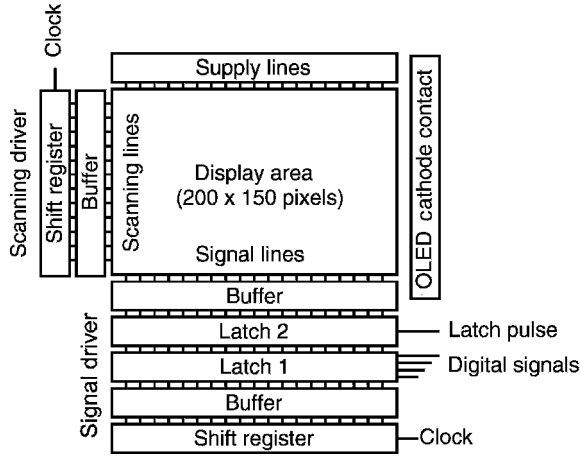


Figure 24.15 Block diagram of the TFT OLED display circuit

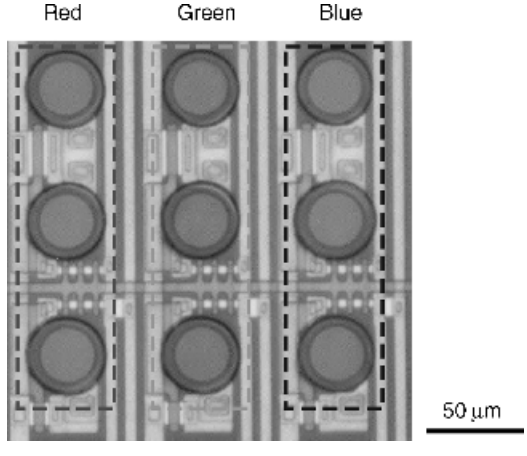


Figure 24.16 Pixel circuit layout of the TFT OLED display circuit

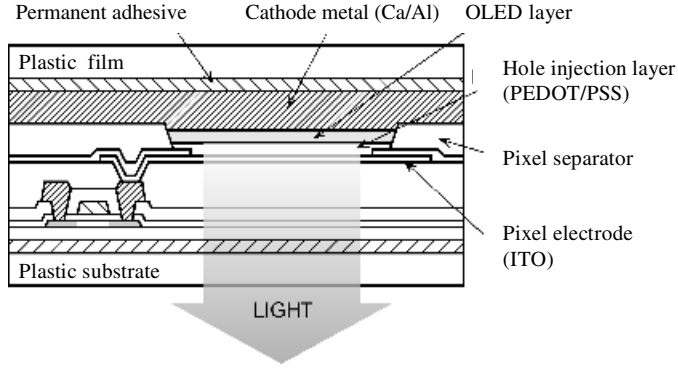


Figure 24.17 Cross section of the pixel circuit of the TFT OLED display circuit

Petitioner Samsung Ex-1011, 0520

given to the area inside the pixel-opening window. Therefore each ink droplet moves of its own accord to the accurate position after landing on the pixel. This procedure gives precise positional accuracy to the patterned OLED materials, even though there is a significant positioning error due to the distortion of the TFT circuit on the plastic film or the error in the landing position of the ink droplet.

After forming the OLED layer, the cathode electrode with its calcium/aluminum bilayer structure was deposited by vacuum deposition. The cathode electrode was encapsulated by gluing a plastic film over it using a permanent adhesive, to protect the OLED layer from moisture invasion. When an electric current flows through the OLED, emitted light is reflected by the cathode electrode and comes out through the plastic film, as shown in Figure 24.17. This type of OLED display is called a bottom emission display. Finally, the FPC was bonded on the side of the display device using ACF, as for the LCD.

Figure 24.18 shows the appearance of the SUFTLA TFT OLED backplane transferred onto the plastic film and Figure 24.19 shows the display image it produces.

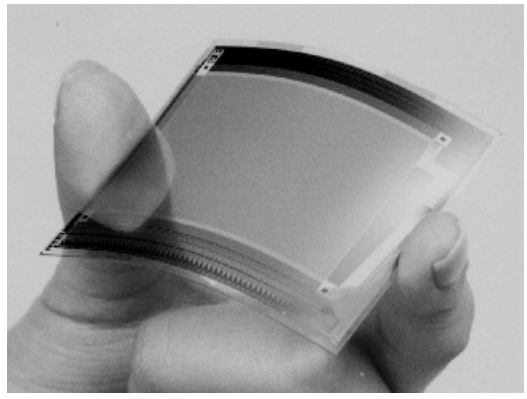


Figure 24.18 Appearance of the TFT OLED display circuit transferred onto the plastic film

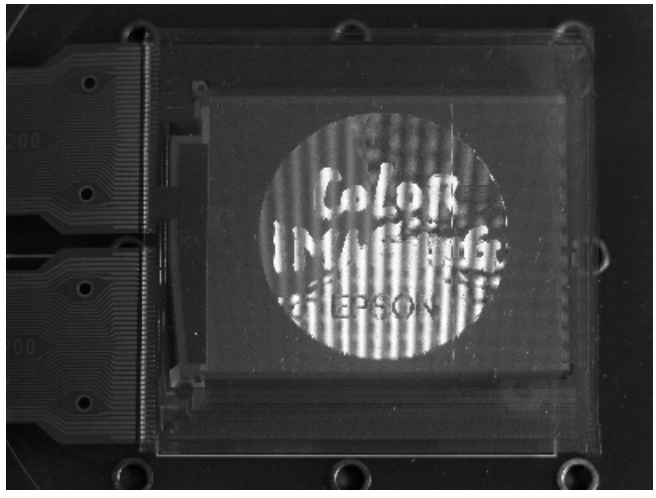


Figure 24.19 The display image sample of the all-plastic substrate SUFTLA TFT OLED display

Petitioner Samsung Ex-1011, 0521

The thickness was 0.7 mm and the weight was only 3.2 g. A clear image was displayed on the all-plastic substrate active matrix OLED display, which shows that the TFT device isn't damaged or degraded by the SUFTLA process. The results demonstrate that the SUFTLA technology has a high potential for flexible display manufacturing.

24.6 Summary

The TFT transfer technology named SUFTLA is based on an excimer laser ablation/annealing technique. High-performance and finely patterned LTPS TFT devices, fabricated on a quartz or glass substrate and then on a sacrificial a-Si thin film, were successfully transferred from the original substrate to the flexible plastic film by means of the SUFTLA technology. The transfer mechanism relies on the release of hydrogen contained in the sacrificial silicon layer, and the void formation due to the hydrogen gas concentration at the interface between the sacrificial layer and the TFT layer.

The TFT device performance was examined after the device was transferred onto the plastic film. The TFT device transferred onto the plastic film performed as well as the conventional LTPS TFT fabricated on the glass substrate. The TFT LCD and the TFT OLED were fabricated as trial display devices to examine the feasibility of the SUFTLA technology, and the display images were successfully observed on the all-plastic film display devices. The results prove the tremendous potential of the SUFTLA technology in the manufacture of thin, lightweight and flexible display devices.

References

Asano, A. *et al.* (2002) Low-temperature polycrystalline-silicon TFT color LCD panel made of plastic substrates. *SID International Symposium Digest of Technical Papers* **33**, 1196.

Asano, A. *et al.* (2003) A plastic 3.8-in. low-temperature polycrystalline silicon TFT color LCD panel. *SID International Symposium Digest of Technical Papers* **34**, 988.

Baeuerle, R. *et al.* (1999) A MIM-driven transmissive display with color filters on 2-in.-diagonal plastic substrates. *SID International Symposium Digest of Technical Papers* **30**, 14.

Dawson, R. M. A. *et al.* (1998) Design of an improved pixel for a polysilicon active-matrix organic LED display. *SID International Symposium Digest of Technical Papers* **29**, 11.

Goh, J.-C. *et al.* (2001) A new poly-Si TFT pixel circuit scheme for an active-matrix organic light emitting diode display. *Proceedings of Asia Display/IDW* **2001**, 319.

Goh, J.-C. *et al.* (2003) A new a-Si:H thin-film transistor pixel circuit for active-matrix organic light-emitting diodes. *IEEE Electron Device Letters* **24**, 583.

Gosain, D. P. *et al.* (2000) High mobility thin film transistors fabricated on a plastic substrate at a processing temperature of 110C. *Japanese Journal of Applied Physics Part 2* **39**, 179.

Inoue, S. *et al.* (2003) Transfer mechanism in surface free technology by laser annealing/ablation (SUFTLA). *SID International Symposium Digest of Technical Papers* **34**, 984.

Kimura, M. *et al.* (2000) An area-ratio gray-scale method to achieve image uniformity in TFT-LEPDs. *SID Journal* **8**(2), 93.

Klauk, H. *et al.* (1999) Fast organic thin-film transistor circuits. *IEEE Electron Device Letters* **20**, 289.

McCormick, C. S. *et al.* (1997) An amorphous silicon thin film transistor fabricated at 125C by dc reactive magnetron sputtering. *Applied Physics Letters* **70**, 226.

Mizukami, M. *et al.* (2000) 6-Bit VGA OLED. *SID International Symposium Digest of Technical Papers* **31**, 912.

Petitioner Samsung Ex-1011, 0522

Okada, Y. *et al.* (2002) A 4-inch reflective color TFT-LCD using a plastic substrate. *SID International Symposium Digest of Technical Papers* **33**, 1204.

Ritter, J. (2001) Active-matrix electrophoretic displays. *Proceedings of Asia Display/IDW* **2001**, 343.

Sameshima, T. (1996) Laser beam application to thin film transistors. *Applications of Surface Science* **96–98**, 352.

Sandoe, J. N. (1998) AMLCD on plastic substrates. *SID International Symposium Digest of Technical Papers* **29**, 293.

Sasaoka, T. *et al.* (2001) A 13-inch AM-OLED display with top emitting structure and adaptive current mode programmed pixel circuit (TAC). *SID International Symposium Digest of Technical Papers* **32**, 384.

Serikawa, T. *et al.* (1989) Low-temperature fabrication of high-mobility poly-Si TFT's for large-area LCD's. *IEEE Tranitions on Electron Devices* **36**, 1929.

Shimoda, T. and Inoue, S. (1999) Surface free technology by laser annealing (SUFTLA). *IEDM 99 Technical Digest*, 289.

Shimoda, T. *et al.* (1999) Technology for active matrix light emitting polymer displays. *IEDM 99 Technical Digest*, 107.

Slikkerveer, P. *et al.* (2002) A fully flexible, cholesteric LC matrix display. *SID International Symposium Digest of Technical Papers* **33**, 27.

Sugimoto, M. (2001) Multi media and display in the 21st century. *Proceedings of Asia Display/IDW* **2001**, 3.

Tsujimura, T. *et al.* (2003) A 20-inch OLED display driven by super-amorphous-silicon technology. *SID International Symposium Digest of Technical Papers* **34**, 6.

Utsunomiya, S. (2002) SUFTLA (surface free technology by laser ablation/annealing). *AM-LCD 02 Digest of Technical Papers*, 37.

Utsunomiya, S. *et al.* (2000) Low-temperature poly-Si TFTs on plastic substrate using surface free technology by laser ablation/annealing (SUFTLA). *SID International Symposium Digest of Technical Papers* **31**, 916.

Utsunomiya, S. *et al.* (2001) Low temperature poly-Si TFT-LCD transferred onto plastic substrate using surface free technology by laser ablation/annealing (SUFTLA). *Proceedings of Asia Display/IDW* **2001**, 339.

Utsunomiya, S. *et al.* (2002a) Flexible TFT-LEPD transferred onto plastic substrate using surface free technology by laser ablation/annealing (SUFTLA). *Eurodisplay 2002 Conference Proceedings*, 79.

Utsunomiya, S. *et al.* (2002b) Low temperature poly-Si TFT transferred onto plastic substrate using surface free technology by laser ablation/annealing (SUFTLA). *SID Journal* **10**(3), 69.

Utsunomiya, S. *et al.* (2003) Flexible color AM-OLED display fabricated using surface free technology by laser ablation/annealing (SUFTLA) and ink-jet printing technology. *SID International Symposium Digest of Technical Papers* **34**, 864.

Wang, Y. W. *et al.* (2001) A new pixel design for improving the uniformity on active matrix OLED. *Proceedings of Asia Display/IDW* **2001**, 323.

Young, N. D. *et al.* (1997) Thin-film-transistor- and diode-addressed AMLCDs on polymer substrates. *SID Journal* **5**(3), 275.

Petitioner Samsung Ex-1011, 0523

25

Markets and Applications of Flexible Displays

Kimberly Allen

iSuppli Corp.

25.1 Introduction

Although it is tempting to begin with a standard opening statement like ''Flexible displays have been generating much recent interest,'' the fact is that flexible displays have fascinated people for at least 50 years, and have been discussed seriously for at least 20 years. The difference now is that display and backplane technology have evolved to the point where reasonably attractive-looking demonstrations of flexible screens are possible (Slikkerveer 2003; Howard 2004).

This has had two effects. It has spurred an intense drive to finally realize the long-time dream of flexible displays. And it also has allowed industry participants to experience directly the real-world challenges of building these displays, rather than granting them the luxury of imagining that products were just around the corner.

Definitions of flexible displays can vary. For the purpose of this chapter, only these displays are included:

- curved or conformed, but not flexed during use;
- mildly flexible, but not designed for severe treatment such as rolling;
- fully flexible, like paper or cloth.

Flexible Flat Panel Displays Edited by G. P. Crawford
© 2005 John Wiley & Sons, Ltd., ISBN 0-470-87048-6

Petitioner Samsung Ex-1011, 0524

This treatment does *not* include displays built on plastic but used in a flat, rigid form, such as those employed solely for ruggedness or light weight. (These flat plastic displays have been commercialized in small quantities for cellphones.) An exception is made for dynamic signage due to the novelty of the application.

The only flexible displays to reach the market so far have been a simple electrophoretic display on plastic, used for in-store dynamic signs in sample quantities, and a curved monochrome LCD on plastic, used for a sports watch. In the time period through 2010, products are expected in other application spaces, such as consumer electronics, automobiles, and smart cards. This first generation of flexible displays will help fire the imaginations of product designers, perhaps spurring new applications that have not yet been conceived.

But this decade will remain firmly in the realm of market experimentation, rather than strong market growth. The manufacturing methods and equipment for flexible displays are very immature at this time. At every step of the fabrication process, from the substrate material through the top barrier layer and packaging, much more development is needed. The next five to seven years will be devoted to establishing processes for several display types and applications.

Resources for the development of flexible displays are increasingly available. Government sponsorship is common, and many large corporations maintain internal research efforts. The prospect of products is close enough that several small and start-up companies are also involved. However, none has emerged as a ''champion'' of flexible displays, devoted to gathering the critical mass needed to grow the industry.

The analysis in this chapter focuses on the technical, manufacturing, and market issues relevant to the flexible display industry. The goal is to define the complex strategic issues in the industry through an explanation and comparison of the existing technologies and a realistic analysis of the market opportunity.

25.2 Why Flexible?

The question as to why a flexible design is desired over a rigid design must be answered. The main reasons to use a flexible substrate are

- to make use of lightweight materials (flexing is a side effect and not a feature);
- to make a tough portable display (flexible for handling abuse);
- to make a curved display (one-time bend);
- to have a flexible or roll-up design (many flexes);
- to implement a roll-to-roll manufacturing process.

Many combinations of the above are possible. For example, the light weight of plastic is also a feature of a rugged portable product. The list draws out the independent benefits. It is also worth noting that the benefit of each of these properties will differ by application and in all cases will have to be weighed against meeting the application need with a rigid approach that is cheaper and more mature.

Overall, the suite of potential advantages for flexible displays is quite broad. And yet, in each case, only a given subset of these benefits is relevant. Companies developing flexible

Petitioner Samsung Ex-1011, 0525

displays must be aware of which benefits their products might bring to the marketplace, and then develop and market them appropriately.

25.2.1 Lightweight Displays

Designers of portable electronic devices for consumers are on a relentless quest to pack more features in a smaller and more lightweight package. In some devices, the display can be a good place to seek weight reduction. Plastic substrates can lighten a display module by 20% to 50%, depending on the architecture (light pipe, frame, driver ICs, etc.).

25.2.2 Rugged Displays

While cellphone, PDA, and notebook computer displays have become thinner over the past few years, the superstructure holding them together has become tougher and lighter. Reinforced composites and lightweight injection-molded metals have led some consumers to assume that the displays are now tough. In fact, the displays are no stronger and cannot be used without the frame or casing.

For future consumer applications, including electronic books and electronic paper, a tough display will be needed, and it will most likely be a flexible display. The desired thickness is 0.2–0.4 mm, and it should be as tough as the sheets of plastic used for overhead slides.

25.2.3 Curved Displays

These displays may be called bent, conformed, or curved. They are shaped during manufacturing, but not intended to be flexed during use. The classic example of such a display is for an automotive application. Flat displays have undesirable optical and mechanical characteristics. Reflections from flat surfaces demand expensive antireflection coatings. A display with a curved surface will eliminate both of these issues, as well as bring aesthetic appeal by matching the other curved surfaces in the auto interior. An effective solution will be embraced by the auto industry, provided that all the performance and cost constraints are met.

Curvature provides additional design freedom over a flat profile in many applications. It is possible to imagine wavy-shaped cellphones, and displays formed around coffee mugs or on jewelry, pet collars, and sneakers. What can be done with this dimension of flexible design is largely unknown at this time; many surprising uses are likely to appear when designers have early products in their hands.

25.2.4 Roll-up Displays

No other application has been used as much as the roll-up display to attract the attention of consumers and investors to the world of flexible displays (Figure 25.1). The immediate appeal is its almost science-fiction-like quality that promises to make computers more compact than their dimensions during use. Given the challenges of creating a full-color,

Petitioner Samsung Ex-1011, 0526



Figure 25.1 Universal Display Corp's flexible OLED concept. Reproduced by the permission of the Universal Display Corporation

active-matrix, high-resolution display, it is not clear from the present state of development when such a product could be commercially available.

25.2.5 Roll-to-roll Manufacturing

The second most cited reason for pursuing flexible displays is the ability or possibility of using roll-to-roll (RTR) manufacturing, regardless of whether the final product is intended to be flexed during use (Chapter 21). But further analysis is necessary to understand this imperative. Roll-to-roll processes are typically used for products with extremely low costs and medium to high volumes: printing newspapers and wallpaper; forming and coating films; making membrane switches, flex circuits, special labels, vinyl notebook binder stock, and many other mass-market items.

A strong case has not yet been built for the display market to shift from sheet-fed batch processing to continuous RTR processing. It is encouraging to see this question beginning to be taken seriously, but more effort is needed.

25.3 Supporting Technologies

The technology of flexible displays includes many components: the flexible substrate, backplane electronics, functional display materials, and various coating, sealing, and packaging technologies. In most cases these components cannot be optimized separately. A flexible display is actually a system of linked parts that must be developed in concert for the total product to function.

The substrate may be plastic, very thin glass, or metal foil. The electronics may be organic or inorganic. The display may be an LCD, OLED, electrophoretic, or other type. And the

Petitioner Samsung Ex-1011, 0527

manufacturing processes may involve vapor deposition, liquid printing, or solid transfer, in batch mode or roll-to-roll. Although not every combination is possible, there are a large number of potential alternatives to create attractive, functional panels appropriate for real-world applications. This is the major challenge for flexible display developers.

This section reviews the major components and processes associated with flexible displays, outlining the advantages and disadvantages of various approaches and combinations. The next section delves into the display technologies themselves.

25.3.1 Substrate Materials

In a sense, the substrate material plays the pivotal role in the viability of the flexible display as a competitive product offering. Substrate materials are key to meeting cost, performance, reliability, and manufacturing goals for flexible electronics and displays. Rather than starting with form and function, the venture into making flexible displays must begin with the choice of a proper substrate material.

Three broad categories of substrates are under consideration: thin glass, metal foil, and plastic. Each offers a different set of advantages, and may be more or less appropriate for a given display technology or application.

Thin glass

Glass that is very thin (~50–200 μm) becomes flexible while still retaining some robustness (Chapter 3). It may be considered for flexible displays because of the valuable qualities it has for rigid displays. It is optically clear, can be made very smooth, and is impermeable to water and oxygen. And most importantly, glass is inexpensive compared to plastic.

However, even when coated with a stabilizing resin, glass does break, which defeats the concept of a rugged flexible display. And it cannot be rolled. In fact, thin, flexible glass substrates are quite difficult to work with even in a batch process due to sagging and the creation of microcracks. Flexible glass may prove to be a good option in particular applications, perhaps automobile dashboards, which require neither dynamic flexing nor ruggedness, but it will need codevelopment of novel handling techniques.

Metal foil

For some display technologies, an opaque backplane is not a problem. This makes metal foil an attractive option because it has the impermeability of glass without the breakability. Usually stainless steel is used because of its resistance to corrosion. The steel must be coated with an insulator to prevent shorts. Metal foil could possibly be used if mild flexing of the display is expected during use, but due to hardening, it is unlikely to perform well under dynamic bending or rolling.

UDC and E Ink have used metal foil as backplanes for OLEDs and electrophoretic displays, respectively. These were demonstration units; such a substrate has not been commercialized for a flexible display.

Petitioner Samsung Ex-1011, 0528

Plastic

Plastic is the usual substrate associated with a flexible display (Chapter 2). Plastics come in a stunning variety of forms limited only by organic chemistry, allowing for many candidates. The performance trade-offs in plastic can be severe, however, making no candidate ideal.

The mechanical, optical, and thermal properties of the plastic must be suitable for a display. Here are some examples of what this means:

- low coefficient of thermal expansion (CTE), well-matched CTEs at adjacent layers, and adequately high working temperature;
- high transparency ($>$ 90–95%, for transmissive displays);
- good surface quality for depositing films;
- resistance to solvents or etchants used in processing the display;
- low birefringence (for LCDs).

Potential candidate materials for flexible display substrates include polycarbonate (PC), polyethylene terephthalate (PET), polyethersulfone (PES), polyetheretherketone (PEEK), and polyethylenenaphthalate (PEN), although literally hundreds are being investigated. In some cases, notably PES, PEEK, and PEN, the material can be ''heat-stabilized'' immediately after extrusion. The heat-stabilization process is done in tension and involves partially aligning the polymer chains. This can greatly improve the dimensional stability of the plastic, meaning the change in size and/or shape due to thermal expansion and contraction.

Barrier layers

Barrier layers are crucial for all types of displays based on a plastic substrate (Chapter 4). Compared with glass, plastic is about 10 million times more permeable to water and oxygen. Moisture and oxygen damage liquid crystals, OLED emitters, and other functional display materials.

A barrier can be as simple as a single-layer coating or as complex as a multilayer stack. A single layer of an inorganic compound such as SiO_2, Al_2O_3, SiN_x, or MgO can be adequate as a barrier layer for LCDs. It is possible that a very dense and amorphous single layer, such as one made by the physical vapor deposition (PVD) process of Symmorphix, would be adequate as an encapsulant for OLED on glass also. But in a flexible display, a single-layer barrier may have difficulty maintaining integrity, especially the oxides or nitrides. These materials will crack readily under tensile stress, leaving openings for moisture and oxygen.

Multilayer barriers tend to be the most robust and forgiving due to built-in redundancy. A defect in one layer does not affect or does not add to a defect in another layer. The process developed by Vitex Systems uses alternating layers of Al_2O_3 and organic acrylate material. Dow Corning is developing barriers based on silicon carbide and silicon oxicarbide. Most companies researching OLEDs and/or flexible displays also have in-house efforts to develop a barrier layer.

Petitioner Samsung Ex-1011, 0529

25.3.2 Semiconductor Material Classes

If the flexible display is to be active matrix, it must have an array of switches, typically thin film transistors (TFTs) on the backplane (Chapters 11, 12, 13, and 14). Silicon transistors have been found to change their mobility and on/off ratio under flexing (for tensile and compressive stress). This can have dramatic effects on the quality of the display image. Furthermore, as noted above for barrier layers, inorganic materials tend to crack under strain.

In the long run, it is clear that an organic material will more adequately serve a fully flexible display. Many challenges arise in replacing silicon with a purely organic material. These include attaining

- adequate mobility,
- process simplicity (hence low cost),
- process stability and repeatability,
- acceptable switching characteristics,
- compatibility with other materials.

Silicon serves as the performance target for the development of organic transistor materials. In its amorphous form, Si has a mobility of 0.5–1.0 cm^2/V s. This makes it ideal as the active matrix switch for an LCD, although not for driver circuitry. Channel dimensions can be made very small, and the speed is great enough to allow all necessary switching times. For OLEDs, it is likely that a higher-current transistor will be necessary. Polycrystalline silicon, in use for AMOLEDs and some AMLCDs, has mobilities of 100–300 cm^2/V s. Pure single-crystal silicon is around 1000 cm^2/V s.

The myriad organic semiconductor materials under investigation cannot be catalogued here, but several promising candidates include pentacene, DH6T (dihexylhexaithiophene), DHADT (dihexylanthradithiophene), P3HT (poly(3-hexythiophene) regioregular), copper hexadecafluorophthalocyanine, and F8T2 (poly-9,9-dioctylfluorene-*co*-bithiophene).

In terms of very basic performance parameters, such as mobility and process temperature, several candidate organic semiconductors already exist, at least under laboratory conditions. But looking deeper brings up several other issues. First, none can yet be made in a truly manufacturable process. That is the key challenge for the near term.

There is a key distinction in organic semiconductor fabrication: pentacene, as a small molecule, can be evaporated, whereas the polymer types are made by solution processing. The evaporation of pentacene is what allows the high mobility, but a price is paid for introducing a vacuum process. Solution processing is more elegant and likely to be less expensive in the long run, but so far has not yielded such high mobilities. The trade-off between performance and ease of processing is well known in the display industry, as it also figures greatly in the evolution of OLED technology.

But more important, the type of semiconductor must be noted. All of the candidates with adequate mobilities are p-type. So far, no n-type materials have been acceptable. Standard silicon devices use CMOS (complementary metal–oxide semiconductor) technology, which requires n-type and p-type semiconductors. Current organics would only be useful for PMOS (positive-channel metal–oxide semiconductor) technology, which is more challenging.

Petitioner Samsung Ex-1011, 0530

Voltage threshold uniformity is the main hurdle; it is faced in a-Si processing and would be even more problematic with the notoriously difficult-to-handle organics.

Thus, organic TFTs are expected to work most effectively in devices that operate on a field effect (also called voltage-driven), e.g. LCDs and electrophoretics. Those that require large currents, e.g. OLEDs, LEDs, and electrochromics, are not as well suited to organic backplanes, at least in the near term.

Looking to the longer term, simply substituting organic materials for silicon in standard semiconductor device structures seems unlikely to produce devices of equivalent performance. Hence concepts such as fully organic computer processors that rival even the ones in use today (much less in the future) seem unrealistic from this vantage point. Organic semiconductors in conventional structures are better suited for lower-performance applications in general, and this is even true within the realm of displays.

25.3.3 Processing Transistors on Plastic

Regardless of whether an inorganic or organic transistor material is to be used, the process of making a transistor array on plastic is nontrivial. Standard process temperatures, even for ''low-temperature'' polysilicon (LTPS), exceed 300 °C, which is unacceptably high for most plastics. Manufacturing of active matrix flexible displays on plastic cannot be achieved until this problem is solved. The early stage of present efforts is indicated by the wide array of options being investigated.

Four main methods have been pursued. One idea is to adapt the LTPS process to even lower temperature so that the array can be built directly on the plastic. A more novel approach is to apply the transistor materials to the plastic as liquids at room temperature, most commonly through inkjet printing (the newest, most embryonic liquid method is to build the transistors through self-assembly). A third way is to use ''solid'' printing, which resembles a carbon-paper approach of applying the layers to the plastic by transferring them from a donor sheet. Finally, a full transfer process can be employed, in which the transistors are built normally on glass, and then the entire array is transferred to a plastic substrate.

Table 25.1 shows the main companies pursuing each type.

Low-temperature direct processes

The reason that low-temperature polysilicon processes are not done at even lower temperature is that inorganic semiconductors made at such low temperatures have poor electrical and chemical properties. In order for LTPS to provide an advantage over a-Si (such

Table 25.1 Companies involved in processing transistors on plastic

Low-temperature direct processes	Liquid processes	Solid processes	Transfer processes
FlexICs	Plastic Logic	Sarnoff/DuPont	Seiko-Epson
Rolltronics	Nanolayers	Samsung SDI	Sony
Samsung Electronics	Nanosys		
Xerox			

Petitioner Samsung Ex-1011, 0531

as the ability to have integrated electronics), its mobility must be at least two orders of magnitude greater. Achieving this to date in a manufacturable way on limited time and budget has meant using a process temperature higher than plastics can tolerate. However, several companies have worked hard to lower that process temperature, even if it means giving up a little bit of mobility.

FlexICs is a start-up firm that has succeeded in reducing process temperatures for poly-Si to a maximum of 115 °C (for all except the final annealing step), such that transistors can be fabricated directly on many types of plastic substrates. Samsung Electronics has chosen to work with a-Si, and has succeeded in making TFTs with a mobility of 0.4 $cm^2/V\,s$ on PES substrates below 150 °C. Rolltronics is tackling the specific task of adapting inorganic electronics to a roll-to-roll process. Displays are one of several key applications it is addressing.

An alternate direct method is being pursued at the Xerox Palo Alto Research Center (PARC). At heart it is traditional lithography, but the process requires no exposure through masks. After a film is deposited, a wax mask is applied by inkjet printing. Then the film is etched to remove all portions not under the wax mask. Xerox has demonstrated this technique to make print-patterned a-Si substrates on glass, and believes that it can be extended to poly-Si and plastic substrates too.

Liquid processes

All of the examples in the previous section concern silicon electronics. Other efforts are under way to fabricate organic electronics on flexible substrates by direct processing at low temperature. The more straightforward way to deal with organics is in liquid form. Hence this type of direct patterning is radically different from standard inorganic processing. It is an elegant solution.

Inkjet printing is the basis of many flexible display, organic transistor, and OLED development programs. Inkjet has great potential for developing into a low-cost manufacturing option for displays and other organic electronic products.

The most important aspect of inkjet printing is that it must be considered as a complete system. This includes ink chemistry and rheology, printheads, substrate surface properties, and drying or treatment processes. The ultimate goal is to enable high-speed, large-area display production using only inkjet technology without other structures such as preformed wells or barriers. Inkjet can enable material efficiency of more than 90%, which is the inverse of the 10% or less expected for vapor deposition.

Droplet size is directly related to the achievable resolution. A drop volume of 7–10 pl (picoliters) will enable a color display with 130 dpi (dots per inch), which is roughly equivalent to a high-resolution monitor or color cellphone display. Inkjet systems sold by Litrex and those developed by Seiko-Epson are capable of this. Epson is reportedly able to reach 2 pl with its multilayer head design.

Throughput is currently about 4 min per layer for a 14 in $\times$ 14 in substrate. This rate will probably improve to 2 min for the next generation of inkjet printers. With the current prices for printers, the most economical solution is to add more systems to enable parallel processing, in which case this throughput would be acceptable.

Positioning accuracy is a complex function of the printhead, speed, aerodynamics of the drop trajectory, and other qualities. Repeatable accuracy to enable printing of 130 dpi over

Petitioner Samsung Ex-1011, 0532

400 mm × 500 mm or eventually 550 mm × 650 mm substrates appears to be achievable. Almost all these initial tests have been done on glass. Polymer OLEDs fabricated on glass by inkjet printing could begin to command a share of the OLED market if they bring cost advantages over vapor-deposited OLEDs. However, flexible displays remain an important secondary goal.

The dual challenge of developing the inkjet printing itself and on an unusual substrate will lengthen the time to market. Established inkjet companies, accustomed to the high-revenue graphics market, have been less than interested in investing in the development of speculative concepts like flexible displays. But in the long run, this type of manufacturing has the potential to replace part of the market served by more expensive conventional techniques.

Another radically new approach to deposition of semiconductor, insulator, and conductive layers is ''nanotech processing,'' in this case self-assembly through molecular layer epitaxy. Companies like Nanolayers, NanoSys, and many others are pursuing these systems. Each layer of material is grown separately and self-assembled to the correct form, building up the device.

Nano-assembly is done through a combination of solution and vacuum processing, usually at less than 200–300 °C. Initial results are suggesting extremely high mobilities, on the order of few × 100 cm^2/V s. Much work remains to be done before these materials and processes are ready for commercialization.

Printing techniques used in traditionally lower-precision industries such as printed circuit boards, decoration, and plasma display processing may eventually be used in some parts of the flexible display industry. These include screen printing, offset printing, and transfer pad printing. But several critical materials problems must first be solved.

Solid processes

The most common ''carbon-paper'' solid process involves transfer of material from a donor substrate to the final plastic substrate by a laser. One current effort in this approach toward flexible displays is a project in the Advanced Technology Program funded by the National Institute of Standards and Technology (NIST) and undertaken by Sarnoff as the lead investigator, along with DuPont and Lucent. The results of the program will be applied to OLED displays by DuPont. Another is the laser-induced thermal imaging (LITI) process of Samsung SDI. LITI was originally applied to manufacturing polymer OLEDs on glass, but Samsung is also working on it at a laboratory stage for flexible displays.

These types of processes are ''clean'' and have been proven for other applications in the printing industry (Creo, a printing industry company, supplies some of the equipment). In the display industry, a similar method was considered for color filter production, but has not panned out. Many challenges remain to be solved. For example, various materials are found not to stick well, or to generate cracks when bent.

Transfer processes

The transfer process is one way of avoiding the dimensional changes that occur when plastic substrates are heated to near their glass transition temperature (Chapter 24). A TFT array is

Petitioner Samsung Ex-1011, 0533

formed on a glass substrate and then transferred to plastic after it is completed. Some intermediate steps are needed to facilitate the transfer. The basic process is as follows:

1. A sacrificial stopper layer is deposited on a conventional glass substrate.
2. The TFT is deposited on top of the stopper layer.
3. The glass with the TFT layer is glued with a removable, but non-water-soluble glue to a temporary plastic substrate.
4. The glass is removed while the sacrificial layer protects the TFTs.
5. The sacrificial layer is removed.
6. Another plastic substrate is adhered in place of the glass with permanent adhesive.
7. The temporary substrate from the other side is removed.

The two main proponents of this method are Seiko-Epson and Sony. Their processes differ only in the choice of sacrificial layer and removal mechanism for the glass substrate. Seiko-Epson calls its technique surface free technology by laser annealing/ablation (SUFTLA). It uses a-Si as the sacrificial layer, called an exfoliation layer. A Xe:Cl excimer laser is used to release the hydrogen in the a-Si, which loosens the glass from the TFT array. Sony uses an etch stop layer as the sacrificial layer and removes the glass by dissolving it in hydrofluoric acid.

This type of full transfer process is obviously a detailed undertaking, but it has been proven to work for PDA-sized LTPS displays. Products have not yet been commercialized.

25.3.4 Flexible Display Manufacturing Processes

Because flexible displays are rather new for the display industry, manufacturers have an opportunity to step back and consider various manufacturing methods.

Sheet-fed or batch processing is the norm across the display industry as well as the entire semiconductor industry. A slight variation on strict batch processing is the cluster-tool concept, where individual sheets are shuttled to parallel processes while inline. This helps balance the line load. Several process steps can be done simultaneously in a cluster-tool setup. The key to cost reduction in batch processing is to load-balance the line at all times. This usually means finding the weakest or slowest link and upgrading it to keep pace with the overall line speed. This might mean adding extra tools, or it might mean working with vendors to increase throughput.

Sheet-fed processing is currently being slighted to some degree by the tremendous interest in pursuing a fully roll-to-roll (RTR) process. Based on the past and current success of TFT-LCD and plasma display (PDP) makers, sheet-fed processing still has many years of useful life before it is retired in favor of roll-to-roll processing. In some areas, it may never be retired.

The concept of roll-to-roll processing, also called reel-to-reel, is to move away from the present batch or cluster-tool process flow to a system more akin to that used in the printing industry. The ultimate vision is to process continuous rolls of display substrates, so that displays of any size or shape can simply be cut from the roll (simpler visions allow for

Petitioner Samsung Ex-1011, 0534

multiple rolls processed in different machines). The roll moves at a continuous speed through a processing line that may include vacuum chambers with deposition, etching, and other processing. The substrate film could be any sort of flexible plastic compatible with the display process. Sometimes the roll is known as the web.

RTR manufacturing is well established in many areas, such as office labels, food packaging, and the newspaper industry, but it has not yet been applied to displays. Although it has become an unquestioned assumption that RTR would dramatically reduce the manufacturing cost of flat panel displays, this may not always be the case. Each batch process must be considered separately to determine whether RTR would be an appropriate replacement. RTR processing can be used beneficially when certain circumstances are in place:

- all tasks in the process fit within the allotted time (based on the speed of the web);
- a high-volume output is desired (and matched with the market);
- all major tasks can be performed inline.

If all three of these conditions are not met, RTR has limited benefits and advantages over batch processing, or may not be advantageous at all. The printing industry provides a clear example of this. Sheet processing is used in the vast majority of printing houses, even though web printing is available. For very high volume runs, such as many newspapers and magazines, RTR processing makes economic sense. For small to medium-sized jobs, sheet-fed printing is advantageous.

Note that in some aspects of adapting RTR, high costs must be paid in creating new infrastructure rather than using what already exists in other industries. Attention must be paid to what is native to RTR, such as handling floppy substrates, and what is not, such as lithography. Also, in standard equipment available today, the web is rarely wider than 30 in; using RTR processing to make very large displays will require moving to larger equipment sizes, not simply adapting processes.

On the market side, most of the highest-volume display applications are focused on large-sized displays, not small-sized displays. The development of RTR processing for flexible displays, however, will probably need to take an evolutionary path from small size to large size, hindering rapid RTR adoption unless there is a major breakthrough in process technology.

25.4 Flexible Display Technologies

So far, the discussion has not focused on particular display technologies. This indicates the multitude of issues with flexible displays that do not even involve the display portion of the system. This section discusses the main display technologies that could be suitable for flexible displays, as well as their advantages and disadvantages in this medium.

25.4.1 Liquid Crystal Displays

LCDs were the first genuine version of flexible displays because they were the only display type that could be made in that format when flexible backplanes were first devised

Petitioner Samsung Ex-1011, 0535

(Chapters 16, 17, 18, 22, and 23). Texas Instruments was working in this area about 20 years ago. The display should operate in reflective mode if it will be flexed during use; otherwise, a flexible backlight or sidelight is also required.

By far the most difficult challenge for the LCD arises from cell gap variations. The visual quality of an LCD relies heavily on having a constant cell gap, as this parameter figures directly in the equations of light management. Flexing the panel creates forces that will cause the liquid crystal to flow, resulting in cell gap variations across the panel. This produces visual distortions and artifacts, which can easily become irreversible. Solutions with support posts and other infrastructures have not worked effectively in a manufacturing environment. It is likely that cell gap problems will prevent LCDs from serving truly dynamically flexible markets, such as realistic electronic paper. However, LCDs face few restrictions in less challenging applications such as curved auto dashboards.

Over the years, many types of LCDs, including less well-known modes like cholesteric and polymer dispersed, have been suggested for use in flexible LCDs. In general, there is no reason to assume these others will be easier to commercialize in flexible form than they are on flat glass. However, bistability is one property of nonstandard LCDs that could be beneficial in some flexible applications. Examples of bistable LCDs include the ''zenithal bistable'' technology of ZBD, the BiNem technology of Nemoptics, and the cholesteric technology of Kent Displays. However, all three companies are planning to start with glass-based products for applications that use bistability, such as electronic books. None considers flexible applications to be a near-term prospect.

Viewing angle is another challenge. When bent, some part of the display will be at an obtuse angle to the viewer. Although modern active matrix LCDs have an excellent range of acceptable viewing angles, this is not the case for many of the simpler LCDs that are being considered for flexible products. Thus, the viewing angle effect may be dramatic.

Finally, it is difficult to include color filters and keep them aligned within a flexible display. Monochrome flexible LCDs will be far simpler. A curved monochrome LCD has been commercialized in the Nike Triax watch. This product also features a display with rounded edges, something much easier to accomplish on a plastic or metal substrate. This gives designers more options.

25.4.2 Organic Light-Emitting Diode Displays

OLEDs are considered the ''natural'' choice for a flexible display, which explains the strong interest among OLED players (Chapter 15). Properties such as Lambertian emission, good colors, no cell gap problem, and the potential for using many promising new solution processing techniques constitute most of the attraction.

But on further consideration, the OLED needs more development before it is suitable for flexible displays. The most substantial challenge is water and oxygen sensitivity, which is a factor on both sides of the display when a polymer substrate is used. As discussed in Section 25.3.1.4, several options are being developed, but none is fully manufacturable yet.

Other challenges for OLEDs derive from the fact that this display technology is still somewhat immature. Manufacturing processes are not well established at this time; some companies are still experiencing poor yields. This is expected to improve rapidly over the next few years. Furthermore, OLED displays still have high power consumption compared to what is expected for eliminating the backlight and color filters that are necessary on an LCD.

Petitioner Samsung Ex-1011, 0536

Improvements in the cell design and materials should help. The power consumption issue is relevant in flexible display development because one reason to choose a plastic substrate in a portable device is to reduce weight and therefore power consumption. This could limit OLED displays entering these early, straightforward applications that are needed to propel the market forward.

Finally, the current-driven nature of the OLED means that above about 160 lines, the display requires an active matrix (AM) driving scheme. The difficulties outlined above for building TFT arrays on plastic indicate that AM flexible displays will not reach the market in the near term. This means that the prospects for OLEDs are limited to small displays until active backplane technology is adequate. Furthermore, as noted in Section 25.3.2, OLED displays are not the ideal candidates to be driven by fully organic backplanes due to their current-driven nature.

In the long run, the OLED is an excellent candidate for flexible applications. Most of the items noted here are temporary barriers that will be overcome with time. However, this longer development timescale must be considered when forecasting the future of the flexible OLED.

25.4.3 Electrophoretic Displays

Electrophoresis means physical motion under a force; electrophoretic displays switch images by movement of particles under voltage (Chapter 19). Many implementations of the concept exist, and have been increasing in popularity. Examples of recent implementations include those by the following companies:

- E Ink (two types of particles suspended in microcapsules);
- Gyricon (bicolored balls rotating in individual sockets);
- SiPix (one type of particle in a dark-colored fluid);
- Bridgestone (two types of particles with no capsules);
- Canon (one type of particle and in-plane addressing).

Electrophoretic displays are almost invariably reflective and bistable. Most lack a threshold to facilitate matrix addressing (SiPix's technology is an exception). Therefore they are combined with an active matrix backplane, built with a triode-type grid, or used in direct-drive mode. One key advantage of electrophoretic displays over OLED displays are the less stringent barrier requirements.

Of all the flexible display technologies, so far only the electrophoretic types can be made in large sizes. The main limitation is slow switching speed (hundreds of milliseconds), making electrophoretics a poor choice for video or even rapid scrolling. This largely eliminates the cellphone and games markets and parts of the auto market.

E Ink and Gyricon's technologies have been field-tested for commercialization in retail dynamic signage applications, good applications for electrophoretic displays because of their bistability. Gyricon is pursuing this option aggressively, having built a roll-to-roll factory for its products.

Petitioner Samsung Ex-1011, 0537

Electronic paper and electronic books are also named as key applications for electrophoretics, again because of their bistability. The initial electronic book products released in 2000 and 2001 did not fare well in the market, but newer display technologies are now available. E Ink plans to commercialize an active matrix monochrome display for an electronic book application in early 2004. Although this display is built on glass, it will be an important trial to see if the market is ready for the next generation of products.

Gyricon has also demonstrated an active matrix panel. It uses inkjet-printed electronics made by Plastic Logic using Dow Chemical's F8T2 material as the channel. This demonstration was on glass.

25.4.4 Other Types of Display

A number of other technologies are being pursued for flexible displays. Electrochromic displays are still under development after decades of research and applications in self-darkening automotive mirrors. Electrochromic displays operate by reversible oxidation–reduction reactions that change a material between two different colors. Unlike previous versions that relied on liquid cells filled with acid, the latest versions are solid-state and can be made flexible.

Dow Chemical has invented an electrochromic technology called Commotion that switches between two colors. It is applied to plastic substrates using screen printing technology that is already available. The initial application was a greeting card but higher-value options, such as time and temperature (TT) labels and smart cards, are also possible.

NTera is a small firm whose electrochromic technology is called Nanochromics. It uses extremely fine particles of titania (6–8 nm) surrounded by an electrolyte and a chromophore (viologen). When a current is applied, the active material forms a monolayer around the titania and turns dark. Contrast of 18:1 with about 50% brightness is reported (this is close to ink on paper). The samples have a switching speed of about 0.1 s and an operating voltage of 2 V. NTera is aiming first at glass-based applications, but has an eye on plastic for the future.

Citala is a start-up that has invented a solid display material that does not rely on polarization to manage the light. The solid formulation means that it can function effectively in a flexible display without changing the cell gap. It also requires less rigorous sealing than a liquid-based display. Picvue Electronics is assisting in manufacturing these displays, which have so far been used in a small batch of novel clock displays.

Ricoh is working on several display technologies specifically suited for electronic paper. The company is also developing special printer technology to work in conjunction with its paper. The most advanced version uses three photochromic materials that become dark under UV exposure, then they can be selectively decolored using visible light to produce colored documents by subtraction. Products are still in a very early stage of development.

The new prospect of viable flexible displays is encouraging companies to explore novel display options. Indeed, with a new medium such as flexible displays, it is not required that the standard, well-known display technologies will be the best suited, especially for currently unimagined applications. However, the already commercialized technologies like LCD and OLED do possess the advantages of more established infrastructures.

Petitioner Samsung Ex-1011, 0538

25.5 Market Forecast

Some care must be taken to define the terms associated with a market forecast. The iSuppli and Stanford Resources forecast covers 2003–10, with 2002 included as a historical year. The data are presented by technology type and application. All dollar values are in 2003 US dollars.

A flexible display panel is considered to be a component, or intermediate product, hence the market for these displays is highly dependent on the market for the end products in which they are used. In some cases the flexible display is enabling a new market, and in others it faces competition from nonflexible alternatives. Two items should be noted:

- The forecast does not include flat plastic displays, such as ruggedized mobile phone panels. An exception is made for dynamic signage due to the novelty of the application. These displays are made by roll-to-roll processing, but are currently affixed to a rigid PCB backplane.
- The prices used to calculate display value are for the display panel or module, whichever is typical for the application. In cases where the display is sold as part of a system, primarily dynamic signage, the price still represents the estimated panel (component) price, *not* the system price.

The appropriate application categories for flexible displays were gleaned from discussions with nearly 30 key industry participants. They represent the most likely target areas as currently envisioned. Table 25.2 gives examples from each category.

Note that in most cases the application constrains many other characteristics of the display (e.g., size, substrate type, degree of flexibility). Table 25.3 lists these characteristics. *Substrate* refers to the three types discussed above (thin glass, metal foil, plastic). The *configuration* refers to the degree of flexibility. A curved display is bent once during fabrication and remains in that bent, curved, or conformed position during use. Another is mildly flexible, but not designed for severe treatment such as rolling. The third is very flexible, like paper or cloth. These three types are called curved, flexible, and rollable, respectively. These applications also tend to have typical sizes associated with them.

Table 25.2 Flexible display applications

Application	Definition and examples
Appliances and other consumer electronics	Home appliances, home electronics, mobile music devices, watches, athletic performance meters
Automotive	Indicators, gauges, navigation, and rear-seat entertainment systems
Mobile phones	Mobile phone handsets
Dynamic signage	Digital signs with communication capability
Electronic books	Electronic readers with attached power source
Electronic paper	Electronic readers without attached power source
PDAs and handheld computers	PDAs and handheld computers
Smart cards	Cards equipped with flex circuits and display
Other	Rollable displays, clothing, and future applications

Petitioner Samsung Ex-1011, 0539

Table 25.3 Related features in flexible displays

Application	Substrate	Configuration	Diagonal size (in)
Appliances/and other consumer electronics	Plastic	Curved	<1 to 3
Automotive	Glass, metal, plastic	Curved	Up to ~7
Mobile phones	Plastic	Curved, flexible	<1 to 2
Dynamic signage	Metal, plastic	Flexible, rollable	~7 to >20
Electronic books	Plastic	Flexible	5–8
Electronic paper	Plastic	Rollable	12–15
PDAs and handheld computers	Plastic	Curved	2–4
Smart cards	Plastic	Flexible	<1

25.5.1 Top-Level Market View

Flexible display panels are currently available only in sample quantities, but by 2005 the market is forecast to reach 45 000 units valued at $311 000, rising to 25.5 million units valued at $17.8 million in 2010 (Figures 25.2, 25.3, and 25.4; the applications are discussed in Section 25.5.3). Many of the units in the later years are low-value smart-card displays, as discussed below, accounting for the low average selling price (ASP). The ASP is simply the market value divided by the units.

A distinct step is seen in 2005, the year when the first infusion of trial products into the market is expected. Another step is around 2007–08, when flexible dynamic signage becomes widely available. The exact timing and size of these steps are nearly unpredictable;

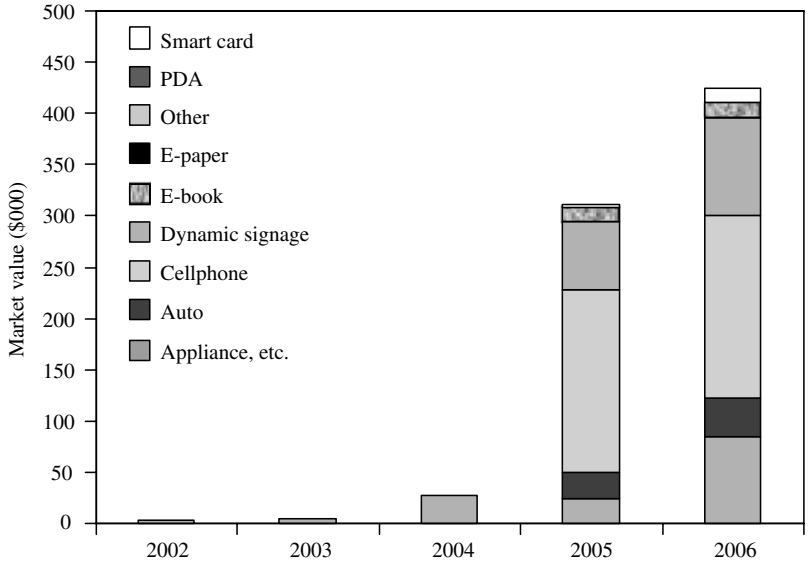


Figure 25.2 Flexible display value by application, 2002–6

Petitioner Samsung Ex-1011, 0540

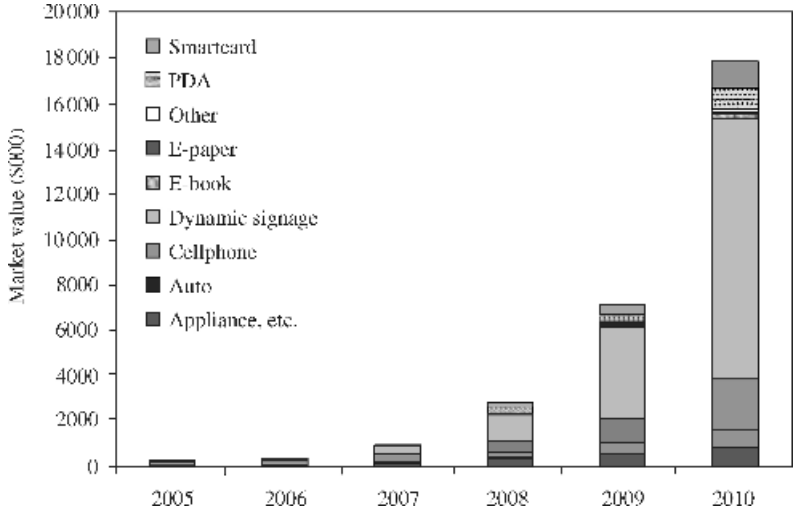


Figure 25.3 Flexible display value by application, 2005–10

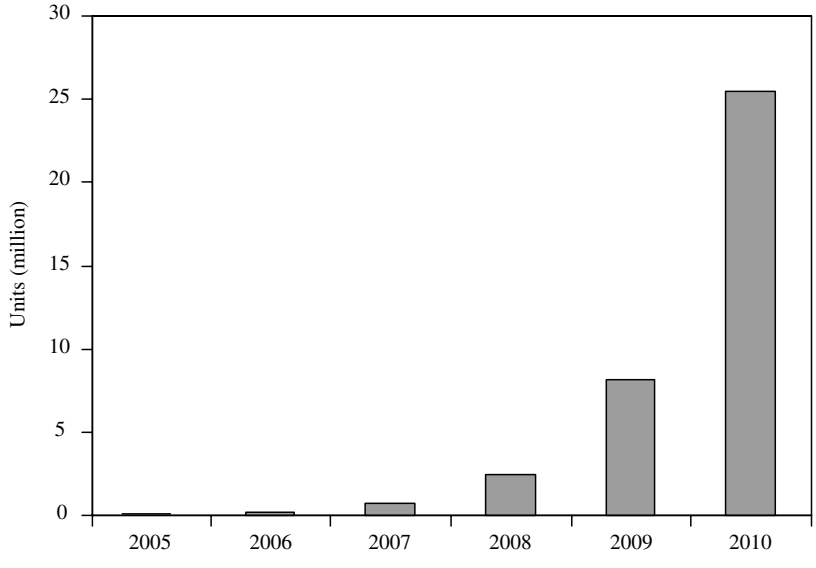


Figure 25.4 Flexible display units, 2005–10

the more important factor is the longer-term vision, independent of such details. Sections 25.6 to 25.8 discuss the logic behind the market forecast presented here.

25.5.2 Market by Display Technology

Due to the huge installed base and decades of manufacturing experience, LCD technology is already mature on glass and has been produced on rigid plastic. Hence it can be converted to

Petitioner Samsung Ex-1011, 0541

flexible substrates with the investment of fewer resources than some other technologies. The key players in Japan developing flexible displays favor the LCD as a near-term candidate. However, flexible LCDs have some technical disadvantages, as noted in Section 25.4.1. They may eventually be supplanted by the more color-capable OLEDs and easier-to-produce electrophoretics in the flexible space. In 2010, LCDs are expected to account for just 19% of the value.

OLED displays are just becoming manufacturable in mass quantities on glass. Interestingly, one barrier to the development of the flexible OLED market is that OLED players are just beginning to taste success in the glass market, and are loath to take resources from that effort to develop plastic. In fact, OLED companies have few resources to spare at this time, due to a combination of the lackluster economy and recent expenditures on first-generation factory equipment. And flexible OLEDs are immature technically, meaning that significant resources will be required to make commercial products. Nonetheless, OLED offers the best combination of speed, color, and viewing angle of all the options.

Thus, it is expected that OLED technology will ramp up slowly in the flexible market, coming into production only near the end of the decade. Another challenge for OLED players in achieving large unit sales will be making appropriate reductions in price. OLEDs will account for 12% of the value in 2010.

Electrophoretic technology is well suited for flexible applications, and almost all companies pursuing this technology are interested in the flexible market. The bistability of electrophoretic displays could offer advantages in several markets. The main challenge is that many applications will require color, but also the manufacturing is still underdeveloped. Electrophoretic may be limited to lower-value, monochrome applications during this decade. Nonetheless, it was the first flexible display type to be commercialized, and is expected to continue increasing in the dynamic signage application. It will grow to 68% of the value in 2010 (the vast majority of which will come from dynamic signage and smart card applications).

Electrochromic technology may find some purchase in the market in some specific cases. And there is always the possibility that a new type of display technology will emerge to fill this new space in the market.

25.5.3 Market by Application

The application distribution for both units and value in these early years of flexible product introduction has less to do with ultimate product success than with the particular structure of the market for each application. Some market segments allow for very small trial runs, while others have minimum order levels of thousands or tens of thousands of units.

The value of the flexible display market by application is shown through 2010 in Figure 25.2 and through 2006 in Figure 25.3. The near-term opportunities are in dynamic signage and mobile phones, although other applications will appear in the next few years also. Looking to the end of the decade, the applications with an early advantage will continue to lead, but others, such as smart cards, will accelerate also.

Figure 25.5 shows the unit forecast excluding smart cards (the extremely high volumes of even trial runs of smart cards are higher than all other applications combined). The figure shows that dynamic signage represents the largest contribution after smart cards. From this vantage point in time, dynamic signage appears to be a promising candidate because product

Petitioner Samsung Ex-1011, 0542

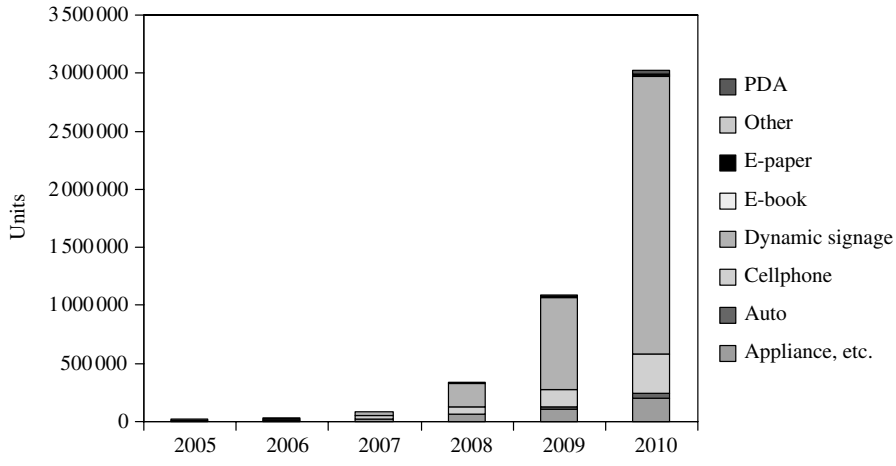


Figure 25.5 Flexible display units by application, excluding smart cards, 2005–10

is already in the market (in field trials) and the means of production exists. These and other key applications are discussed below.

Smart cards

The idea of the display-equipped smart card is to include a small display on an identification, phone, security, or credit card that shows some of the information carried in its embedded electronics. The display must be bistable, rugged, and slightly flexible. It can be changed by interfacing the card with a powered read/write device. Direct-drive monochrome characters are acceptable. LCD and electrophoretic are the most likely technology choices, but electrochromic is also an option in some select cases.

Note that ''smart card'' is also a more general term meaning cards equipped with electronic chips to perform functions. These are becoming more common in applications such as national ID cards and security badges, and could see even wider use. However, not all such smart cards have displays, or even a need for a display. Thus, the total market will be smaller than that for all smart cards.

Price is a tremendous challenge; only pennies per card will be tolerated by the market. When these cards can be easily and inexpensively produced, it is possible to imagine a scenario in which enormous numbers of units are needed. However, the low price point means that these cards will remain a small source of revenue in the long run. A good plan would be to combine their production with other products on a high-volume line.

This application is nearing commercial viability. It is possible that trial runs of products could occur within the next six to eight quarters. Anticipating that large volumes will not occur until the second generation of devices, the market does not make a large uptick until the end of the forecast period. This is likely to be when electrophoretic and LCD devices can be manufactured in large volumes with technical qualities that match the requirements for smart cards.

Petitioner Samsung Ex-1011, 0543

Smart cards dominate the flexible displays unit forecast (97% in 2010) simply because so many can be made; each display is far less than an inch in diagonal. In terms of value, the smart card market is also somewhat significant ($1.1 million; 13% of total value in 2010).

Dynamic signage

The concept of dynamic signage is to turn retail signs into displays that can be changed by a few keystrokes rather than by physically swapping the sign. This might be done remotely if the signs are connected by wires to a local network (say, through a cord that suspends them from the ceiling) or locally by beaming a signal from a handheld device. It can save effort in labor and also allows the store greater flexibility in the message on the sign. It is even possible to imagine tailoring the sign's content every few hours depending on which customers are likely to pass by at that time of day.

Dynamic signs do not have to be flexible displays. Indeed, much of the interest in this market currently concerns LCD and PDP technology, which are large, bright, video-capable displays perfect for attracting attention. (Another segment of the market concerns dynamic outdoor signs or billboards, which can be LEDs, video walls, or various other technologies.) The appeal of a flexible display for indoor signs could come from its smaller size, lower price, lighter weight, and multiplicity of hanging and mounting options compared to LCDs and PDPs.

This is potentially a large market, given the enormous number of signs used in stores (estimated at close to 100 million in North America alone). However, in light of the limited budget of many such operations, it is not clear how large a fraction of signage could be converted to digital. The flexible displays will be a subset of the total. Because of the novelty of this product, and the fact that the display portion is printed on a roll-to-roll line, even flat, rigid displays are included (they are rigid because at this time they are driven by a stiff printed circuit board backplane).

As E Ink and Gyricon have become aware, it pays to offer a total solution. Store owners are not necessarily high-tech enthusiasts, and even if they are, they probably have a tight budget. Many prefer options that are simple, fast, and cheap – essentially ''plug and play.'' (And yet they will also have high standards for the display quality, especially the brightness and color because the sign must be eye-catching.) This means creating a product that includes both hardware and software, with an intuitive interface. Note that the price in the database represents the ''display price,'' which can be difficult to extract from a total-solution product. Nonetheless, it can be estimated from the system cost.

The price differences partially result from the expected sizes, although the preferred sizes in this nascent market have hardly been established. Electrophoretic displays are the only type so far that can be made in fairly large sizes (up to 30 in wide using standard roll-to-roll equipment). They also have the big advantage of bistability. LCDs could serve in smaller sizes. OLEDs will come into the market later because the technology will not be ready for manufacturing on flexible substrates in the near term. The increase in potential size for OLEDs near the end of the forecast counterbalances the dropping price in each size range. Dai Nippon Printing is exploring this application for OLED. The company recently received a Cambridge Display Technology license with the intent to make polymer OLEDs on plastic sheeting for retail signage in Japan. However, most of this market is expected to remain electrophoretic.

Petitioner Samsung Ex-1011, 0544

One important question in the market's evolution is the potential for color. Monochrome products are in demand at this time, but history shows that most display markets evolve irreversibly toward color. Electrophoretic displays cannot easily use color at this time, although companies are working on ways to achieve color. The market is expected to reach 2.4 million units valued at $11 million in 2010.

Mobile phones

The large number of mobile phone units in Figure 25.5 is driven by the requirement that mobile phone shipments exceed about 10 000 units, even for test products, simply to fill the channel. When a handset maker decides to test a flexible product, these volumes will be required, and it is expected that some design wins will occur in the near term. The total mobile phone market stands at well over 500 million units, so the flexible portion represents a small fraction in the foreseeable future.

Taking very thin panels based on plastic or metal foil and incorporating them into mobile phones would be highly desirable for the weight reduction and increased ruggedness. However, this treatment does not cover *flat* plastic or metal panels that are used only for their light weight. The relevant mobile phones are those using curved panels or even dynamically flexible ones. These designs might be chosen for their visual appeal as a means of product differentiation. So the important question becomes, What is the product? One challenge is that flexible displays, like most new technologies, would seem likely to enter the market in a high-end product. Also, they would probably begin as a subdisplay (also called secondary or external display) because these require fewer pixels. But high-end mobile phones currently have an active matrix main display. This type of display is unlikely to be made in curved form until late in the decade (due to technical challenges). If the main display is flat and rigid, why would the subdisplay be curved?

Thus, the initial product most easily imagined at this point is a curved mobile phone with either a single passive matrix display or two such displays. DuPont Displays has shown a concept demonstration of this type, although it did not have a functioning display. These are likely to be niche markets at the time such products arrive (around 2005 for LCDs). Near the end of the forecast, curved or flexible active matrix displays could be reaching the market, which would open up new options.

More speculative product possibilities also exist. One can imagine a rigid main display with some kind of ''flap'' cover (like some current PDA cases) that could be slightly flexible. This flap could contain a flexible subdisplay.

A longer-term option could be a disposable mobile phone that looks something like a large smart card: it would have a display, a few buttons, a small flat battery, and some kind of communication link. Some companies have already talked about such concepts, and given the popularity of disposable phone cards, the product would already have a place in the market, as well as distribution channels into convenience stores worldwide. This could have very large numbers of units, but would need a price of just pennies per display.

LCD and OLED will provide the basis for this market, with OLED gaining the upper hand in the long run due to its superior viewing angle (which is important in a curved display). The slow speed of electrophoretic displays will limit participation in this market until perhaps the very end of the decade, when they might serve some of the more speculative items discussed.

Petitioner Samsung Ex-1011, 0545

Electronic paper

This application has been a vision in the display industry for many years. Sheets of rewritable paper that can interface with computers or printers seem to represent the ultimate in convenience, combining the best aspects of computers and standard paper.

The technological challenges are enormous. This product is required to be fully bistable and reasonably high resolution. It must also be durable in that it might be crammed into a briefcase or pressed against with a ballpoint pen. From this vantage point, LCD and OLED seem to be unlikely candidates. Various electrophoretic options are promising, and some companies are even inventing new technologies in combination with the printer that will create the documents (e.g. Ricoh and Xerox).

The use paradigm has yet to be established. Calling this still-hypothetical product ''electronic paper'' conjures images of replacing every piece of plain, noninteractive paper with a dynamic counterpart. However, it is clear on reflection that the cost of this would be prohibitive. Instead, it is likely that paper used only for certain purposes will become electronic.

Even more intriguing is to imagine that the electronic paper does not replace paper, but rather replaces a laptop computer in certain situations. For example, when attending a meeting, it is common to bring a laptop because it has some important document or file that will be shared (alternatively, the file may be printed by one person, or sent by email ahead of time and printed by many people). Instead, the document could be printed onto electronic paper and shared among meeting attendees, and then the paper could be reused (possibly after notes written on it in the meeting were uploaded back to a computer).

The appeal of the second concept is that the price of the sheets could be quite high. If each person only needs a small number of sheets (say, less than 10) to carry around in lieu of a laptop occasionally, a price of $25 or more could be acceptable. Attempting to fit electronic paper into a ''paper'' paradigm could require price more than two orders of magnitude smaller, although savings due to continual recycling help offset the cost. These costs need to be studied in much more detail.

This market is expected to emerge slowly near the end of the decade. The technical and business challenges of the product make it likely that only samples will be available in small quantities by 2010.

Automotive

The automobile industry is extremely interested in curved displays for car interiors. These will solve several mechanical and optical problems with flat displays. Furthermore, this is a time of rising interest in displays in general on the part of automakers. Displays are adding value to many parts of the car, allowing for differentiation and new options.

However, along with the increased attention comes an increased discrimination in quality. Requirements for color, resolution, brightness, and environmental characteristics are becoming more stringent. Even today's AMLCDs are struggling to meet the standards in some cases. By the end of the decade, standards will be even higher. And the price is always expected to be low.

Nonetheless, flexible displays (curved) are expected to do well in this market. New technologies tend to penetrate the auto market slowly, with the average time from market

Petitioner Samsung Ex-1011, 0546

readiness to widespread deployment in cars being about 15 years. Thus, by 2010, the market will be small but accelerating. Curved displays will begin in high-end vehicles and may pass through a phase in rental vehicles to gain the attention of average buyers. Only then can they penetrate mainstream cars.

Other applications

Flexible displays may potentially be used in a wide range of other applications, from athletic equipment and clothing to industrial products. Perhaps the most intriguing possibilities are those that have not yet been conceived. When flexible displays have been in the market for a few years (say, near the end of this decade), designers will find new ways to use them that cannot be envisioned today. This will pave the way for additional market growth beyond 2010.

25.6 Regional Development

The flexible display industry is developing differently in various regions of the world. It is too early to make strong statements about market leaders, but some general comments can be made about regional development activity.

Japanese companies started the plastic displays business several years ago with small-scale production of rigid passive LCDs on plastic, mainly by Sharp, Ricoh, and Matsushita. These were intended as rugged displays for handheld devices (primarily cellphones), but were not overly successful due to high price and comparatively poor visual quality. At the time, some announcements were made of intentions to build factories, but with the subdued market reception, these plans did not materialize.

With this experience in rigid plastic and other aspects of display technology, Japanese companies have become strong developers of flexible display technology. In particular, a government–industry–university consortium has arisen to develop flexible displays. Led by Sumitomo Bakelite, the program is called the Next Generation Mobile Display Materials Development. It consists of the following corporate members: Sumitomo Bakelite, Sumitomo Chemical, Konika, JSR, Dai Nippon Ink, Dai Nippon Printing, Toray, Toppan, NEC, and Hitachi Chemical.

The New Energy and Industrial Technology Development Organization (NEDO) has built a laboratory at Tokyo Noko University, where these companies can perform development in conjunction with university researchers. It started in 2002 and will proceed for five years. The main focus is LCD technology because OLED is perceived as a longer-term opportunity. It is likely that Japanese companies will proceed into the market with caution due to their inital experience with plastic production.

The major Korean players have also shown interest in flexible technology. With their manufacturing strength, these companies could quickly enter the flexible market when needed. But other technologies are taking precedence at this time. Taiwanese players have been quieter in the flexible displays arena, focusing more energy on nearer-term prospects.

As often happens with early-stage technologies, a large R&D effort is being carried out in the United States and Europe. In the US, the Advanced Technologies Program (ATP) of the

Petitioner Samsung Ex-1011, 0547

National Institute of Standards and Technology (NIST) is actively sponsoring research in areas relevant to flexible displays. NIST ATP programs have a specific charter to support cutting-edge research in areas that represent significant commercial potential in the 10- to 15-year timeframe. Currently, two major ATP programs related to flexible displays are going on: Dow Chemical, Motorola, and Xerox are developing organic semiconductors for TFTs; and Sarnoff, DuPont, and Lucent are developing printed active matrix backplanes.

Further support of flexible displays is coming from the Army Research Laboratory (ARL), which has instituted a large grant program that is now seeking applicants. The United States Display Consortium (USDC) holds an annual conference on flexible displays to which the ARL (which funds USDC) sends representatives in charge of the grant program.

In Europe, the Sixth European Union Framework Program for Research and Technological Development (FP6) is considering funding a program called PolyApply. FP6 is an EU-level financial instrument intended to help create an internal market for science and technology. PolyApply is a program designed by European chemical and other technical companies to develop polymer electronics (polytronics) for a variety of applications, including RF ID tags, ICs, solar cells, and display backplanes.

The concept of PolyApply emerged in late 2002 from a workshop called PolyScene, which was organized by the following companies: Siemens AG (Germany), Interuniversitair Micro-Electronica Centrum VZW (Belgium), Philips Electronics (Netherlands), Fraunhofer Gesellschaft zur Förderung der Angewandten Forschung EV (Germany), Commissariat al'Energie Atomique (France), Acreo AB (Sweden), Infineon Technologies AG (Germany), STMicroelectronics SA (France), Motorola GmbH (Germany), VDI/VDE Technologiezentrum Informationstechnik GmbH (Germany), Thomson Multimedia R&D (France), and Avecia Ltd (UK).

These players and others are contributing to the strong European interest in developing polymer electronics. If funded, PolyApply could receive up to €50 million over a three-year period, and would also be eligible for continuation and further funding if progress is made.

Overall, the prevalence of academic contributors at conferences indicates the embryonic nature of this industry. When manufacturing seems to be a serious possibility, Asian companies will move to the task. This changeover cannot be seen clearly yet, which is one reason that the forecast remains modestly sized for many years.

25.7 Investment and Commitment

One unavoidable issue is that ramping up the flexible display market will require money. At this time, the industry activity consists of a moderate amount of R&D funding and the first batch of regular conferences. More bluntly, factory plans do not exist.

That is not to say that factory plans *could* not exist. The technology for flexible displays is just becoming robust enough to glimpse future products. The demand side has shown itself to be at least interested in the prospect of a flexible display. An especially enterprising company could take the lead at this time.

Several factors dampen the enthusiasm, however. One is certainly the poor economic conditions worldwide. Large display companies are loath to spend internal resources on long-term prospects, and investors of all sizes are holding back on supporting start-ups. It is easy to observe that a large fraction of conference papers on flexible displays are from

Petitioner Samsung Ex-1011, 0548

universities. Another factor is the lack of solid cost analysis at this time. It is unclear whether the most cost-effective plan is to convert an existing depreciated factory or build new equipment and a new factory. (To some degree this depends on the intended display technology and application but it is also true that, in general, players feel unsure about how even to approach such cost analysis.) Further technology development will probably help to elucidate the costs.

Thus, a crucial point in the development of the flexible display market will be when the first player steps forth and declares publicly its commitment to manufacture these displays. At what point this prospect will seem appealing depends on both technical and business factors. What is certain is that even to achieve the forecast in the previous section will require more resources than have been committed to date.

25.8 What Will It Take?

Getting down to the strategic heart of the flexible display prospect, it is now possible to gather all the technology, market, and other business information discussed so far into a set of fundamental needs facing the industry:

- new substrate material,
- full-color process,
- a ''champion'' leading to critical mass,
- compelling applications,
- ultra low cost manufacturing.

These are the sticking points that must be overcome in order for the flexible market to blossom.

25.8.1 New Substrate Material

Despite the large selection of potential substrate materials that have been proposed for flexible displays, none can yet provide the functionality, price, and reliability that glass offers. The ideal material would be transparent, flexible, low-cost, chemically inert to solvents and acids, dimensionally stable to 250 °C or higher, and would provide inherent barrier properties. Currently, each of these features is found individually or in limited numbers in different polymers, but no material yet offers all. Glass and metal foil also have limitations.

The current selection of materials introduces many cost additions or performance limitations. For example, polyimide film is attractive for its high-temperature stability, but its dark orange color prevents it from being used as a substrate for a backlit LCD. Another cost addition is the barrier layer. For both OLEDs and LCDs, a robust barrier must be added to prevent oxygen and water from reacting with the functional materials. If this barrier layer were inherent in the substrate, a simple lamination of two film sheets would be sufficient.

Petitioner Samsung Ex-1011, 0549

25.8.2 Full-Color Process

In the case of CRT, LCD, and plasma technology, large market values did not develop until large-area, full-color displays were available. This phenomenon is being experienced right now in the rigid OLED display market, and will also come to pass in the flexible display market. The market prices are set by competitive offerings and currently range from around $10 per square inch for small displays to $2 per square inch for large displays in full color. The prices of monochrome displays are less than a third as high. In order to achieve a flexible display market value of several hundred million dollars, full-color capability is required.

Inkjet printing offers the best current opportunity for a low-cost process to make full-color displays. However, the display technology best suited for inkjet – OLED – suffers from a lack of blue emitters that can be deposited by this method. As a result, inkjet printing remains in the development stage for the display industry. It is expected to play a more prominent role in the future. Laser-induced thermal imaging (LITI) requires better materials stability before it progresses to pilot or full production. But it too may provide a path to full color.

25.8.3 A "Champion" Leading to Critical Mass

The current flexible displays industry resembles an Olympic-size swimming pool with the players arrayed around the outside surveying the water. Perhaps a few have waded into the shallow end, but overall, the splash of someone taking a full plunge has not been heard.

Markets grow large when they achieve so-called critical mass – a body of players, supported by a robust supply chain that has enough momentum to propel itself over market barriers. Bootstrapping an industry from an embryonic stage to critical mass requires a ''champion,'' or preferably several, to generate interest and excitement in its potential partners and customers, as well as inspire the fear of being left behind in its potential competitors.

At the research stage, this champion can be a government agency or academic group, but to create genuine revenue, the champions must be corporate. Furthermore, it should possess significant financial resources and have a well-recognized name on the global stage. The flexible display industry does not yet have a champion, and is far from achieving critical mass. Until such a figure appears – through the act of committing a large sum to build a factory, for instance – it is unlikely that the market will blossom. Who will take the plunge?

25.8.4 Compelling Applications

Perhaps the greatest impediment to a large and flourishing flexible display market is the lack of a truly compelling business/consumer application. All successful display application segments have ultimately been driven by business/consumer adoption, rather than industrial, military, or medical niches. This implies that large numbers of consumers must find value in the new product and that they must be willing to pay to acquire it. Flexible display panels, so far, are in the position of providing alternatives to established rigid displays, which are already fairly low cost and offer very good performance.

Petitioner Samsung Ex-1011, 0550

What is needed is a new (not replacement) application, enabled by a flexible display that will drive unit sales into the millions over the next few years. Imagine a flexible product of the stature of the PDA, camcorder, digital camera, or CD player. Crucially, new applications cannot demand a major change in behavior. This has been a hurdle to the broader commercialization of head-mounted displays. While a casual observer could visualize using such displays for some novel purposes, everyday usage would require a major change in established habits. Such a major change by millions of consumers is rare, so applications that demand this often have disappointing market results.

However, it may be that the novel applications are not the places to start. Radically new applications may be forthcoming only after samples and the first generation of products have been introduced. This phenomenon is common. Camera-based cellphones, USB flash memory sticks, and car entertainment systems are examples. New applications for flexible displays that can be imagined at this time include some type of electronic paper for personal or commercial usage, folding or roll-up displays, and some types of ultra lightweight displays for handheld electronic products.

Based on the current state of flexible display performance, totally new applications are unlikely to reach the market within the next few years, although they are expected to appear at some point in the future. Even after their initial appearance, market development will take time. This conjecture has a major influence on the forecast.

25.8.5 Ultra Low Cost Production

Even after compelling applications for flexible are found (replacement or novel), the market growth may be hindered by high costs of production, hence high prices. The surest path to developing a large market is to rapidly drop the selling price of a product with advanced technology. This has been the key to the exploding markets for LCD monitors and plasma Tiffs. Flexible displays are not yet at the maturity level for rapid price and cost reductions, but they have the potential to reach this point in about five years.

With ultra low costs and prices, very high volume applications will become available. These might include electronic greeting cards, disposable products such as book covers or even wrapping paper. When this point is reached, the technology and products have become fully commoditized and are sold in an ultra competitive market at near manufacturing cost. This stage will not occur for at least 10–15 years. It is not always welcome by producers, but it is worth realizing that it must happen if such huge markets are to be tackled.

25.9 Conclusion

As expected, more questions than answers have been brought up. But it is hoped that in this final chapter the key issues have been teased apart so that players in the flexible industry have a full awareness of the technology, manufacturing, and competitive challenges on the road ahead.

Flexible displays are just barely reaching the market. The true ‘‘first generation’’ of products is yet to come. It is certainly an exciting time, and it may feel like a vulnerable time, but the industry will grow. It has 50 years of imagination behind it that can finally be

Petitioner Samsung Ex-1011, 0551

manifested technologically. The unfolding will occur fully over more than the coming decade, but those present at this early stage will likely remember these first steps as highly significant.

References

Howard, W. E. (2004) Better displays with organic Films. *Scientific American* **290**, 76–81.
Slikkerveer, P. J. (2003) Bending the rules. *Information Display* **3**, 20–24.

Petitioner Samsung Ex-1011, 0552

Index

Active Matrix OLED (AMOLED), 306
Additive Printing Digital, 238
addressing, 24, 164, 223, 246, 256, 260, 289–290, 306, 340–341, 353, 364, 367, 374–377, 380, 383, 385–386, 391–392, 393, 397, 401–404, 406–407, 414, 503, 508
Aluminosilicate, 36
AMOLED, 304
amorphous silicon TFT, 480
amorphous silicon, 8, 121, 123, 132, 214, 219–220, 229, 243, 246, 261, 263, 265, 414, 447, 452, 461–462, 463, 480, 493
antireflection coatings, 190

Barnier Cochings, 13
barrier layer, 6, 255, 413, 466, 477, 496, 500, 520
barrier layers, 3, 6, 9, 22, 32, 57, 63–64, 67–69, 73, 75–76, 119, 165, 179, 290, 292–293, 312
bias stress, 224, 226–228, 236, 242
Bichroreal, 397
birefringence, 14, 37, 164, 183, 185–186, 345, 361, 371, 498
black and white displays, 345
boro silicate, 36–37
bottom gate architecture, 247
brittle films, 102, 109–110
buckling failure, 113
buckling strain, 114–116
buffer layer, 125–132, 418, 465

Ca test, 32, 61–63, 68, 77, 292
calcium tests, 62
cell thickness, 337, 339
channel effects, 223, 226, 241, 306
charge carrier transport, 230
charge retention, 221
chemical oxidative polymerization, 139
chemical reductive polymerization, 140
chemical vapor disposition, 481
chip on glass, 459
chip on plastic, 450
cholesteric displays, 164, 177, 332, 334, 338, 341–342, 344, 350–353
cholesteric domains, 334
cholesteric film polarizers, 185
coefficient of thermal expansion (CTE), 39, 100, 119, 294
color filters, 7, 179, 186–188, 191–192, 299, 332, 355, 460, 493, 507
color patterning, 343, 345
color TFT-LCD, 462, 477, 493
conducting polymers, 5, 7, 32, 59, 76, 81, 160, 242, 261, 310, 352
conjugated polymers, 143, 158, 160, 231, 242–243, 286–287, 309
contact printing, 197, 216
contact resistance, 171, 223–226, 236
crack density, 103–104, 122, 130
critical strain, 104, 106, 117, 167–168, 173, 293
cumulative driving, 342
current decay, 227
current-drain, 223

defect, 20, 23, 58, 61–64, 70–74, 89–90, 97, 104, 107–108, 110–112, 291, 314–315, 326, 335, 411, 416, 450, 500
defect-free, 304

Flexible Flat Panel Displays Edited by G. P. Crawford

© 2005 John Wiley & Sons, Ltd., ISBN 0-470-87048-6

Petitioner Samsung Ex-1011, 0554

delamination, 100, 112, 114, 116–117, 119–120, 122, 364–365
diffusion path, 69–71, 73
Dinonylnaphtalene Sulfonic Acid (DNNSA-PANI), 203–206
direct addressing, 374–377
dispersion, 155, 185, 217, 238, 243, 302, 317, 346–351
doped polymer, 136, 224
double layer structure, 123–125
Down Draw (DD), 41
dram source current, 470–471
driver, 221–223, 246, 248, 257, 307, 341, 369, 388, 424, 467–470, 480, 487–490, 497, 501
drivers, 27, 221, 246, 256–258, 261, 306, 311–312, 401–402, 424, 463, 469–470, 473, 490
driving voltage, 318, 326, 469, 473, 486–488
droplet dispersions, 332, 334, 345–347, 349–351
droplet morphology, 347, 349
dynamic driving, 341

edge impact test, 47
electrical receptivity, 132
electrochemical polymerizations, 144
electroluminiscence (EL), 287
electron spin resonance, 484
electrophoretic displays, 12, 14, 246, 261, 328, 372, 377–378, 380–385, 387, 389–390, 494, 499, 508, 513, 515–516
electrophoretic mobility, 373, 384
electrophoretics, 7–8, 164–165, 220, 314, 502, 508–509, 513
encapsulated liquid crystals, 314–315, 317–318
evaporation, 58, 85, 91, 96, 205, 207, 214, 224, 300–301, 303, 311, 346, 348, 364, 418, 423, 444–445, 485, 501

ferroelectric liquid crystal, 326, 328
film stress, 80, 301
float glass, 41
four-point bending, 46
full color display, 299, 344

gas barrier, 32, 58–60, 76, 100, 449
Gate-source Voltage (VGS), 304–305
glass cleaning, 51–52
glass reinforcement, 48–49
glass transition temperature (Tg), 319
glass transition temperature, 165, 290, 319–320, 357, 504
Gyricon, 393

hardcoat, 20, 48
Hexadecadluorophthalocyanine (FCuPc), 207
Hole Injection Transport Layer (HITL), 288
hole mobility, 288
hydraulic trap, 397

image sticking, 378
indanthrone disulfonate, 180–181
indium binary oxides, 84
Indium tin oxide (ITO), 100, 165, 212, 355
indium tin oxide, 14, 76, 84, 86, 90, 97, 100, 120, 165, 212, 249, 310–312, 355
In-plane Switching (IPS), 368
interdigitated electrodes, 206, 359, 362, 366
ITO, 7, 58, 80–81, 83–96, 98, 100–110, 112–117, 119, 121–123, 126–132, 152, 158–159, 164–170, 173–175, 225, 288, 295–296, 299–301, 304, 308–312, 340, 350–351, 359, 417, 423, 431, 458, 468, 474–475, 490

K bonding
Kumda coupling, 141

lamination, 48, 164, 203, 206, 208, 214–217, 237, 383, 420, 425, 431, 520
leakage current, 29, 223, 229, 251–253, 288, 306, 451, 454–455
linear electrode array (Stylus ward), 401
liquid crystal display (LCD), 1, 12, 59, 479
liquid crystal displays (LCDs), 122
lithography-digital, 237
loading, 32, 102, 104–106, 117–118, 151, 166, 169–175, 309, 328, 428
Low Temperature Polycrystalline Silicon (LPTS), 464
Low Temperature Polysilicon (LTPS), 306
Lyotropic Liquid Crystals (LLC), 180

market forecats, 510
mechanical stress, 42, 123, 127, 131, 263–264, 424
metal bus disposition, 301
microcellular displays, 383–385
microcontact printing, 30, 198–199, 212–213
microencapsulated displays, 378, 380–382
mobility, 14, 29–30, 82–83, 90, 92, 94, 96, 196, 207–208, 210–211, 215, 220, 222–224, 226, 229–233, 235–236, 240–243, 250–254, 256, 288, 295, 305–307, 309, 384, 449–451, 455–456, 463, 472–473, 477, 480, 486, 493, 501, 503
monochrome display, 289, 306, 509
moth-fixed image addressing, 402
multidomain, 190, 192
multilayer barriers, 32
multiplexing, 338, 340

nanotransfer printing (nTP), 200

OLED, 6, 8, 11–12, 14–15, 18, 23–24, 29–31, 33, 50, 53, 57–62, 72–76, 175, 285–286, 288–294, 296, 298–300, 302–308, 310–312, 410, 418, 420, 424–425, 442–444, 479,

Petitioner Samsung Ex-1011, 0555

488, 490–494, 498, 500–504, 507–509, 513, 515–518, 521
OLEDs, 477
O-Octahedra, 87
Organic Light-Emitting Diode (OLED), 6, 99, 479
Organic Light Emitting Diode Displays (OLED Displays), 507
organic light-emitting diodes (OLEDs), 122
organic, 5–9, 12, 28–30, 32–33, 40, 51, 79, 81, 97, 99–100, 122–123, 128–129, 142, 146, 150–152, 159–161, 163–164, 175–176, 179–180, 191–192, 196–197, 202, 204–209, 213, 215–217, 263–266, 318, 356, 388, 402, 404, 406, 418, 420, 424, 447–449, 454–457, 462, 479, 493, 498, 500–503, 507–508, 519, 523
organic semi-conductor, 247
Organic TFT (OTFT), 307
Overlay Registration (OVL), 296–301
oxide layers, 58, 63–64, 67, 70, 176

Passive Matrix OLED (PMOLED), 298
PECVD, 33, 60, 224, 239, 299, 413–414, 453, 456–458, 461–462, 465
PEDOT : PSS (Polyethylene dioxythiophene: Polystyrene sulfonate), 317
permeability, 23–24, 40, 58–59, 61, 64–65, 67–68, 74–75, 293, 423
permeating, 63
phase separation, 93, 316, 318, 320, 326, 329–330, 346–348, 356–359, 362, 365, 368
photo alignment layers, 188
Pi bonds, 135
planarization layer, 363–364
Plyethylene Teraphthalate (PET), 290, 296, 297
2-point Bend Test, 103
poly (dialkylquarter thiophene), 235
poly (dialkylteriophene), 232
poly(dimethylsiloxane) (PDMS), 198
poly thiophene, 231
polyacetylene, 136–139, 145–147
polyaniline, 81, 138–139, 144–145, 148–150, 152, 156–157, 203, 288, 312
Polyethylene Dioxythiophene / Polystyrene Sulfonate (PEDOT:PSS), 288
polyethylene naphthalate, 13–15, 17–18, 20, 24–27, 29–30, 248
Polyethylene Teraphthalate (PET), 122
polyethylene terephthalate, 13–18, 20, 24, 27–28, 30, 290, 470, 500
Polyethylene Teriphthalate(PET), 316
polyheterocycle, 205
polyimide (PI), 13, 467
polymer dispersed liquid crystal (PDLC), 163
polymer-dispersed liquid crystals, 7–8, 176, 313, 316, 319, 321, 326–327, 368
polymerization induced phase separation, 348, 351
polymerization phase separation, 356
polymer walls, 115, 346, 360–362, 364–365
polypyrrole, 138–139, 144–145, 153, 156–157
poly-Si TFT, 261, 478, 480–481, 493–494
polythiopene, 153, 156
poly(vinyl 4-methoxycinnamate), 189
power consumption, 249, 285, 306, 313, 331–332, 342–343, 352, 369–370, 374, 507–508
printable display, 307
Π*-band, 286

reel-to-reel, 216, 365, 367, 505
reflectance, 53, 191, 323–324, 335–336, 339–340, 347, 380–382, 395
ring on ring procedure, 46

scattering imaging films, 370–371
sealant, 422, 460–461
self-assembled monolayer, 199–200, 224
semiconductor materials, 195, 211, 214, 229–230, 242, 501
semiconductor polymers, 230
sequential coating, 356
shift registers, 248, 256–261
Sigma Bonds, 135
silicon ribbons, 211
Silver (Ag), 81
singlet state, 288
Single-walled Carbon Nanotube (SWNT), 203–205
small molecule OLED, 285
small molecular semiconductors, 230
soda lime glass, 36
solvent induced phase separation, 348
source drain current, 208–211, 214
source drain voltage, 208–210, 214
source gate voltage, 470–471
spacers, 316, 320, 355, 385, 468
stacked color display, 344
stamp printing, 197
steady-state transmission tests, 61
stille coupling, 143
stress relaxation, 321–322
stresses, 29, 46, 102, 107, 109, 113, 117–119, 122–123, 128, 132–133, 264–265, 293–295, 304, 311–312, 364, 455
substrate materials, 53, 80, 165, 499, 520
subtractive printing digital, 237
Surface Free Technology by Laser Annealing Lablation (SUFTLA), 505
surface roughness, 40, 42, 60, 290, 485

Petitioner Samsung Ex-1011, 0556

surface treatment, 29, 334
Suzuki coupling, 142

tantalum (Ta), 128
tensilic test, 103
tension, 15, 27, 40, 45, 103–104, 109, 117, 119–120, 302, 312, 326, 346, 406, 417–418, 421–422, 426–427, 429–431, 435–437, 439, 500
TFT Deposition, 147
TFT-LCD, Assembly, 487
TFT transfer mechanism, 483
TFT Transfer, 8, 307, 479–484, 486, 488, 490, 492–494
thermal shrinkage, 39
thermal transfer printing, 30, 202–205, 214
TFT-LCD, SUFTLA, 485
thermally induced phase separation, 348
thin film disposition, 464
Thin Film Encapsulation (TFE), 303
thin film polarizer, 180
thin film polarizers, 7, 179, 181, 192, 368
thin film retarders, 184
Thin Film Transistors (TFT), 410
thin film transistors, 7, 24, 28, 121, 123, 176, 179, 199, 206, 211, 215–216, 219, 241, 261, 263, 309–310, 312, 410, 445, 460–461, 477, 493–494
thin film vapor barrier systems, 57
threshold voltage, 29–30, 196, 223–224, 229–230, 250, 254, 305, 307, 320, 375, 383, 398, 401, 449–451, 455–456, 486
Titanium Nitride (TiN)m
touch panels, 42, 53–54
transfer process, 28, 216, 246, 425, 464–470, 474–475, 477, 480–481, 485, 502, 504–505
Transparent Conducting Oxides (TCO), 80
Transparent Conductive Oxide (TCO), 122
triple-layer structure, 125, 131
triplet state, 288

ultimate tensile strength, 448
UV exposure, single step, 359
UV exposure, two-step, 359

viewing angle, 180, 184, 189–190, 324, 330, 335–336, 368, 369
viewing angle, 507, 513, 516
viscous drag, 394
voltage threshold, 338, 502

Water Vapor Transmission Rate (WVTR), 291

Young's moduli, 126
Young's modulus, 24, 100–102, 122–128, 131–132, 185, 294, 298, 456–457

zeta potential, 373
Zinc Oxide - amorphous, 92

Petitioner Samsung Ex-1011, 0557